EMERGING INFECTIOUS DISEASES®

CDC
CENTERS FOR DISEASE CONTROL AND PREVENTION

Fastidious Bacteria

January 2024

Jan Verkolje (1650–1693), *Portrait of Anthonie van Leeuwenhoek, Natural Philosopher and Zoologist in Delft, 1680–1686.*
Oil on canvas, 22 in × 18.7 in/56 cm × 47.5 cm. Public domain image courtesy of Rijksmuseum, Amsterdam, Netherlands.

EMERGING INFECTIOUS DISEASES®

Emerging Infectious Diseases is published monthly by the Centers for Disease Control and Prevention, 1600 Clifton Rd NE, Mailstop H16-2, Atlanta, GA 30329-4018, USA. Telephone 404-639-1960; email, eideditor@cdc.gov

EMERGING INFECTIOUS DISEASES®

Fastidious Bacteria **January 2024**

On the Cover

Jan Verkolje (1650–1693), *Portrait of Anthonie van Leeuwenhoek, Natural Philosopher and Zoologist in Delft,* 1680–1686. Oil on canvas, 22 in x 18.7 in/56 cm × 47.5 cm. Public domain image courtesy of Rijksmuseum, Amsterdam, Netherlands.

About the Cover p. 208

Perspective

Synopses

Research

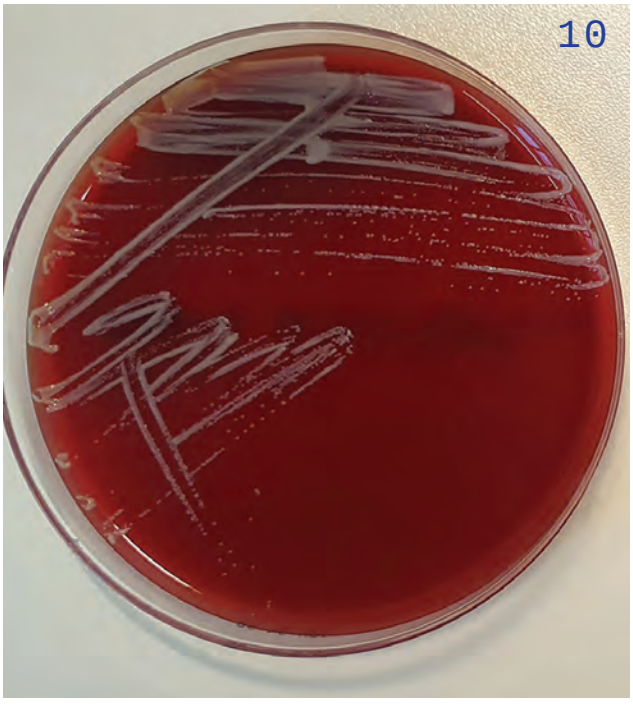

Dispatches

EMERGING INFECTIOUS DISEASES®
January 2024

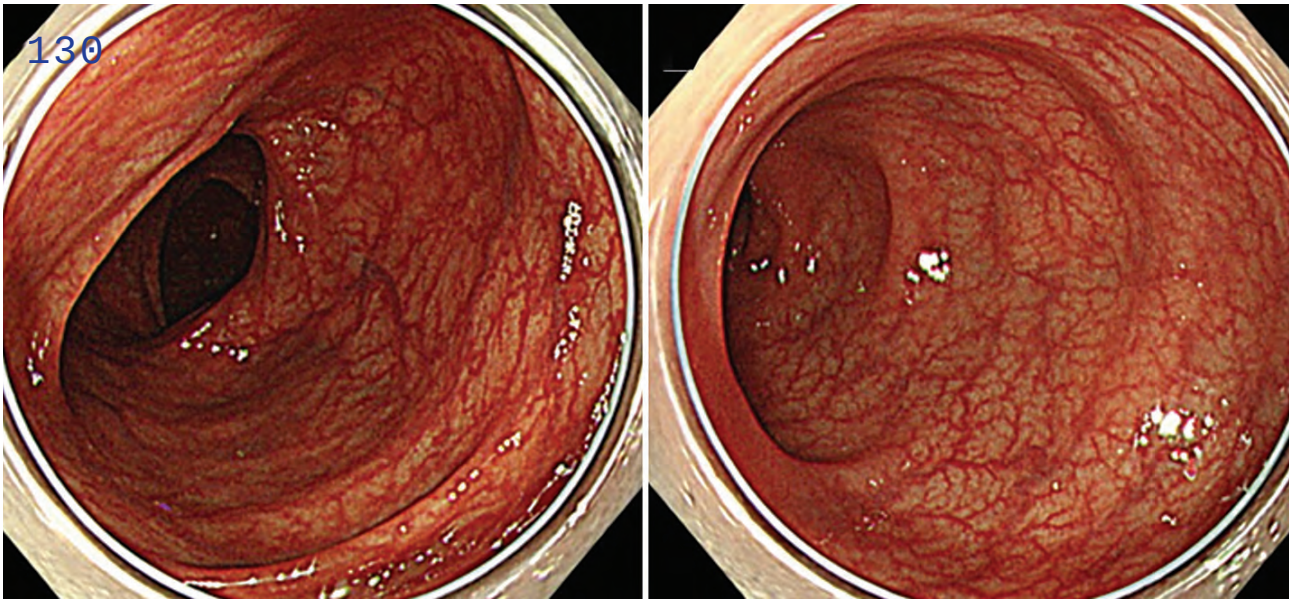

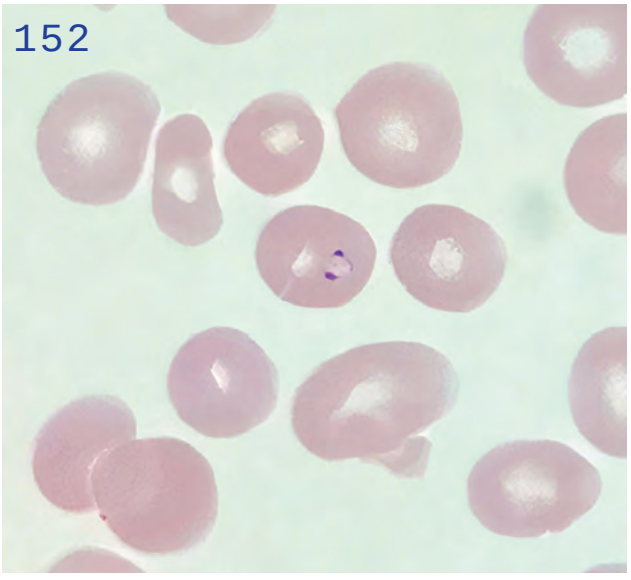

Research Letters

EMERGING INFECTIOUS DISEASES®
January 2024

Comment Letters

About the Cover

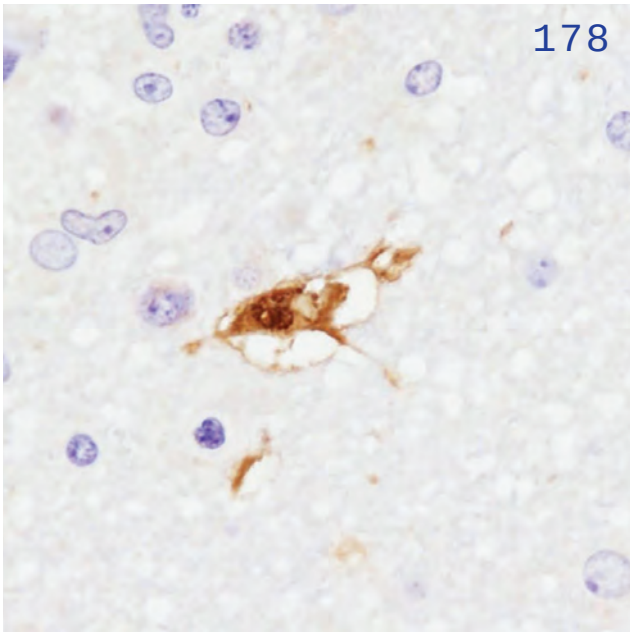

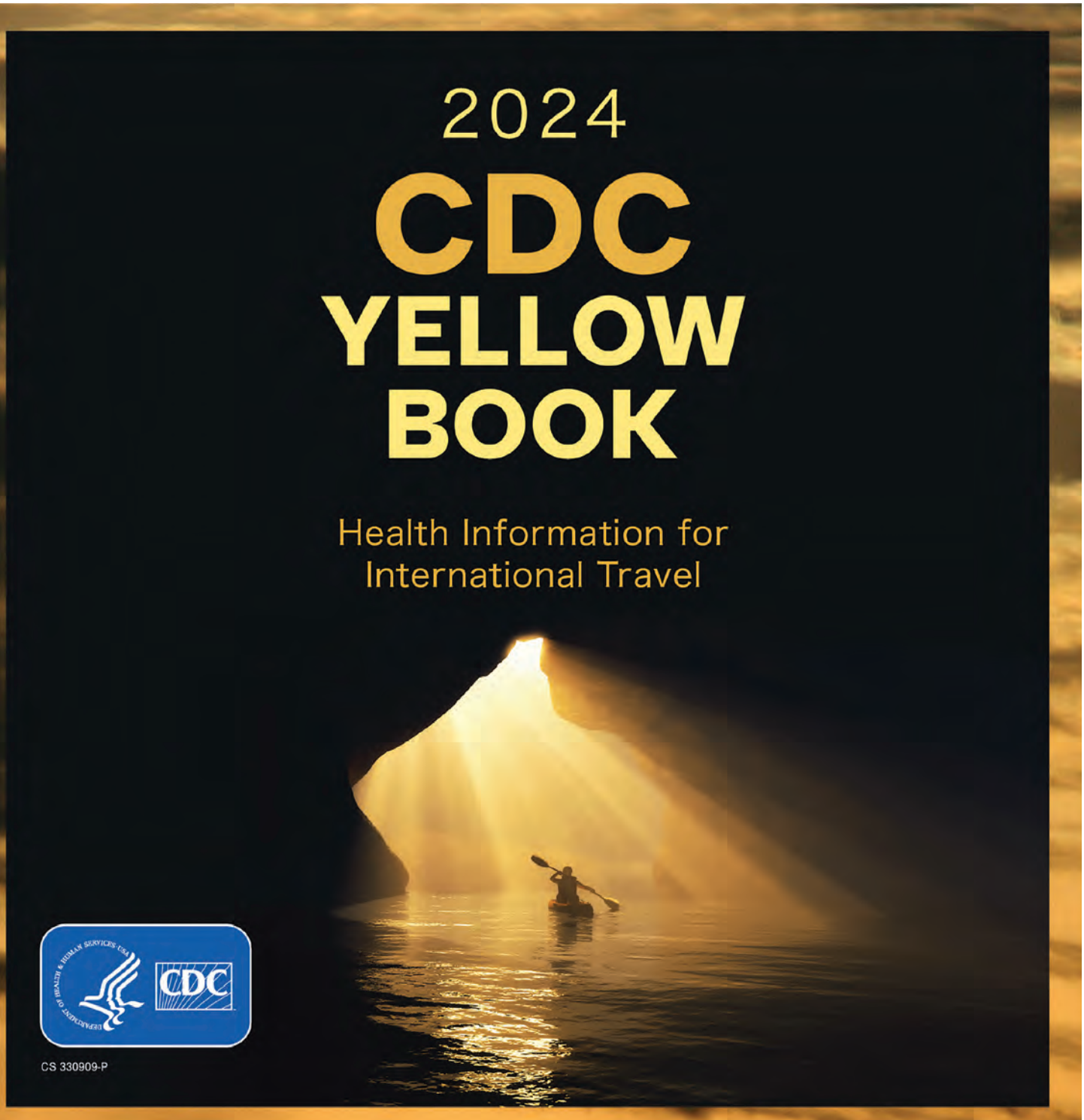

Launch of CDC Yellow Book 2024 – A Trusted Travel Medicine Resource

CDC is pleased to announce the launch of the CDC Yellow Book 2024. The CDC Yellow Book is a source of the U.S. Government's recommendations on travel medicine and has been a trusted resource among the travel medicine community for over 50 years. Healthcare professionals can use the print and digital versions to find the most up-to-date travel medicine information to better serve their patients' healthcare needs.

The CDC Yellow Book is available in print through Oxford University Press and online at www.cdc.gov/yellowbook.

Efficacy of Unregulated Minimum Risk Products to Kill and Repel Ticks

Lars Eisen

Human-biting ticks threaten public health in the United States. Registration by the Environmental Protection Agency of products to kill host-seeking ticks or repel ticks contacting humans is indicative of their safety and effectiveness. Unregulated minimum risk products, exempt from Environmental Protection Agency registration and often based on botanical oils, are proliferating in the marketplace, but there is concern about their effectiveness to kill and repel ticks. Evaluations of such products are limited in the published literature. A review showed considerable variability among minimum risk products to kill host-seeking blacklegged ticks, with effectiveness similar to chemical pesticide products for some minimum risk products but minimal impact on the ticks for other products. Evaluations of minimum risk tick repellents have typically focused on individual active ingredients rather than formulated products, which often combine multiple active ingredients. Consumers should be aware that effectiveness to kill and repel ticks can differ among unregulated minimum risk products.

Human-biting ticks threaten public health in the United States. The blacklegged tick (*Ixodes scapularis*) is a frequent human-biter and vector of viral, bacterial, and parasitic agents causing human illness, including Lyme disease (*1*). Strategies to prevent human tick bites include broadcast of pesticide products (toxicants) to kill host-seeking ticks in the environment and potentially reduce the likelihood of encountering ticks, as well as use of repellent products applied to skin or clothing to reduce the chance of a tick encounter leading to a bite (*2*). In both cases, consumers can choose to use either products registered by the US Environmental Protection Agency (EPA) or minimum risk products, also called 25(b) exempt products, that are exempt from EPA registration because the active and inert ingredients they contain are considered to pose little to no risk to human health or the environment (*3*).

Active ingredients allowable in a minimum risk 25(b) exempt product include botanicals (e.g., cinnamon, citronella, cloves, garlic, peppermint, rosemary, sesame, spearmint, thyme, and white pepper), botanical oils (e.g., castor oil, cedarwood oil, cinnamon oil, citronella oil, clove oil, corn oil, eugenol oil, garlic oil, geraniol oil, geranium oil, lemongrass oil, linseed oil, peppermint oil, rosemary oil, sesame oil, soybean oil, spearmint oil, and thyme oil), and some other types of compounds (e.g., citric acid, lauryl sulfate, malic acid, potassium sorbate, and sodium chloride) (*4*). Most compounds allowable as active ingredients are readily understood by the public to be of natural origin. Active ingredients in EPA-registered tick toxicant or repellent products often represent synthetic compounds (e.g., N,N-diethyl-meta-toluamide [DEET], IR3535, and picaridin for skin repellents; permethrin for clothing treatment; and various carbamates and pyrethroids to kill host-seeking ticks) but can also be compounds of natural origin in the case of repellents (citronella, citronella oil, and oil of lemon eucalyptus) (*5*).

Consequently, antitick products on the market fall into 3 categories: unregulated products based on minimum risk 25(b) exempt active and inert ingredients; EPA-regulated products containing active ingredients of natural origin; and EPA-regulated products containing synthetic (chemical) active ingredients. Citronella is unique in that it is included both in some EPA-registered repellent products labeled for ticks (*5*) and in minimum risk 25(b) exempt tick repellent products.

Registration by EPA of products to kill host-seeking ticks or repel ticks contacting humans is indicative of product effectiveness. Unregulated minimum risk 25(b) exempt products are proliferating in the marketplace but there is concern about their effectiveness to kill and repel ticks, as expressed in the 2020 report by the Tick Biology, Ecology, and Control subcommittee of the Tick-Borne Disease Working Group established by the US Department of Health and Human Services (*6*). In this perspective, I focus on what is known about the efficacy of EPA-registered versus minimum risk 25(b) exempt products to kill and repel ticks, and how end-users choose among these product types.

Author affiliation: Centers for Disease Control and Prevention, Fort Collins, Colorado, USA

DOI: https://doi.org/10.3201/eid3001.230813

Consumer Choice of EPA-Registered versus Unregulated Minimum Risk 25(b) Exempt Tick Toxicant and Repellent Products

Surveys conducted in Lyme disease–endemic areas of the United States provide information on levels of use of synthetic versus natural tick toxicants (*7*–*9*) and repellents (*8*,*10*). However, survey questions were not phrased specifically to distinguish between EPA-registered and minimum risk 25(b) exempt products. Moreover, no survey has addressed the reasons why members of the public choose to use EPA-registered versus minimum risk 25(b) exempt tick toxicant and repellent products. A reasonable assumption is that choice of an EPA-registered product is driven by a belief that the registration ensures the product will be safe and effective in killing or repelling ticks when used according to label recommendations. Use of EPA-registered products also is recommended by public health agencies, including the Centers for Disease Control and Prevention (*11*). Conversely, it is reasonable to assume that choice of a minimum risk 25(b) exempt product is driven, in part, by the belief that it is safer than a synthetic product for the user, other family members, pets, wildlife, or the environment. It is not clear to what extent the consumer assumes a minimum risk 25(b) exempt product will be as effective as an alternative EPA-registered product in killing or repelling ticks.

Tick Toxicants for Use in the Environment

Two studies in the northeastern United States (*7*,*8*) each reported similar levels of use of synthetic versus natural products to kill host-seeking ticks on residential properties. One study (*7*) used the phrasings chemical pesticide (reportedly used by 23% of respondents to control ticks) and natural pesticide (reportedly used by 15% of respondents). However, it is not clear if pesticides considered to be natural by the respondents were minimum risk 25(b) exempt products. The other study (*8*) used the phrasings of synthetic pesticides (e.g., bifenthrin) versus natural/organic pesticides (e.g., cedar oil), with both types of pesticides reportedly being used by 2%–3% of respondents to control ticks. Those phrasings provided an example of an EPA-registered active ingredient (bifenthrin) and a minimum risk 25(b) exempt active ingredient (cedarwood oil) but still fall short of explicitly comparing EPA-registered versus minimum risk 25(b) exempt products.

Another study explored willingness to pay for natural versus chemical pesticide yard treatments to kill host-seeking ticks (*9*). Of those willing to pay for yard treatment, 95% were willing to use a natural pesticide, compared with 63% for a chemical pesticide. In both cases, most respondents (63%–66%) were only willing to pay up to $99/year for the treatment, and few respondents (<5%) were willing to pay $500 or more. Additional information came from an assessment of commercial tick control practices on residential properties in the Northeast (*12*). Most (80%) firms offering tick control services reported applying synthetic pesticide products (carbaryl and various pyrethroids) to kill host-seeking ticks. A smaller proportion (34%) of firms reported applying natural or organic pesticide products; those were based on a variety of natural active ingredients, including minimum risk 25(b) exempt compounds (cedar oil, geraniol oil, peppermint oil, rosemary oil, and thyme oil) and other compounds of natural origin (pyrethrin). Primary reasons for the firms to not offer natural products to kill host-seeking ticks included efficacy concerns, followed by lack of client request and cost. In an earlier survey in the northeastern United States, safety concerns was the most common reason for not using synthetic pesticides for tick control on residential properties, but similar information was not provided for natural pesticides (*13*).

Tick Repellents

Two studies in the Upper Midwest (*10*) and northeastern (*8*) United States each reported similar levels of use, or willingness to use, for synthetic versus natural tick repellents. The survey in the Upper Midwest made the distinction between natural and synthetic repellents (respondent preference of use among these product types was 24% for natural repellents only versus 19% for synthetic repellents only), but the EPA-registered oil of lemon eucalyptus active ingredient was used as the example of a natural repellent (*10*). Therefore, the survey findings cannot be interpreted in the context of EPA-registered versus minimum risk 25(b) exempt repellents. The survey in the Northeast (*8*) used the more explicit phrasings of spray containing EPA-approved repellent (e.g., DEET), which reportedly was being used by 13%–17% of respondents, versus natural/organic spray repellent, which reportedly was being used by 8% of respondents. However, it is not clear in which category respondents would place an EPA-approved repellent based on compounds understood to be of natural origin, such as oil of lemon eucalyptus or citronella.

Efficacy of Unregulated Minimum Risk 25(b) Exempt Products to Kill Host-Seeking Ticks

With 1 notable exception (*14*), field trials of commercial minimum risk 25(b) exempt products have compared a single product with a negative control (untreated or sprayed with water) and often also a positive control (an EPA-registered synthetic pesticide). Additional

factors to consider when interpreting the results of such field evaluations include whether sprays were applied at low or high pressure and the timepoints sampled after application. Products based on synthetic pyrethroids effectively suppress host-seeking blacklegged ticks for at least 6 weeks, with similar results for low- and high-pressure spray applications (*15*). Those pesticides are stable in the environment and their efficacy is not dependent on being applied at high pressure to increase penetration of vegetation and the litter and duff layers; they will affect both the ticks they reach during the spray event itself and ticks that contact them weeks later while moving around in duff and litter layers or ascending vegetation while seeking a host. Minimum risk 25(b) exempt pesticide products appear to be less stable in the environment and therefore highly effective in suppressing blacklegged ticks only for a shorter period of time, often 1–3 weeks, thus requiring more frequent applications to achieve the same level of tick suppression as synthetic pesticides (*15*). It may be that efficacy of minimum risk 25(b) exempt pesticide products to suppress host-seeking ticks is higher when they are applied at high spray pressure and therefore are able to penetrate vegetation and the litter and duff layers to reach ticks more effectively during the application event. Application of EPA-registered synthetic pesticide products labeled for ticks has, with 1 notable exception (*16*), uniformly resulted in high (>80%) tick killing efficacy (*15,17–20*). In contrast, tremendous variability in killing efficacy has been observed among different minimum risk 25(b) exempt pesticide products, including for a study by using standardized methods to simultaneously compare multiple minimum risk 25(b) exempt pesticide products (*14*).

Products Based on Rosemary and Peppermint Oils

Multiple studies have investigated the efficacy of minimum risk 25(b) exempt products containing rosemary and peppermint oils to suppress blacklegged ticks when applied to naturally infested field plots. Two studies conducted in Maine (*21,22*) evaluated the product Eco-Exempt IC2 (containing 10% rosemary oil and 2% peppermint oil). Applied by high-pressure spraying by a pest control firm on a single occasion, this minimum risk 25(b) exempt product was as effective as a positive control product (SpeckoZ) containing the synthetic pyrethroid bifenthrin in reducing the abundance of host-seeking blacklegged ticks for several months after application. Two other studies conducted in New Jersey (*17,23*) evaluated similar products: EcoTrol T&O (containing 10% rosemary oil, 2% peppermint oil, and 0.5% sodium lauryl sulfate) and Essentria IC^3 (containing 10% rosemary oil, 5% geraniol oil, and 2% peppermint oil). Applied by low-pressure spraying, those products did not maintain a high level (>90%) of suppression of nymphal blacklegged ticks for more than 1–3 weeks and required multiple applications to remain moderately to highly effective (>70% suppression) over a longer period. In the study with Essentria IC^3 (*17*), a positive control product (Talstar P) containing bifenthrin provided 100% suppression of nymphal blacklegged ticks for 9 weeks after a single spray event. A follow-up study (*24*) to compare the effect of Essentria IC^3 applied by low-pressure versus high-pressure spraying did not find an extended duration of suppression for nymphal blacklegged ticks with the high pressure-spraying: regardless of spray pressure, the level of suppression decreased to <60% after 2 weeks and 20% after 3 weeks. Moreover, the low-pressure spraying unexpectedly outperformed the high-pressure spraying to suppress nymphs at some timepoints after application in this trial.

Both Eco-Exempt IC2 and Essentria IC^3 also were evaluated in a standardized field microplot trial where nymphal blacklegged ticks were introduced into field arenas (*14*). Eco-Exempt IC2 showed 87% suppression of ticks placed in the arenas before spraying (knockdown effect), but when ticks instead were introduced 2 weeks after the spray event (residual effect), the level of suppression fell to 30%. Essentria IC^3 was evaluated in 3 different years in the study; knockdown suppression ranged from 15% to 53% and residual suppression from 0% to 6%. Two additional products (Private Label 1 and 2), based on the original Eco-Exempt IC2 formulation and including rosemary oil, peppermint oil, and geraniol oil, also were evaluated: knockdown suppression ranged from 0% to 37% and residual suppression from 0% to 17%. A follow-up study (T.N. Mather, University of Rhode Island, pers. comm., 2023 Aug 16) using the same experimental system reported low levels of knockdown suppression (0%–16%) and residual suppression (0%–15%) for multiple products, based on oils from rosemary or peppermint, together with oils from clove and thyme. Knockdown and residual killing efficacy for Talstar P (bifenthrin) were 98%–100% in both studies (*14*; T.N. Mather, University of Rhode Island, pers. comm., 2023 Aug 16). The highly variable findings across different studies for minimum risk 25(b) exempt products based on rosemary and peppermint oils underscore the difficulty in making recommendations about unregulated products based solely on the active ingredients they contain.

Products Based on Cedarwood Oil

Natural product pesticides based on cedarwood oil are commonly offered by commercial firms providing

tick control services in the northeastern United States (*12*). Laboratory studies (*25*–*27*) have demonstrated toxicity of cedarwood oil toward multiple tick species, including the blacklegged tick, but there are no published data on the efficacy of minimum risk 25(b) exempt products based on cedarwood oil to suppress blacklegged ticks in naturally infested areas. However, 2 products based on cedarwood oil (CedarCide PCO Choice and Tick Killz) were evaluated in the standardized field microplot system (*14*). Neither product provided more than minimal tick knockdown (5%–6%) or residual tick suppression after 2 weeks (0%–8%). A follow-up study (T.N. Mather, University of Rhode Island, pers. comm., 2023 Aug 16) using the same experimental system found similar results for 3 products based primarily on cedarwood oil; tick knockdown ranged from 0% to 24% and residual tick suppression from 0% to 15%.

Product Based on Garlic

A product called Mosquito Barrier (99.3% garlic juice, 0.5% citric acid, and 0.2% potassium sorbate), labeled as repellent rather than toxicant, was evaluated on naturally tick-infested plots in Connecticut (*28*). A laboratory trial showed the product to repel but not be toxic to blacklegged ticks at the label application rate (*28*). When applied by high-pressure spraying in the field, the product provided short-term (1–3 weeks), moderate (37%–59%) suppression of host-seeking nymphal blacklegged ticks, presumably due to repellency keeping the nymphs down in grass thatch or leaf litter rather than a toxicant effect.

Efficacy of Unregulated Minimum Risk 25(b) Exempt Products to Repel Ticks

Studies on repellency against ticks of natural substances, or fractionated compounds from these substances, were reviewed previously (*29*–*32*). Experimental studies typically focused on active ingredients; published studies comparing commercial products available in the United States are rare and restricted to EPA-registered products (*33*–*36*). EPA registration indicates a product will effectively repel ticks for a label-specified duration of time, and the online tool for repellent products provided by the EPA (*5*) indicates the number of hours protection is expected to last for a specific product. Essential considerations (already accounted for in the case of EPA-registered repellents) regarding minimum risk 25(b) exempt repellent products include their efficacy to repel ticks, as well as the duration of repellency after application. Similar to tick toxicant products (*6*), there is concern that minimum risk 25(b) exempt tick repellent products might be less effective and have a shorter duration of protection than repellent products based on synthetic chemicals, such as DEET or picaridin. The evaluations outlined here focus specifically on minimum risk 25(b) active ingredients and repellent products, excluding studies on fractionated compounds from the active ingredients.

Minimum Risk 25(b) Exempt Commercial Repellent Products Available in the United States

Published evaluations of minimum risk 25(b) exempt repellent products are limited to 3 studies (*37*–*39*). Two studies (*37*,*38*) focused on EcoSMART Organic Insect Repellent (containing 1% geraniol oil, and 0.5% oils of each of rosemary, cinnamon, and lemongrass). The repellency of this product was compared with a permethrin product (Repel Permanone) by application to tick drags that then were used to collect ticks from natural areas (*37*) or to coveralls used by the investigators to walk through tick-infested vegetation (*38*). The repellent efficacy (based on numbers of ticks still remaining on treated versus untreated textile 3 min after contact with vegetation ended) of the EcoSMART Organic Insect Repellent was similar to that of Repel Permanone for blacklegged ticks and lone star ticks (*Amblyomma americanum*). Repellency was uniformly >90% against both tick species up to 2 days after textiles were treated with the EcoSMART Organic Insect Repellent. The third study (*39*) was on experimental formulations called TT-4228 and TT-4302 (containing 5% geraniol oil as the active ingredient), subsequently marketed under the product name Guardian. Those experimental formulations were as effective as a 15% DEET product (OFF! Active Insect Repellent) in repelling blacklegged ticks, lone star ticks, American dog ticks (*Dermacentor variabilis*), and brown dog ticks (*Rhipicephalus sanguineus* sensu lato) in an in vitro assay, and TT-4228 outperformed the DEET product in repelling lone star ticks when applied to socks worn in a field trial (treatments applied 2.5–3.5 hours before the trial). Although the results of the field trials with minimum risk 25(b) exempt repellent products outlined above are promising, none included evaluation of application to skin, which might differ in repellency from application to textiles. Published data from laboratory studies using the EPA-recommended human skin bioassay (*40*) to assess repellency are entirely lacking for minimum risk 25(b) exempt repellent products labeled for use against ticks. To be most informative, such studies should include the main human-biting life stages of multiple tick species of medical concern.

Evaluations of Minimum Risk 25(b) Exempt Active Ingredients against Ticks of Medical Concern in the United States

A recent study (*41*) compared the repellency of 19 minimum risk 25(b) exempt active ingredients (as 10% lotion emulsions) against female blacklegged ticks by using the EPA-recommended human skin bioassay. Complete protection times in this assay ranged from less than 10 minutes (castor oil, corn oil, cottonseed oil, linseed oil, rosemary oil, sesame oil, and soybean oil) to more than 10 minutes but less than 1 hour (cedarwood oil, citronella oil, cornmint oil, garlic oil, geranium oil, lemongrass oil, peppermint oil, spearmint oil, and thyme oil) and 1–2 hours (cinnamon oil, clove oil, and geraniol oil). No minimum risk 25(b) exempt active ingredient had a complete protection time >2 hours, whereas the positive DEET control provided complete protection for the entire 6-hour observation period. Similar results for peppermint oil and rosemary oil against nymphs of the blacklegged tick were reported for human skin bioassays in another recent study (*42*): a positive DEET control remained effective (>80% repellency) over a 6-hour period, whereas initially high repellent efficacy of peppermint oil fell below 20% after 2 hours, and rosemary oil was not repellent at any timepoint after application. Another study (*43*) compared repellency of multiple minimum risk 25(b) exempt active ingredients against nymphal lone star ticks in an in vitro assay: lower concentrations of clove oil and thyme oil repelled 95% of ticks, compared with cinnamon oil, cedarwood oil, and peppermint oil. Additional studies, using variable methods to assess repellency for 1 or 2 minimum risk 25(b) exempt active ingredients, included evaluations of repellency against blacklegged ticks or lone star ticks for cedarwood oil (*27*,*44*), geraniol oil (*45*), geranium oil (*46*), or lemongrass oil (*45*).

Evaluations of Minimum Risk 25(b) Exempt Active Ingredients against Ticks of Medical Concern in Europe

Studies on the castor bean tick (*Ix. ricinus*) have evaluated repellency of minimum risk 25(b) exempt active ingredients in laboratory assays (*47*–*49*). One noteworthy study (*47*) compared multiple minimum risk 25(b) exempt active ingredients, demonstrating sustained repellency against nymphal ticks up to 8 hours after application of 10% solutions of citronella oil (83% repellency by the 8-hour time point), clove oil (78%), and geraniol oil (67%). Those compounds had similar or better repellency than a 10% DEET solution (71% repellency by 8 hours). In contrast, peppermint oil showed moderate repellency (50%) up to 4 hours but only minimal repellency after 6 hours (10%), and geranium oil had no repellency 4 hours after application.

Conclusions

The review of published literature yielded more information for the effectiveness of minimum risk 25(b) exempt products intended to kill host-seeking ticks compared with tick repellent products. Considerable variability has been documented among marketed minimum risk 25(b) exempt products to kill host-seeking blacklegged ticks, with effectiveness similar to chemical products for some minimum risk products but minimal effect on ticks for other products. Moreover, different products based on the same active ingredients (e.g., rosemary and peppermint oils) can have highly variable tick killing efficacy, underscoring the difficulty in making recommendations about unregulated minimum risk products based solely on the active ingredients they contain. Evaluations of minimum risk 25(b) exempt tick repellents have typically focused on individual active ingredients rather than formulated commercial products, which often combine multiple active ingredients together with inert ingredients. In the near absence of studies on repellency of formulated products with similar and variable combinations of minimum risk active ingredients, it is not possible to make recommendations about unregulated minimum risk tick repellent products based solely on the active ingredients they contain. Consumers should be aware that effectiveness to kill and repel ticks can differ among unregulated minimum risk products, and independent sources of information on the effectiveness of specific products are most often lacking. There also is a need to better understand the reasons why members of the public choose to use EPA-registered versus minimum risk 25(b) exempt tick toxicant and repellent products, based on perceptions about effectiveness and safety for humans, pets, and the environment.

Acknowledgments

I thank Susan Jennings and Tom Mather for providing helpful comments on a draft of this paper and Tom Mather for providing unpublished data on field efficacy of minimum risk 25(b) exempt products to kill host-seeking ticks.

About the Author

Dr. Eisen is a research entomologist in the Division of Vector-Borne Diseases, National Center for Emerging and Zoonotic Infectious Diseases, Centers for Disease Control and Prevention, Fort Collins, Colorado. His primary research interest is control of ticks and tickborne diseases in the United States.

References

1. Eisen L. Tick species infesting humans in the United States. Ticks Tick Borne Dis. 2022;13:102025. https://doi.org/10.1016/j.ttbdis.2022.102025
2. Eisen L, Stafford KC III. Barriers to effective tick management and tick-bite prevention in the United States (Acari: Ixodidae). J Med Entomol. 2021;58:1588–600. https://doi.org/10.1093/jme/tjaa079
3. United States Environmental Protection Agency. Minimum risk pesticides exempted from FIFRA registration [cited 2023 Sep 23]. https://www.epa.gov/minimum-risk-pesticides
4. United States Environmental Protection Agency. Active ingredients eligible for minimum risk pesticide products (updated December 2015) [cited 2023 Sep 23]. https://www.epa.gov/sites/default/files/2018-01/documents/minrisk-active-ingredients-tolerances-jan-2018.pdf
5. United States Environmental Protection Agency. Repellents: protection against mosquitoes, ticks and other arthropods [cited 2023 Sep 23]. https://www.epa.gov/insect-repellents
6. United States Department of Health and Human Services. Tick Biology, Ecology, and Control Subcommittee Report to the Tick-Borne Disease Working Group 2020 [cited 2023 Sep 23]. https://www.hhs.gov/ash/advisory-committees/tickbornedisease/reports/tick-biology-ecology-control-subcommittee-report/index.html
7. Niesobecki S, Hansen A, Rutz H, Mehta S, Feldman K, Meek J, et al. Knowledge, attitudes, and behaviors regarding tick-borne disease prevention in endemic areas. Ticks Tick Borne Dis. 2019;10:101264. https://doi.org/10.1016/j.ttbdis.2019.07.008
8. Kopsco HL, Mather TN. Tick-borne disease prevention behaviors among participants in a tick surveillance system compared with a sample of master gardeners. J Community Health. 2022;47:246–56. https://doi.org/10.1007/s10900-021-01041-9
9. Niesobecki S, Rutz H, Niccolai L, Hook S, Feldman K, Hinckley A. Willingness to pay for select tick-borne disease prevention measures in endemic areas. J Public Health Manag Pract. 2022;28:E37–42. https://doi.org/10.1097/PHH.0000000000001295
10. Beck A, Bjork J, Biggerstaff BJ, Eisen L, Eisen R, Foster E, et al. Knowledge, attitudes, and behaviors regarding tick-borne disease prevention in Lyme disease-endemic areas of the Upper Midwest, United States. Ticks Tick Borne Dis. 2022;13:101925. https://doi.org/10.1016/j.ttbdis.2022.101925
11. Centers for Disease Control and Prevention. Fight the bite! Prevent mosquito and tick bites [cited 2023 Sep 23]. https://www.cdc.gov/ncezid/dvbd/about/prevent-bites.html
12. Jordan RA, Schulze TL. Availability and nature of commercial tick control services in three Lyme disease endemic states. J Med Entomol. 2020;57:807–14. https://doi.org/10.1093/jme/tjz215
13. Gould LH, Nelson RS, Griffith KS, Hayes EB, Piesman J, Mead PS, et al. Knowledge, attitudes, and behaviors regarding Lyme disease prevention among Connecticut residents, 1999–2004. Vector Borne Zoonotic Dis. 2008;8:769–76. https://doi.org/10.1089/vbz.2007.0221
14. Dyer MC, Requintina MD, Berger KA, Puggioni G, Mather TN. Evaluating the effects of minimal risk natural products for control of the tick, *Ixodes scapularis* (Acari: Ixodidae). J Med Entomol. 2021;58:390–7.
15. Eisen L, Dolan MC. Evidence for personal protective measures to reduce human contact with blacklegged ticks and for environmentally based control methods to suppress host-seeking blacklegged ticks and reduce infection with Lyme disease spirochetes in tick vectors and rodent reservoirs. J Med Entomol. 2016;53:1063–92. https://doi.org/10.1093/jme/tjw103
16. Hinckley AF, Meek JI, Ray JAE, Niesobecki SA, Connally NP, Feldman KA, et al. Effectiveness of residential acaricides to prevent Lyme and other tick-borne diseases in humans. J Infect Dis. 2016;214:182–8. https://doi.org/10.1093/infdis/jiv775
17. Schulze TL, Jordan RA. Synthetic pyrethroid, natural product, and entomopathogenic fungal acaricide product formulations for sustained early season suppression of host-seeking *Ixodes scapularis* (Acari: Ixodidae) and *Amblyomma americanum* nymphs. J Med Entomol. 2021;58:814–20. https://doi.org/10.1093/jme/tjaa248
18. Jordan RA, Schulze TL, Eisen L, Dolan MC. Ability of three general use, over-the-counter pesticides to suppress *Ixodes scapularis* and *Amblyomma americanum* (Acari: Ixodidae) nymphs. J Am Mosq Control Assoc. 2017;33:50–5. https://doi.org/10.2987/16-6610.1
19. Schulze TL, Jordan RA. Early season applications of bifenthrin suppress *Ixodes scapularis* and *Amblyomma americanum* (Acari: Ixodidae) nymphs. J Med Entomol. 2020;57:797–800. https://doi.org/10.1093/jme/tjz202
20. Bron GM, Lee X, Paskewitz SM. Do-it-yourself tick control: granular gamma-cyhalothrin reduces *Ixodes scapularis* (Acari: Ixodidae) nymphs in residential backyards. J Med Entomol. 2021;58:749–55. https://doi.org/10.1093/jme/tjaa212
21. Rand PW, Lacombe EH, Elias SP, Lubelczyk CB, St Amand T, Smith RP Jr. Trial of a minimal-risk botanical compound to control the vector tick of Lyme disease. J Med Entomol. 2010;47:695–8. https://doi.org/10.1093/jmedent/47.4.695
22. Elias SP, Lubelczyk CB, Rand PW, Staples JK, St Amand TW, Stubbs CS, et al. Effect of a botanical acaricide on *Ixodes scapularis* (Acari: Ixodidae) and nontarget arthropods. J Med Entomol. 2013;50:126–36. https://doi.org/10.1603/ME12124
23. Jordan RA, Dolan MC, Piesman J, Schulze TL. Suppression of host-seeking *Ixodes scapularis* and *Amblyomma americanum* (Acari: Ixodidae) nymphs after dual applications of plant-derived acaricides in New Jersey. J Econ Entomol. 2011;104:659–64. https://doi.org/10.1603/EC10340
24. Schulze TL, Jordan RA. Relative efficacy of high-pressure versus backpack sprayer applications of 2 natural product-based acaricides for control of host-seeking *Ixodes scapularis* and *Amblyomma americanum* nymphs. J Med Entomol. 2023;60:1131–5. https://doi.org/10.1093/jme/tjad074
25. Panella NA, Karchesy J, Maupin GO, Malan JC, Piesman J. Susceptibility of immature *Ixodes scapularis* (Acari:Ixodidae) to plant-derived acaricides. J Med Entomol. 1997;34:340–5. https://doi.org/10.1093/jmedent/34.3.340
26. Dolan MC, Dietrich G, Panella NA, Montenieri JA, Karchesy JJ. Biocidal activity of three wood essential oils against *Ixodes scapularis* (Acari: Ixodidae), *Xenopsylla cheopis* (Siphonaptera: Pulicidae), and *Aedes aegypti* (Diptera: Culicidae). J Econ Entomol. 2007;100:622–5. https://doi.org/10.1603/0022-0493(2007)100[622:BAOTWE]2.0.CO;2
27. Flor-Weiler LB, Behle RW, Eller FJ, Muturi EJ, Rooney AP. Repellency and toxicity of a CO_2-derived cedarwood oil on hard tick species (Ixodidae). Exp Appl Acarol. 2022;86:299–312. https://doi.org/10.1007/s10493-022-00692-0
28. Bharadwaj A, Hayes LE, Stafford KC III. Effectiveness of garlic for the control of *Ixodes scapularis* (Acari: Ixodidae) on residential properties in western Connecticut. J Med Entomol. 2015;52:722–5. https://doi.org/10.1093/jme/tjv044

29. Bissinger BW, Roe RM. Tick repellents: past, present, and future. Pestic Biochem Physiol. 2010;96:63–79. https://doi.org/10.1016/j.pestbp.2009.09.010
30. Dolan MC, Panella NA. A review of arthropod repellents. In: Paluch GE, Coats JR, editors. Recent developments in invertebrate repellents. Washington (DC): American Chemical Society; 2011. p. 1–19.
31. Nwanade CF, Wang M, Wang T, Yu Z, Liu J. Botanical acaricides and repellents in tick control: current status and future directions. Exp Appl Acarol. 2020;81:1–35. https://doi.org/10.1007/s10493-020-00489-z
32. Benelli G, Pavela R. Repellence of essential oils and selected compounds against ticks: a systematic review. Acta Trop. 2018;179:47–54. https://doi.org/10.1016/j.actatropica.2017.12.025
33. Foster E, Fleshman AC, Ford SL, Levin ML, Delorey MJ, Eisen RJ, et al. Preliminary evaluation of human personal protective measures against the nymphal stage of the Asian longhorned tick, *Haemaphysalis longicornis* (Acari: Ixodidae). J Med Entomol. 2020;57:1141–8. https://doi.org/10.1093/jme/tjaa008
34. Bissinger BW, Apperson CS, Sonenshine DE, Watson DW, Roe RM. Efficacy of the new repellent BioUD against three species of ixodid ticks. Exp Appl Acarol. 2009;48:239–50. https://doi.org/10.1007/s10493-008-9235-x
35. Semmler M, Abdel-Ghaffar F, Al-Rasheid KA, Mehlhorn H. Comparison of the tick repellent efficacy of chemical and biological products originating from Europe and the USA. Parasitol Res. 2011;108:899–904. https://doi.org/10.1007/s00436-010-2131-4
36. Bissinger BW, Zhu J, Apperson CS, Sonenshine DE, Watson DW, Roe RM. Comparative efficacy of BioUD to other commercially available arthropod repellents against the ticks *Amblyomma americanum* and *Dermacentor variabilis* on cotton cloth. Am J Trop Med Hyg. 2009;81:685–90. https://doi.org/10.4269/ajtmh.2009.09-0114
37. Schulze TL, Jordan RA, Dolan MC. Experimental use of two standard tick collection methods to evaluate the relative effectiveness of several plant-derived and synthetic repellents against *Ixodes scapularis* and *Amblyomma americanum* (Acari: Ixodidae). J Econ Entomol. 2011;104:2062–7. https://doi.org/10.1603/EC10421
38. Jordan RA, Schulze TL, Dolan MC. Efficacy of plant-derived and synthetic compounds on clothing as repellents against *Ixodes scapularis* and *Amblyomma americanum* (Acari: Ixodidae). J Med Entomol. 2012;49:101–6. https://doi.org/10.1603/ME10241
39. Bissinger BW, Schmidt JP, Owens JJ, Mitchell SM, Kennedy MK. Activity of the plant-based repellent, TT-4302 against the ticks *Amblyomma americanum, Dermacentor variabilis, Ixodes scapularis* and *Rhipicephalus sanguineus* (Acari: Ixodidae). Exp Appl Acarol. 2014;62:105–13. https://doi.org/10.1007/s10493-013-9719-1
40. United States Environmental Protection Agency. Product Performance Test Guidelines: OPPTS 810.3700: Insect Repellents to be Applied to Human Skin [EPA 712-C-10–001] (July 2010 [cited 2023 Sep 23]. https://www.regulations.gov/document/EPA-HQ-OPPT-2009-0150-0011
41. Luker HA, Salas KR, Esmaeili D, Holguin FO, Bendzus-Mendoza H, Hansen IA. Repellent efficacy of 20 essential oils on *Aedes aegypti* mosquitoes and *Ixodes scapularis* ticks in contact-repellency assays. Sci Rep. 2023;13:1705. https://doi.org/10.1038/s41598-023-28820-9
42. Burtis JC, Ford SL, Parise CM, Foster E, Eisen RJ, Eisen L. Comparison of in vitro and in vivo repellency bioassay methods for *Ixodes scapularis* nymphs. Parasit Vectors. 2023;16:228. https://doi.org/10.1186/s13071-023-05845-7
43. Meng H, Li AY, Costa Junior LM, Castro-Arellano I, Liu J. Evaluation of DEET and eight essential oils for repellency against nymphs of the lone star tick, *Amblyomma americanum* (Acari: Ixodidae). Exp Appl Acarol. 2016;68:241–9. https://doi.org/10.1007/s10493-015-9994-0
44. Carroll JF, Tabanca N, Kramer M, Elejalde NM, Wedge DE, Bernier UR, et al. Essential oils of *Cupressus funebris, Juniperus communis*, and *J. chinensis* (Cupressaceae) as repellents against ticks (Acari: Ixodidae) and mosquitoes (Diptera: Culicidae) and as toxicants against mosquitoes. J Vector Ecol. 2011;36:258–68. https://doi.org/10.1111/j.1948-7134. 2011.00166.x
45. Faraone N, MacPherson S, Hillier NK. Behavioral responses of *Ixodes scapularis* tick to natural products: development of novel repellents. Exp Appl Acarol. 2019;79:195–207. https://doi.org/10.1007/s10493-019-00421-0
46. Tabanca N, Wang M, Avonto C, Chittiboyina AG, Parcher JF, Carroll JF, et al. Bioactivity-guided investigation of geranium essential oils as natural tick repellents. J Agric Food Chem. 2013;61:4101–7. https://doi.org/10.1021/jf400246a
47. Thorsell W, Mikiver A, Tunón H. Repelling properties of some plant materials on the tick *Ixodes ricinus* L. Phytomedicine. 2006;13:132–4. https://doi.org/10.1016/j.phymed.2004.04.008
48. Elmhalli F, Garboui SS, Borg-Karlson AK, Mozūraitis R, Baldauf SL, Grandi G. The repellency and toxicity effects of essential oils from the Libyan plants *Salvadora persica* and *Rosmarinus officinalis* against nymphs of *Ixodes ricinus*. Exp Appl Acarol. 2019;77:585–99. https://doi.org/10.1007/s10493-019-00373-5
49. Jaenson TG, Garboui S, Pålsson K. Repellency of oils of lemon eucalyptus, geranium, and lavender and the mosquito repellent MyggA natural to *Ixodes ricinus* (Acari: Ixodidae) in the laboratory and field. J Med Entomol. 2006;43:731–6. https://doi.org/10.1093/jmedent/43.4.731

Address for correspondence: Lars Eisen, Centers for Disease Control and Prevention, 3156 Rampart Rd, Fort Collins, CO 80521, USA; email: evp4@cdc.gov

Auritidibacter ignavus, an Emerging Pathogen Associated with Chronic Ear Infections

Sophie Roth, Maximilian Linxweiler, Jacqueline Rehner, Georges-Pierre Schmartz, Sören L. Becker, Jan Philipp Kühn

Medscape CME Activity

In support of improving patient care, this activity has been planned and implemented by Medscape, LLC and Emerging Infectious Diseases. Medscape, LLC is jointly accredited with commendation by the Accreditation Council for Continuing Medical Education (ACCME), the Accreditation Council for Pharmacy Education (ACPE), and the American Nurses Credentialing Center (ANCC), to provide continuing education for the healthcare team.

Medscape, LLC designates this Journal-based CME activity for a maximum of 1.00 ***AMA PRA Category 1 Credit(s)™***. Physicians should claim only the credit commensurate with the extent of their participation in the activity.

Successful completion of this CME activity, which includes participation in the evaluation component, enables the participant to earn up to 1.0 MOC points in the American Board of Internal Medicine's (ABIM) Maintenance of Certification (MOC) program. Participants will earn MOC points equivalent to the amount of CME credits claimed for the activity. It is the CME activity provider's responsibility to submit participant completion information to ACCME for the purpose of granting ABIM MOC credit.

All other clinicians completing this activity will be issued a certificate of participation. To participate in this journal CME activity: (1) review the learning objectives and author disclosures; (2) study the education content; (3) take the post-test with a 75% minimum passing score and complete the evaluation at http://www.medscape.org/journal/eid; and (4) view/print certificate. For CME questions, see page 211.

NOTE: It is Medscape's policy to avoid the use of Brand names in accredited activities. However, in an effort to be as clear as possible, the use of brand names should not be viewed as a promotion of any brand or as an endorsement by Medscape of specific products.

Release date: December 20, 2023; Expiration date: December 20, 2024

Learning Objectives

Upon completion of this activity, participants will be able to:

- Analyze the microbiology of *Auritidibacter ignavus*
- Assess risk factors for *A. ignavus* otitis
- Distinguish antimicrobial resistance patterns of *A. ignavus*
- Identify physical findings associated with *A. ignavus* otitis

CME Editor

Thomas J. Gryczan, MS, Technical Writer/Editor, Emerging Infectious Diseases. *Disclosure: Thomas J. Gryczan, MS, has no relevant financial relationships.*

CME Author

Charles P. Vega, MD, Health Sciences Clinical Professor of Family Medicine, University of California, Irvine School of Medicine, Irvine, California. *Disclosure: Charles P. Vega, MD, has the following relevant financial relationships: served as an advisor or consultant for Boehringer Ingelheim; GlaxoSmithKline; Johnson & Johnson Services, Inc.*

Authors

Sophie Roth, MD; Maximilian Linxweiler, MD; Jacqueline Rehner, MSc; Georges-Pierre Schmartz, MSc; Sören L. Becker, MD, PhD; Jan Philipp Kühn, MD.

Author affiliation: Saarland University Institute of Medical Microbiology and Hygiene, Homburg/Saar, Germany

DOI: https://doi.org/10.3201/eid3001.230385

We describe detection of the previously rarely reported gram-positive bacterium *Auritidibacter ignavus* in 3 cases of chronic ear infections in Germany. In all 3 cases, the patients had refractory otorrhea. Although their additional symptoms varied, all patients had an ear canal stenosis and *A. ignavus* detected in microbiologic swab specimens. A correct identification of *A. ignavus* in the clinical microbiology laboratory is hampered by the inability to identify it by using matrix-assisted laser desorption/ionization time-of-flight mass spectrometry. Also, the bacterium might easily be overlooked because of its morphologic similarity to bacterial species of the resident skin flora. We conclude that a high index of suspicion is warranted to identify *A. ignavus* and that it should be particularly considered in patients with chronic external otitis who do not respond clinically to quinolone ear drop therapy.

Auritidibacter ignavus is an aerobic gram-positive, rod-shaped bacterium that was described by Yassin et al. in 2011 after isolation from an ear swab specimen (*1*). Thus far, all published cases with microbiological detection of *A. ignavus* were associated with ear infection that clinically manifested as otitis externa with otorrhea, which indicates a specific role of this pathogen in inflammatory diseases of the outer ear (*1*–*3*). However, only a limited number of cases have been published, and scant data are hampering valid conclusions on the clinical relevance and therapeutic implications of this pathogen. In addition, there are discrepant results with regard to susceptibility testing (*1*,*2*).

We describe 3 cases of patients with otorrhea caused by *A. ignavus* detected during March 2021 and October 2022 at the Saarland University Institute of Medical Microbiology and Hygiene (Homburg/Saar, Germany); the total number of ear swab specimens analyzed for diagnostic purposes in the institute's microbiology laboratory during 2021 and 2022 was 922. We provide an in-depth description of the clinical isolates, including their antimicrobial drug susceptibility patterns and strain comparison by whole-genome sequencing. Furthermore, we review the available literature pertaining to *A. ignavus*.

Case Reports

Written informed consent was obtained from the 3 patients to publish this case report. Patient 1 was a 50-year-old man who sought care for a chronic right-sided otorrhea caused by treatment-resistant external otitis, which had caused symptoms for several months. An outpatient topical treatment with ciprofloxacin ear drops for several weeks did not result in clinical improvement. At initial examination, the patient described persistent itching and otalgia on the affected ear. Clinical examination showed an extensive stenosis of the external auditory canal caused by multiple exostoses that narrowed the lumen by >50%. The ear canal appeared swollen and red by ear microscopy (Figure 1, panel A). The eardrum was covered with black fungal spores. Microbiological wound swab specimens showed *A. ignavus* and the dematiaceous fungus *Exophiala dermatitidis*. Thus, an alternating topical therapy with povidone-iodine drops and ethanol drops was initiated. Four weeks later, the patient reported major clinical improvement and absence of any symptoms. The examination showed a dry ear canal without any abnormal findings.

Patient 2 was a 72-year-old woman who sought care for slowly progressing conductive hearing loss of the right ear and occasional otorrhea. She denied any pain, dizziness, or tinnitus. Although an otologic examination of the left ear showed unremarkable findings, the right side showed a fibrotic, moist auditory canal with stenosis, which was suggestive of a postinflammatory acquired atresia of the external auditory canal (Figure 1, panel B). Audiometry showed an air bone gap of up to 20 dB on the right side with bilateral sensorineural normacusis. To exclude middle and inner ear affection or malformations, computed tomography was performed and showed a partial obstruction of the right external auditory canal by fibrous tissue without any additional pathologic findings. To widen the external auditory canal and to help with outer ear drainage, we performed a meatoplasty. Because the otorrhea did not subside postoperatively, we obtained a microbiological swab specimen, which grew *A. ignavus*. A topical therapy with ethanol drops and nourishing oil drops led to a long-lasting improvement of symptoms without recurring otorrhea.

Patient 3 was a 76-year-old man who had lichen planus and sought care for recurrent otorrhea of both ears for >2 months. He reported no otalgia, vertigo, or tinnitus. A symmetric presbycusis had remained unchanged for years and was treated with conventional hearing aids. On examination, both auditory canals were moist and constricted, clinically manifesting as inflammatory meatal fibrosis, a common finding in patients who have lichen planus. Result of a computed tomography scan showed a bilateral circumferential bony overgrowth of the osseous external auditory canal. A microbiological swab specimen led to the identification of *A. ignavus* in both ears. Thus, a topical therapy with ethanol drops and a tincture of isopropyl alcohol, glycerin, acetic acid, and peppermint

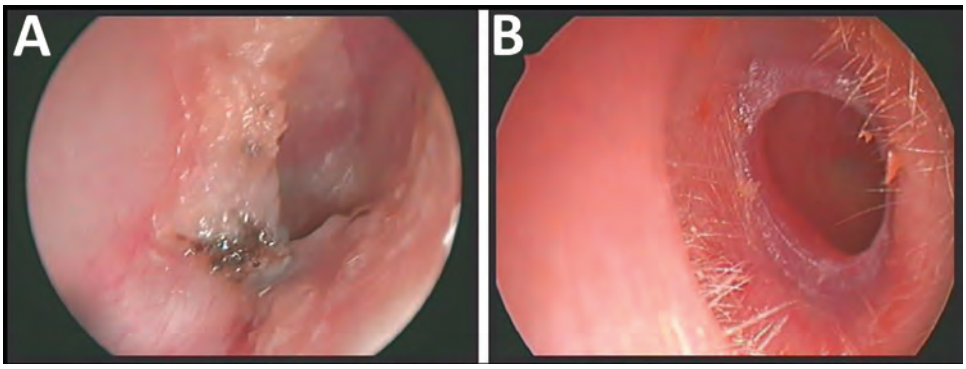

Figure 1. Right ears of 2 patients with chronic ear infections who were infected with *Auritidibacter ignavus*, Germany. A) Patient 1. Auditory canal was swollen and red and contained fungal spores. B) Patient 2. Fibrotic stenosis in the cartilaginous part of the ear canal, which was suggestive of a postinflammatory acquired atresia of the external auditory canal.

oil was initiated. At follow-up after 3 weeks, both auditory canals were dry and without signs of acute infection but with an unchanged fibrotic stenosis.

Microbiological Characteristics of *A. ignavus*

In all 3 cases, microbiological ear swab specimens were subjected to standard microbiological culture methods (i.e., incubation on tryptic soy blood agar and chocolate agar for ≥48 hours). After 1 day of incubation, small white-gray colonies appeared (Figure 2), which changed to a gray-yellow appearance with a slimy surface over the course of few days. On Gram staining, gram-positive rods were observed, with a partially coccoid morphology.

No distinct identification was achieved by matrix-assisted laser desorption/ionization time-of-flight mass spectrometry (Bruker Daltonics). Thus, we performed a 16S broad-range PCR and subsequent Sanger sequencing. Analysis using a BLAST search (https://www.ncbi.nlm.nih.gov/BLAST) based on the National Center for Biotechnology Information genome database showed a sequence homology ≥99% for *A. ignavus* in all 3 cases.

We performed antimicrobial susceptibility testing using epsilometry on Mueller-Hinton agar with 5% sheep blood. In the absence of specific species-related clinical breakpoints for *A. ignavus*, we assessed the MICs by using the non–species-related breakpoints put forth by the European Committee on Antimicrobial Susceptibility Testing (https://www.eucast.org). We consistently noted high MICs for ciprofloxacin, which are likely to be associated with clinical failure of this drug. In contrast, all isolates were susceptible to β-lactam antimicrobial drugs and vancomycin (Table).

We extracted whole-genome DNA from isolates of *A. ignavus* by using the ZymoBIOMICS DNA Miniprep Kit (Zymo Research Corp.). We performed subsequent whole-genome sequencing by using Illumina PE150 (HiSeq), conducted by Novogene UK Ltd.. We performed quality control of sequencing output by using Fastp version 0.23.2 and MultiQC version 1.13a. We aligned reads against the reference genome of *A. ignavus* (CP031746.1 *Auritidibacter* sp. NML130574) by using Bowtie2 version 2.4. Variant calling using Freebayes version 1.3.2, filtering using Vcftools version 0.1.16 with a set threshold of 20, and comparison with Vcftools suggested that all 3 isolates were unrelated and had only 5,246 single-nucleotide polymorphisms in common (Figure 3).

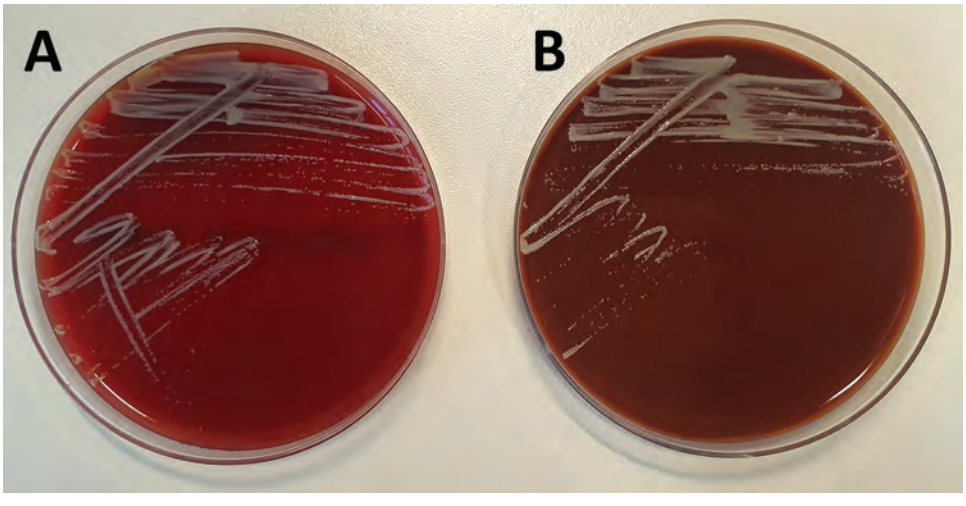

Figure 2. Small white-gray colonies of *Auritidibacter ignavus* in a sample from a chronic ear infection patient, Germany. Colonies are shown after 2 days of incubation at 37°C on tryptic soy blood agar (A) and chocolate agar (B).

Table. Antimicrobial drug susceptibility patterns for 10 drugs of 3 *Auriditibacter ignavus* isolates from patients with chronic ear infections, Germany*

	MIC, mg/L									
Isolate	PEN	CRX	AMS	MEM	VAN	LIN	CLI	DOX	SXT	CIP
1	0.38	0.5	0.25	1.5	0.064	0.5	32	0.5	0.094	32
2	0.19	0.094	0.125	0.38	0.125	0.75	2	0.064	0.008	16
3	0.125	0.125	0.25	0.5	0.064	0.38	1.5	0.125	0.19	12

*Testing was performed by using epsilometry on Mueller-Hinton-Agar with 5% sheep blood. AMS, ampicillin/sulbactam; CIP, ciprofloxacin; CLI, clindamycin; CRX, cefuroxime; DOX, doxycycline; LIN, linezolid; MEM, meropenem; PEN, penicillin, SXT, trimethoprim/sulfamethoxazole; VAN, vancomycin.

Discussion

Auritidibacter spp. infections have rarely been reported in the literature. A systematic PubMed/MEDLINE search using the search term "*Auritidibacter*" yielded only 3 results. In 2011, Yassin et al. (*1*) provided a detailed account of this bacterium with a microbiological, biochemical, and phylogenic characterization. The phenotypic culture morphology pattern described in their work matched our own observations. Eight years later, Seth-Smith et al. (*3*) published a complete genome assembly of an isolate from Switzerland and compared it with 4 global genomes, which showed a high diversity within the species. That finding is consistent with our findings of only 24.4%–29.1% single-nucleotide polymorphism identity between the 3 different isolates from the 3 case-patients (Ai_01, 29.1%; Ai_02, 24.4%; Ai_03, 26.5%). More recently, Bernard et al. (*2*) investigated 4 isolates of the genus *Auriditibacter* by microbiological and biochemical detection methods, as well as whole-genome sequencing, to assess their relatedness to the species *A. ignavus*.

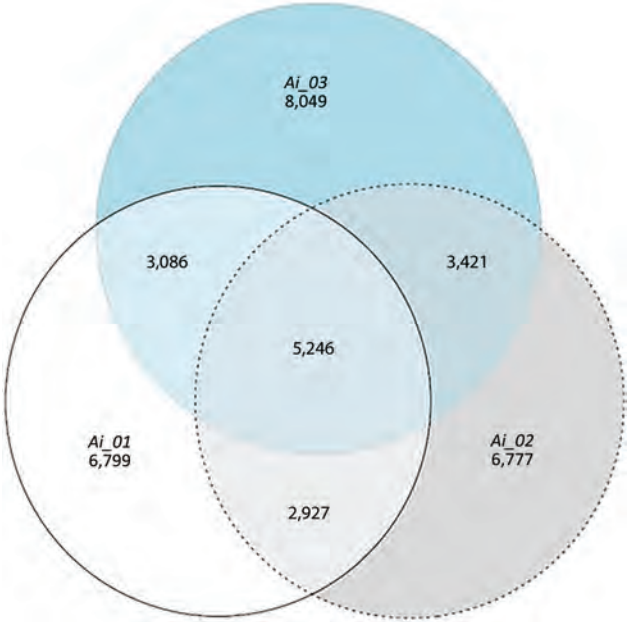

Figure 3. Venn diagram showing overlapping single-nucleotide polymorphism information among *Auritidibacter ignavus* isolates (Ai_01, Ai_02, and Ai_03) from 3 chronic ear infection patients, Germany.

All of those studies reported only little clinical data of the included patients. We present a report that includes details on the patients' clinical courses, including the clinical treatment response. Whereas no clear associations of *A. ignavus* infections with predisposing factors was found, outer ear canal stenosis was observed in all 3 patients. This anatomic feature seems to favor the colonization and probably also the infection with this pathogen. However, limited data make it difficult to explicitly establish a causal link between both conditions. Thus, additional studies or case series of a larger number of patients, including a control group of patients with ear canal stenosis and no clinical symptoms suggestive of acute inflammation, would be necessary to distinguish between colonization and infection.

According to Yassin et al. (*1*), *A. ignavus* is usually susceptible to β-lactam antimicrobial drugs, whereas Bernard et al. (*2*) reported resistance to cefepime. Such discrepancies might partially be explained by different antimicrobial testing methods, which underscores the need for coordinating testing recommendations for rare bacteria such as *A. ignavus*. Particular attention should be paid to our observation of ciprofloxacin resistance in all isolates, a finding that is consistent with the report by Bernard et al. (*2*).

Ciprofloxacin ear drops are commonly prescribed in clinical practice. Although MICs enable only limited conclusions on the clinical effectiveness of local antimicrobial drug therapy, we suggest that patients with therapeutic failure after empiric topical treatment with ciprofloxacin ear drops should be assessed for *A. ignavus* by using microbiological tests. The clinical suspicion should be reported to the microbiology laboratory because there is a serious risk of overlooking *A. ignavus* caused by its morphologic similarity to bacterial species belonging to the residential skin flora.

No specific request for an in-depth analysis was made by the treating clinicians in the cases we describe. Thus, increased awareness among the clinical microbiologists was caused by the repeated receipt of ear swab specimens from the patients with the clinical information otorrhea in context with the bacterial

growth of presumed physiologic flora in large quantities, which led to a low threshold to submit bacterial colonies to additional testing for species identification. Finally, the absence of *A. ignavus* in matrix-assisted laser desorption/ionization time-of-flight mass spectrometry databases poses an additional threat to correct identification in the clinical microbiology laboratory, as has been reported for other pathogens (*4*).

In conclusion, *A. ignavus* is a novel, potentially underrecognized pathogen that seems to be associated with a distinct clinical pattern in patients with ear infections. A high level of disease awareness and accurate microbiological diagnostics are required for correct identification. In patients who have a clinical course of chronic external otitis and who do not respond to empirical treatment with quinolone ear drops, *Auritidibacter* infection should be considered and further investigated.

About the Author

Dr. Roth is a physician at the Institute of Medical Microbiology and Hygiene, Saarland University, Homburg/Saar, Germany. Her primary research interest is improved and faster diagnostic of bacterial infections.

References

1. Microbiology Society. *Auritidibacter ignavus* gen. nov., sp. nov., of the family Micrococcaceae isolated from an ear swab of a man with otitis externa, transfer of the members of the family Yaniellaceae Li et al. 2008 to the family Micrococcaceae and emended description of the suborder Micrococcineae [cited 2023 Feb 24]. https://www.microbiologyresearch.org/content/journal/ijsem/10.1099/ijs.0.019786-0#tab2
2. Bernard KA, Pacheco AL, Burdz T, Wiebe D, Beniac DR, Hiebert SL, et al. Emendation of the genus *Auritidibacter* Yassin et al. 2011 and *Auritidibacter ignavus* Yassin et al. 2011 based on features observed from Canadian and Swiss clinical isolates and whole-genome sequencing analysis. Int J Syst Evol Microbiol. 2020;70:83–8. https://doi.org/10.1099/ijsem.0.003719
3. Seth-Smith HM, Goldenberger D, Bernard KA, Bernier AM, Egli A. Complete genome assembly of an *Auritidibacter ignavus* isolate obtained from an ear infection in Switzerland and a comparison to global isolates. Microbiol Resour Announc. 2019;8:e00291–19. https://doi.org/10.1128/MRA.00291-19
4. Chen XF, Hou X, Xiao M, Zhang L, Cheng JW, Zhou ML, et al. Matrix-assisted laser desorption/ionization time of flight mass spectrometry (MALDI-TOF MS) analysis for the identification of pathogenic microorganisms: a review. Microorganisms. 2021;9:1536. https://doi.org/10.3390/microorganisms9071536

Address for correspondence: **S**ophie Roth, Institute of Medical Microbiology and Hygiene, Saarland University, Kirrberger Strasse, Bldg 43, Homburg 66421, Germany; email: mikrobiologie@uks.eu

Incidence of Legionnaires' Disease among Travelers Visiting Hotels in Germany, 2015–2019

Udo Buchholz, Bonita Brodhun, Ann-Sophie Lehfeld

We determined whether the incidence rates of travel-associated Legionnaires' disease (TALD) in hotels in Germany increased after a previous occurrence and whether control measures required by the European Legionnaires' Disease Surveillance Network after a cluster (≥2 cases within 2 years) restored the rate to baseline. We analyzed TALD surveillance data from Germany during 2015–2019; a total of 307 TALD cases (163 domestic, 144 nondomestic) in hotels were reported. The incidence rate ratio was 5.5 (95% CI 3.6–7.9) for a second case and 25 (95% CI 11-50) for a third case after a cluster had occurred, suggesting that control measures initiated after the occurrence of TALD clusters might be inadequate to restore the incidence rate to baseline. Our findings indicate that substantial LD preventive measures should be explored by hotels or other accommodations after the first TALD case occurs to reduce the risk for future infections.

Legionnaires' disease (LD) is caused by bacteria of the genus *Legionella*, predominantly by *Legionella pneumophila* serogroup 1. Humans are infected via contaminated aerosols. The list of confirmed infection sources is long and includes drinking water piping systems, evaporative condensers, and whirlpool spas (*1*). Usually, proof of an infection source for individual cases is difficult. However, exposures within 2–10 days (incubation period) before symptom onset are categorized as community-acquired LD cases (≈75% of all cases in Germany), travel-associated LD (TALD) cases (≈20% of all cases in Germany), or hospital/healthcare–acquired LD cases (≈5% of all cases in Germany) (*2*). Whereas large LD outbreaks are rare, TALD clusters occur frequently.

TALD cases are associated with hotels or other commercial accommodations (e.g., campsites or holiday apartments). Those accommodations are often at higher risk because they frequently have complex water systems, might be periodically unoccupied, and sometimes offer additional facilities, such as whirlpool spas, to their guests; all of those factors are associated with an increased risk for LD (*3*,*4*).

In Europe, TALD cases are reported by national public health authorities to the European Legionnaires' Disease Surveillance Network (ELDSNet, https://www.ecdc.europa.eu/en/about-us/partnerships-and-networks/disease-and-laboratory-networks/eldsnet) that is hosted by the European Centre for Disease Prevention and Control in Stockholm, Sweden. ELDSNet collects TALD case data and informs countries about commercial accommodations that persons with LD had visited. Since the end of 2012, Germany has participated in ELDSNet and reports TALD cases for residents of the country who have been associated with a commercial accommodation in Germany or abroad.

In 2012, the TALD incidence rate in Europe was estimated at 0.3 cases/1 million nights (*5*). When restricting those data to countries that reported the most cases of TALD to ELDSNet (implying that they reported more completely than other countries), results suggested that the incidence rate among nondomestic travelers (travelers from outside of the country where the hotel was located) might be 2-fold higher on average.

According to ELDSNet, a TALD cluster is defined as a commercial accommodation where ≥2 case-patients with TALD stayed within 2 years and LD developed within 2–10 days after their stay. After a cluster is reported, local health departments responsible for the respective commercial accommodations are required to initiate an investigation that includes creating a risk assessment, taking environmental samples, and introducing control measures, if deemed suitable, such as thermal disinfection, cleaning, or structural improvements (*6*). The health department judges the adequacy of control measures and confirms that they were initiated appropriately (*6*). Within accommodations where a TALD cluster had occurred, the risk for

Author affiliation: Robert Koch Institute, Berlin, Germany

DOI: https://doi.org/10.3201/eid3001.231064

a further case (reoffender) was estimated at ≈12.4/100 accommodation-years (*3*). Another study found that the probability of a second TALD case at the same accommodation site varies according to the country and size of the hotel (*7*).

Examining the incidence rate of TALD in hotels with 0, 1, or 2 previous LD cases by using person-time as the denominator would be useful to investigate whether the incidence rate for TALD among hotels with a first case might be higher than baseline. In addition, preventive measures taken after the occurrence of a cluster might substantially reduce the incidence rate for further TALD cases. Knowing the values of those indicators might enhance the evidence base used for recommendations on managing accommodations that have 1 or 2 LD cases. Thus, the objectives of this study were to estimate the incidence rate of all TALD cases associated with hotels in Germany in general (traveler incidence), estimate the incidence rate of hotels in Germany that had their first LD case after the start of the study period (January 1, 2015), evaluate the incidence rates among accommodations after 1 or 2 LD cases occurred, and determine the incidence rate when 2 cases were associated with the same accommodation within 2 years (cluster).

Methods

Similar to other countries in Europe, LD is notifiable in Germany. As part of the notification process, the patient's exposure history, particularly travel history, is also reported. We analyzed data on accommodations in Germany that were associated with ≥1 case-patient with TALD who resided in Germany or abroad during 2015–2019. We selected those dates because TALD case data were still relatively incomplete before 2015, and the COVID-19 pandemic had started and influenced travel behavior of the population after 2019 (*8*). We restricted analyses to case-patients with TALD who had stayed in hotels, guesthouses, or boarding houses (hereinafter hotels) and excluded ships, campsites, and other types of commercial accommodations, such as holiday apartments. If a case-patient had stayed in >1 hotel, each hotel was categorized as having been associated with a TALD case.

We assumed that hotels had a stable bed capacity (i.e., we assumed no structural changes had occurred during 2015−2019). Moreover, we assumed that the occupancy rate was constant and consistently applied to all accommodations. According to 2017 data from Statista (https://www.statista.com), we assumed a conservative general bed occupancy rate of 70% (*9*).

We calculated 4 indicators. The first indicator was the number of all cases of TALD/number of nights spent by all travelers in hotels in Germany during 2015–2019 (traveler incidence). The second indicator was the number of hotels in Germany that had a first TALD case/number of nights spent by all travelers either until a first case occurred or, for hotels without a case, until the end of the 2019 observation period (first-case incidence). The third indicator was the number of hotels in Germany that had a second TALD case/number of nights spent in those hotels after the first case and until the occurrence of a second case or, for hotels without a further case, until the end of 2019 (second-case incidence). The fourth indicator was the number of German hotels that had a third TALD case/number of nights spent in those hotels after the second case until the occurrence of a third case or, for hotels without a further case, until the end of 2019 (third-case incidence). We also calculated the third-case incidence for hotels that previously had 2 cases within 2 years (defined as a cluster or reoffending hotel).

The 4 indicators were calculated as the number of TALD cases or number of hotels that had a TALD occurrence per million nights spent in hotels in Germany. To calculate indicators, we searched Eurostat (https://ec.europa.eu/eurostat) to identify the number of nights that guests spent in hotels in Germany during 2015–2019; we searched all countries that reported TALD incidents to ELDSNet, which included 26 European Union countries (Cyprus and Slovakia were excluded) plus Norway, Switzerland, and the United States, for a total of 29 countries (designated all-hotel-nights-29 for calculations) (*10*). Data from those countries comprised 94% of all nights that guests stayed in hotels in Germany. For the first indicator (traveler incidence), we divided the total number of TALD cases by the number of all-hotel-nights-29. In addition, we calculated the traveler incidence separately for domestic travelers (residents of Germany) and nondomestic travelers (residents of 28 countries reporting to ELDSNet other than Germany) as well as for travelers from those countries reporting >10 TALD cases that included a stay in a hotel in Germany. For the second indicator (first-case-incidence), we needed to subtract the number of nights among hotels that had a first case from all-hotel-nights-29. To perform this subtraction, we researched the bed capacity of every hotel that was associated with ≥1 TALD case. In some hotels, we estimated the number of beds on the basis of the number of rooms. Because we knew the date when the cases occurred, we could calculate the number of nights that guests spent in hotels after the first TALD case before the end of 2019. To determine the number of nights in hotels after

the occurrence of a first case (spent in hotels in Germany by visitors only from the countries reporting to ELDSNet), we estimated this number as: bed capacity of all hotels with a first case × 70% occupancy rate × number of days after the occurrence of the first case × 94%; we then subtracted that number from all-hotel-nights-29 to obtain the denominator for indicator 2 (Figure 1). The numerator was the number of hotels with a first case during 2015–2019.

To estimate the third (second-case-incidence) and fourth (third-case-incidence) indicators, we used a similar concept (Figure 1). For the third indicator, we calculated the denominator as the number of hotel nights after the occurrence of a first case until the end of 2019 or until the occurrence of the second case. The numerator was the number of hotels with a second TALD case. For the fourth indicator, we calculated the denominator as the number of hotel nights after occurrence of a second case until the end of 2019 or until the occurrence of the third case. The numerator was the number of hotels with a third TALD case.

We also calculated the third-case incidence among hotels that had TALD clusters (reoffending hotels), where measures deemed necessary had been taken to prevent further cases. ELDSNet permits 6 weeks for health departments and hotels to take preventive measures; we added another 2 weeks to account for the *Legionella* incubation period. Thus, we calculated the risk of having another TALD case ≥8 weeks after the cluster notification.

To examine hotel size as a potential confounding or effect-modifying factor, we stratified the second-case and third-case incidences according to hotel size (<200 beds was small, ≥200 beds was large) and compared those incidence rates. This calculation was not possible for traveler or first-case incidence rates because we did not know the distribution of nights spent among small and large hotels.

Sampling results from on-site investigations were mainly available for hotels associated with ≥2 cases. In addition, *Legionella* sp. strains were only sporadically typed (e.g., by using monoclonal antibody subtyping).

Results

During 2015–2019, a total of 384 TALD cases (case-patients residing in Germany or abroad) associated with any commercial accommodation in Germany were reported. Of those, 307 TALD cases were associated with hotels; 163 were domestic and 144 nondomestic cases (Table 1). Of the 144 nondomestic cases, 62 were reported from the Netherlands, 14 from Denmark, and 13 from France; the remaining cases were reported from 13 other countries. The 307 case-patients named 357 hotels, which partially overlapped, for a total of 309 different hotels. Of the 307 case-patients, 274 (89%) stayed in 1 hotel and 33 (11%) stayed in ≥2 hotels in Germany. The average number of named hotels per case was 1.2 (range 1–6). The number of TALD cases in hotels in Germany increased from 22 cases in 2015 to 94 cases in 2019.

Overall, 103 (34%) case-patients were <60 and 203 (66%) were ≥60 years of age; 238 (78%) were male and 68 (22%) were female. For 1 case, no information was available for age or gender. Age group, gender, or the number of named hotels did not differ between domestic and nondomestic TALD cases. However, compared with domestic case-patients, nondomestic TALD case-patients visited larger hotels (p = 0.008) (Table 1).

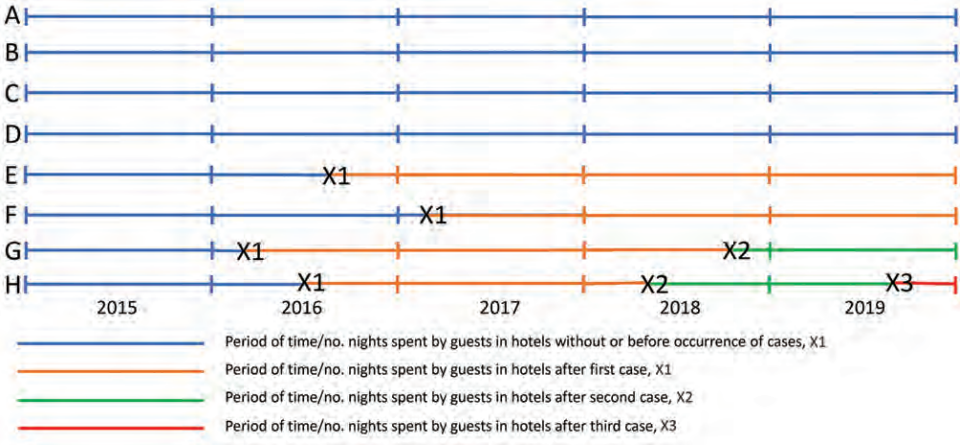

Figure 1. Schematic diagram showing typical timelines used to calculate first-, second-, and third-case incidence rates for Legionnaires' disease among travelers visiting hotels in Germany, 2015–2019. Data were collected from 29 countries that reported cases of travel-associated Legionnaires' disease (TALD) to the European Legionnaires' Disease Surveillance Network (https://www.ecdc.europa.eu/en/about-us/partnerships-and-networks/disease-and-laboratory-networks/eldsnet) after stays in hotels in Germany. Reports were from 26 European Union countries (Cyprus and Slovakia were excluded), Norway, Switzerland, and the United States. A–H indicates different hotels; X1 shows the occurrence of first TALD cases, X2 second TALD cases, and X3 third TALD cases. LD, Legionnaires' disease.

Table 1. Main characteristics of case-patients and hotels in study of incidence of Legionnaires' disease among travelers visiting hotels in Germany, 2015–2019*

Characteristics	All TALD cases	Domestic TALD cases	Nondomestic TALD cases	p value
No. case-patients	307	163	144	
Age, y†				
<60	103 (34)	59 (36)	44 (31)	
≥60	203 (66)	104 (64)	99 (69)	0.32
Sex†				
M	238 (78)	130 (80)	108 (76)	
F	68 (22)	33 (20)	35 (24)	0.38
No. visited hotels				
1	274 (89)	147 (90)	127 (88)	
>1	33 (11)	16 (10)	17 (12)	0.57
Median (mean; range)	1 (1.16; 1–6)	1 (1.15; 1–4)	1 (1.18; 1–6)	0.58
Hotel size‡				
≤50 beds	109 (30)	66 (35)	43 (25)	
51−199 beds	135 (38)	70 (37)	65 (38)	
≥200 beds	113 (32)	51 (27)	62 (37)	0.07
Median (range) no. beds	90 (4–1,920)	76 (4–1,402)	125 (9–1,920)	0.008

*Values are no. (%) except as indicated. Data were stratified according to domestic and nondomestic cases of TALD; nondomestic cases were from any of 28 countries reporting to the European Legionnaires' Disease Surveillance Network (https://www.ecdc.europa.eu/en/about-us/partnerships-and-networks/disease-and-laboratory-networks/eldsnet) other than Germany. TALD, travel-associated Legionnaires' disease.
†No information was available for 1 case.
‡Hotel size was categorized according to the number of beds. Multiple visited hotels per case were possible.

Hotels Associated with TALD Cases

Of the 309 hotels identified, 281 (91%) were associated with 1 TALD case, 16 (5.2%) with 2 cases, 8 (2.6%) with 3 cases, 1 (0.3%) with 4 cases, 2 (0.7%) with 5 cases, and 1 (0.3%) with 6 cases. The median number of beds was 71 in hotels with 1 case, 159 in hotels with 2 cases, and 208 in hotels with >2 cases. All 309 hotels had a first TALD case (i.e., the hotel was associated with a TALD case for the first time after January 1, 2015), 28 hotels had ≥2 cases, and 12 hotels had ≥3 cases. The ratio of domestic:nondomestic cases was 52:48 among hotels when the first case occurred, 50:50 among hotels when the second case occurred, and 67:33 among hotels when the third case occurred. Among hotels with ≥2 cases, the second case occurred at a median of 375 (range 0−1,559) days after the first case occurred.

TALD Incidence

During 2015–2019, guests residing in countries reporting to ELDSNet spent 1,351,540,219 nights in hotels in Germany. TALD incidence rate was 0.227/1 million nights (traveler incidence). The first-case incidence (referent) was 0.233/1 million nights, the second-case incidence was 1.3/million nights, and the third-case incidence was 9.4/1 million nights (Table 2). The third-case incidence for hotels that had a cluster according to the ELDSNet definition (reoffending hotels) was 5.9/1 million nights. The incidence rate ratios (IRRs) were 5.5 for second-case incidence and 40 for third-case incidence (Table 2; Figure 2); the difference was statistically significant.

The traveler incidence rate was 0.15/1 million nights for domestic travelers and 0.58/1 million nights for nondomestic travelers staying at hotels in Germany. The traveler incidence rate was 2.05/1 million nights for persons from the Netherlands, 1.12/1 million nights for travelers from Denmark, and 0.89/1 million nights for travelers from France.

Among smaller hotels (<200 beds) that had a first case, guests stayed 6,135,216 nights and 15 second cases of TALD occurred (incidence rate, 2.4 cases/1 million nights), whereas, among smaller hotels with a second case, guests stayed 215,433 nights and 6 third cases occurred (incidence rate, 28 cases/1 million nights; IRR, 11 [95% CI 4.2–25]). Among larger hotels that had a first case, guests stayed 15,770,216 nights and 13 second cases occurred (incidence rate 0.82 cases/1 million nights), whereas, among larger hotels with a second case, guests stayed 1,059,327 nights and 6 third cases occurred (incidence rate 5.7 cases/1 million nights); the IRR was 6.9 (95% CI 2.5–15.0). The IRRs for smaller and larger hotels were not significantly different.

In 5 hotels, monoclonal antibody MAb 3/1–positive *Legionella* strains were detected, but it is unknown how many times the antibody typing was performed. Of those 5 hotels, 3 were associated with >1 case.

Discussion

According to surveillance data from ELDSNet and Germany, our findings show that a substantially increased incidence rate for TALD was associated with hotels in Germany that had only 1 TALD case-patient during 2015–2019. The incidence rate increased further after 2 TALD cases were associated with a hotel. The incidence rates also increased further among hotels that had a TALD cluster after preventive measures had already been performed.

The per-hotel LD risk has been reported to increase with increasing hotel size (*7*); we also showed that the median size increased for hotels that had second or third TALD cases compared with those that had only a first case. Therefore, the increase in IRR (from baseline to hotels that had a second TALD case) observed in this study might be partially explained if larger hotels had an increased incidence rate. Because we did not know the distribution of nights spent among small and large hotels in Germany for traveler incidence and first-case incidence, we could only calculate the ratio for second-case and third-case incidences. Our finding that the increasing IRR applied to both smaller and larger hotels (with no significant difference) suggests that no effect-modifying factors existed and that our overall findings likely apply to both smaller and larger hotels.

Our overall incidence rate of TALD cases in hotels in Germany (0.227/1 million nights) is a composite of the rates among domestic and nondomestic travelers; the incidence rate for domestic travelers (0.15/1 million nights) was substantially lower than that for nondomestic travelers (0.58/1 million nights). One reason for this difference could be that the TALD surveillance systems of other countries in Europe are more sensitive than the system in Germany. The incidence rate for nondomestic travelers during 2015–2019 was lower than that estimated in 2009 for any accommodation (0.79/1 million nights) (*5*). The lower rate during 2015–2019 might be explained, in part, by an increasing number of younger travelers (*11*), and it is also possible that primary prevention of LD in hotels and other accommodations improved between 2009 and 2015.

In this study, we show increased incidence rates for accommodations that experienced first and second TALD cases. A previous study estimated the TALD incidence rate for all cases per total number of hotel nights but did not determine the incidence rates after first or second cases occurred (*5*). Another study calculated the number of cases among accommodations after ≥2 LD cases occurred but used accommodation-years in the denominator rather than the number of nights spent (*3*). Because the type of hotel can vary substantially from 1 hotel to another, we used the number of nights spent at the respective site as the denominator in our study.

Knowing that the incidence rates of TALD cases increase with each additional case can inform preventive measures to reduce LD infections. The increased TALD incidence rate observed among hotels that had a first case compared with baseline (IRR 5.5) suggests that risk assessments and taking preventive measures might be beneficial after the first occurrence. Furthermore, the even higher IRR among hotels that experienced a cluster (IRR 25) is inconsistent with the requirement of those hotels to investigate the drinking water system and take preventive measures that are

Table 2. Incidence rates for first, second, and third occurrences of Legionnaires' disease among travelers visiting hotels in Germany, 2015–2019*

Constellation	No.	TALD cases/1 million nights	IRR (95% CI)
First-case incidence rate†			
No. nights in hotels in Germany during 2015–2019	1,351,540,219	NA	NA
No. nights from first TALD case until end of 2019	24,568,957	NA	NA
No. nights in hotels that did not have a TALD case or until occurrence of first case	1,326,971,262	NA	NA
No. hotels that had a first TALD case	309	NA	NA
First-case incidence	NA	0.23	Referent
Second-case incidence rate among hotels that had a first case			
No. nights among hotels that had a first case until the end of 2019 or until the occurrence of a second case	21,905,432	NA	NA
No. hotels that had a second TALD case	28	NA	NA
Second-case incidence	NA	1.3	5.5 (3.6–7.9)
Third-case incidence rate among hotels that had a second case			
No. nights among hotels that had a second case until the end of 2019 or until the occurrence of a third case	1,274,759	NA	NA
No. hotels that had a third TALD case	12	NA	NA
Third-case incidence	NA	9.4	40 (21–71)
Third-case incidence rate among cluster or reoffending hotels			
No. nights among cluster hotels until the end of 2019 or until the occurrence of a third case ≥8 wk after cluster notification	1,350,676	NA	NA
No. reoffending hotels that had a third TALD case	8	NA	NA
Reoffender incidence	NA	5.9	25 (11–50)

*Data were reported by 29 countries (including Germany) to the European Legionnaires' Disease Surveillance Network (https://www.ecdc.europa.eu/en/about-us/partnerships-and-networks/disease-and-laboratory-networks/eldsnet); numbers of nights are provided for travelers of those 29 countries. IRR, incidence rate ratio; NA, not applicable; TALD, travel-associated Legionnaires' disease.
†Baseline/referent incidence rate among all hotels.

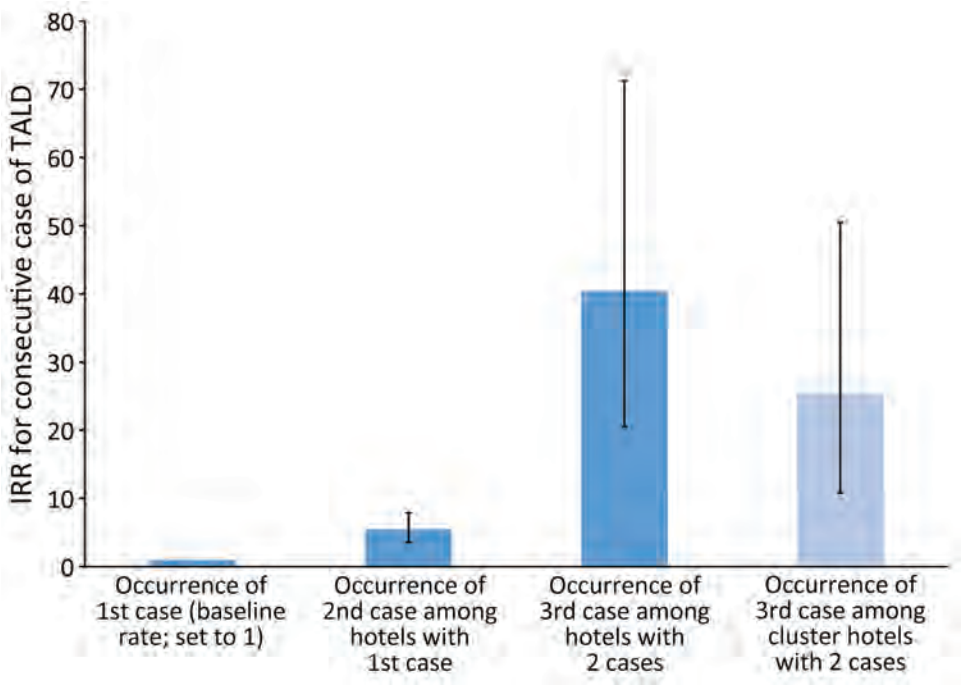

Figure 2. Incidence rate ratios for Legionnaires' disease cases among travelers visiting hotels in Germany, 2015–2019. IRRs were calculated for hotels that had a second or third TALD case or experienced a cluster of cases. Cluster hotels had 2 cases within 2 years; reoffending hotels were cluster hotels that had 2 cases and another case ≥8 weeks after the cluster notification. First-case incidence was the referent. Error bars indicate 95% CIs. IRR, incidence rate ratio; TALD, travel-associated Legionnaires' disease.

deemed adequate by the local health department. If preventive measures are effective, the incidence rate would be expected to return to baseline. However, according to ELDSNet data, many hotels or accommodations have a high propensity to be associated with ≥1 further TALD cases after a cluster occurs (*3*,*4*,*12*), suggesting that eradicating virulent *Legionella* strains from drinking water installations might be difficult. Assuming that exposure to *Legionella* strains dwelling in piping systems (and conceding that other factors might also play a role) is constant, we postulate that a large proportion of the human population is immune to virulent *Legionella* bacteria. Also, assuming that hotels with 2 associated cases are contaminated with virulent *Legionella* bacteria and are a source for TALD cases and considering that travelers stay 2 days in a hotel on average (*13*), we postulate that 9.4 persons/500,000 travelers (1 million nights divided by 2) are at risk for LD.

The first limitation of our study is that we used a different method to obtain the denominator for the first-case incidence rate than for the second- and third-case incidence rates. Using the same method would require access to a complete list of all hotels and their bed capacity and multiplying those numbers by the assumed 70% occupancy rate, as was done to estimate the denominator for the second- and third-case incidence rates; however, this information was not available for first-case incidence rate calculations. Nevertheless, we believe that the numbers of nights spent at a hotel in Germany provided by the Eurostat website were accurate and already accounted for a 70% occupancy rate. Second, to obtain denominators for the second- and third-case incidence rates, we had to make certain assumptions regarding hotel size or capacities. Third, we assumed that TALD cases were associated with the hotel that the patient visited, although some case-patients might have acquired their infection elsewhere during their travel or at home. Fourth, we assumed that all reported hotels had no LD cases before 2015. Finally, some TALD cases might not have been detected because exposure history could not be determined or because the case-patient resided in a country that did not participate in ELDSNet. Both of those possibilities could have led to underestimation of the traveler incidence as well as first-, second-, and third-case incidence rates.

In conclusion, we have shown that incidence rates of TALD increase significantly after the occurrence of a first case in hotels in Germany and, to a greater extent, after the occurrence of a second case. Local health departments and hotels should explore substantial LD preventive measures after the first TALD occurrence rather than after a cluster to reduce the infection risk for future guests.

Acknowledgment

We thank colleagues in other countries of Europe for their thorough collaboration with ELDSNet, the managers of ELDSNet for database maintenance, colleagues in district and federal state health departments for their conscientious contributions to TALD case reporting and

investigating accommodations in Germany that had TALD cases, and Stefan Kröger and Walter Haas for their thoughtful manuscript comments.

This study was conducted using data from the mandatory surveillance system in Germany and from data provided by ELDSNet. According to the Infectious Diseases Prevention Act (Infektionsschutzgesetz) of Germany, the Robert Koch Institute is authorized and obliged to process, analyze, and publish the respective surveillance data. No personal data were reported to the Robert Koch Institute, and the analyses shown here are restricted to highly aggregated data.

About the Author

Dr. Buchholz is an epidemiologist at the Robert Koch Institute. His main research interests are influenza and other respiratory viruses, participatory surveillance systems, and Legionnaires' disease.

References

1. Phin N, Parry-Ford F, Harrison T, Stagg HR, Zhang N, Kumar K, et al. Epidemiology and clinical management of Legionnaires' disease. Lancet Infect Dis. 2014;14:1011–21. https://doi.org/10.1016/S1473-3099(14)70713-3
2. Robert Koch Institut. Legionellosis, RKI guide. September 5, 2019 [cited 2022 Mar 30]. https://www.rki.de/DE/Content/Infekt/EpidBull/Merkblaetter/Ratgeber_Legionellose.html
3. Beauté J, Sandin S, de Jong B, Hallström LP, Robesyn E, Giesecke J, et al.; European Legionnaires' Disease Surveillance Network. Factors associated with Legionnaires' disease recurrence in hotel and holiday rental accommodation sites. Euro Surveill. 2019;24:1800295. PubMed https://doi.org/10.2807/1560-7917.ES.2019.24.20.1800295
4. Ricketts KD, Yadav R, Rota MC, Joseph CA; European Working Group for Legionella Infections. Characteristics of reoffending accommodation sites in Europe with clusters of Legionnaires disease, 2003–2007. Euro Surveill. 2010;15:19680.
5. Beauté J, Zucs P, de Jong B. Risk for travel-associated Legionnaires' disease, Europe, 2009. Emerg Infect Dis. 2012;18:1811–6. https://doi.org/10.3201/eid1811.120496
6. European Centre for Disease Prevention and Control. European Legionnaires' Disease Surveillance Network (ELDSNet): operating procedures for the surveillance of travel-associated Legionnaires' disease in the EU/EEA. 2017 [cited 2023 Sep 11]. https://www.ecdc.europa.eu/sites/default/files/documents/ELDSNET_2017-revised_guidelines_2017-web.pdf
7. Ricketts KD, Slaymaker E, Verlander NQ, Joseph CA. What is the probability of successive cases of Legionnaires' disease occurring in European hotels? Int J Epidemiol. 2006;35:354–60. https://doi.org/10.1093/ije/dyi317
8. Brodhun B, Buchholz U. Development of cases of Legionnaires' disease before the background of the COVID-19 pandemic, Jan–Jul 2020 [in German]. Epid Bull. 2020;44:3–9. https://doi.org/10.25646/7195
9. Statista. Utilized capacity of hotels in Germany from 2008–2018 in the first half year [in German]. 2018 [cited 2023 Jun 15]. https://de.statista.com/statistik/daten/studie/167521/umfrage/zimmerauslastung-der-hotellerie-seit-1997
10. Eurostat. Nights spent at tourist accommodation establishments by country of origin of the tourist [in German]. [cited 2023 Jul 3]. https://ec.europa.eu/eurostat/databrowser/view/TOUR_OCC_NINRAW__custom_6730510/default/table?lang=de
11. Reise vor9. ADV: proportion of younger and female passengers is heavily on the rise [in German]. [cited 2023 Sep 24]. https://www.reisevor9.de/inside/adv-anteil-junger-und-weiblicher-passagiere-steigt-stark
12. Lehfeld AS, Buchholz U, Brodhun B. Did infection of travel-associated cases of Legionnaires' disease actually occur during travel? [in German]. Epid Bull. 2023;23:3–21. https://doi.org/10.25646/11412
13. Statistisches Bundesamt. Monthly tourism statistics. Arrivals and overnight stays in accommodations: Germany, years, type of accommodation, residence of guests. Table 45412–0012 [in German]. [cited 2023 Jun 23]. https://www-genesis.destatis.de/genesis//online?operation=table&code=45412-0012&bypass=true&levelindex=0&levelid=1699984141222#abreadcrumb

Address for correspondence: Udo Buchholz, Robert Koch Institute, Seestrasse 10, 13353 Berlin, Germany; email: buchholzu@rki.de

Early-Onset Infection Caused by *Escherichia coli* Sequence Type 1193 in Late Preterm and Full-Term Neonates

Célie Malaure,[1] Guillaume Geslain,[1] André Birgy, Philippe Bidet, Isabelle Poilane, Margaux Allain, Mathilde Liberge, Nizar Khattat, Paola Sikias, Stéphane Bonacorsi

In support of improving patient care, this activity has been planned and implemented by Medscape, LLC and Emerging Infectious Diseases. Medscape, LLC is jointly accredited with commendation by the Accreditation Council for Continuing Medical Education (ACCME), the Accreditation Council for Pharmacy Education (ACPE), and the American Nurses Credentialing Center (ANCC), to provide continuing education for the healthcare team.

Medscape, LLC designates this Journal-based CME activity for a maximum of 1.00 ***AMA PRA Category 1 Credit(s)™***. Physicians should claim only the credit commensurate with the extent of their participation in the activity.

Successful completion of this CME activity, which includes participation in the evaluation component, enables the participant to earn up to 1.0 MOC points in the American Board of Internal Medicine's (ABIM) Maintenance of Certification (MOC) program. Participants will earn MOC points equivalent to the amount of CME credits claimed for the activity. It is the CME activity provider's responsibility to submit participant completion information to ACCME for the purpose of granting ABIM MOC credit.

All other clinicians completing this activity will be issued a certificate of participation. To participate in this journal CME activity: (1) review the learning objectives and author disclosures; (2) study the education content; (3) take the post-test with a 75% minimum passing score and complete the evaluation at http://www.medscape.org/journal/eid; and (4) view/print certificate. For CME questions, see page 212.

NOTE: It is Medscape's policy to avoid the use of Brand names in accredited activities. However, in an effort to be as clear as possible, the use of brand names should not be viewed as a promotion of any brand or as an endorsement by Medscape of specific products.

Release date: December 21, 2023; Expiration date: December 21, 2024

Learning Objectives

Upon completion of this activity, participants will be able to:

- Assess the prevalence and complications of early-onset neonatal sepsis (EOS)
- Compare characteristics of *Escherichia coli* isolates from EOS and healthy vaginal carriage in the current study
- Analyze characteristics of sequence type 1193 EOS in the current study
- Evaluate similarities and differences in *E. coli* EOS among preterm and term infants in the current study

CME Editor

Tony Pearson-Clarke, MS, Technical Writer/Editor, Emerging Infectious Diseases. *Disclosure: Tony Pearson-Clarke, MS, has no relevant financial relationships.*

CME Author

Charles P. Vega, MD, Health Sciences Clinical Professor of Family Medicine, University of California, Irvine School of Medicine, Irvine, California. *Disclosure: Charles P. Vega, MD, has the following relevant financial relationships: served as an advisor or consultant for Boehringer Ingelheim; GlaxoSmithKline; Johnson & Johnson Services, Inc.*

Authors

Célie Malaure, PharmD; Guillaume Geslai, MD; André Birgy, PharmD, PhD; Philippe Bidet, MD, PhD; Isabelle Poilane, PharmD; Margaux Allain, PharmD; Mathilde Liberge, PharmD; Nizar Khattat, MD; Paola Sikias, MD; Stéphane Bonacorsi, MD, PhD.

Using whole-genome sequencing, we characterized *Escherichia coli* strains causing early-onset sepsis (EOS) in 32 neonatal cases from a 2019–2021 prospective multicenter study in France and compared them to *E. coli* strains collected from vaginal swab specimens from women in third-trimester gestation. We observed no major differences in phylogenetic groups or virulence profiles between the 2 collections. However, sequence type (ST) analysis showed the presence of 6/32 (19%) ST1193 strains causing EOS, the same frequency as in the highly virulent clonal group ST95. Three ST1193 strains caused meningitis, and 3 harbored extended-spectrum β-lactamase. No ST1193 strains were isolated from vaginal swab specimens. Emerging ST1193 appears to be highly prevalent, virulent, and antimicrobial resistant in neonates. However, the physiopathology of EOS caused by ST1193 has not yet been elucidated. Clinicians should be aware of the possible presence of *E. coli* ST1193 in prenatal and neonatal contexts and provide appropriate monitoring and treatment.

Extraintestinal pathogenic *Escherichia coli* and *Streptococcus agalactiae* are bacterial pathogens that commonly cause early-onset neonatal sepsis (EOS) in industrialized countries. EOS is confirmed by a blood or cerebrospinal fluid culture positive for the causative pathogen ≤72 hours after birth. EOS incidence is ≈1/1,000 live births (*1*,*2*); 10% of cases are complicated by meningitis, which can lead to neurologic sequelae in up to 50% and death in 10% of cases in industrialized countries (*3*).

EOS caused by *S. agalactiae* can be prevented by peripartum antimicrobial prophylaxis but not EOS caused by *E. coli*. *E. coli* strains that cause neonatal meningitis have been well characterized, but *E. coli* strains that cause EOS less so (*4*,*5*). Neonatal meningitis *E. coli* strains belong mainly to phylogenetic group B2/sequence type complex (STc) 95 (*6*) and are frequently O18:K1, O1:K1, O83:K1, or $O45_{S88}$:K1 serotypes (*7*,*8*). Most STc95 strains are distributed worldwide and still largely susceptible to antimicrobials (*9*). However, other strains that can cause EOS, notably in preterm neonates, might be resistant to probabilistic antimicrobial therapy. In a recent study in Israel (*10*), maternal carriage rates of extended-spectrum β-lactamase (ESBL)–producing *E. coli* were 17.5% for mothers and 12.9% for preterm neonates; in China, ESBL accounted for up to 48% of *E. coli* infections in neonates (*11*).

Characterizing *E. coli* strains that cause EOS would constitute a critical first step towards better understanding the pathophysiology of this condition and developing potential preventive strategies. We conducted a prospective study covering a large area in France to estimate annual incidence and pathogen distribution of EOS in neonates born at ≥34 weeks of gestation during 2019–2021 (*12*). In total, we recorded 107 cases of bacteremia including 35 caused by *E. coli*, 15 (incidence 0.89/1,000 births) in late-preterm and 20 (0.06/1,000 births) in full-term infants. We prospectively recorded data on maternal and infant demographics, maternal antimicrobial therapy, peripartum antimicrobial prophylaxis, and outcomes (*12*). We aimed to use whole-genome sequencing (WGS) to characterize *E. coli* strains that caused EOS in cases from this prospective study and stratify results according to these data. In addition, we determined to compare those strains to *E. coli* strains obtained from cultures from vaginal swabs collected to screen for *S. agalactiae* carriage at 34–38 weeks of gestation from woman with newborns who had no history of EOS. The ethics committee institutional review board (Ramsay Santé Recherche & Enseignement, IRB00010835) authorized the study (*12*).

Methods

Bacterial Strains

We recorded 35 cases of EOS caused by *E. coli* during a prospective study in 81 maternity wards of the Ile de France area during 2019–2021 (*12*). Thirty-two *E. coli* isolates were sent to the National Reference Center in Robert-Debré Hospital to be further characterized. For comparison with the isolates from the

Author affiliations: *Escherichia coli* National Reference Center, Robert-Debré University Hospital, Assistance Publique–Hôpitaux de Paris, Paris, France (C. Malaure, A. Birgy, P. Bidet, S. Bonacorsi); Paediatric Intensive Care Unit, Robert-Debré University Hospital, Assistance Publique–Hôpitaux de Paris, Paris (G. Geslain); Paris Cité University, Paris (G. Geslain, A. Birgy, P. Bidet, S. Bonacorsi); Avicenne University Hospital, Assistance Publique–Hôpitaux de Paris, Bobigny, France (I. Poilane); Louis Mourier University Hospital, Assistance Publique–Hôpitaux de Paris, Colombes, France (M. Allain); Saint Louis University Hospital, Assistance Publique–Hôpitaux de Paris, Paris (M. Liberge); Neonatal Care Unit, Robert-Debré University Hospital, Assistance Publique–Hôpitaux de Paris, Paris (N. Khattat); Hôpital Privé d'Antony, Ramsay Santé, Antony, France (P. Sikias)

DOI: https://doi.org/10.3201/eid3001.230851

[1]These authors contributed equally to this article.

Table 1. Characteristics of mothers and their newborns with early-onset sepsis caused by *Escherichia coli* strains, France*

Case ID	Birth city†	Pregnancy term, wk	Prepartum antimicrobial‡	Meningitis§	Serotypes¶	FimH type	ST (STc)#	ESBL
APIMF52	Pontoise	37	–	–	O18:K1	fimH15	95	–
APIMF53	Antony	38	–	–	O13:K1	fimH21	357	–
APIMF54	Paris (Robert Debre)	35	+	–	O7:K5	fimH27	93 (168)	–
APIMF56	Orsay	41	+	–	O84	fimH38	2040	–
APIMF57	Clamart	40	+	–	O8	fimH32	58 (155)	–
APIMF58	Clichy	36	+	–	O18:K5	fimH27	14	–
APIMF59	Paris (Necker)	36	–	–	O25:K5	fimH30	131	+
APIMF60	Paris (Clinique Bleuets)	37	+	+	O75:K1	fimH64	1193 (14)	+
APIMF63	Quincy Sous Senart	39	–	–	O2:K1	fimH34	10	–
APIMF67	Mantes-La-Jolie	39	–	–	O18:K1	fimH107	95	–
APIMF68	Paris (Pitie)	40	–	–	O2:K1	fimH27	95	–
APIMF69	Saint Cloud	35	–	–	O18:K1	fimH15	95	–
APIMF70	Saint Denis	40	–	–	O25:K1	fimH41	59	–
APIMF71	Paris (Trousseau)	37	–	–	O7:K1	fimH1	80 (568)	–
APIMF72	Aulnay	36	–	–	O1:K1	fimH41	95	–
APIMF73	Villeneuve Saint-Georges	34	+	–	O75:K1	fimH64	1193 (14)	+
APIMF76	Colombes	41	–	–	O75:K1	fimH64	1193 (14)	–
APIMF77	Nogent Sur Marne	41	–	–	O17/O77:K52	Unknown	394	–
APIMF78	Coulommiers	41	–	+	O75:K1	fimH64	1193 (14)	–
APIMF79	Longjumeau	38	–	–	O6:K23	fimH103	73	–
APIMF80	Eaubonne	38	–	–	O4:K96	fimH5	12	–
APIMF81	Jossigny	34	–	–	O75:K5	fimH27	14	–
APIMF82	Meaux	34	+	–	O25:K5	fimH28	2279 (131)	–
APIMF83	Saint-Maurice	39	+	–	O8	fimH29	58 (155)	–
APIMF84	Creteil	39	+	–	O15:K96	fimH30	69	–
APIMF85	Arpajon	41	–	–	O4:Ku	fimH8–like	12	–
APIMF87	Paris (Trousseau)	35	–	+	O7:K1	fimH44	62	–
APIMF88	Marne La Vallee	36	+	+	O7:K1	fimH44	62	–
APIMF89	Creteil	36	+	+	O75:K1	fimH64	1193 (14)	+
APIMF90	Levallois Perret	36	+	–	O75:K1	fimH64	1193 (14)	–
APIMF91	Melun	34	–	–	O1:K1	fimH41	59	–
APIMF92	Beaumont Sur Oise	40	+	+	O18:K1	fimH15	95	–

*ESBL, extended spectrum β-lactamase; FimH, type 1 fimbriae D-mannose specific adhesin; ID, identification; Ku, unknown serogroup capsular; +, positive for condition; –, negative for condition.
†For Paris birthplaces, name of hospital where born is indicated in parentheses.
‡Amoxicillin was the only antimicrobial prescribed within 3 days before labor.
§Early onset neonatal meningitis.
¶O antigen predicted with SerotypeFinder 2.0 and serogroup capsular predicted by the Center for Genomic Epidemiology (https://genomicepidemiology.org).
#Sequence type complex (STc) indicated in parentheses if different from ST number.

Ile de France study, we included 50 *E. coli* isolates obtained from cultures from vaginal swabs collected from 4 maternity wards to screen pregnant woman for *S. agalactiae* carriage at 34–38 weeks of gestation. We found healthy vaginal carriage (HVC) among all; that is, none of the infants of the pregnant women from the *S. agalactiae* screening developed EOS caused by *E. coli*.

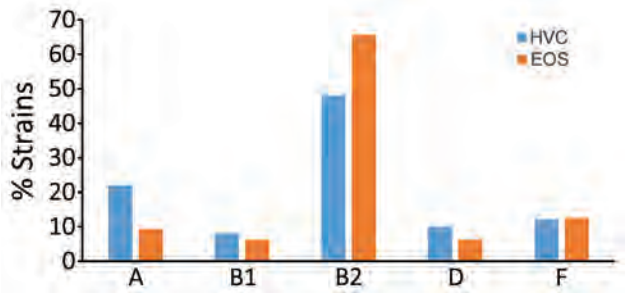

Figure 1. Phylogroup distribution among 32 EOS *Escherichia coli* strains from neonates and 50 HVC strains, France. No significant difference was observed in each group. EOS, early-onset neonatal sepsis; HVC, healthy vaginal carriage.

Antimicrobial Susceptibility Testing and Phenotypic Characterization

We determined antimicrobial susceptibility of the *E. coli* strains using disk diffusion on Mueller-Hinton agar plates (bioMérieux, https://www.biomerieux.com), as recommended by Comité de l'Antibiogramme de la Société Française de Microbiologie (https://www.sfm-microbiologie.org) guidelines. We defined ESBL production by synergy between clavulanic acid and ≥1 extended-spectrum cephalosporin or aztreonam.

Molecular Characterization

We performed WGS on 82 isolates, 32 described elsewhere (*12*) and 50 from the HVC/*S. agalactiae* screening. We extracted bacterial genomic DNA using the DNeasy UltraClean Microbial Kit

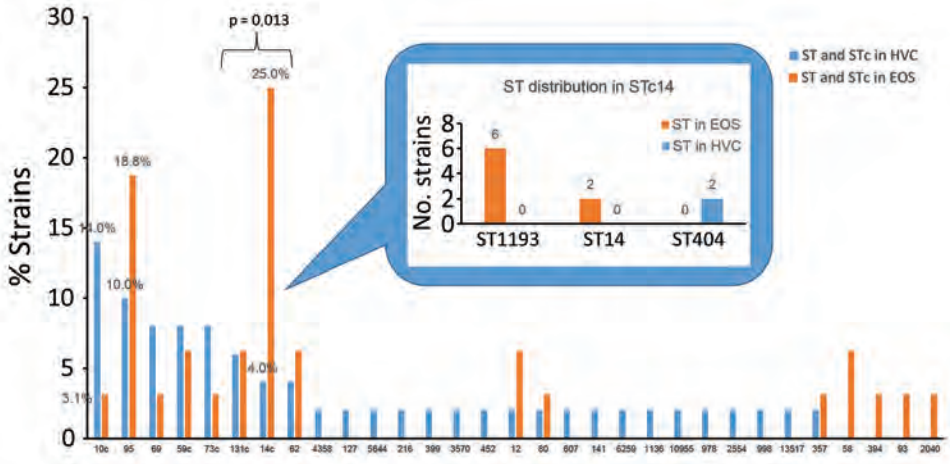

Figure 2. ST and STc distributions of EOS neonate and HVC *Escherichia coli* strains, France. STc14 distribution is detailed. STc10 includes ST10, ST13795, ST6826, and ST13957; STc59 includes ST59, ST415, and ST13796; STc11 includes ST73 and ST355; STc131 includes ST131 and ST2279. EOS, early-onset neonatal sepsis; HVC, healthy vaginal carriage; ST, sequence type; STc, ST complex.

(QIAGEN, https://www.qiagen.com) and prepared libraries using Nextera Flex/DNA Prep library kits (Illumina, https://www.illumina.com) as specified by the manufacturers. We performed sequencing using 2 × 150 bp MiniSeq technology (Illumina) and assembled models using SPAdes (https://github.com/ablab/spades). We estimated quality of sequencing data using standard metrics, including N50 and mean coverage (Appendix, https://wwwnc.cdc.gov/EID/article/30/1/23-0851-App1.pdf). We determined phylogenetic groups, serotypes, fimH type, sequence type (ST), and STcs (which regroup all STs of ≤1 allele difference), whole-genome multilocus sequence typing (MLST), and hierarchical clustering of core genome MLST using Enterobase (https://enterobase.warwick.ac.uk) (*13*). We used the Center for Genomic Epidemiology website (https://genomicepidemiology.org) to search for resistance and virulence genes. We also used a local BLAST with a collection of virulence genes as described elsewhere (*14*). We used Fisher exact analysis for statistical comparisons among groups.

Results

Bacterial Collection and Demographic and Clinical Features of Patients

We studied 82 *E. coli* isolates. Birth locations of the neonates within Ile de France were diverse (30 different locations among 32 EOS case-patients). Babies were delivered at full term (≥37 weeks of gestation) in 59% (19/32) and preterm (<37 weeks of gestation) in 41% (13/32) of cases. In 6 (31%) cases from the full-term group and 7 cases (54%) from the preterm group, mothers received antimicrobial treatment ≤3 days before labor. We observed 6 cases of meningitis, 3 each from the full-term and preterm neonate groups (Table 1).

Diversity and Phylogenetics of EOS and HVC *E. coli* Strain Collections

Five of 7 major *E. coli* phylogroups—A, B1, B2, D, and F, but not C or E—were represented in similar proportions in both the Ile de France study and vaginal swab collections (p>0.05). The exceptions to this trend were phylogroup A being more common in vaginal swab (22%) than EOS (9.4%) isolates and group B2 more common in EOS (65.6%) than vaginal swab (48%) isolates (Figure 1). Among the 3 most frequent ST/STc variants in our study, STc10 (phylogroup A) was present in more HVC strains, whereas ST95 and STc14 (phylogroup B2) were more common in EOS strains. The imbalance was striking for STc14, which was present in 25% of EOS strains but only 4% of HVC strains (p = 0.01) (Figure 2). STc14 isolates included 6 ST1193, 2 ST14, and 2 ST404. Of note, the 6 ST1193 isolates were found exclusively in the EOS collection.

Virulence and Antimicrobial Resistance

We observed no significant difference in distribution of virulence factors between the EOS and HVC strain

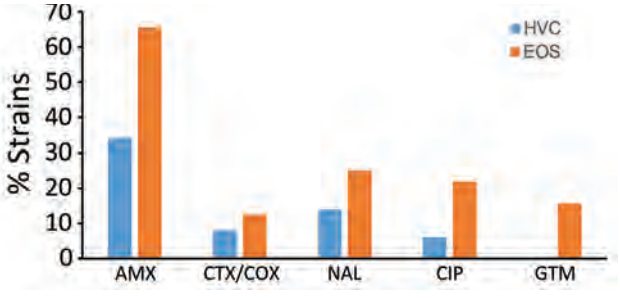

Figure 3. Antibiotic resistance rates among EOS neonate and HVC *Escherichia coli* strains, France. AMX, amoxicillin; CIP, ciprofloxacin; CTX/COX, cefotaxime/ceftriaxone; EOS, early-onset neonatal sepsis; GTM, gentamicin; HVC, healthy vaginal carriage; NAL, nalidixic acid.

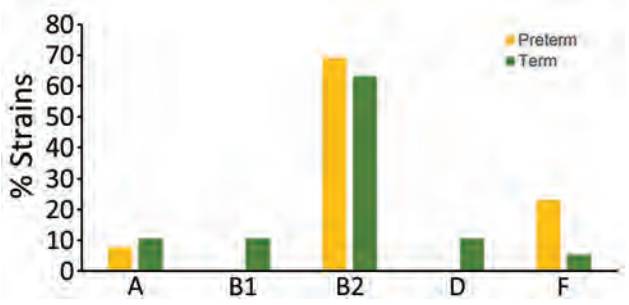

Figure 4. Phylogroup distributions according to birth term among 32 neonates with early-onset sepsis, France. EOS, early-onset neonatal sepsis.

collections, except for genes encoding the K1 capsule, which were present significantly more in the EOS collection (Appendix Table 1). In contrast, antimicrobial resistance differed markedly between collections (Figure 3). Aminopenicillin resistance was ≈2 times higher among EOS (65.6%) than HVC (34%) collection strains (p = 0.007); ESBL was present in 12.5% of EOS and 8% of HVC strains (p>0.05). Resistance to fluoroquinolone and gentamicin were also more common among EOS strains (Figure 3).

We examined the distribution of phylogenetic groups and ST/STc frequency among EOS strains stratified by gestational term of newborns. Differences in rates of B2 phylogroup strains in the 2 subpopulations (69% in preterm, 63% in full-term neonates) were not statistically significant (Figure 4). STc14 (ST14/ST1193) was >2 times as frequent in the preterm (38.5%) as the full-term subpopulation (15.8%), but the difference was not statistically significant (p>0.05). Distribution of ST95, the second most frequent ST, was similar between preterm (15.4%) and full-term (21.1%) subpopulations (Figure 5). There were more mothers with STc14 *E. coli* isolates (5/13 [38.5%]) among those who received antimicrobial therapy ≤3 days before delivery than those who did not (3/19 [15.8%]) (p>0.05) (Figure 6). In contrast, there were fewer ST95 isolates among mothers receiving prenatal antimicrobial therapy (1/13 [7.69%]) than those receiving no therapy (5/19 [26.32%]) (p>0.05).

Main Features of EOS Caused by ST1193 *E. coli* and Characterization of Isolates

All 6 ST1193 EOS strains were isolated from different maternity hospitals. Half (3/6) of neonates with ST1193 EOS were born at full term. Three neonates had meningitis, 2 full-term and 1 preterm. Four (67%) mothers with ST1193 strains received prenatal antimicrobial therapy compared with nine (35%) for the non-ST1193 strains (p>0.05) (Table 1; Figure 6). All strains were resistant to fluoroquinolones, 3 were resistant to azithromycin, and 3 others harbored an ESBL phenotype (Table 2). All strains were lactose nonfermenters (data not shown).

We assessed presence of putative virulence factors among the 6 ST1193 isolates (Table 2; Appendix Table 2) and identified presence of factors with a significant difference (p<0.05) among ST1193 compared with non-ST1193 strains: adherence protein *Iha*, colicin Ia immunity protein *Imm*, major pilin subunit *PapA_F43*, plasmid-encoded enterotoxin *SenB*, serine protease *Sat*, vacuolating autotransporter toxin *Vat*, and Type 1 fimbrin D-mannose specific adhesion 64.

Three strains harbored ESBL phenotypes contained the β-lactamase–encoding genes $bla_{\text{CTX-M-15}}$ and $bla_{\text{OXA-1}}$ associated with the *aac(6')-Ib-cr* genes, and 3/6 strains harbored the *mph(A)* gene (macrolide 2'-phosphotransferase), which inactivates macrolides, reinforcing observed phenotypic resistance to azithromycin. None of the non-ST1193 strains carried that gene. One strain was resistant only to fluoroquinolones (Table 2). All strains had different hierarchical cluster 10 (HC10) but the same HC20 (571), whereas ribosomal MLST (rMLST) split the strains into 2 main populations:

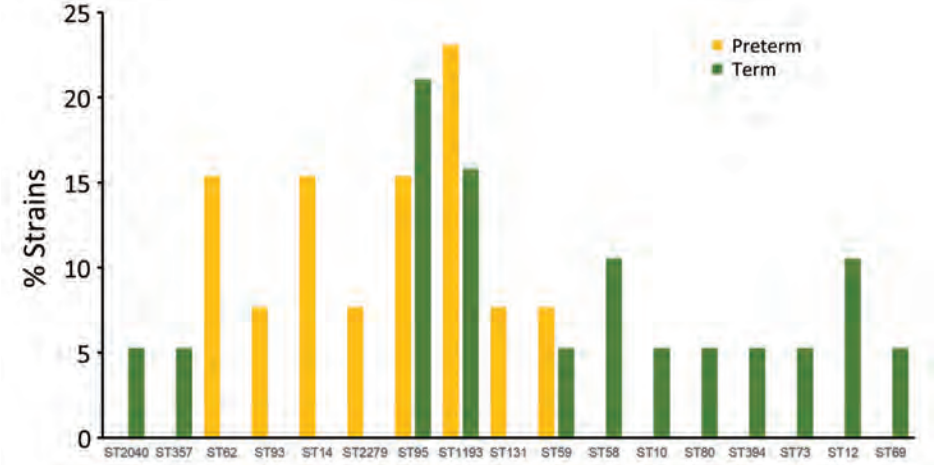

Figure 5. ST distributions according to birth term among 32 neonates with early-onset neonatal sepsis. ST, sequence type.

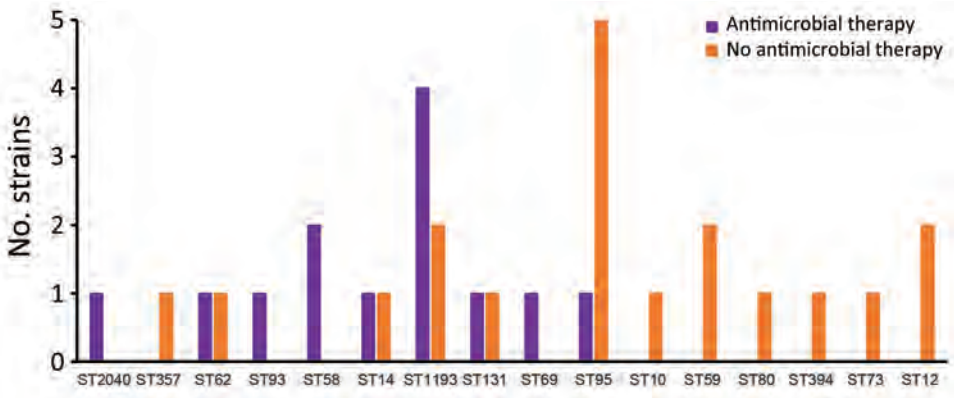

Figure 6. Distribution of maternal antimicrobial therapy within 3 days before delivery according to *Escherichia coli* ST among 32 neonates with early-onset neonatal sepsis, France. ST, sequence type.

rMLST 33503, which regroups the 3 ESBL-producing strains, and rMLST 1674, which contains 2 less-resistant isolates.

Discussion

In our study, we used WGS to characterize *E. coli* strains causing EOS from a prospective multicenter study in France (*12*) and compared them to *E. coli* strains obtained from vaginal samples from pregnant women at 34–38 weeks of gestation. Although we observed no major differences between the EOS study and vaginal sample collections in distribution of phylogroups or virulence factors except the K1 antigen, we identified emerging ST1193 strains as major causes of EOS. Three isolates of the ST1193 clonal group caused meningitis, and half harbored an ESBL. *E. coli* ST1193 thus appears to be the most virulent and antimicrobial-resistant *E. coli* group that causes EOS.

Among major phylogroups, B2 and, to a lesser extent, D are associated with extraintestinal infections, whereas A and B1 are most associated with commensal strains or intestinal infections (*15*). We also observed predominance of B2 strains in our EOS population, regardless of the term of birth of the newborns. Although the proportion of phylogroup A strains was higher in the HVC than the EOS population, B2 strains largely predominated in the HVC collection, as reported in previous studies (*16*,*17*). However, sequence typing enabled a finer comparison between the 2 collections. Among the HVC strains, phylogroup A/STc10 (ST10, ST13795, ST6826, and ST13957) was predominant but was rarely observed among the EOS patients, in which ST95 and STc14 (notably ST14 and ST1193) were largely predominant. The high frequency of ST95 was expected because of its virulence in neonates, notably those with neonatal meningitis, which is well known worldwide (*6*,*18*). Of note, ST95 was second most common among HVC strains, suggesting its capacity to colonize the vagina, at least temporarily. Five of 6 mothers with EOS caused by ST95 received no prepartum antimicrobials. In contrast, ST14 and ST1193 strains were frequently associated with women receiving prepartum antimicrobials (5/8), and those strains were not present among HVC patients, suggesting the vaginal environment might inhibit the presence of ST14 and ST1193 strains. Of note, STc14 but not ST95 was more prevalent among preterm neonates with EOS, and 3/6 infections caused by ST1193 strains occurred in preterm newborns. It might be that ST1193 strains are less virulent than ST95 strains commonly found in full-term neonates. However, almost all women with preterm newborns received antimicrobial drugs, which might favor the selection of resistant strains, such as ST1193.

ST1193 was identified within STc14 approximately 25 years ago; its prevalence in extraintestinal infections could become a public health burden (*19*–*21*). One study observed an increased rate of ST1193 causing bloodstream infections, mostly in elderly patients in Canada during 2016–2018 (*22*). In an analysis of the population structure of 218 ESBL–producing *E. coli* in urinary tract infections in febrile children in France during 2014–2017, we noted prevalence of ST1193 rose from 0% to 9% (*23*). Large epidemiologic studies of ST1193 prevalence in neonatal infection have only recently been conducted. In 2 studies, ST1193 was shown to be a major cause of neonatal sepsis; however, because the definition of EOS in those studies differed from ours, data are difficult to compare (*11*,*24*). The finding of a worrying percentage of ST1193 among EOS patients (19%) in our study population indicates that in the future that ST should be closely monitored using microbiologic detection.

One epidemiologic study of intracranial infections in neonates caused by *E. coli* (*25*) found ST1193 to be the most prevalent ST (28%). All 8 ST1193 isolates caused late-onset infections, although none caused EOS. Only 1 recent case of early-onset meningitis caused by *E. coli* ST1193 has been reported, but cases of meningitis caused by ST1193 occurring >72 hours after birth were described in another study (*24*,*26*).

Table 2. Characteristics of newborns with early onset sepsis caused by ST1193 *Escherichia coli* and genetic and phenotypic features of the isolates*

APIMF case ID	EOS clinical features		Genetic and phenotypic characteristic of *E. coli* strains ST1193					
	Term, wk†	Antimicrobial prepartum‡	Virulence genes§	Antimicrobial resistance genes§	Phenotypic AMR	HC10¶	HC20¶	rMLST#
60**	37	Amoxicillin	*aslA*, *chuA*, *csgA*, *fdeC*, *fimH*, *fyuA*, *gad*, *iha*, *irp2*, *iucC*, *iutA*, *kpsE*, *kpsMII_K1*, *neuC*, *nlpI*, *ompT*, *papA_F43*, *sat*, *senB*, *shiA*, *sitA*, *terC*, *tia*, *usp*, *vat*, *yehA*, *yehB*, *yehC*, *yehD*, *yfcV*	*dfrA17*, *aph(6)-Id*, *aac(6')-Ib-cr*, *aac(3)-IIa*, *aph(3")-Ib*, *sul2*, *catB3*,*mph(A)*, *sitABCD*, *tet(B)*, $bla_{CTX-M-15}$, bla_{TEM-1B}, bla_{OXA-1}	AMX, CTX, CIP, SXT, GTM, AZI, TET, CMP, ESBL	132,558	571	33,503
73	34	Amoxicillin	*aslA*, *chuA*, *csgA*, *fdeC*, *fimH*, *fyuA*, *gad*, *iha*, *irp2*, *iucC*, *iutA*, *kpsE*, *kpsMII_K1*, *neuC*, *nlpI*, *ompT*, *papA_F43*, *sat*, *senB*, *sitA*, *terC*, *usp*, *vat*, *yehA*, *yehB*, *yehC*, *yehD*, *yfcV*	*catB3*, *tet(B)*, $bla_{CTX-M-15}$, bla_{OXA-1}, *aph(6)-Id*, *aac(3)-IIa*, *aph(3")-Ib*, *aac(6')-Ib-cr*, *sul2*, *aac(6')-Ib-cr*, *qnrB19*, *dfrA17*	AMX, CTX, CIP, SXT, GTM, TET, ESBL	148,092	571	33,503
76	41	None	*aslA*, *ccl*, *chuA*, *clbB*, *csgA*, *fdeC*, *fimH*, *fyuA*, *gad*, *iha*, *irp2*, *iucC*, *iutA*, *kpsE*, *kpsMII_K1*, *neuC*, *nlpI*, *ompT*, *papA_F43*, *sat*, *senB*, *sitA*, *terC*, *usp*, *vat*, *yehA*, *yehB*, *yehC*, *yehD*, *yfcV*	None	CIP	227,323	571	1,674
78**	41	None	*AslA*, *chuA*, *csgA*, *fdeC*, *fimH*, *fyuA*, *gad*, *iha*, *irp2*, *iucC*, *iutA*, *kpsE*, *kpsMII_K1*, *neuC*, *nlpI*, *ompT*, *papA_F43*, *sat*, *senB*, *sitA*, *terC*, *usp*, *vat*, *yehA*, *yehB*, *yehC*, *yehD*, *yfcV*	*aadA5*, *dfrA17*, *mph(A)*	CIP, AZI, SXT	11,740	571	1,674
89**	36	Amoxicillin/ gentamicin	*AslA*, *astA*, *chuA*, *colE7*, *csgA*, *fdeC*, *fimH*, *fyuA*, *gad*, *iha*, *irp2*, *iucC*, *iutA*, *kpsE*, *kpsMII_K1*, *neuC*, *nlpI*, *ompT*, *papA_F43*, *sat*, *senB*, *shiA*, *sitA*, *terC*, *tia*, *usp*, *vat*, *yehA*, *yehB*, *yehC*, *yehD*, *yfcV*	*aac(3)-IIa*, *aac(6')Ib-cr*, $bla_{CTX-M-15}$, bla_{OXA-1}, *catB3*	AMX, CTX, CIP, GTM, CMP, ESBL	4,073	571	33,503
90	36	Amoxicillin	*AslA*, *chuA*, *csgA*, *fdeC*, *fimH*, *fyuA*, *gad*, *iha*, *irp2*, *iucC*, *iutA*, *kpsE*, *kpsMII_K1*, *neuC*, *nlpI*, *ompT*, *papA_F43*, *sat*, *senB*, *sitA*, *terC*, *usp*, *vat*, *yehA*, *yehB*, *yehC*, *yehD*, *yfcV*	bla_{TEM-1B}, *dfrA17*, *mph(A)*, *aph(6)-Id*, *aph(3")-Ib*, *sul2*, *tet(B)*	AMX, CIP, SXT, AZI, TET	227,336	571	New

*AMR, antimicrobial resistance; AMX, amoxicillin; AZI, azithromycin; cgMLST, core genome multilocus sequence typing; CIP, ciprofloxacin; CMP, chloramphenicol; CTX, cefotaxime; EOS, early-onset neonatal sepsis; ESBL, extended spectrum β-lactamase; GTM, gentamicin; HC, human chromosome; ID, identification; rMLST, ribosomal multilocus sequence typing; ST, sequence type; SXT, trimethoprim/sulfamethoxazole; TET, tetracycline.
†Term of pregnancy at birth in weeks.
‡Antimicrobial treatment within 3 days before labor began.
§Search for antimicrobial resistance genes and replicon/plasmid sequence types run using Center for Genomic Epidemiology website (https://genomicepidemiology.org) and local BLAST.
¶Hierarchical clustering of distances between genomes calculated using 10 (HC10) or 20 (HC20) shared core genome MLST alleles and genomes linked on a single-linkage clustering criteria.
#Approach that indexes variation of the 53 genes encoding the bacterial ribosome protein subunits.
**Early-onset neonatal sepsis with meningitis.

The recent case occurred in a late-preterm neonate with a history of prolonged rupture of the membrane with prepartum and peripartum antimicrobial drugs administered, as in most of our cases.

Given that 3/6 ST1193 strains caused neonatal meningitis, such strains were shown to have high invasive disease potential in newborns. Several virulence factors and genetic determinants have been shown to be involved in the pathophysiology of neonatal meningitis, such as capsule K1, siderophore salmochelin, plasmid *pS88*, and invasin *IbeA* (*27*). Of note, among these determinants, only the K1 capsule was present in the ST1193 strains. Several virulence factors (Iha, Imm, plasmid-encoded enterotoxin SenB, Sat) were present in all ST1193 strains, with a significant p value ($p<0.05$) compared with non-ST1193 (Appendix Table 2) strains, and were present in >85% of ST1193 strains in the large collection of 1 study (*28*). Therefore, without in vivo study, it is difficult to determine the specific roles of these key factors in the invasiveness of ST1193 in cerebrospinal fluid.

Except for consistency of fluoroquinolone resistance and carrying the fimH64 allele, which characterized all ST1193 *E. coli* strains described in previous studies, multiple plasmid-borne resistance genes have been reported but are inconsistently associated with ST1193 (*19*,*28*,*29*). No isolates harbored the same phenotypic antimicrobial resistance pattern, highlighting their diversity. The co-occurrence of $bla_{CTX\text{-}M\text{-}15}$/$bla_{OXA\text{-}1}$/*aac(6')-Ib-cr*, which we observed in 3/6 of EOS strains, has been frequently described, initially in ST131 but also more recently in emerging lineages of ST1193 (*30*). Half of our strains, similar to findings from other studies (*28*), carried the *mph*A resistance gene and had a high azithromycin MIC (>32 mg/L) (data not shown), which might have contributed to the emergence of ST1193 given that azithromycin is among the most-prescribed antimicrobial drugs worldwide among adult outpatients (*31*).

As of May 2023, sequences of 2,031 *E. coli* ST1193 strains from all over the world are available in Enterobase (*13*). Of those, 80% belong to HC20 571, as did our strains, and most (82%) harbor rMLST 1674, whereas rMLST 33503 is found in only 8%. Hierarchical clustering analysis did not suggest the presence of a particular clone in our collection. Distribution of rMLSTs was notably different: half of our ST1193 strains belonged to rMLST 33503. Whether this subgroup is emerging or has specific invasive disease potential in neonates has yet to be determined.

Among its strengths, our prospective epidemiologic study, conducted in a large area of France, estimated annual incidence and pathogen distribution in EOS patients (*12*) and documented the unique molecular and phenotypic characteristics of the strains in our study. We were limited by the small number of patients; results, especially implication of ST1193 in infections in very preterm neonates, need to be confirmed in larger study populations.

In conclusion, our findings suggest that ST1193 is emerging as a major *E. coli* pathogen that can cause EOS and early-onset neonatal meningitis in full-term and late-preterm newborns and might surpass ST95 in incidence and causing illness because of its potential virulence combined with its resistance to multiple antimicrobials. Pediatricians and microbiologists should be aware of the public health threat from *E. coli* ST1193 and the benefits of prepartum/peripartum EOS treatment with effective antimicrobials. Isolating ST1193 *E. coli* strains in the neonatal context (from mother, newborn, or both) will require careful, sustained clinical monitoring of newborns. It might also require implementing measures to limit spread, especially in neonatal wards. On the basis of microbiologic evidence, ST1193 should be suspected when 3 properties are all present: high resistance to ciprofloxacin, K1 capsule, and non–lactose-fermenting colonies, each of which can easily be tested for in a microbiology laboratory. Further studies should help to define the genetic determinants of ST1193 virulence in neonates and confirm and subsequently explain its inability or weak ability to colonize the vagina. Clinicians need to be aware of the possible presence of *E. coli* ST1193 in prenatal and neonatal contexts and provide appropriate monitoring and treatment.

This work was funded in part by l'Agence Nationale de la Recherche (project ANR-Seq-N-Vac).

C.M., G.G., and S.B. contributed conceptualization, methodology, and writing of the original draft; P.B., C.M., and G.G., formal analysis; P.S. and S.B., investigation; P.S., I.P., M.A., K.N., and M.L., resources; S.B., supervision; and all authors, writing, review, and editing.

About the Author

Dr. Malaure is a medical resident in clinical microbiology at Robert Debré Hospital, Université Paris Cité, Paris, France. Her main research interests are bacterial pathogens, molecular typing, and bacterial resistance.

References

1. Shane AL, Sánchez PJ, Stoll BJ. Neonatal sepsis. Lancet 2017;390:1770–80.
2. Stoll BJ, Puopolo KM, Hansen NI, Sánchez PJ, Bell EF, Carlo WA, et al.; Eunice Kennedy Shriver National Institute of Child Health and Human Development Neonatal Research Network. Early-onset neonatal sepsis 2015 to 2017, the rise of *Escherichia coli*, and the need for novel prevention strategies. JAMA Pediatr. 2020;174:e200593. https://doi.org/10.1001/jamapediatrics.2020.0593
3. Gaschignard J, Levy C, Romain O, Cohen R, Bingen E, Aujard Y, et al. Neonatal bacterial meningitis: 444 cases in 7 years. Pediatr Infect Dis J. 2011;30:212–7. https://doi.org/10.1097/INF.0b013e3181fab1e7
4. Joshi NS, Huynh K, Lu T, Lee HC, Frymoyer A. Epidemiology and trends in neonatal early onset sepsis in California, 2010–2017. J Perinatol. 2022;42:940–6. https://doi.org/10.1038/s41372-022-01393-7
5. Miselli F, Cuoghi Costantini R, Creti R, Sforza F, Fanaro S, Ciccia M, et al. *Escherichia coli* is overtaking group B *Streptococcus* in early-onset neonatal sepsis. Microorganisms. 2022;10:10. https://doi.org/10.3390/microorganisms10101878
6. Basmaci R, Bonacorsi S, Bidet P, Biran V, Aujard Y, Bingen E, et al. *Escherichia coli* meningitis features in 325 children from 2001 to 2013 in France. Clin Infect Dis. 2015;61:779–86. https://doi.org/10.1093/cid/civ367
7. Bonacorsi S, Clermont O, Houdouin V, Cordevant C, Brahimi N, Marecat A, et al. Molecular analysis and experimental virulence of French and North American *Escherichia coli* neonatal meningitis isolates: identification of a new virulent clone. J Infect Dis. 2003;187:1895–906. https://doi.org/10.1086/375347
8. Peigne C, Bidet P, Mahjoub-Messai F, Plainvert C, Barbe V, Médigue C, et al. The plasmid of *Escherichia coli* strain S88 (O45:K1:H7) that causes neonatal meningitis is closely

related to avian pathogenic *E. coli* plasmids and is associated with high-level bacteremia in a neonatal rat meningitis model. Infect Immun. 2009;77:2272–84. https://doi.org/10.1128/IAI.01333-08
9. Riley LW. Pandemic lineages of extraintestinal pathogenic *Escherichia coli*. Clin Microbiol Infect. 2014;20:380–90. https://doi.org/10.1111/1469-0691.12646
10. Frank Wolf M, Abu Shqara R, Naskovica K, Zilberfarb IA, Sgayer I, Glikman D, et al. Vertical transmission of extended-spectrum, beta-lactamase-producing *Enterobacteriaceae* during preterm delivery: a prospective study. Microorganisms. 2021;9:506. https://doi.org/10.3390/microorganisms9030506
11. Gu S, Lai J, Kang W, Li Y, Zhu X, Ji T, et al. Drug resistance characteristics and molecular typing of *Escherichia coli* isolates from neonates in class A tertiary hospitals: a multicentre study across China. J Infect. 2022;85:499–506. https://doi.org/10.1016/j.jinf.2022.09.014
12. Sikias P, Biran V, Foix-L'Hélias L, Plainvert C, Boileau P, Bonacorsi S; EOS study group. Early-onset neonatal sepsis in the Paris area: a population-based surveillance study from 2019 to 2021. Arch Dis Child Fetal Neonatal Ed. 2023;108:114–20. https://doi.org/10.1136/archdischild-2022-324080
13. Zhou Z, Alikhan N-F, Mohamed K, Fan Y, Achtman M; Agama Study Group. The EnteroBase user's guide, with case studies on *Salmonella* transmissions, *Yersinia pestis* phylogeny, and *Escherichia* core genomic diversity. Genome Res. 2020;30:138–52. https://doi.org/10.1101/gr.251678.119
14. Cointe A, Birgy A, Mariani-Kurkdjian P, Liguori S, Courroux C, Blanco J, et al. Emerging multidrug-resistant hybrid pathotype Shiga toxin–producing *Escherichia coli* O80 and related strains of clonal complex 165, Europe. Emerg Infect Dis. 2018;24:2262–9. https://doi.org/10.3201/eid2412.180272
15. Denamur E, Clermont O, Bonacorsi S, Gordon D. The population genetics of pathogenic *Escherichia coli*. Nat Rev Microbiol. 2021;19:37–54. https://doi.org/10.1038/s41579-020-0416-x
16. Sáez-López E, Cossa A, Benmessaoud R, Madrid L, Moraleda C, Villanueva S, et al. Characterization of vaginal *Escherichia coli* isolated from pregnant women in two different African sites. PLoS One. 2016;11:e0158695. https://doi.org/10.1371/journal.pone.0158695
17. Watt S, Lanotte P, Mereghetti L, Moulin-Schouleur M, Picard B, Quentin R. *Escherichia coli* strains from pregnant women and neonates: intraspecies genetic distribution and prevalence of virulence factors. J Clin Microbiol. 2003;41:1929–35. https://doi.org/10.1128/JCM.41.5.1929-1935.2003
18. Johnson TJ, Wannemuehler Y, Johnson SJ, Stell AL, Doetkott C, Johnson JR, et al. Comparison of extraintestinal pathogenic *Escherichia coli* strains from human and avian sources reveals a mixed subset representing potential zoonotic pathogens. Appl Environ Microbiol. 2008;74:7043–50. https://doi.org/10.1128/AEM.01395-08
19. Pitout JDD, Peirano G, Chen L, DeVinney R, Matsumura Y. *Escherichia coli* ST1193: following in the footsteps of *E. coli* ST131. Antimicrob Agents Chemother. 2022;66:e0051122. https://doi.org/10.1128/aac.00511-22
20. Crémet L, Caroff N, Giraudeau C, Reynaud A, Caillon J, Corvec S. Detection of clonally related *Escherichia coli* isolates producing different CMY β-lactamases from a cystic fibrosis patient. J Antimicrob Chemother. 2013;68:1032–5. https://doi.org/10.1093/jac/dks520
21. Platell JL, Trott DJ, Johnson JR, Heisig P, Heisig A, Clabots CR, et al. Prominence of an O75 clonal group (clonal complex 14) among non-ST131 fluoroquinolone-resistant *Escherichia coli* causing extraintestinal infections in humans and dogs in Australia. Antimicrob Agents Chemother. 2012;56:3898–904. https://doi.org/10.1128/AAC.06120-11
22. Peirano G, Matsumara Y, Nobrega D, DeVinney R, Pitout J. Population-based epidemiology of *Escherichia coli* ST1193 causing blood stream infections in a centralized Canadian region. Eur J Clin Microbiol Infect Dis. 2021. Online ahead of print.
23. André Birgy A, Fouad Madhi F, Camille Jung C, Corinne Levy C, Aurélie Cointe A, Philippe Bidet P, et al. Diversity and trends in population structure of ESBL-producing *Enterobacteriaceae* in febrile urinary tract infections in children in France from 2014 to 2017. J Antimicrob Chemother. 2020;75:96–105.
24. Ding Y, Zhang J, Yao K, Gao W, Wang Y. Molecular characteristics of the new emerging global clone ST1193 among clinical isolates of *Escherichia coli* from neonatal invasive infections in China. Eur J Clin Microbiol Infect Dis. 2021;40:833–40. https://doi.org/10.1007/s10096-020-04079-0
25. Zhong Y-M, Zhang X-H, Ma Z, Liu W-E. Prevalence of *Escherichia coli* ST1193 causing intracranial infection in Changsha, China. Trop Med Infect Dis. 2022;7:217. https://doi.org/10.3390/tropicalmed7090217
26. Oldendorff F, Linnér A, Finder M, Eisenlauer P, Kjellberg M, Giske CG, et al. Case report: fatal outcome for a preterm newborn with meningitis caused by extended-spectrum β-lactamase-producing *Escherichia coli* sequence type 1193. Front Pediatr. 2022;10:866762. https://doi.org/10.3389/fped.2022.866762
27. De Francesco MA, Bertelli A, Corbellini S, Scaltriti E, Risso F, Allegri R, et al. Emergence of pandemic clonal lineage sequence types 131 and 69 of extraintestinal *Escherichia coli* as a cause of meningitis: is it time to revise molecular assays? Microbiol Spectr. 2023;11:e0327422. https://doi.org/10.1128/spectrum.03274-22
28. Wyrsch ER, Bushell RN, Marenda MS, Browning GF, Djordjevic SP. Global phylogeny and f virulence plasmid carriage in pandemic *Escherichia coli* ST1193. Microbiol Spectr. 2022;10:e0255422. https://doi.org/10.1128/spectrum.02554-22
29. Johnson TJ, Elnekave E, Miller EA, Munoz-Aguayo J, Flores Figueroa C, Johnston B, et al. Phylogenomic analysis of extraintestinal pathogenic *Escherichia coli* sequence type 1193, an emerging multidrug-resistant clonal group. Antimicrob Agents Chemother. 2018;63:e0191318. https://doi.org/10.1128/AAC.01913-18
30. Jackson N, Belmont CR, Tarlton NJ, Allegretti YH, Adams-Sapper S, Huang YY, et al. Genetic predictive factors for nonsusceptible phenotypes and multidrug resistance in expanded-spectrum cephalosporin-resistant uropathogenic *Escherichia coli* from a multicenter cohort: insights into the phenotypic and genetic basis of coresistance. MSphere. 2022;7:e0047122. https://doi.org/10.1128/msphere.00471-22
31. Hicks LA, Taylor TH Jr, Hunkler RJ. U.S. outpatient antibiotic prescribing, 2010. N Engl J Med. 2013;368:1461–2. https://doi.org/10.1056/NEJMc1212055

Address for correspondence: Stéphane Bonacorsi, Service de Microbiologie, Hôpital Universitaire Robert-Debré, AP-HP, 48 Boulevard Sérurier 75019 Paris, France; email: stephane.bonacorsi@aphp.fr

Molecular Evolution and Increasing Macrolide Resistance of *Bordetella pertussis*, Shanghai, China, 2016–2022

Pan Fu,[1] Jinlan Zhou,[1] Chao Yang, Yaxier Nijiati, Lijun Zhou, Gangfen Yan, Guoping Lu, Xiaowen Zhai, Chuanqing Wang

Resurgence and spread of macrolide-resistant *Bordetella pertussis* (MRBP) threaten global public health. We collected 283 *B. pertussis* isolates during 2016–2022 in Shanghai, China, and conducted 23S rRNA gene A2047G mutation detection, multilocus variable-number tandem-repeat analysis, and virulence genotyping analysis. We performed whole-genome sequencing on representative strains. We detected pertussis primarily in infants (0–1 years of age) before 2020 and older children (>5–10 years of age) after 2020. The major genotypes were *ptxP1/prn1/fhaB3/ptxA1/ptxC1/fim2–1/fim3–1* (48.7%) and *ptxP3/prn2/fhaB1/ptxA1/ptxC2/fim2-1/fim3-1* (47.7%). MRBP increased remarkably from 2016 (36.4%) to 2022 (97.2%). All MRBPs before 2020 harbored *ptxP1*, and 51.4% belonged to multilocus variable-number tandem-repeat analysis type (MT) 195, whereas *ptxP3*-MRBP increased from 0% before 2020 to 66.7% after 2020, and all belonged to MT28. MT28 *ptxP3*-MRBP emerged only after 2020 and replaced the resident MT195 *ptxP1*-MRBP, revealing that 2020 was a watershed in the transformation of MRBP.

Whooping cough (pertussis) is a contagious respiratory illness caused by *Bordetella pertussis*. The introduction of the whole-cell vaccine (WCV) successfully decreased the incidence of pertussis. Although vaccination has been successful, replacement of the WCV with an acellular vaccine (ACV) has correlated with reemergence of pertussis, especially in adolescents and infants (*1*). In China, ACV was developed in the late 1990s and has replaced WCV and been exclusively used in China since 2012 (*2*,*3*). However, a multicenter study showed that the levels of protective antibodies against pertussis were already very low in immunized children 2–20 years of age (*4*).

Resurgence of pertussis has been widely reported and is mainly found in age groups of unvaccinated or incompletely vaccinated children or those whose immunity has waned (*5*,*6*). Mooi et al. (*7*,*8*) first identified the antigenic divergence between circulating isolates and vaccine strains in 1998, which explained the reemergence of pertussis and the distinct epidemiology of pertussis in different regions. Since then, a series of studies have demonstrated antigenic changes in bacterial virulence genes that might compromise vaccine-mediated immunity against *B. pertussis* (*9*–*11*). Virulence antigens, such as filamentous hemagglutinin (FHA), pertactin (Prn), pertussis toxin (PT), fimbriae2 (Fim2), and fimbriae3 (Fim3), are the essential components of ACV (*12*). PT export genes are regulated by the *ptx* promoter (*ptxP*) and may be required for efficient translation of *ptx* mRNA in *B. pertussis* strains (*13*). The *ptxP* region include 2 major alleles *ptxP1* and *ptxP3*, and *ptxP3* produces more PT than the *ptxP1* allele (*14*).

In many countries, circulating *B. pertussis* harbors different virulence genotypes compared with vaccine strains (*15*,*16*). Different alleles of *ptxP*, *fhaB, ptxA, ptxC*, *fim2*, and *fim3* have been reported in many studies (*6*,*17*,*18*). Among those virulence-related genes, the *ptxC* alleles *ptxC1* and ptxC2 have been described; those alleles differ at a single nucleotide, resulting in a silent mutation (*19*). Compared with the major *ptxP1/fhaB1/prn1/ptxA2* genotype of vaccine strains, the *ptxP3/fhaB3/prn2/ptxA1* genotype have emerged in the circulating *B. pertussis* population in China (*6*,*20*,*21*).

Author affiliations: National Children's Medical Center, Shanghai, China (P. Fu, J. Zhou, Y. Nijiati, L. Zhou, G. Yan, G. Lu, X. Zhai, C. Wang); Chinese Academy of Sciences, Shanghai (C. Yang)

DOI: https://doi.org/10.3201/eid3001.221588

[1]These first authors contributed equally to this article.

Despite the variation in virulence genotypes in circulating strains, different *B. pertussis* subtypes are prevalent in the world. The multilocus variable-number tandem-repeat analysis (MLVA) type (MT) 27 strain carrying the genotype of *ptxP3/ptxA1/prn2/fim3–1* has become the predominant *B. pertussis* strain in many countries (*22*). However, MT27 has seldomly been reported in China, whereas the MT55, MT195, or MT104 strains harboring the *ptxP1* allele have been reported to circulate in some regions of China (*23*,*24*). Macrolide-resistant *B. pertussis* (MRBP), which carries an A-to-G transition at nucleotide position 2047 (A2047G mutation) in a region critical for erythromycin binding, emerged in some countries, but was only frequently detected in China (*15*,*16*,*25*–*27*). MRBPs generally carry *ptxP1* and *fhaB3*, but 2 novel MRBPs belonging to MT28 and MT27 carrying *ptxP3* and *fhaB1* were reported in mainland China (*15*,*28*).

Our recent study reported that MT28 *ptxP3*-MRBP has emerged and spread in Shanghai, China, during 2021–2022 (*29*). However, several urgent questions remain to be resolved. For example, was *ptxP3*-MT28 MRBP dominant in Shanghai in the long term, or did it emerge in 2021 and 2022? Why and when did *ptxP3*-MT28 MRBP emerge in Shanghai, and how did they evolve? To resolve those questions, we conducted further research during 2016–2022 to reveal the evolution of MRBP in Shanghai. We collected a total of 283 *B. pertussis* isolates during 2016–2022 in Shanghai and systematically analyzed the antimicrobial resistance and molecular evolution of those strains.

Methods

Enrollment of Case-Patients with *B. pertussis* Infection

We included in the study a total of 1,065 children admitted to the Children's Hospital of Fudan University and diagnosed with pertussis during January 2016–October 2022, who had nasopharyngeal swab (NP) samples collected and delivered to the microbiology laboratory for *B. pertussis* culture, antimicrobial resistance testing, and PCR detection. We extracted DNA from NP samples and performed real-time PCR (LightCycler 480; Roche, https://www.roche.com) to detect nucleic acids according to the protocol of a pertussis bacteria nucleic acid detection kit based on the PCR-fluorescent probe method (Yilifang Biotechnology, http://www.yilifangbio.com). The laboratory testing results and data collection were based on electronic medical records during hospitalization or clinic visits, and all data analysis was anonymous. The study protocol was approved by the Ethics Committee of the Children's Hospital of Fudan University (approval no. 2022-66).

PCR and Sequencing for 23S rRNA A2047G Mutation Detection and Virulence Genotyping Analysis

We obtained 692 *B. pertussis* strains in 2016 (11 strains), 2017 (177 strains), 2018 (165 strains), 2019 (169 strains), 2020 (1 strain), 2021 (30 strains), and 2022 (139 strains). Because very few strains were obtained from 2016, 2020, and 2021, we selected all 42 strains for this study. We chose other isolates by the systematic sampling method, yielding 50 strains in 2017, 45 strains in 2018, 74 strains in 2019, and 72 strains in 2022. We gave each strain a number and then chose it by a random method to ensure each strain had an equal chance of being chosen through the use of an unbiased selection method. We selected a total of 283 isolates for further analysis.

We prepared genomic DNA of *B. pertussis* isolates by using a QIAamp DNA Mini Kit (QIAGEN, https://www.qiagen.com). We performed PCR-based sequencing of the A2047G mutation as described in a previous study (*30*). We also performed PCR and sequencing of virulence-related genes (*ptxP*, *ptxA*, *ptxC*, *prn*, *fim2*, *fim3*) as previously described (*6*). By using a convention for *fhaB* allele naming that defined *fhaB1* and *fhaB2* alleles by the A2493C mutation and defined the novel *fhaB3* allele by the C5330T mutation, as previously described (*23*,*31*), we identified *fhaB* alleles by detecting and sequencing these 2 mutations. The primers for *fhaB*-2493 were forward, 5′-GATGTAGGCAAGGTTTCCGC-3′, and reverse, 5′-CGCTCGACACATGCAGAC-3′; the primers for *fhaB*-5330 were forward, 5′-ATATCGACAACAAGCAGGCC-3′, and reverse, 5′-TTGACATAGCCGATACCGCT-3′. We retrieved reported DNA sequences from GenBank and analyzed them by using BLAST (https://blast.ncbi.nlm.nih.gov) to determine the allele of each virulence gene.

MLVA

We performed MLVA by following the procedures described by Schouls et al. (*32*). We amplified 5 loci (variable-number tandem-repeat [VNTR] 1, VNTR3a/VNTR3b, VNTR4, VNTR5, and VNTR6) by using PCR detection. We calculated the number of repeats at each VNTR locus from the DNA fragment length. We assigned an MT on the basis of the combination of repeat counts for VNTRs 1, 3a, 3b, 4, 5, and 6, as described in previous reports (*15*,*32*).

DNA Extraction and Whole-Genome Sequencing

We further subjected 4 representative BP strains, including 1 MT27 *ptxP3* macrolide-sensitive *B. pertussis* (MSBP) (BP1-Shanghai-2016), 1 MT195 *ptxP1*-MRBP (BP7-Shanghai-2016), 1 MT28 *ptxP3*-MSBP (P20-Shanghai-2017), and 1 MT28 *ptxP3*-MRBP

(P745-Shanghai-2022) to whole-genome sequencing (WGS) analysis. We extracted genomic DNA by using the sodium dodecyl sulphate method (*33*). We constructed libraries for single-molecule real-time sequencing with an insert size of 10 kb by using the SMRTbell Template Prep Kit 1.0 (PacBio, https://www.pacb.com). We generated sequencing libraries for the Illumina platform by using the NEBNext Ultra DNA Library Prep Kit for Illumina (New England BioLabs, https://www.neb.com). We sequenced the whole genomes by using the PacBio Sequel platform and Illumina NovaSeq PE150 at Beijing Novogene Bioinformatics Technology Co., Ltd (Beijing, China). We deposited the sequencing data into GenBank (accession nos. CP118023–6).

Public Genome Dataset

We included a total of 1,491 public genomes of *B. pertussis* strains from China (*15*,*21*,*28*) and global *B. pertussis* P strains in this study for comparison (Appendix 1 Table, https://wwwnc.cdc.gov/EID/article/30/1/23-1588-App1.xlsx). We sequenced the public genomes for various purposes, and they covered 27 countries from 8 geographic areas (Appendix 1 Table). We downloaded raw short-read sequencing data from the National Center for Biotechnology Information Sequence Read Archive (https://www.ncbi.nlm.nih.gov/sra). We filtered sequencing reads by using Trimmomatic (*34*), and we performed de novo genome assembly of public data by using SPAdes (*35*) with default settings.

Single-Nucleotide Polymorphism Calling and Phylogenetic Analysis

We identified core-genome (regions present in >99% of isolates) single-nucleotide polymorphisms (SNPs), as previously described (*36*). In brief, we aligned the assemblies against the reference genome (GenBank accession no. NC_002929.2, Tohama I) by using MUMmer (*37*) to generate whole-genome alignment. We performed SNP calling by using SNP-Sites (*38*) on the basis of the alignment. We identified the repetitive regions of the reference genome by using Tandem repeats finder and self-aligning by blastn (https://blast.ncbi.nlm.nih.gov). We excluded SNPs located in repetitive regions from further analysis. We constructed a maximum-likelihood phylogenetic tree by using RAxML-NG (*39*) under the general time-reversible with gamma distribution model.

Statistical Analysis

We analyzed data by using the t test, χ^2 test, or Fisher exact test, as appropriate. We performed all statistical analyses by using the SPSS Statistics 13.0 (IBM, https://www.ibm.com). We considered $p<0.05$ to be statistically significant.

Results

Clinical Characteristics of Children with BP Infection

A total of 1,065 children had pertussis diagnosed at the Children's Hospital of Fudan University during January 2016–October 2022 (Appendix 2 Table 1, https://wwwnc.cdc.gov/EID/article/30/01/22-1588-App1.pdf). Of those, 65.0% (692) had culture-proven pertussis, and the others were culture-negative but verified by PCR or clinical symptoms. The case-patients were 470 girls (44.1%) and 595 boys (55.9%), and the average age was 2.6 years (range 23 days–11.5 years). Approximately 93.8% of the case-patients (999) had cough symptoms; average duration of cough was of 20.7 days (range 1–130 days). Most of the patients (75.5% [804]) were treated with antibiotics before sampling, among which macrolides were used in 60.1% (640) of patients. The age distributions of pertussis changed from 2016 to 2022; pertussis was detected primarily in infants (0–1 years of age) (84.7%–100%) before 2020 but was mostly detected in older children and adolescents (>5–10 years of age) (50.3%–56.8%) after 2020 ($p<0.001$) (Figure 1).

MLVA Types of *B. pertussis* strains

We identified 14 MLVA types in this study, and the major MLVA types were MT195 (26.9%), MT28 (26.1%), MT27 (20.8%), MT104 (13.4%), and MT55 (6.4%) (Appendix 2 Table 2). The other MLVA types were MT158 (1.1%), MT 16 (1.1%), MT29 (0.7%), MT114 (0.7%), MT30 (0.4%), MT32 (0.4%), untyped-1 (0.4%), untyped-2 (1.1%), and untyped-3 (0.4%).

Only 1 strain was isolated in 2020, so we deleted the analysis of 2020. MT27 was the main subtype during 2016–2019 (29.1%–54.5%). However, MT28, which accounted for 0–4.1% before 2020, accounted for 40.0% in 2021 and 77.8% in 2022 (Figure 2, panel A).

We further analyzed the MT distributions in different age groups. MT28, which was seldomly detected in infants (3.6% [6/169]) and absent in noninfants (>1–12 years of age) (0% [0/11]) during 2016–2019, was predominantly isolated from all age groups during 2021–2022, accounting for 64.9% (24/37) in infants, and 66.7% (44/66) in noninfants (Figure 2, panel B).

Virulence Gene Alleles and Genotype Profiles of *B. pertussis* Strains

We identified 2 *ptxP* alleles; we identified *ptxP1* in 49.8% and *ptxP3* in 50.2% of *B. pertussis* strains. *ptxP3*,

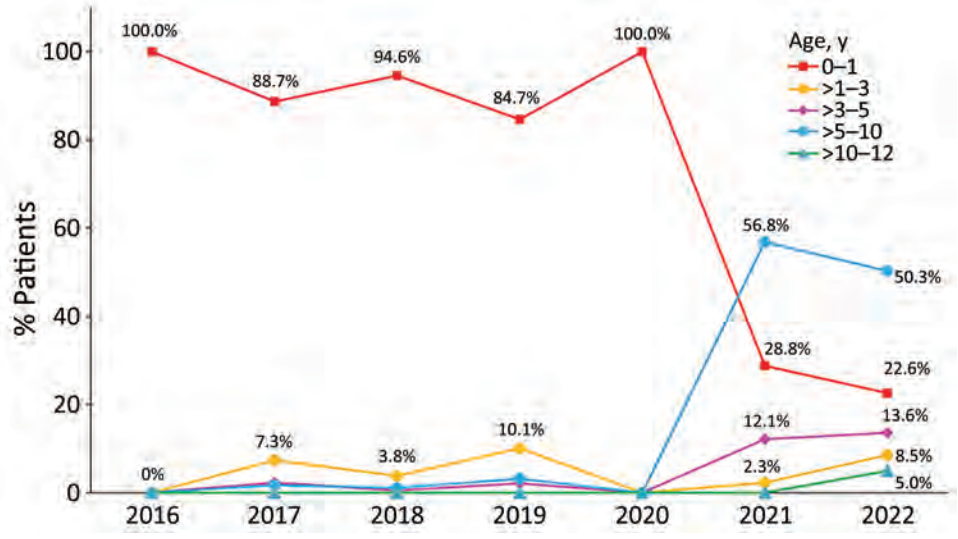

Figure 1. Distributions of pertussis patients in different age groups, Shanghai, China, 2016–2022. Pertussis was primarily detected from infants (0–1 years of age) before 2020 but mostly from older children and adolescents (>5–10 years of age) after 2020.

which accounted for only 37.2% before 2020, became the major allele (73.5%) after 2020. Moreover, we identified 4 types of *prn* (*prn1*, *prn2*, *prn3*, and *prn9*), 2 types of *fhaB* (*fhaB1* and *fhaB3*), 3 types of *ptxC* (*ptxC1*, *ptxC2*, and *ptxC3*), 1 type of *ptxA* (*ptxA1*), 1 type of *fim2* (*fim2–1*), and 3 types of *fim3* (*fim3–1*, *fim3–2*, and *fim3–4*).

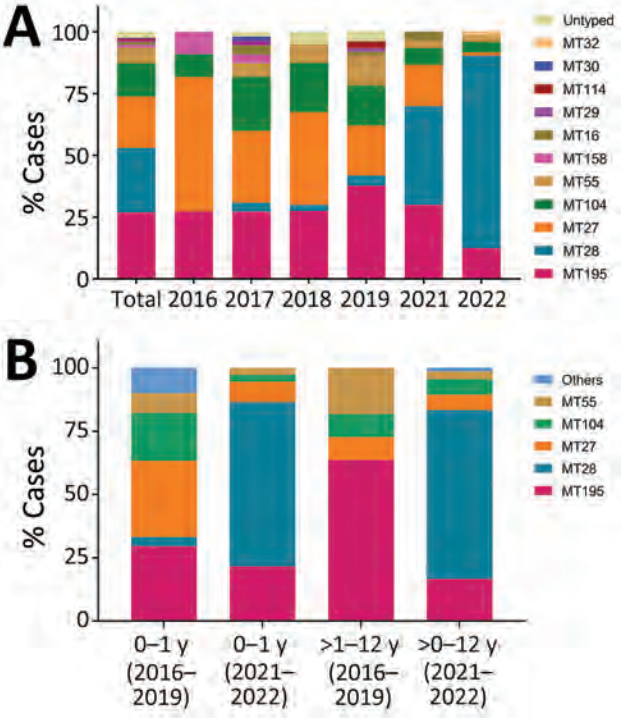

Figure 2. Distributions of prevalent *Bordetella pertussis* subtypes over time (A) and by age group (B), Shanghai, China, 2016–2022. Fourteen MTs were identified in this study. MT27 was the major strain during 2016–2019, whereas MT28 isolates increased quickly during 2021–2022 (panel A). MT distributions in infants (0–1 years of age) and noninfants (>1–12 years of age) change substantially from 2016–2019 to 2021–2022 (panel B). MT, multilocus variable-number tandem-repeat analysis type.

ptxP1 was mostly linked to *prn1* and *fhaB3*, whereas *ptxP3* linked closely to *prn2* and *fhaB1*. The major genotypes were *ptxP1/prn1/fhaB3/ptxC1/ptxA1/fim2–1/fim3–1* (48.7%) and *ptxP3/prn2/fhaB1/ptxC2/ptxA1/fim2–1/fim3–1* (47.7%): the former included 7 subtypes (MT16, MT27, MT30, MT55, MT104, MT195, and untyped-3), and the latter involved 6 subtypes (MT27, MT28, MT32, MT114, MT158, and untyped-2). (Appendix 2 Table 3).

A2047G mutation and Antimicrobial-Resistance Profiles of *B. pertussis* Strains

B. pertussis was highly resistant to macrolides, and MRBP accounted for 72.4% (205/283) of strains (Table 1). A total of 97.2% of *ptxP1/prn1/fhaB3*-BP and 91.9% of MT28 *ptxP3/prn2/fhaB1*-BP belonged to MRBP, whereas all non-MT28 *ptxP3/prn2/fhaB1*-BP were MSBP.

We frequently detected the A2047G mutation in 205 *B. pertussis* strains (72.4%) that showed 100% resistance to erythromycin, azithromycin, and clarithromycin. The A2047G mutation accounted for 61.0% before 2020 and 93.1% after 2020. All MT195, MT55, and MT104 carried the A2047G mutation, but none of the MT27 acquired this mutation. A2047G mutation in MT28 increased from 0% before 2020 to 100% after 2020.

MRBP increased from 36.4% in 2016 to 97.2% in 2022, including *ptxP1*-MRBP (48.4% [137/283]) and *ptxP3*-MRBP (24.0% [68/283]). Most (100% in 2016, 2018, and 2021; 94.3% in 2017; 98.0% in 2019, and 93.3% in 2022) of the *ptxP1* strains belonged to MRBP. However, macrolide resistance in *ptxP3* strains increased from 0% before 2020 to 70.6% in 2021 and 98.2% in 2022. Of note, macrolides resistance in MT28 *ptxP3*-strains switched from 0% before 2020 to

Table. Antimicrobial-resistance profiles and virulence genotypes of 283 *Bordetella pertussis* isolates, Shanghai, China, 2016–2022*

Antibiotic	MIC, μg/mL	Total, no (%)	Frequency of genotype profiles, no (%)		
			ptxP1/prn1/fhaB3 non-MT28, n = 141	*ptxP3/prn2/fhaB1* non-MT28,† n = 68	*ptxP3/prn2/fhaB1* MT28,‡ n = 74
Erythromycin	Resistant, >256	205 (72.4)	137 (97.2)	0	68 (91.9)
	Sensitive, <0.064	78 (27.6)	4 (2.8)	68 (100)	6 (8.1)
Azithromycin	Resistant, 128 to >256	205 (72.4)	137 (97.2)	0	68 (91.9)
	Sensitive, <0.064	78 (27.6)	4 (2.8)	68 (100)	6 (8.1)
Clarithromycin	Resistant, 128 to >256	205 (72.4)	137 (97.2)	0	68 (91.9)
	Sensitive, <0.064	78 (27.6)	4 (2.8)	68 (100)	6 (8.1)
Sulfamethoxazole/ trimethoprim	Resistant, >32	0	0	0	0
	Sensitive, 0.064 to <0.008	283 (100)	141 (100)	68 (100)	74 (100)

*MT, multilocus variable-number tandem-repeat analysis type.
†Includes 1 MT27-*ptxP3/prn3/ptxC2* strain.
‡Includes 1 MT28-*ptxP3/prn9/fhaB1* strain.

100% after 2020, whereas all non-MT28 *ptxP3* isolates showed sensitivity to macrolides (Figure 3, panel A). *ptxP1*-MRBP was prevalent before 2020 (111 [61.7%]); of those 111 strains, of which 57 (51.4%) were MT195. *ptxP3*-MRBP, which was absent before 2020, increased to 66.7% after 2020, and all of them belonged to MT28 (Figure 3, panel B; Figure 4).

Combination of MLVA Types, Virulence Genotypes, and A2047G Mutations

MT195, MT55, and MT104 all carried *ptxP1/prn1/fhaB3* and the A2047 mutation (Figure 4). As 2 closely related MLVA types, 98.3% of MT27-BP and 98.6% of MT28-BP carried the genotype of *ptxP3/prn2/fhaB1*. However, the A2047G mutation was highly detected

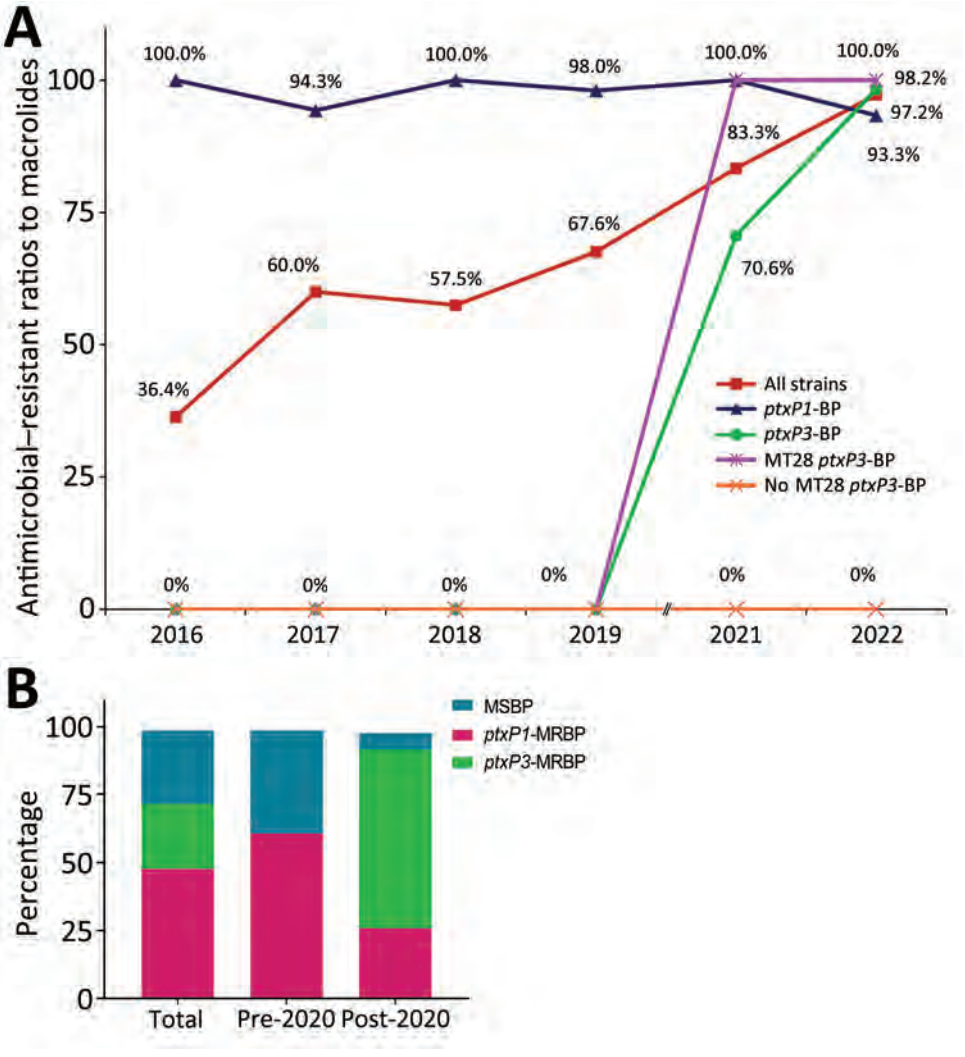

Figure 3. Changing macrolide resistance of circulating *Bordetella pertussis* strains, Shanghai, China, 2016–2022. A) *ptxP3*-strains showed very high resistance to macrolides after 2020. Resistance to macrolides was different in non-MT28 (0%) and MT28 (100%) isolates. B) Percentages of macrolide-sensitive BP, *ptxP1*-MRBP, and *ptxP3*-MRBP before and after 2020 show that *ptxP1*-MRBP strain was prevalent before 2020 but predominately *ptxP3*-MRBP spread after 2020. MRBP, macrolide-resistant *Bordetella pertussis*; MT, multilocus variable-number tandem-repeat analysis type.

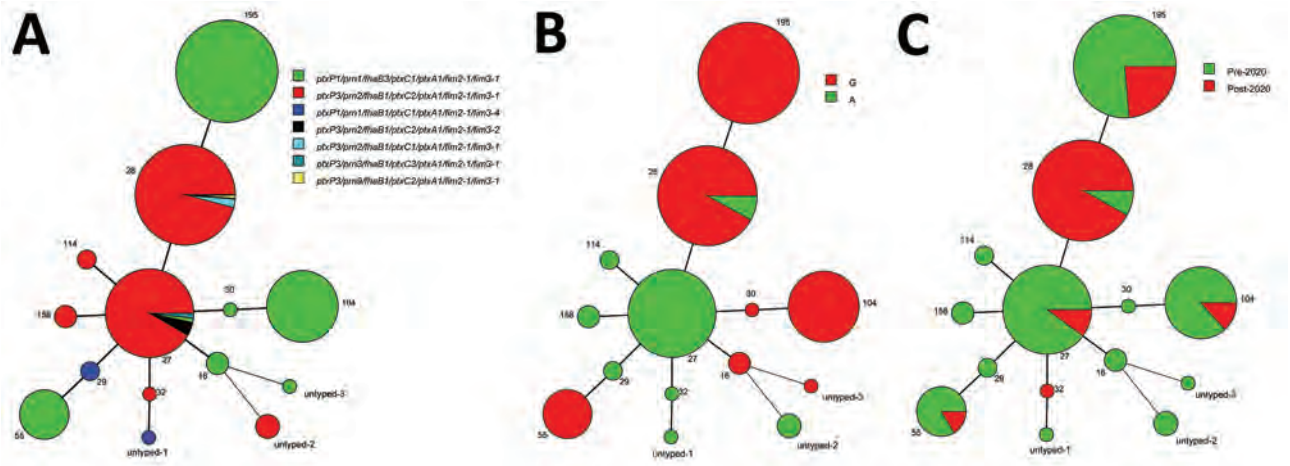

Figure 4. Minimum-spanning tree of 283 *Bordetella pertussis* MTs, Shanghai, China, 2016–2022. A) Virulence genotype profiles; B) A2047G mutations; C) pre-2020 versus post-2020. Circle sizes indicate the number of each MT. Differences in the length and thickness of the lines linking 2 circles indicate differences in the number of variable-number tandem repeats between the 2 linked MTs. MT, multilocus variable-number tandem repeat analysis type.

in MT28 (91.9%) but absent (0%) in MT27 (Figure 4, panels A, B). MT195, MT27, and MT104 were the major subtypes before 2020, whereas MT28 emerged and spread quickly after 2020 (Figure 4, panel C).

WGS Analysis

Four *B. pertussis* strains (MT27 *ptxP3*-MSBP, MT195 *ptxP1*-MRBP, MT28 *ptxP3*-MSBP, and MT28 *ptxP3*-MRBP) were chosen for further WGS analysis. We constructed a maximum-likelihood phylogenetic tree of 4 Shanghai and 1,491 global strains. *B. pertussis* isolates in Shanghai were closely related to other isolates from China but differed from other international strains isolated from the United States, Europe, Australia, Argentina, Africa, Japan, Iran, Israel, and other regions and countries (Figure 5). Of note, MT28-MRBP (P745) was prevalent after 2020 and was closely related to MT28 *ptxP3*-MSBP (P20) but was quite heterogeneous to MT195-MRBP (BP7) and MT27 *ptxP3*-MSBP (BP1) before 2020. Moreover, P745 was highly homologous to a previously reported MT28-MRBP (B19005) in Anhui Province, China.

Discussion

In this study, we systematically investigated the clinical characteristics, antimicrobial resistance profiles, and molecular evolution of *B. pertussis* strains in Shanghai, China, during 2016–2022. Pertussis was primarily diagnosed in infants before 2020 but mostly in older children and adolescents after 2020. MRBPs remarkably increased, from 36.4% in 2016 to 97.2% in 2022. MT28 *ptxP3/prn2/fhaB1*-MRBP emerged only after 2020 and replaced MT195 *ptxP1/prn1/fhaB3*-MRBP, which was prevalent before 2020, indicating that 2020 was a watershed in the transformation of MRBP in Shanghai, China.

The first MRBP in China was reported in Shandong Province in 2011 (*40*). MRBPs in China was thought less likely to cause epidemics in other countries because the MRBPs in China were mostly assigned to *ptxP1* lineage, whereas *ptxP3* strains are currently endemic in other countries (*21*,*27*). In China, *ptxP1*-MRBPs were reported to contribute 75.4% (Zhejiang Province, 2016), 48.6% (Shenzhen Province, 2015–2017), and 84.9% (a multicenter study during 2017–2019) of the circulating *B. pertussis* strains in China (*15*,*41*,*42*). Previous studies showed that MRBP was mostly linked to the *ptxP1* allele and that the *ptxP3* strain was isolated from MSBP without exception (*6*,*20*,*41*). Our recent study demonstrated that the *ptxP3* allele had a close linkage with MRBP (*29*). In this study, *ptxP1*-MRBP was the major (61.7%) strain during 2016–2020, whereas *ptxP3*-MRBP, which emerged only after 2020, replaced *ptxP1*-MRBP and became predominant (66.7%) after 2020.

MRBP strains were widely prevalent in western China and mainly linked to MT195, MT104, and MT55 (*26*). Wu et al. (*15*) showed that MT28 MRBP with genotype of *ptxP3/fhaB1/prn9* was first identified in Anhui Province, China, revealing the emergence of *ptxP3*-MRBP in mainland China (*15*). In this study, the circulating *B. pertussis* strains changed greatly from 2016 to 2022. MT195 presented the VNTR profiles of 8-6-0-7-6-8, whereas MT28 showed the profiles of 8-7-0-7-6-8, and MT27 showed the profiles of 8-7-0-7-6-7. Although those subtypes have minor differences on VNTR3a or VNTR6, their virulence genotypes and A2047G mutation carriages

were quite different, making the circulating strains very heterologous. All MRBPs before 2020 harbored *ptxP1* and 51.4% belonged to MT195, whereas *ptxP3*-MRBP, which was absent before 2020, increased to 66.7% after 2020, and all belonged to MT28. WGS analysis further revealed that MT28-MRBP was quite heterologous with MT195-MRBP, revealing the different molecular characteristics of MRBP prevalent before and after 2020 in Shanghai.

MT28-MRBP in this study was quite different from the international strains but represented close relevance to MT28-MSBP isolated before 2020, which indicates that MT28-MRBP was not reported from other countries but more likely because the resident MT28-MSBP acquired the A2047G mutation and became resistant to macrolides. Moreover, the emergence and spread of MT28 *ptxP3*-MRBP in Shanghai were probably related to the selection pressure from high usage of macrolides and vaccination. Macrolides were excessively used for treating pertussis, which might participate in the selection of *ptxP3*-MRBP. Of interest, although MRBPs are highly resistant to macrolides, most (60.1%) of the MRBP patients were still treated with macrolides in this study. In addition, compared with vaccine strains in China with the genotype of *ptxP1/fhaB1/prn1/ptxA2/ptxC1*, MT28 harbored more gene variants, including *ptxP3*, *prn2*, *ptxA1*, and *ptxC2* than MT195, which carried *fhaB3* and *ptxA1*. Currently, 2 types of diphtheria, tetanus, and pertussis (DTaP) vaccine formulations are licensed in China: one is the 2-component DTaP vaccine containing PT and FHA, another is the 3-component DTaP vaccine containing PT, FHA, and PRN (*43*). The circulating *B. pertussis* has evolved, mainly changed from *ptxP1* to *ptxP3* lineage, indicating the *ptxP3* variation reflect selective advantage under high coverage with acellular pertussis vaccine (*42*). Previous study showed that *prn2* variation affected the efficacy of commercial vaccine, and mice studies suggested that the incorporation of *prn2* to vaccine could enhance the ACV's efficacy (*44*). Moreover, studies from Safarchi et al. (*45*) and Van Gent et al. (*46*) demonstrate that *ptxP3/*

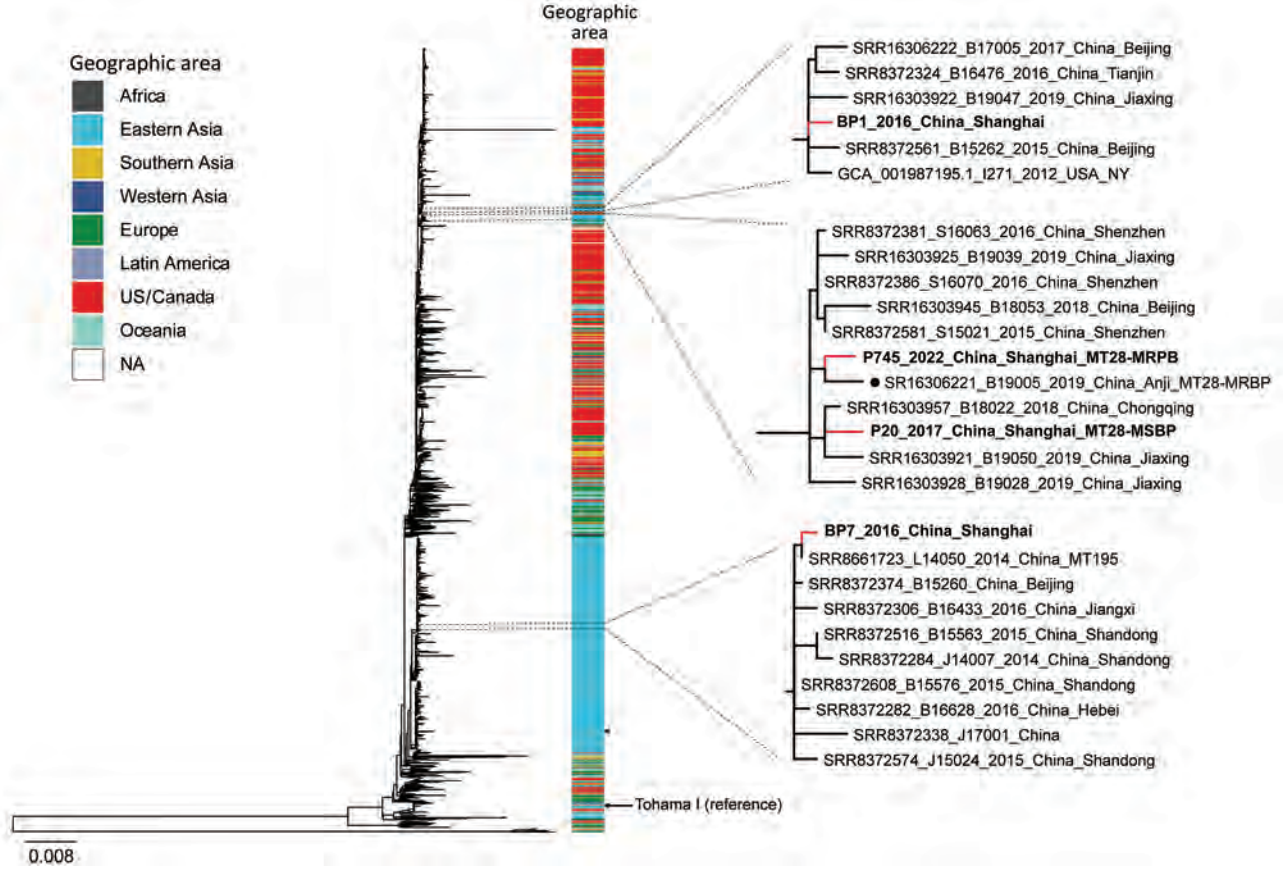

Figure 5. Maximum-likelihood phylogenetic tree of 4 Shanghai, China, and 1,491 global *Bordetella pertussis* strains, by geographic area, 2016–2022. Red lines indicate Shanghai strains; bold indicates 2 MT28 strains. Black dot indicates MT28-MRBP (B19005) strain from Anhui Province, China. Arrow indicates reference strain Tohama I. Shanghai strains associated phylogenetic subclades are enlarged for visualization. MSBP, macrolide-sensitive *Bordetella pertussis*; MT, multilocus variable-number tandem-repeat analysis type; NA, not applicable.

prn2-BP colonized better than the *ptxP1/prn3*-BP strain and provide the evidence for increased fitness and better immune evasion of *ptxP3/prn2* strains in a mouse model involving mice immunized with 3-component ACVs. Therefore, we hypothesized that *prn2* and *ptxP3* variation in MT28 strains may play a role in better fitness and immune evasion compared with ACVs in China, causing MT28-BP to be selected by the vaccination and then to spread quickly. The exact relationship between *prn2*/*ptxP3* variant and vaccine escape needs further study.

In this study, pertussis was primarily detected in infants before 2020 but was mostly detected in older children after 2020. We propose 2 potential hypotheses for this age shift. First, the age shift was closely related to the emergence of MT28-MRBP; *ptxP3/ptxA1/ptxC2/prn2*-carrying MT28 strains, which emerged and spread after 2020 could avoid the immunity of vaccine and weaken the vaccine effects, making the pertussis populations shift from unvaccinated or incompletely vaccinated infants to vaccinated population. Second, the COVID-19 pandemic increased the public awareness of microbiologic laboratory testing in children with respiratory symptoms, so more older children who were not considered as the primary pertussis population before 2020 accepted *B. pertussis* testing and were diagnosed with pertussis after 2020, making 2020 become the watershed moment for the shift of pertussis population.

In conclusion, we systematically investigated the molecular evolution of MRBPs to clarify the evolution of MRBP from MT195 to MT28 in Shanghai, China, during 2016–2022, revealing that 2020 was watershed in the transformation of MRBPs from MT195 *ptxP1/prn1/fhaB3*-alleles to MT28 *ptxP3/prn2/fhaB1*-alleles in Shanghai. The emergence and spread of MT28 *ptxP3*-MRBP strains are likely attributable to the A2047G mutation and the selection pressure from vaccination and high usage of macrolides, which will further complicate the epidemiology of pertussis and evolve to pose a looming threat to global public health. Therefore, worldwide surveillance of the molecular evolution and AMR profiles of circulating *B. pertussis*, especially *ptxP3*-MRBP, is urgent.

This study was funded by the National Key Research and Development Program of China (grant nos. 2021YFC2701800 and 2021YFC2701801), the Key Development Program of the Children's Hospital at Fudan University (grant no. EK2022ZX05), and the National Natural Science Foundation of China (grant no. 82202567).

Author contribution: C.W., X.Z., and P.F. designed the experiments and revised the manuscript. C.Y. performed WGS analysis, analyzed the data, and revised the manuscript. P.F. analyzed the data and wrote the manuscript. J.Z. performed most of the experiments. G.L. performed experiments guidance. Y.N., G.Y., and L.Z. participated in the experiments.

About the Author

Dr. Fu is an associate professor at the Clinical Microbiology Laboratory at Children's Hospital of Fudan University. Her primary research interests include pediatric infectious diseases and multidrug-resistant organisms. Dr. J. Zhou is a master candidate at Children's Hospital of Fudan University. Her primary research interests include infectious diseases and organisms in pediatric ICU department.

References

1. Scheller EV, Cotter PA. *Bordetella* filamentous hemagglutinin and fimbriae: critical adhesins with unrealized vaccine potential. Pathog Dis. 2015;73:ftv079. https://doi.org/10.1093/femspd/ftv079
2. Xu Y, Zhang L, Tan Y, Wang L, Zhang S, Wang J. Genetic diversity and population dynamics of *Bordetella pertussis* in China between 1950–2007. Vaccine. 2015;33:6327–31. https://doi.org/10.1016/j.vaccine.2015.09.040
3. Litt DJ, Neal SE, Fry NK. Changes in genetic diversity of the *Bordetella pertussis* population in the United Kingdom between 1920 and 2006 reflect vaccination coverage and emergence of a single dominant clonal type. J Clin Microbiol. 2009;47:680–8. https://doi.org/10.1128/JCM.01838-08
4. Wang CQ, Zhu QR. Seroprevalence of *Bordetella pertussis* antibody in children and adolescents in China. Pediatr Infect Dis J. 2011;30:593–6. https://doi.org/10.1097/INF.0b013e31820eaf88
5. Mooi FR, Van Der Maas NA, De Melker HE. Pertussis resurgence: waning immunity and pathogen adaptation—two sides of the same coin. Epidemiol Infect. 2014;142:685–94. https://doi.org/10.1017/S0950268813000071
6. Fu P, Wang C, Tian H, Kang Z, Zeng M. *Bordetella pertussis* infection in infants and young children in Shanghai, China, 2016–2017: clinical features, genotype variations of antigenic genes and macrolides resistance. Pediatr Infect Dis J. 2019;38:370–6. https://doi.org/10.1097/INF.0000000000002160
7. Mooi FR, van Oirschot H, Heuvelman K, van der Heide HG, Gaastra W, Willems RJ. Polymorphism in the *Bordetella pertussis* virulence factors P.69/pertactin and pertussis toxin in The Netherlands: temporal trends and evidence for vaccine-driven evolution. Infect Immun. 1998;66:670–5. https://doi.org/10.1128/IAI.66.2.670-675.1998
8. Mooi FR, He Q, van Oirschot H, Mertsola J. Variation in the *Bordetella pertussis* virulence factors pertussis toxin and pertactin in vaccine strains and clinical isolates in Finland. Infect Immun. 1999;67:3133–4. https://doi.org/10.1128/IAI.67.6.3133-3134.1999
9. Cassiday P, Sanden G, Heuvelman K, Mooi F, Bisgard KM, Popovic T. Polymorphism in *Bordetella pertussis* pertactin and pertussis toxin virulence factors in the United States, 1935–1999. J Infect Dis. 2000;182:1402–8. https://doi.org/10.1086/315881
10. Elomaa A, Advani A, Donnelly D, Antila M, Mertsola J, Hallander H, et al. Strain variation among *Bordetella pertussis*

isolates in Finland, where the whole-cell pertussis vaccine has been used for 50 years. J Clin Microbiol. 2005;43:3681–7. https://doi.org/10.1128/JCM.43.8.3681-3687.2005
11. Mastrantonio P, Spigaglia P, Oirschot HV, van der Heide HGJ, Heuvelman K, Stefanelli P, et al. Antigenic variants in *Bordetella pertussis* strains isolated from vaccinated and unvaccinated children. Microbiology (Reading). 1999; 145:2069–75. https://doi.org/10.1099/13500872-145-8-2069
12. Guiso N. *Bordetella pertussis*: why is it still circulating? J Infect. 2014;68(Suppl 1):S119–24. https://doi.org/10.1016/j.jinf.2013.09.022
13. Baker SM, Masi A, Liu DF, Novitsky BK, Deich RA. Pertussis toxin export genes are regulated by the *ptx* promoter and may be required for efficient translation of *ptx* mRNA in *Bordetella pertussis*. Infect Immun. 1995;63:3920–6. https://doi.org/10.1128/iai.63.10.3920-3926.1995
14. Mooi FR, van Loo IH, van Gent M, He Q, Bart MJ, Heuvelman KJ, et al. *Bordetella pertussis* strains with increased toxin production associated with pertussis resurgence. Emerg Infect Dis. 2009;15:1206–13. https://doi.org/10.3201/eid1508.081511
15. Wu X, Du Q, Li D, Yuan L, Meng Q, Fu Z, et al. A cross-sectional study revealing the emergence of erythromycin-resistant *Bordetella pertussis* carrying *ptxP3* alleles in China. Front Microbiol. 2022;13:901617. https://doi.org/10.3389/fmicb.2022.901617
16. Ivaska L, Barkoff AM, Mertsola J, He Q. Macrolide resistance in *Bordetella pertussis*: current situation and future challenges. Antibiotics (Basel). 2022;11:1570. https://doi.org/10.3390/antibiotics11111570
17. Moriuchi T, Vichit O, Vutthikol Y, Hossain MS, Samnang C, Toda K, et al. Molecular epidemiology of *Bordetella pertussis* in Cambodia determined by direct genotyping of clinical specimens. Int J Infect Dis. 2017;62:56–8. https://doi.org/10.1016/j.ijid.2017.07.015
18. Advani A, Gustafsson L, Ahrén C, Mooi FR, Hallander HO. Appearance of Fim3 and *ptxP3*-*Bordetella pertussis* strains, in two regions of Sweden with different vaccination programs. Vaccine. 2011;29:3438–42. https://doi.org/10.1016/j.vaccine.2011.02.070
19. van Loo IHM, Mooi FR. Changes in the Dutch *Bordetella pertussis* population in the first 20 years after the introduction of whole-cell vaccines. Microbiology (Reading). 2002;148:2011–8. https://doi.org/10.1099/00221287-148-7-2011
20. Yang Y, Yao K, Ma X, Shi W, Yuan L, Yang Y. Variation in *Bordetella pertussis* susceptibility to erythromycin and virulence-related genotype changes in China (1970–2014). PLoS One. 2015;10:e0138941. https://doi.org/10.1371/journal.pone.0138941
21. Yao K, Deng J, Ma X, Dai W, Chen Q, Zhou K, et al. The epidemic of erythromycin-resistant *Bordetella pertussis* with limited genome variation associated with pertussis resurgence in China. Expert Rev Vaccines. 2020;19:1093–9. https://doi.org/10.1080/14760584.2020.1831916
22. Kamachi K, Yao SM, Chiang CS, Koide K, Otsuka N, Shibayama K. Rapid and simple SNP genotyping for *Bordetella pertussis* epidemic strain MT27 based on a multiplexed single-base extension assay. Sci Rep. 2021;11:4823. https://doi.org/10.1038/s41598-021-84409-0
23. Xu Z, Wang Z, Luan Y, Li Y, Liu X, Peng X, et al. Genomic epidemiology of erythromycin-resistant *Bordetella pertussis* in China. Emerg Microbes Infect. 2019;8:461–70. https://doi.org/10.1080/22221751.2019.1587315
24. Du Q, Wang X, Liu Y, Luan Y, Zhang J, Li Y, et al. Direct molecular typing of *Bordetella pertussis* from nasopharyngeal specimens in China in 2012–2013. Eur J Clin Microbiol Infect Dis. 2016;35:1211–4. https://doi.org/10.1007/s10096-016-2655-3
25. Wu S, Hu Q, Yang C, Zhou H, Chen H, Zhang Y, et al. Molecular epidemiology of *Bordetella pertussis* and analysis of vaccine antigen genes from clinical isolates from Shenzhen, China. Ann Clin Microbiol Antimicrob. 2021;20:53. https://doi.org/10.1186/s12941-021-00458-3
26. Zhang J, Zhang D, Wang X, Wei X, Li H. Macrolide susceptibility and molecular characteristics of *Bordetella pertussis*. J Int Med Res. 2022;50:3000605221078782. https://doi.org/10.1177/03000605221078782
27. Feng Y, Chiu CH, Heininger U, Hozbor DF, Tan TQ, von König CW. Emerging macrolide resistance in *Bordetella pertussis* in mainland China: findings and warning from the global pertussis initiative. Lancet Reg Health West Pac. 2021;8:100098. https://doi.org/10.1016/j.lanwpc.2021.100098
28. Koide K, Yao S, Chiang CS, Thuy PTB, Nga DTT, Huong DT, et al. Genotyping and macrolide-resistant mutation of *Bordetella pertussis* in East and South-East Asia. J Glob Antimicrob Resist. 2022;31:263–9. https://doi.org/10.1016/j.jgar.2022.10.007
29. Fu P, Zhou J, Meng J, Liu Z, Nijiati Y, He L, et al. Emergence and spread of MT28 *ptxP3* allele macrolide-resistant *Bordetella pertussis* from 2021 to 2022 in China. Int J Infect Dis. 2023;128:205–11. https://doi.org/10.1016/j.ijid.2023.01.005
30. Wang Z, Cui Z, Li Y, Hou T, Liu X, Xi Y, et al. High prevalence of erythromycin-resistant *Bordetella pertussis* in Xi'an, China. Clin Microbiol Infect. 2014;20:O825–30. https://doi.org/10.1111/1469-0691.12671
31. van Loo IH, Heuvelman KJ, King AJ, Mooi FR. Multilocus sequence typing of *Bordetella pertussis* based on surface protein genes. J Clin Microbiol. 2002;40:1994–2001. https://doi.org/10.1128/JCM.40.6.1994-2001.2002
32. Schouls LM, van der Heide HG, Vauterin L, Vauterin P, Mooi FR. Multiple-locus variable-number tandem repeat analysis of Dutch *Bordetella pertussis* strains reveals rapid genetic changes with clonal expansion during the late 1990s. J Bacteriol. 2004;186:5496–505. https://doi.org/10.1128/JB.186.16.5496-5505.2004
33. Lim HJ, Lee EH, Yoon Y, Chua B, Son A. Portable lysis apparatus for rapid single-step DNA extraction of *Bacillus subtilis*. J Appl Microbiol. 2016;120:379–87. https://doi.org/10.1111/jam.13011
34. Bolger AM, Lohse M, Usadel B. Trimmomatic: a flexible trimmer for Illumina sequence data. Bioinformatics. 2014; 30:2114–20. https://doi.org/10.1093/bioinformatics/btu170
35. Bankevich A, Nurk S, Antipov D, Gurevich AA, Dvorkin M, Kulikov AS, et al. SPAdes: a new genome assembly algorithm and its applications to single-cell sequencing. J Comput Biol. 2012;19:455–77. https://doi.org/10.1089/cmb.2012.0021
36. Yang C, Li Y, Jiang M, Wang L, Jiang Y, Hu L, et al. Outbreak dynamics of foodborne pathogen *Vibrio parahaemolyticus* over a seventeen year period implies hidden reservoirs. Nat Microbiol. 2022;7:1221–9. https://doi.org/10.1038/s41564-022-01182-0
37. Delcher AL, Salzberg SL, Phillippy AM. Using MUMmer to identify similar regions in large sequence sets. Curr Protoc Bioinformatics. 2003 Feb;Chapter 10:Unit 10.3. https://doi.org/10.1002/0471250953.bi1003s00
38. Page AJ, Taylor B, Delaney AJ, Soares J, Seemann T, Keane JA, et al. SNP-sites: rapid efficient extraction of SNPs from multi-FASTA alignments. Microb Genom. 2016;2:e000056. https://doi.org/10.1099/mgen.0.000056

39. Kozlov AM, Darriba D, Flouri T, Morel B, Stamatakis A. RAxML-NG: a fast, scalable and user-friendly tool for maximum likelihood phylogenetic inference. Bioinformatics. 2019;35:4453–5. https://doi.org/10.1093/bioinformatics/btz305
40. Zhang Q, Li M, Wang L, Xin T, He Q. High-resolution melting analysis for the detection of two erythromycin-resistant *Bordetella pertussis* strains carried by healthy schoolchildren in China. Clin Microbiol Infect. 2013;19:E260–2. https://doi.org/10.1111/1469-0691.12161
41. Zhang JS, Wang HM, Yao KH, Liu Y, Lei YL, Deng JK, et al. Clinical characteristics, molecular epidemiology and antimicrobial susceptibility of pertussis among children in southern China. World J Pediatr. 2020;16:185–92. https://doi.org/10.1007/s12519-019-00308-5
42. Wang Z, Luan Y, Du Q, Shu C, Peng X, Wei H, et al. The global prevalence *ptxP3* lineage of *Bordetella pertussis* was rare in young children with the co-purified aPV vaccination: a 5 years retrospective study. BMC Infect Dis. 2020;20:615. https://doi.org/10.1186/s12879-020-05332-9
43. Wang L, Lei D, Zhang S. Acellular pertussis vaccines in China. Vaccine. 2012;30:7174–8. https://doi.org/10.1016/j.vaccine.2012.10.009
44. Quintana-Vázquez D, Coizeau E, Alvarez A, Delgado M, Cárdenas T, Ramos Y, et al. Recombinant hybrid proteins from pertactin type 1 and 2 of *Bordetella pertussis* are more immunogenic in mice than the original molecules. Biotecnología Aplicada. 2014;31:33–42.
45. Safarchi A, Octavia S, Luu LD, Tay CY, Sintchenko V, Wood N, et al. Better colonisation of newly emerged *Bordetella pertussis* in the co-infection mouse model study. Vaccine. 2016;34:3967–71. https://doi.org/10.1016/j.vaccine.2016.06.052
46. van Gent M, van Loo IH, Heuvelman KJ, de Neeling AJ, Teunis P, Mooi FR. Studies on Prn variation in the mouse model and comparison with epidemiological data. PLoS One. 2011;6:e18014. https://doi.org/10.1371/journal.pone.0018014

Address for correspondence: Wang Chuanqing, Pan Fu, or Xiaowen Zhai, Children's Hospital of Fudan University, 399 Wanyuan Rd, Shanghai 201102, China; email: chuanqing523@163.com, fup1028@163.com, or xwxhai@fudan.edu.cn

Disease-Associated *Streptococcus pneumoniae* Genetic Variation

Shimin Yang,[1] Jianyu Chen,[1] Jinjian Fu,[1] Jiayin Huang, Ting Li, Zhenjiang Yao, Xiaohua Ye

Streptococcus pneumoniae is an opportunistic pathogen that causes substantial illness and death among children worldwide. The genetic backgrounds of pneumococci that cause infection versus asymptomatic carriage vary substantially. To determine the evolutionary mechanisms of opportunistic pathogenicity, we conducted a genomic surveillance study in China. We collected 783 *S. pneumoniae* isolates from infected and asymptomatic children. By using a 2-stage genomewide association study process, we compared genomic differences between infection and carriage isolates to address genomic variation associated with pathogenicity. We identified 8 consensus k-mers associated with adherence, antimicrobial resistance, and immune modulation, which were unevenly distributed in the infection isolates. Classification accuracy of the best k-mer predictor for *S. pneumoniae* infection was good, giving a simple target for predicting pathogenic isolates. Our findings suggest that *S. pneumoniae* pathogenicity is complex and multifactorial, and we provide genetic evidence for precise targeted interventions.

Streptococcus pneumoniae is a pathogen that causes community-associated infections in young children <5 years of age (*1*,*2*). It can asymptomatically colonize the nasopharynx and upper airway in healthy children (up to 60%) and can also invade sterile sites and lead to infections from mild to life-threatening, which can result in substantial illness and death worldwide (*1*,*3*,*4*). Despite the widespread use of pneumococcal vaccines to immunize children, *S. pneumoniae* remains the leading cause of life-threatening diseases. Worldwide, the increasing disease burden of *S. pneumoniae* is alarming; an estimated 1 million children <5 years of age die of pneumococcal disease every year (*5*). All pneumococcal diseases arise from bacterial colonization, and the adaptability of the virulence characteristics enhances pneumococcal persistence in colonization of the host respiratory tract, suggesting that nasopharyngeal carriage of *S. pneumoniae* plays a key role in development and transmission of pneumococcal diseases (*6*). Pneumococcal disease is one of the most common infectious diseases caused by asymptomatic *S. pneumoniae* colonization in humans. Eliminating this opportunistic pathogenic bacterium requires knowledge of the pathogenicity-associated genetic elements that distinguish infection from carriage isolates. Previous studies have been limited to exploring virulence factors and molecular characterization of invasive *S. pneumoniae* isolates (*7*,*8*).

Whole-genome sequencing (WGS) has become a powerful tool for bacterial genotyping; costs have been decreasing as accessibility increases. The high-dimensional genomic data can provide unprecedented resolution for identifying subtle genomic variations. Genomewide association studies (GWAS) are increasingly used to detect novel genes and genetic elements associated with bacterial phenotypes, which may provide insight for future preventive strategies and control measures (*9*–*12*). In brief, traditional GWAS methods can be used to identify large numbers of common genetic variants, usually single-nucleotide polymorphisms (SNPs), to determine the genetic basis of bacterial phenotypes of interest. However, considering the high genomic plasticity of many species of bacteria, traditional GWAS methods can only partially identify the phenotype-associated genetic variants. To avoid the limitations of SNP-based GWAS, we used k-mers (DNA words of length k) as an alternative method, which can capture different types of variants (*13*,*14*).

To determine whether genetic variation is unevenly enriched in *S. pneumoniae* infection isolates, we used multiple GWAS analyses to compare genomic differences between infection and carriage isolates. Study protocols were approved by the Ethics Committee of Guangdong Pharmaceutical

Author affiliations: Guangdong Pharmaceutical University, Guangzhou, China (S. Yang, J. Chen, J. Huang, T. Li, Z. Yao, X. Ye); Liuzhou Maternity and Child Health Care Hospital, Liuzhou, China (J. Fu)

DOI: https://doi.org/10.3201/eid3001.221927

[1]These authors contributed equally to this article.

University (2019–19) and the Ethics Committee of Liuzhou Maternity and Child Healthcare Hospital (2018–84). We obtained written informed consent from parents or legal guardians on behalf of the children.

Methods

Sampling

During 2015–2021, we collected clinical samples from infected children and nasal swab samples from healthy children in southern China (Guangxi and Guangdong Provinces). From hospitalized infected children, we collected 349 nonrepetitive pneumococcal isolates (e.g., blood, bronchoalveolar lavage fluid, sputum, middle ear fluid), of which 342 were noninvasive and 7 invasive. The eligibility criteria for infected children were having clinical infectious manifestations such as cough, respiratory secretions, abnormal lung sounds, dyspnea, or fever >38°C, with or without infiltrates seen on chest radiographs; having *S. pneumoniae* infection diagnosed by clinical doctors on the basis of signs and symptoms; and having *S. pneumoniae* isolated from clinical infection sites. In terms of asymptomatic carriage isolates, we sampled 434 isolates from healthy children in kindergarten.

Whole-Genome Sequencing

We performed high-throughput genome sequencing on a Hiseq 2000 machine (Illumina, https://www.illumina.com) to obtain paired-end 150-bp reads. We assessed the quality of the raw sequenced reads by using FastQC version 0.11.5 (https://github.com/s-andrews/FastQC) and trimmed for low quality reads and adaptor regions by using Trimmomatic version 0.36 (https://github.com/usadellab/Trimmomatic). We then assembled trimmed reads by using SPAdes version 3.6.1 (https://github.com/ablab/spades). We used PathogenWatch (https://pathogen.watch) to predict global pneumococcal sequencing cluster (GPSC), multilocus sequence typing (MLST), and serotyping for all genomes.

Phylogenetic Analyses

To generate the variant sites with SNPs, we mapped assembled contigs to a standard reference genome *S. pneumoniae* R6 by using Snippy version 4.4.5 (https://github.com/tseemann/snippy). We used the generated core SNP alignment to construct a maximum-likelihood phylogenetic tree by using the generalized time reversible plus gamma model and 100 bootstrap replicates with FastTree version 2.1.10 (http://www.microbesonline.org/fasttree). We visualized and annotated the phylogenetic tree by using ChiPlot (https://www.chiplot.online).

Counting and Annotating k-mers

We scanned all k-mers that were 9- to 100-bp long from all assembled reads by using fsm-lite (https://github.com/nvalimak/fsm-lite) and filtered them to obtain 10,591,337 k-mers seen on 1%–99% of the total samples. To identify the relevant genes by using BWA-MEM (the Burrows-Wheeler Aligner with maximal exact matches alignment tool, https://github.com/lh3/bwa), we mapped all k-mers to 10 *S. pneumoniae* reference genomes (CGSP14, D39, Hungary^{19A}-6, R6, Taiwan^{19F}-14, TIGR4, Spain^{23F}-ST81, ATCC 49619, EF3030, and MDRSPN001) obtained from the Virulence Factor Database (http://www.mgc.ac.cn/VFs) and previous studies. We determined gene ontology annotations by using the UniProt (https://beta.uniprot.org).

Multiple GWAS Analyses of Disease-Associated k-mers

To explore the genomewide associations between genetic elements (k-mers) and *S. pneumoniae* disease status (infection or carriage), and thus to identify infection-associated k-mers, we used GWAS methods. Because of the high-dimensional genomic data structures, we used multiple GWAS methods: the linear mixed model (LMM; (https://github.com/mgalardini/pyseer), phylogenetic-based approach (Scoary; https://github.com/AdmiralenOla/Scoary), variable selection using random forests (VSURF; https://github.com/robingenuer/VSURF), and least absolute shrinkage and selection operator (LASSO; https://scikit-learn.org/stable/modules/generated/sklearn.linear_model.Lasso.html) regression.

In brief, we used a 2-stage analysis process to detect the infection-associated k-mers by comprehensive GWAS analyses (Figure 1). First, we fitted a univariate LMM to initially screen infection-associated k-mers by using the Pyseer tool (version 1.3.10) (*15*). To correct for the population structure, we used the similarity pyseer command of Pyseer, which computes a similarity kinship matrix on the basis of the core genome SNPs. For covariates, the GWAS analysis used host age (years) and sex. Second, we used multiple methods (Scoary, LASSO, and VSURF) to minimize false-positive associations and identify consensus infection-associated k-mers by Venn diagram. In the GWAS analyses, we used the Bonferroni correction (α/N) to control for

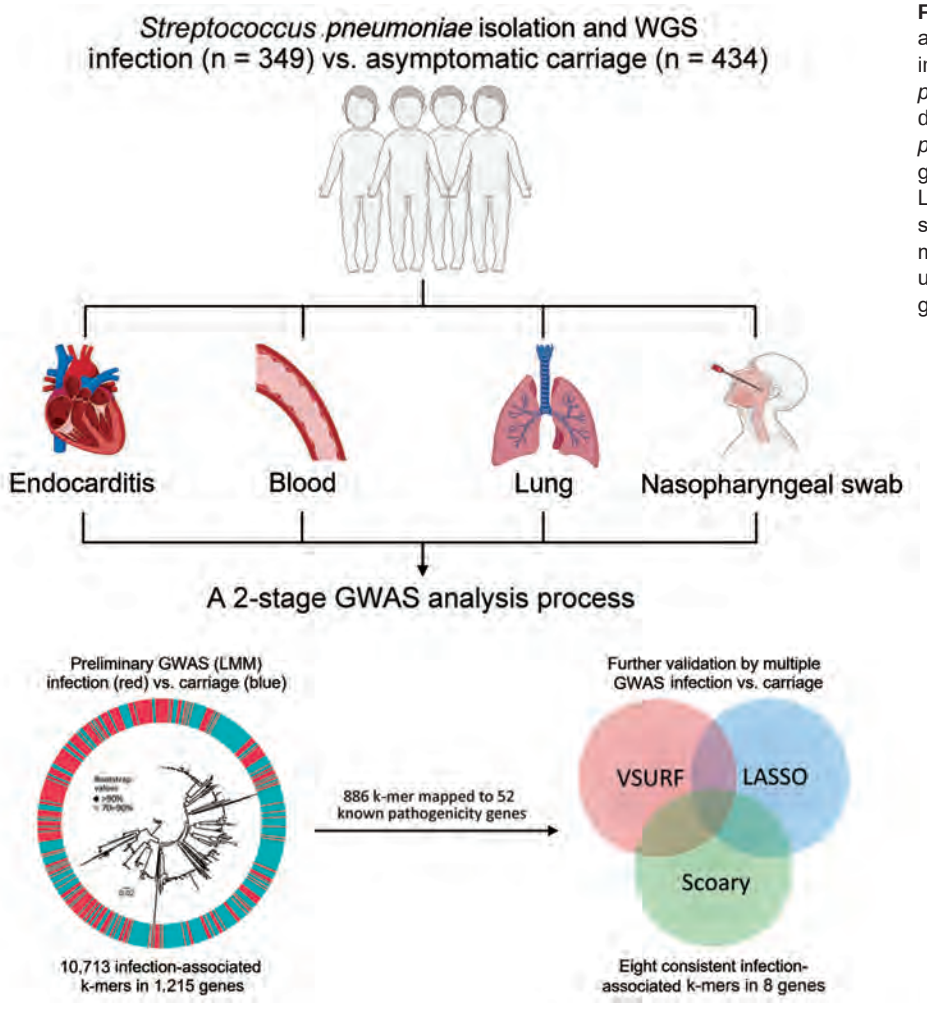

Figure 1. Two-stage GWAS analysis process used to detect infection-associated *Streptococcus pneumoniae* k-mers in study of disease-associated *Streptococcus pneumoniae* genetic variation. GWAS, genome-wide association studies; LASSO, least absolute shrinkage and selection operator; LMM, linear mixed model; VSURF, variable selection using random forests; WGS, whole-genome sequencing.

false-positive rates resulting from multiple comparisons of 1,418,815 k-mers (adjusted p value threshold 3.52×10^{-8}). Scoary is an ultrafast software tool for GWAS analyses that uses a phylogenetic-based method to adjust population structure. The LASSO regression is suitable for high-dimensional data structures, and the coefficients of nonrelevant variables can be compressed to zero to solve the problem of model overfitting (*16*). We used VSURF, based on random forest (RF), to perform a 2-step feature selection on the variables (*17*). Initially, VSURF ranks the variables according to the importance measure by using the RF permutation-based score of importance to obtain a subset of important variables, and then it uses a stepwise forward strategy for variable introduction based on the smallest out-of-bag error. More precisely, a variable is added only if the error decrease is larger than a threshold. We ranked the importance of k-mers by the mean decrease in impurity (mean decrease Gini), which is a measure of the predictor's contribution to the correct sample classification. We compiled associated phenotype data for all 783 isolates (Appendix Table 1, https://wwwnc.cdc.gov/EID/article/30/1/22-1927-App1.pdf) and deposited sequences in the National Center for Biotechnology Information Sequence Read Archive database (https://www.ncbi.nlm.nih.gov/sra; projection no. PRJNA976286). The k-mer sequences and output results files from several GWAS analyses are publicly available (https://doi.org/10.6084/m9.figshare.24466606.v3).

Results

Characteristics of *S. pneumoniae* Isolates

Of the 349 children with *S. pneumoniae* infection, 342 (98.0%) had noninvasive disease (264 pneumonia, 49 bronchitis, 13 otitis media, 9 upper respiratory infection, 6 nasosinusitis, and 1 corneal ulcer), and 7 (2.0%) had invasive disease (6 bacteremia and 1 endocarditis). χ^2 test results indicated no differences between infection and carriage isolates with regard to host sex

(p = 0.359) but significant differences with regard to age (p<0.001) (Appendix Table 2).

Association between Genotypes and Disease Status

The most prevalent GPSCs for infection isolates were GPSC1 (45.9%), GPSC321 (9.2%), and GPSC852 (5.4%); the predominant GPSCs for carriage isolates were GPSC321 (16.1%), GPSC1 (15.4%), and GPSC23 (15.0%). In terms of sequence types (STs), the most common genotypes for infection isolates were ST271 (29.2%), ST320 (9.5%), and ST902 (7.2%); the predominant genotypes for carriage isolates were ST902 (15.9%), ST90 (13.8%), and ST271 (8.5%). The most prevalent serotypes for infection isolates were 19F (43.0%), 6B (15.2%), and 23F (8.3%); and the predominant serotypes for carriage isolates were 6B (32.7%), 19F (13.1%), and 15A (11.1%). The results indicated potential genotype differences between infection and carriage isolates. In addition, the phylogenetic tree based on core SNPs revealed that several genotypes (GPSCs/STs/serotypes) from infection and carriage isolates clustered in the same branches (Figure 2). Moreover, we found statistically significant differences in the proportion of specific GPSCs/STs/serotypes between infection and carriage isolates (Table 1), indicating that these isolates are associated with infection.

Preliminary Screening for Infection-Associated K-Mers by LMM

We identified 10,591,337 k-mers from the assemblies of 783 *S. pneumoniae* isolates and then filtered out low-frequency k-mers for a reduced matrix with 1,418,815 k-mers. Using those k-mers for GWAS, we performed a univariate LMM analysis to initially identify 22,790 infection-associated k-mers; 10,713 k-mers were successfully mapped to 1,215 unique genes (Figure 3, panel A; Appendix Figure 1). In the initial model with 10,713 k-mers, we used the RF model to assess the prediction effect. The classification balanced accuracy based on cross-validation was 93.60% (95% CI 91.48%–95.72%) (Table 2); the area under the curve (AUC), based on the out-of-bag risk scores of the classifier, was 0.98. In the LMM analysis, the QQ-plot indicated that population structure was well controlled at low p values (p<0.01) (Appendix Figure 2). Because of the considerable redundancy among the genetic elements in risk prediction, studying all k-mer combinations had little benefit; therefore, we used a simpler model with 886 k-mers successfully mapped to 52 antibiotic resistance or virulence genes (Appendix Table 3). The classification balanced accuracy was 91.28% (95% CI 89.34%–93.22%) (Table 2); the AUC was 0.96, suggesting that the power of these 886 k-mers for

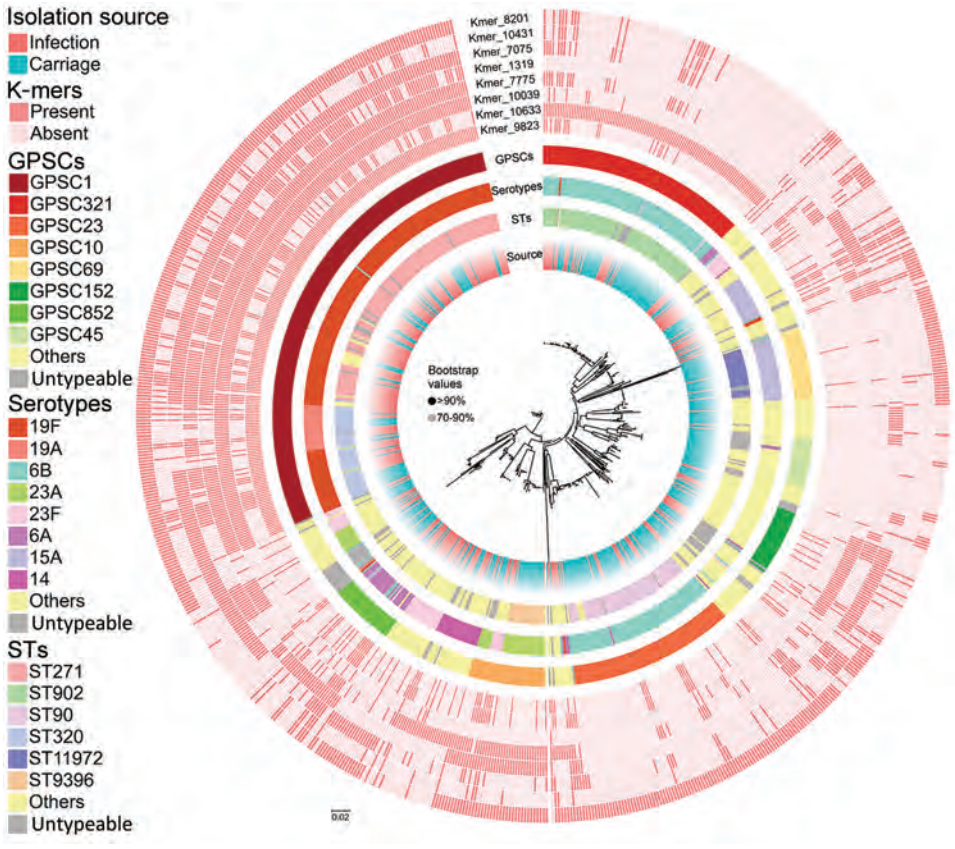

Figure 2. Whole-genome phylogenetic tree showing genetic similarity of 783 *Streptococcus pneumoniae* isolates in a study of disease-associated *Streptococcus pneumoniae* genetic variation. The colored strips at the tips of the tree (from inner to outer) represent isolate metadata (source, STs, serotypes, and GPSCs) and infection-associated k-mers found in the final model. GPSC, global pneumococcal sequencing cluster; ST, sequence type.

Table 1. Association analysis between dominant genotypes and disease status from study of disease-associated *Streptococcus pneumoniae* genetic variation*

Genotype	Infection isolates, no. (%), n = 349	Carriage Isolates, no. (%), n = 434	χ^2	p value	OR (95% CI)
ST					
ST271	102 (29.2)	37 (8.5)	56.78	**<0.001**	4.43 (2.95–6.67)
ST902	25 (7.2)	69 (15.9)	13.97	**<0.001**	0.41 (0.25–0.66)
ST90	13 (3.7)	60 (13.8)	23.34	**<0.001**	0.24 (0.13–0.45)
ST320	33 (9.5)	24 (5.5)	4.42	**0.036**	1.78 (1.03–3.08)
ST11972	3 (0.9)	24 (5.5)	12.67	**<0.001**	0.15 (0.04–0.50)
ST9396	1 (0.3)	22 (5.1)	15.52	**<0.001**	0.05 (0.01–0.40)
Serotype					
19F	150 (43.0)	57 (13.1)	88.61	**<0.001**	4.99 (3.51–7.08)
6B	53 (15.2)	142 (32.7)	31.80	**<0.001**	0.37 (0.26–0.53)
15A	12 (3.4)	48 (11.1)	15.88	**<0.001**	0.29 (0.15–0.55)
23F	29 (8.3)	21 (4.8)	3.90	0.056	1.78 (0.96–3.35)
23A	10 (2.9)	32 (7.4)	7.74	**0.005**	0.37 (0.18–0.77)
6A	24 (6.9)	10 (2.3)	9.74	**0.002**	3.13 (1.48–6.64)
19A	15 (4.3)	11 (2.5)	1.87	0.171	1.73 (0.78–3.81)
14	15 (4.3)	11 (2.5)	1.87	0.171	1.73 (0.78–3.81)
GPSC					
GPSC1	160 (45.9)	67 (15.4)	88.88	**<0.001**	4.64 (3.32–6.48)
GPSC321	32 (9.2)	70 (16.1)	8.27	**0.004**	0.52 (0.34–0.82)
GPSC23	15 (4.3)	65 (15.0)	24.05	**<0.001**	0.25 (0.14–0.45)
GPSC10	9 (2.6)	28 (6.5)	6.44	**0.011**	0.38 (0.18–0.81)
GPSC69	3 (0.9)	31 (7.1)	18.39	**<0.001**	0.11 (0.04–0.35)
GPSC152	13 (3.7)	18 (4.2)	0.09	0.763	0.89 (0.44–1.83)
GPSC852	19 (5.4)	12 (2.8)	3.65	0.056	2.02 (0.98–4.17)

*Boldface indicates statistical significance. GPSC, global pneumococcal sequencing cluster; OR, odds ratio; ST, sequence type.

predicting disease status was close to that of the model with 10,713 k-mers.

In addition, we sorted the 886 disease-associated k-mers according to estimated importance (Figure 3, panel B). The k-mers were mainly associated with antimicrobial resistance (34%), adherence (20%), immune modulation (17%), and exoenzyme (1%). Moreover, the k-mers were divided into 3 functional gene ontology categories. Among those categories, proteolysis and cell wall organization were the largest subcategories in the biological process, membrane was the most enriched term in the cellular component, and serine-type D-Ala-D-Ala carboxypeptidase activity was the top term in the molecular function (Figure 3, panel C).

Further Validation of Infection-Associated k-mers by Multiple GWAS Analyses

To reduce the complexity of the model, we used 3 methods to identify consensus infection-associated k-mers (Figure 4). On the basis of the 886 k-mers screened above, we observed consensus on genomewide statistically significant associations for pathogenicity k-mers; 8 k-mers were identified by all 3 methods. When we used the simplest model with the 8 k-mers, the classification balanced accuracy was 90.89% (95% CI 89.48%–92.31%) (Table 2), and the AUC value was 0.93 (Figure 5, panel A**)**, suggesting that the power of the 8 k-mers to predict disease status was comparable to that of the model with 886 k-mers. Of note, the k-mer predictors still exhibited high classification balanced accuracy in the predominant GPSCs (95.34% for GPSC1 and 92.79% for GPSC321). The importance of the selected k-mers in the final model indicated that these predictors were mainly associated with adherence function (Figure 5, panel B). The highest ranked predictor (Kmer_9823 in sortase [*srtG1*]) achieved a classification accuracy of 79.57% on its own and also showed high classification accuracy in the predominant GPSCs (70.04% for GPSC1 and 85.29% for GPSC321). In addition, the best predictor (in *srtG1*) was associated with GPSC1 and GPSC321 (all $p<0.05$). For the additional validation analysis that used the best RF classifier k-mer (in *srtG1*), 2 independent datasets of *S. pneumoniae* genomes with genotype distribution similar to that of our study were available on the National Center for Biotechnology Information Assembly database (https://www.ncbi.nlm.nih.gov/assembly (data1: 60 noninvasive vs. 60 carriage isolates; data2: 60 invasive versus 60 carriage isolates; the prevalence of the predominant GPSCs [GPSC1 and GPSC321] was 58.3% for noninvasive, 55.0% for invasive and 30.0% for carriage isolates) (Appendix Table 4). Classification accuracy was 75.83% for data1 and 74.17% for data2, similar to that in the larger primary dataset in our study.

The proportion of k-mers differed significantly between infection and carriage isolates (all $p<0.05$) (Figure 5, panel C), indicating that the proportion of k-mers was substantially higher in infection

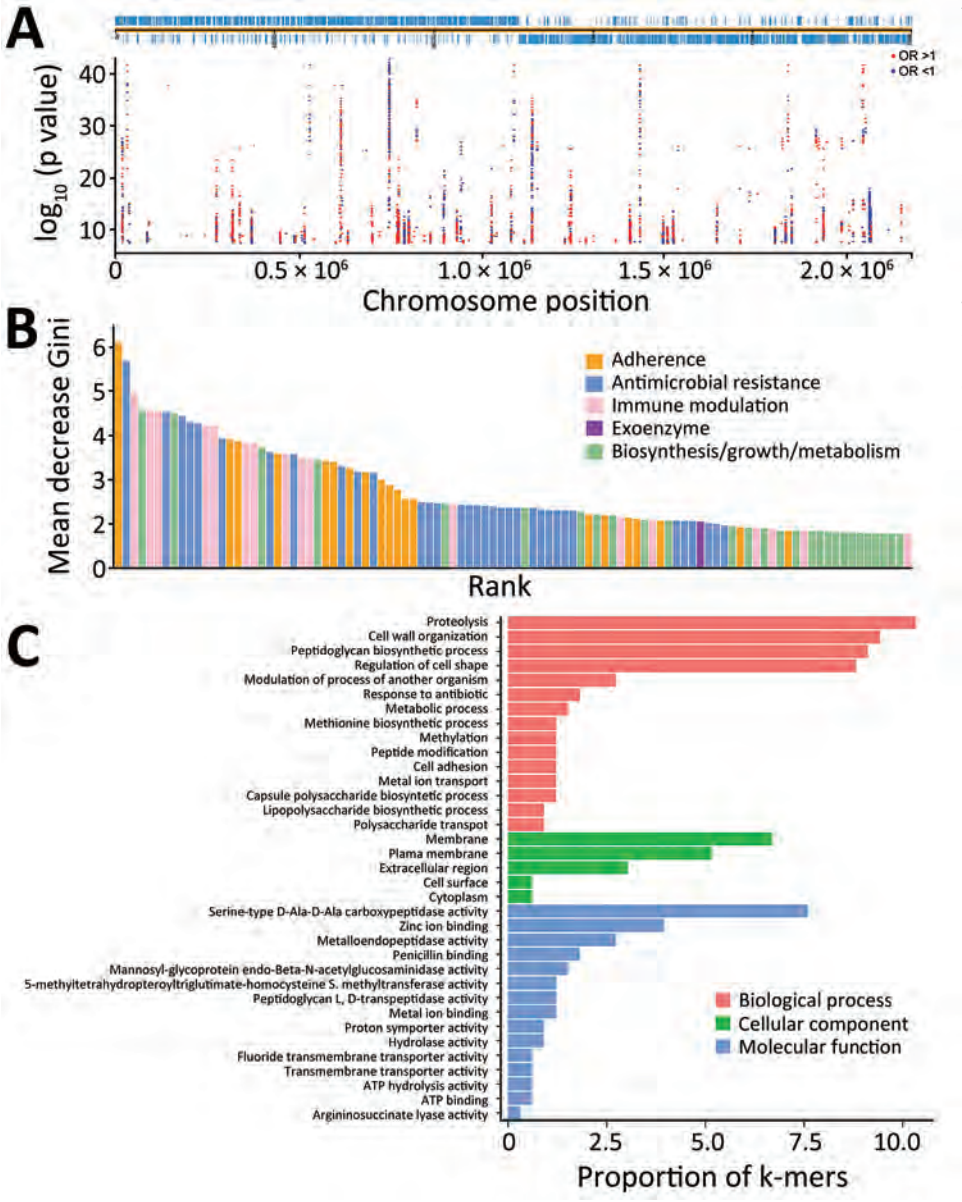

Figure 3. Preliminary screening for infection-associated k-mers by linear mixed model in study of disease-associated *Streptococcus pneumoniae* genetic variation. A) Manhattan plot showing statistical significance and chromosomal location of k-mers mapped to a complete reference genome (TIGR4; GenBank accession no. NC_003028.3). B) Importance of the top 100 k-mer predictors in a simpler model with 886 k-mers. C) Gene ontology annotations of the top 100 k-mer predictors. OR, odds ratio.

isolates than in carriage isolates. The effect of each k-mer on the estimated risk score (Figure 5, panel D), indicated by a point above the diagonal, indicates that the risk score is increased when the k-mer profile is present. The presence of k-mers associated with adherence genes markedly increased the risk for *S. pneumoniae* infection (odds ratio [OR] 1.88 for Kmer_9823, OR 1.65 for Kmer_10039, and OR 1.69 for Kmer_10431) (Table 3).

Discussion

To explore genomic differences between infection and carriage isolates, linking infection-associated genotypes with disease status is necessary. In our study, the most common serotypes for infection isolates (19F, 6B, 23F) were consistent with the results from other regions of China (*18*–*20*) but differed from those from the United States and Japan (*21*,*22*). Moreover, we observed considerable ST diversity among infection isolates; the most prevalent genotypes were ST271, ST320, and ST902, a finding consistent with those of previous studies in China but different from those in developed and developing countries (*23*–*25*). The resolution of MLST and serotyping for inferring isolate relatedness is limited, so we also used GPSCs to characterize and compare different lineages (*26*). The most prevalent GPSCs among the infection isolates were GPSC1, GPSC321, and GPSC852, which

Table 2. Resubstitution estimate and cross-validation results based on random forest models used in study of disease-associated *Streptococcus pneumoniae* genetic variation*

	10,713 k-mer predictors		886 k-mer predictors		8 k-mer predictors	
Evaluation indicators	Resubstitution estimate	10-fold cross-validation estimate	Resubstitution estimate	10-fold cross-validation estimate	Resubstitution estimate	10-fold cross-validation estimate
Accuracy	98.60	93.23	96.42	90.81	90.93	90.04
Balanced accuracy	98.65	93.60	96.61	91.28	91.48	90.89
Sensitivity	99.13	94.48	97.91	92.87	94.27	93.72
Specificity	98.18	92.71	95.31	89.69	88.70	88.07
PPV	97.71	90.27	93.98	86.27	84.81	83.65
NPV	99.31	95.63	98.39	94.48	95.85	95.18
Kappa	0.97	0.86	0.93	0.81	0.81	0.80

*Values are percentages except for kappa, which is reported as a value ranging from –1 to 1. NPV, negative predictive value; PPV, positive predicitive value.

differed from those in the United States and South Africa (*27*). Our findings suggest that discrepancy in genotypes on a global scale may be associated with different pathogenicity and evolutionary directions. In our study, associations between specific genotypes (such as 19F and GPSC1) and disease status differed significantly, which is consistent with findings from a study in India (*28*). Our findings indicate that the presence of specific pathogenic clones may promote infection. In a simple pathogenicity model, all pathogenic clones would belong to specific clusters of genetically related disease-causing isolates (i.e., pathogenic clone hypothesis; Figure 6, panel A), which has been observed for *Staphylococcus aureus* and *S. pneumoniae* isolates (*29*,*30*). That pathogenicity model is not suitable for all *S. pneumoniae* clones because many infection isolates clustered in the same branches of phylogenetic tree as carriage isolates. In addition, traditional genotypes provide little power for identifying small genetic variations at the genomic level (*29*), suggesting that those genotypes only partially explain the pathogenicity of *S. pneumoniae*.

Using high-throughput genome sequencing technologies and bacterial GWAS methods to further explore high-dimensional genetic variation between infection and carriage isolates is essential, thereby revealing the pathogenicity-associated genetic elements of *S. pneumoniae*. According to the phylogenetic tree, we observed that infection isolates were markedly unevenly distributed across the phylogeny and also clustered with carriage isolates within several lineages, indicating that most lineages are capable of causing infection (i.e., opportunistic pathogenicity hypothesis; Figure 6, panel B). If this hypothesis is reasonable, then GWAS analyses would not detect numerous pathogenicity-associated k-mers. However, the LMM-based GWAS in our study detected 22,790 pathogenicity-associated k-mers. These findings suggest that the enrichment of genetic elements encoding pathogenicity traits may increase the pathogenicity of *S. pneumoniae* (i.e., pathogenic-determinant hypothesis; Figure 6, panel C), which is consistent with *Staphylococcus epidermidis* and avian pathogenic *Escherichia coli* (*30*,*31*). In this pathogenic-determinant model, horizontal gene transfer could spread genetic determinants in bacteria such as *S. pneumoniae* and *Klebsiella pneumoniae* (*32*–*34*), leading various clones to successfully cause disease.

High-throughput genomic data have brought substantial challenges to data analysis because of high-dimensional and highly correlated data structures. In our study, we identified infection-associated k-mers by using a 2-stage comprehensive GWAS analysis process, including LMM for initially screening

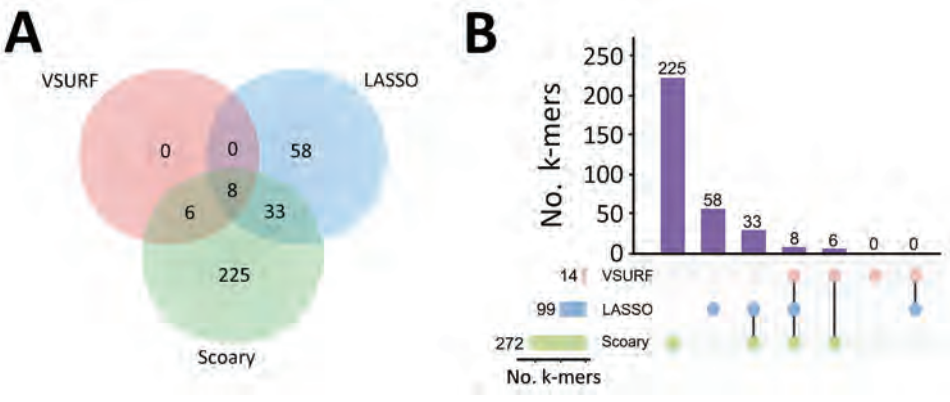

Figure 4. Further validation of infection-associated k-mers by multiple GWAS analyses in study of disease-associated *Streptococcus pneumoniae* genetic variation. A) Venn diagram visualization of the k-mers identified by 3 methods. B) UpSet plot visualization of the k-mers identified by 3 methods. LASSO, least absolute shrinkage and selection operator; VSURF, variable selection using random forests.

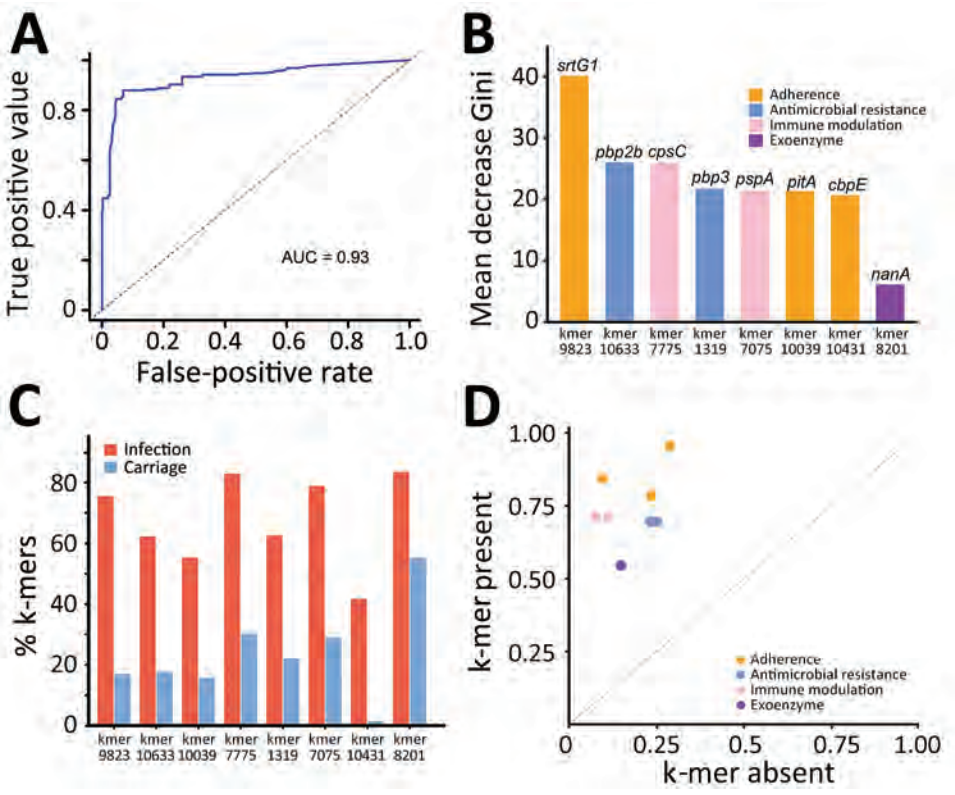

Figure 5. Prediction effect of the 8 k-mers identified in the final model used in study of disease-associated *Streptococcus pneumoniae* genetic variation. A) Receiver operating characteristic curve of the final model. B) Predictor importance of the 8 k-mers in the final model. C) Proportion of k-mer predictors between infection and carriage isolates. D) Change in risk score for a specific k-mer profile when the k-mer is present (y-axis) compared to absent (x-axis). AUC, area under the curve.

pathogenic k-mers and multiple GWAS methods for further validation. In the final prediction model, we identified 8 k-mer predictors, which mapped to genes associated with adherence, immune regulation, antibiotic resistance, and exoenzyme. Of the adherence-related genes, *srtG1* and the LPxTG-type surface-anchored protein (*pitA*) are important components of the pneumococcal pilus-2, which plays a crucial role in promoting adhesion, colonization, and cellular invasion (*35*,*36*). Classification accuracy of the most important k-mer in *srtG1* was high by itself, and that of the additional validation RF analysis based on open datasets was similar, suggesting that this predictor has great potential for predicting pathogenic isolates in a clinical setting. Phosphorylcholine esterase (*cbpE*) plays an important role in modulating both the phosphorylcholine decoration of its surface and choline-bound surface adhesins, which may contribute to pneumococcal adherence and invasiveness (*37*). Capsular polysaccharide (CPS) is a major virulence factor in *S. pneumoniae*. Capsular polysaccharide protein C (CpsC) has been shown to affect the level of CPS expression and also regulate the assembly, export, and attachment of CPS to the cell wall (*38*). Pneumococcal surface protein A (PspA) plays role in preventing complement-mediated opsonization and is also capable of binding to lactoferrin, thereby preventing it from killing pneumococci (*39*). The infection-associated genes reported in our study (*cpsC* and *pspA*) are homologous to the genes associated with invasive pneumococci (*cpsA*, *cpsD*, and *pspC*) identified in previous studies (*11*,*12*), providing more evidence for

Table 3. Association analysis between k-mers and disease status used in study of disease-associated *Streptococcus pneumoniae* genetic variation*

k-mer	Genes	Infection isolates, no. (%), n = 349	Carriage isolates, no. (%), n = 434	p value	OR (95%CI)
Kmer_9823	*srtG1*	264 (75.6)	75 (17.3)	8.55×10^{-45}	1.88 (1.79–1.96)
Kmer_10633	*pbp2b*	218 (62.5)	78 (18.0)	2.68×10^{-37}	1.77 (1.71–1.84)
Kmer_10039	*pitA*	194 (55.6)	69 (15.9)	1.47×10^{-31}	1.65 (1.51–1.79)
Kmer_7775	*cpsC*	290 (83.1)	132 (30.4)	6.59×10^{-49}	1.75 (1.66–1.83)
Kmer_1319	*pbp3*	219 (62.8)	96 (22.1)	9.95×10^{-31}	1.79 (1.70–1.87)
Kmer_7075	*pspA*	276 (79.1)	126 (29.0)	4.31×10^{-44}	1.64 (1.55–1.72)
Kmer_10431	*cbpE*	146 (41.8)	7 (1.6)	3.38×10^{-45}	1.69 (1.62–1.76)
Kmer_8201	*nanA*	292 (83.7)	241 (55.5)	4.68×10^{-17}	1.66 (1.55–1.76)

*OR, odds ratio.

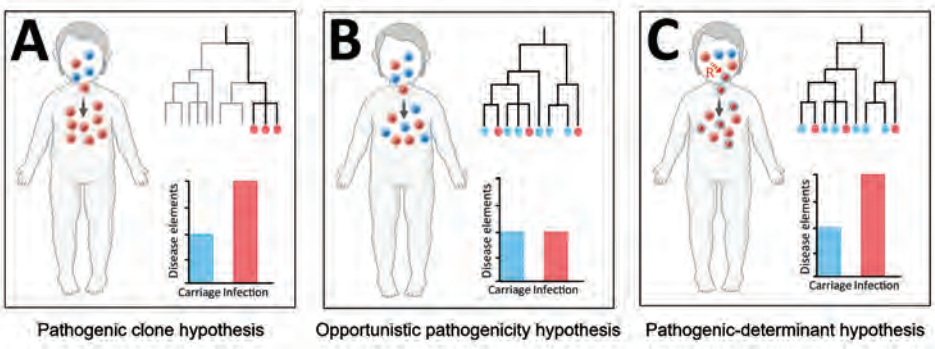

Figure 6. Pathogenicity models for genetically related disease-causing isolates used in study of disease-associated *Streptococcus pneumoniae* genetic variation. A) Pathogenic clone hypothesis; B) opportunistic pathogenicity hypothesis; C) pathogenic-determinant hypothesis.

S. pneumoniae pathogenicity. Neuraminidase A encoded by the *nanA* gene is an essential colonization factor for *S. pneumoniae* and promotes growth and survival of the bacteria in the upper respiratory tract (*40*). Antimicrobial drug use and abuse not only induce widespread multidrug-resistant pneumococci but also increase the susceptibility to invasive disease (*41*). For decades, penicillin has been the first choice for treatment of pneumococcal infection, and mutations in penicillin-binding proteins (PBPs) are essential for high-level penicillin resistance (*42*). Li et al. demonstrated that *pbp2b* and *pbp3* are associated with pneumococcal infection (*42*). One reason is that PBP2B and PBP3 are involved in the synthesis and growth of bacterial cell walls, which are crucial for the survival and virulence of pneumococci (*43*). In addition, a previous study revealed a potential association between penicillin resistance and GPSC1 (*44*), and our findings also showed that GPSC1 was associated with pneumococcal infection, suggesting that it cannot support a causal link between resistance and pneumococcal infection and may result from a lineage confounder. In summary, these infection-associated k-mers provide genetic evidence for revealing optimal risk factors for infection isolates, which may offer a theoretical basis for precise targeted interventions.

In this study, we attempted to use the comprehensive analysis strategy to identify pathogenic k-mers by well-characterized *S. pneumoniae* isolates from a single location so we could reduce redundancy of k-mer predictors, minimize false-positive associations, and avoid geographic variation. Our consensus findings of pathogenic k-mers from multiple GWAS methods may provide sufficient evidence for clarifying the complex multifactorial pathogenicity of *S. pneumoniae*. However, among the potential limitations, the first is that *S. pneumoniae* pathogenesis is a multifactorial and interacting process, but traditional GWAS methods identify the main effect of each genetic variation and ignore the complex gene-gene interactions (*45*). Therefore, future studies should use the enrichment theory to determine the core functions or pathways for risk genes, which may provide new insights for understanding pathogenesis at functional levels (*46*,*47*). Second, although k-mers can reflect variation in bacterial genomes, we mapped infection-associated k-mers in our study to reference genomes to identify pathogenic genes, which cannot cover complete genomic variation in the entire species. To overcome those issues, we developed the extended k-mer–based GWAS methods to detect phenotype-specific k-mers without relying on prior annotations or reference genomes (*48*,*49*). Third, our study focused mainly on noninvasive rather than invasive isolates, and *S. pneumoniae* can transition from carriage to infection, suggesting potential similarity in carriage and noninvasive infection isolates. To improve the statistical power and comparability of exploring disease-associated markers, we included infection isolates from children with confirmed associated symptoms and carriage isolates from asymptomatic healthy children.

In conclusion, our 2-stage GWAS analyses identified a subset of 8 pathogenic k-mers associated with adherence, antimicrobial resistance, and immune modulation, indicating that the enrichment of genetic elements encoding pathogenicity traits may increase the pathogenicity of *S. pneumoniae.* The best predictor for *S. pneumoniae* infection achieved a high classification accuracy, giving a very simple target for predicting pathogenic isolates in a clinical setting. These findings suggest the complex multifactorial nature of *S. pneumoniae* pathogenicity and provide genetic evidence for the evolution of virulence and development of precise targeted interventions.

Acknowledgments

We sincerely thank all study children included in this study. We also thank the research staff and students at Guangdong Pharmaceutical University, China.

This work was supported by the National Natural Science Foundation of China (grant nos. 81973069 and 81602901),

the Guangdong Basic and Applied Basic Research Foundation (grant no. 2023A1515011583), and the Key Scientific Research Foundation of Guangdong Educational Committee (grant no. 2022ZDZX2033). The funders had no role in the study design, data collection, and analysis, or interpretation of the data.

About the Author

Ms. Yang is a graduate student at the Guangdong Pharmaceutical University, China. Her research interests include the pneumococcal disease, evolution of virulence, and genome-wide association study.

References

1. Henriques-Normark B, Tuomanen EI. The pneumococcus: epidemiology, microbiology, and pathogenesis. Cold Spring Harb Perspect Med. 2013;3:a010215. https://doi.org/10.1101/cshperspect.a010215
2. Mancuso G, Midiri A, Gerace E, Biondo C. Bacterial antibiotic resistance: the most critical pathogens. Pathogens. 2021;10:1310. https://doi.org/10.3390/pathogens10101310
3. Subramanian K, Henriques-Normark B, Normark S. Emerging concepts in the pathogenesis of the *Streptococcus pneumoniae*: from nasopharyngeal colonizer to intracellular pathogen. Cell Microbiol. 2019;21:e13077. https://doi.org/10.1111/cmi.13077
4. Bogaert D, De Groot R, Hermans PW. *Streptococcus pneumoniae* colonisation: the key to pneumococcal disease. Lancet Infect Dis. 2004;4:144–54. https://doi.org/10.1016/S1473-3099(04)00938-7
5. Yao KH, Yang YH. *Streptococcus pneumoniae* diseases in Chinese children: past, present and future. Vaccine. 2008;26:4425–33. https://doi.org/10.1016/j.vaccine.2008.06.052
6. Kadioglu A, Weiser JN, Paton JC, Andrew PW. The role of *Streptococcus pneumoniae* virulence factors in host respiratory colonization and disease. Nat Rev Microbiol. 2008;6:288–301. https://doi.org/10.1038/nrmicro1871
7. Piet JR, Geldhoff M, van Schaik BD, Brouwer MC, Valls Seron M, Jakobs ME, et al. *Streptococcus pneumoniae* arginine synthesis genes promote growth and virulence in pneumococcal meningitis. J Infect Dis. 2014;209:1781–91. https://doi.org/10.1093/infdis/jit818
8. Tunjungputri RN, Mobegi FM, Cremers AJ, van der Gaast-de Jongh CE, Ferwerda G, Meis JF, et al. Phage-derived protein induces increased platelet activation and is associated with mortality in patients with invasive pneumococcal disease. MBio. 2017;8:e01984–16. https://doi.org/10.1128/mBio.01984-16
9. Chaguza C, Ebruke C, Senghore M, Lo SW, Tientcheu PE, Gladstone RA, et al. Comparative genomics of disease and carriage serotype 1 pneumococci. Genome Biol Evol. 2022;14:evac052. https://doi.org/10.1093/gbe/evac052
10. The CRyPTIC Consortium. Genome-wide association studies of global *Mycobacterium tuberculosis* resistance to 13 antimicrobials in 10,228 genomes identify new resistance mechanisms. PLoS Biol. 2022;20:e3001755. https://doi.org/10.1371/journal.pbio.3001755
11. Lees JA, Ferwerda B, Kremer PHC, Wheeler NE, Serón MV, Croucher NJ, et al. Joint sequencing of human and pathogen genomes reveals the genetics of pneumococcal meningitis. Nat Commun. 2019;10:2176. https://doi.org/10.1038/s41467-019-09976-3
12. Obolski U, Gori A, Lourenço J, Thompson C, Thompson R, French N, et al. Identifying genes associated with invasive disease in *S. pneumoniae* by applying a machine learning approach to whole genome sequence typing data. Sci Rep. 2019;9:4049. https://doi.org/10.1038/s41598-019-40346-7
13. Lees JA, Vehkala M, Välimäki N, Harris SR, Chewapreecha C, Croucher NJ, et al. Sequence element enrichment analysis to determine the genetic basis of bacterial phenotypes. Nat Commun. 2016;7:12797. https://doi.org/10.1038/ncomms12797
14. Gupta PK. Quantitative genetics: pan-genomes, SVs, and k-mers for GWAS. Trends Genet. 2021;37:868–71. https://doi.org/10.1016/j.tig.2021.05.006
15. Lees JA, Galardini M, Bentley SD, Weiser JN, Corander J. pyseer: a comprehensive tool for microbial pangenome-wide association studies. Bioinformatics. 2018;34:4310–2. https://doi.org/10.1093/bioinformatics/bty539
16. Pedregosa F, Varoquaux G, Gramfort A, Michel V, Thirion B, Grisel O, et al. Scikit-learn: machine learning in Python. J Mach Learn Res. 2011;12:2825–30. https://doi.org/10.48550/arXiv.1201.0490
17. Genuer R, Poggi J-M, Tuleau-Malot C. VSURF: an R package for variable selection using random forests. R J. 2015;7:19–33. https://doi.org/10.32614/RJ-2015-018
18. Geng Q, Zhang T, Ding Y, Tao Y, Lin Y, Wang Y, et al. Molecular characterization and antimicrobial susceptibility of *Streptococcus pneumoniae* isolated from children hospitalized with respiratory infections in Suzhou, China. PLoS One. 2014;9:e93752. https://doi.org/10.1371/journal.pone.0093752
19. Shi W, Li J, Dong F, Qian S, Liu G, Xu B, et al. Serotype distribution, antibiotic resistance pattern, and multilocus sequence types of invasive *Streptococcus pneumoniae* isolates in two tertiary pediatric hospitals in Beijing prior to PCV13 availability. Expert Rev Vaccines. 2019;18:89–94. https://doi.org/10.1080/14760584.2019.1557523
20. Yu YY, Xie XH, Ren L, Deng Y, Gao Y, Zhang Y, et al. Epidemiological characteristics of nasopharyngeal *Streptococcus pneumoniae* strains among children with pneumonia in Chongqing, China. Sci Rep. 2019;9:3324. https://doi.org/10.1038/s41598-019-40088-6
21. Suaya JA, Mendes RE, Sings HL, Arguedas A, Reinert RR, Jodar L, et al. *Streptococcus pneumoniae* serotype distribution and antimicrobial nonsusceptibility trends among adults with pneumonia in the United States, 2009–2017. J Infect. 2020;81:557–66. https://doi.org/10.1016/j.jinf.2020.07.035
22. Yanagihara K, Kosai K, Mikamo H, Mukae H, Takesue Y, Abe M, et al. Serotype distribution and antimicrobial susceptibility of *Streptococcus pneumoniae* associated with invasive pneumococcal disease among adults in Japan. Int J Infect Dis. 2021;102:260–8. https://doi.org/10.1016/j.ijid.2020.10.017
23. Yan Z, Cui Y, Huang X, Lei S, Zhou W, Tong W, et al. Molecular characterization based on whole-genome sequencing of *Streptococcus pneumoniae* in children living in southwest China during 2017–2019. Front Cell Infect Microbiol. 2021;11:726740. https://doi.org/10.3389/fcimb.2021.726740
24. Kellner JD, Ricketson LJ, Demczuk WHB, Martin I, Tyrrell GJ, Vanderkooi OG, et al. Whole-genome analysis of *Streptococcus pneumoniae* serotype 4 causing outbreak of invasive pneumococcal disease, Alberta, Canada. Emerg Infect Dis. 2021;27:1867–75. https://doi.org/10.3201/eid2707.204403
25. Vorobieva S Jensen V, Furberg AS, Slotved HC, Bazhukova T, Haldorsen B, Caugant DA, et al. Epidemiological and

molecular characterization of *Streptococcus pneumoniae* carriage strains in pre-school children in Arkhangelsk, northern European Russia, prior to the introduction of conjugate pneumococcal vaccines. BMC Infect Dis. 2020;20:279. https://doi.org/10.1186/s12879-020-04998-5
26. Gladstone RA, Lo SW, Lees JA, Croucher NJ, van Tonder AJ, Corander J, et al.; Global Pneumococcal Sequencing Consortium. International genomic definition of pneumococcal lineages, to contextualise disease, antibiotic resistance and vaccine impact. EBioMedicine. 2019;43:338–46. https://doi.org/10.1016/j.ebiom.2019.04.021
27. Lo SW, Gladstone RA, van Tonder AJ, Lees JA, du Plessis M, Benisty R, et al.; Global Pneumococcal Sequencing Consortium. Pneumococcal lineages associated with serotype replacement and antibiotic resistance in childhood invasive pneumococcal disease in the post-PCV13 era: an international whole-genome sequencing study. Lancet Infect Dis. 2019;19:759–69. https://doi.org/10.1016/S1473-3099(19)30297-X
28. Nagaraj G, Govindan V, Ganaie F, Venkatesha VT, Hawkins PA, Gladstone RA, et al. *Streptococcus pneumoniae* genomic datasets from an Indian population describing pre-vaccine evolutionary epidemiology using a whole genome sequencing approach. Microb Genom. 2021;7:000645. https://doi.org/10.1099/mgen.0.000645
29. Harris SR, Feil EJ, Holden MT, Quail MA, Nickerson EK, Chantratita N, et al. Evolution of MRSA during hospital transmission and intercontinental spread. Science. 2010;327:469–74. https://doi.org/10.1126/science.1182395
30. Méric G, Mageiros L, Pensar J, Laabei M, Yahara K, Pascoe B, et al. Disease-associated genotypes of the commensal skin bacterium *Staphylococcus epidermidis*. Nat Commun. 2018;9:5034. https://doi.org/10.1038/s41467-018-07368-7
31. Mageiros L, Méric G, Bayliss SC, Pensar J, Pascoe B, Mourkas E, et al. Genome evolution and the emergence of pathogenicity in avian *Escherichia coli*. Nat Commun. 2021;12:765. https://doi.org/10.1038/s41467-021-20988-w
32. Arnold BJ, Huang IT, Hanage WP. Horizontal gene transfer and adaptive evolution in bacteria. Nat Rev Microbiol. 2022;20:206–18. https://doi.org/10.1038/s41579-021-00650-4
33. Wyres KL, Wick RR, Judd LM, Froumine R, Tokolyi A, Gorrie CL, et al. Distinct evolutionary dynamics of horizontal gene transfer in drug resistant and virulent clones of *Klebsiella pneumoniae*. PLoS Genet. 2019;15:e1008114. https://doi.org/10.1371/journal.pgen.1008114
34. Salvadori G, Junges R, Morrison DA, Petersen FC. Competence in *Streptococcus pneumoniae* and close commensal relatives: mechanisms and implications. Front Cell Infect Microbiol. 2019;9:94. https://doi.org/10.3389/fcimb.2019.00094
35. Bagnoli F, Moschioni M, Donati C, Dimitrovska V, Ferlenghi I, Facciotti C, et al. A second pilus type in *Streptococcus pneumoniae* is prevalent in emerging serotypes and mediates adhesion to host cells. J Bacteriol. 2008;190:5480–92. https://doi.org/10.1128/JB.00384-08
36. Dzaraly ND, Muthanna A, Mohd Desa MN, Taib NM, Masri SN, Rahman NIA, et al. Pilus islets and the clonal spread of piliated *Streptococcus pneumoniae*: a review. Int J Med Microbiol. 2020;310:151449. https://doi.org/10.1016/j.ijmm.2020.151449
37. Hermoso JA, Lagartera L, González A, Stelter M, García P, Martínez-Ripoll M, et al. Insights into pneumococcal pathogenesis from the crystal structure of the modular teichoic acid phosphorylcholine esterase Pce. Nat Struct Mol Biol. 2005;12:533–8. https://doi.org/10.1038/nsmb940
38. Kadioglu A, Weiser JN, Paton JC, Andrew PW. The role of *Streptococcus pneumoniae* virulence factors in host respiratory colonization and disease. Nat Rev Microbiol. 2008;6:288–301. https://doi.org/10.1038/nrmicro1871
39. Marquart ME. Pathogenicity and virulence of *Streptococcus pneumoniae*: cutting to the chase on proteases. Virulence. 2021;12:766–87. https://doi.org/10.1080/21505594.2021.1889812
40. Brittan JL, Buckeridge TJ, Finn A, Kadioglu A, Jenkinson HF. Pneumococcal neuraminidase A: an essential upper airway colonization factor for *Streptococcus pneumoniae*. Mol Oral Microbiol. 2012;27:270–83. https://doi.org/10.1111/j.2041-1014.2012.00658.x
41. Navarro-Torné A, Dias JG, Hruba F, Lopalco PL, Pastore-Celentano L, Gauci AJ; Invasive Pneumococcal Disease Study Group. Risk factors for death from invasive pneumococcal disease, Europe, 2010. Emerg Infect Dis. 2015;21:417–25. https://doi.org/10.3201/eid2103.140634
42. Li Y, Metcalf BJ, Chochua S, Li Z, Gertz RE Jr, Walker H, et al. Penicillin-binding protein transpeptidase signatures for tracking and predicting β-lactam resistance levels in *Streptococcus pneumoniae*. MBio. 2016;7:e00756–16. https://doi.org/10.1128/mBio.00756-16
43. Gibson PS, Veening JW. Gaps in the wall: understanding cell wall biology to tackle amoxicillin resistance in *Streptococcus pneumoniae*. Curr Opin Microbiol. 2023;72:102261. https://doi.org/10.1016/j.mib.2022.102261
44. Egorova E, Kumar N, Gladstone RA, Urban Y, Voropaeva E, Chaplin AV, et al. Key features of pneumococcal isolates recovered in central and northwestern Russia in 2011–2018 determined through whole-genome sequencing. Microb Genom. 2022;8:mgen000851. https://doi.org/10.1099/mgen.0.000851
45. Bai G, Vidal JE. Editorial: molecular pathogenesis of *Pneumococcus*. Front Cell Infect Microbiol. 2017;7:310. https://doi.org/10.3389/fcimb.2017.00310
46. Chen L, Zhang YH, Wang S, Zhang Y, Huang T, Cai YD. Prediction and analysis of essential genes using the enrichments of gene ontology and KEGG pathways. PLoS One. 2017;12:e0184129. https://doi.org/10.1371/journal.pone.0184129
47. Kanehisa M, Furumichi M, Sato Y, Kawashima M, Ishiguro-Watanabe M. KEGG for taxonomy-based analysis of pathways and genomes. Nucleic Acids Res. 2023;51(D1):D587–92. https://doi.org/10.1093/nar/gkac963
48. Jaillard M, Lima L, Tournoud M, Mahé P, van Belkum A, Lacroix V, et al. A fast and agnostic method for bacterial genome-wide association studies: bridging the gap between k-mers and genetic events. PLoS Genet. 2018;14:e1007758. https://doi.org/10.1371/journal.pgen.1007758
49. Aun E, Brauer A, Kisand V, Tenson T, Remm M. A k-mer-based method for the identification of phenotype-associated genomic biomarkers and predicting phenotypes of sequenced bacteria. PLOS Comput Biol. 2018;14:e1006434. https://doi.org/10.1371/journal.pcbi.1006434

Address for correspondence: Xiaohua Ye, Guangdong Pharmaceutical University, 283# Jianghai Dadao, Haizhu District, Guangzhou, China; email: smalltomato@163.com

Effect of 2020–21 and 2021–22 Highly Pathogenic Avian Influenza H5 Epidemics on Wild Birds, the Netherlands

Valentina Caliendo, Erik Kleyheeg, Nancy Beerens, Kees C.J. Camphuysen, Rommert Cazemier, Armin R.W. Elbers, Ron A.M. Fouchier, Leon Kelder, Thijs Kuiken, Mardik Leopold, Roy Slaterus, Marcel A.H. Spierenburg, Henk van der Jeugd, Hans Verdaat, Jolianne M. Rijks

The number of highly pathogenic avian influenza (HPAI) H5-related infections and deaths of wild birds in Europe was high during October 1, 2020–September 30, 2022. To quantify deaths among wild species groups with known susceptibility for HPAI H5 during those epidemics, we collected and recorded mortality data of wild birds in the Netherlands. HPAI virus infection was reported in 51 bird species. The species with the highest numbers of reported dead and infected birds varied per epidemic year; in 2020–21, they were within the Anatidae family, in particular barnacle geese (*Branta leucopsis*) and in 2021–22, they were within the sea bird group, particularly Sandwich terns (*Thalasseus sandvicensis*) and northern gannet (*Morus bassanus*). Because of the difficulty of anticipating and modeling the future trends of HPAI among wild birds, we recommend monitoring live and dead wild birds as a tool for surveillance of the changing dynamics of HPAI.

The dynamics of highly pathogenic avian influenza (HPAI) virus infection of the H5 GS/GD lineage (clade 2.3.4.4b) have dramatically changed for wild birds. For 2 recent epidemic seasons (2020–21 and 2021–22), HPAI H5 viruses have adapted to survive long term in wild bird populations; they are now considered enzootic in wild birds (*1*–*3*). This change in status was supported by the shift in HPAI epidemiology during summer 2021, as the virus circulated continuously in northwestern Europe and Scandinavia (*1*,*4*). High rates of virus detection in wild and captive birds continued in 2022 for the largest epidemic observed to date in Europe (*4*). The circulation of HPAI virus during the 2022 breeding season exposed several colony-breeding seabird species along the northwest coast of Europe to infection (*4*–*7*), culminating in a high number of HPAI virus detections in dead wild birds during June–August 2022. At that time several seabird species exhibited widespread and massive deaths from HPAI H5N1 virus at their breeding colonies in Germany, the Netherlands, France, and the United Kingdom (*4*–*8*). Authorities have recommended reporting the number of wild birds found dead or ill during HPAI-associated dieoffs, both to contribute to the understanding of the ecologic effect of HPAI outbreaks and for targeted, evidence-based policy making (*4*,*9*).

The extent to which bird species are associated with HPAI largely depends on how often each species has tested positive (*10*). Several factors play a role in this assessment: species-specific susceptibility to clinical disease, local population size, geographic and climate circumstances, reporter effort, and number of birds screened during surveillance.

Author affiliations: Utrecht University, Utrecht, the Netherlands (V. Caliendo, J.M. Rijks); Sovon, Dutch Centre for Field Ornithology, Nijmegen, the Netherlands (E. Kleyheeg, R. Slaterus); Wageningen Bioveterinary Research, Lelystad, the Netherlands (N. Beerens); Royal Netherlands Institute for Sea Research, Den Burg, the Netherlands (K.C.J. Camphuysen); Wetterskip Fryslan, Leeuwarden, the Netherlands (R. Cazemier); Wageningen Bioveterinary Research, Lelystad (A.R.W. Elbers); Erasmus University Medical Center, Rotterdam, the Netherlands (R.A.M. Fouchier, T. Kuiken); Staatsbosbeheer, Amersfoort, the Netherlands (L. Kelder); Wageningen Marine Research, Den Helder, the Netherlands (M. Leopold, H. Verdaat); Netherlands Food and Consumer Product Safety Authority, Utrecht (M.A.H. Spierenburg); Vogeltrekstation—Dutch Centre for Avian Migration and Demography NIOO-KNAW, Wageningen, the Netherlands. (H. van der Jeugd); Waarneming.nl, Stichting Observation International, Den Helder (H. Verdaat)

DOI: http://doi.org/10.3201/eid3001.230970

In the Netherlands, the AI-Impact working group, a consortium of ornithologists, virologists, epidemiologists, nature managers, and animal health organizations, has been active since 2020 to provide up-to-date information on wild bird mortalities during HPAI outbreaks. The aims of the consortium are to identify the range of wild bird species exposed and affected by HPAI, and to estimate the HPAI-associated level of mortality of wild birds, also relative to their population size.

For this study, we collected dead-bird reports and virologic diagnoses from a variety of sources to estimate species-specific mortality prevalence caused by the 2020–21 and 2021–22 HPAI H5 epidemics in the Netherlands. During the epidemics, mortality data were collected monthly and provided near–real-time information on the trend of the epidemic for interested organizations.

Methods

The methods for this study were similar to those used by Kleyheeg et al. (*11*). In brief, we collected wild bird mortality data from 2 complete bird influenza seasons, October 1, 2020–September 30, 2021, and October 1, 2021–September 30, 2022. The national competent authorities reported dead wild birds to the AI-Impact consortium as part of the national animal infectious disease surveillance program and by citizen scientists who were invited to report sightings of dead birds on the web platforms of the AI-Impact members (https://dwhc.nl/dode-vogels-melden/, https://www.sovon.nl/nl/content/vogelgriep, https://www.nvwa.nl/onderwerpen/vogelgriep-preventie-en-bestrijding, https://waarneming.nl). In addition, all seabird strandings data along the Dutch North Sea and Wadden Sea coasts were analyzed as part of a long-term monitoring project and checked for unusually high numbers of stranded birds with effort correction (number per km of coastline searched, n km^{-1}) (*12*,*13*). Unusually high densities (i.e., stranded birds per area) were ≥5 times background densities, as measured using identical surveys from the previous 40 years in any given month. Double counts did not occur in this dataset because carcasses were marked.

We categorized reports by bird species, date, and location of finding. Double counts (e.g., multiple entries for the same species on the same date, at the same location from the same observer) were excluded as much as possible. Consistent with similar studies, we found it highly likely that the number of reported carcasses substantially underestimates actual deaths; for example, collection rates of water bird carcasses during typical avian botulism outbreaks are 10%–25% (*14*).

We categorized wild bird mortality reports into 4 groups: Anatidae (i.e., geese, swans, ducks), other water birds (including gulls, grebes, herons, cormorants, waders, rallids), raptors, and other land birds. We classified birds of the families Podicipedidae, Laridae, Stercorariidae, Alcidae, Gaviidae, Procellariidae, Sulidae, and Phalacrocoracidae, in 1 subgroup, sea birds. We analyzed mortality data of selected species individually, because they experienced particularly high mortality rates during either the 2020–21 epidemic (i.e., barnacle goose [*Branta leucopsis*], common buzzard [*Buteo buteo*], peregrine falcon [*Falco peregrinus*], great black-backed gull [*Larus marinus*]), or during the 2021–22 epidemic (i.e., Sandwich tern [*Thalasseus sandvicensis*], northern gannet [*Morus bassanus*]). We used data from the public database of Sovon (Dutch Centre for Field Ornithology, Nijmegen, the Netherlands; https://www.sovon.nl) to compare the number of reported dead wild birds per avian group during October–March (classified as winter mortality) and April–September (classified as summer mortality) between the 2020–21 and 2021–22 epidemics; we then compared data for the same months of 2010–11 with 2015–16 as described by Kleyheeg et al. (*11*). In the later period (2010–2016), there had been no outbreaks of HPAI in wild birds in the Netherlands. We tested a limited number of wild bird carcasses (Appendix 1 Table, https://wwwnc.cdc.gov/EID/article/30/1/23-0970-App1.xlsx) for HPAI virus by real-time reverse transcription PCR on oropharyngeal and cloacal swabs as previously described (*15*,*16*). We submitted groups of ≥3 dead wild birds of certain categories (i.e., Anatidae, water birds) found dead at the same location, and single birds of other susceptible species (i.e., raptors) that were suspected of being HPAI virus-infected, for virologic analysis.

We used species data on live population estimates from the public database of Sovon to evaluate mortality rates by bird species (Table; Appendix 1 Table). Population size represents the estimated lowest and highest number of birds wintering in the Netherlands, based on census data for 2013–2020 from Sovon. For summer migratory species, population size represents the estimated lowest and highest number of birds migrating to the Netherlands, based on census data for 2016–2021 from Sovon.

Results

A total of 16,631 wild birds of 160 species were reported dead in the Netherlands in October 1, 2020–September 30, 2021. Water birds including Anatidae accounted for 70% of the total deaths reported and land birds, including raptors, the remaining 30% (Table 1).

Table. Reported bird species, nonbreeding population size estimates, number of carcasses, and RT-PCR test results for wild birds sampled during 2020–21 and 2021–22 HPAI epidemics, the Netherlands*

Avian group and species	Maximum estimated nonbreeding population size, ×1,000	No. carcasses (mortality rate, %)†		No. carcasses HPAI positive/no. tested	
		2020–21	2021–22	2020–21	2021–22
Anatidae		7,901	14,309	361/628	173/416
Geese		4,802	8,867	234/332	154/260
Barnacle goose	710–870	3,435 (1.5–4.8)	5,310 (2.4–7.4)	147/171	77/104
Graylag goose	550–670	390 (0.2–0.7)	1,054 (0.7–1.9)	30/59	53/60
Unidentified species	NA	607	1,653	35/59	36/60
Swans		996	1,453	60/136	2/17
Mute swan	41–48	305 (2.5–7.4)	479 (3.9–11)	38/93	0
Unidentified species	NA	629	969	19/54	2/17
Ducks		2,103	3,985	67/160	17/139
Eurasian wigeon	820–950	125 (<0–0.01)	300 (0.1–0.3)	12/13	1/9
Tufted duck	220–280	45 (0.6–2.5)	34 (0.01–0.1)	1/19	0
Other waterbirds		4,068	21,895	19/162	95/245
Grebes	NA	62	164	0/2	4/10
Herons	NA	250	232	0/33	3/23
Cormorants	NA	234	371	2/14	2/35
Waders	NA	1,045	1,713	9/49	10/14
Rallids	NA	327	472	0/2	1/23
Sea bird		2,371	19,340	16/102	75/140
Gulls		1,074	5,538	7/61	37/100
Great black-backed gull	25–100	137 (0.01–5.4)	372 (1.4–14.8)	1/1	1/3
Sandwich tern	27–120‡	0	5,166 (17.2–>90)§	0	29/33
Northern gannet	4–27	203	2,215 (32.8–>90)	0	6/11
Raptors		1,011	763	42/155	83/149
Common buzzard	30–50	365 (2.9–12.1)	363 (2.9–12.1)	27/91	55/81
Peregrine falcon	0.5–0.6	27 (18–54)	28 (18–56)	4/5	9/11
Other land birds		3,651	3,850	2/40	6/59
Corvids	NA	271	363	1/24	4/26
Total		16,631	41,519	427/985	357/869

*Data from Sovon (Dutch Centre for Field Ornithology, Nijmegen, the Netherlands). HPAI, highly pathogenic avian influenza; NA, not available; RT-PCR, reverse transcription PCR.
†Expressed as fraction of the nonbreeding population. Lower and higher values are calculated considering the 10%–25% collection rates, as described by Kleyheeg et al. (*11*).
‡Estimated migration maximum.
§Expressed as fraction of the migrant population.

Anatidae by themselves represented 50% of the total deaths reported. Of the bird carcasses identified to species, by far the highest number of deaths were reported for barnacle geese (n = 3,435). The next highest numbers of dead animals were reported for graylag geese (n = 390), common buzzards (n = 365), and mute swans (*Cygnus olor*) (n = 305). HPAI virus infection was reported in 45 species (Appendix 1 Table). The species with the highest numbers of reported dead and infected birds were within the Anatidae group: barnacle geese, graylag geese, and mute swans. Common buzzard was the species with the highest numbers of reported dead and infected birds within the raptor group. Expressed as fraction of the nonbreeding population, and after accounting for detection probability, the reported dead birds represented up to 4.8% of barnacle geese, 0.7% of graylag geese, and 7.4% of mute swans (Table 1). We found the highest mortality rates occurred in raptors and scavenging species: relative to their wintering populations, up to 54% of peregrine falcons, 12.1% of common buzzards, and 5.4% of great black-backed gulls may have died.

A total of 41,519 wild birds of 158 species were reported dead in the Netherlands during October 1, 2021–September 30, 2022. Water birds including Anatidae accounted for 80% and land birds including raptors for the remaining 20% of the total deaths reported (Table 1). Sea birds represented >40% and Anatidae 30% of the total deaths. Of the bird carcasses identified to species, the highest number was reported for the barnacle goose (n = 5,310). The next highest numbers of dead individuals were reported for Sandwich terns (n = 5,166), and northern gannets (n = 2,215). HPAI virus infection was confirmed in 51 species (Appendix 1 Table). The species with the highest numbers of reported dead and infected birds were within the sea bird and Anatidae groups, and the species most represented were the Sandwich tern and the barnacle goose. Expressed as a fraction of the nonbreeding population, and after accounting for detection probability, the reported dead birds represented 32.8%–90% of northern gannets and up to 7.4% of barnacle geese (Table 1). The Sandwich tern appears as a summer breeder in the Netherlands;

after accounting for detection probability, the reported dead birds represented 17.2%–90% of the estimated migrant population of Sandwich terns. We found that high mortality rates also occurred in raptors: up to 56% of wintering populations of peregrine falcons and 12.1% of common buzzards may have died. Mortality rates in winter or summer months were higher than the average estimates in previous years (i.e., compared to the same timeframe in 2011–2016, years in which major wild bird mortalities from outbreaks of HPAI virus did not occur). In particular, the number of reported carcasses was >50 times higher for geese in winter 2022 and >1,000 times higher for Sandwich terns in summer 2022 (Figure 1).

During the 2020–21 epidemic in the Netherlands, wild bird deaths clustered in 2 peaks, the first in November 2020 and the second, smaller peak in April–May 2021 (Figure 2). During both peaks, barnacle geese were among the species most severely affected. During the 2021–22 epidemic in the Netherlands, wild bird deaths also showed 2 peaks, the first in January 2022 and the second in June 2022 (Figure 2). During the first peak, barnacle geese were again among the species most severely affected, and during the second peak, sea birds were the most severely affected. The virus was still detected in October 2022, but that date was considered the start of the new HPAI 2022–23 outbreak.

Discussion

HPAI dynamics in wild birds are constantly evolving. The 2020–21 HPAI H5 epidemic was more devastating than earlier HPAI H5 epidemics in Europe, causing high numbers of HPAI infections and deaths in many species of wild birds (*4*,*9*,*17*–*19*). Goose species, such as the barnacle goose, accounted for the highest number of casualties. During that epidemic, high prevalence of infection in geese was also reported in Germany and United Kingdom (*2*). In our study, several duck species consistently tested positive for HPAI H5 virus during the epidemic; however, reported deaths for those species were lower than for goose species. This finding represents a different scenario than that of the 2016–17 HPAI H5 epidemic, in which duck species, such as Eurasian wigeons (*Mareca penelope*) and tufted ducks (*Aythya fuligula*), experienced the highest number of deaths (*11*). The high mortality rate of barnacle geese during the 2020–21 HPAI H5 epidemic is unprecedented. Barnacle geese are one of the most abundant geese species in the Netherlands

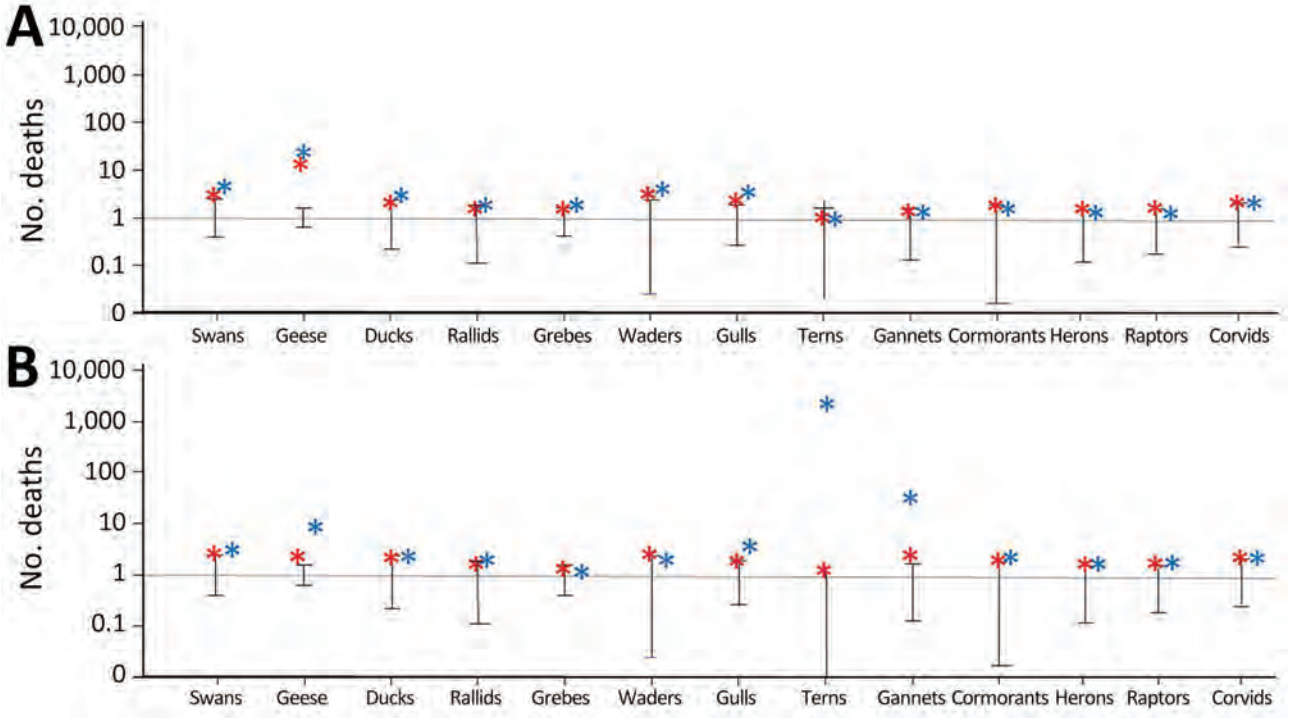

Figure 1. Relative number of reported deaths during the highly pathogenic avian influenza epidemics of 2020–21 (red asterisks), and 2021–22 (blue asterisks), the Netherlands. Deaths are relative to the normalized number of deaths reported over the same period from 2011–2012 to 2015–2016 (average is 1; data from Sovon, Dutch Centre for Field Ornithology, Nijmegen, the Netherlands). A) Deaths reported in the winter months, October–March. B) Deaths reported in the summer months, April–September. The y-axis is on a log scale; reported relative number of deaths among geese during winter 2021–22 was >50 larger than in the previous years. Error bars indicate maximum and minimum deaths.

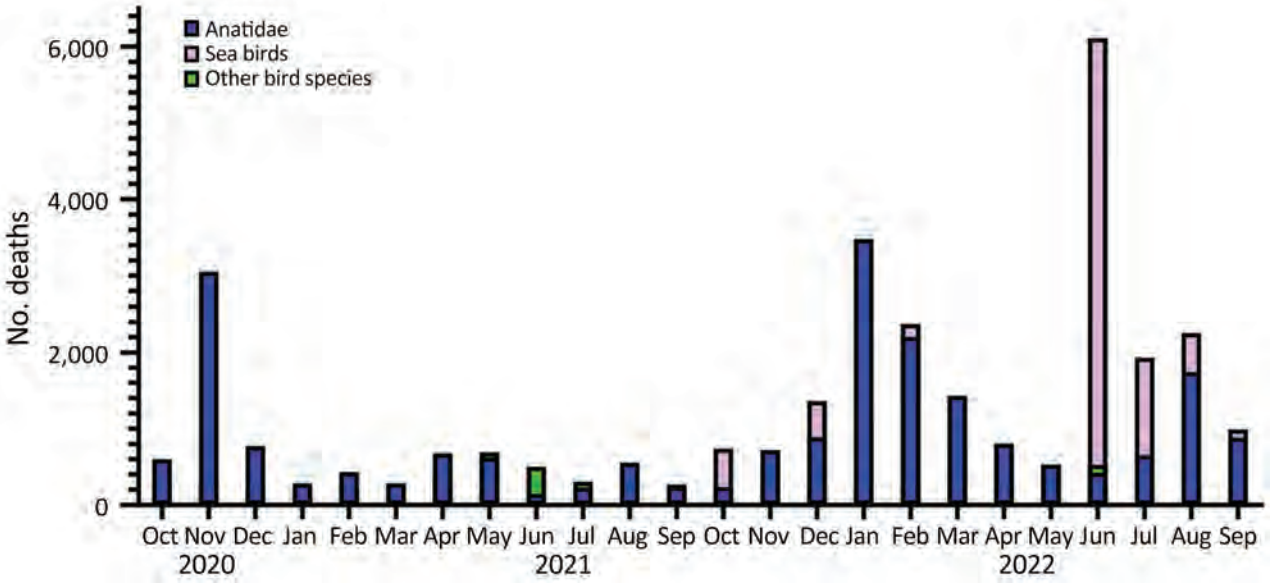

Figure 2. Temporal pattern of wild bird deaths during the 2020–21 and 2021–22 highly pathogenic avian influenza epidemics, the Netherlands. Sea birds include the bird families of Podicipedidae, Laridae, Stercorariidae, Alcidae, Gaviidae, Procellariidae, Sulidae, and Phalacrocoracidae.

(*19*,*20*); they are gregarious, herbivorous birds with a preference for coastal grassland and water-rich agricultural fields (*21*,*22*). Barnacle geese share their wintering habitat with other herbivorous birds, such as Eurasian wigeons and mute swans (*Cygnus olor*). The large number of geese and their gregarious behavior likely enabled the intraspecies transmission of the virus by direct or indirect contact (e.g., contaminated grass, contaminated water). The abundant circulation of HPAI H5 virus in new host species indicates that the virus has become well adapted to transmission in those species. During the 2020–21 epidemic, HPAI H5 virus was recovered from wild bird populations in the Netherlands for >1 year, indicating that it can be spread and maintained long-term in those populations (*4*,*9*), a new observation since the 2016–17 HPAI H5 epidemic, in which viral circulation was mainly limited to autumn and winter (*11*). A consequence of the unusual persistence of the virus into summer was that naive, newly hatched birds, especially juvenile Anseriformes such as mute swans and graylag geese and raptors such as white-tailed eagle (*Haliaeetus albicilla*), were exposed to the virus and died from infection during spring and summer 2021 (*9*). The large number of infected wild birds, either ill or dead, was a likely determinant for interspecies viral transmission to hunting or scavenger bird species. Raptors, for example, are exposed to infection by ingesting infected prey (*23*). During the epidemic, 11 different raptor species were found to be infected, and the highest number of infections and deaths occurred in the common buzzard (Table; Appendix 1 Table). Among the nonraptor scavenger species, we found 6 different species of gulls (Laridae) and 4 species of corvid (Corvidae) to be infected (Table; Appendix). Because the populations certain raptor species, such as the peregrine falcon, are relatively small, HPAI may represent a new threat for their conservation. Clinical signs of the infection in wild raptors were mainly neurologic, such as incoordination, body tremors, and torticollis, and were associated with brain lesions and a high level of neurotropism (*23*).

The 2021–22 HPAI H5 virus epidemic has caused the highest number of casualties among wild birds ever recorded in Europe (*4*). A significant change in the dynamic of the infections was that, since summer 2021, the virus has been enzootic in wild bird populations in Europe (*1*,*2*). This unprecedented, continuous circulation of virus during spring and summer also exposed colonial sea birds to infection (*5*). During the spring, colonial sea birds congregate in high number at their coastal breeding grounds. In this setting the virus could spread widely within and between breeding colonies, causing outbreaks that resulted in high adult and chick deaths (*6*,*7*). Sandwich terns were among the sea bird species that were more severely affected by the HPAI epidemic in the Netherlands. The sandwich tern is a vulnerable, migratory species that only breeds in a limited number of colonies across Europe seasonally, during April–September. Infection-associated mass mortality, with a mortality peak in June, was seen in 9 of the 10 Sandwich tern

breeding colonies in the Netherlands (*6*). The HPAI-associated mass mortality event is a severe threat for the conservation of this species. Mass dieoffs in the breeding colonies will most likely have long-term repercussions for the Sandwich tern population (*6*). Constant monitoring of the surviving birds will be necessary to assess the long-term effect of HPAI on this species in the coming years.

The northern gannet is another colonial sea bird species that seasonally occurs off the coast of the Netherlands, although it does not breed in the Netherlands, and that was severely affected by the HPAI epidemic. The HPAI-associated infections started in April and reached a peak in July 2022. We recorded high mortality of breeding gannets on nests; large numbers of carcasses of gannets were sighted afloat near several of the largest or most important breeding colonies and widespread in the North Sea basin (*7*). The ecology and pattern of mortalities of northern gannets have been studied in the Netherlands since 1980. Data from this long-term study enabled accurate evaluation of the 2022 mortality event in relation to background mortality and corrected per observer effort (*24*). For the northern gannet the number of reported corpses in July 2022 was 66 times larger than average in previous years, the highest spike in deaths over the past 40 years (*24*).

During the 2021–22 epidemic, high mortality rates in sea bird species were also reported in other countries in and outside of Europe. For example, Dalmatian pelicans (*Pelecanus crispus*) in Greece and great skuas (*Stercorarius skua*) on Foula, United Kingdom, both had 60%–70% declines of their populations because of HPAI virus infection during colonial breeding (*7*,*8*,*25*). The high density of birds and their close contact during colonial breeding probably enabled the rapid spread of the infection within the colonies. Field data suggest that HPAI-positive birds could shed virus for some period before death, providing opportunities for direct bird-to-bird or environmental transmission (*26*). Bird species such as great skuas have been reported to bathe and socialize at freshwater lochs and pools, providing possible opportunities for conspecific infection (*7*). Scavenging activities are another possible source of infection. Unattended chicks from dead parents most likely died because of lack of parental care. Maternal antibodies have been described in chicks of previously infected parents, but clinical protection is short-lived and requires high maternal antibody titers (*27*,*28*). Furthermore, maternal antibodies are only relevant if the infection has occurred before egg laying. Infected birds of certain Anatidae species can survive HPAI virus infection with limited clinical consequences (*29*,*30*). Experimentally serially infected ducks can develop a long-term immunity that confers protection from subsequent HPAI virus infection (*29*). It is possible that sea bird species will also develop flock immunity protective at future reinfection. The surviving birds should be tested for the presence of serum antibodies to gather data about flock immunity over the next several years.

The massive number of dead birds at colonies posed a biosecurity issue through the risk for viral spillover; cleaning up was an overwhelming task for the involved authorities. The AI-Impact consortium, together with the competent health authorities, provided a decision tree for the cleanup of dead birds to reduce the environmental contamination with minimal disturbance for the remaining birds (Appendix 2, https://wwwnc.cdc.gov/EID/article/30/1/23-0970-App2.pdf; Appendix 3, https://wwwnc.cdc.gov/EID/article/30/1/23-0970-App3.pdf). Carcass removal is necessary to reduce the amount of infected material that could spread the infection in the environment (*6*). Thus, we recommend controlled studies to optimize carcass removal.

During spring 2021, for the first time since the 2005–06 HPAI H5 epidemic, the virus was detected in Europe in several carnivore species, European foxes (*Vulpes vulpes*), gray seals (*Halichoerus grypus*), and harbor seals (*Phoca vitulina*); they were most likely infected through contact with or ingestion of infected wild birds (*9*,*31*). HPAI H5 viruses were once again detected in wild mammal species in Europe during the 2021–22 season and showed genetic markers of adaptation to replication in mammals (*16*). Therefore, we recommend planned year-round active and passive surveillance of wild mammals. The zoonotic risk for infection for humans of this particular H5 virus strain is considered low for the general population and low to medium for occupationally exposed workers, such as culling operators, wild animal rehabilitators, and workers involved in carcass removal (*16*). Persons at occupational risk should wear adequate personal protective equipment and be immunized with preventive annual vaccination against human influenza to avoid reassortment with HPAI H5 virus. In case of potential infection, those persons should be monitored for respiratory symptoms, neurologic symptoms, or conjunctivitis for 10 days after exposure (*16*), and diagnostic testing, if necessary, should be conducted at the competent national health authority.

Since the end of 2016, mass mortality events among wild birds caused by HPAI H5 infection in the

Netherlands have occurred in various species in various years, including Eurasian wigeon (2016), tufted duck (2016), barnacle goose (2020–2022), Sandwich tern (2022), and black-headed gull (*Chroicocephalus ridibundus*) (2023) (*16*). One characteristic those species have in common is that they live in dense groups at certain times of the year (*10*) and live close to open water. We suspected that this combination is an important risk factor for infection, because such groups have more opportunities for virus exposure and transmission and for possible species-specific adaptation of the virus (*10*). However, susceptibility to disease from HPAI virus infection seems to vary enormously between species. For example, disease and death can peak in one species while other species similarly present in the same area show hardly any signs of disease (*10*).

Because it remains difficult to anticipate and to model the future trends of HPAI among wild birds, we recommend constant monitoring of live and dead wild birds as an essential tool for surveillance of the evolving dynamics of HPAI. This method has several limitations; one is that it is difficult to exclude double-counted reports. Another is that not all the reported dead birds can be tested for HPAI virus infection, and not all will have died from HPAI infection. Two main improvements that we propose for HPAI surveillance in wild birds are long-term monitoring of HPAI-associated wild bird deaths, corrected for observer effort, and testing apparently healthy wild birds, particularly candidate reservoir species, for both HPAI virus and antibodies to HPAI virus. For the constant monitoring of wild bird deaths in the Netherlands during the 2020–21 and 2021–22 HPAI H5 epidemics, citizen scientists were a fundamental resource and made it possible to obtain a wider impression of the actual scale of mortality in wild birds, which otherwise would have been limited to the data from official surveillance. In addition to surveillance for HPAI, we recommend recording of wild bird deaths and encouraging and systematically endorsing the work of citizen scientists and international citizen-science platforms.

Acknowledgments

We thank the members of the AI-Impact group for their contribution.

All data are available in the article and appendices.

This research was financed by Horizon 2020 Framework Programme Deltaflu (grant no. 727922), and in part by the Dutch Ministry of Agriculture, Nature and Food Quality (project no. WOT-01-003-012).

Author contributions: Conceptualization: V.C., E.K., J.R., T.K. Methodology: V.C., E.K., J.R. Investigation: all authors. Visualization: V.C., E.K. Supervision: J.R., T.K. Writing, original draft: V.C. Writing, review and editing: all authors.

About the Author

Dr. Caliendo is a postdoctoral researcher at the Dutch Wildlife Health Centre in Utrecht, the Netherlands. Her primary research interests are wildlife medicine and diseases.

References

1. Pohlmann A, King J, Fusaro A, Zecchin B, Banyard AC, Brown IH, et al. Has epizootic become enzootic? Evidence for a fundamental change in the infection dynamics of highly pathogenic avian influenza in Europe, 2021. MBio. 2022;13:e0060922. https://doi.org/10.1128/mbio.00609-22
2. King J, Harder T, Globig A, Stacker L, Günther A, Grund C, et al. Highly pathogenic avian influenza virus incursions of subtype H5N8, H5N5, H5N1, H5N4, and H5N3 in Germany during 2020–21. Virus Evol. 2022;8:veac035. https://doi.org/10.1093/ve/veac035
3. Caliendo V, Lewis NS, Pohlmann A, Baillie SR, Banyard AC, Beer M, et al. Transatlantic spread of highly pathogenic avian influenza H5N1 by wild birds from Europe to North America in 2021. Sci Rep. 2022;12:11729. https://doi.org/10.1038/s41598-022-13447-z
4. European Food Safety Authority; European Centre for Disease Prevention and Control; European Reference Laboratory for Avian Influenza; Adlhoch C, Fusaro A, Gonzales JL, Kuiken T, Marangon S, Niqueux É, et al. Avian influenza overview June–September 2022. EFSA Journal 2022;20:7597. https://doi.org/10.2903/j.efsa.2022.7597
5. Wille M, Barr IG. Resurgence of avian influenza virus. Science. 2022;376:459–60. https://doi.org/10.1126/science.abo1232
6. Rijks JM, Leopold MF, Kühn S, In 't Veld R, Schenk F, Brenninkmeijer A, et al. Mass mortality caused by highly pathogenic influenza A(H5N1) virus in Sandwich terns, the Netherlands, 2022. Emerg Infect Dis. 2022;28:2538–42. https://doi.org/10.3201/eid2812.221292
7. Camphuysen CJ, Gear SC, Furness RW. Avian influenza leads to mass mortality of adult great skuas in Foula in summer 2022. Scott. Birds. 2022;42:312–23.
8. Banyard AC, Lean FZX, Robinson C, Howie F, Tyler G, Nisbet C, et al. Detection of highly pathogenic avian influenza virus H5N1 Clade 2.3.4.4b in great skuas: a species of conservation concern in Great Britain. Viruses. 2022;14:212. https://doi.org/10.3390/v14020212
9. European Food Safety Authority, European Centre for Disease Prevention and Control, European Reference Laboratory for Avian Influenza; Adlhoch C, Fusaro A, Gonzales JL, Kuiken T, Marangon S, Niqueux E, et al. Avian influenza overview September–December 2021. 2021 Dec 22. https://doi.org/10.2903/j.efsa.2021.7108
10. Slaterus R, Schekkerman H, Kleyheeg E, Sierdsema H, Foppen R. Impact of highly pathogenic avian influenza in bird populations in the Netherlands [in Dutch]. Nijmegen (the Netherlands): Sovon Vogelonderzoek Nederland; 2022.

11. Kleyheeg E, Slaterus R, Bodewes R, Rijks JM, Spierenburg MAH, Beerens N, et al. Deaths among wild birds during highly pathogenic avian influenza A(H5N8) virus outbreak, the Netherlands. Emerg Infect Dis. 2017;23:2050–4. https://doi.org/10.3201/eid2312.171086
12. Camphuysen CJ, Heubeck M. Marine oil pollution and beached bird surveys: the development of a sensitive monitoring instrument. Environ Pollut. 2001;112:443–61. https://doi.org/10.1016/S0269-7491(00)00138-X
13. Camphuysen CJ. Beached bird surveys in the Netherlands, autumn 2021 and winter 2021/22. NIOZ Report, RWS Centrale Informatievoorziening BM 22.18. Texel (the Netherlands): Royal Netherlands Institute for Sea Research; 2022.
14. Bollinger TK, Evelsizer DD, Dufour KW, Soos C, Clark RG, Wobeser G, et al. Ecology and management of avian botulism on the Canadian prairies. 2011 [cited 2017 Jun 20]. http://www.phjv.ca/pdf/BotulismReport_FINAL_FullReport_Aug2011.pdf
15. Poen MJ, Venkatesh D, Bestebroer TM, Vuong O, Scheuer RD, Oude Munnink BB, et al. Co-circulation of genetically distinct highly pathogenic avian influenza A clade 2.3.4.4 (H5N6) viruses in wild waterfowl and poultry in Europe and East Asia, 2017-18. Virus Evol. 2019;5:vez004. https://doi.org/10.1093/ve/vez004
16. Beerens N, Heutink R, Bergervoet SA, Harders F, Bossers A, Koch G. Multiple reassorted viruses as cause of highly pathogenic avian influenza A(H5N8) virus epidemic, the netherlands, 2016. Emerg Infect Dis. 2017;23:1974–81. https://doi.org/10.3201/eid2312.171062
17. Adlhoch C, Baldinelli F, Fusaro A, Terregino C. Avian influenza, a new threat to public health in Europe? Clin Microbiol Infect. 2022;28:149–51. https://doi.org/10.1016/j.cmi.2021.11.005
18. European Food Safety Authority, European Centre for Disease Prevention and Control, European Reference Laboratory for Avian Influenza; Adlhoch, C, Fusaro, A, Gonzales, JL, Kuiken, T, Marangon, S, Stahl, K, et al., 2023. Scientific report: avian influenza overview December 2022–March 2023. EFSA Journal. 2023;21:7917. https://doi.org/10.2903/j.efsa.2023.7917
19. van der Jeugd HP, Kwak A. Management of a Dutch resident barnacle goose *Branta* leucopsis population: How can results from counts, ringing and hunting bag statistics be reconciled? Ambio. 2017;46(Suppl 2):251–61. https://doi.org/10.1007/s13280-017-0900-3
20. Voslamber B, van der Jeugd H, Koffijberg K. Numbers, trends, and distribution of breeding goose populations in the Netherlands. Limosa. 20107;80:1–17.
21. Koffijberg K, Schekkerman H, van der Jeugd H, Hornman M, van Winden E. Responses of wintering geese to the designation of goose foraging areas in The Netherlands. Ambio. 2017;46(Suppl 2):241–50. https://doi.org/10.1007/s13280-016-0885-3
22. Si Y, Skidmore A, Wang T, de Boer WF, Toxopeus AG, Schlerf M, et al. Distribution of barnacle geese *Branta leucopsis* in relation to food resources, distance to roosts, and the location of refuges. Ardea. 2011;99:217–26. https://doi.org/10.5253/078.099.0212
23. Caliendo V, Leijten L, van de Bildt MWG, Fouchier RAM, Rijks JM, Kuiken T. Pathology and virology of natural highly pathogenic avian influenza H5N8 infection in wild common buzzards (*Buteo buteo*). Sci Rep. 2022;12:920. https://doi.org/10.1038/s41598-022-04896-7
24. Camphuysen KCJ, Kelder L, Zuhorn C, Fouchier R. Avian influenza panzootic leads to mass strandings of northern gannets in the Netherlands, April–October 2022. Limosa. 2022;95:4.
25. Alexandrou O, Malakou M, Catsadorakis G. The impact of avian influenza 2022 on Dalmatian pelicans was the worst ever wildlife disaster in Greece. Oryx. 2022;56:813. https://doi.org/10.1017/S0030605322001041
26. Prosser DJ, Schley HL, Simmons N, Sullivan JD, Homyack J, Weegman M, et al. A lesser scaup (*Aythya affinis*) naturally infected with Eurasian 2.3.4.4 highly pathogenic H5N1 avian influenza virus: movement ecology and host factors. Transbound Emerg Dis. 2022;69:e2653–60. https://doi.org/10.1111/tbed.14614
27. Christie KF, Poulson RL, Seixas JS, Hernandez SM. Avian influenza virus status and maternal antibodies in nestling white ibis (*Eudocimus albus*). Microorganisms. 2021;9:2468. https://doi.org/10.3390/microorganisms9122468
28. Maas R, Rosema S, van Zoelen D, Venema S. Maternal immunity against avian influenza H5N1 in chickens: limited protection and interference with vaccine efficacy. Avian Pathol. 2011;40:87–92. https://doi.org/10.1080/03079457.2010.541226
29. Caliendo V, Leijten L, van de Bildt MWG, Poen MJ, Kok A, Bestebroer T, et al. Long-term protective effect of serial infections with H5N8 highly pathogenic avian influenza virus in wild ducks. J Virol. 2022;96:e0123322. https://doi.org/10.1128/jvi.01233-22
30. Gobbo F, Fornasiero D, De Marco MA, Zecchin B, Mulatti P, Delogu M, et al. Active surveillance for highly pathogenic avian influenza viruses in wintering waterbirds in northeast Italy, 2020–2021. Microorganisms. 2021;9:2188. https://doi.org/10.3390/microorganisms9112188
31. Rijks JM, Hesselink H, Lollinga P, Wesselman R, Prins P, Weesendorp E, et al. Highly pathogenic avian influenza A(H5N1) virus in wild red foxes, the Netherlands, 2021. Emerg Infect Dis. 2021;27:2960–2. https://doi.org/10.3201/eid2711.211281</jrn>

Address for correspondence: Valentina Caliendo, Dutch Wildlife Health Centre, Faculteit Diergeneeskunde, Universiteit Utrecht, Yalelaan 1, 3584 CL, Utrecht, the Netherlands; email: v.caliendo@uu.nl

COVID-19–Related School Closures, United States, July 27, 2020–June 30, 2022

Nicole Zviedrite, Ferdous Jahan, Sarah Moreland,[1] Faruque Ahmed, Amra Uzicanin

As part of a multiyear project that monitored illness-related school closures, we conducted systematic daily online searches during July 27, 2020–June 30, 2022, to identify public announcements of COVID-19–related school closures (COVID-SCs) in the United States lasting ≥1 day. We explored the temporospatial patterns of COVID-SCs and analyzed associations between COVID-SCs and national COVID-19 surveillance data. COVID-SCs reflected national surveillance data: correlation was highest between COVID-SCs and both new PCR test positivity (correlation coefficient [r] = 0.73, 95% CI 0.56–0.84) and new cases (r = 0.72, 95% CI 0.54–0.83) during 2020–21 and with hospitalization rates among all ages (r = 0.81, 95% CI 0.67–0.89) during 2021–22. The numbers of reactive COVID-SCs during 2020–21 and 2021–22 greatly exceeded previously observed numbers of illness-related reactive school closures in the United States, notably being nearly 5-fold greater than reactive closures observed during the 2009 influenza (H1N1) pandemic.

Although unplanned school closures occur every year, outside of a pandemic, only a small minority (≈1%) are associated with infectious disease, whereas most are attributable to weather and natural disasters (*1*). However, the initial months (February–June 2020) of the COVID-19 pandemic in the United States led to unprecedented, nearly simultaneous, nationwide implementation of kindergarten through 12th grade (K–12) school closures throughout the United States as a part of a wider effort to slow virus transmission and reduce disease prevalence (*2*). In most communities, those early pandemic-related closures were implemented preemptively as a nonpharmaceutical intervention before community transmission was high. In contrast, the subsequent COVID-19–related school closures occurring in the 2020–21 and 2021–22 school years were predominantly reactive (i.e., occurring after infection had affected students, staff, or both).

As school reconvened for 2020–21 and 2021–22, schools and districts were faced with the challenge of providing in-person education and services during the ongoing pandemic. In a previous analysis, we described the transition to online learning that occurred during February–June 2020 after the COVID-19–related preemptive closures of schools and school districts (*2*). The subsequent 2 pandemic-affected school years (2020–21 and 2021–22) were characterized by the deployment of various education modalities, including education that was fully in-person, fully distance learning, or a hybrid model (*3*–*5*). In both years, among schools offering in-person learning (fully or hybrid), school closures continued to be implemented in response to local transmission dynamics and policies and to other consequences of the pandemic (e.g., vaccination of staff and students and side effects of vaccination, teacher and staff shortages, and pandemic-related mental health issues).

In this study, we describe trends in reactive COVID-19–related K–12 school closures (COVID-SCs) in the United States during July 27, 2020–June 30, 2022. We also analyze associations between COVID-SCs and national level COVID-19 epidemiologic surveillance data.

Methods

Data Collection

We conducted daily systematic online searches during July 27, 2020–June 30, 2022, to identify public

Author affiliations: Centers for Disease Control and Prevention, Atlanta, Georgia, USA (N. Zviedrite, F. Jahan, S. Moreland, F. Ahmed, A. Uzicanin); Cherokee Nation Operational Solutions, LLC, Tulsa, Oklahoma, USA (F. Jahan); Oak Ridge Institute for Science and Education, Oak Ridge, Tennessee, USA (S. Moreland)

DOI: https://doi.org/10.3201/eid3001.231215

[1]Current affiliation: Henry M. Jackson Foundation, Bethesda, Maryland, USA.

announcements of unplanned, illness-related K–12 school closures in the United States. We conducted searches in Google and Google News by using the following terms: "school closed" and either "COVID," "COVID-19," or "coronavirus." In addition, we used in a Google Alert the search string "(academy OR school OR district OR class) AND (close OR closing OR closure OR cancel OR cancelled) AND (coronavirus OR corona OR 'COVID-19' OR COVID OR 'novel coronavirus')." We also checked publicly available COVID-19–related school closure dashboards identified during those routine searches, including those published online by school districts, state and local education authorities, and private entities. We saved all school closure announcements as PDFs before data abstraction. We included for analysis only announcements mentioning COVID-19 as a reason for closure. Additional details on the search strategy and data abstraction processes have been published previously (*1*,*2*). We did not collect data during July 1–25, 2021, because this period coincided with school summer break in the United States.

We classified fully in-person and hybrid learning modalities as open, and we classified modalities without in-person learning (i.e., fully distanced learning and closed) as closed. We defined unplanned closure as a transition from being open to being closed for in-person instruction for ≥1 day. If a school or district reopened for ≥1 day and then closed again, we counted the subsequent closure as a new occurrence of closure. For closures that spanned both unplanned and planned closure days, such as those contiguous with weekends or planned holidays, we counted only unplanned closure days. For closures for which a reopening date could not be identified after closure, we assumed the length of closure to be 1 day. Delay of in-person learning at the start of the school year, through closure or full distance-learning modalities, was not captured in this data collection. For each identified COVID-SC, we abstracted school or school district name, state, dates of closure and reopening, and reasons for closure as reported in the announcements.

Contextualizing School Closures

To better understand the characteristics of schools and districts experiencing COVID-SCs, we matched each closure event to publicly available data downloaded from the National Center for Education Statistics (NCES) by using the respective NCES district or school identification (identified using district or school name and location) (*6*,*7*). Some districts and schools experienced multiple COVID-SC events during the study period and therefore appear >1 time in the resulting dataset. For each public school and public school district, we matched COVID-SC data with the respective year (i.e., 2020–21 or 2021–22) of NCES data, and for private schools, we matched COVID-SCs with the most recent year of data available (2019–20) in NCES. NCES data include information such as the number of schools per district, number of students and staff, number of students eligible in the federal free or reduced-price school lunch programs (only for public schools and public school districts), urbanicity, and grade span data. We excluded school districts with no schools; schools with no student enrollment; vocational, special education, and alternative schools with missing values for student enrollment; schools with prekindergarten, transitional kindergarten, or adult students only; and permanent distance learning–only schools (Appendix, https://wwwnc.cdc.gov/EID/article/30/01/23-1215-App1.pdf).

Epidemiologic Data

We gathered publicly available COVID-19 surveillance data during July 27, 2020–June 30, 2022, including daily new cases and death counts (*8*), weekly hospitalization rates (*9*), and daily PCR positivity (*10*) for the duration of the study period. We reported hospitalization rates per epidemiologic week, and we calculated corresponding weekly figures for new cases, deaths, and PCR positivity at the national level. Epidemiologic weeks run Sunday through Saturday; epidemiologic week 1 was the first week to hold ≥4 days from the new calendar year.

Data Analysis

We described characteristics of school closures according to the data abstracted from public announcements. We summarized specific reasons for COVID-SCs by grouping them into 12 non–mutually exclusive categories under 2 primary themes: transmission-related reasons and non–transmission-related reasons (Appendix). Transmission-related reasons included COVID-19 cases, suspected cases, increased student absenteeism, increased staff absenteeism, cluster or widespread transmission in the community, state or local guidance or mandate to close schools in response to COVID-19, cleaning or disinfecting school facilities, and other reasons related to COVID-19 mitigation, including testing, contact tracing, quarantine of students and staff, prevention of holiday-related surge, death of staff member, critical lack of community resources (e.g., contact tracers), and noncompliance with governor's executive orders regarding nonpharmaceutical interventions. Non–transmission-related reasons

included COVID-19 vaccinations, teacher or staff shortages, student or staff mental health, and other reasons associated with COVID-19, including staff protests of in-person learning, protests over mask policies, transportation issues specific to COVID-19, lack of resources specific to COVID-19, and work on the COVID-19 mitigation plan. We estimated in-person student-days lost because of COVID-SCs by multiplying the number of students per school by the respective number of unplanned closures days experienced.

We compared weekly patterns of COVID-SCs with COVID-19 epidemiologic surveillance data at the national level (new cases and deaths, hospitalization rates, and laboratory test positivity). We calculated Spearman rank correlations (r) and 95% CIs to evaluate these relationships ($\alpha = 0.05$) during the school years. We excluded from analysis the final week of each calendar year because this week coincides with school winter break in the United States (Appendix). We calculated p values for the Spearman rank correlation on the basis of the Fisher Z-transformation. We conducted analysis by using SAS version 9.4 (SAS Institute Inc., https://www.sas.com) and visualized results by using Excel and Power BI (Microsoft, https://www.microsoft.com). In addition, we calculated in-person school days lost, the frequency and patterns of repeat closures of schools for COVID-19, and cumulative incidence of COVID-SCs by states, and we conducted bivariate and multivariable regression analyses (Appendix).

Results

School Year 2020–21

During July 27, 2020–June 30, 2021, a total of 16,890 unique schools experienced an estimated 19,273 COVID-SCs (Table 1). Approximately 75% closed as part of districtwide closures. More than 11 million students were affected, and >159 million in-person student-days were lost. Most COVID-SCs were observed in the first half of the school year (August–December), and they peaked in epidemiologic week 47, the week before the US Thanksgiving holiday (Figure 1). The median number of in-person schools days lost per closure nationally was 10 days (interquartile range [IQR] 3–23 days) (Appendix Figure 1); however, this figure reached >20 days in 7 states (California, Colorado, Illinois, Indiana, Kentucky, Minnesota, and Nevada) (Appendix Figure 2). Most schools experiencing COVID-SCs experienced only 1 COVID-SC during the school year (Appendix Table 1). However, 2,036 schools (12.1%) experienced 2–7 COVID-SCs during the school year; 2 was most common (1,756 schools [86.2%]).

Among the announcements reporting reasons for closure, the most common reasons were having positive COVID-19 cases in the school (47.4% of district-level and 58.5% of school-level events) and clusters or widespread transmission in the community (47.8% of district-level and 32.5% of school-level events) (Table 2). In addition, state and local mandates to close schools in response to COVID-19 accounted for >20% of closures. When analysis was restricted to the 7 states with the highest median closure lengths (California, Colorado, Illinois, Indiana, Kentucky, Minnesota, and Nevada), clusters or widespread transmission in the community accounted for greater proportions of district-level (83.1%) and school-level (55.4%) closure events (Appendix Table 2). Similarly, closure events attributable to state and local mandates were proportionally higher in these states at the district level (28.8%) and school level (30.7%) than in the nation as a whole (Appendix Table 2). Mandates were issued either as part of an ongoing policy triggered by reaching a COVID-19 threshold, such as the positivity rate of testing (*13*), or in response to local surges in cases (*14*,*15*). Although few COVID-SCs were attributed to non–transmission-related reasons, such as vaccination of staff and students or nonspecific teacher shortages attributed to the pandemic, nearly 30% of COVID-SCs during epidemiologic weeks 6–11 of 2021 were attributable to vaccination of staff and side effects of vaccination (Figure 1).

Transmission-related COVID-SCs were strongly correlated with weekly COVID-19 testing positivity rates (r = 0.73, 95% CI 0.56–0.84) and with new COVID-19 cases (r = 0.72, 95% CI 0.54–0.83) (Table 3). Transmission-related COVID-SCs were moderately correlated with both new COVID-19 deaths by week (r = 0.51, 95% CI 0.25–0.69) and weekly laboratory confirmed COVID-19–associated hospitalization rates for all ages (r = 0.64, 95% CI 0.42–0.78) (Table 4). Age-specific correlation with hospitalization rates varied; the 5–17-year age group, which aligns with the K–12 student population, had the weakest correlation (r = 0.37, 95% CI 0.09–0.60), and correlations strengthened for each subsequent older age group (Table 4). The peak in weekly COVID-SCs preceded the peaks in COVID-19 disease surveillance indicators (new cases, new deaths, percentage positive PCR tests, and hospitalization rates) by roughly 6–8 weeks (Figure 2, panels A–D; Figure 3, panel A).

School Year 2021–22

During August 1, 2021–June 30, 2022, more than 14.6 million students in the United States were affected

Table 1. Characteristics of COVID-19–associated school closures, by school year, United States, July 27, 2020–June 30, 2022*

Characteristics of COVID-19–associated school closures	Total	School year†	
		2020–21	2021–22
No. school closures‡	10,884	6,322 (58.1)	4,562 (41.9)
Districtwide	3,443 (31.6)	1,528 (24.2)	1,915 (42.0)
Individual school	7,441 (68.4)	4,794 (75.8)	2,647 (58.0)
Total estimated no. unique schools closed	36,761	16,890 (45.9)	19,871 (54.1)
Total estimated no. closed schools§¶	45,180	19,273 (42.7)	25,907 (57.3)
Closure type			
Districtwide	37,739 (83.5)	14,479 (75.1)	23,260 (89.8)
Individual school	7,441 (16.5)	4,794 (24.9)	2,647 (10.2)
School type			
Public	44,463 (98.4)	18,620 (96.6)	25,843 (99.8)
Private	717 (1.6)	653 (3.4)	64 (0.3)
School grade level§			
Elementary school: K–5th grade	18,273 (40.4)	7,701 (40.0)	10,572 (40.8)
Elementary–middle school: K–8th grade	8,241 (18.2)	3,037 (15.8)	5,204 (20.1)
Elementary–high school: K–12th grade	1,107 (2.5)	461 (2.4)	646 (2.5)
Middle school: 6–8th grade	6,405 (14.2)	2,751 (14.3)	3,654 (14.1)
Middle–high school: 6–12th grade	2,137 (4.7)	969 (5.0)	1,168 (4.5)
High school: 9–12th grade	8,587 (19.0)	4,048 (21.0)	4,539 (17.5)
Not specified	430 (1.0)	306 (1.6)	124 (0.5)
Season			
Fall: Sep–Nov	18,298 (40.5)	11,660 (60.5)	6,638 (25.6)
Winter: Dec–Feb	22,651 (50.1)	5,694 (29.5)	16,957 (65.5)
Spring: Mar–May	2,818 (6.2)	1,642 (8.5)	1,176 (4.5)
Summer: Jun–Aug	1,413 (3.1)	277 (1.4)	1,136 (4.4)
Urbanicity			
City	17,689 (39.2)	6,734 (34.9)	10,955 (42.3)
Suburban	13,609 (30.1)	6,116 (31.7)	7,493 (28.9)
Town	4,429 (9.8)	1,959 (10.2)	2,470 (9.5)
Rural	9,098 (20.1)	4,181 (21.7)	4,917 (19.9)
Not specified	355 (0.8)	283 (1.5)	72 (0.3)
HHS region#			
HHS 1	1,906 (4.2)	1,301 (6.8)	605 (2.3)
HHS 2	4,556 (10.1)	3,146 (16.3)	1,410 (5.4)
HHS 3	5,642 (12.5)	2,886 (15.0)	2,756 (10.6)
HHS 4	9,399 (20.8)	3,978 (20.6)	5,421 (20.9)
HHS 5	9,646 (21.4)	3,627 (18.8)	6,019 (23.1)
HHS 6	5,103 (11.3)	1,050 (5.5)	4,053 (15.6)
HHS 7	2,217 (4.9)	588 (3.1)	1,634 (6.3)
HHS 8	2,493 (5.5)	872 (4.5)	1,621 (6.3)
HHS 9	2,334 (5.2)	1,453 (7.5)	881 (3.4)
HHS 10	1,879 (4.2)	372 (1.9)	1,507 (5.8)
No. students affected§**	25,837,466	11,232,072 (43.5)	14,605,394 (56.5)
No. teachers affected§††	1,710,459	752,264 (44.0)	958,195 (56.0)
% Students eligible for free or reduced-price lunch,§‡‡ median (IQR)	57.2 (33.2–83.2)	52.0 (28.8–79.1)	60.9 (37.0–85.7)
No. in-person student-days lost§§	205,689,158	159,968,778 (77.8)	45,720,380 (22.2)
No. unplanned closure days,¶¶ median (IQR)	4 (1–10)	10 (3–23)	2 (1–4)

*Values are no. (%) except as indicated. HHS, US Department of Health and Human Services; ID, identification; IQR, interquartile range; K, kindergarten; NCES, National Center for Education Statistics; PSS, the Private School Universe Survey.
†School years: 2020–21 (July 27, 2020–June 30, 2021), 2021–22 (August 1, 2021–June 30, 2022).
‡School closures were defined as a transition from being opened to being closed for in-person instruction excluding any scheduled days off; fully in-person and hybrid learning modalities were classified as open, and fully remote and closed were classified as closed. Closure events were documented at either the district-level or the individual school level on the basis of the source and scope of the closure decision as reported in the announcements.
§Schools were counted once for each time they were part of a school closure event at either the district-level or school level.
¶Number of schools closed in district-wide closures, total number of students, total number of teachers, number of students eligible for federal free or reduced-priced lunch, and number of schools by urbanicity and grade levels were estimated by matching the public school district ID or public school ID with the district or school data with the respective year, as obtained from NCES and private school ID with the 2019–20 private school data, as obtained from PSS. Because of missing information on urbanicity in 2021–22 NCES public school data, the information on urbanicity for the 2021–22 school year public school closures was obtained from the 2020–21 NCES public school data (*6*,*7*). School NCES ID was not found for 168 schools (124 for 2020–21 school year and 44 for 2021–22 school year), which were categorized as public or private by manual search on the basis of the location of schools in the school closure announcements.
#HHS regions defined at https://www.hhs.gov/about/agencies/regional-offices/index.html.
**Students were counted once for each school closure event. The number of students was missing for 562 schools (public, 325; private, 237).
††Teachers were counted once for each school closure event. Part-time teaching positions were reported as a fraction of 1 full-time position. The number of teachers was missing for 1,041 schools (public, 804; private, 237).
‡‡Data only for public schools.
§§In-person student-days lost estimated by multiplying the number of students per school by the number of unplanned closure days.
¶¶2,075 schools did not have reopening dates and defaulted to a 1-day closure; among these, 1,996 (96%) were during the 2020–21 school year.

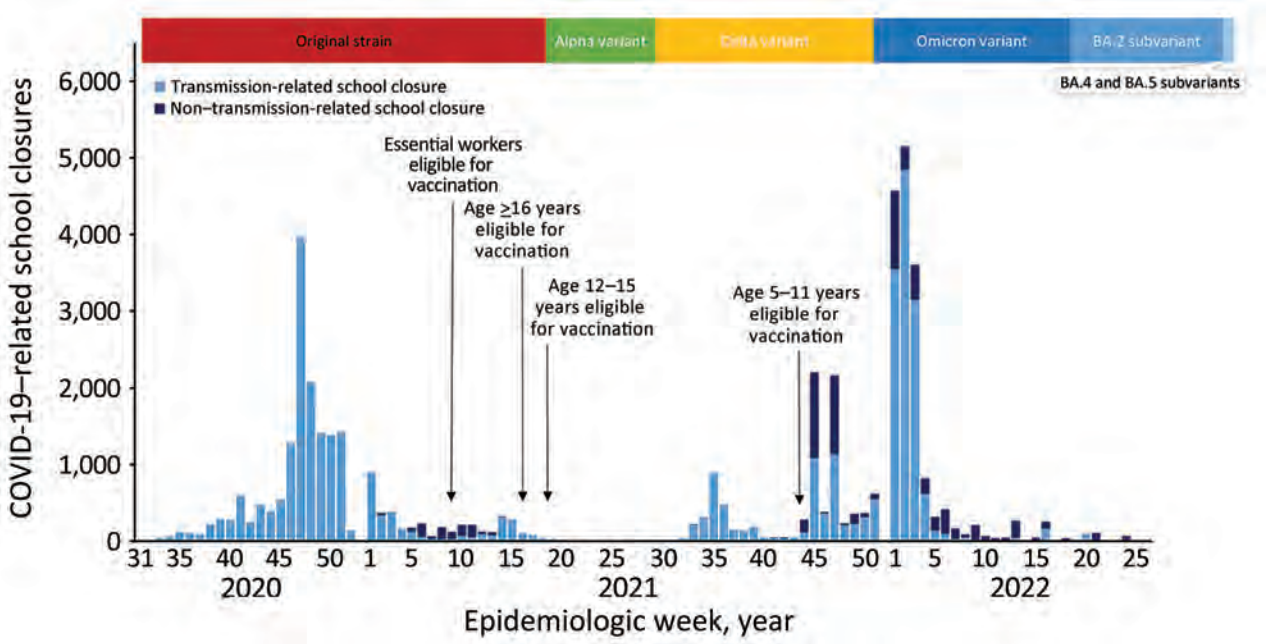

Figure 1. COVID-19–related school closures, dominant COVID-19 variants, and timing of vaccination availability, United States, July 27, 2020–June 30, 2022. School closure was defined as a transition from being open to being closed for in-person instruction excluding any scheduled days off; fully in-person and hybrid learning modalities were classified as open, and fully remote and closed were classified as closed. Transmission-related reasons were COVID-19 cases, suspected cases, increased student absenteeism, increased staff absenteeism, cluster or widespread transmission in the community, state or local guidance or mandate to close schools in response to COVID-19, to clean or disinfect school facilities, and other. Non–transmission-related reasons were COVID-19 vaccinations and side effects of vaccination of staff or students, teacher or staff shortage, for student or staff mental health, and other reasons associated with COVID-19. Timeline of COVID-19 variants derived from Centers for Disease Control and Prevention Museum COVID-19 Timeline (*11*) and defined as the point at which a variant accounted for the largest proportion of cases. Emergency Use Authorization by the Food and Drug Administration authorized COVID-19 vaccination for teachers and staff as part of the essential workforce on March 2, 2021, and all persons ≥16 years of age on April 19, 2021 (*12*). Advisory Committee on Immunization Practices recommended COVID-19 vaccination for persons 12–15 years of age on May 12, 2021, and for persons 5–11 years of age on November 2, 2021 (*11*).

by an estimated 25,907 COVID-SCs (Table 1). Among unique schools that experienced COVID-SCs, most closed once (77.5%), whereas >20% closed 2–8 times (Appendix Table 1). Most closures occurred in the first 3 weeks of 2022, peaking at epidemiologic week 2 (Figure 1). The median number of in-person school days lost per closure was 2 days (IQR 1–4 days) (Appendix Figure 1).

Closures occurred in all 50 states and the District of Columbia; >1,000 closures occurred in each of 7 states (Georgia, Illinois, Missouri, North Carolina, Ohio, Tennessee, and Texas) (Appendix Figure 3, panel A), accounting for more than one third of all COVID-SCs observed during the school year. COVID-SCs were experiences by more than half of the schools in Alabama (51.6%), Nevada (51.3%), and Oregon (51.2%) and by 40%–50% of schools in 8 additional states Colorado, Kentucky, Maryland, Nebraska, Oklahoma, Tennessee, Utah, and Virginia) (Appendix Figure 3, panel B).

Most COVID-SC events were attributed to positive cases in the schools (58.5% of district-level and 61.5% of school-level events) (Table 2). Non–transmission-related reasons accounted for a greater number of COVID-SCs than in the prior school year, particularly those attributable to long-term teacher or staff shortages (e.g., shortages related to hiring and retention challenges rather than directly linked to current disease transmission).

Transmission-related COVID-SCs were strongly correlated with weekly hospitalization rates for all ages (r = 0.81, 95% CI 0.67–0.89), among which correlation was moderate for the 5–17-year age group (r = 0.69, 95% CI 0.47–0.82) and strong for the 3 adult age groups (Table 4). Transmission-related COVID-SCs were moderately correlated with new COVID-19 cases (r = 0.61, 95% CI 0.38–0.76) and new COVID-19 deaths (r = 0.58, 95% CI 0.35–0.74), whereas we observed no significant correlation for percentage positive COVID-19 PCR tests (Table 3). The peak in

weekly COVID-SCs occurred within 1–2 weeks of the peaks in weekly new COVID-19 cases, percentage PCR positivity, and hospitalization rates and preceded the peak in weekly new COVID-19 deaths by 3 weeks (Figure 4, panels A–D; Figure 3, panel B).

Discussion

Our study describes COVID-19 school closures in the United States as school systems and communities grappled with ongoing disease transmission during a rapidly evolving pandemic. The COVID-SCs we analyzed reflect SARS-CoV-2 spread among school-aged children and staff, as demonstrated by the correlation between COVID-SCs and COVID-19 epidemiologic surveillance. The large increase in illness-related closures during the 2020–21 and 2021–22 school years, which was nearly 5-fold higher than those observed during severe influenza seasons, including the 2009 influenza (H1N1) pandemic (*16*) and subsequent moderate and severe influenza seasons (e.g., 2017–18, 2018–19, and 2019–20), was nearly fully attributed to COVID-19 (Zviedrite et al., unpub. data, https://doi.org/10.1101/2023.08.28.23294732). This increase probably reflected both ongoing transmission of SARS-CoV-2 and the greater clinical severity of COVID-19 infection among children compared with influenza, as demonstrated by both higher rates of hospitalization and higher rates of intensive care unit admission among those ≤18 years of age (*17*,*18*).

The most frequently documented reason for closure in both school years was COVID-19 cases in the school or school district. School year 2020–21 also had a significant number of closures attributable to increased community transmission and to state or local mandates to close schools in response to COVID-19, consistent with the changing incidence of COVID-19 among both the general population and children during the study period (*8*,*9*). COVID-SCs attributable to teacher absenteeism (because of illness in themselves or others) and teacher or staff shortages were more common in 2021–22 than in SY 2020–21. Although

Table 2. Reasons for COVID-19–related K–12 school closure, United States, July 27, 2020–June 30, 2022*

Reasons for school closure decision stated in closure announcement†	Total		2020–21‡		2021–22‡	
	District	School	District	School	District	School
COVID-19–related closure	3,443	7,441	1,528	4,794	1,915	2,647
COVID-19 only	85 (2.5)	123 (1.7)	43 (2.8)	76 (1.6)	42 (2.2)	49 (1.9)
COVID-19 and specific reasons	3,358 (97.5)	7,318(98.3)	1,485 (97.2)	4,718 (98.4)	1,873 (97.8)	2,598 (98.1)
Transmission-related reasons						
Positive case	1,845 (53.6)	4,511 (60.6)	724 (47.4)	2,829 (59.0)	1,121 (58.5)	1,682 (61.5)
In student	758 (22.0)	1,412 (19.0)	233 (15.2)	651 (13.6)	525 (27.4)	761 (28.7)
In staff member	763 (22.2)	1,359 (18.3)	226 (14.8)	575 (12.0)	537 (28.0)	784 (29.6)
In household member§	15 (0.4)	24 (0.3)	11 (0.7)	12 (0.3)	4 (0.2)	12 (0.5)
In visitor	2 (0.1)	0	2 (0.1)	0	0	0
Suspected case	78 (2.3)	224 (3.0)	64 (4.2)	173 (3.6)	14 (0.7)	51 (1.9)
In student	23 (0.7)	70 (0.9)	21 (1.4)	48 (1.0)	2 (0.1)	22 (0.8)
In staff member	33 (1.0)	71 (1.0)	27 (1.8)	53 (1.1)	6 (0.3)	18 (0.7)
In household member§	0	5 (0.1)	0	5 (0.1)	0	0
Increased student absenteeism	515 (15.0)	732 (9.8)	56 (3.7)	132 (2.8)	459 (24.0)	600 (31.3)
Increased staff absenteeism	1,022 (29.7)	1,955 (26.3)	183 (12.0)	536 (11.2)	839 (43.8)	1,419 (53.6)
Cluster or widespread transmission¶	1,096 (31.8)	1,918 (25.8)	727 (47.8)	1,556 (32.5)	369 (19.3)	362 (13.7)
State or local guidance or mandate	348 (10.1)	1,146 (15.4)	318 (20.8)	1,091 (22.8)	30 (1.6)	55 (2.1)
To clean or disinfect#	240 (7.0)	682 (9.2)	102 (6.7)	562 (11.7)	138 (7.2)	120 (4.5)
Other**	356 (10.3)	750 (10.1)	146 (9.6)	532 (11.1)	210 (11.0)	218 (8.2)
Non–transmission-related reasons						
Vaccination of staff or students	83 (2.4)	56 (0.8)	66 (4.3)	49 (1.0)	17 (0.9)	7 (0.3)
Side effects of vaccination	9 (0.3)	18 (0.2)	9 (0.6)	18 (0.4)	0	0
Teacher shortage	135 (3.9)	158 (2.1)	20 (1.3)	26 (0.5)	115 (6.0)	132 (5.0)
Mental health	158 (4.6)	48 (0.6)	0	0	158 (8.3)	48 (1.8)
Other††	17 (0.5)	32 (0.4)	0	10 (0.2)	17 (0.9)	22(0.8)

*Values are no. (%) except as indicated.
†Reasons are recorded as stated in the school closure announcements. Categories are not mutually exclusive because a closure announcement may attribute the closure to >1 factor, there may be >1 announcement that contributes the closure to different factors, or both.
‡School year: 2020–21 (July 27, 2020–June 30, 2021), 2021–22 (August 1, 2021–June 30, 2022).
§Of student or staff.
¶In the community.
#Classrooms, buildings, and facilities
**Other reasons were contact tracing, quarantine of students and staff, prevention of holiday-related surge, precautionary measure as a concern of community spread because of union wanting work stoppage, death of staff member, inability to find substitute teachers, transportation issues, critical lack of community resources (including contact tracers), testing, out of an abundance of caution, influenza or other respiratory virus-related or enteric virus-related illnesses, internet outage, facility issues, and noncompliance with governor's executive orders regarding nonpharmaceutical interventions.
††Other reasons were staff protesting in-person learning, protest over mask policy, transportation issue, lack of resources, allowing time for testing, and work on the COVID-19 mitigation plan.

Table 3. Weekly correlation between COVID-19–related school closures and COVID-19–related cases, deaths, and PCR positivity, by school year, United States, July 27, 2020–June 30, 2022*

			Weeks considered as winter school break†			
	Weeks 52–53		Weeks 52–53 or weeks 51–52		Weeks 53–1 or weeks 52–1	
School closure type	r (95% CI)	p value	r (95% CI)	p value	r (95% CI)	p value
Transmission-related school closures‡						
COVID-19 cases§						
2020–21	0.721 (0.544–0.832)	<0.001	0.728 (0.552–0.837)	<0.001	0.707 (0.521–0.824)	<0.001
2021–22	0.609 (0.384–0.760)	<0.001	0.591 (0.358–0.750)	<0.001	0.583 (0.346–0.744)	<0.001
COVID-19 deaths§						
2020–21	0.507 (0.255–0.688)	<0.001	0.510 (0.256–0.692)	<0.001	0.482 (0.221–0.673)	<0.001
2021–22	0.580 (0.346–0.741)	<0.001	0.592 (0.359–0.750)	<0.001	0.571 (0.331–0.736)	<0.001
PCR positivity¶						
2020–21	0.734 (0.563–0.840)	<0.001	0.748 (0.581–0.850)	<0.001	0.720 (0.540–0.832)	<0.001
2021–22	0.280 (−0.011–0.523)	0.056	0.245 (−0.052–0.497)	0.102	0.232 (−0.065–0.487)	0.122
Total school closures#						
COVID-19 cases§						
2020–21	0.772 (0.620–0.864)	<0.001	0.790 (0.645–0.876)	<0.001	0.761 (0.601–0.858)	<0.001
2021–22	0.511 (0.257–0.693)	<0.001	0.486 (0.223–0.678)	<0.001	0.478 (0.213–0.672)	0.001
COVID-19 deaths§						
2020–21	0.577 (0.345–0.737)	<0.001	0.589 (0.358–0.747)	<0.001	0.557 (0.316–0.725)	<0.001
2021–22	0.596 (0.367–0.751)	<0.001	0.610 (0.382–0.762)	<0.001	0.587 (0.353–0.747)	<0.001
PCR positivity¶						
2020–21	0.695 (0.506–0.815)	<0.001	0.721 (0.542–0.833)	<0.001	0.679 (0.480–0.806)	<0.001
2021–22	0.190 (−0.105–0.451)	0.202	0.149 (−0.149–0.420)	0.325	0.136 (−0.162–0.409)	0.369

*School closure is defined as a transition from being open to being closed for in-person instruction excluding any scheduled days off; fully in-person and hybrid learning modalities are classified as open, and fully remote and closed are classified as closed. School year: 2020–21 (July 27, 2020–June 30, 2021), 2021–22 (August 1, 2021–June 30, 2022). Spearman rank correlation (r) was used to evaluate the relationship between COVID-19–associated cases, deaths, and PCR positivity (epidemiologic weeks 31–26).

†School winter break was excluded from the analysis. The break is understood to be ≈2 weeks in length; however, the start and end dates vary by school and district. Winter breaks consistently overlap on the last week of the year, which was epidemiologic week 53 in 2020 and epidemiologic week 52 in 2021. In 2020, we calculated correlations excluding winter break at epidemiologic week 53, weeks 52–53, and weeks 53–1. In 2021, correlations were calculated excluding winter break at epidemiologic week 52, weeks 51–52, and weeks 52–1.

‡Transmission-related reasons were COVID-19 cases, suspected cases, increased student absenteeism, increased staff absenteeism, cluster or widespread transmission in the community, state or local guidance or mandate to close schools in response to COVID-19, to clean or disinfect school facilities, and other.

§Data on COVID-19 cases and COVID-19–associated deaths available from Centers for Disease Control and Prevention (*8*).

¶PCR positivity was calculated from the number of new positive results divided by the total number of new results reported. Data on PCR testing were available from US Department of Health and Human Services (*10*).

#Total school closures were both transmission and non–transmission-related school closures. Transmission-related reasons were COVID-19 cases, suspected cases, increased student absenteeism, increased staff absenteeism, cluster or widespread transmission in the community, state or local guidance or mandate to close schools in response to COVID-19, to clean or disinfect school facilities, and other. Non–transmission-related reasons were COVID-19 vaccinations and side effects of vaccination of staff or students, teacher or staff shortage, for student or staff mental health, and other reasons associated with COVID-19.

teacher shortages also were reported before the pandemic, they were exacerbated by the pandemic (*19*,*20*).

In 2020–21, the number of schools open to in-person education varied throughout the semester; some schools were teaching in-person, some relied solely on distance learning, some used hybrid or mixed methods, and others moved among different modalities in response to disease transmission and related guidance throughout the school year (*5*). COVID-19 transmission during 2020–21 was primarily dominated by the ancestral strain of SARS-CoV-2, which would only later be supplanted by new variants as the predominating virus in circulation (*21*,*22*). Most COVID-SCs in 2020–21 occurred in the first semester (August– December 2020) before peaks in COVID-19 epidemiologic surveillance data; the bulk occurred in the 2 weeks leading up to the 2020 Thanksgiving holiday break. The wording of reasons for closure as abstracted from some school closure announcements suggested that, amidst increasing transmission, schools and school districts were trying to take advantage of a planned break and lengthen the total time outside of the classroom by closing schools early. Despite recommendations from the Centers for Disease Control and Prevention against travel during the holiday (*23*), travel during Thanksgiving week of 2020 (November 22–28, 2020) was at its highest since the start of the pandemic 8 months prior (*24*,*25*). During this time of increased social gatherings and movement, many schools that closed before Thanksgiving chose to stay shuttered until after the subsequent winter break (*26*–*28*). Annual (school year) COVID-19 peaks in the epidemiologic surveillance data occurred in January 2021. After Emergency Use Authorization was issued by the Food and Drug Administration for the first COVID-19 vaccine in December 2020 (*29*), teachers and staff became eligible for vaccination as part of the

essential workforce on March 2, 2021, and all those ≥16 years of age became eligible for vaccination on April 19, 2021 (*12*). Subsequently, the succeeding Alpha variant began to predominate in early April 2021 (*11*,*22*), holding that position until June as the number of COVID-SCs slowed and remained comparably low.

Thereafter, the Delta variant, which was more transmissible and more severe than both the ancestral strain or Alpha variant (*30*,*31*), predominated through the start of school year 2021–22 until mid-December (*22*). During that period, the Food and Drug Administration's Emergency Use Authorizations for COVID-19 vaccines were extended to persons 12–15 years of age in May 2021 and to those 5–11 years of age in October 2021 (*11*), whereby all K–12 students, teachers, and staff were eligible for vaccination during the first half of the 2021–22 school year. Prior to the start of that school year, nearly 90% of teachers were vaccinated nationally (*32*). Expanded vaccine eligibility and high uptake among teachers and staff coincided with a return to in-person learning for nearly all schools in the United States in 2021–22 (*3*,*5*). In that school year, according to the epidemiologic surveillance data, COVID-19 peaked in January 2022 amid the domination of the Omicron variant, thus far characterized as the

Table 4. Weekly correlation between COVID-19–related school closures and laboratory-confirmed COVID-19–associated hospitalizations, by school year and age group, United States, July 27, 2020–June 30, 2022*

			Weeks considered as winter school break†			
	Weeks 52–53		Weeks 52–53 or weeks 51–52		Weeks 53–1 or weeks 52–1	
School closure type	r (95% CI)	P value	r (95% CI)	p value	r (95% CI)	p value
Transmission-related school closures‡						
2020–21						
All ages	0.639 (0.420–0.783)	<0.001	0.650 (0.431–0.791)	<0.001	0.618 (0.387–0.770)	<0.001
0–4 y	0.403 (0.119–0.620)	0.006	0.406 (0.120–0.625)	0.006	0.367 (0.074–0.596)	0.014
5–17 y	0.373 (0.085–0.598)	0.011	0.378 (0.087–0.604)	0.011	0.339 (0.043–0.575)	0.024
18–49 y	0.548 (0.298–0.722)	<0.001	0.548 (0.294–0.723)	<0.001	0.520 (0.258–0.705)	<0.001
50–64 y	0.622 (0.396–0.771)	<0.001	0.630 (0.404–0.778)	<0.001	0.599 (0.362–0.758)	<0.001
≥65 y	0.669 (0.461–0.802)	<0.001	0.685 (0.480–0.813)	<0.001	0.650 (0.431–0.791)	<0.001
2021–22						
All ages	0.812 (0.667–0.894)	<0.001	0.803 (0.650–0.890)	<0.001	0.798 (0.641–0.886)	<0.001
0–4 y	0.357 (0.051–0.596)	0.021	0.321 (0.006–0.572)	0.043	0.308 (−0.008–0.563)	0.053
5–17 y	0.687 (0.474–0.818)	<0.001	0.676 (0.454–0.813)	<0.001	0.663 (0.436–0.805)	<0.001
18–49 y	0.761 (0.586–0.864)	<0.001	0.750 (0.565–0.858)	<0.001	0.743 (0.555–0.854)	<0.001
50–64 y	0.827 (0.692–0.903)	<0.001	0.820 (0.677–0.899)	<0.001	0.814 (0.668–0.896)	<0.001
≥65 y	0.700 (0.494–0.827)	<0.001	0.685 (0.468–0.818)	<0.001	0.677 (0.457–0.814)	<0.001
Total school closures§						
2020–21						
All ages	0.651 (0.437–0.791)	<0.001	0.675 (0.467–0.807)	<0.001	0.631 (0.405–0.779)	<0.001
0–4 y	0.386 (0.100–0.608)	0.008	0.401 (0.114–0.621)	0.007	0.349 (0.054–0.582)	0.020
5–17 y	0.351 (0.060–0.581)	0.018	0.368 (0.075–0.596)	0.014	0.315 (0.016–0.557)	0.037
18–49 y	0.533 (0.278–0.712)	<0.001	0.5444 (0.288–0.721)	<0.001	0.503 (0.237–0.693)	<0.001
50–64 y	0.630 (0.407–0.776)	<0.001	0.651 (0.432–0.791)	<0.001	0.608 (0.373–0.763)	<0.001
≥65 y	0.720 (0.535–0.834)	<0.001	0.752 (0.580–0.855)	<0.001	0.705 (0.510–0.826)	<0.001
2021–22						
All ages	0.708 (0.518–0.827)	<0.001	0.693 (0.492–0.818)	<0.001	0.689 (0.486–0.815)	<0.001
0–4 y	0.470 (0.200–0.668)	0.001	0.442 (0.162–0.650)	0.002	0.433 (0.152–0.644)	0.003
5–17 y	0.646 (0.429–0.787)	<0.001	0.630 (0.404–0.778)	<0.001	0.621 (0.391–0.772)	<0.001
18–49 y	0.645 (0.427–0.786)	<0.001	0.625 (0.397–0.775)	<0.001	0.620 (0.390–0.771)	<0.001
50–64 y	0.723 (0.539–0.836)	<0.001	0.708 (0.514–0.828)	<0.001	0.704 (0.508–0.825)	<0.001
≥65 y	0.677 (0.472–0.806)	<0.001	0.659 (0.443–0.797)	<0.001	0.654 (0.437–0.793)	<0.001

*School closure is defined as a transition from being open to being closed for in-person instruction excluding any scheduled days off; fully in-person and hybrid learning modalities are classified as open, and fully remote and closed are classified as closed. School year: 2020–21 (July 27, 2020–June 30, 2021), 2021–22 (August 1, 2021–June 30, 2022). Data on laboratory-confirmed COVID-19–associated hospitalizations was available from COVID-NET (*9*). Spearman rank correlation (r) was used to evaluate the relationship between COVID-19–associated cases, deaths, and PCR-positivity (epidemiologic weeks 31–26).

†School winter break was excluded from the analysis. The break is understood to be ≈2 weeks in length; however, the start and end dates vary by school and district. Winter breaks consistently overlap on the last week of the year, which was epidemiologic week 53 in 2020 and epidemiologic week 52 in 2021. In 2020, we calculated correlations excluding winter break at epidemiologic week 53, weeks 52–53, and weeks 53–1. In 2021, correlations were calculated excluding winter break at epidemiologic week 52, weeks 51–52, and weeks 52–1.

‡Transmission-related reasons were COVID-19 cases, suspected cases, increased student absenteeism, increased staff absenteeism, cluster or widespread transmission in the community, state or local guidance or mandate to close schools in response to COVID-19, to clean or disinfect school facilities, and other.

§Total school closures were both transmission and non–transmission-related school closures. Transmission-related reasons were COVID-19 cases, suspected cases, increased student absenteeism, increased staff absenteeism, cluster or widespread transmission in the community, state or local guidance or mandate to close schools in response to COVID-19, to clean or disinfect school facilities, and other. Non–transmission-related reasons were COVID-19 vaccinations and side effects of vaccination of staff or students, teacher or staff shortage, for student or staff mental health, and other reasons associated with COVID-19.

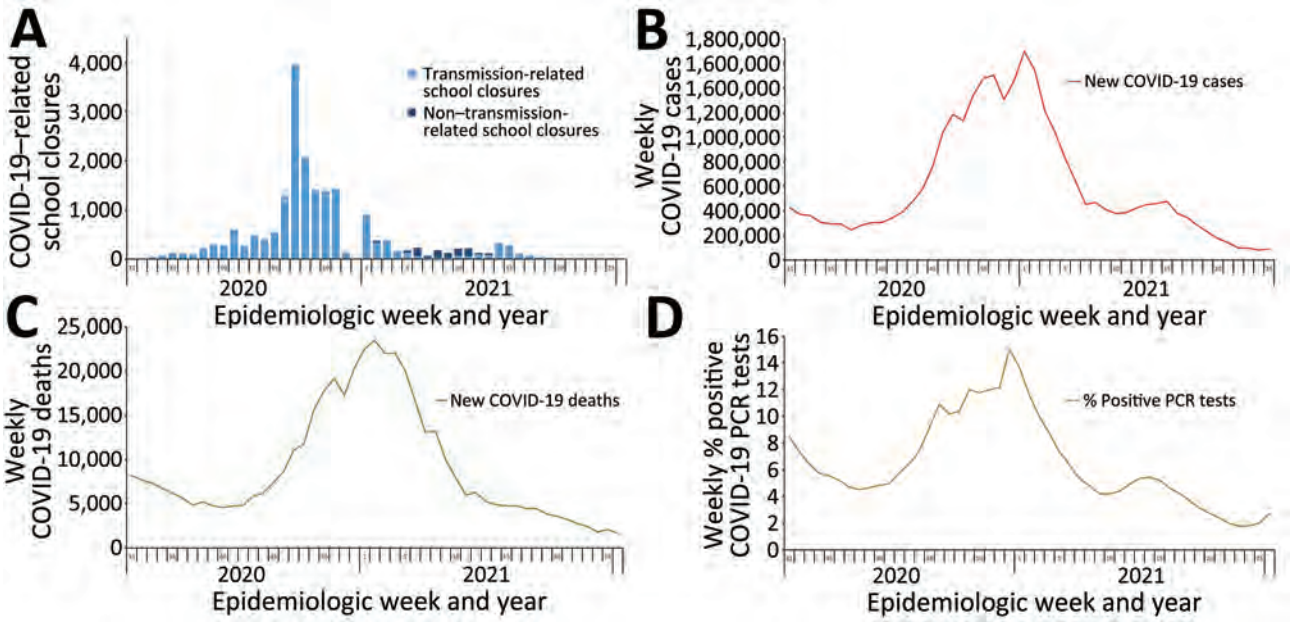

Figure 2. COVID-19–related school closures and COVID-related cases, deaths, and PCR positivity by school year, United States, July 27, 2020–June 30, 2021. School closure, transmission-related reasons, and non–transmission-related reasons are defined in the Figure 1 legend. Data on COVID-19 cases and COVID-19–associated deaths available from Centers for Disease Control and Prevention (*8*). PCR positivity was calculated from the number of new positive results divided by the total number of new results reported. Data on PCR testing were available from US Department of Health and Human Services (*10*). School year: 2020–21 (July 27, 2020–June 30, 2021).

fastest-spreading variant (*33*), and was matched with the highest weekly counts of COVID-SCs. Although we observed lower correlation of COVID-SCs with COVID-19 cases and percentage PCR positivity in 2021–22 than in the previous year, correlations with new deaths and hospitalization rates were both higher.

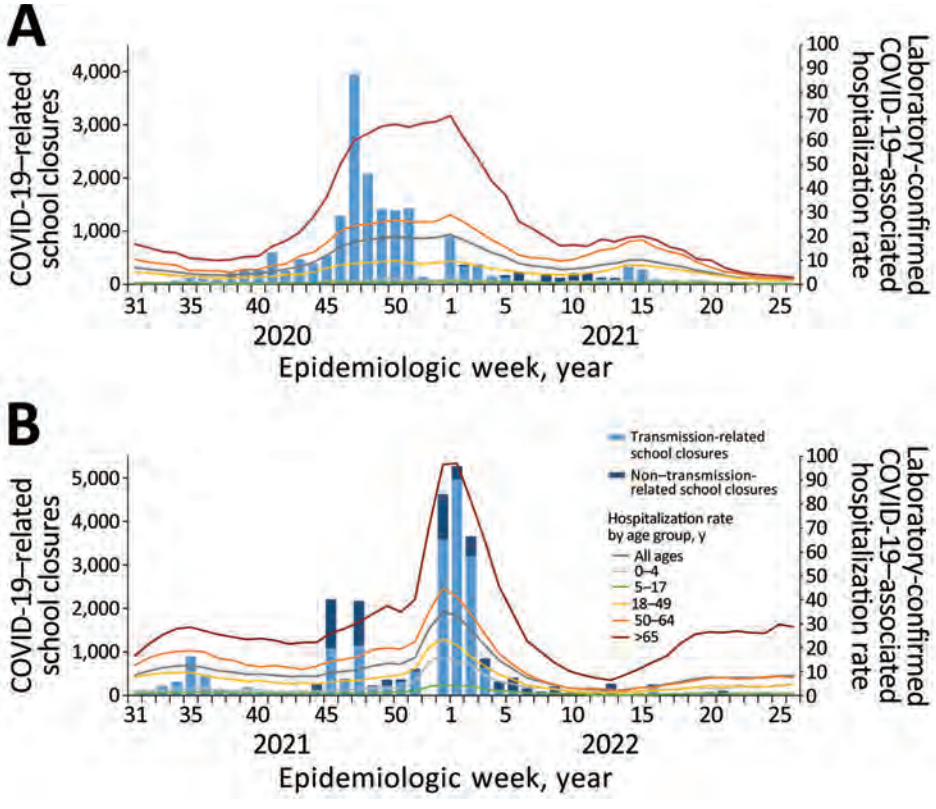

Figure 3. COVID-19–related school closures and laboratory-confirmed COVID-19–related hospitalizations by age group, United States, July 27, 2020–June 30, 2022. A) School year 2020–21 (July 27, 2020–June 30, 2021); B) school year 2021–22 (August 1, 2021–June 30, 2022). School closure, transmission-related reasons, and non–transmission-related reasons are defined in the Figure 1 legend. Data on laboratory-confirmed COVID-19–associated hospitalizations available from COVID-NET (*9*).

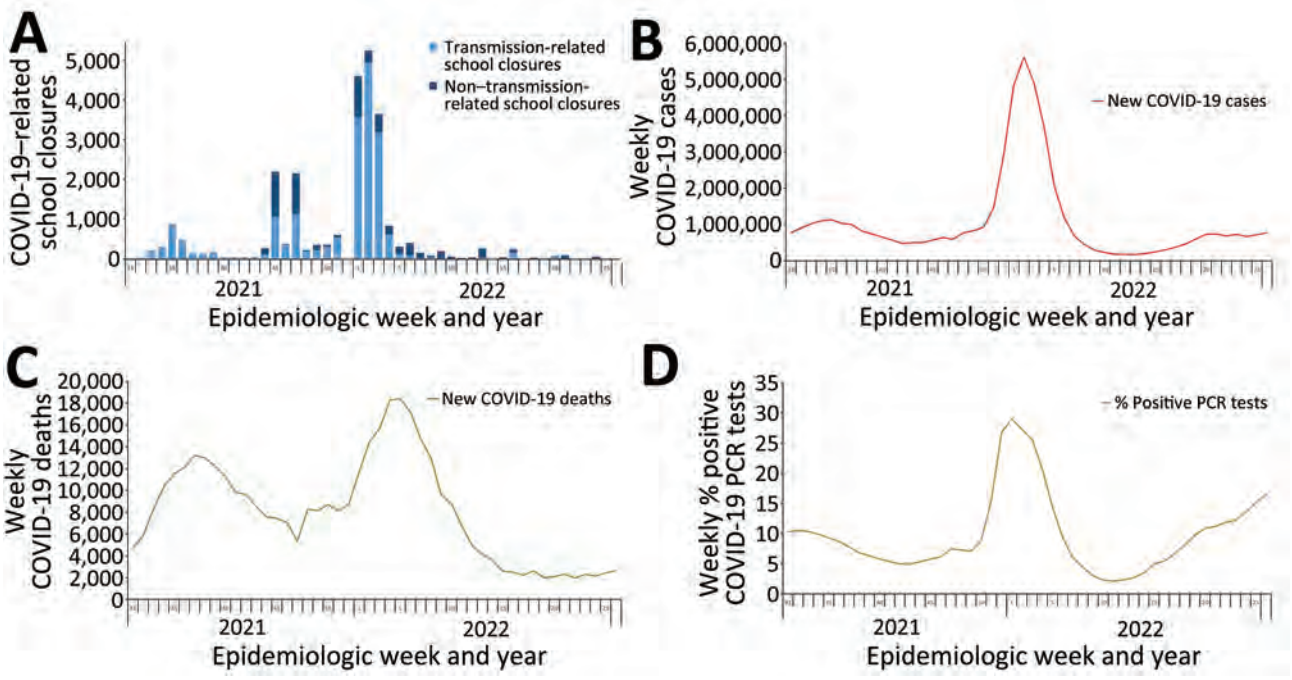

Figure 4. COVID-19–related school closures and COVID-related cases, deaths, and PCR positivity by school year, United States, August 1, 2021–June 30, 2022. School closure, transmission-related reasons, and non–transmission-related reasons are defined in the Figure 1 legend. Data on COVID-19 cases and COVID-19–associated deaths available from Centers for Disease Control and Prevention (*8*). PCR positivity was calculated from the number of new positive results divided by the total number of new results reported. Data on PCR testing were available from US Department of Health and Human Services (*10*). School year: 2021–22 (August 1, 2021–June 30, 2022).

Strong correlation between COVID-SCs and hospitalization rates may suggest that COVID-SCs are not only associated with disease prevalence but also with the severity of the dominant circulating variant.

Various prevention measures were implemented in schools and districts to prevent the spread of SARS-CoV-2 (*34*) and thereby reduce the number of COVID-SCs. However, disparities in their implementation have been observed across locales and school poverty levels (*34*). Infection-prevention measures include nonpharmaceutical interventions that can be rapidly implemented in schools, such as masking, social distancing, and quarantining, all of which have previously been shown to be effective at slowing influenza transmission in community congregate settings (*35*); at least 1 study documented that use of face masks reduces SARS-CoV-2 infection incidence in K–12 schools (*36*).

One limitation of our study is that reports are limited to publicly available data, and some closures may have been missed depending on how they were reported. In addition, data may be incomplete for various reasons, including delays in identifying public announcements of school closures, incomplete or unavailable public announcements, or lags in data entry. Moreover, lengths of closure may be unknown when the specific date of reopening cannot be ascertained or because the school or district remains closed. Furthermore, learning modality may not be specified in the data abstraction source (the announcement, website, or both) and the data may therefore not capture all transitions from in-person to distance learning. However, the data were collected without burdening schools or districts and were readily available in near real-time. Those limitations probably lead to underestimation of the number and duration of school closures. Therefore, our results likely convey the lower range of the impact of COVID-SCs during this period.

The COVID-SC data we describe were collected as part of an ongoing research project to document how school closures occur outside of an influenza pandemic (*1*). In the absence of a true surveillance system, those data were the most timely and comprehensive data available on COVID-SCs from the early days of the pandemic. This project documented near-simultaneous nationwide closures implemented as a mitigation strategy during the spring of 2020 (*2*) and an unprecedented number of illness-related reactive school closures during the 2 subsequent school years, 2020–21 and 2021–22. These data could be used

in conjunction with epidemiologic surveillance and other data for future computer simulations to explore the impact of the COVID-19 pandemic at various geographic levels and to help evaluate effectiveness of contemporaneous pandemic interventions. Specifically, we encourage further research, including high-resolution modeling studies, for locales where early reactive closures occurred (i.e., those with closures occurring in the weeks before COVID-19 peaks were observed in the epidemiologic data) to explore the effects of these closures on communitywide transmission. Given that COVID-19 is already established as an endemic disease and respiratory pathogens other than SARS-CoV-2 will reestablish circulation, local outbreaks of COVID-19, influenza, and other diseases will probably continue to occur, and some will cause reactive school closures. The continued monitoring of disease-related school closures should preserve the ability to detect their occurrence in near–real-time as a component of community-based surveillance during pandemics and severe outbreaks. In addition, ongoing surveillance for disease-related school closures would help in understanding their underlying causes, scale, and distribution and would enable evaluation of their effects on schools and communities.

Acknowledgments

We thank the data collection team, including our unit ORISE Fellows (Livvy Shafer, Pallavi Malla, and Larry Ayer) and contractors (Tamara Cummings, Jasminn Evans, Atea Francis, Elisha Gilbert, Esther Amoakohene, and Zaneta Oliver).

This work was supported by the Centers for Disease Control and Prevention (CDC). The coauthors are or were employees of CDC (N.Z., F.A., and A.U.), contractors at CDC (F.J.), or ORISE Fellows (S.M.) at the time of the study. F.J. is employed by Cherokee Nation Operational Solutions, LLC. The funder (Cherokee Nation Operational Solutions, LLC) provided support in the form of salary for the author (F.J.), but did not have any additional role in the study design, data collection and analysis, decision to publish, or preparation of the manuscript. During the study period, S.M. was a fellow appointed through the Research Participation Program at CDC administered by the Oak Ridge Institute for Science and Education through an interagency agreement between the US Department of Energy and CDC.

About the Author

Ms. Zviedrite is an epidemiologist at CDC's National Center for Emerging and Zoonotic Infectious Diseases in the Division of Global Migration Health. Her primary research interests include the use of nonpharmaceutical interventions in response to influenza and other respiratory diseases, particularly in school settings, and, more recently, infectious disease epidemiology in the United States–Mexico border region.

References

1. Wong KK, Shi J, Gao H, Zheteyeva YA, Lane K, Copeland D, et al. Why is school closed today? Unplanned K–12 school closures in the United States, 2011–2013. PLoS One. 2014;9:e113755. https://doi.org/10.1371/journal.pone.0113755
2. Zviedrite N, Hodis JD, Jahan F, Gao H, Uzicanin A. COVID-19-associated school closures and related efforts to sustain education and subsidized meal programs, United States, February 18–June 30, 2020. PLoS One. 2021; 16:e0248925. https://doi.org/10.1371/journal.pone.0248925
3. Parks SE, Zviedrite N, Budzyn SE, Panaggio MJ, Raible E, Papazian M, et al. COVID-19–related school closures and learning modality changes—United States, August 1–September 17, 2021. MMWR Morb Mortal Wkly Rep. 2021;70:1374–6. https://doi.org/10.15585/mmwr.mm7039e2
4. MCH Strategic Data. COVID-19 impact: school district operational status, updates for Spring 2021. 2021 [cited 2022 Nov 18]. https://www.mchdata.com/covid19/schoolclosings
5. Burbio, Inc. K–12 school opening tracker. 2022 [cited 2022 Nov 18]. https://about.burbio.com/school-opening-tracker
6. National Center for Education Statistics. Common core of data. [cited 2023 Apr 5]. http://nces.ed.gov/ccd
7. National Center for Education Statistics. Private School Universe Survey [cited 2022 Mar 21]. https://nces.ed.gov/surveys/pss
8. Centers for Disease Control and Prevention, COVID-19 response. COVID-19 case surveillance public data access, summary, and limitations [cited 2023 Mar 15]. https://data.cdc.gov/Case-Surveillance/COVID-19-Case-Surveillance-Public-Use-Data/vbim-akqf
9. Centers for Disease Control and Prevention. COVID-NET: COVID-19–Associated Hospitalization Surveillance Network [cited 2023 Mar 7]. https://gis.cdc.gov/grasp/covidnet/covid19_5.html
10. US Department of Health and Human Services. COVID-19 diagnostic laboratory testing (PCR testing) time series [cited 2023 Mar 15]. https://beta.healthdata.gov/dataset/COVID-19-Diagnostic-Laboratory-Testing-PCR-Testing/j8mb-icvb
11. Centers for Disease Control and Prevention. CDC Museum COVID-19 timeline [cited 2023 Apr 7]. https://www.cdc.gov/museum/timeline/covid19.html
12. US Department of Health and Human Services. Coronavirus: COVID-19 vaccines. 2022 [cited 2023 Apr 7]. https://www.hhs.gov/coronavirus/covid-19-vaccines/index.html
13. Shapiro E. New York City to close public schools again as virus cases rise. The New York Times. 2021 [cited 2023 Feb 21]. https://www.nytimes.com/2020/11/18/nyregion/nyc-schools-covid.html
14. Commonwealth of Kentucky Office of the Governor. Executive order 2020-969: state of emergency. 2020 Nov 18 [cited 2023 Feb 21]. https://governor.ky.gov/attachments/20201118_Executive-Order_2020-969_State-of-Emergency.pdf
15. Michigan Department of Health and Human Services. Emergency order under MCL 333.2253: gatherings and face mask order. 2020 Nov 15 [2023 Feb 21].

https://www.michigan.gov/coronavirus/resources/orders-and-directives/lists/executive-directives-content/gatherings-and-face-mask-order-4
16. Kann L, Kinchen S, Modzelski B, Sullivan M, Carr D, Zaza S, et al. ILI-related school dismissal monitoring system: an overview and assessment. Disaster Med Public Health Prep. 2012;6:104–12. https://doi.org/10.1001/dmp.2012.13
17. Delahoy MJ, Ujamaa D, Taylor CA, Cummings C, Anglin O, Holstein R, et al. Comparison of influenza and coronavirus disease 2019-associated hospitalizations among children younger than 18 years old in the United States: FluSurv-NET (October–April 2017–2021) and COVID-NET (October 2020–September 2021). Clin Infect Dis. 2023;76:e450–9. https://doi.org/10.1093/cid/ciac388
18. Shein SL, Carroll CL, Remy KE, Rogerson CM, McCluskey CK, Lin A, et al. Epidemiology and outcomes of SARS-CoV-2 infection or multisystem inflammatory syndrome in children vs influenza among critically ill children. JAMA Netw Open. 2022;5:e2217217. https://doi.org/10.1001/jamanetworkopen.2022.17217
19. Schmitt J, deCourcy K. The pandemic has exacerbated a long-standing national shortage of teachers. 2022 Dec 6 [cited 2023 May 8]. https://www.epi.org/publication/shortage-of-teachers
20. National Center for Education Statistics. US schools report increased teacher vacancies due to COVID-19 pandemic, new NCES data show. 2022 Mar 3 [cited 2023 May 8]. https://nces.ed.gov/whatsnew/press_releases/3_3_2022.asp
21. Centers for Disease Control and Prevention. COVID data tracker. 2023 Mar 21 [cited 2023 Mar 21]. https://covid.cdc.gov/covid-data-tracker
22. Hodcroft EB. CoVariants. 2021 [cited 2023 Apr 7]. https://covariants.org
23. Fox M. CDC recommends against travel for Thanksgiving. CNN. 2020 Nov 19 [cited 2023 Mar 28]. https://www.cnn.com/2020/11/19/health/cdc-thanksgiving-travel-wellness-bn/index.html
24. US Bureau of Transportation Statistics. Thanksgiving week travel: total number of trips down, long distance trips up over last year. 2020 [cited 2023 Mar 28]. https://www.bts.gov/data-spotlight/thanksgiving-travel-long-distance-trips-are-up
25. Perrone M, Renault M. Heading into holidays, US COVID-19 testing strained again. AP News. 2020 [cited 2023 Mar 8]. https://apnews.com/article/us-covid-19-testing-strained-holidays-db20ebbcc1fa8a411be8f9ebc241af3b
26. Mangrum M. All metro Nashville public schools students to stay remote after Thanksgiving. The Tennessean. 2020 [cited 2023 Mar 8]. https://www.tennessean.com/story/news/education/2020/11/23/mnps-schools-stay-closed-after-thanksgiving-coronavirus-spike/6342873002
27. Kelley JP. Dayton schools to hold no classes for next 6 weeks, go to school in June instead. Dayton [Ohio] Daily News. 2020 [cited 2023 Mar 2]. https://www.daytondailynews.com/local/six-week-break-part-of-big-change-to-dps-academic-calendar/V6ML2EHHVZCEPOU2YJJJDFT33E
28. Sawchuk S, Gewertz C. Schools are retreating to remote learning as COVID-19 surges. Do they have to? Education Week. 2020 [cited 2023 Mar 2]. https://www.edweek.org/leadership/schools-are-retreating-to-remote-learning-as-covid-19-surges-do-they-have-to/2020/11
29. US Food and Drug Administration. FDA approves first COVID-19 vaccine—approval signifies key achievement for public health. 2021 Aug 23 [cited 2023 Apr 7]. https://www.fda.gov/news-events/press-announcements/fda-approves-first-covid-19-vaccine
30. Earnest R, Uddin R, Matluk N, Renzette N, Turbett SE, Siddle KJ, et al.; New England Variant Investigation Team. Comparative transmissibility of SARS-CoV-2 variants Delta and Alpha in New England, USA. Cell Rep Med. 2022;3:100583. https://doi.org/10.1016/j.xcrm.2022.100583
31. Twohig KA, Nyberg T, Zaidi A, Thelwall S, Sinnathamby MA, Aliabadi S, et al.; COVID-19 Genomics UK (COG-UK) Consortium. Hospital admission and emergency care attendance risk for SARS-CoV-2 Delta (B.1.617.2) compared with Alpha (B.1.1.7) variants of concern: a cohort study. Lancet Infect Dis. 2022;22:35–42. https://doi.org/10.1016/S1473-3099(21)00475-8
32. White House. Fact sheet: President Biden to announce new actions to get more Americans vaccinated and slow the spread of the Delta variant. 2021 [cited 2023 Mar 22]. https://www.whitehouse.gov/briefing-room/statements-releases/2021/07/29/fact-sheet-president-biden-to-announce-new-actions-to-get-more-americans-vaccinated-and-slow-the-spread-of-the-delta-variant
33. Liu Y, Rocklöv J. The effective reproductive number of the Omicron variant of SARS-CoV-2 is several times relative to Delta. J Travel Med. 2022;29:taac037. https://doi.org/10.1093/jtm/taac037
34. Pampati S, Rasberry CN, Timpe Z, McConnell L, Moore S, Spencer P, et al. Disparities in implementing COVID-19 prevention strategies in public schools, United States, 2021–22 school year. Emerg Infect Dis. 2023;29:937–44. https://doi.org/10.3201/eid2905.221533
35. Qualls N, Levitt A, Kanade N, Wright-Jegede N, Dopson S, Biggerstaff M, et al. Community mitigation guidelines to prevent pandemic influenza—United States, 2017. MMWR Recomm Rep. 2017;66:1–34.
36. Donovan CV, Rose C, Lewis KN, Vang K, Stanley N, Motley M, et al. SARS-CoV-2 incidence in K–12 school districts with mask-required versus mask-optional policies—Arkansas, August–October 2021. MMWR Morb Mortal Wkly Rep. 2022;71:384–9. https://doi.org/10.15585/mmwr.mm7110e1

Address for correspondence: Nicole Zviedrite, Centers for Disease Control and Prevention, 1600 Clifton Rd NE, Mailstop V18-2, Atlanta, GA 30329-4018, USA; email: jmu6@cdc.gov

Effectiveness of Vaccines and Antiviral Drugs in Preventing Severe and Fatal COVID-19, Hong Kong

Yue Yat Harrison Cheung,[1] Eric Ho Yin Lau,[1] Guosheng Yin, Yun Lin, Benjamin J. Cowling, Kwok Fai Lam

We compared the effectiveness and interactions of molnupiravir and nirmatrelvir/ritonavir and 2 vaccines, CoronaVac and Comirnaty, in a large population of inpatients with COVID-19 in Hong Kong. Both the oral antiviral drugs and vaccines were associated with lower risks for all-cause mortality and progression to serious/critical/fatal conditions (study outcomes). No significant interaction effects were observed between the antiviral drugs and vaccinations; their joint effects were additive. If antiviral drugs were prescribed within 5 days of confirmed COVID-19 diagnosis, usage was associated with lower risks for the target outcomes for patients ≥60, but not <60, years of age; no significant clinical benefit was found if prescribed beyond 5 days. Among patients ≥80 years of age, 3–4 doses of Comirnaty vaccine were associated with significantly lower risks for target outcomes. Policies should encourage COVID-19 vaccination, and oral antivirals should be made accessible to infected persons within 5 days of confirmed diagnosis.

Since the outbreak of the COVID-19 pandemic in 2019, scientists around the world have raced to discover effective treatments and vaccinations that mitigate the spread of this highly contagious disease; many old drugs have been repurposed for COVID-19 treatment (*1*). Molnupiravir, approved by the US Food and Drug Administration (*2*) for medical use in December 2021, is one of the first oral antiviral drugs shown to inhibit the replication of SARS-CoV-2 virus and to be effective in treating COVID-19 patients (*3*). A double-blind, randomized, controlled, phase 2 trial of unvaccinated and vaccinated patients with early SARS-CoV-2 infection was conducted in the United Kingdom during November 18, 2020–March 16, 2022; results showed molnupiravir recipients had faster median time from randomization to a negative SARS-CoV-2 PCR (primary outcome) than nonrecipients (*4*). Results from MOVe-OUT and MOVe-IN trials suggest that molnupiravir is most effective when treatment is initiated early to patients with mild to moderate COVID-19 who do not require hospitalization but have high risk for severe disease (*5*,*6*). The oral nirmatrelvir/ritonavir combination, also approved by the US Food and Drug Adminstration for medical use in December 2021 (*7*), is another weapon in the arsenal against COVID-19. MOVe-IN, MOVe-OUT, and EPIC-HR trials evaluating nirmatrelvir/ritonavir efficacy suggest that the combination can effectively reduce risks for death and progression to severe disease for patients with mild to moderate COVID-19 (*8*,*9*).

Vaccination is another available tool to mitigate the spread of COVID-19. CoronaVac (Sinovac, http://www.sinovac.com), a whole inactivated virus vaccine, is a popular vaccine choice in the pan-Pacific region and in many developing countries. A double-blind, randomized, controlled, phase 3 trial conducted in Turkey showed CoronaVac has a good safety profile and can effectively reduce the risk for PCR-confirmed, symptomatic SARS-CoV-2 infection and severe COVID-19 (*10*). Results from a large-scale, prospective cohort study in Chile suggested that CoronaVac can effectively prevent SARS-CoV-2 infection and reduce the risks of COVID-19–induced hospitalization, severe disease, and death. Whereas early clinical trials demonstrated the safety and tolerability of CoronaVac among the elderly (*11*), children (*12*), and persons with autoimmune rheumatic diseases (*13*), recent trials have compared the safety and efficacy of the CoronaVac booster with other vaccines

Author affiliations: The University of Hong Kong, Hong Kong, China (Y.Y.H. Cheung, E.H.Y. Lau, G. Yin, Y. Lin, B.J. Cowling, K.F. Lam); Hong Kong Science and Technology Park, Hong Kong (E.H.Y. Lau, B.J. Cowling); Imperial College London, London, UK (G. Yin); Duke-NUS Medical School, Singapore (K.F. Lam)

DOI: https://doi.org/10.3201/eid3001.230414

[1]These first authors contributed equally to this manuscript.

(*14*,*15*). Comirnaty (Pfizer-BioNTech, https://www.pfizer.com), an mRNA-based vaccine, is another popular vaccination choice to prevent COVID-19. Similar to the case for CoronaVac, abundant clinical trials and studies have proven safety and efficacy of the Comirnaty vaccine against COVID-19–related hospitalization, death, and severe outcomes (*16*–*19*).

Although clinical trials and studies have demonstrated the efficacy of oral antiviral drugs and vaccinations against COVID-19, real-world evidence is needed to determine the effectiveness of such interventions when used in combination. Furthermore, it would be of interest to explore and evaluate potential interactions, if any, between oral antiviral drugs, vaccinations, and age. Therefore, we compared the effectiveness and interactions of molnupiravir and nirmatrelvir/ritonavir and 2 vaccines, CoronaVac and Comirnaty, in a large population of inpatients with COVID-19.

Methods

Study Design

We analyzed data from a territory-wide population cohort of adult hospital inpatients in Hong Kong who had confirmed diagnoses of SARS-CoV-2 infection during March 16–October 31, 2022. Our study received ethics approval from the Institutional Review Board of The University of Hong Kong.

Data Sources and Study Population

We used data from electronic health records of hospital patients with SARS-CoV-2 infections extracted from the Clinical Management System of Hong Kong Hospital Authority, which is the statutory body that manages all public hospitals in Hong Kong. The deidentified records contained patient age (which we stratified into groups 18–59, 60–79, and ≥80 years) (*20*–*22*), gender, occupation, symptomatic status, chronic disease history, dates of confirmed SARS-CoV-2 infection, symptom onset, admission date, discharge date, whether infection developed into serious/critical/fatal conditions, and oral antiviral drug prescriptions. We matched and merged patient records with anonymized population-based vaccination records provided by the Centre for Health Protection, Hong Kong Department of Health, via a unique identification key. Vaccination variables were vaccination type, vaccination date, and number of doses. License restrictions apply to the availability of the research data used in this study.

We included adult inpatients if they had a confirmed diagnosis of SARS-CoV-2 infection and were admitted to a local public hospital during the study period. We excluded patients who received both types of oral antiviral drugs (1,421 patients received both molnupiravir and nirmatrelvir/ritonavir), received both types of vaccinations (1,540 patients received both CoronaVac and Comirnaty) or nonlocal vaccinations (167 patients), had missing vaccination dates (49 patients), or received oral antiviral drugs during or after infection developed into a serious or critical condition (362 patients). We evaluated the study population according to treatment and vaccination status (Appendix Table 1, https://wwwnc.cdc.gov/EID/article/30/1/23-0414-App1.pdf).

Time-Dependent Variable

We indexed the hazard function according to calendar day; oral treatment status was time-dependent. The use of time-dependent treatment status can address the issue of immortal time bias, which arises in many retrospective studies when determining a patient's treatment status involves a waiting period (e.g., waiting for a prescription to be dispensed). During this waiting period, treated patients are considered immortal because they have to survive until the treatment definition is fulfilled (*23*). To address the issue of immortal time bias, patients who lived long enough to receive treatment were defined as unexposed to the treatment before prescription and only defined as exposed to the treatment on the prescription day and thereafter. When compared with patients who were too ill and did not live long enough to receive the oral treatment, an unexposed treatment status helped resolve the issue of immortal time interval between infection and treatment prescription. If an oral antiviral drug was prescribed, we further indicated whether the prescription was made within or after 5 days of the confirmed COVID-19 diagnosis (*24*–*27*).

We also considered age, gender, Charlson comorbidity index, vaccination type, and number of doses as predictors in our analyses. For generalized-likelihood ratio tests, we evaluated those variables with the first and second order interaction effects between age, vaccination, and oral treatment status.

Outcomes and Follow-Up Period

The primary outcome was all-cause mortality. The secondary outcome was disease development into a serious/critical/fatal case, comprising a composite outcome of disease progression (all-cause mortality, 3 L/min oxygen supplementation required, intensive care unit admission, intubation, extracorporeal membrane oxygenation, or shock).

The follow-up period for each patient was 28 days, starting from the date of confirmed COVID-19 diagnosis (*28*). We censored data from hospitalized patients who were discharged or never experienced the events of interest within the follow-up period. In the analyses related to the secondary outcome, we defined the date of the event as the date the illness turned serious or critical or the date of in-hospital death, whichever came first.

Statistical Analysis

We used a proportional hazards regression model with a calendar day setting (*29*–*32*) and time-dependent variables to estimate and compare the effectiveness of molnupiravir and nirmatrelvir/ritonavir treatments and CoronaVac or Comirnaty vaccines against death or progression to severe COVID-19 among hospitalized patients. The hazard function of a patient on calendar day t was defined as the baseline hazard function of day t multiplied by a function of a predictor, such as age, sex, vaccination status, time-dependent oral treatment status, or their interactions. Because the hazard function was indexed by calendar day, patients were only compared if they had a confirmed COVID-19 diagnosis and were hospitalized during roughly the same period (i.e., with overlapping follow-up windows). Thus, confounding factors arising from the ever-changing baseline hazard function during different waves and periods of the COVID-19 pandemic could then be addressed.

We used the partial-likelihood estimation method to estimate the coefficients of the predictors; each calendar day contributed to 1 term in the log-likelihood function. We adopted the Breslow estimator to estimate the conditional likelihood for the days that had >1 event (i.e., tied observations) and applied the large sample theory to produce approximate variance-covariance matrices for the estimated coefficients.

We initially fitted a full model with all marginal effects and first and second order interaction effects between age, oral treatment status, vaccination type and number of doses. We conducted generalized-likelihood ratio (GLR) tests to analyze the first and second order interaction effects. According to GLR test results, we fitted a reduced model with all marginal effects and significant interactions. We conducted GLR tests to analyze the interaction effects between oral antiviral drugs and vaccinations, between age and oral antiviral drugs, and between age and vaccinations; we then performed subgroup analyses. For each age group, we ran a reduced model with marginal effects only and included the variables age, gender, vaccination type and number of doses, the time-dependent oral treatment status (and whether

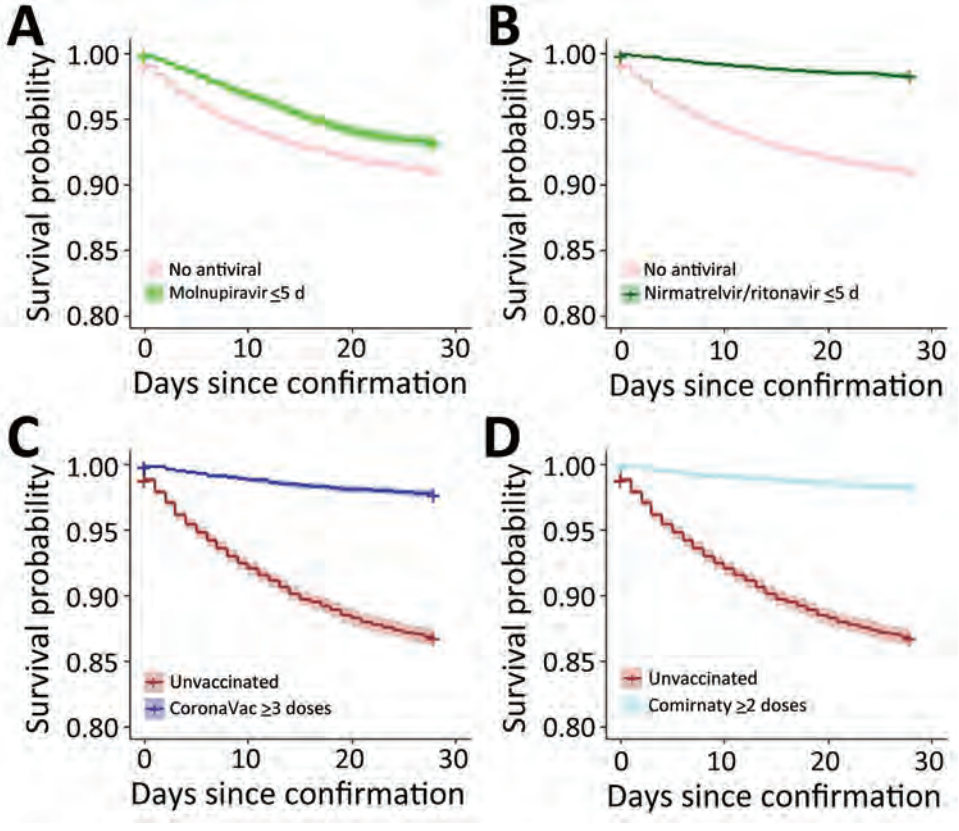

Figure 1. Survival curves for all-cause mortality outcome in study of effectiveness of vaccines and antiviral drugs in preventing severe and fatal COVID-19, Hong Kong. Survival curves were generated to compare patients who did not receive antiviral drugs with those prescribed molnupiravir (A) or nirmatrelvir/ritonavir (B) within 5 days after confirmation of COVID-19 diagnosis and to compare unvaccinated patients with those vaccinated with CoronaVac (C) or Comirnaty (D) vaccines.

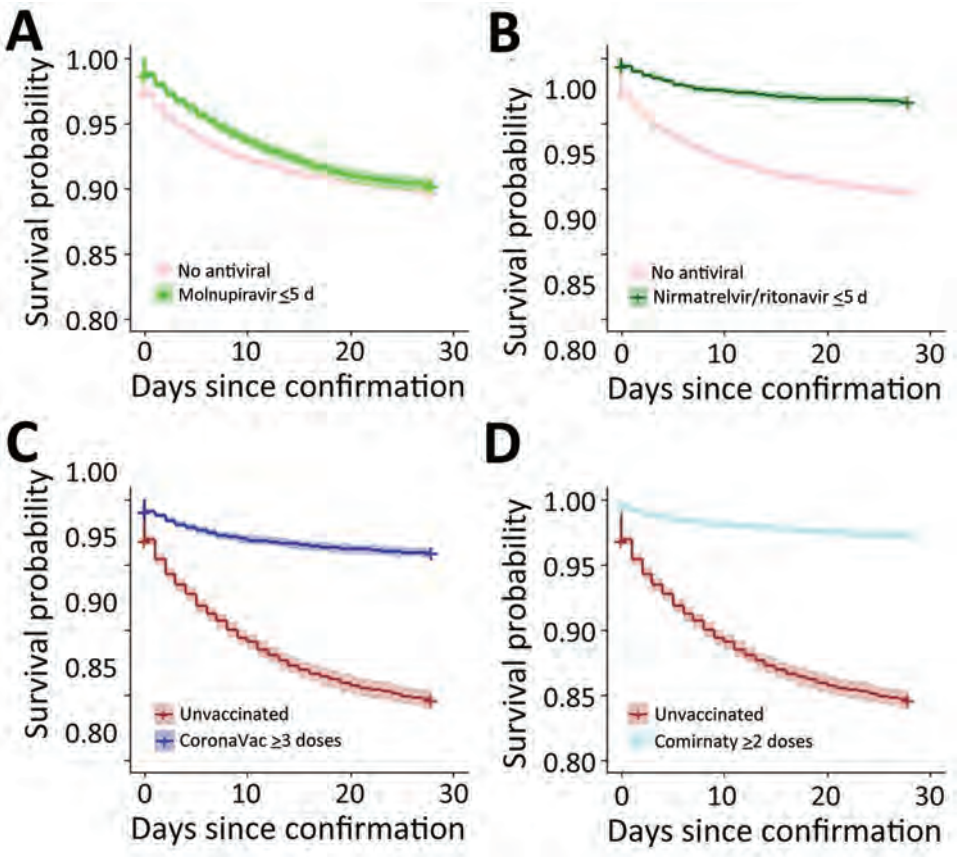

Figure 2. Survival curves for progression to serious/critical/fatal illness outcome in study of effectiveness of vaccines and antiviral drugs in preventing severe and fatal COVID-19, Hong Kong. Survival curves were generated to compare patients who did not receive antiviral drugs with those prescribed molnupiravir (A) or nirmatrelvir/ritonavir (B) within 5 days after confirmation of COVID-19 diagnosis and to compare unvaccinated patients with those vaccinated with CoronaVac (C) or Comirnaty (D) vaccines.

the treatment was prescribed within 5 days of confirmed diagnosis), and the Charlson comorbidity index. We performed Z-tests for the difference in population means to compare the relative size effects of different oral antiviral drugs, different vaccinations, the same type of vaccination with different numbers of doses, and effects between the antiviral drugs and vaccinations.

We performed all statistical tests and analyses by using RStudio (https://www.rstudio.com) in R version 4.2.1 (The R Project for Statistical Computing, https://www.r-project.org). All statistical tests were 2-sided; we considered $p<0.05$ statistically significant.

Results

We identified a total of 39,627 hospitalized adults who had a confirmed diagnosis of SARS-CoV-2 infection during March 16–October 31, 2022, of whom 9,616 received molnupiravir and 10,873 received nirmatrelvir/ritonavir during their hospital stays. Among the 20,489 patients prescribed oral antiviral drugs, 8,708 were ≥80, 8,996 were 60–79, and 2,785 were <60 years of age. A total of 10,291 hospitalized patients were unvaccinated at the time of confirmed diagnosis, 10,346 had received 1–2 doses of CoronaVac vaccine, 10,166 had received 3–4 doses of CoronaVac vaccine, 576 had received 1 dose of Comirnaty vaccine, and 8,248 had received 2–4 doses of Comirnaty vaccine (Appendix Table 1). Patients were observed during the 28-day follow-up period if they were not discharged or did not experience the outcomes of interest (death or progression to serious illness).

The cumulative incidences of all-cause mortality were 847 for molnupiravir users, 245 for nirmatrelvir/ritonavir users, and 1,987 for those who did not receive antiviral drugs (controls); cumulative incidences of progression to a serious/critical/fatal case were 1,076 for molnupiravir users, 407 for nirmatrelvir/ritonavir users, and 2,052 for controls (Appendix Table 2). The cumulative incidences of all-cause mortality were 959 for patients partially vaccinated with CoronaVac, 291 for those fully vaccinated with CoronaVac, 51 for those partially vaccinated with Comirnaty, 180 for those fully vaccinated with Comirnaty, and 1,598 for unvaccinated patients; cumulative incidences of progression to a serious/critical/fatal case were 1,104 for those partially vaccinated with CoronaVac, 447 for those fully vaccinated with CoronaVac, 56 for those partially vaccinated with Comirnaty, 248

for those fully vaccinated with Comirnaty, and 1,680 for unvaccinated patients (Appendix Table 3). We defined fully vaccinated status as having ≥3 doses of CoronaVac and ≥2 doses of Comirnaty vaccines.

The second-order interaction effects among age, oral antivirals, and vaccinations were not significant for all-cause mortality (p = 0.604) and for progression to serious illness (p = 0.584). Furthermore, the interaction effects between oral antiviral drugs and vaccinations were not significant for all-cause mortality (p = 0.280) and for progression to serious illness (p = 0.341) (Appendix Table 4). The joint effects of oral antiviral drugs and vaccinations were additive. For both target outcomes, significant (or moderate) interaction effects were found between age and oral antiviral drugs and between age and vaccinations (p<0.05) (Appendix Table 4).

Receipt of oral antiviral drugs within 5 days of confirmed COVID-19 diagnosis was associated with significantly lower risk for all-cause mortality in patients ≥60 years of age (Appendix Table 5). For molnupiravir, the hazard ratios (HRs) for all-cause mortality were 0.65 (95% CI 0.55–0.78) for the 60–79-year age group and 0.61 (95% CI 0.55–0.67) for the ≥80-year group. For nirmatrelvir/ritonavir, HRs for all-cause mortality were 0.38 (95% CI 0.29–0.49) for the 60–79-year age group and 0.31 (95% CI 0.26–0.36) for the ≥80-year group. Lower risk for progression to a serious/critical/fatal condition was also observed with antiviral treatments; for molnupiravir, HRs were 0.78 (95% CI 0.67–0.91) for the 60–79-year age group and 0.73 (95% CI 0.67–0.81) for the ≥80-year group; for nirmatrelvir-ritonavir, HRs were 0.55 (95% CI 0.45–0.67) for the 60–79-year age group and 0.44 (95% CI 0.38–0.51) for the ≥80-year group. For both age groups, receipt of nirmatrelvir/ritonavir was associated with lower risks than molnupiravir for all-cause mortality and progression to a serious/critical/fatal conditions (p<0.001). No significant clinical benefit was found if the antiviral drugs were prescribed beyond 5 days of confirmed diagnosis or for patients who were <60 years of age, as the corresponding CIs for the HRs contained the value of 1 (Appendix Table 5).

Among patients ≥60 years of age, receipt of CoronaVac or Comirnaty vaccines was generally associated with lower risks for all-cause mortality and progression to a serious/critical/fatal condition; a greater number of vaccine doses was associated with lower risks. HRs for all-cause mortality in the 60–79-year age group were 0.70 (95% CI 0.56–0.88) for 1 dose of CoronaVac, 0.58 (95% CI 0.47–0.71) for 2 doses,

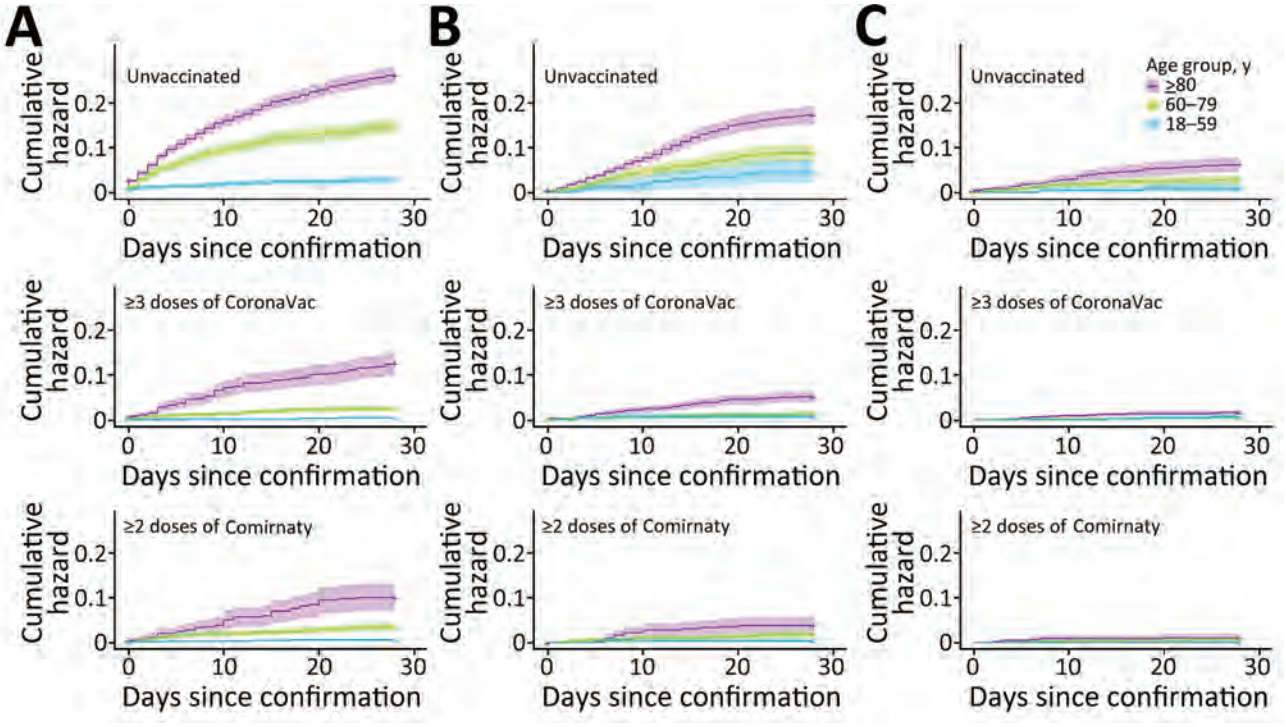

Figure 3. Cumulative hazards for all-cause mortality outcome events in study of effectiveness of vaccines and antiviral drugs in preventing severe and fatal COVID-19, Hong Kong. Cumulative hazards were compared among age groups, patients prescribed oral antiviral drugs, and those unvaccinated or vaccinated with CoronaVac or Comirnaty vaccines. A) No antiviral drugs, B) molnupiravir, C) nirmatrelvir/ritonavir. Antiviral drugs were prescribed within 5 days after confirmation of a COVID-19 diagnosis. Colors indicate age groups within each treatment group.

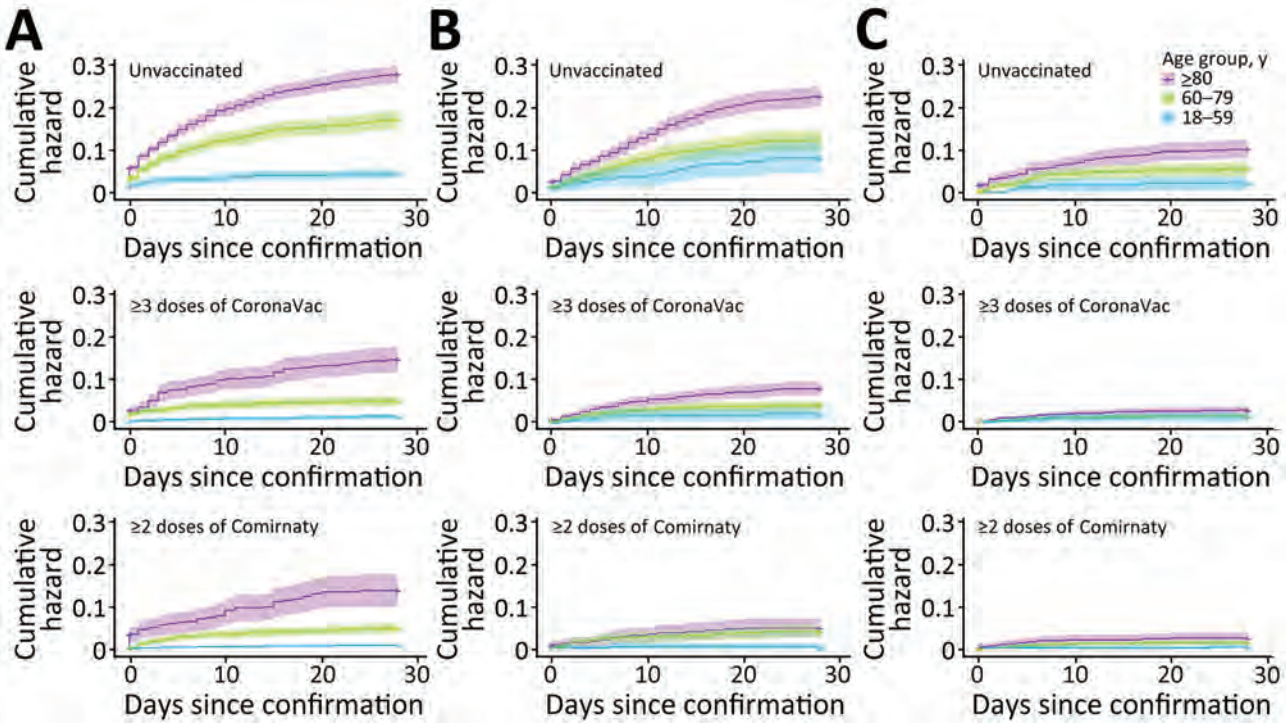

Figure 4. Cumulative hazards for serious/critical/fatal condition outcome events in study of effectiveness of vaccines and antiviral drugs in preventing severe and fatal COVID-19, Hong Kong. Cumulative hazards were compared among age groups, patients prescribed oral antiviral drugs, and those unvaccinated or vaccinated with CoronaVac or Comirnaty vaccines. A) No antiviral drugs, B) molnupiravir, C) nirmatrelvir/ritonavir. Antiviral drugs were prescribed within 5 days after confirmation of a COVID-19 diagnosis. Colors indicate age groups within each treatment group.

0.32 (95% CI 0.24–0.42) for 3 doses, and 0.12 (95% CI 0.04–0.37) for 4 doses. HRs for all-cause mortality in the ≥80-year age group were 0.91 (95% CI 0.81–1.02) for 1 dose of CoronaVac, 0.73 (95% CI 0.64–0.83) for 2 doses, 0.57 (95% CI 0.48–0.69) for 3 doses, and 0.35 (95% CI 0.18–0.69) for 4 doses. For those receiving the Comirnaty vaccine, HRs for all-cause mortality in the 60–79-year age group were 0.70 (95% CI 0.44–1.11) for 1 dose, 0.66 (95% CI 0.50–0.87) for 2 doses, 0.28 (95% CI 0.18–0.43) for 3 doses, and 0.09 (95% CI 0.01–0.65) for 4 doses; in the ≥80-year age group, HRs were 1.26 (95% CI 0.87–1.81) for 1 dose, 0.56 (95% CI 0.42–0.76) for 2 doses, 0.37 (95% CI 0.25–0.55) for 3 doses, and 0.28 (95% CI 0.07–1.11) for 4 doses. For patients 18–59 years of age, receipt of 3 doses of CoronaVac or Comirnaty was associated with lower risks of all-cause mortality (CoronaVac, HR 0.36 [95% CI 0.19–0.71]; Comirnaty, HR 0.18 [95% CI 0.07–0.45]) and progression to a serious/critical/fatal condition (CoronaVac, HR 0.54 [95% CI 0.34–0.85]; Comirnaty, HR 0.29 [95% CI 0.16–0.51]), whereas no significant benefit was observed for 1 or 2 doses.

Comparisons between CoronaVac and Comirnaty vaccinations showed no significant differences in risks for all-cause mortality or progression to a serious/critical/fatal condition when patients received 1 or 2 doses of either vaccine. For the ≥80-year age group, those who received 3 doses of Comirnaty vaccine had significantly lower risks for all-cause mortality ($p = 0.038$) and progression to a serious/critical/fatal condition ($p = 0.026$) than those who received 3 doses of CoronaVac vaccine.

Survival was greater for patients who received oral antiviral drugs (within 5 days of diagnosis) than for those who did not receive antiviral drugs (Figures 1, 2). Survival was also greater for patients who received ≥3 doses of CoronaVac or ≥2 doses of Comirnaty vaccines than for those who were unvaccinated. Survival curves showed that both oral antivirals and vaccinations effectively reduced the risk for all-cause mortality. Similarly, cumulative hazards for patients who received oral antiviral drugs or vaccinations were lower than for those who did not receive the antiviral drugs and were unvaccinated (Figures 3, 4). Furthermore, vaccination and use of oral antivirals was more effective for patients ≥80 years of age than for those in the younger age groups.

Discussion

We conducted a real-world study to compare the effectiveness of SARS-CoV-2 oral antiviral drugs and vaccinations, to examine their interaction effects in a unified model setting, and to address immortal time bias. Hospitalized COVID-19 patients in Hong Kong who received nirmatrelvir/ritonavir had significantly lower all-cause mortality and disease progression risks than those receiving molnupiravir. Interaction effects between the oral antiviral drugs and vaccinations were not significant. The oral antiviral drugs provided greater clinical benefits to the adult patients ≥60 years of age than to those <60 years of age. Vaccinations generally provided greater clinical benefits for patients <60 years of age.

Several observational studies have been performed to examine the effectiveness of oral antiviral drugs in patients with mild to moderate COVID-19. A retrospective cohort study of hospitalized patients with confirmed SARS-CoV-2 diagnoses was conducted during February 26–April 26, 2022; the study used propensity score matching to evaluate the effectiveness of molnupiravir and nirmatrelvir/ritonavir for patients who did not require supplemental oxygen at admission (*33*). Our findings on interaction between age and oral antivirals agreed with that study; however, we did not find a significant interaction effect between oral antiviral drugs and vaccinations, which disagreed with that study. We covered a longer study period, and our study population was more inclusive because of the application of the calendar day setting and time-dependent treatment and outcome variables. Another cohort study of nonhospitalized patients showed molnupiravir and nirmatrelvir/ritonavir were effective for patients with mild to moderate COVID-19 (*34*). Compared with that study, the strength of our study population could be attributed to the inpatient setting where clinical outcomes and procedures were systematically documented, and medication adherence was guaranteed. Our findings offer additional insight into the effectiveness of oral antiviral drugs and vaccinations. A different observational study was performed using inverse probability of treatment weighting to adjust the baseline differences between treatment and control groups (*35*). Unlike that study, our analyses involved vaccination records of patients and examined the effectiveness of oral antiviral drugs and vaccinations in a unified model that addressed immortal time bias.

Despite having some advantages over previous studies, the first limitation of our study is that our analyses were inevitably subject to selection bias; therefore, our inpatient setting suggests that the generalizability of our results to outpatients or other settings is questionable. Second, we did not have compliance data for the oral antiviral drugs, and an intention-to-treat handling of the prescription data could underestimate the effects of the oral treatments. However, inpatients are more likely to have a high level of compliance. Third, we were not able to further differentiate all-cause mortality from deaths directly caused by SARS-CoV-2 as opposed to other causes. Fourth, in our modeling of vaccination effect, we did not consider the elapsed time between doses and the potential waning effect of vaccination. Fifth, the difference in treatment timing could have caused bias in our comparison between the 2 types of treatments (i.e., vaccination and oral antiviral drugs). All vaccinated patients prescribed antiviral drugs were vaccinated before they received the drug. The difference in treatment timing could have caused bias in our comparisons between vaccine and antiviral drug effects, as well as during examination of their interaction effects.

In conclusion, this retrospective study of hospitalized patients with COVID-19 showed that the use of vaccinations and oral antiviral drugs was associated with substantial reductions in risks for all-cause mortality and disease progression. Oral molnupiravir and nirmatrelvir/ritonavir were more effective in reducing the risks of target outcomes for adults ≥60 than for those <60 years of age. In contrast, vaccinations were relatively more effective in reducing the risks for target outcomes for adults <60 than for those ≥60 years of age. We did not observe significant interaction effects on target outcomes between the use of vaccinations and oral antiviral drugs, and the joint effects of vaccinations and antivirals were additive. Policies should be introduced to encourage COVID-19 vaccinations; oral antivirals should be the standard care for hospitalized patients who have SARS-CoV-2 infection and should be provided within 5 days of confirmed diagnosis.

The data custodians (the Hospital Authority and Department of Health of the Government of the Hong Kong Special Administrative Region) provided the underlying individual-patient data to The University of Hong Kong for the purpose of scientific research. Restrictions apply to the availability of those data, which were used under license for this study. Authors must not transmit or release the data, in whole or in part, and in whatever form or media, or to any other parties or place outside of Hong Kong and must fully comply with the duties under the law relating to the protection of personal data, including those under the Personal Data (Privacy)

Ordinance and its principles in all aspects. All computer code related to this article has been made publicly available at the Open Science Framework (https://doi.org/10.17605/OSF.IO/2DR6M).

This project was supported by the Health and Medical Research Fund of the Health Bureau, Government of the Hong Kong Special Administrative Region, China (grant no. CID-HKU2-12). The funding bodies had no role in the design of the study; collection, analysis, and interpretation of data; or writing of the manuscript.

B.J.C. consults for AstraZeneca, Fosun Pharma, GlaxoSmithKline, Haleon, Moderna, Pfizer, Roche, and Sanofi Pasteur. The other authors report no other potential conflicts of interest.

About the Author

Mr. Cheung is a PhD candidate in the Department of Statistics and Actuarial Science at The University of Hong Kong. His academic interests include biostatistics and causal inference.

References

1. Zhou Y, Wang F, Tang J, Nussinov R, Cheng F. Artificial intelligence in COVID-19 drug repurposing. Lancet Digit Health. 2020;2:e667–76. https://doi.org/10.1016/S2589-7500(20)30192-8
2. US Food and Drug Administration. Coronavirus (COVID-19) update: FDA authorizes additional oral antiviral for treatment of COVID-19 in certain adults. 2021 [cited 2022 Nov 2]. https://www.fda.gov/news-events/press-announcements/coronavirus-covid-19-update-fda-authorizes-additional-oral-antiviral-treatment-covid-19-certain
3. Masyeni S, Iqhrammullah M, Frediansyah A, Nainu F, Tallei T, Emran TB, et al. Molnupiravir: a lethal mutagenic drug against rapidly mutating severe acute respiratory syndrome coronavirus 2—a narrative review. J Med Virol. 2022;94:3006–16. https://doi.org/10.1002/jmv.27730
4. Khoo SH, FitzGerald R, Saunders G, Middleton C, Ahmad S, Edwards CJ, et al.; AGILE CST-2 Study Group. Molnupiravir versus placebo in unvaccinated and vaccinated patients with early SARS-CoV-2 infection in the UK (AGILE CST-2): a randomised, placebo-controlled, double-blind, phase 2 trial. Lancet Infect Dis. 2023;23:183–95. https://doi.org/10.1016/S1473-3099(22)00644-2
5. Castillo Almeida NE, Kalil AC. Molnupiravir: is it time to move in or move out? NEJM Evid. 2022;1:1–3. https://doi.org/10.1056/EVIDe2100048
6. Jayk Bernal A, Gomes da Silva MM, Musungaie DB, Kovalchuk E, Gonzalez A, Delos Reyes V, et al.; MOVe-OUT Study Group. Molnupiravir for oral treatment of COVID-19 in nonhospitalized patients. N Engl J Med. 2022;386:509–20. https://doi.org/10.1056/NEJMoa2116044
7. US Food and Drug Administration. Coronavirus (COVID-19) update: FDA authorizes first oral antiviral for treatment of COVID-19. 2021 [cited 2022 Nov 2]. https://www.fda.gov/news-events/press-announcements/coronavirus-covid-19-update-fda-authorizes-first-oral-antiviral-treatment-covid-19
8. Reis S, Metzendorf MI, Kuehn R, Popp M, Gagyor I, Kranke P, et al. Nirmatrelvir combined with ritonavir for preventing and treating COVID–19. Cochrane Database Syst Rev. 2022;9:CD015395. PubMed https://doi.org/10.1002/14651858.CD015395.pub2
9. Hammond J, Leister-Tebbe H, Gardner A, Abreu P, Bao W, Wisemandle W, et al.; EPIC-HR Investigators. Oral nirmatrelvir for high-risk, nonhospitalized adults with COVID-19. N Engl J Med. 2022;386:1397–408. https://doi.org/10.1056/NEJMoa2118542
10. Tanriover MD, Doğanay HL, Akova M, Güner HR, Azap A, Akhan S, et al.; CoronaVac Study Group. Efficacy and safety of an inactivated whole-virion SARS-CoV-2 vaccine (CoronaVac): interim results of a double-blind, randomised, placebo-controlled, phase 3 trial in Turkey. Lancet. 2021;398:213–22. https://doi.org/10.1016/S0140-6736(21)01429-X
11. Wu Z, Hu Y, Xu M, Chen Z, Yang W, Jiang Z, et al. Safety, tolerability, and immunogenicity of an inactivated SARS-CoV-2 vaccine (CoronaVac) in healthy adults aged 60 years and older: a randomised, double-blind, placebo-controlled, phase 1/2 clinical trial. Lancet Infect Dis. 2021;21:803–12. https://doi.org/10.1016/S1473-3099(20)30987-7
12. Han B, Song Y, Li C, Yang W, Ma Q, Jiang Z, et al. Safety, tolerability, and immunogenicity of an inactivated SARS-CoV-2 vaccine (CoronaVac) in healthy children and adolescents: a double-blind, randomised, controlled, phase 1/2 clinical trial. Lancet Infect Dis. 2021;21:1645–53. https://doi.org/10.1016/S1473-3099(21)00319-4
13. Medeiros-Ribeiro AC, Aikawa NE, Saad CGS, Yuki EFN, Pedrosa T, Fusco SRG, et al. Immunogenicity and safety of the CoronaVac inactivated vaccine in patients with autoimmune rheumatic diseases: a phase 4 trial. Nat Med. 2021;27:1744–51. https://doi.org/10.1038/s41591-021-01469-5
14. Mok CKP, Chen C, Yiu K, Chan T-O, Lai KC, Ling KC, et al. A randomized clinical trial using CoronaVac or BNT162b2 vaccine as a third dose in adults vaccinated with two doses of CoronaVac. Am J Respir Crit Care Med. 2022;205:844–7. https://doi.org/10.1164/rccm.202111-2655LE
15. Li J, Hou L, Guo X, Jin P, Wu S, Zhu J, et al. Heterologous AD5-nCOV plus CoronaVac versus homologous CoronaVac vaccination: a randomized phase 4 trial. Nat Med. 2022;28:401–9. https://doi.org/10.1038/s41591-021-01677-z
16. Thomas SJ, Moreira ED Jr, Kitchin N, Absalon J, Gurtman A, Lockhart S, et al.; C4591001 Clinical Trial Group. Safety and efficacy of the BNT162b2 mRNA COVID-19 vaccine through 6 months. N Engl J Med. 2021;385:1761–73. https://doi.org/10.1056/NEJMoa2110345
17. Polack FP, Thomas SJ, Kitchin N, Absalon J, Gurtman A, Lockhart S, et al.; C4591001 Clinical Trial Group. Safety and efficacy of the BNT162b2 mRNA COVID-19 vaccine. N Engl J Med. 2020;383:2603–15. https://doi.org/10.1056/NEJMoa2034577
18. Kim Y-Y, Choe YJ, Kim J, Kim RK, Jang EJ, Park SK, et al. Effectiveness of second mRNA COVID-19 booster vaccine in immunocompromised persons and long-term care facility residents. Emerg Infect Dis. 2022;28:2165–70. https://doi.org/10.3201/eid2811.220918
19. Zaidi A, Harris R, Hall J, Woodhall S, Andrews N, Dunbar K, et al. Effects of second dose of SARS-CoV-2 vaccination on household transmission, England. Emerg Infect Dis. 2023;29:127–32. https://doi.org/10.3201/eid2901.220996
20. Launer LJ, Harris T; Ad Hoc Committee on the Statistics of Anthropometry and Aging. Weight, height and body mass index distributions in geographically and ethnically diverse samples of older persons. Age Ageing. 1996;25:300–6. https://doi.org/10.1093/ageing/25.4.300

21. Qin W, Xu L, Sun L, Li J, Ding G, Wang Q, et al. Association between frailty and life satisfaction among older people in Shandong, China: the differences in age and general self-efficacy. Psychogeriatrics. 2020;20:172–9. https://doi.org/10.1111/psyg.12482
22. Sung VW, Weitzen S, Sokol ER, Rardin CR, Myers DL. Effect of patient age on increasing morbidity and mortality following urogynecologic surgery. Am J Obstet Gynecol. 2006;194:1411–7. https://doi.org/10.1016/j.ajog.2006.01.050
23. Lévesque LE, Hanley JA, Kezouh A, Suissa S. Problem of immortal time bias in cohort studies: example using statins for preventing progression of diabetes. BMJ. 2010;340:b5087. https://doi.org/10.1136/bmj.b5087
24. Fragoulis GE, Koutsianas C, Fragiadaki K, Mariolis I, Panopoulos S, Tsalapaki C, et al. Oral antiviral treatment in patients with systemic rheumatic disease at risk for development of severe COVID-19: a case series. Ann Rheum Dis. 2022;81:1477–9. https://doi.org/10.1136/annrheumdis-2022-222845
25. Lewnard JA, McLaughlin JM, Malden D, Hong V, Puzniak L, Ackerson BK, et al. Effectiveness of nirmatrelvir-ritonavir in preventing hospital admissions and deaths in people with COVID-19: a cohort study in a large US health-care system. Lancet Infect Dis. 2023;23:806–15. https://doi.org/10.1016/S1473-3099(23)00118-4
26. Massetti GM, Jackson BR, Brooks JT, Perrine CG, Reott E, Hall AJ, et al. Summary of guidance for minimizing the impact of COVID-19 on individual persons, communities, and health care systems—United States, August 2022. MMWR Morb Mortal Wkly Rep. 2022;71:1057–64. https://doi.org/10.15585/mmwr.mm7133e1
27. Xie Y, Choi T, Al-Aly Z. Association of treatment with nirmatrelvir and the risk of post–COVID-19 condition. JAMA Intern Med. 2023;183:554–64. https://doi.org/10.1001/jamainternmed.2023.0743
28. World Health Organization. Therapeutics and COVID-19: living guideline, 24 September 2021 [cited 2022 Nov 2]. https://iris.who.int/bitstream/handle/10665/345356/WHO-2019-nCoV-therapeutics-2021.3-eng.pdf
29. Lin D-Y, Gu Y, Wheeler B, Young H, Holloway S, Sunny S-K, et al. Effectiveness of COVID-19 vaccines over a 9-month period in North Carolina. N Engl J Med. 2022;386:933–41. https://doi.org/10.1056/NEJMoa2117128x
30. Cheung YB, Ma X, Lam KF, Yung CF, Milligan P. Modelling non-linear patterns of time-varying intervention effects on recurrent events in infectious disease prevention studies. J Biopharm Stat. 2023;33:220–33. https://doi.org/10.1080/10543406.2022.2108826
31. Cheung YB, Xu Y, Tan SH, Cutts F, Milligan P. Estimation of intervention effects using first or multiple episodes in clinical trials: the Andersen-Gill model re-examined. Stat Med. 2010;29:328–36. https://doi.org/10.1002/sim.3783
32. Xu J, Lam KF, Chen F, Milligan P, Cheung YB. Semiparametric estimation of time-varying intervention effects using recurrent event data. Stat Med. 2017;36:2682–96. https://doi.org/10.1002/sim.7319
33. Wong CKH, Au ICH, Lau KTK, Lau EHY, Cowling BJ, Leung GM. Real-world effectiveness of early molnupiravir or nirmatrelvir-ritonavir in hospitalised patients with COVID-19 without supplemental oxygen requirement on admission during Hong Kong's Omicron BA.2 wave: a retrospective cohort study. Lancet Infect Dis. 2022;22:1681–93. https://doi.org/10.1016/S1473-3099(22)00507-2
34. Wong CKH, Au ICH, Lau KTK, Lau EHY, Cowling BJ, Leung GM. Real-world effectiveness of molnupiravir and nirmatrelvir plus ritonavir against mortality, hospitalisation, and in-hospital outcomes among community-dwelling, ambulatory patients with confirmed SARS-CoV-2 infection during the Omicron wave in Hong Kong: an observational study. Lancet. 2022;400:1213–22. https://doi.org/10.1016/S0140-6736(22)01586-0
35. Wai AKC, Chan CY, Cheung AWL, Wang K, Chan SCL, Lee TTL, et al. Association of molnupiravir and nirmatrelvir-ritonavir with preventable mortality, hospital admissions and related avoidable healthcare system cost among high-risk patients with mild to moderate COVID-19. Lancet Reg Health West Pac. 2023;30:100602. https://doi.org/10.1016/j.lanwpc.2022.100602

Address for correspondence: Kwok Fai Lam, Department of Statistics and Actuarial Science, The University of Hong Kong, Pokfulam Road, Hong Kong; email: hrntlkf@hku.hk

Costs of Digital Adherence Technologies for Tuberculosis Treatment Support, 2018–2021

Ntwali Placide Nsengiyumva, Amera Khan, Maricelle Ma. Tarcela S. Gler, Mariecef L. Tonquin, Danaida Marcelo, Mark C. Andrews, Karine Duverger, Shahriar Ahmed, Tasmia Ibrahim, Sayera Banu, Sonia Sultana, Mona Lisa Morales, Andre Villanueva, Egwumo Efo, Baraka Onjare, Cristina Celan, Kevin Schwartzman

Digital adherence technologies are increasingly used to support tuberculosis (TB) treatment adherence. Using microcosting, we estimated healthcare system costs (in 2022 US dollars) of 2 digital adherence technologies, 99DOTS medication sleeves and video-observed therapy (VOT), implemented in demonstration projects during 2018–2021. We also obtained cost estimates for standard directly observed therapy (DOT). Estimated per-person costs of 99DOTS for drug-sensitive TB were $98 in Bangladesh (n = 719), $119 in the Philippines (n = 396), and $174 in Tanzania (n = 976). Estimated per-person costs of VOT were $1,154 in Haiti (87 drug-sensitive), $304 in Moldova (173 drug-sensitive), $452 in Moldova (135 drug-resistant), and $661 in the Philippines (110 drug-resistant). 99DOTS costs may be similar to or less expensive than standard DOT. VOT is more expensive, although in some settings, labor cost offsets or economies of scale may yield savings. 99DOTS and VOT may yield savings to local programs if donors cover infrastructure costs.

As part of the mission to cure and ultimately eliminate tuberculosis (TB), maintaining treatment adherence poses a substantial barrier (*1*). Persons with TB must complete multidrug regimens typically lasting ≥6 months. Even small lapses in adherence can be associated with poorer treatment outcomes, including relapse with the potential for further transmission (*2*). TB prevention and care programs have often sought to improve adherence, and hence treatment outcomes, by using directly observed therapy (DOT) (*3*,*4*). However, healthcare system barriers (mostly resource limitations), coupled with stigma, loss of autonomy, and the heavy burden of DOT clinic visits, can result in subpar outcomes and adherence that may not exceed that of self-administered treatment (*5*–*8*). Those limitations have led the World Health Organization (WHO) to recommend community or home-based DOT over healthcare facility–based DOT or unsupervised treatment (*4*).

WHO defines a DOT provider as any person who observes the person with TB taking their medications in real time (*4*). By leveraging current advances in mobile technologies, person-centered treatment observation can be achieved by digital adherence technologies (DATs) such as medication sleeves, smart pill boxes, and video-supported therapy. Moreover, real-time digital adherence information offers the possibility of tailoring treatment support to individual needs. However, before TB programs adopt those technologies as a central strategy for treatment support, evidence for their effectiveness must be robust. Demonstration projects highlighting feasibility and acceptability of DATs for TB treatment support provide substantial evidence; to date, evidence is more limited for clinical outcomes with use of DATs than for other forms of treatment observation or self-administered treatment (*9*–*11*). In principle, DATs can enable expansion of TB treatment supervision and support while reducing the burden on persons with TB and their providers.

Information about the cost to TB programs of those technologies and their real-world cost-effectiveness comes largely from pilot and modeling studies (*11*,*12*). To estimate the cost of 2 DATs currently recommended for use by WHO (*4*), we used data from

Author affiliations: McGill International Tuberculosis Centre and Research Institute, McGill University Health Centre, Montreal, Quebec, Canada (N.P. Nsengiyumva, K. Schwartzman); Stop TB Partnership, Geneva, Switzerland (A. Khan); De La Salle Medical and Health Sciences Institute, Makati City, Philippines (M.M.T.S. Gler, M.L. Tonquin, D. Marcelo); Health Through Walls, Port au Prince, Haiti (M.C. Andrews, K. Duverger); icddr,b, Dhaka, Bangladesh (S. Ahmed, T. Ibrahim, S. Banu, S. Sultana); KNCV, Manila, Philippines (M.L. Morales, A. Villanueva); KNCV, Dar es Salaam, Tanzania (E. Efo, B. Onjare); Center for Health Policies and Studies, Chisinau, Moldova (C. Celan)

DOI: https://doi.org/10.3201/eid3001.230427

implementation studies in Bangladesh, Haiti, Moldova, the Philippines, and Tanzania. Each demonstration project participating in this study received local institutional ethics review board approval.

Methods

Study Design and Tools

Our multicountry cost analysis reflects DAT implementation projects funded by TB REACH Wave 6 (*13*). Our goal was to estimate capital and recurrent costs of DATs. We developed questionnaires and measurement tools to describe the current standard of care (without DATs) for treatment of drug-susceptible TB (DS-TB) and drug-resistant TB (DR-TB); document how the DATs used in each project were integrated into the local standard of care and what practice changes resulted from their introduction; and capture all cost components of the DAT used during each project, including all related interventions and practice changes. Participating programs were given a series of cost analysis questionnaires, available online (*14*) and were trained in their use via webinars. Our report is limited to cost analyses and does not address cost-effectiveness. During execution of each project, we collected data prospectively.

Study Populations

During 2018–2021, we enrolled eligible adolescents and adults receiving treatment for DS-TB and DR-TB in DAT implementation projects in Bangladesh, Haiti, Moldova, the Philippines, and Tanzania (Table 1). The projects were either 99DOTS (a technology-enabled supplement to enhanced DOT (https://www.99dots.org/About.html) medication sleeves or video-observed therapy (VOT; also referred to as video-supported therapy).

Cost Analyses

We performed a combination of bottom-up and top-down microcosting for 6 TB REACH (https://tbreach.org) DAT implementation projects. Seven other implementation projects pursued separate costing analyses, some of which have been published elsewhere (e.g., the Ugandan project [*15*]). Bottom-up costing applied to most cost components, but top-down microcosting incorporated total amounts spent for DAT platform/infrastructure, systems/data management and technical support, and training activities. Bottom-up microcosting involves a detailed enumeration of cost component data points obtained from the service provider to estimate unit costs (*16*,*17*). Top-down microcosting uses total costs for relevant elements and then prorates them to calculate unit costs (e.g., per patient treated, per service delivered) (*18*,*19*).

We conducted our analysis from the healthcare system perspective; hence, we did not tabulate costs borne by patients and their families. All costs were converted to 2022 US dollars by using the respective countries' inflation and exchange rates from the World Bank (*20*,*21*). Costs reflected project expenses reported by staff and were grouped into 2 categories: fixed and variable. Variable costs fell into 7 categories: 1) phones and accessories; 2) systems/data management; 3) mobile data use; 4) adherence monitoring by healthcare workers (HCWs) using the DAT platform; 5) HCW escalation/intervention in cases of nonadherence; 6) trainers; and 7) trainees. Two additional variable cost categories were specific to 99DOTS: 1) printing and shipping of medication sleeves, and 2) medication preparation (in case medication blister packs were not packaged within 99DOTS sleeves by the supplier). Fixed costs were those of the DAT platform and required infrastructure (Appendix, https://wwwnc.cdc.gov/EID/article/30/1/23-0427-App1.pdf).

For each project, we estimated total costs and then prorated them per person treated for TB. Because certain fixed costs (e.g., acquisition of the relevant platforms and computing infrastructure) can be substantial, we performed scenario analyses in which the DAT was scaled up to support more persons during treatment. In those scenarios, most variable costs remained unchanged, but we annuitized fixed technology costs as well as computer and phone purchases for HCWs and patients on the basis of a 5-year lifespan. We also explored scenarios in which fixed technology/platform introduction and maintenance costs would be shared across expanded user numbers (i.e., 2× study population, 5× study population, 10× study population, and 100× study population) while maintaining the same variable costs as previously estimated.

To situate the DAT costs relative to the local standard of care; we evaluated per-person costs for DATs compared with in-person DOT, accounting for each study setting (i.e., duration of treatment and salary/wages of the persons observing treatment). We supplemented this analysis by considering DOT costs from the existing literature. To capture the patient volumes at which DAT scale-up might become cost saving, we also performed a threshold analysis.

An additional scenario analysis accounted for the high fixed up-front costs, which can pose a substantial barrier to DAT adoption. In that scenario analysis, we assumed that the costs were covered separately by

international donor funds. Thus, we excluded them from the analysis, which was therefore restricted to variable costs borne by the local TB program, including computer and phone purchases for HCWs and patients. We then compared those estimates with the cost estimates for DOT.

Results

During 2018–2021, the three 99DOTS projects enrolled a total of 2,091 patients: 719 in Bangladesh, 396 in the Philippines and 976 in Tanzania. During the same period, the 3 VOT projects enrolled a total of 505 patients: 87 in Haiti, 308 in Moldova, and 110 in the Philippines (Tables 1, 2; Appendix Tables 2–4, 6–9).

99DOTS

The estimated total costs of 99DOTS in the 3 implementation projects were $70,756 overall and $98 per person treated for DS-TB in Bangladesh, $47,074 overall and $119 per person in the Philippines, and $169,536 overall and $174 per person in Tanzania. Variable costs accounted for 79% of the total in Bangladesh, 70% in the Philippines, and 94% in Tanzania (Appendix Tables 3, 5, 6).

The main cost drivers for 99DOTS varied across project sites. Key components included adherence monitoring by personnel in Bangladesh (25% of costs), platform and infrastructure in the Philippines (29%), and systems/data management in Tanzania (34%).

For scenario analyses, we evaluated variation in per-person costs if 99DOTS were potentially scaled to larger numbers of persons receiving TB treatment and of their providers, while maintaining the same total fixed costs and the same variable costs per patient. When the number of persons served by the platform was increased 100-fold, we estimated a 39% decrease in cost per patient to $60 in Bangladesh, a 30% decrease to $83 in the Philippines, and an 8% decrease to $160 in Tanzania (Figure 1). In all scenario analyses, the most influential cost components remained the same (they all belonged to the variable cost category).

VOT

For the project in Haiti (DS-TB), estimated overall costs for VOT were $100,436 and costs per person treated were $1,154; for Moldova (all TB patients), $114,336 and $372; and for the Philippines (DR-TB),

Table 1. Implementation projects and participants in study of costs of digital adherence technologies for tuberculosis treatment support*

Country	DAT	Organization	Project description	Participants
Bangladesh	99DOTS†	icddr,b	Implementation of 99DOTS in private sector TB screening and treatment centers established by icddr,b under its social enterprise model in Dhaka	719 adults with DS-TB (mean age 34 y, SD 27) enrolled in the project, April 2019–July 2020.
Philippines	99DOTS	KNCV	A project to assess 99DOTS use in the private sector in the Philippines, where data suggest that 50% of patients in the country seek care	396 adults (>15 y) with DS-TB enrolled on 99DOTS at 3 private clinics based in metro Manila area, December 2018–June 2020.
Tanzania	99DOTS	KNCV	The project involved mining communities in Tanzania in 4 rural districts using 99DOTS with SMS-targeted educational messages and reminders. Patient dosing histories were used for counseling and for differentiated care (more intensive patient management)	976 adult miners (>15 y) with DS-TB from 11 public health facilities recruited at treatment initiation or during medication refill. 22 DOT nurses and 11 community health workers were engaged in the project, February 2019–June 2020.
Haiti	VOT	Health through Walls, Inc.	A project using VOT to improve TB treatment adherence and outcomes for current and former prisoners in Haiti	87 incarcerated persons with DS-TB enrolled in the project, February 2019–February 2020. The project used a commercial VOT platform.
The Philippines	VOT	Hermano (San) Miguel Febres Cordero Medical Education Foundation, Inc	A pilot study to determine feasibility and acceptability of VOT in a high-burden, resource constrained DR-TB clinic in the Philippines, where smartphone penetration is moderate and growing	110 adolescents and adults (>13 y) with DR-TB enrolled to use VOT at 6 DR-TB clinics. Everyone received a smartphone with the VOT application pre-installed and with SIM cards, December 2018–June 2021. The project used a commercial VOT platform.
Moldova	VOT	Centre for Health Policies and Studies	A pilot project to scale up a locally developed VOT application	173 adults with DS-TB and 135 adults with DR-TB enrolled on a locally developed VOT platform, April 2020–June 2021.

*Numbers indicate participants in the costing exercise; the overall parent study might have had more participants. CHW, community health worker; DAT, digital adherence technology; DR-TB, drug-resistant TB; DS-TB, drug-susceptible TB; KNCV, Koninklijke Nederlandse Centrale Vereniging tot bestrijding der Tuberculose; TB, tuberculosis; VOT, video-observed therapy; VST, video-supported therapy; SMS,short message service.
†https://www.99dots.org.

Table 2. Costs of digital adherence technologies for tuberculosis treatment support determined in study of costs of digital adherence technologies for tuberculosis treatment support*

	Variable costs, US$		Fixed costs, US$		Total costs, US$	
Adherence technology	Variable overall	Variable per patient	Fixed overall	Fixed per patient	Total overall	Total per patient
Observed project costs						
99DOTS†						
Bangladesh, n = 71	55,985	78	14,772	21	70,756	98
The Philippines, n = 396	33,173	84	13,901	35	47,074	119
Tanzania, n = 976	159,028	163	10,509	11	169,536	174
VOT						
Haiti, n = 87	69,287	796	31,149	358	100,436	1,154
Moldova, DS-TB, n = 173	34,248	198	18,429	107	52,677	304
Moldova DR-TB, n = 135	40,088	293	21,571	160	61,659	452
Moldova all TB, n = 308	74,336	242	40,000	130	114,336	372
The Philippines, n = 110	45,330	412	27,327	248	72,656	661
Project costs annuitized over the 5-y life span of servers and phones						
99DOTS						
Bangladesh, n = 719		60		21		81
The Philippines, n = 396		83		8.84		92
Tanzania, n = 976		160		3.61		163
VOT						
Haiti, n = 87		702		358		1,060
Moldova DS-TB, n = 173		151		21		172
Moldova DR-TB, n = 135		222		32		254
Moldova All TB, n = 308		185		26		211
The Philippines, n = 110		247		248		495

*DR-TB, drug-resistant TB; DS-TB, drug-susceptible TB; TB, tuberculosis; VOT, video-observed treatment.
†https://www.99dots.org.

$72,656 and $661. Variable costs accounted for 69% of the total in Haiti (DS-TB), 65% in Moldova (all TB patients), and 62%, in the Philippines (DR-TB) (Appendix Tables 6–8).

The largest cost component in Haiti was associated with systems/data management and technical support, which together accounted for 54% of the total. VOT platform and infrastructure accounted for 35% of the total cost in Moldova and 38% in the Philippines.

For the scenario analysis, when the number of persons served by the same platform was increased 100-fold, we estimated a 31% decrease in cost with per-person costs falling to $800 in Haiti (DS-TB), 12% falling to $185 in Moldova (all TB patients), and 50% falling to $151 in the Philippines (DR-TB) (Figure 2). In that scenario, the largest cost component in Haiti (DS-TB) remained systems/data management and technical support at 91%; adherence monitoring then accounted for 55% of the total per patient cost in Moldova (all TB patients) and 88% in the Philippines.

99DOTS Versus DOT

The 99DOTS projects were conducted in settings in which TB treatment is ordinarily observed by health facility workers, community health workers, or family members. Program personnel estimated that 30% of patients would continue traditional DOT after the introduction of 99DOTS in Bangladesh, 20% in the Philippines, and 0 in Tanzania. Such persons included those receiving TB retreatment, persons without access to a mobile phone, persons residing outside the clinic's catchment area, hospitalized patients, persons with extrapulmonary TB receiving ≥12-month treatment regimens, and persons unwilling to provide consent. From the Tanzania healthcare system perspective, DOT itself does not imply healthcare system costs, and hence DOT costs to the healthcare system are not offset by use of 99DOTS because treatment support is ordinarily provided (unpaid) by family members.

In a threshold analysis, we explored the patient volumes required for 99DOTS to be cost saving when compared with DOT. In Bangladesh, when we used study DOT cost estimates, 99DOTS was associated with a $7 increase per patient enrolled; when we used DOT costs published elsewhere, the incremental cost was $45 (22). We estimated that an increase of >47% in patient volumes from the study population would render 99DOTS cost saving. In the Philippines, 99DOTS was cost saving with existing patient volumes according to study DOT cost estimates and those published elsewhere (23). In Tanzania, there was no possibility of healthcare system cost savings with 99DOTS compared with DOT because DOT relied on family members at no cost to the healthcare system.

For the scenario in which fixed costs are paid by donors, 99DOTS was cost saving in Bangladesh and the Philippines. In that scenario, TB programs would be able to support treatment for $60 per patient by using 99DOTS compared with $74 per patient by using DOT in Bangladesh, $83 compared with $176 in the Philippines, and $160 compared with $0 per patient in Tanzania.

VOT versus DOT

Program personnel estimated that 15% of persons treated for TB would remain on traditional DOT after the implementation of VOT in Haiti, 10% in Moldova, and 50% in the Philippines (Table 3). Use of VOT in Haiti was associated with $646 additional cost per patient compared with study DOT cost estimates and $1,011 compared with published DOT cost estimates (*25*). In Moldova, VOT was cost-saving with existing patient volumes according to our own DOT cost estimates; 77% of the DS-TB and 75% of the DR-TB study populations actually enrolled would have been sufficient to generate cost savings in Moldova. In Bangladesh and the Philippines, VOT costs per patient exceeded those for DOT even with all fixed costs excluded, meaning that expanding the number of patients covered by VOT (i.e., economies of scale for fixed costs) could not result in savings.

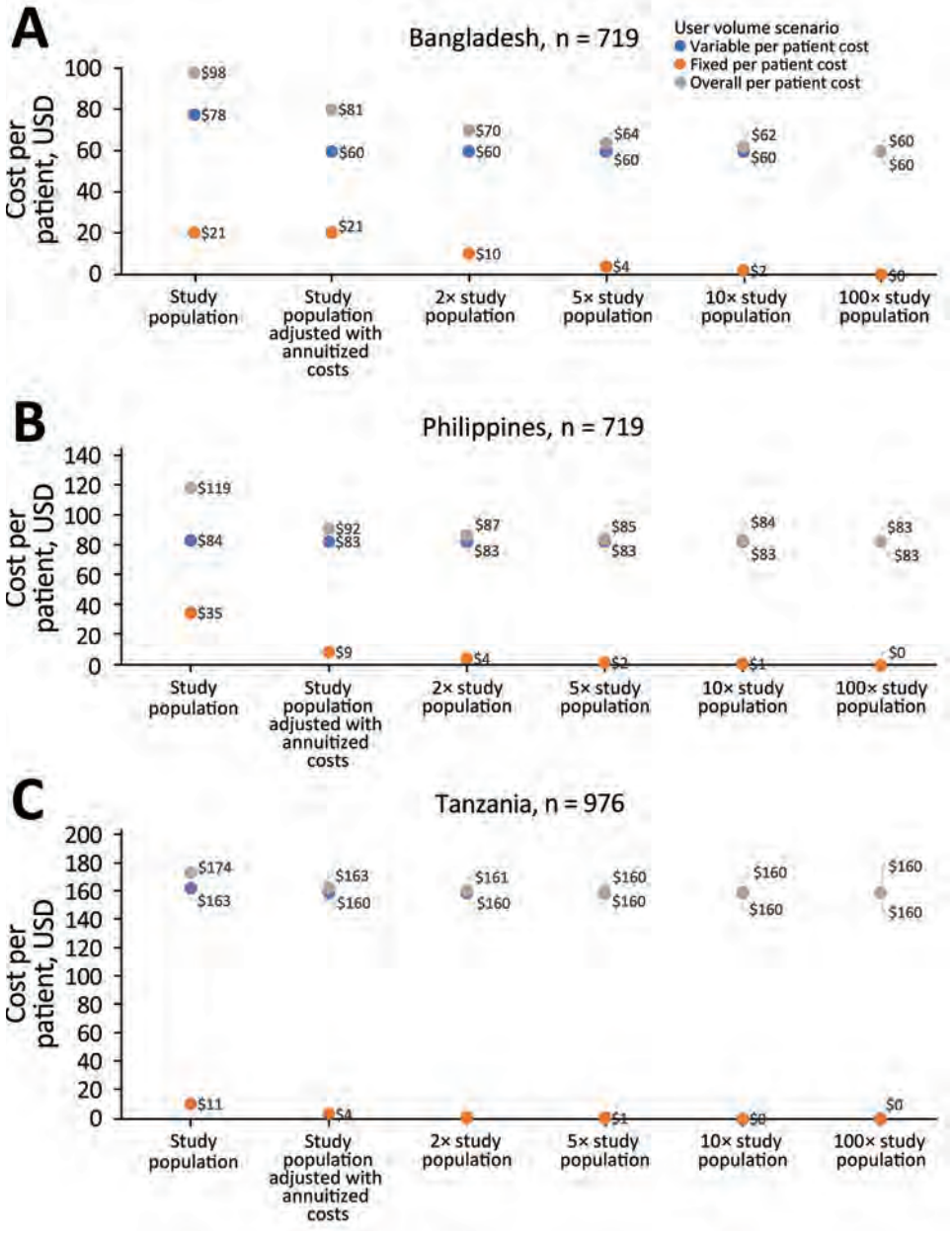

Figure 1. Directly observed tuberculosis therapy scale-up scenario analysis for 3 countries: A) Bangladesh; B) the Philippines; C) Tanzania. In each scenario, fixed technology/platform introduction and maintenance costs are shared across expanded user numbers (i.e., 2× study population, 5× study population, 10× study population, and 100× study population) while maintaining the same variable costs.

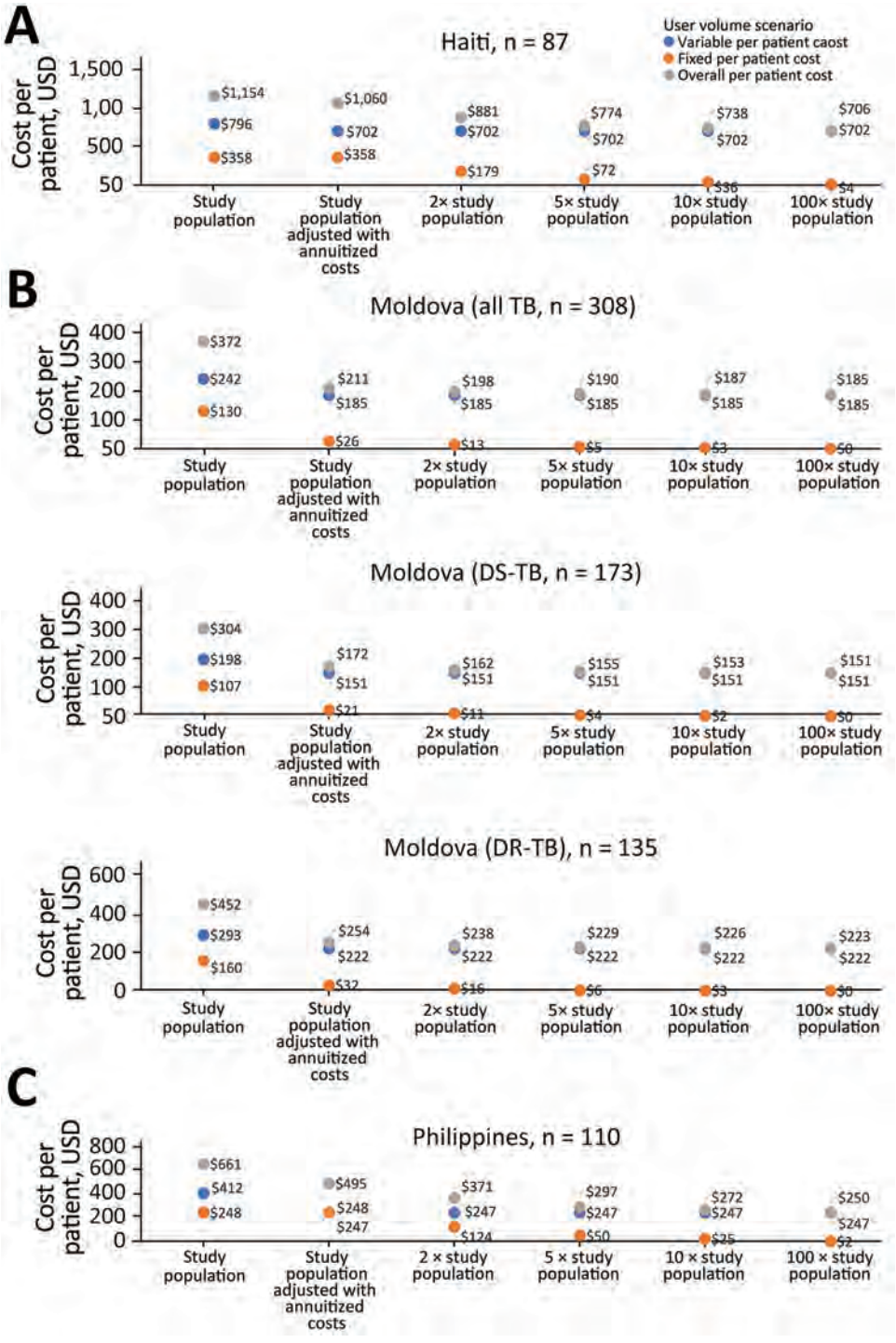

Figure 2. Video-observed tuberculosis therapy scale-up scenario analysis for 3 countries: A) Haiti; B) Moldova; C) the Philippines. In each scenario, fixed technology/platform introduction and maintenance costs are shared across expanded user numbers (i.e., 2× study population, 5× study population, 10× study population, and 100× study population) while maintaining the same variable costs. All TB, all TB patients; DR-TB, drug-resistant TB; DS-TB, drug-susceptible TB; TB, tuberculosis.

For the scenario in which fixed costs are covered by donors, VOT was cost saving in Moldova but not in Haiti or the Philippines. In that scenario, TB programs would be able to support treatment with VOT for $702 per patient compared with $414 per patient with DOT in Haiti, $151 compared with $336 in Moldova (DS-TB), $222 compared with $504 in Moldova (DR-TB), $185 compared with $427 in Moldova (all TB patients), and $247 compared with $17 per patient in the Philippines.

Discussion

Our cost analysis for 2 DATS covered a wide range of settings with diverse populations, socioeconomic conditions, and TB epidemiology. Implementation costs, particularly infrastructure and training costs,

were substantial when limited to a small number of persons with TB. However, if the DAT programs are scaled up to cover larger numbers of persons, the healthcare system cost per treatment course would fall and could become less expensive than paid in-person DOT.

The same infrastructure can be stretched only so far; a better knowledge of its capacity will be essential for understanding cost and budgetary effects of DAT expansion. Moving forward, it will also be useful to account for potential cost savings to the healthcare system, to the extent that in-person DOT is reduced and especially for potential cost savings to persons and families affected by TB.

Among the strengths of our analysis are a diversity of real-world settings, reflective of those in which TB care is provided, and the use of carefully gathered microcosting data. We explicitly considered scenarios in which user volume could be expanded to better harness the necessary technical infrastructure. However, the numbers of persons with TB included in these projects varied, and the project settings were not always representative of the available resources and infrastructure in some places where persons with TB obtain care. According to questionnaire responses from local project personnel, DOT visits were substantially longer in the Philippines and Bangladesh than at the other project sites. Nonetheless, those data provide relevant insights for managers and policy makers considering adding those technologies to their TB treatment programs.

We did not evaluate effectiveness of the DATs, which has been addressed in other related publications; an analysis of the feasibility and acceptability of DATs in the TB REACH projects is forthcoming (*26*). Limitations of the technologies themselves have been recognized: for example, messages received or not received by the 99DOTS platform do not necessarily equate with medication ingestion or lack thereof (*27*,*28*). Hence, direct comparisons of DAT and DOT costs are only appropriate to the extent that clinical outcomes with the DAT in question are similar to or better than standard care; we explicitly did not address that point in our analysis. Our study considered only economies of scale resulting from sharing of fixed infrastructure and equipment costs by more users. We did not have specific information as to how variable costs (e.g., HCW time, phones, and data charges) might fall with increased user numbers (e.g., greater HCW efficiency, discounted phones, and data with larger bulk purchasing). Clearly, any reductions in variable costs at scale would be relevant to providers and payers.

Of note, we did not evaluate costs or savings for patients and family members with regard to constraints such as missed work hours or childcare needs, which may be mitigated when in-person DOT is replaced by digital treatment support. Other studies have highlighted the value of such savings in the DAT context (*29*,*30*).

Among the limitations to our comparison of DATs with DOT, the total estimated cost for DOT was

Table 3. Digital adherence technologies compared with directly observed therapy costs*

Cost	99DOTS sites, US$			VOT sites, US$				
	Bangladesh, healthcare facility	Philippines, health care facility	Tanzania, home	Haiti, prison	Moldova, health facility			Philippines, healthcare facility or home
					DS-TB	DR-TB	All TB	
Crude estimate for DOT cost for the standard of care derived from the costing tool								
Hourly wage of person offering DOT support	0.83	1.40	0.00	4.60	11.20	11.20	11.20	2.88
Duration of DOT visit, min	45	45	0	45	15	15	15	2
Total per patient cost								
DOT cost from study data	74	176	0	414	336	504	427	17
DOT cost from the literature	36 (*22*)	155 (*23*)	89 (*24*)	49 (*25*)				166 (*23*)
Annuitized cost of DAT	81	92	163	1,060	172	254	211	495
Variable DAT costs only	60	83	160	702	151	222	185	247
Incremental per patient cost for the DAT versus standard of care								
Study data as comparator†	7	–84	163	646	–164	–250	–216	478
Prior published data as comparator‡	45	–63	74	1,011	–	–	–	329
Incremental per patient cost for the DAT using variable costs only versus standard of care, assuming fixed costs are already sunk								
Study data as comparator†	–14	–93	160	288	–185	–282	–242	230
Prior published data as comparator‡	24	–72	71	653	–	–	–	81

*DAT, digital adherence technologies; DOT, directly observed therapy; –, no prior published data available for comparison.
†Negative incremental costs indicate savings for the DAT relative to standard of care.
‡There is no available literature documenting the cost of DOT in Moldova; therefore, we did not calculate incremental costs when published literature was the comparator.

based on the reported staff time cost per DOT visit multiplied by the number of DOT visits expected for a complete course of treatment (perfect attendance). However, for 99DOTS and VOT, we included only the costs of the actual calls made and videos sent. On the other hand, we had explicit microcosting information, which enabled us to include the cost of escalation (additional phone calls and home visits) in the case of suboptimal adherence detected with the DATs. We did not have such granular data available for escalation costs in the event of suboptimal adherence during DOT. Similarly, we did not include DOT training costs because we did not have data for those.

The high costs of DATs, especially VOT, are driven largely by up-front infrastructure costs such as computing equipment and phones, initial configuration, and software licensing (Appendix Table 3). For Haiti and Moldova, where the cost of purchasing phones accounted for a substantial portion of the per patient cost, the loan of phones to patients or their use of personal phones would drastically lower the cost of implementing VOT. The per-patient cost was notably higher in Haiti because of higher hardware cost at the beginning of the project; there was a learning curve when evaluating whether tablets or phones were best suited for the intervention.

Asynchronous VOT offsets some recurrent costs associated with synchronous VOT and improves flexibility by allowing persons with TB to record medication ingestion within an agreed range of time, even if they did not have internet access at that moment (*31*). Similarly, the use of compressed video files can lower data-use costs. Less worker time is needed if the recordings are reviewed at higher playback speed or if computer-assisted recognition of pill swallowing is used (*32*; J.N. Sekandi, unpub. data, https://doi.org/10.2139/ssrn.4074672). However, those adaptations may not be sufficient to make VOT easily accessible to TB programs in low- and lower middle-income countries. Our scenario analysis suggests that the initial capital investment would have to be covered by donor funds for this technology to become cost saving to local TB programs in these settings.

Global DAT initiatives for TB are addressing the infrastructure cost burden by improving market access, procurement mechanisms, and supply chains (*33*). Our study complements this work by carefully documenting capital and operating expenditures, allowing for better planning and decisions by TB treatment programs (*34*). Our cost estimates for 99DOTS are similar to those from other TB programs that have used this technology (*15*,*35*). A recent study from the United States estimated that VOT was less expensive than in-person DOT provided by healthcare staff (*29*) for both the healthcare system and for persons with TB and their families. The extent that DATs offload HCWs from in-person observation will reduce their net cost.

However, local factors also further shape overall costs, such as the cost of internet and SMS (short message service), the DAT and platform used, specific infrastructure used and patient population served, labor costs, varying nature of services, and treatment duration. Barriers beyond internet connectivity and infrastructure include restricted availability, accessibility, and affordability of some technologies for persons in resource-limited areas and, similarly, the availability and affordability of technical personnel needed to support the TB clinics (*26*,*36*). Hence, real-world cost, effectiveness, and implementation data from high TB-incidence, lower-income settings will remain paramount.

In conclusion, advances in the usability and acceptability of DATs, coupled with widespread internet access and mobile phone use, make them viable tools for person-centered adherence support. However, economic evaluations are limited to date. Our analysis suggests that 99DOTS may be affordable to TB programs in diverse settings, particularly if used at scale. VOT appears less affordable for lower-income countries, although costs for both technologies could be reduced if the same infrastructure and hardware could support more patients, and both technologies would be cost saving should their fixed cost be covered by international donor funds. Our work is a step toward future cost-effectiveness analysis of DATs as more clinical outcome data become available.

Acknowledgments

We acknowledge Olivia Oxlade, who substantially contributed to the development of the data collection tools, and Jonathon Campbell, who provided invaluable guidance during the analysis.

This study was supported by a grant from TB REACH, Wave 6 through funding from the Bill and Melinda Gates Foundation (grant no. OPP1139029) and Global Affairs Canada (grant no. CA-3-D000920001).

K.S., A.K., and N.P.N. contributed to study concept and design; all authors contributed to data collection and curation; A.K., N.P.N., and K.S. contributed to data harmonization and analysis; N.P.N., A.K., and K.S. contributed to drafting the manuscript: and all authors contributed to manuscript revisions and intellectual content.

About the Author

Mr. Nsengiyumva is a research analyst with degrees in applied mathematics and health informatics. He is part of the McGill International TB Centre, where his current research uses modeling of TB epidemiology and cost-effectiveness analysis to evaluate TB interventions. He is currently evaluating the potential scale-up of latent TB infection screening of immigrants to Canada.

References

1. Stop TB, World Health Organization. An expanded DOTS framework for effective tuberculosis control. Int J Tuberc Lung Dis. 2002;6:378–88.
2. Imperial MZ, Nahid P, Phillips PPJ, Davies GR, Fielding K, Hanna D, et al. A patient-level pooled analysis of treatment-shortening regimens for drug-susceptible pulmonary tuberculosis. Nat Med. 2018;24:1708–15. https://doi.org/10.1038/s41591-018-0224-2
3. World Health Organization. What is DOTS? A guide to understanding the WHO-recommended TB control strategy known as DOTS [cited 2023 Mar 17]. https://apps.who.int/iris/handle/10665/65979
4. World Health Organization. Guidelines for treatment of drug-susceptible tuberculosis and patient care [cited 2023 Mar 17]. https://apps.who.int/iris/bitstream/handle/10665/255052/9789241550000-eng.pdf
5. Karumbi J, Garner P. Directly observed therapy for treating tuberculosis. Cochrane Database Syst Rev. 2015;2015:CD003343. https://doi.org/10.1002/14651858.CD003343.pub4
6. Pasipanodya JG, Gumbo T. A meta-analysis of self-administered vs directly observed therapy effect on microbiologic failure, relapse, and acquired drug resistance in tuberculosis patients. Clin Infect Dis. 2013;57:21–31. https://doi.org/10.1093/cid/cit167
7. Volmink J, Garner P. Directly observed therapy for treating tuberculosis. Cochrane Database Syst Rev. 2007; 4:CD003343. https://doi.org/10.1002/14651858.CD003343.pub3
8. Tian J-H, Lu ZX, Bachmann MO, Song FJ. Effectiveness of directly observed treatment of tuberculosis: a systematic review of controlled studies. Int J Tuberc Lung Dis. 2014;18:1092–8. https://doi.org/10.5588/ijtld.13.0867
9. Ngwatu BK, Nsengiyumva NP, Oxlade O, Mappin-Kasirer B, Nguyen NL, Jaramillo E, et al.; Collaborative Group on the Impact of Digital Technologies on TB. The impact of digital health technologies on tuberculosis treatment: a systematic review. Eur Respir J. 2018;51:1701596. https://doi.org/10.1183/13993003.01596-2017
10. Subbaraman R, de Mondesert L, Musiimenta A, Pai M, Mayer KH, Thomas BE, et al. Digital adherence technologies for the management of tuberculosis therapy: mapping the landscape and research priorities. BMJ Glob Health. 2018;3:e001018. https://doi.org/10.1136/bmjgh-2018-001018
11. Story A, Aldridge RW, Smith CM, Garber E, Hall J, Ferenando G, et al. Smartphone-enabled video-observed versus directly observed treatment for tuberculosis: a multicentre, analyst-blinded, randomised, controlled superiority trial. Lancet. 2019;393:1216–24. https://doi.org/10.1016/S0140-6736(18)32993-3
12. Nsengiyumva NP, Mappin-Kasirer B, Oxlade O, Bastos M, Trajman A, Falzon D, et al. Evaluating the potential costs and impact of digital health technologies for tuberculosis treatment support. Eur Respir J. 2018;52:1801363. https://doi.org/10.1183/13993003.01363-2018
13. Stop TB Partnership. Wave 6 digital adherence technology projects [cited 2023 Mar 17]. https://stoptb.org/global/awards/tbreach/wave6dat.asp
14. Stop TB Partnership. Costing tool—Wave 6 digital adherence technology projects [cited 2023 Mar 17]. https://www.stoptb.org/wave-6/wave-6-digital-adherence-technology-projects
15. Thompson RR, Kityamuwesi A, Kuan A, Oyuku D, Tucker A, Ferguson O, et al. Cost and cost-effectiveness of a digital adherence technology for tuberculosis treatment support in Uganda. Value Health. 2022;25:924–30. https://doi.org/10.1016/j.jval.2021.12.002
16. Chapko MK, Liu CF, Perkins M, Li YF, Fortney JC, Maciejewski ML. Equivalence of two healthcare costing methods: bottom-up and top-down. Health Econ. 2009;18:1188–201. https://doi.org/10.1002/hec.1422
17. Batura N, Pulkki-Brännström AM, Agrawal P, Bagra A, Haghparast-Bidgoli H, Bozzani F, et al. Collecting and analysing cost data for complex public health trials: reflections on practice. Glob Health Action. 2014;7:23257. https://doi.org/10.3402/gha.v7.23257
18. Flessa S, Moeller M, Ensor T, Hornetz K. Basing care reforms on evidence: the Kenya health sector costing model. BMC Health Serv Res. 2011;11:128. https://doi.org/10.1186/1472-6963-11-128
19. Conteh L, Walker D. Cost and unit cost calculations using step-down accounting. Health Policy Plan. 2004;19:127–35. https://doi.org/10.1093/heapol/czh015
20. World Bank. Inflation, consumer prices (annual %) [cited 2022 Jul 22]. https://data.worldbank.org/indicator/FP.CPI.TOTL.ZG
21. World Bank. Official exchange rate (LCU per US$, period average [cited 2022 Jul 22]. https://data.worldbank.org/indicator/PA.NUS.FCRF
22. Gomez GB, Dowdy DW, Bastos ML, Zwerling A, Sweeney S, Foster N, et al. Cost and cost-effectiveness of tuberculosis treatment shortening: a model-based analysis. BMC Infect Dis. 2016;16:726. https://doi.org/10.1186/s12879-016-2064-3
23. Tupasi TE, Gupta R, Quelapio MID, Orillaza RB, Mira NR, Mangubat NV, et al. Feasibility and cost-effectiveness of treating multidrug-resistant tuberculosis: a cohort study in the Philippines. PLoS Med. 2006;3:e352. https://doi.org/10.1371/journal.pmed.0030352
24. Wandwalo E, Robberstad B, Morkve O. Cost and cost-effectiveness of community based and health facility based directly observed treatment of tuberculosis in Dar es Salaam, Tanzania. Cost Eff Resour Alloc. 2005;3:6. https://doi.org/10.1186/1478-7547-3-6
25. Jacquet V, Morose W, Schwartzman K, Oxlade O, Barr G, Grimard F, et al. Impact of DOTS expansion on tuberculosis related outcomes and costs in Haiti. BMC Public Health. 2006;6:209. https://doi.org/10.1186/1471-2458-6-209
26. Casalme DJO, Marcelo DB, Dela Cuesta DM, Tonquin M, Frias MVG, Gler MT. Feasibility and acceptability of asynchronous VOT among patients with MDR-TB. Int J Tuberc Lung Dis. 2022;26:760–5. https://doi.org/10.5588/ijtld.21.0632
27. Thomas BE, Kumar JV, Chiranjeevi M, Shah D, Khandewale A, Thiruvengadam K, et al. Evaluation of the accuracy of 99DOTS, a novel cellphone-based strategy for monitoring adherence to tuberculosis medications: comparison of DigitalAdherence data with urine isoniazid testing. Clin Infect Dis. 2020;71:e513–6. https://doi.org/10.1093/cid/ciaa333

28. de Groot LM, Straetemans M, Maraba N, Jennings L, Gler MT, Marcelo D, et al. Time trend analysis of tuberculosis treatment while using digital adherence technologies-an individual patient data meta-analysis of eleven projects across ten high tuberculosis-burden countries. Trop Med Infect Dis. 2022;7:65. https://doi.org/10.3390/tropicalmed7050065
29. Beeler Asay GR, Lam CK, Stewart B, Mangan JM, Romo L, Marks SM, et al. Cost of tuberculosis therapy directly observed on video for health departments and patients in New York City; San Francisco, California; and Rhode Island (2017-2018). Am J Public Health. 2020;110:1696–703. https://doi.org/10.2105/AJPH.2020.305877
30. Au-Yeung KY, DiCarlo L. Cost comparison of wirelessly vs. directly observed therapy for adherence confirmation in anti-tuberculosis treatment. Int J Tuberc Lung Dis. 2012;16:1498–504. https://doi.org/10.5588/ijtld.11.0868
31. Garfein RS, Doshi RP. Synchronous and asynchronous video observed therapy (VOT) for tuberculosis treatment adherence monitoring and support. J Clin Tuberc Other Mycobact Dis. 2019;17:100098. https://doi.org/10.1016/j.jctube.2019.100098
32. Kumwichar P, Chongsuvivatwong V, Prappre T. Development of a video-observed therapy system to improve monitoring of tuberculosis treatment in Thailand: mixed-methods study. JMIR Form Res. 2021;5:e29463. https://doi.org/10.2196/29463
33. TB Digital Adherence. Procurement [cited 2023 Mar 12]. https://tbdigitaladherence.org/implement/procure
34. TB Digital Adherence. Financial planning for DATs [cited 2023 Mar 13]. https://tbdigitaladherence.org/implement/budget
35. Adherence Support Coalition to End TB (ASCENT). Digital adherence technologies: technical guidance & budget for Global Fund funding request [cited 2023 Mar 17]. https://www.thearcadygroup.com/wp-content/uploads/2020/07/TAG_Digital-Adherence-Technologies-Technical-Guidance-1.0.pdf
36. Bommakanti KK, Smith LL, Liu L, Do D, Cuevas-Mota J, Collins K, et al. Requiring smartphone ownership for mHealth interventions: who could be left out? BMC Public Health. 2020;20:81. https://doi.org/10.1186/s12889-019-7892-9

Address for correspondence: Kevin Schwartzman, Centre for Outcomes Research and Evaluation, Research Institute of the McGill University Health Centre, 5252 Boulevard de Maisonneuve Ouest, Rm 3D.63, Montreal, QB H4A 3S5, Canada; email: kevin.schwartzman@mcgill.ca

etymologia revisited

Trichinella spiralis

[tri kuh neh′ luh spr a′ luhs]

Trichinella is derived from the Greek words *trichos* (hair) and *ella* (diminutive); *spiralis* means spiral. In 1835, Richard Owen (1804–1892) and James Paget (1814–1899) described a spiral worm (*Trichina spiralis*)–lined sandy diaphragm of a cadaver. In 1895, Alcide Raillet (1852–1930) renamed it as *Trichinella spiralis* because *Trichina* was attributed to an insect in 1830. In 1859, Rudolf Virchow (1821–1902) described the life cycle. The genus includes many distinct species, several genotypes, and encapsulated and nonencapsulated clades based on the presence/absence of a collagen capsule.

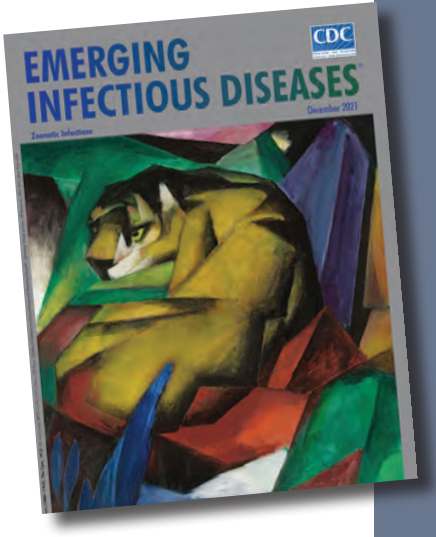

Originally published in December 2021

References

1. Campbell WC. History of trichinosis: Paget, Owens and the discovery of *Trichinella spiralis*. Bull Hist Med. 1979;53:520–52.
2. Centers for Disease Control and Prevention. Trichinellosis: general information [cited 2021 May 11]. https://www.cdc.gov/parasites/trichinellosis/gen_info/faqs.html
3. Gottstein B, Pozio E, Nöckler K. Epidemiology, diagnosis, treatment, and control of trichinellosis. Clin Microbiol Rev. 2009;22:127–45. https://doi.org/10.1128/CMR.00026-08
4. Observations on *Trichina spiralis*. Boston Med Surg J. 1860; 63:294–8. https://doi.org/10.1056/NEJM186011080631504
5. Zarlenga D, Thompson P, Pozio E. *Trichinella* species and genotypes. Res Vet Sci. 2020;133:289–96. https://doi.org/10.1016/j.rvsc.2020.08.012

https://wwwnc.cdc.gov/eid/article/27/12/et-2712_article

Doxycycline Prophylaxis for Skin and Soft Tissue Infections in Naval Special Warfare Trainees, United States[1]

Jeffrey Spiro, Piotr Wisniewski, Julia Schwartz, Alfred G. Smith, Sara Burger, Drake H. Tilley, Ryan C. Maves

In 2015, several severe cases of skin and soft tissue infection (SSTI) among US Naval Special Warfare trainees prompted the introduction of doxycycline prophylaxis during the highest-risk portion of training, Hell Week. We performed a retrospective analysis of the effect of this intervention on SSTI incidence and resulting hospital admissions during 2013–2020. In total, 3,371 trainees underwent Hell Week training during the study period; 284 SSTIs were diagnosed overall, 29 of which led to hospitalization. After doxycycline prophylaxis was introduced, admission rates for SSTI decreased from 1.37 to 0.64 admissions/100 trainees (p = 0.036). Overall SSTI rates remained stable at 7.42 to 8.86 SSTIs/100 trainees (p = 0.185). Hospitalization rates per diagnosed SSTI decreased from 18.4% to 7.2% (p = 0.009). Average length of hospitalization decreased from 9.01 days to 4.33 days (p = 0.034). Doxycycline prophylaxis was associated with decreased frequency and severity of hospitalization for SSTIs among this population.

Skin and soft tissue infections (SSTIs) are common and potentially severe medical conditions that occur regularly in both military and nonmilitary populations. Military members, however, have a 21% higher incidence of SSTI than do similarly aged nonmilitary populations because of a variety of factors, such as increased rate of minor traumatic injuries and intermittently poor hygiene practices often associated with field exercises and deployments to austere locations (*1*). Furthermore, a disproportionate burden of SSTI in the military occurs in recruit and training settings, likely resulting from increased crowding, decreased adherence to good personal hygiene, and environmental contamination (*1*,*2*).

United States Naval Special Warfare (NSW) training in Coronado, California, USA, exposes trainees to extreme physical stresses and environmental conditions that create an ideal setting for increased frequency and severity of SSTIs. In 2015, medical staff at the Naval Special Warfare Center (NSWCEN) identified a concerning trend in its trainees, when a series of severe SSTIs were identified as being caused by invasive gram-negative saltwater-associated pathogens, including *Shewanella algae* and *Vibrio* spp. (*3*). Those severe SSTIs primarily occurred during the highest-risk phase of training, Hell Week, which consists of 5 days of intense exertion with minimal rest and continuous exposure to wet and cold environments.

As a result, starting in September 2015, all NSW trainees entering Hell Week received 100 mg oral doxycycline daily as prophylaxis primarily aimed at limiting the incidence of severe SSTIs, particularly those caused by invasive gram-negative saltwater-associated pathogens. Trainees started prophylaxis 2 days before Hell Week and stopped the day after completing the training exercise (8 total doses). For this study, we reviewed data from 2013–2020 to determine whether this intervention had any significant effect on the rate, severity, or quality of SSTIs in the NSW trainee population during Hell Week.

Methods

Our study was a retrospective cohort study of all NSW trainees who participated in the Hell Week phase of

Author affiliations: Naval Medical Center, San Diego, California, USA (J. Spiro, P. Wisniewski, D.H. Tilley, R.C. Maves); Naval Health Research Center, San Diego (P. Wisniewski); Naval Special Warfare Center, Coronado, California, USA (J. Schwartz, S. Burger); Naval Medical Center, Portsmouth, Virginia, USA (A.G. Smith); Wake Forest University School of Medicine, Winston-Salem, North Carolina, USA (R.C. Maves)

DOI: https://doi.org/10.3201/eid3001.230890

[1]Preliminary findings were presented at IDWeek 2019, Washington, DC, USA, October 2–6, 2019.

training during April 2013–February 2020 at the NSW Center in Coronado, California. We selected this timeframe because of limited data availability: NSWCEN used nonelectronic medical records before April 2013 that were no longer available at the time of this analysis. The study was approved as minimal risk with a waiver of informed consent by the Naval Medical Center San Diego (NMCSD) institutional review board on July 26, 2021 (approval no. NMCSD.2021.0007).

Overall, 42 separate Hell Weeks occurred during the study timeframe, roughly every 2 months. NMCSD is the principal care location for NSW trainees requiring emergency or inpatient care. To this end, we requested hospital admission data for all NSW trainees admitted to NMCSD during the study period. We narrowed the search further by only requesting data from the 42 Hell Week periods. Each Hell Week period was specifically defined as the training exercise itself (5 days) plus the 7 days after its completion. This timeframe helped to account for SSTIs that likely began during Hell Week but were not diagnosed until several days after its conclusion. Once admission data were obtained, investigators (primarily J. Spiro) reviewed data from each admission to determine whether the primary reason for hospitalization was treatment of an SSTI. Once those target cases were identified, we compiled and analyzed relevant data points. Separately, a limited amount of deidentified data was also provided from the NSWCEN medical staff directly. Those data consisted only of the number of NSW trainees who participated in each Hell Week, as well as the number of SSTIs diagnosed locally at the NSWCEN clinic during each Hell Week period, regardless of whether that trainee ultimately required hospitalization. The case definition of SSTI at NSWCEN was consistent throughout the study period and was based on clinical manifestations, mainly skin erythema, edema, and warmth with or without concurrent abscess, which led to initiation of treatment-dose antimicrobial therapy. Of note, data regarding common side effects related to doxycycline use were not readily available from NSWCEN, so we did not analyze side effect incidence during the study timeframe. Although specific documentation of medication adherence was not available, all doxycycline doses were administered under directly observed therapy by NSWCEN medical personnel for the duration of prophylaxis. Last, to assess for development of resistance to doxycycline over the study timeframe, the NMCSD microbiology department provided antibiotic susceptibility data for blood and wound cultures positive with *Staphylococcus aureus* from all NSW trainees during the study period, regardless of whether they were participating in Hell Week or hospitalized for an SSTI.

The primary outcome of this study was hospital admission rates for SSTI during Hell Week periods before and after initiating doxycycline prophylaxis. September 2015 was the first Hell Week period during which trainees received doxycycline prophylaxis and marked the beginning of the post-doxycycline prophylaxis cohort. Secondary outcomes included overall incidence of SSTIs (regardless of hospital admission), percentage of diagnosed SSTIs that led to hospitalization, length of hospitalization, and assessment for notable changes in blood and wound culture data before and after the doxycycline prophylaxis. The NMCSD microbiology department performed all blood and wound culture analysis per hospital protocol and procedures did not differ during the study period. Minimal changes were made to training protocols during Hell Week at NSWCEN during the study timeframe, so the preintervention cohort served as the functional control group for this analysis. In addition, given that Hell Week periods occurred roughly every 2 months during the study timeframe, their seasonal distribution did not meaningfully differ before and after doxycycline prophylaxis, and we did not perform analysis incorporating seasonal incidence of disease.

Statistical analysis of hospital admission rates for SSTI, general incidence of SSTI, and percentage of diagnosed SSTI leading to hospitalization all involved comparison of incidence rates for which we determined 2-tailed z-scores with a p value cutoff of <0.05. We used the Byar method to develop rate ratios when applicable. We treated length of hospital stay before and after the intervention as independent groups and analyzed them with unpaired t-tests, again using a p value of <0.05 as significant. We used OpenEpi version 3 (https://www.openepi.com/Menu/OE_Menu.htm) for calculations. We limited analysis of blood and wound culture data to descriptive statistics given the more nuanced nature of the data and the smaller sample size.

Results

A total of 3,371 NSW trainees participated in the 42 Hell Week training periods during April 2013–February 2020. From that population, 70 patients were admitted to NMCSD for all medical conditions; 29 of those admissions were primarily for treatment of SSTI. Specific demographic data on the 3,371 trainees were limited because of variable attrition rates in each class throughout the training process. However, all trainees were men 18–33 years of age. Most trainees

were enlisted personnel, and most enlisted and officer trainees had no previous active military experience. The 29 trainees hospitalized for SSTIs were all men; age range was 19–28 years (mean 23.4 years). Of 29 hospital admissions, 13/29 (44.8%) occurred during Hell Week, and 16/29 (55.2%) occurred in the 7 days after each Hell Week. Mean time from start of Hell Week to hospital admission was 6.24 days. Twenty cases involved SSTI in 1 or both lower extremities, 3 cases involved a combination of upper and lower extremities, and 6 cases involved an isolated upper extremity. Seven patients had clear abscesses or another complication that required incision and drainage or other surgical intervention. Four patients required treatment in the intensive care unit. No deaths occurred among the 29 trainees hospitalized for SSTI during the study period.

Doxycycline prophylaxis during Hell Week started in September 2015. Fifteen Hell Weeks involving 1,024 trainees occurred before doxycycline prophylaxis began, and 27 Hell Weeks involving 2,347 trainees took place after the intervention. Fourteen of 29 cases of SSTI requiring hospital admission occurred before doxycycline prophylaxis was implemented, a rate of 1.37 hospitalizations/100 trainees. Fifteen of 29 cases took place after the intervention began, a rate of 0.64 hospitalizations/100 trainees. Those values correspond to a rate ratio of 0.468 (95% CI 0.226–0.968; p = 0.036) for SSTI leading to hospitalization after implementing doxycycline prophylaxis and a theoretical number needed to treat of 137.3 trainees to prevent 1 hospitalization for SSTI (Table 1).

A total of 284 SSTIs were diagnosed locally at the NSWCEN medical clinic during the study period; 76 infections occurred before the doxycycline prophylaxis was enacted and 208 after (Figure). The more general incidence of SSTI before the intervention was 7.42 SSTIs per 100 trainees, whereas the incidence after the intervention was 8.86 SSTIs per 100 trainees. Those data correspond to a rate ratio of 1.19 (95% CI 0.918–1.55; p = 0.185) for SSTI after doxycycline prophylaxis was begun. In the preintervention period, 14 hospitalizations among 76 SSTI cases resulted in an 18.4% admission rate, whereas 15 hospitalizations among 208 SSTIs in the postintervention period produced a 7.2% admission rate. The hospitalizations per infection rate ratio was 0.392 (95% CI 0.189–0.811; p = 0.0089) after doxycycline prophylaxis was started (Table 1). The average length of hospitalization in trainees admitted for SSTI in the predoxycycline prophylaxis period was a mean of 9.07 days (median 7 days); average length in the postdoxycycline prophylaxis period was a mean of 4.33 days (median 4 days). The difference of those means was 4.74 days (95% CI 0.40–9.08; p = 0.034) (Table 1).

Blood and wound culture data from the 29 trainees hospitalized for SSTI revealed 7 case-patients with positive wound cultures and 3 cases of bacteremia before initiation of doxycycline prophylaxis. In the postintervention population, data revealed 8 case-patients with positive blood cultures and 2 cases of bacteremia. *S. aureus* and *Streptococcus pyogenes* were the most commonly identified pathogens both before and after doxycycline prophylaxis was introduced (Table 2). We observed a notable change in invasive infections with gram-negative saltwater-associated pathogens. Four cases of *S. algae* infection (3 from wound culture, 1 from blood culture) and 2 cases of *Vibrio* spp. (from both wound and blood cultures) were identified preintervention, whereas 1 case of *S. algae* infection (from blood culture) and 1 case of *Vibrio* spp. infection (wound culture) were seen postintervention.

Blood and wound culture data regarding *S. aureus* antibiotic susceptibility in all NSW trainees throughout the study period (including those outside of Hell Week training) showed 37 *S. aureus* isolates with documented tetracycline class sensitivities, reported for minocycline in all cases. There were 10 isolates in the predoxycycline cohort, all of which were sensitive to minocycline (MIC ≤0.5). In the postdoxycycline cohort, 27 isolates had documented sensitivities; 25 were minocycline-sensitive (MIC ≤0.5), 1 had intermediate sensitivity to minocycline (MIC <8), and 1 was resistant to minocycline (MIC >16).

Discussion

The principal finding of our study was that the introduction of doxycycline prophylaxis to NSW trainees entering Hell Week was associated with a decreased

Table 1. Primary and secondary outcome data in study of doxycycline prophylaxis for SSTIs in Naval Special Warfare trainees, United States*

Outcome	Preprophylaxis	Postprophylaxis	Rate ratio (95% CI)	p value
Hospital admission rate per 100 trainees	1.37 (14/1,024)	0.64 (15/2,347)	0.468 (0.226–0.968)	0.036
Mean hospital admission length, d	9.07	4.33	NA	0.034
Overall SSTI incidence rate per 100 trainees	7.42 (76/1,024)	8.86 (208/2,347)	1.19 (0.918– 1.55)	0.185
Hospital admission rate per diagnosed SSTI	18.4 (14/76)	7.2 (15/208)	0.392 (0.189–0.811)	0.0089

*Values are % (no. patients/total no. in category) except as indicated. NA, not applicable; SSTI, skin and soft tissue infection.

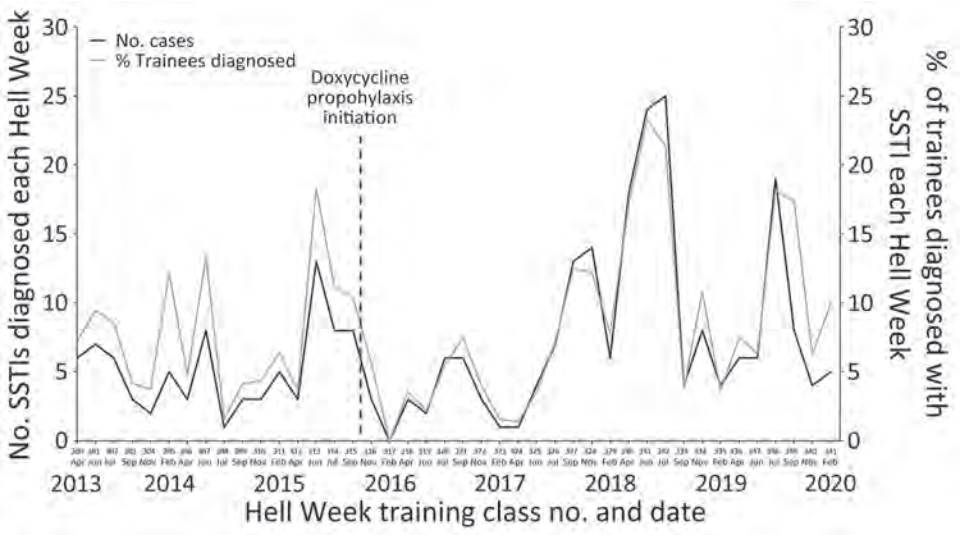

Figure. Total number of SSTIs diagnosed at the Naval Special Warfare Center medical clinic during each Hell Week with corresponding percentage of Naval Special Warfare trainees diagnosed with SSTI in each training class, United States. Each Hell Week is labeled by month, year, and training class number (300–341). Date of doxycycline prophylaxis initiation is indicated. SSTI, skin and soft tissue infection.

incidence of hospitalization for severe SSTI. In addition, secondary findings of significantly decreased rate of hospitalization per diagnosed SSTI and decreased length of hospitalization after doxycycline prophylaxis further support an overall decrease in the severity of SSTIs in the study population. The overall incidence of SSTI (regardless of hospitalization status) did not change significantly, possibly suggesting that mild-to-moderate SSTIs were less affected by doxycycline prophylaxis. This application of doxycycline prophylaxis focused on reducing severe SSTIs caused by occupational or recreational exposure. Other investigations into doxycycline as prophylaxis against skin infection have mostly centered on prevention of iatrogenic complications, such as surgical site infections (*4*–*6*), or severe infections related to toxicities of antineoplastic agents, such as cetuximab or panitumumab (*7*,*8*). In military populations, efforts to prevent SSTIs (largely aimed at *S. aureus* infections) have been limited to decolonizing strategies, such as intranasal mupirocin or topical chlorhexidine, in addition to several more recent vaccination trials (*9*).

Doxycycline has a well-established history for use as prophylaxis against other infections, such as malaria (*10*,*11*) and, more recently, syphilis (*12*–*14*). Doxycycline has also been used as prophylaxis against potential bioterrorism agents, such as anthrax and tularemia (*15*,*16*), as well as against Lyme disease (*17*), leptospirosis (*18*), and other zoonoses. Dosing of doxycycline for those purposes has varied depending on the study, but typically is either intermittent 200 mg doses (given either before or after exposure) or daily 100 mg doses. Pharmacokinetic data indicate that a 200 mg dose is largely eliminated from the body after roughly 3–5 days, and some studies have questioned the efficacy of 200 mg weekly dosing schedules (*19*,*20*). Regardless, the choice of dosing schedule is typically tailored to the recipient and environment, particularly because less frequent drug administration might sometimes be the only practical option. Overall, this large body of evidence is indicative of doxycycline's relative safety and tolerability for populations at high risk for polypharmacy or drug side effects.

Table 2. Wound and blood culture data from Naval Special Warfare trainees hospitalized for skin and soft tissue infections in the periods before and after implementation of doxycycline prophylaxis, United States

	Preprophylaxis		Postprophylaxis	
Pathogen	Positive wound cultures	Positive blood cultures	Positive wound cultures	Positive blood cultures
Staphylococcus aureus	6	1	5	1
Group A *Streptococcus*	4	0	4	0
Shewanella algae	3	1	0	1
Vibrio spp.	2	1	1	0
Coagulase-negative *Staphylococcus*	2	0	1	1
Staphylococcus lugdunensis	1	0	0	0
Diptheroids	1	0	2	0
Enterococcus faecalis	2	0	0	1
Acinetobacter hemolyticus	2	0	0	0
Pseudomonas aeruginosa	1	0	0	0
Providencia rettgeri	0	0	1	0

The nature and intensity of NSW training places the subjects of this study at particularly high risk for SSTIs, both from common causes like *S. pyogenes* and *S. aureus* and from rarer saltwater-associated organisms, such as *Vibrio* spp. and *S. algae*. The reasons for this higher risk are multifactorial. NSW trainees during Hell Week experience substantial and often diffuse skin breakdown and extremity edema because of the intensity of the physical training and near-constant exposure to ocean water. In addition, NSW trainees might have a component of functional immune impairment as a result of minimal sleep, high stress, and frequent transmission of more minor communicable illnesses. Antibiotic prophylaxis in such settings is not novel; chemoprophylaxis has long been used to target invasive infections from group A *Streptococcus* in military training populations (*21*). The doxycycline prophylaxis analyzed in this study was specifically started in 2015 to limit severe invasive infections caused by saltwater-associated gram-negative pathogens such as *Vibrio* spp. and *S. algae* in the setting of a previous outbreak. Doxycycline is still considered a first-line agent for treating *Vibrio* spp. SSTIs with minimal documented resistance (*22*,*23*). Invasive *S. algae* infections are uncommon in otherwise young and healthy persons, as discussed in a recent case series from our center (*3*). Antibiotic susceptibility patterns are less well studied, but data from some areas show high rates of susceptibility to third-generation cephalosporins, fluoroquinolones, tetracycline, and aminoglycosides (*24*).

A review of doxycycline as long-term malaria prophylaxis by the Centers for Disease Control and Prevention in 2011 found mild-to-moderate gastrointestinal symptoms (nausea, abdominal pain) to be the most common adverse effect, occurring in 4%–33% of patients (*25*). An investigation of US Marines in Okinawa, Japan, in 2014 taking 200 mg doxycycline weekly reported side effects, primarily nausea, in 18% of 291 study participants. Peace Corps volunteers receiving long-term malarial prophylaxis reported gastrointestinal side effects in 40% of survey respondents taking doxycycline, but few of those persons reported severe symptoms, and symptoms did not frequently lead participants to discontinue the medication (*26*). More severe gastrointestinal manifestations, such as pill-induced esophagitis, occur in <1% of doxycycline recipients, although that number might be an underestimate (*25*,*27*,*28*). Phototoxicity has been reported in 7%–21% of persons taking doxycycline for long-term malaria prophylaxis, depending on the degree of sun exposure (*25*,*29*). Most of those side effects might be mitigated through some simple precautions (e.g., remaining upright after taking medications and taking them with adequate water to prevent pill esophagitis, wearing sunscreen and avoidance of direct skin exposure to sun for phototoxicity). In our investigation, a previously healthy population was exposed to doses of 100 mg doxycycline daily for 8 days. Although specific side effects were not actively solicited at the time, we noted no overt increase in attributable symptoms.

One possible concern with the type of intervention analyzed in this study is development of resistance against doxycycline. One relevant retrospective study from 2016 (*30*) analyzed 168 *S. aureus* isolates collected from wounded US military personnel returning from Iraq and Afghanistan during 2009–2012 with regard to tetracycline class resistance and doxycycline exposure, primarily in the form of long-term antimalarial prophylaxis. That study found overall resistance rates of 23% (tetracycline), 15% (doxycycline), and 14% (minocycline) and identified no significant association between doxycycline exposure and resistance to the tetracycline antimicrobial class (*30*). In our study, we assessed *S. aureus* sensitivity to tetracycline class antibiotics from blood and wound cultures and found 2 of 27 isolates with poor sensitivity (1 with intermediate resistance and 1 fully resistant) in the postdoxycycline prophylaxis period, compared with no documented resistance in the predoxycycline period. However, the 2 nonsensitive isolates were from 2015 and 2016 (relatively recently after initiation of doxycycline prophylaxis), and no documented resistance was seen in the 22 isolates from 2017–2020. On the basis of those limited data, we did not identify a concerning pattern for development of resistance to tetracycline-class antibiotics over the course of the study period. In addition, the intervention we analyzed was periodic, rather than continuous, possibly reducing any selective pressure to promote widespread resistance. Furthermore, the otherwise healthy population of trainees is unlikely to have extensive interaction within the medical setting after their Hell Week training, thereby reducing the likelihood of spreading more resistant clones to potentially immune-suppressed patients.

The first limitation of our study is that it was not a randomized trial, where rates of infection can be directly compared with minimal bias. However, given the limited changes to Hell Week training over the past 10 years, as well as the generally stable demographics of NSW trainees, the study population before doxycycline prophylaxis can reasonably be considered internal controls in this setting. Second,

this study was a retrospective analysis, preventing the assignment of any true causality to doxycycline prophylaxis. Data regarding adverse reactions in the study population were not reliably obtainable, and therefore we cannot be certain that a rise in minor iatrogenic issues was not present. In addition, after doxycycline prophylaxis was implemented, NSWCEN medical providers' increased awareness of serious SSTI complications could have led to their recognizing and treating infections earlier, ultimately limiting the severity of illness in the postintervention cohort. Finally, the total number of hospital admissions for SSTI was relatively small, thereby increasing the chance that the lower incidence of SSTI noted after the intervention was coincidental.

The overall goal of this study was to determine whether introducing doxycycline prophylaxis to NSW trainees entering Hell Week had an effect on the severity, rate, and quality of SSTI. Our data indicate that doxycycline prophylaxis in this population was associated with a significantly decreased rate of hospitalization for SSTI, decreased rate of hospitalization per identified SSTI, and a decreased length of hospitalization for SSTI treatment. General rates of SSTI diagnosed by clinic medical providers were not significantly different before and after doxycycline prophylaxis. Fewer cases of severe SSTI caused by invasive gram-negative saltwater-associated pathogens (*Shewanella* spp., *Vibrio* spp.) were associated doxycycline prophylaxis, but because of the small number of those infections, we did not measure the decrease statistically.

In conclusion, doxycycline appears generally well tolerated and was associated with a decrease in severe SSTIs requiring hospitalization, as well as a decrease in cases caused by aquatic gram-negative pathogens. In special populations whose circumstances include prolonged saltwater exposure and participation in activities that place them at high risk for skin trauma, doxycycline prophylaxis at the time of highest risk appears safe and might reduce the risk for severe SSTIs.

Acknowledgments

We thank the medical and training staff at the Naval Special Warfare Center for their assistance with this project.

J. Spiro performed the primary literature search and data analysis, wrote and edited the manuscript, and created figures. P.W. assisted with the literature search and wrote and edited the manuscript. J. Schwartz assisted in collating and analyzing data from NSWCEN. A.S., S.B., D.T., and R.M. assisted in study design, data analysis, and manuscript preparation.

About the Author

Dr. Spiro is a naval officer and infectious diseases fellow at the Naval Medical Center San Diego in San Diego, California. He previously served as an undersea medical officer at the Naval Special Warfare Center in Coronado, California.

References

1. Stahlman S, Williams VF, Oh GT, Millar EV, Bennett JW. Skin and soft tissue infections, active component, U.S. Armed Forces, 2013–2016. MSMR. 2017;24:2–11.
2. Leamer NK, Clemmons NS, Jordan NN et al. Update: community-acquired MRSA skin and soft tissue infection surveillance among active duty military personnel at Fort Benning GA, 2008–2010. Mil Med. 2013;178:914–20.
3. Bauer MJ, Stone-Garza KK, Croom D, et al. *Shewanella algae* infections in United States Naval Special Warfare Trainees. Open Forum Infect Dis. 2019; 6:ofz442. https://doi.org/10.1093/ofid/ofz442 PMID 31696143
4. Giske A, Nymo LS, Fuskevåg OM, Amundsen S, Simonsen GS, Lassen K. Systemic antibiotic prophylaxis prior to gastrointestinal surgery—is oral administration of doxycycline and metronidazole adequate? Infect Dis (Lond). 2017;49:785–91. https://doi.org/10.1080/23744235.2017.1342044
5. Namdari S, Nicholson T, Parvizi J, Ramsey M. Preoperative doxycycline does not decolonize *Propionibacterium acnes* from the skin of the shoulder: a randomized controlled trial. J Shoulder Elbow Surg. 2017;26:1495–9. https://doi.org/10.1016/j.jse.2017.06.039
6. Rao AJ, Chalmers PN, Cvetanovich GL, et al. Preoperative doxycycline does not reduce *Propionibacterium acnes* in shoulder arthroplasty. J Bone Joint Surg Am. 2018; 100:958–964.
7. Bachet JB, Peuvrel L, Bachmeyer C, Reguiai Z, Gourraud PA, Bouché O, et al. Folliculitis induced by EGFR inhibitors, preventive and curative efficacy of tetracyclines in the management and incidence rates according to the type of EGFR inhibitor administered: a systematic literature review. Oncologist. 2012;17:555–68. https://doi.org/10.1634/theoncologist.2011-0365
8. Petrelli F, Borgonovo K, Cabiddu M, Coinu A, Ghilardi M, Lonati V, et al. Antibiotic prophylaxis for skin toxicity induced by antiepidermal growth factor receptor agents:

a systematic review and meta-analysis. Br J Dermatol. 2016;175:1166–74. https://doi.org/10.1111/bjd.14756
9. Milllar EV, Schlett CD, Law NN, et al. Opportunities and obstacles in the prevention of skin and soft-tissue infections among military personnel. Mil Med. 2019;184:35–43.
10. Hickey PW, Mitra I, Fraser J, Brett-Major D, Riddle MS, Tribble DR. Deployment and travel medicine Knowledge, Attitudes, Practices, and Outcomes Study (KAPOS): malaria chemoprophylaxis prescription patterns in the military health system. Am J Trop Med Hyg. 2020;103:334–43.
11. Gaillard T, Madamet M, Pradines B. Tetracyclines in malaria. Malar J. 2015;14:445. https://doi.org/10.1186/s12936-015-0980-0
12. Grant JS, Stafylis C, Celum C, Grennan T, Haire B, Kaldor J, et al. Doxycycline prophylaxis for bacterial sexually transmitted infections. Clin Infect Dis. 2020;70:1247–53. https://doi.org/10.1093/cid/ciz866
13. Bolan RK, Beymer MR, Weiss RE, Flynn RP, Leibowitz AA, Klausner JD. Doxycycline prophylaxis to reduce incident syphilis among HIV-infected men who have sex with men who continue to engage in high-risk sex: a randomized, controlled pilot study. Sex Transm Dis. 2015;42:98–103. https://doi.org/10.1097/OLQ.0000000000000216
14. Molina JM, Charreau I, Chidiac C, Pialoux G, Cua E, Delaugerre C, et al.; ANRS IPERGAY Study Group. Post-exposure prophylaxis with doxycycline to prevent sexually transmitted infections in men who have sex with men: an open-label randomised substudy of the ANRS IPERGAY trial. Lancet Infect Dis. 2018;18:308–17. https://doi.org/10.1016/S1473-3099(17)30725-9
15. Hendricks KA, Wright ME, Shadomy SV, Bradley JS, Morrow MG, Pavia AT, et al.; Workgroup on Anthrax Clinical Guidelines. Centers for Disease Control and Prevention expert panel meetings on prevention and treatment of anthrax in adults. Emerg Infect Dis. 2014;20:e130687. https://doi.org/10.3201/eid2002.130687
16. Dennis DT, Inglesby TV, Henderson DA, Bartlett JG, Ascher MS, Eitzen E, et al.; Working Group on Civilian Biodefense. Tularemia as a biological weapon: medical and public health management. JAMA. 2001;285:2763–73. https://doi.org/10.1001/jama.285.21.2763
17. Lantos PM, Rumbaugh J, Bockenstedt LK, Falck-Ytter YT, Aguero-Rosenfeld ME, Auwaerter PG, et al. Clinical practice guidelines by the Infectious Diseases Society of America (IDSA), American Academy of Neurology (AAN), and American College of Rheumatology (ACR): 2020 guidelines for the prevention, diagnosis and treatment of Lyme disease. Clin Infect Dis. 2021;72:1–8. https://doi.org/10.1093/cid/ciaa1215
18. Takafuji ET, Kirkpatrick JW, Miller RN, Karwacki JJ, Kelley PW, Gray MR, et al. An efficacy trial of doxycycline chemoprophylaxis against leptospirosis. N Engl J Med. 1984;310:497–500. https://doi.org/10.1056/NEJM198402233100805
19. Agwuh KN, MacGowan A. Pharmacokinetics and pharmacodynamics of the tetracyclines including glycylcyclines. J Antimicrob Chemother. 2006;58:256–65. https://doi.org/10.1093/jac/dkl224
20. Dierks J, Servies T, Do T. A study on the leptospirosis outbreak among US Marine trainees in Okinawa, Japan. Mil Med. 2018;183:e208–12. https://doi.org/10.1093/milmed/usx013
21. Webber BJ, Kieffer JW, White BK, Hawksworth AW, Graf PCF, Yun HC. Chemoprophylaxis against group A streptococcus during military training. Prev Med. 2019;118:142–9. https://doi.org/10.1016/j.ypmed.2018.10.023
22. Brehm TT, Berneking L, Rohde H, Chistner M, Schlickewei C, Sena Martins M, et al. Wound infection with *Vibrio harveyi* following a traumatic leg amputation after a motorboat propeller injury in Mallorca, Spain: a case report and review of literature. BMC Infect Dis. 2020;20:104. https://doi.org/10.1186/s12879-020-4789-2
23. Heng SP, Letchumanan V, Deng CY, Ab Mutalib NS, Khan TM, Chuah LH, et al. *Vibrio vulnificus*: an environmental and clinical burden. Front Microbiol. 2017;8:997. https://doi.org/10.3389/fmicb.2017.00997
24. McAuliffe GN, Hennessy J, Baird RW. Relative frequency, characteristics, and antimicrobial susceptibility patterns of *Vibrio* spp., *Aeromonas* spp., *Chromobacterium violaceum*, and *Shewanella* spp. in the northern territory of Australia, 2000–2013. Am J Trop Med Hyg. 2015;92:605–10. https://doi.org/10.4269/ajtmh.14-0715
25. Tan KR, Magill AJ, Parise ME, Arguin PM; Centers for Disease Control and Prevention. Doxycycline for malaria chemoprophylaxis and treatment: report from the CDC expert meeting on malaria chemoprophylaxis. Am J Trop Med Hyg. 2011;84:517–31. https://doi.org/10.4269/ajtmh.2011.10-0285
26. Korhonen C, Peterson K, Bruder C, Jung P. Self-reported adverse events associated with antimalarial chemoprophylaxis in Peace Corps volunteers. Am J Prev Med. 2007;33:194–9. https://doi.org/10.1016/j.amepre.2007. 04.029
27. Affolter K, Samowitz W, Boynton K, Kelly ED. Doxycycline-induced gastrointestinal injury. Hum Pathol. 2017;66:212–5. https://doi.org/10.1016/j.humpath.2017.02.011
28. Morris TJ, Davis TP. Doxycycline-induced esophageal ulceration in the U.S. Military service. Mil Med. 2000;165:316–9. https://doi.org/10.1093/milmed/165.4.316
29. Lim DS, Murphy GM. High-level ultraviolet A photoprotection is needed to prevent doxycycline phototoxicity: lessons learned in East Timor. Br J Dermatol. 2003;149:213–4. https://doi.org/10.1046/j.1365-2133.2003.05389.x
30. Mende K, Beckius ML, Zera WC, Yu X, Li P, Tribble DR, et al.; Infectious Disease Clinical Research Program Trauma Infectious Disease Outcomes Study Investigative Team. Lack of doxycycline antimalarial prophylaxis impact on Staphylococcus aureus tetracycline resistance. Diagn Microbiol Infect Dis. 2016;86:211–20. https://doi.org/10.1016/j.diagmicrobio.2016.07.014

Address for correspondence: Jeffrey Spiro or Piotr Wisniewski, Naval Medical Center San Diego, Division of Infectious Diseases, 34800 Bob Wilson Dr, San Diego, CA 92134, USA; email: jeffrey.d.spiro.mil@health.mil or piotr.wisniewski.mil@health.mil

Predictive Mapping of Antimicrobial Resistance for *Escherichia coli*, *Salmonella*, and *Campylobacter* in Food-Producing Animals, Europe, 2000–2021

Ranya Mulchandani, Cheng Zhao, Katie Tiseo, João Pires, Thomas P. Van Boeckel

In Europe, systematic national surveillance of antimicrobial resistance (AMR) in food-producing animals has been conducted for decades; however, geographic distribution within countries remains unknown. To determine distribution within Europe, we combined 33,802 country-level AMR prevalence estimates with 2,849 local AMR prevalence estimates from 209 point prevalence surveys across 31 countries. We produced geospatial models of AMR prevalence in *Escherichia coli*, nontyphoidal *Salmonella*, and *Campylobacter* for cattle, pigs, and poultry. We summarized AMR trends by using the proportion of tested antimicrobial compounds with resistance >50% and generated predictive maps at 10 × 10 km resolution that disaggregated AMR prevalence. For *E. coli*, predicted prevalence rates were highest in southern Romania and southern/eastern Italy; for *Salmonella*, southern Hungary and central Poland; and for *Campylobacter*, throughout Spain. Our findings suggest that AMR distribution is heterogeneous within countries and that surveillance data from below the country level could help with prioritizing resources to reduce AMR.

Antimicrobial resistance (AMR) is a substantial threat to the health of humans and animals. Among humans, in 2019 an estimated 1.27 million deaths were associated with bacterial AMR (*1*). Among food-producing animals (i.e., animals that are used for or produce food items for human consumption), estimates of global AMR burden are still lacking. However, recent work has suggested that among common indicator bacteria of food-producing animals in low- and middle-income countries, the proportion of antimicrobials with resistance >50% increased from 12%–15% in 2000 to 34%–41% in 2018 (*2*), an increase that may have harmful consequences for humans (*3*). Moreover, the loss of treatment effectiveness in animals is a long-term threat for animal production and the millions of persons who rely on raising animals for subsistence (*4*,*5*). Therefore, monitoring AMR in food-producing animals has become a global priority for effective prevention strategies.

Since 2009, the European Food Safety Authority (EFSA) has led a harmonized surveillance system for AMR in food-producing animals and products (*6*). The system includes AMR prevalence estimates for *Escherichia coli*, nontyphoidal *Salmonella*, and *Campylobacter* among cattle and pigs (odd years) and chickens and turkeys (even years) (*7*). Data collected by EFSA have been instrumental for monitoring AMR and for guiding policy decisions in the European Union (e.g., the 2018 ban on prophylactic use of antimicrobials in animals [*8*]). The efforts to document AMR have also enabled comparison between countries in Europe by estimating prevalence of AMR at the national level. However, recent works have shown that resistance levels in humans and animals can vary at a fine spatial scale, and accumulation of resistance genes in those areas may create geographic hotspots for AMR (*2*,*9*). Identifying geographic hotspots of AMR within countries could help with targeting interventions against AMR, such as improved farm biosecurity and targeted surveillance, where they might have the greatest benefits (*10*–*12*).

In that context, point prevalence surveys (PPSs) of AMR among food-producing animals, with data points collected at individual geographic locations,

Author affiliations: ETH Zürich, Zurich, Switzerland (R. Mulchandani, C. Zhao, K. Tiseo, J. Pires, T.P. Van Boeckel); One Health Trust, Washington, DC, USA (T.P. Van Boeckel)

DOI: https://doi.org/10.3201/eid3001.221450

provide an opportunity to supplement the national estimates of AMR assembled by EFSA (*2*). The resulting mapped predictions could be used to help design regional antibiotic stewardship campaigns or target local investment in farm biosecurity (*12*). However, generating robust predictions of AMR pose at least 3 challenges. First, comparisons need to be made between the resistance trends inferred from PPSs and EFSA; second, subnational predictions should reflect resistance levels reported by EFSA at the national level; and third, an appropriate geospatial modeling approach must be developed to combine data collected at different spatial scales.

In this study, we disaggregated trends in AMR prevalence of *E. coli,* nontyphoidal *Salmonella*, and *Campylobacter* among cattle, pigs, and poultry. We used stacked geospatial models that supplement data from EFSA with individual PPSs to map predictions of AMR prevalence at a resolution of 10 × 10 km for 31 countries in Europe.

Materials and Methods

EFSA Data Collection

We reviewed annual EFSA reports published during 2011–2022 (*13*). We extracted country-level data on AMR prevalence (2009–2020), focusing on the percentage resistance to antimicrobials against *E. coli*, *Salmonella*, *Campylobacter coli*, and *Campylobacter jejuni*. We extracted information on country, year of isolation, animal type (cattle, pigs, chickens, turkeys), sample origin (slaughtered animal, living animal, or meat), bacteria, species, number of samples, antimicrobial tested, and resistance prevalence. We followed European Committee on Antimicrobial Susceptibility Testing (EUCAST) guidelines to assess microbiological resistance and used microdilution methods and epidemiologic cutoff (ECOFF) values (*14*). We retained only antimicrobial/bacteria combinations recommended by the World Health Organization Advisory Group on Integrated Surveillance of Antimicrobial Resistance (*15*) for antimicrobial susceptibility testing (Appendix Table 1, https://wwwnc.cdc.gov/EID/article/30/1/22-1450-App1.pdf).

PPS Data Collection

We systematically reviewed PPSs (Appendix) reporting AMR prevalence at individual locations in Europe (Appendix Figure 1). We searched PubMed, Web of Science, and Scopus for PPSs reporting AMR prevalence for *E. coli*, nontyphoidal *Salmonella*, and *Campylobacter* in healthy cattle, pigs, and poultry (combined data for chickens, turkeys, or other poultry), as well as their products (meat and dairy) in Europe during 2000–2021. Environmental samples (e.g., water, soil) were not included. We also extracted information on the geographic location of the PPS (Appendix), the year the PPS was conducted, the year the bacteria was isolated (but not species identification methods used), sample types collected (cecal, cloacal, lymph, or fecal samples taken from living animals, slaughtered animals, dairy products, or meat), animal species, number of samples collected and tested, susceptibility testing guidelines used, and susceptibility guidelines used for resistance interpretation.

We assessed microbiological resistance across PPSs by using different methods (disk diffusion vs. broth dilution), guidelines (Clinical and Laboratory Standards Institute [https://www.clsi.org] 52%, EUCAST 29%, other 14.6%) and cutoffs (clinical break points vs. ECOFFs [*15*]). We attempted to account for these differences by using a harmonization approach developed by Van Boeckel et al. (*2*) (Appendix). We calibrated data from PPSs by using antimicrobial susceptibility testing, guidelines, and breakpoints reported in each study to match those of EUCAST guidelines each year, to enable comparison between those data and data reported by EFSA. As with EFSA data, we retained only antimicrobial/bacteria combinations recommended by the World Health Organization Advisory Group on Integrated Surveillance of Antimicrobial Resistance (*15*). In addition, for our analysis we retained only countries that reported to EFSA and that had reported >50 samples during the study period. All prevalence estimates extracted from PPS are available at resistancebank.org (https://resistancebank.org) (*16*).

Comparative Analysis of Data Sources

We used the proportion of antimicrobials with >50% resistance (P50s) to summarize trends in resistance across each drug/bacteria combination, as in previous works (*2*,*12*,*17*); all P50s can be recalculated by using the data available at resistancebank.org. To assess the difference in AMR prevalence between PPS and EFSA data, as well as the implications that that could have for geospatial modeling, we compared the average P50 in countries reporting at >1 PPS and to EFSA during 2018–2020 (Appendix Table 3). A ratio <1 indicated a lower 3-year mean P50 using PPS data, and a ratio >2 meant a more than double 3-year mean P50 from PPS data compared with EFSA data.

Geospatial Modeling of P50

We mapped predicted subnational antimicrobial resistance in food-producing animals at a resolution of

0.08333 decimal degrees, corresponding to ≈10 km at the equator. To create the map, we used a 3-step procedure (Appendix Figure 2).

In the first step, we trained 3 child models (one of the individual models that are combined to form the final model) to quantify the relationship between P50 and a set of 9 environmental and anthropogenic covariates (Appendix Table 2). We selected those covariates because of their suspected association with AMR in animals (*2*,*12*,*17*–*19*). The models used for the first step were boosted regression trees (*20*); LASSO (least absolute shrinkage and selection operator) applied to logistic regression (*21*); and overlapped grouped LASSO penalties for General Additive Models selection (A. Chouldechova, unpub. data, https://arxiv.org/abs/1506.03850). We calculated the importance of each covariate by comparing the areas under the receiver operator curve (AUCs) between a full model that contained all covariates and a model without each covariate. To evaluate the relative importance of each covariate to the full model, we repeated the procedure sequentially (Appendix Table 5).

We weighted all models by the number of isolates tested in each survey and conducted 10 Monto Carlo simulations on the models to account for the variation introduced by transformation of prevalence estimates into binary variables. The models were trained by using 4-fold spatial cross-validation to prevent overfitting and ensure generalization in geographic regions poorly represented in the training dataset. We defined the 4 spatial folds by using a k-means clustering algorithm (*22*). The algorithm clustered the surveys according to their spatial distances and partitioned them into 4 spatially disjointed sets with equal sizes (Appendix). No predictions were made in urban settlements; there were areas defined as artificial surfaces in GlobCover 2009 (*23*). We conducted sensitivity analyses by restricting PPSs to 2009–2020 only (to match EFSA reporting period), to 6 or 7 of the most common antimicrobial/bacteria combinations only, and to P50 calculated by class (rather than compound) (Appendix).

In the second step, we ensembled predictions from the 3 models according to the models' predictive ability, assessed by using the AUC. We calculated the resulting map of P50 as the mean of the 3 model predictions weighted by their AUC values. We calculated the associated map of prediction uncertainty as the SD of predicted P50 values from the 10 Monte Carlo simulations (Appendix Figure 4, panel A).

In the third step, we adjusted the P50 predictions in each country, using P50 values calculated from EFSA reports. Concretely, we multiplied P50 values in each pixel by the ratio of country-level P50 as reported by EFSA and the mean P50 of all pixels across each country as predicted by the geospatial model. That step ensured that the country-level mean of P50 values corresponded to reports from EFSA while preserving geographic variations in AMR levels within each country. To assess the variations in P50 values within each country, we calculated country-level SDs of P50s (Appendix Figure 4, panel C).

Last, we created the predictive maps of AMR hotspots for each pathogen. The threshold value for a pixel to be classified as a hotspot corresponded to the 95th percentile of all P50 values across the map and varied for each pathogen (Appendix Figure 4, panel B). We obtained estimated animal densities associated with those areas from Gilbert et al. (*24*). Using those estimates, for each country we calculated the percentage of each animal species living in the hotspot areas.

Results

EFSA Surveillance

At the country level, EFSA data for 2009–2020 provided 33,802 AMR prevalence estimates (resulting in 2,996 P50s). The data were for *E. coli*, nontyphoidal *Salmonella*, *C. coli*, and *C. jejuni* in cattle, pigs, and poultry across 31 countries in Europe.

PPSs

At the local level, for 2000–2021 we identified 209 PPSs, which provided 2,849 AMR prevalence estimates (resulting in 368 P50s). The data were for *E. coli*, nontyphoidal *Salmonella*, and *Campylobacter* in food-producing animals and derived products from 21 countries in Europe. In terms of AMR prevalence, *E. coli* accounted for 44.4%, *Salmonella* for 34.2%, and *Campylobacter* for 21.4%. Poultry accounted for approximately half of the AMR prevalence (n = 1,429, 50.2%), followed by pigs (28.1%) and cattle (21.8%). One third of the sample types tested were meat (34.7%, n = 988), followed by fecal samples (23.4%). Across the countries included in the analysis, geographic coverage was on average 4.21 PPSs (interquartile range 0–11.7)/100,000 km^2. Half of the PPSs identified were from the combination of Spain (20.5%), Italy (18.7%), and Germany (10.5%) (Figure 1). The average number of PPSs published by year increased from 3 during 2000–2005 to 14 during 2015–2021 (Figure 1, panel B).

Comparison of PPS and EFSA

AMR prevalence estimates varied considerably between data sources and country. For 2018–2020, Greece, Poland, and Germany accounted for more

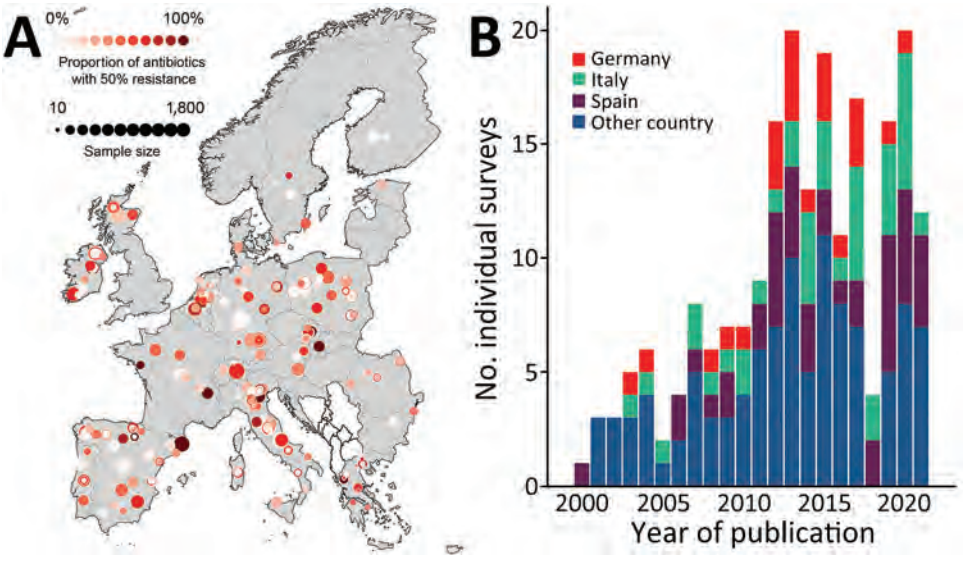

Figure 1. Data from study of predictive mapping for antimicrobial resistance of *Escherichia coli*, *Salmonella*, and *Campylobacter* in food-producing animals, Europe, 2000–2021. A) Geographic distribution of point prevalence surveys (PPSs). B) Number of PPSs published per year. Additional information is provided in the Appendix (https://wwwnc.cdc.gov/EID/article/30/1/22-1450-App1.pdf).

than double the national average P50 calculated from PPS data compared with P50s calculated from EFSA (Table 1). Conversely, the national average P50 calculated from PPS data from Portugal and Switzerland was ≤30% lower than that calculated from EFSA.

The highest resistance prevalence estimates were for tetracycline (57.9%–36.4%), ampicillin (58.6%–34.9%), ciprofloxacin (64.6%–13.1%), and nalidixic acid (60.9%–25.5%). The difference in mean P50 between PPSs and EFSA data ranged from 15.2% to −17.4% for *Salmonella* and from 19.1% to −7.96% for *E. coli*. For *Campylobacter*, systematically higher prevalence estimates were obtained from PPSs; differences ranged from 12.1% to 0.78% (Figure 2).

Geospatial Modeling

We mapped predicted P50s at 10 × 10 km resolution for each of the 3 bacteria across Europe (Figure 3). In the final models, the predicted P50 values ranged from 0 to 79% for *E. coli*, 0 to 40% for *Salmonella*, and 0 to 100% for *Campylobacter* (Figure 3, panel A; prediction uncertainty, Appendix Figure 3, panel A). P50 cutoffs for hotspots of AMR (calculated as the top 95% of the values on the map) were 0.43 for *E. coli*, 0.23 for *Salmonella*, and 0.60 for *Campylobacter*. AMR hotspots for *E. coli* were predicted to be located in southern Romania (Muntenia, Dobrogea) and southern and eastern Italy (Sicily, Emilia-Romagna, Apulia); and for *Salmonella*, predicted hotspots were in southern Hungary, northern Italy, and central Poland. More than 90% of hotspot areas for *Campylobacter* were predicted to be throughout mainland Spain (Figure 3, panel B).

For *E. coli*, the highest geographic variations in predicted P50 levels were in Romania (13% pixel-level SDs), Bulgaria (11%), Greece 1(2%), and Italy (11%). For *Campylobacter*, the highest geographic variations in P50 were in France (10%) and Germany (10%; Appendix Figure 4, panel C). No countries had high spatial variations in predicted P50s for *Salmonella*. Cold spots for all 3 bacteria were identified in Sweden, Norway, Finland, and Iceland (data not shown). Spatial variations of P50 for countries containing coldspots were small, with pixel-level standard deviations of 3.2% (*E. coli*), 0.9% (*Salmonella*), and 1.0% (*Campylobacter*). Restricting PPS by year and antimicrobial bacteria combinations resulted in little difference (mean Pearson correlation coefficient 0.992; mean absolute error 0.932%) to the overall model predictions (Appendix Table 4). In addition, we found little difference when P50 was calculated by antimicrobial class rather than individual compound (Pearson correlation coefficient 0.995, mean absolute error 0.66%) (Appendix Table 4, Figure 4). Importance of environmental covariates to the models varied by pathogen (Appendix Table 5). For *E. coli* and *Salmonella*, the covariate with highest importance was the percentage of tree coverage

Table 1. Three-year mean of proportion of antimicrobial drugs with >50% resistance from PPS and EFSA data and ratios of P50 for countries reporting to both data sources, Europe, 2018–2020*

Country	Mean P50 from PPSs	Mean P50 from EFSA	PPS and EFSA P50 ratio
Poland	0.64	0.26	2.47
Germany	0.60	0.25	2.42
Greece	0.39	0.19	2.02
Spain	0.39	0.24	1.67
Belgium	0.29	0.21	1.34
Romania	0.31	0.28	1.10
Italy	0.23	0.25	0.92
Switzerland	0.17	0.22	0.77
Portugal	0.18	0.32	0.57

*EFSA, European Food Safety Authority; PPS, point prevalence surveys; P50, >50% antimicrobial resistance.

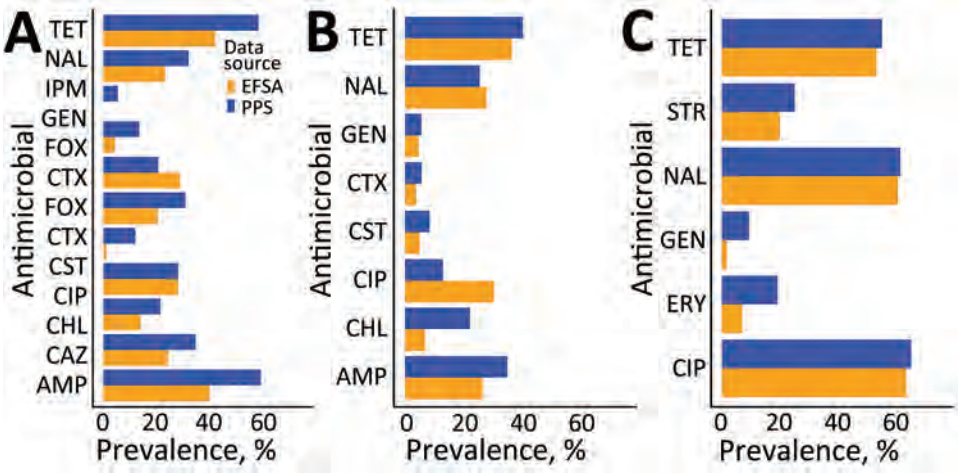

Figure 2. Mean prevalence for antimicrobial class and bacteria combinations, split by data source, Europe, 2009–2020. A) *Escherichia coli*; B) *Salmonella*; C) *Campylobacter*. AMP, ampicillin; CAZ, ceftazidime; CHL, chloramphenicol; CIP, ciprofloxacin; CST, colistin; CTX, clavulanic acid; EFAS, European Food Safety Authority; FOX, cefoxitin; GEN, gentamicin; IPM, imipenem; NAL, nalidixic acid; PPS, point prevalence survey; STR, streptomycin; TET, tetracycline.

(ΔAUC 0.106 for *E. coli* and 0.078 for *Salmonella*). For *Campylobacter*, the covariate with highest importance was antimicrobial use in animals (ΔAUC 0.037), closely followed by yearly average of minimum monthly temperature (ΔAUC 0.034).

In 9 of the 31 countries in Europe, >50% of cattle, pigs, or poultry are estimated to be raised in the predicted AMR hotspot areas (Table 2). For instance, 93% of poultry in Spain, 90% of poultry in Greece, and 97% of poultry and 92% of pigs in Cyprus are raised in AMR hotspots.

Discussion

In this study, we geographically disaggregated AMR prevalence for *E. coli*, nontyphoidal *Salmonella*, and *Campylobacter* reported among food-producing animals across Europe by supplementing national EFSA data with subnational PPS data to produce maps of estimated AMR prevalence. For multiple countries, such as Italy, Romania, and Poland, rather than consistently high countrywide AMR levels, in our final model we predicted specific geographic hotspots of high AMR prevalence that may coexist within regions

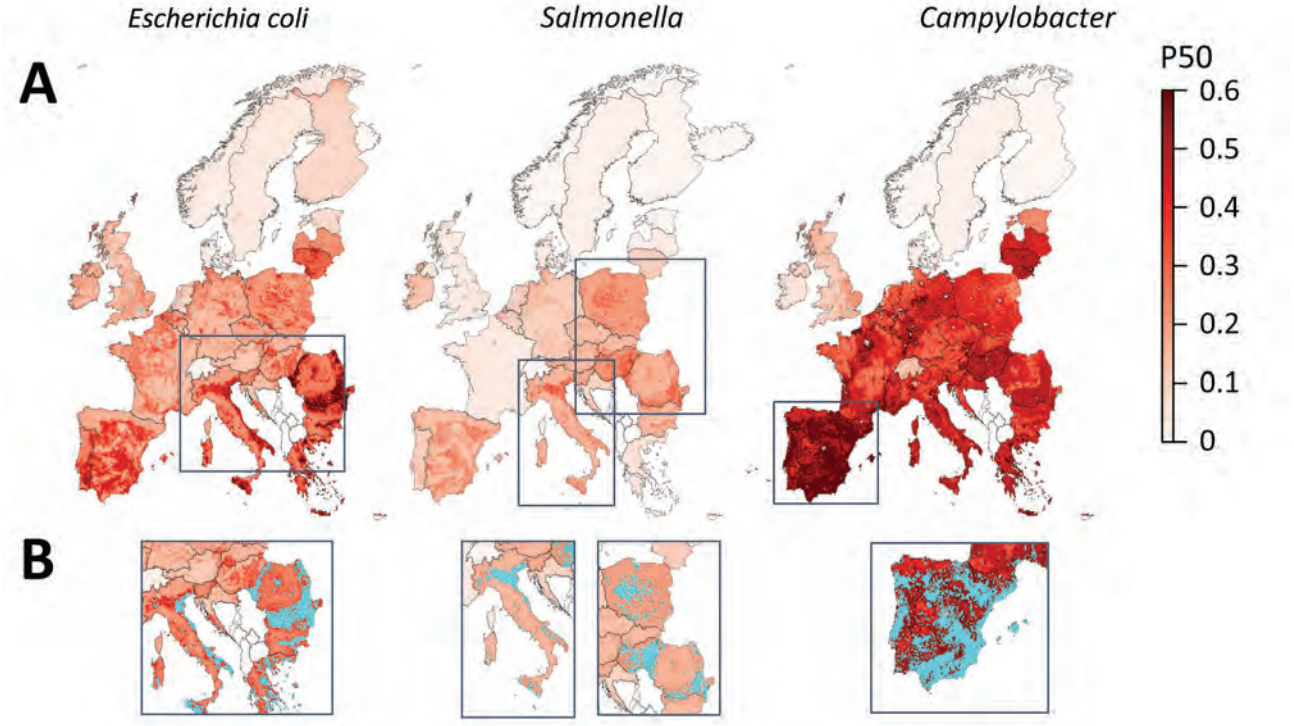

Figure 3. Mapping of predicted P50s and hotspot areas for antimicrobial resistance of *Escherichia coli*, *Salmonella*, and *Campylobacter*, Europe. A) Predicted proportions of antimicrobials with P50 at 10 × 10 km resolution per bacteria. B) Antimicrobial resistance hotspots (light blue) in eastern Europe, Italy, and Spain. Cutoffs: *E. coli*, 0.43; *Salmonella*, 0.23; *Campylobacter*, 0.6 (95% percentile). P50, >50% antimicrobial resistance.

of lower AMR prevalence in the same countries. In specific regions, countries in which AMR seems to be consistently high may have made more progress against AMR than previously thought (with only some, rather than all, areas containing high levels) by interpretation of EFSA data or nationally published reports. Further improvements could be made in those countries by targeting interventions (e.g., improved farm biosecurity and targeted surveillance in hotspots where AMR levels remain high). In contrast, largely diffuse and geographically uniform (low) countrywide AMR prevalence was found in countries with low AMR levels (e.g., Sweden, Norway, and Iceland); uncertainty in these predictions were higher for *Campylobacter* than for *E. coli* and *Salmonella*.

For all 3 bacteria studied, AMR prevalence was substantially lower in Norway, Sweden, Denmark, and Switzerland than the average for Europe. Those countries were among the first to establish animal AMR surveillance (i.e., DANMAP in Denmark in 1995 [*25*]) and have now integrated surveillance of zoonotic bacteria in humans and animals. For several decades, they have been guiding national and international control strategies. For instance, in the 1990s, increased prevalence of vancomycin-resistant enterococci reported by DANMAP was instrumental to banning use of antimicrobial drugs for growth promotion in livestock (*25*).

In contrast, countries in which a high proportion of food-producing animals are raised in areas predicted as hotspots of resistance by our study are Cyprus, Portugal, and Spain. In 2018, one fifth (20.8%) of the pigs in the European Union were reared in Spain (*26*), where 88% of its pigs were predicted to be raised in geographic hotspots of *Campylobacter* resistance, primarily in Aragon and Catalonia. However, that finding was not the case for other high-density pig regions such as Brittany (France), northwest Germany (Lower Saxony and North Rhine-Westphalia), and Denmark (*27*). Those findings suggest that high AMR is not necessarily associated with high animal densities but possibly with other drivers such as farming practices, biosecurity measures, and antimicrobial use (*28*).

Across Europe, the highest prevalence of resistance in our models was reported for antimicrobial drugs commonly used in animal production: tetracyclines, quinolones, penicillins, and aminoglycosides (gentamicin and streptomycin). Of particular concern were the compounds considered critically important antimicrobials for human medicine (*29*) and for which AMR prevalence was predicted to be >50% (ampicillin in *E. coli* [58.6%] and ciprofloxacin in *Campylobacter* [64.6%]).

Table 2. Percentages of food-producing animals raised in each country that fall within an antimicrobial resistance hotspot area (95th percentile per pathogen) for France, Germany, Spain, and countries in which pathogen percentage >50% for ≥1 animal species*

Pathogen, country	Cattle, %	Pigs, %	Poultry, %
Escherichia coli			
France	0	0	0
Germany	0	0	0
Spain	2.1	2.3	1.8
Bulgaria	34.4	51.5	57.8
Cyprus	33.8	68.9	68.5
Greece	39.4	57.9	35.5
Romania	34.8	77.5	57.8
Salmonella			
France	0	0	0
Germany	0	0	0
Spain	8.8	28.2	24.8
Cyprus	51.8	91.6	96.6
Hungary	63.5	64.7	80.6
Italy	52.0	70.2	64.0
Poland	21.6	66.0	74.3
Romania	17.0	65.2	45.0
Campylobacter			
France	0.5	4.6	6.2
Germany	1.8	14.9	23.2
Spain	32.3	87.9	93.0
Cyprus	26.0	44.9	66.3
Greece	10.9	58.4	90.3
Portugal	22.1	74.9	88.0

*Antimicrobial resistance for *Escherichia coli*, nontyphoidal *Salmonella*, and *Campylobacter*.

In our study, estimates of P50 for *Salmonella* were much lower than those for *E. coli* and *Campylobacter*, which could potentially be attributed to the success of targets imposed by the European Union (e.g., reducing *Salmonella* prevalence in poultry over the past decade [*30*]). In addition, several countries had already implemented *Salmonella* control strategies before European Union–wide initiatives. For instance, in the 1970s, the United Kingdom set up national AMR surveillance for *Salmonella*, and in 1969, France had similar initiatives for *Salmonella* and *E. coli* (*25*). Switzerland also implemented a stringent control program for *Salmonella* Enteritidis in 1993 (*31*), more than a decade earlier than the first European Union–wide initiative (*30*).

When we compared estimates of resistance (P50) derived from PPS and EFSA data, the average P50 from PPSs seemed to more closely match national EFSA prevalence values in some countries more than in others. For instance, in Spain and Italy, the ratios of P50 inferred from PPS and EFSA data were close to 1 over the past 3 years. One reason may be the higher number of PPSs from these countries (17 in Spain and 13 in Italy), which average out closer to the EFSA values. In contrast, in countries with P50 ratios >2 or <0.8 (Poland, Germany, Greece, Portugal) inferred from PPS and EFSA data, only 1–4 studies have been conducted in the past 3 years. Therefore, although

smaller sample sizes may be insufficient for comparing national averages (PPS vs. EFSA) they may still represent subnational heterogeneity in AMR not observed in the national average from EFSA. A higher coverage of PPSs may further improve the confidence in subnational model predictions.

Among the limitations of our modeling study, the first is that our literature search for PPSs published in Europe during 2000–2021 resulted in a mere 209 PPSs that were associated with geographic information. In contrast, for the same period, 446 PPSs with geographic information were published in China (*12*). Torres et al. also assembled AMR studies of food-producing animals during 1957–2018; however, of the 510 papers from Europe identified, the breakdown of their surveys corresponding to our search criteria was not available in open access (*32*). Thus, the limited number of surveys that satisfied our inclusion criteria, particularly the reporting of geographic information, precluded mapping AMR prevalence for individual drug/bacteria combinations or animal species.

Second, with regard to using PPSs for regional estimations, differences in sampling strategy and sample sizes may affect the comparability of surveys and potentially explain why prevalence calculated from PPSs was in some instances higher than the prevalence estimates reported by EFSA. In particular, targeted sampling for bacteria that probably have high-resistance profiles, such as extended-spectrum beta lactamase–producing *E. coli* (*33*), could lead to comparatively higher AMR in PPS data than in the general population, which are more likely to be observed with the EFSA sampling scheme. In terms of microbiology, the set of tested antimicrobials differed between PPSs, which necessitated use of a composite metric. In addition, there were some transparency issues in terms of which methods or breakpoints were used (i.e., assumptions had to be made in the case of missing data [such as guideline year] and in the harmonization approach used for PPSs that used different guidelines, which may have led to some unintended bias), as well as a diversity of breakpoints used. Despite attempts to reduce variability between surveys, some variability may still exist and therefore efforts should be made to develop standardized protocols in the future, such as for all PPSs to shift to using ECOFF values and to release raw data. The creation of a consensus breakpoint table that could be used by all would also greatly assist with the comparability of those data and reduce the need for such adjustments. Because most studies reported only sampling location or region by name rather than specific coordinates, coordinates and size of region were estimated (and may not always represent the location of the farms where the animals were raised), which may have led to further uncertainty in our models.

Third, because of the limited number of PPSs, as well as their heterogenous distribution across the study period, incorporating the temporal dimension into the modeling framework remains challenging at this stage. Therefore, countries that have had considerably reduced AMR levels since 2009, such as the Netherlands (*34*), may be associated with higher AMR prevalence in our maps than that in the latest reports. However, as the number of surveys grows in the future, other spatio-temporal approaches, such as the Integrated Nested Laplace Approximation (*35*), could be used to account for not only spatial but also temporal variations in AMR prevalence extracted from PPSs.

Last, because of the static framework of geospatial modeling, it was not possible to incorporate all relevant data. That limitation may have a dynamic effect on AMR prevalence estimates, notably animal movement.

In conclusion, high-resolution maps that predict subnational hotspots can help support targeted resource allocation and control strategies for reducing AMR burden. Such strategies could include improving farm biosecurity and targeted surveillance. The accuracy of these maps could be gradually improved in the future should countries routinely report geographic location data along with microbiological sampling results.

Acknowledgments

We thank Roger Stephan for providing critical feedback and Nicola G. Criscuolo for uploading estimates of prevalence of resistance to resistancebank.org.

R.M. and K.T. were supported by the EU Horizon 2020 grant for MOOD (MOnitoring Outbreaks for Disease Surveillance) in a data science context. C.Z. was supported by the Branco Weiss Foundation, J.P. was supported by the NRP72 program of the Swiss National Science Foundation, and T.P.V.B. was supported by The Swiss National Science Foundation Eccellenza Fellowship. The project has received funding from the EU Horizon 2020 Research and Innovation program under grant agreement no. 874850. The contents of this publication are the sole responsibility of the authors and do not necessarily reflect the views of the European Commission.

R.M. contributed to data analysis and drafted the manuscript; C.Z. contributed to geospatial analysis and revision of the manuscript; K.T. contributed to literature

review and data extraction; J.P. contributed to interpretation and revision of the manuscript; T.V.B. contributed to study conception and design, data interpretation, supervision, revision of the manuscript, and final approval.

About the Author

Ms. Mulchandani is a research assistant at ETH Zurich, where she is researching AMR in animals. Her main research interests are zoonotic diseases and outbreak responses.

References

1. Antimicrobial Resistance Collaborators. Global burden of bacterial antimicrobial resistance in 2019: a systematic analysis. Lancet. 2022;399:629–55. https://doi.org/10.1016/S0140-6736(21)02724-0
2. Van Boeckel TP, Pires J, Silvester R, Zhao C, Song J, Criscuolo NG, et al. Global trends in antimicrobial resistance in animals in low- and middle-income countries. Science. 2019;365:eaaw1944. https://doi.org/10.1126/science.aaw1944
3. Muloi D, Ward MJ, Pedersen AB, Fèvre EM, Woolhouse MEJ, van Bunnik BAD. Are food animals responsible for transfer of antimicrobial-resistant Escherichia coli or their resistance determinants to human populations? A systematic review. Foodborne Pathog Dis. 2018;15:467–74. https://doi.org/10.1089/fpd.2017.2411
4. Food and Agriculture Organization of the United Nations. The economic lives of smallholder farmers: an analysis based on household data from nine countries [cited 2022 Apr 29]. https://www.fao.org/3/i5251e/i5251e.pdf
5. Bengtsson B, Greko C. Antibiotic resistance—consequences for animal health, welfare, and food production. Ups J Med Sci. 2014;119:96–102. https://doi.org/10.3109/03009734.2014.901445
6. Deruelle T. A tribute to the foot soldiers: European health agencies in the fight against antimicrobial resistance. Health Econ Policy Law. 2021;16:23–37. https://doi.org/10.1017/S1744 3120000213
7. European Food Safety Authority; European Centre for Disease Prevention and Control. The European Union summary report on antimicrobial resistance in zoonotic and indicator bacteria from humans, animals and food in 2018/2019. EFSA J. 2021;19:e06490.
8. European Union. Regulation (EU) 2019/6 of the European Parliament and of the Council of 11 December 2018 on veterinary medicinal products and repealing Directive 2001/82/EC [cited 2022 Apr 27]. http://data.europa.eu/eli/reg/2019/6/oj/eng
9. Ramos DA, Pulgarín JAH, Gómez GAM, Alzate JA, Gómez JCO, Bonilla IC, et al. Geographic mapping of Enterobacteriaceae with extended-spectrum β-lactamase (ESBL) phenotype in Pereira, Colombia. BMC Infect Dis. 2020;20:540.
10. Agersø Y, Aarestrup FM. Voluntary ban on cephalosporin use in Danish pig production has effectively reduced extended-spectrum cephalosporinase-producing Escherichia coli in slaughter pigs. J Antimicrob Chemother. 2013;68:569–72. https://doi.org/10.1093/jac/dks427
11. Raasch S, Collineau L, Postma M, Backhans A, Sjölund M, Belloc C, et al. on behalf of the MINAPIG Consortium. Effectiveness of alternative measures to reduce antimicrobial usage in pig production in four European countries. Porcine Health Manag. 2020;6:6. https://doi.org/10.1186/s40813-020-0145-6
12. Zhao C, Wang Y, Tiseo K, Pires J, Criscuolo NG, Van Boeckel TP. Geographically targeted surveillance of livestock could help prioritize intervention against antimicrobial resistance in China. Nat Food. 2021;2:596–602. https://doi.org/10.1038/s43016-021-00320-x
13. EFSA (European Food Safety Authority) and ECDC. The European Union Summary report on antimicrobial resistance in zoonotic and indicator bacteria from humans, animals and food in 2019–2020. EFSA J. 2022;20:e07209.
14. European Society of Clinical Microbiology and Infectious Diseases. Standard operating procedure: MIC distributions and the setting of epidemiological cut-off (ECOFF) values [cited 2023 Jan 1]. https://www.eucast.org/fileadmin/src/media/PDFs/EUCAST_files/EUCAST_SOPs/EUCAST_SOP_10.1_MIC_distributions_and_epidemiological_cut-off_value__ECOFF__setting_20191130.pdf
15. World Health Organization. Integrated surveillance of antimicrobial resistance in foodborne bacteria: application of a One Health approach: guidance from the WHO Advisory Group on Integrated Surveillance of Antimicrobial Resistance (AGISAR). Geneva: The Organization; 2017.
16. Criscuolo NG, Pires J, Zhao C, Van Boeckel TP. Resistancebank.org, an open-access repository for surveys of antimicrobial resistance in animals. Sci Data. 2021;8:189.
17. Schar D, Zhao C, Wang Y, Larsson DGJ, Gilbert M, Van Boeckel TP. Twenty-year trends in antimicrobial resistance from aquaculture and fisheries in Asia. Nat Commun. 2021;12:5384. https://doi.org/10.1038/s41467-021-25655-8
18. MacFadden DR, McGough SF, Fisman D, Santillana M, Brownstein JS. Antibiotic resistance increases with local temperature. Nat Clim Chang. 2018;8:510–4. https://doi.org/10.1038/s41558-018-0161-6
19. Tang KL, Caffrey NP, Nóbrega DB, Cork SC, Ronksley PE, Barkema HW, et al. Restricting the use of antibiotics in food-producing animals and its associations with antibiotic resistance in food-producing animals and human beings: a systematic review and meta-analysis. Lancet Planet Health. 2017;1:e316–27. https://doi.org/10.1016/S2542-5196(17)30141-9
20. Elith J, Leathwick JR, Hastie T. A working guide to boosted regression trees. J Anim Ecol. 2008;77:802–13. https://doi.org/10.1111/j.1365-2656.2008.01390.x
21. Tibshirani R. Regression shrinkage and selection via the lasso: a retrospective. J R Stat Soc Series B Stat Methodol. 2011;73:273–82. https://doi.org/10.1111/j.1467-9868.2011.00771.x
22. Hartigan JA, Wong M. Algorithm AS 136: A k-means clustering algorithm. J R Stat Soc Ser C Appl Stat. 1979;28:100–8.
23. Bontemps S, Defourny P, Van Bogaert E, Arino O, Kalogirou V, Ramos Perez J. GlobCover 2009 [cited 2023 Jan 1]. http://due.esrin.esa.int/page_globcover.php
24. Gilbert M, Conchedda G, Van Boeckel TP, Cinardi G, Linard C, Nicolas G, et al. Income disparities and the global distribution of intensively farmed chicken and pigs. PLoS One. 2015;10:e0133381. https://doi.org/10.1371/journal.pone.0133381
25. Simjee S, McDermott P, Trott DJ, Chuanchuen R. Present and future surveillance of antimicrobial resistance in animals: principles and practices. Microbiol Spectr. 2018;6:6.4.06. https://doi.org/10.1128/microbiolspec.ARBA-0028-2017

26. European Parlaiment. The EU pig meat sector [cited 2022 Apr 27]. https://www.europarl.europa.eu/RegData/etudes/BRIE/2020/652044/EPRS_BRI(2020)652044_EN.pdf
27. Eurostat. Archive: Pig farming sector—statistical portrait 2014 [cited 2022 Apr 27]. https://ec.europa.eu/eurostat/statistics-explained/index.php?title=Archive:Pig_farming_sector_-_statistical_portrait_2014
28. Huber L, Agunos A, Gow SP, Carson CA, Van Boeckel TP. Reduction in antimicrobial use and resistance to Salmonella, Campylobacter, and Escherichia coli in broiler chickens, Canada, 2013-2019. Emerg Infect Dis. 2021;27:2434–44. https://doi.org/10.3201/eid2709.204395
29. World Health Organization. Critically important antimicrobials for human medicine: 6th revision [cited 2022 Apr 29]. https://apps.who.int/iris/bitstream/handle/10665/312266/9789241515528-eng.pdf
30. EUR-Lex. Commission Regulation (EC) no. 1177/2006 of 1 August 2006 implementing Regulation (EC) no. 2160/2003 of the European Parliament and of the Council as regards requirements for the use of specific control methods in the framework of the national programmes for the control of salmonella in poultry [cited 2022 Apr 19]. https://eur-lex.europa.eu/legal-content/EN/ALL/?uri=CELEX:32006R1177
31. Hoop RK. The Swiss control programme for Salmonella Enteritidis in laying hens: experiences and problems. Rev Sci Tech. 1997;16:885–90. https://doi.org/10.20506/rst.16.3.1063
32. Torres RT, Carvalho J, Fernandes J, Palmeira JD, Cunha MV, Fonseca C. Mapping the scientific knowledge of antimicrobial resistance in food-producing animals. One Health. 2021;13:100324. https://doi.org/10.1016/j.onehlt.2021.100324
33. Geser N, Stephan R, Kuhnert P, Zbinden R, Kaeppeli U, Cernela N, et al. Fecal carriage of extended-spectrum β-lactamase-producing Enterobacteriaceae in swine and cattle at slaughter in Switzerland. J Food Prot. 2011;74:446–9. https://doi.org/10.4315/0362-028X.JFP-10-372
34. Hesp A, Veldman K, van der Goot J, Mevius D, van Schaik G. Monitoring antimicrobial resistance trends in commensal Escherichia coli from livestock, the Netherlands, 1998 to 2016. Euro Surveill. 2019;24:1800438. https://doi.org/10.2807/1560-7917.ES.2019.24.25.1800438
35. Blangiardo M, Cameletti M, Baio G, Rue H. Spatial and spatio-temporal models with R-INLA. Spat Spatio-Temporal Epidemiol. 2013;4:33–49.

Address for correspondence: Thomas Van Boeckel, ETH Zurich, CHN H 72 Universitätstrasse 16 8092 Zürich Schweiz, Zurich, Switzerland; email: thomas.van.boeckel@gmail.com

etymologia revisited

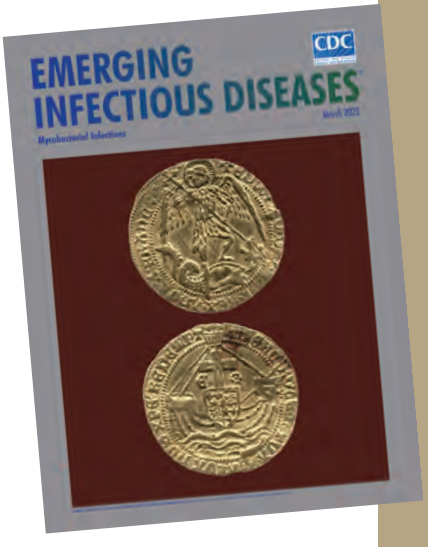

Originally published in March 2022

Schizophyllum commune

[skiz-of′-ĭ-ləm kom′-yoon]

Schizophyllum commune, or split-gill mushroom, is an environmental, wood-rotting basidiomycetous fungus. *Schizophyllum* is derived from "*Schíza*" meaning split because of the appearance of radial, centrally split, gill like folds; "*commune*" means common or shared ownership or ubiquitous. Swedish mycologist, Elias Magnus Fries (1794–1878), the Linnaeus of Mycology, assigned the scientific name in 1815. German mycologist Hans Kniep in 1930 discovered its sexual reproduction by consorting and recombining genomes with any one of numerous compatible mates (currently >2,800).

References

1. Chowdhary A, Kathuria S, Agarwal K, Meis JF. Recognizing filamentous basidiomycetes as agents of human disease: a review. Med Mycol. 2014;52: 782–97. https://doi.org/10.1093/mmy/myu047
2. Cooke WB. The genus *Schizophyllum*. Mycologia. 1961;53:575–99. https://doi.org/10.1080/00275514.1961.12017987
3. Greer DL. Basidiomycetes as agents of human infections: a review. Mycopathologia. 1978;65:133–9. https://doi.org/10.1007/BF00447184
4. O'Reilly P. *Schizophyllum commune*, split gill fungus, 2016 [cited 2021 Aug 23]. https://www.first-nature.com/fungi/schizophyllum-commune.php
5. Raper CA, Fowler TJ. Why study *Schizophyllum*? Fungal Genet Rep. 2004;51:30–6. https://doi.org/10.4148/1941-4765.1142

https://wwwnc.cdc.gov/eid/article/28/3/et-2803_article

Population-Based Study of Pertussis Incidence and Risk Factors among Persons >50 Years of Age, Australia

Rodney Pearce, Jing Chen, Ken L. Chin, Adrienne Guignard, Leah-Anne Latorre, C. Raina MacIntyre, Brittany Schoeninger, Sumitra Shantakumar

Despite vaccination programs, pertussis has been poorly controlled, especially among older adults in Australia. This longitudinal, retrospective, observational study aimed to estimate the incidence and risk factors of pertussis among persons ≥50 years of age in Australia in the primary care setting, including those with underlying chronic obstructive pulmonary disease (COPD) or asthma. We used the IQVIA general practitioner electronic medical record database to identify patients ≥50 years of age with a clinical diagnosis of pertussis during 2015–2019. Pertussis incidence rates ranged from 57.6 to 91.4 per 100,000 persons and were higher among women and highest in those 50–64 years of age. Patients with COPD or asthma had higher incidence rates and an increased risk for pertussis compared with the overall population ≥50 years of age. Our findings suggest that persons ≥50 years of age in Australia with COPD or asthma have a higher incidence of and risk for pertussis diagnosis.

Pertussis, or whooping cough, a bacterial respiratory infection caused by *Bordetella pertussis*, is typically characterized by paroxysms of coughing with a whooping sound during inhalation. In Australia, pertussis is one of the least well-controlled vaccine-preventable diseases (*1*). Robust childhood and maternal immunization programs prevent pertussis-related hospitalizations and mortality in infants and children, but breakthrough disease can occur at any age, because naturally acquired and vaccine-induced immunity against pertussis is not lifelong (*2*,*3*). Although older adults can be a source of transmission and adversely affected by infection, vaccination programs are prioritized for pregnant women (preferably 20–32 weeks' gestation), infants and children (i.e., ages 2, 4, 6 and 18 months, and 4 years), and adolescents (11–13 years of age) (*1*). Consequently, pertussis in older adults constitutes a considerable reservoir of infection and contributes to substantial disease burden, healthcare utilization, and other pertussis-associated costs (*1*).

Recent research has offered a clearer assessment of pertussis cases among adults ≥50 years of age (*4*). In Australia, pertussis-containing (i.e., combined diphtheria, tetanus, and acellular pertussis) vaccines are recommended for adults at 50 years and 65 years of age by the Australian Technical Advisory Group on Immunisation (*1*,*5*,*6*) but are not funded by the National Immunisation Program. Both confirmed and probable cases of pertussis must be reported to the Commonwealth's National Notifiable Diseases Surveillance System (NNDSS) (*5*). However, pertussis infections are often underdiagnosed and underreported, owing to difficulties in diagnosis because of unspecific symptoms, delays in seeking healthcare, underuse of diagnostic testing by general practitioners (GPs), and other coexisting respiratory diseases. Accordingly, NNDSS notification data tend to underestimate the true number of pertussis infections and are more likely to capture persons with severe disease (*7*), posing serious challenges to policy considerations for pertussis vaccination in adults ≥50 years of age. Given the underuse of diagnostic testing by GPs, pertussis diagnoses are based frequently on clinical evidence. Beyond NNDSS data, alternative sources of data, including electronic medical records (EMRs), may inform understanding of the burden of pertussis

Author affiliations: Medical HQ Family Practice, Glynde, South Australia, Australia (R. Pearce); GSK, Singapore (J. Chen, S. Shantakumar); IQVIA, Melbourne, Victoria, Australia (K.L. Chin); Monash University, Melbourne (K.L. Chin); GSK, Wavre, Belgium (A. Guignard); GSK, Melbourne (L.-A. Latorre); University of New South Wales, Sydney, New South Wales, Australia (C.R. MacIntyre); IQVIA, Sydney (B. Schoeninger)

DOI: http://doi.org/10.3201/eid3001.230261

in persons ≥50 years of age in Australia (hereafter Australians ≥50 years) in the primary care setting.

Patients with underlying respiratory conditions, such as asthma and chronic obstructive pulmonary disease (COPD), have an increased risk for pertussis, leading to more severe outcomes and exacerbation of asthma and COPD (*8*–*10*). The considerable overlap in the clinical manifestations of those conditions can complicate the diagnosis of pertussis in such patients. In this study, we estimated the incidence rate (IR) of pertussis based on clinical diagnoses and determined the risk factors of pertussis among Australians ≥50 years, including those with COPD or asthma, using the IQVIA GP EMR database.

Methods

Data Sources

We conducted a longitudinal, retrospective, observational study by using records in the IQVIA GP EMR database dated January 2015–December 2019. The IQVIA GP EMR database contains de-identified patient records collected from the EMR software of consenting GPs in Australia, covering 2,286,308 patients across 2,500 GPs and averaging 6 years' follow-up per patient. The database provides rich data that includes demographic and biometric profiles, medical profiles, prescribing information, and prescriber characteristics.

Study Population

The study population included patients ≥50 years of age whose records were collected in the IQVIA GP EMR database during January 2015–December 2019, with pertussis as the outcome of interest. We identified pertussis cases in the overall study population and in patients with COPD or asthma (Figure 1). We used search terms to identify pertussis, COPD, and asthma cases for the primary and sensitivity analyses (Appendix Table 1, https://wwwnc.cdc.gov/EID/article/30/1/23-0261-App1.pdf). We performed sensitivity analyses on a secondary patient population, applying a broader pertussis definition to assess the robustness of estimates, including patients with prolonged coughing potentially related to undiagnosed pertussis, treated empirically as atypical pneumonia or upper respiratory tract infections (Appendix Table 2).

We excluded patients with a diagnosis of pertussis before April 30, 2015, because a run-in period was required to rule out prevalent cases carried forward from the end of 2014. We also excluded patients without a history of diagnosed pertussis during the study period who visited their GP for pertussis vaccination or travel immunization.

Study Objectives

The primary objective of our study was to estimate pertussis incidence based on clinical evidence captured in the IQVIA GP EMR database in Australians ≥50 years, including those with COPD or asthma. The secondary objective was to determine the risk factors for pertussis in this population.

Data Analysis

We calculated the IR of pertussis (cases/100,000 persons) in the overall study population and in patients with COPD or asthma per calendar year as the number of new cases of pertussis divided by the corresponding population in the dataset for each year. We parametrically estimated IRs with 95% CIs by fitting Poisson or negative binomial distributions as appropriate. We compared qualitative or discrete variables by using Pearson χ^2 or Fisher exact tests, and we compared quantitative variables by using 2-sample Student t-test or analysis of variance, after checking equality of variance (Fisher test) and normality (Shapiro–Wilk test). We used Wilcoxon, Mann–Whitney, or Kruskal–Wallis tests if equality of variance and normality were not confirmed.

To determine risk factors for pertussis, we compared patients with diagnosed pertussis with controls by using a nested case-control design. We defined controls as patients who had never received a diagnosis of pertussis during the study period. We matched case patients and controls based on age group (in 5-year groups ≥50 years of age), sex, postal code, and year of GP visit, by using a 1:3 ratio within the same calendar year. We used conditional logistic regression to estimate odds ratios (ORs) and 95% CIs. We examined all exposure variables for univariate associations and constructed a multivariable model that included age, sex, and any variables with p value ≤0.2 in univariate analyses. We also performed multivariable logistic regressions based on forward and backward elimination methods to confirm robustness of the estimates. Given its association with pertussis diagnoses in a previous report, asthma was retained in the final model a priori, irrespective of statistical significance (*11*). Likewise, use of angiotensin-converting enzyme inhibitors (known to induce cough) or angiotensin receptor blockers (known to protect against pertussis infection) and history of pertussis vaccination (during the study period) were retained in the final model a priori, irrespective of statistical significance (*4*,*12*). We performed additional exploratory analyses to evaluate health-seeking behavior by estimating the number of GP visits per year before pertussis diagnosis and antibiotic prescriptions for

cough 1 month before pertussis diagnosis; we then further stratified these data by age, sex, and underlying COPD or asthma. We performed all analyses by using R version 4.3 (The R Foundation for Statistical Computing, https://www.r-project.org).

Results

Study Population

The total population of Australians ≥50 years in the IQVIA GP EMR database covered 252,227–415,201 patients for each year during 2015–2019. We selected 992 patients with pertussis, including those not tested for pertussis, for inclusion in the primary analysis based on the diagnosis label (Table 1). Laboratory tests for pertussis were ordered for 243 (24%) patients and results documented for 205 (21%) patients, of which only 10 (0.01%) tested positive for pertussis. Because of the limited diagnostic testing performed for patients with diagnosed pertussis in GP clinics, our study relied instead on the clinical diagnosis of pertussis.

Among 992 patients with diagnosed pertussis, 66% were women, 41% had a history of cardiovascular disease, 19% had COPD, and 12% had asthma; mean age was 63.3 (95% CI 62.7–63.9) years. Fourteen percent of patients had a record of pertussis immunization during the study period and before pertussis diagnosis. A total of 2,543 patients with pertussis met the extended definition of pertussis for the sensitivity analysis (Appendix Tables 3, 4).

Incidence of Pertussis

We observed differences in annual incidence of pertussis among Australians ≥50 years in 2015–2019

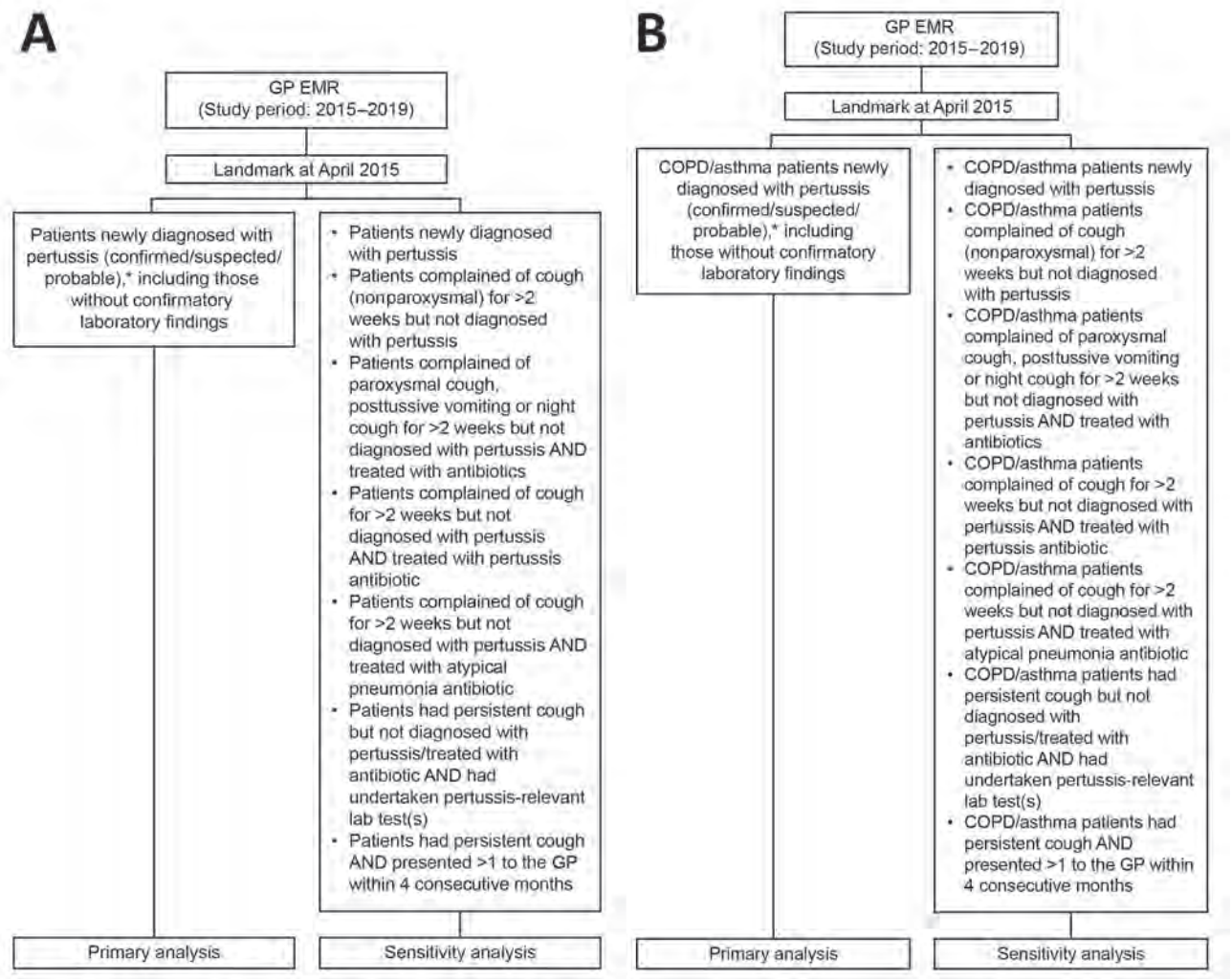

Figure 1. Identification of pertussis cases in population-based study of pertussis incidence and risk factors among persons ≥50 years of age, Australia. A) Overall study population; B) patients with COPD/asthma. *Differentiation between confirmed, probable, and suspected cases was not possible because lab testing is not routinely being performed in all patients and cases were identified from the GP EMR based on the diagnosis label. COPD, chronic obstructive pulmonary disease; EMR, electronic medical record; GP, general practitioner.

Table 1. Baseline patient characteristics for persons ≥50 years of age with pertussis identified in the overall study population, Australia*

Characteristics	Year						p value†
	2015, n = 253	2016, n = 251	2017, n = 219	2018, n = 162	2019, n = 148	Total, n = 992	
Age, y							
Mean (95% CI)	62.5 (61.3–63.7)	63.1 (61.9–64.3)	63.1 (61.9–64.2)	65 (63.4–66.5)	63.8 (62.3–65.4)	63.3 (62.7–63.9)	0.22
Median (IQR)	61 (54–68)	61 (54–68)	63 (56.5–69.5)	63 (56–70)	63 (55.6–70.5)	62 (55.5–68.5)	0.15
Sex‡							
M	91 (36)	77 (31)	73 (33)	56 (35)	49 (33)	332 (33)	0.61
F	162 (64)	173 (69)	146 (67)	105 (65)	99 (67)	658 (67)	0.61
Smoking status							
Never	101 (41)	107 (45)	94 (44)	67 (41)	70 (47)	433 (44)	0.61
Past	49 (20)	45 (19)	53 (25)	51 (31)	33 (22)	216 (22)	0.46
Current	15 (6)	22 (9)	17 (8)	14 (9)	9 (6)	75 (8)	0.61
Unknown	79 (32)	63 (27)	51 (24)	30 (19)	36 (24)	268 (27)	0.13
Alcohol consumption/d§							
None	94 (39)	97 (41)	86 (40)	75 (46)	75 (51)	426 (43)	0.09
≤1 unit	39 (16)	32 (14)	35 (16)	28 (17)	28 (19)	161 (16)	0.13
>1 unit	18 (7)	12 (5)	14 (7)	15 (9)	18 (12)	76 (8)	0.13
Unknown	93 (38)	96 (41)	80 (37)	44 (27)	27 (18)	329 (33)	0.09
Vaccination history¶							
Pertussis	36 (14)	29 (12)	36 (16)	31 (19)	25 (17)	140 (14)	0.22
Influenza	2 (1)	49 (20)	68 (31)	71 (44)	59 (40)	241 (24)	0.09
Pneumococcal	8 (3)	11 (4)	15 (7)	11 (7)	21 (14)	60 (7)	0.04
Residence							
New South Wales	83 (34)	54 (23)	51 (24)	34 (21)	49 (33)	282 (29)	0.81
Victoria	64 (26)	78 (33)	71 (33)	40 (25)	29 (20)	258 (26)	0.31
Queensland	29 (12)	26 (11)	27 (13)	15 (9)	9 (6)	111 (11)	0.22
Western Australia	21 (9)	17 (7)	15 (7)	12 (7)	7 (5)	70 (7)	0.10
South Australia	12 (5)	10 (4)	6 (3)	3 (2)	6 (4)	38 (4)	0.31
Tasmania	5 (2)	11 (5)	12 (6)	35 (22)	30 (20)	89 (9)	0.09
Australian Capital Territory	26 (11)	31 (13)	23 (11)	14 (9)	11 (7)	105 (11)	0.13
Northern Territory	4 (2)	10 (4)	10 (5)	9 (6)	7 (5)	39 (4)	0.13
Comorbidities#							
COPD	41 (16)	51 (20)	40 (18)	38 (23)	25 (17)	185 (19)	0.81
Asthma	25 (10)	35 (14)	27 (12)	24 (15)	16 (11)	117 (12)	0.81
CVD	101 (40)	111 (44)	96 (44)	78 (48)	57 (39)	409 (41)	0.61
Heart failure	4 (2)	4 (2)	3 (1)	2 (1)	9 (6)	16 (2)	0.61
Diabetes mellitus	32 (13)	32 (13)	36 (16)	34 (21)	18 (12)	144 (14)	0.61
History of stroke	3 (1)	3 (1)	3 (2)	2 (1)	9 (6)	21 (2)	0.27
Chronic kidney disease	5 (2)	4 (2)	10 (5)	4 (2)	5 (3)	27 (3)	0.58
Cancer, active or remission	23 (9)	45 (18)	32 (15)	29 (18)	22 (15)	136 (14)	0.79

*Values are no. (%) except as indicated. Variables were defined as those at baseline (i.e., restricted to those recorded during the study period or until the time of pertussis diagnosis). COPD, chronic obstructive pulmonary disease; CVD, cardiovascular disease (except heart failure); IQR, interquartile range.
†Pearson χ^2 or Fisher exact test for categorical variables, Student t-test/Wilcoxon/Kruskal Wallis tests for continuous variables, as appropriate. There were significant differences in smoking status, alcohol consumption, state of residence (Western Australia, Australian Capital Territory), COPD, and diabetes between males and females.
‡Two patients had sex documented as unknown.
§One unit of alcohol is defined as containing 10 g of alcohol according to Australia's national alcohol guidelines.
¶History of pertussis immunization was defined as the presence of pertussis immunization record throughout the study period, as recorded in the Australia general practitioner electronic medical records database.
#History of CVD, chronic kidney disease, and cancer were defined as those at baseline and were restricted to those recorded during the study period, or until the time of pertussis diagnosis, as applicable.

(Figure 2, panel A; Appendix Table 5). Pertussis IRs per 100,000 persons were 91.4 (95% CI 84.1–98.7) in 2015 and 58.7 (95% CI 51.4–66.0) in 2019 (Figure 2, panel A). In age subgroups, IRs were consistently highest among those 50–64 years of age and 65–74 years of age (Figure 2, panel B; Appendix Table 5). Overall, pertussis IRs varied across all age groups during 2015–2019 (Figure 2, panel B).

When stratified by sex, pertussis IRs among women were 110.5 (95% CI 102.3–118.7) in 2015 and 74.5 (95% CI 66.3–82.7) in 2019. Lower IRs of 70.6 (95% CI 64.3–76.8) in 2015 and 41.6 (95% CI 35.4–47.8) in 2019 were observed among men (Figure 2, panel C). Similar trends were reported by the NNDSS, although pertussis IRs were lower than those in our study population (Figure 2).

In patients with COPD, pertussis IRs throughout the study period ranged from 304.4 (95% CI 290.7–318.1) in 2015 to 194.3 (95% CI 180.5–207.9) in 2019 (Figure 3, panel A; Appendix Table 6). Similarly, in patients

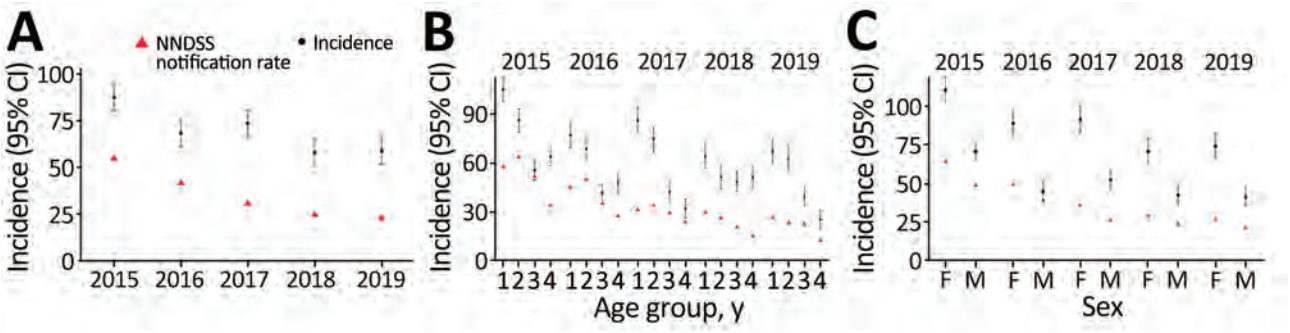

Figure 2. National notification rates compared with annual incidence of pertussis in population-based study of pertussis incidence and risk factors among persons ≥50 years of age, Australia. A) Overall study population; B) by age group: group 1, 50–64 y; group 2, 65–74 y; group 3, 75–84 y; group 4, ≥85 y; C) by sex. Incidence rates are reported per 100,000 persons; error bars indicate 95% CIs. Both NNDSS and GP EMR data consist of persons ≥50 years of age. Data in 2015 were projected to 12-month period because a run-in period/landmark was applied to rule out prevalent pertussis cases carried forward from the previous year. Data for 2016–2019 are as observed. EMR, electronic medical records; GP, general practitioner; NNDSS, National Notifiable Diseases Surveillance System.

with asthma, pertussis IRs ranged from 473.0 (95% CI 454.0–492.0) in 2015 to 376.8 (95% CI 357.8–395.8) in 2019 (Figure 4, panel A; Appendix Table 7). Although pertussis IRs among patients with COPD or asthma were higher than the overall study population, variations between age groups were generally consistent (Figure 3, panel B; Figure 4, panel B). Consistent with the overall study population, pertussis IRs in women with COPD or asthma were higher than in men with COPD (Figure 3, panel C; Appendix Table 6) or in men with asthma (Figure 4, panel C; Appendix Table 7).

In the sensitivity analysis, based on an extended definition of pertussis, annual IRs were 197.6 (95% CI 185.5–209.7) in 2015 and 196.7 (95% CI 184.5–208.8) in 2019 (Appendix Figure 1, panel A). Overall, the lowest IRs were observed in patients ≥85 years of age (Appendix Figure 1, panel B). IRs remained higher among women versus men (Appendix Figure 1, panel C). In the sensitivity analysis, IRs among patients with COPD or asthma were higher than those in the overall study population (Appendix Figure 2, panel A, Figure 3, panel A). In 2016–2018, pertussis IRs in patients with COPD or asthma were highest in patients 65–74 years of age (Appendix Figure 2, panel B, Figure 3, panel B). Overall, IRs by age group and sex in patients with COPD or asthma were higher than IRs for the same group in the primary analysis and NNDSS, consistent with trends observed in the primary analysis (Appendix Figure 2, panels B, C, Figure 3, panels B, C). Trends observed in the monthly number of pertussis cases defined within the primary and sensitivity analyses cohorts and those reported in the NNDSS data were generally consistent and peaked in winter (June–September) (Figure 5).

Risk Factor Modeling

Conditional univariable logistic regression models predicted that concurrent diabetes, asthma, or COPD, use of angiotensin-converting enzyme inhibitors or angiotensin receptor blockers, and prior use of antibiotics within 1 month increased the risk for a

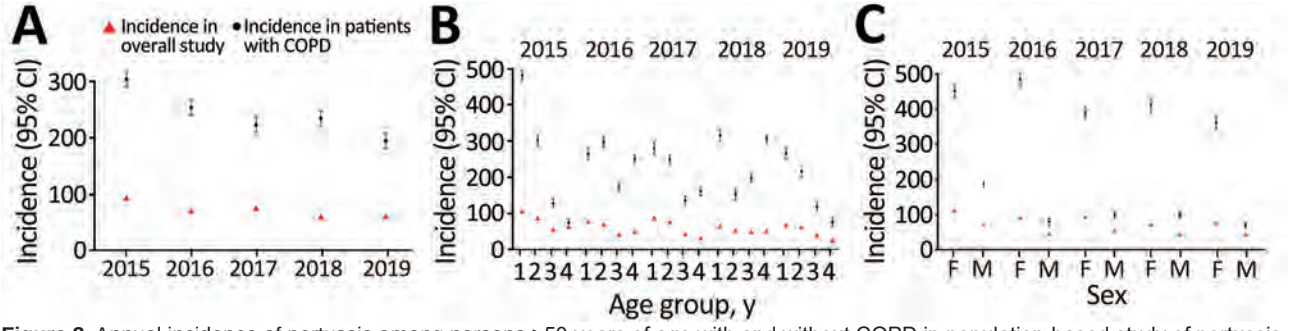

Figure 3. Annual incidence of pertussis among persons ≥50 years of age with and without COPD in population-based study of pertussis incidence and risk factors, Australia. A) Overall study population; B) by age group: group 1, 50–64 y; group 2, 65–74 y; group 3, 75–84 y; group 4, ≥85 y; C) by sex.Incidence rates are reported per 100,000 persons; error bars indicate 95% CIs. COPD cases were defined based on diagnosis label or prescription of reliever/corticosteroid inhaler (≥1 refill of the same product). Data in 2015 were projected to 12-month period because a run-in period/landmark was applied to rule out prevalent pertussis cases carried forward from the previous year. Data for 2016–2019 are as observed. COPD, chronic obstructive pulmonary disease.

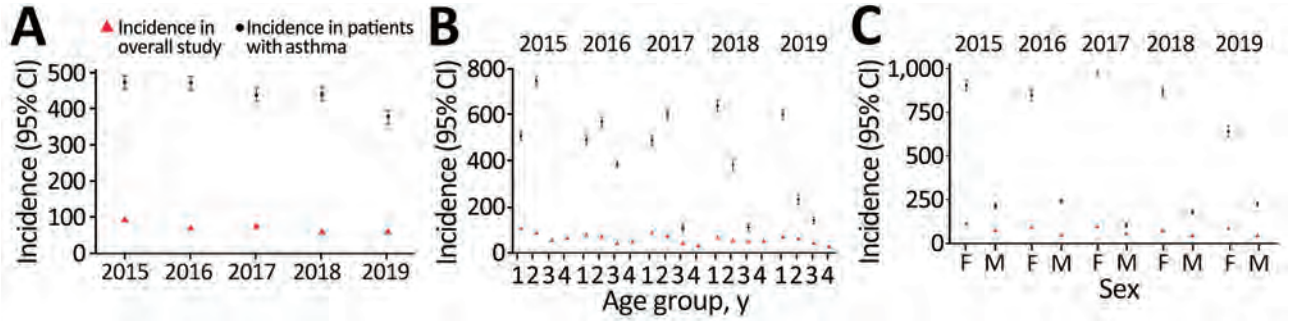

Figure 4. Annual incidence of pertussis among persons ≥50 years of age with and without asthma in population-based study of pertussis incidence and risk factors, Australia. A) Overall study population; B) by age group: group 1, 50–64 y; group 2, 65–74 y; group 3, 75–84 y; group 4, ≥85 y; C) by sex. Incidence rates are reported per 100,000 persons; error bars indicate 95% CIs. Asthma cases were defined based on diagnosis label or prescription of reliever/corticosteroid inhaler (≥1 refill of the same product). Data in 2015 were projected to 12-month period because a run-in period/landmark was applied to rule out prevalent pertussis cases carried forward from the previous year. Data for 2016–2019 are as observed.

pertussis diagnosis; history of influenza vaccination was associated with reduced risk for a pertussis diagnosis (Table 2). The adjusted multivariable logistic regression model suggested that prior prescription of an antibiotic for cough within 1 month (OR 7.00 [95% CI 4.21–11.64]), asthma (OR 2.94 [95% CI 1.71–5.04]), and COPD (OR 1.88 [95% CI 1.23–2.86]) were predictors of pertussis diagnosis, but the risk for pertussis diagnosis was lower for patients with a history of influenza vaccination (OR 0.38 [95% CI 0.26–0.55]; Table 3).

Healthcare-Seeking Behavior and Antibiotic Prescriptions

We compared the number of GP visits for men and women in terms of asthma status, COPD status, and across age groups (Appendix Figure 4, panel A). We observed no sex-specific differences (p = 0.12) among patients with COPD or asthma (women, median 11, interquartile range [IQR] 10, vs. men, median 10, IQR 13).

In the overall study population, the median number of GP visits within 1 year before pertussis diagnosis was significantly higher (p = 0.001) for women (median 8, IQR 10) than for men (median 6, IQR 9). The median number of GP visits increased with presence of COPD or asthma for both women and men. In patients without COPD or asthma, the median number of GP visits was also significantly higher (p = 0.01) in women (median 6, IQR 8) compared with men (median 5, IQR 9). Furthermore, the number of GP visits increased with age, independent of sex and COPD or asthma status (Appendix Figure 4, panels B, C).

To investigate the observed reduced risk for pertussis associated with history of influenza vaccination within the risk factor modeling, we also looked at the distributed number of GP visits among those with or without history of influenza vaccination before pertussis diagnosis. Persons vaccinated for influenza before pertussis diagnosis had a higher median number of GP visits compared with those without influenza vaccination across all age groups (Table 4).

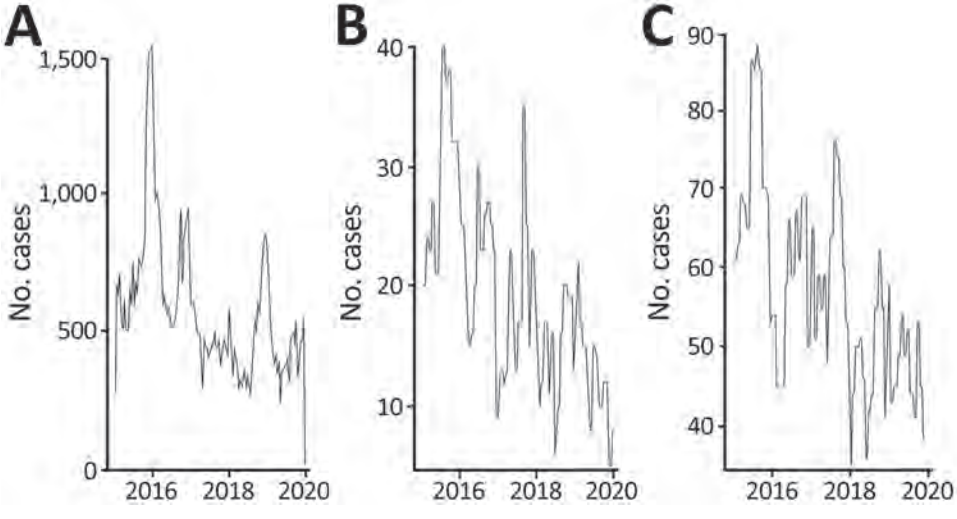

Figure 5. Comparison of the monthly number of pertussis cases reported to the NNDSS and identified in the primary and sensitivity analyses of population-based study of pertussis incidence and risk factors among persons ≥50 years of age, Australia. A) Cases captured by the NNDSS; B) cases in the primary overall study population; C) cases in the sensitivity analysis cohort. NNDSS, National Notifiable Diseases Surveillance System.

Overall, 252 (25%) patients diagnosed with pertussis in the primary analysis were prescribed antibiotics for cough 1 month before their pertussis diagnosis. The most prescribed antibiotics were macrolides (83%) and broad-spectrum penicillin (24%), followed by tetracyclines (5%), cephalosporins (4%), and trimethoprim combinations (1%) (Table 5).

Discussion

By using the IQVIA GP EMR database, we estimated IRs and risk factors for clinically diagnosed pertussis among Australians ≥50 years, including those with COPD or asthma (Appendix Figure 5). IRs were highest among patients 50–64 years of age and were 2 times higher in women than in men. Furthermore, compared with the overall study population, IRs in patients with COPD were ≈3–4 times higher and in patients with asthma were ≈5–8 times higher.

In a systematic literature review reporting results from 85 publications, IRs in older adults broadly ranged 2–16,670/100,000 population, depending on the definition of pertussis and study methodology (*4*). Our findings are largely consistent with previously published global studies and studies in Australia, also reporting higher pertussis IRs in women compared with men (*11*,*13*,*14*). The higher IRs in women may be attributed to healthcare-seeking behavior, increased exposure to children and elderly persons infected with pertussis through caretaker roles, and biological and immune response differences (*14*).

For the extended definition of pertussis in the sensitivity analysis, we noted pertussis IRs to be higher than those in the primary analysis, likely attributable in part to the inclusion of nonpertussis seasonal respiratory diseases. In patients with COPD or asthma, we found IRs in the sensitivity analysis to be >3 times higher than those observed in the primary analysis, although the overall trends were consistent.

Trends observed in IRs were largely consistent between GP EMR data and NNDSS data, aligning with the known cyclic trend of pertussis epidemics in Australia. Contemporary data suggest that pertussis outbreaks occur periodically every 3 to 4 years (*5*,*15*); the 2 most recent epidemics of pertussis in Australia peaked in 2011 and 2015 (*16*). Evidence of seasonal fluctuations in pertussis incidence has been noted in other countries as well (*17*–*21*). There are conflicting findings in the context of Australia; several studies report higher incidence peaks in spring and summer months (November–January) and others report such peaks in winter months (June–September) (*22*–*24*). Pertussis was also found to be a common pathogen in infants hospitalized for acute lower respiratory tract infection, including pertussis co-infection, during winter in the Netherlands (*25*). It is therefore likely that the incidence spikes of pertussis observed in our study were confounded by circulating influenza viruses or respiratory syncytial virus outbreaks because of the the non–laboratory-confirmed definition of pertussis cases.

Conditional multivariable regression analysis showed that prior use of antibiotics within 1 month and concurrent asthma and COPD were predictors of pertussis diagnosis. Because only 24% of patients with pertussis in this study were tested for pertussis, antibiotics prescribed for concurrent asthma and COPD may have influenced prediction of pertussis diagnosis.

Patients with a history of influenza vaccination had a 62% lower risk for pertussis diagnosis than those without that history. A post-hoc analysis from a clinical trial among pregnant women suggested that influenza vaccination may have a positive effect on rates of pertussis infection and called for further investigation into the possible mechanisms in the upper respiratory tract that can lead to the synergy between

Table 2. Predictors of pertussis in persons ≥50 years of age from conditional univariable logistic regression models in the overall study population, Australia*

Variable	OR (95% CI)	p value
Smoking status		
No	Referent	
Yes	1.18 (0.88–1.58)	0.80
Alcohol consumption/d†		
None	Referent	
≤1 unit	1.02 (0.71–1.46)	0.93
>1 unit	1.04 (0.67–1.63)	0.86
Immunization history‡		
Pertussis	0.77 (0.48–1.24)	0.28
Influenza	0.52 (0.37–0.73)	<0.001
Pneumococcal	0.70 (0.41–1.17)	0.17
Comorbidities§		
CVD	1.30 (0.97–1.74)	0.08
Heart failure	0.93 (0.33–2.63)	0.90
Diabetes mellitus	1.65 (1.13–2.42)	<0.001
Stroke	0.88 (0.32–2.42)	0.80
Chronic kidney disease	0.90 (0.42–1.92)	0.78
Cancer	1.45 (0.98–2.15)	0.06
Asthma	2.46 (1.54–3.93)	<0.001
COPD	2.01 (1.38–2.93)	<0.001
Asthma/COPD	2.2 (1.59–3.05)	<0.001
Use of ACEi-ARB	1.45 (1.09–1.93)	<0.001
Prior use of antibiotics	7.19 (4.42–11.69)	<0.001

*Variables were defined as those at baseline (i.e., restricted to those recorded during the study period or until the time of pertussis diagnosis). In this analysis, patients with missing data were excluded. ACEi-ARB, angiotensin-converting enzyme inhibitors–angiotensin receptor blockers; COPD, chronic obstructive pulmonary disease; CVD, cardiovascular disease (except heart failure); OR, odds ratio.
†One unit of alcohol is defined as containing 10 g of alcohol.
‡History of pertussis immunization was defined as the presence of pertussis immunization record throughout the study period, as recorded in the Australia general practitioner electronic medical records database.
§History of CVD, chronic kidney disease, and cancer were defined as those at baseline and were restricted to those recorded during the study period, or until the time of pertussis diagnosis, as applicable.

Table 3. Predictors of pertussis in persons ≥50 years of age from conditional multivariable logistic regression models, Australia*

Variables	aOR (95%CI)
Prior prescription of antibiotics for cough	7.00 (4.21–11.64)
Asthma	2.94 (1.71–5.04)
COPD	1.88 (1.23–2.86)
Diabetes mellitus	1.47 (0.68–2.27)
Use of ACEi-ARB	1.37 (1.00–1.85)
History of pertussis immunization†	1.03 (0.62–1.69)
History of influenza vaccination	0.38 (0.26–0.55)

*Variables were defined as those at baseline (i.e., restricted to those recorded during the study period or until the time of pertussis diagnosis). In this analysis, patients with missing data were excluded. ACEi-ARB, angiotensin-converting enzyme inhibitors–angiotensin receptor blockers; COPD, chronic obstructive pulmonary disease.
†History of pertussis immunization was defined as the presence of pertussis immunization record throughout the study period, as recorded in the Australia general practitioner electronic medical records database.

the 2 pathogens (*26*). Influenza-vaccinated persons have a lower risk for influenza-related worsening of other respiratory diseases (*27*); thus, fewer potentially misdiagnosed pertussis cases may contribute to artifacts rather than true association between influenza vaccination history and pertussis diagnosis. Given the low pertussis testing rates in this study, these findings should be treated with caution. Notably, the Australian government offers free influenza vaccines through the National Immunisation Program for seniors ≥65 years of age, which may have contributed to a higher influenza vaccination rate in the study population. In addition, patients in better health or who are health-conscious are more likely to get vaccinated (i.e., healthy vaccinee bias) and seek health care when experiencing respiratory symptoms (*28*).

The risk for pertussis diagnosis in patients with underlying COPD and asthma was previously reported to be higher than for patients with pertussis but without those conditions (*29*). Contemporary data also suggest that patients with COPD and asthma have a higher pertussis incidence, risk for pertussis infection, and greater subsequent disease burden than patients with pertussis but without such concurrent conditions (*9*,*29*–*31*). Furthermore, asthma, COPD, and other chronic inflammatory pulmonary diseases can be exacerbated by *B. pertussis* infection (*29*). Increased risk for pertussis in patients with COPD or asthma may be explained by potential adverse effects of inhaled or systemic corticosteroids, altered airway architecture, impairment of innate and acquired immunity, waning humoral immunity over time, and influence of concurrent conditions on immunogenicity (*30*).

In this study, women, older age groups, and those with a history of influenza vaccination were associated with a higher median number of GP visits in a year, likely resulting in a higher chance of pertussis being recognized or diagnosed. Those observations might be due to women and older adults (who may have other concurrent conditions) visiting the GP more often (*32*–*34*). The higher median number of GP visits in persons with a history of influenza vaccination versus without suggests that those persons are more health conscious (i.e., healthy vaccinee bias) or had other conditions that required more GP visits. Among all patients diagnosed with pertussis, antibiotic prescriptions within 1 month before pertussis diagnosis were more common for those with COPD or asthma, men, and younger age groups (50–74 years); macrolides and penicillin were the most prescribed. Of note, persistent cough is a criterion for asthma and COPD exacerbation according to Australia guidelines (*35*,*36*), possibly explaining why antibiotics were more commonly prescribed and why pertussis may not have been recognized or diagnosed earlier in these patients. Because macrolides are the preferred treatment for pertussis, an adequate dosage and treatment duration may reduce likelihood of pertussis diagnosis (*37*), which may have skewed the estimated pertussis IRs in the populations described in this study, particularly among patients with COPD or asthma.

Because of differing case definitions in this study and the lack of routine laboratory testing in the primary care setting, the pertussis IRs in Australians ≥50 years may be higher than those reported to the NNDSS. NNDSS data rely on GP clinical, laboratory, or empirical diagnoses to identify confirmed and probable cases of pertussis. The surveillance case definition for pertussis requires confirmed cases to have either laboratory-definitive evidence or laboratory-suggestive evidence and clinical evidence, whereas probable cases require clinical and epidemiologic evidence (*38*). In our study, we identified cases based on clinical diagnosis, and only a small proportion of patients had pertussis-related diagnostic laboratory tests performed and documented in the EMR. Therefore, the approach we used in this study captured more cases that did not meet the NNDSS case definition of pertussis. Estimating the true impact of pertussis vaccination is not feasible, given the low vaccination rate and underdocumentation of vaccination history in the EMR database. Previous studies have shown that pertussis-related hospitalizations, healthcare burden,

Table 4. Comparison of median number of GP visits within 1 year before pertussis diagnosis by history of influenza vaccination and age groups in persons ≥50 years of age, Australia*

	History of influenza vaccination, median (IQR) visits		
Age group, y	No	Yes	p value†
50–64	5 (8)	9 (8)	<0.001
65–74	6 (9.5)	13 (9)	<0.001
75–84	8 (12)	13 (15)	<0.001
≥85	8 (10.5)	15 (17)	0.01

*GP, general practitioner; IQR, interquartile range.
†Differences in median number of GP visits within 1 year before the pertussis diagnosis within each age group.

concurrent conditions, and risk for death increase with age (*4*,*11*,*39*). However, because the GP EMR database is based in the primary care setting, it is not representative of all Australians ≥50 years and does not allow further evaluation of pertussis severity and its association with hospitalization, healthcare burden, and mortality. Given the known underdiagnosis and underreporting of pertussis, our incidence and risk factor analysis can still provide useful guidance related to pertussis prevention in the primary care setting. Nevertheless, it will be important to further validate the findings of this study by using a more specific and validated case definition of pertussis cases.

From a public health standpoint, this study highlights the importance of pertussis prevention for Australians ≥50 years, especially among those with COPD or asthma, thus improving community awareness and uptake of immunization at age 50 and 65 years, which is currently suboptimal (*40*,*41*). An effective vaccination strategy is necessary to reduce complications and increased healthcare costs associated with pertussis among patients with COPD or asthma (*4*,*29*). For patients with COPD or asthma who have unrecognized or undiagnosed pertussis, inappropriately prescribed antibiotics may empirically treat pathogens causing other respiratory illnesses but delay the diagnosis and control of pertussis. Conversely, timely pertussis vaccinations can protect vaccinated persons against pertussis development and prevent community-level transmission. Other strategies include increasing pertussis testing by GPs to improve ascertainment of cases and ensure timely treatment (*40*).

Table 5. Distribution of antibiotics prescribed within 1 month before pertussis diagnosis in persons ≥50 years of age, Australia*

Category	No. pertussis cases	Antibiotic prescription		Antibiotic category				
		No	Yes	Broad-spectrum penicillin	Cephalosporins	Macrolides	Tetracyclines	Trimethoprim combinations
All pertussis patients								
Overall	992	740 (75)	252 (25)	61 (24)	11 (4)	209 (83)	12 (5)	2 (1)
Age group, y								
50–64	598	444 (74)	154 (26)	33 (21)	4 (3)	130 (84)	6 (4)	1 (1)
65–74	260	190 (73)	70 (27)	17 (24)	6 (9)	60 (86)	1 (1)	0 (0)
75–84	95	76 (80)	19 (20)	8 (42)	1 (5)	11 (58)	5 (26)	0 (0)
≥85	39	30 (77)	9 (23)	3 (33)	0 (0)	8 (89)	0 (0)	1 (11)
Sex								
F	658	497 (76)	161 (24)	36 (22)	9 (6)	134 (83)	7 (4)	2 (1)
M	332	242 (73)	90 (27)	25 (28)	2 (2)	74 (82)	5 (6)	0 (0)
Pertussis patients with asthma								
Overall	117	75 (64)	42 (36)	14 (33)	7 (17)	34 (81)	0	NA
Age group, y								
50–64	72	47 (65)	25 (35)	7 (28)	3 (12)	21 (84)	0	
65–74	38	21 (14)	17 (86)	6 (35)	4 (24)	14 (82)	0	NA
75–84	7	6 (86)	1 (14)	1 (100)	0	0	0	
≥85	0	0	0	0	0	0	0	
Sex								
F	86	55 (64)	31 (36)	10 (32)	7 (23)	26 (84)	0	NA
M	31	20 (65)	11 (35)	4 (36)	0	8 (73)	0	
Pertussis patients with COPD								
Overall	185	139 (75)	46 (25)	17 (37)	2 (4)	38 (83)	3 (7)	NA
Age group, y								
50–64	81	61 (75)	20 (25)	7 (35)	0	16 (80)	1 (5)	
65–74	60	44 (73)	16 (27)	6 (38)	2 (13)	14 (88)	0	NA
75–84	29	22 (76)	7 (24)	2 (29)	0	6 (86)	2 (29)	
≥85	15	11 (73)	4 (27)	2 (50)	0	3 (75)	0	
Sex								
F	143	110 (77)	33 (23)	8 (24)	2 (6)	29 (88)	2 (6)	NA
M	42	29 (69)	13 (31)	9 (69)	0	9 (69)	1 (8)	
Pertussis patients without asthma/COPD								
Overall	709	534 (75)	175 (25)	34 (19)	4 (2)	147 (84)	9 (5)	2 (1)
Age group, y								
50–64	452	337 (75)	115 (25)	21 (18)	1 (1)	99 (86)	5 (4)	1 (1)
65–74	173	129 (75)	44 (25)	7 (16)	2 (5)	38 (86)	1 (2)	0
75–84	60	49 (82)	11 (18)	5 (45)	1 (9)	5 (45)	3 (27)	0
≥85	24	19 (79)	5 (21)	1 (20)	0	5 (100)	0	1 (20)
Sex								
F	443	337 (76)	106 (24)	21 (20)	2 (2)	87 (82)	5 (5)	2 (2)
M	264	196 (74)	68 (26)	13 (19)	2 (3)	59 (87)	4 (6)	0

*Values are no. (%) except as indicated. Percentages were calculated within each row. Because some patients may have received combination of antibiotics, the sum of number of patients in antibiotics category do not equal to total number of pertussis cases in each row. Likewise, percentages do not sum up to 100%. COPD, chronic obstructive pulmonary disease; NA, not applicable.

Future studies might consider the effect of policy interventions on pertussis vaccination behavior, underuse of pertussis vaccines, and cost-effectiveness of potential new models of pertussis immunization programs to address policy gaps in the present program. In summary, a sizeable burden of pertussis in older adults in Australia has a greater impact on persons with COPD or asthma. This study highlights the importance of pertussis prevention for Australians ≥50 years of age.

Acknowledgments

We thank Roeland Van Kerckhoven for publication management and Co Luu for providing medical insight supporting the interpretation of study results. The authors also thank Costello Medical for editorial assistance and publication coordination, on behalf of GSK, and acknowledge Loveena Sharma for medical writing and editorial assistance based on the authors' input and direction.

The data and datasets that support the findings of this study are not publicly available because they are owned by IQVIA.

This study was sponsored by GlaxoSmithKline Biologicals SA (Study identifier eTrack: EPI-pertussis-066). Support for third-party writing assistance for this article, provided by Loveena Sharma, Costello Medical, Singapore, and Claire Hews, Costello Medical, UK, was funded by GSK in accordance with Good Publication Practice (GPP3) guidelines (http://www.ismpp.org/gpp3).

R.P. has received honoraria from GSK group of companies and Pfizer for educational speaking events and advisory board participation. J.C., A.G., and S.S. are employees of and hold shares in the GSK group of companies. L.-A.L. is an employee of the GSK group of companies. K.L.C., B.S., and G.S. are employees of IQVIA and received fees related to the conduct of this study from the GSK group of companies. C.R.M. reports nothing to disclose.

Substantial contributions to study conception and design: R.P., J.C., K.L.C., A.G., L.-A.L., C.R.M., B.S., G.S., and S.S.; substantial contributions to analysis and interpretation of the data: R.P., J.C., K.L.C., A.G., L.-A.L., B.S., G.S., and S.S.; drafting the article or revising it critically for important intellectual content: R.P., J.C., K.L.C., A.G., L.-A.L., C.R.M., B.S., G.S., and S.S.; final approval of the version of the article to be published: R.P., J.C., K.L.C., A.G., L.-A.L., C.R.M., B.S., G.S., and S.S.

About the Author

Dr. Pearce is a practicing grass-roots general practitioner and policy adviser in Australia who serves as chairman of the Immunisation Coalition and member of the Asia Pacific Alliance for the Control of Influenza.

References

1. Australian Government Department of Health. Pertussis (whooping cough) 2021 [cited 2023 Jul 13]. https://immunisationhandbook.health.gov.au/vaccine-preventable-diseases/pertussis-whooping-cough
2. Burdin N, Handy LK, Plotkin SA. What is wrong with pertussis vaccine immunity? The problem of waning effectiveness of pertussis vaccines. Cold Spring Harb Perspect Biol. 2017;9:a029454. https://doi.org/10.1101/cshperspect.a029454
3. Crowcroft NS, Pebody RG. Recent developments in pertussis. Lancet. 2006;367:1926–36. https://doi.org/10.1016/S0140-6736(06)68848-X
4. Kandeil W, Atanasov P, Avramioti D, Fu J, Demarteau N, Li X. The burden of pertussis in older adults: what is the role of vaccination? A systematic literature review. Expert Rev Vaccines. 2019;18:439–55. https://doi.org/10.1080/14760584.2019.1588727
5. Australian Technical Advisory Group on Immunisation (ATAGI). Pertussis. In: The Australian immunisation handbook, 10th edition. Canberra: Australian Government Department of Health; 2015. p. 312–26.
6. Australian Government Department of Health and Aged Care. Australian Technical Advisory Group on Immunisation (ATAGI) 2023 [cited 2023 Jul 13]. https://www.health.gov.au/committees-and-groups/australian-technical-advisory-group-on-immunisation-atagi
7. Karki S, McIntyre P, Newall AT, MacIntyre CR, Banks E, Liu B. Risk factors for pertussis hospitalizations in Australians aged 45 years and over: a population based nested case-control study. Vaccine. 2015;33:5647–53. https://doi.org/10.1016/j.vaccine.2015.08.068
8. Hashemi SH, Nadi E, Hajilooi M, Seif-Rabiei MA, Samaei A. High seroprevalence of *Bordetella pertussis* in patients with chronic obstructive pulmonary disease: a case-control study. Tanaffos. 2015;14:172–6.
9. Bhavsar A, Aris E, Harrington L, Simeone JC, Ramond A, Lambrelli D, et al. Burden of pertussis in individuals with a diagnosis of asthma: a retrospective database study in England. J Asthma Allergy. 2022;15:35–51. https://doi.org/10.2147/JAA.S335960
10. Jenkins VA, Savic M, Kandeil W. Pertussis in high-risk groups: an overview of the past quarter-century. Hum Vaccin Immunother. 2020;16:2609–17. https://doi.org/10.1080/21645515.2020.1738168
11. Liu BC, McIntyre P, Kaldor JM, Quinn HE, Ridda I, Banks E. Pertussis in older adults: prospective study of risk factors and morbidity. Clin Infect Dis. 2012;55:1450–6. https://doi.org/10.1093/cid/cis627
12. Dicpinigaitis PV. Angiotensin-converting enzyme inhibitor-induced cough: ACCP evidence-based clinical practice guidelines. Chest. 2006;129(Suppl):169S–73S. https://doi.org/10.1378/chest.129.1_suppl.169S
13. Leong RNF, Wood JG, Liu B, Menzies R, Newall AT. Estimating pertussis incidence in general practice using a large Australian primary care database. Vaccine. 2021;39:4153–9. https://doi.org/10.1016/j.vaccine.2021.05.079
14. Peer V, Schwartz N, Green MS. A multi-country, multi-year, meta-analytic evaluation of the sex differences in age-specific pertussis incidence rates. PLoS One. 2020;15:e0231570. https://doi.org/10.1371/journal.pone.0231570

15. Quinn HE, McIntyre PB. Pertussis epidemiology in Australia over the decade 1995-2005—trends by region and age group. Commun Dis Intell Q Rep. 2007;31:205–15.
16. NNDSS Annual Report Working Group. Australia's notifiable disease status, 2016: annual report of the National Notifiable Diseases Surveillance System. Canberra: Australian Government Department of Health; 2021 [cited 2022 Oct 19]. https://www1.health.gov.au/internet/main/publishing.nsf/Content/5C71FABF639650F6CA2586520081286B/$File/australia_s_notifiable_disease_status_2016_annual_report_of_the_national_notifiable_diseases_surveillance_system.pdf
17. Gu W, Wang K, Zhang X, Hao C, Lu Y, Wu M, et al. Pathogen analysis of pertussis-like syndrome in children. BMC Infect Dis. 2020;20:353. https://doi.org/10.1186/s12879-020-05074-8
18. Skowronski DM, De Serres G, MacDonald D, Wu W, Shaw C, Macnabb J, et al. The changing age and seasonal profile of pertussis in Canada. J Infect Dis. 2002;185:1448–53. https://doi.org/10.1086/340280
19. Ghorbani GR, Zahraei SM, Moosazadeh M, Afshari M, Doosti F. Comparing seasonal pattern of laboratory confirmed cases of pertussis with clinically suspected cases. Osong Public Health Res Perspect. 2016;7:131–7. https://doi.org/10.1016/j.phrp.2016.02.004
20. Bhatti MM, Rucinski SL, Schwab JJ, Cole NC, Gebrehiwot SA, Patel R. Eight-year review of *Bordetella pertussis* testing reveals seasonal pattern in the United States. J Pediatric Infect Dis Soc. 2017;6:91–3. https://doi.org/10.1093/jpids/piv079
21. Public Health England. Laboratory confirmed cases of pertussis in England: annual report for 2019. London: Public Health England; 2020 [cited 2022 Aug 15]. https://assets.publishing.service.gov.uk/media/5ea6bcf5e90e07048c84e801/hpr0820_PRTSSS_annual.pdf
22. Leong RNF, Wood JG, Turner RM, Newall AT. Estimating seasonal variation in Australian pertussis notifications from 1991 to 2016: evidence of spring to summer peaks. Epidemiol Infect. 2019;147:e155. https://doi.org/10.1017/S0950268818003680
23. Kaczmarek MC, Ware RS, Nimmo GR, Robson JMB, Lambert SB. Pertussis seasonality evident in polymerase chain reaction and serological testing data, Queensland, Australia. J Pediatric Infect Dis Soc. 2016;5:214–7. https://doi.org/10.1093/jpids/piu144
24. Huang X, Lambert S, Lau C, Soares Magalhaes RJ, Marquess J, Rajmokan M, et al. Assessing the social and environmental determinants of pertussis epidemics in Queensland, Australia: a Bayesian spatio-temporal analysis. Epidemiol Infect. 2017;145:1221–30. https://doi.org/10.1017/S0950268816003289
25. van den Brink G, Wishaupt JO, Douma JC, Hartwig NG, Versteegh FGA. *Bordetella pertussis*: an underreported pathogen in pediatric respiratory infections, a prospective cohort study. BMC Infect Dis. 2014;14:526. https://doi.org/10.1186/1471-2334-14-526
26. Nunes MC, Cutland CL, Madhi SA. Influenza vaccination during pregnancy and protection against pertussis. N Engl J Med. 2018;378:1257–8. https://doi.org/10.1056/NEJMc1705208
27. Centers for Disease Control and Prevention. Vaccine effectiveness: how well do flu faccines work? 2022 [cited 2022 Dec 13]. https://www.cdc.gov/flu/vaccines-work/vaccineeffect.htm
28. Remschmidt C, Wichmann O, Harder T. Frequency and impact of confounding by indication and healthy vaccinee bias in observational studies assessing influenza vaccine effectiveness: a systematic review. BMC Infect Dis. 2015;15:429. https://doi.org/10.1186/s12879-015-1154-y
29. Buck PO, Meyers JL, Gordon L-D, Parikh R, Kurosky SK, Davis KL. Economic burden of diagnosed pertussis among individuals with asthma or chronic obstructive pulmonary disease in the USA: an analysis of administrative claims. Epidemiol Infect. 2017;145:2109–21. https://doi.org/10.1017/S0950268817000887
30. Capili CR, Hettinger A, Rigelman-Hedberg N, Fink L, Boyce T, Lahr B, et al. Increased risk of pertussis in patients with asthma. J Allergy Clin Immunol. 2012;129:957–63. https://doi.org/10.1016/j.jaci.2011.11.020
31. Aris E, Harrington L, Bhavsar A, Simeone JC, Ramond A, Papi A, et al. Burden of pertussis in COPD: a retrospective database study in England. COPD. 2021;18:157–69. https://doi.org/10.1080/15412555.2021.1899155
32. Thompson AE, Anisimowicz Y, Miedema B, Hogg W, Wodchis WP, Aubrey-Bassler K. The influence of gender and other patient characteristics on health care-seeking behaviour: a QUALICOPC study. BMC Fam Pract. 2016;17:38. https://doi.org/10.1186/s12875-016-0440-0
33. Wang Y, Hunt K, Nazareth I, Freemantle N, Petersen I. Do men consult less than women? An analysis of routinely collected UK general practice data. BMJ Open. 2013;3:e003320. https://doi.org/10.1136/bmjopen-2013-003320
34. Xu KT, Borders TF. Gender, health, and physician visits among adults in the United States. Am J Public Health. 2003;93:1076–9. https://doi.org/10.2105/AJPH.93.7.1076
35. COPD-X. Manage eXacerbations. The COPD-X Plan: Australian and New Zealand guidelines for the management of chronic obstructive pulmonary disease. 2021 [cited 2022 Aug 15]. https://copdx.org.au/copd-x-plan/x-manage-exacerbations
36. National Asthma Council Australia. Managing flare-ups in adults. Australian Asthma Handbook. 2022 [cited 2023 Jul 13]. https://www.asthmahandbook.org.au/management/adults/flare-ups
37. Bergquist SO, Bernander S, Dahnsjö H, Sundelöf B. Erythromycin in the treatment of pertussis: a study of bacteriologic and clinical effects. Pediatr Infect Dis J. 1987; 6:458–61. https://doi.org/10.1097/00006454-198705000-00009
38. Australian Government Department of Health and Aged Care. Pertussis (whooping cough)—surveillance case definition. 2022 [cited 2023 Oct 5]. https://www.health.gov.au/resources/publications/pertussis-whooping-cough-surveillance-case-definition
39. Ridda I, Yin JK, King C, Raina MacIntyre C, McIntyre P. The importance of pertussis in older adults: a growing case for reviewing vaccination strategy in the elderly. Vaccine. 2012;30:6745–52. https://doi.org/10.1016/j.vaccine.2012.08.079
40. Bayliss J, Randhawa R, Oh KB, Kandeil W, Jenkins VA, Turriani E, et al. Perceptions of vaccine preventable diseases in Australian healthcare: focus on pertussis. Hum Vaccin Immunother. 2021;17:344–50. https://doi.org/10.1080/21645515.2020.1780848
41. Hoe Nam L, Chiu C-H, Heo JY, Ip M, Jung K-S, Menzies R, et al. The need for pertussis vaccination among older adults and high-risk groups: a perspective from advanced economies of the Asia Pacific region. Expert Rev Vaccines. 2021;20:1603–17. https://doi.org/10.1080/14760584.2021.1990759

Address for correspondence: Jing Chen, GSK Asia House, 23 Rochester Park, 139234, Singapore; email: jing.j.chen@gsk.com

Racial and Ethnic Disparities in Tuberculosis Incidence, Arkansas, USA, 2010–2021

Maheen Humayun, Leonard Mukasa, Wen Ye, Joseph H. Bates, Zhenhua Yang

We conducted an epidemiologic assessment of disease distribution by race/ethnicity to identify subpopulation-specific drivers of tuberculosis (TB). We used detailed racial/ethnic categorizations for the 932 TB cases diagnosed in Arkansas, USA, during 2010–2021. After adjusting for age and sex, racial/ethnic disparities persisted; the Native Hawaiian/Pacific Islander (NHPI) group had the highest risk for TB (risk ratio 173.6, 95% CI 140.6–214.2) compared with the non-Hispanic White group, followed by Asian, Hispanic, and non-Hispanic Black. Notable racial/ethnic disparities existed across all age groups; NHPI persons 0–14 years of age were at a particularly increased risk for TB (risk ratio 888, 95% CI 403–1,962). The risks for sputum smear–positive pulmonary TB and extrapulmonary TB were both significantly higher for racial/ethnic minority groups. Our findings suggest that TB control in Arkansas can benefit from a targeted focus on subpopulations at increased risk for TB.

Globally, tuberculosis (TB) is the 13th leading cause of death and a leading infectious killer, second to COVID-19 (*1*,*2*). In 2021, TB affected 10.6 million persons and caused 1.6 million deaths worldwide (*2*). Moreover, a quarter of the world's population is latently infected with *Mycobacterium tuberculosis*, which puts them at a 5%–10% lifetime risk of developing active disease (*2*–*4*). Global trends indicate that the World Health Organization's (WHO) End TB Strategy milestones will likely be missed because TB incidence has reduced by only 10% and TB deaths by 5.9% during 2015–2021, compared with the desired goals of 20% reduction in incidence and 35% reduction in deaths (*2*,*5*). The COVID-19 pandemic has further disrupted TB notification and treatment, reversing the progress toward global TB elimination while widening existing inequalities (*2*,*6*).

The TB epidemic is considered a major challenge in low-resource, high-burden countries; 30 high-burden countries represent 87% of the global burden (*2*). However, the epidemiology of TB in low-incidence countries is characterized by concentration of the TB burden, sometimes as high as in high-burden countries, among socially and historically marginalized populations (*7*,*8*). Before the impact of COVID-19 on TB notification, TB incidence continued to decline during 1993–2019 in the United States; however, the annual rate at which TB declined plateaued during the later years (*9*). Similarly, a recent study from Arkansas reported no significant decline in TB incidence during 2009–2020 (*10*). To move toward preelimination (1 case/100,000 population) and eventually elimination (<1 case/100,000 population), current TB interventions should be adapted to unique local challenges focusing on populations at increased risk for TB as suggested by WHO's action framework for TB elimination in low-incidence countries (*7*,*8*). This framework calls for epidemiologic assessment of disease distribution in the local population by important sociodemographic variables; however, such disaggregated analysis is typically not available in TB surveillance reports, limiting the ability of public health programs to develop pro-equity policies (*7*,*8*,*11*,*12*).

In the United States, race is a strong social determinant of health because it serves as a proxy for systemic and structural barriers to equitable opportunities for education, employment, earning, housing, and healthcare, which perpetuates racial discrimination and unjust distribution of resources that lead to adverse health outcomes (*13*,*14*). In this study from Arkansas, USA, a state with TB incidence below the national average of 2.4 cases/100,000 population, we quantify the racial/ethnic disparities in TB incidence

Author affiliations: University of Michigan, Ann Arbor, Michigan, USA (M. Humayun, W. Ye, Z. Yang); Arkansas Department of Health, Little Rock, Arkansas, USA (L. Mukasa, J.H. Bates); University of Arkansas for Medical Sciences, Little Rock, Arkansas, USA (L. Mukasa, J.H. Bates)

DOI: http://doi.org/10.3201/eid3001.230778

at the population level using detailed racial/ethnic categorizations that have not been widely used in previous TB studies in Arkansas (*15*–*17*). This study will not only help map subpopulations at an increased risk for TB in a low-burden setting but also guide the development of targeted TB interventions in light of the underlying factors that differentially drive TB incidence across racial/ethnic groups.

This study used de-identified patient data that we retrospectively retrieved from the TB surveillance database maintained by the Arkansas Health Department. The University of Michigan Health Sciences and Behavioral Sciences Institutional Review Board (IRBHSBS) determined that this study was not regulated.

Methods

Study Population

This study included all 932 TB cases diagnosed in Arkansas during 2010–2021. All of these cases met the Centers for Disease Control and Prevention (CDC)'s definition of a verified TB case. These verified cases met either laboratory or clinical case definition, including those verified by provider diagnosis as described in CDC's TB case reporting manual (*18*).

Data Collection and Data Sources

Demographic and clinical data available in this dataset were collected on verified TB cases using the standard CDC TB reporting form. We obtained US Census Bureau official population estimates for 2010–2019 from annual resident population estimates for 6 race groups (5 race-alone groups and 2 or more races) by age, sex and Hispanic origin for states and the District of Columbia from April 1, 2010–July 1, 2019; April 1, 2020; and July 1, 2020. We obtained population estimates for 2020 and 2021 from annual state resident population estimates for 6 race groups (5 race-alone groups and 2 or more races) by age, sex, and Hispanic origin from April 1, 2020–July 1, 2021 (*19*).

Data Analysis

This study had 4 objectives. The objectives were to characterize racial/ethnic disparities in TB risk; to determine if the observed racial/ethnic disparities were a result of underlying differences in sex and age distribution; to track age-specific incidence for racial/ethnic groups to draw inferences related to the underlying drivers of TB incidence; and to characterize racial/ethnic differences in advanced TB disease at diagnosis.

From the TB surveillance dataset, we created a combined variable for race and ethnicity with 5 categories so that we did not consider racial/ethnic identities in isolation (*20*). The Hispanic category included all racial subcategories. We categorized non-Hispanic persons into Asian, non-Hispanic Black, Native Hawaiian/Pacific Islander (NHPI), and non-Hispanic White categories. We did not include American Indian/Alaska Native (n = 4) and multirace (n = 1) categories in race/ethnicity-stratified results because of their small sample sizes. We categorized age as 0–14 years, 15–24 years, 25–44 years, 45–64 years, and ≥65 years. Consistent with the definition used by CDC, US-born persons included those who were eligible for US citizenship at the time of birth regardless of place of birth.

To address the first objective, we calculated the overall TB incidence for the period 2010–2021, with corresponding 95% CI for the state and the 5 racial/ethnic groups mentioned. We calculated TB incidence per 100,000 population using the population estimates from the US Census Bureau (*19*). We estimated TB incidence in the overall population and stratified by race/ethnicity and age group using Poisson regression with an offset term for the total population size. To further characterize TB-related disparities, we calculated risk ratio (RR) estimates for the race/ethnicity-combined variable, sex, and age group using Poisson regression. Because age and sex are important determinants of TB risk, we calculated race/ethnicity RRs that were adjusted for both age and sex concurrently using Poisson regression to achieve our second objective. In the absence of genotyping data, age-specific TB incidence can help draw inferences related to the underlying mechanisms that drive TB incidence. Previous studies demonstrated that TB among older adults strongly reflects reactivation of latent TB infection (LTBI) in low-burden settings, whereas TB is typically a result of recent transmission among young children (*21*,*22*). Hence, the third objective determined how racial disparities tracked across age groups by reporting RRs for race/ethnicity from age-specific Poisson models adjusted for sex. In addition, to track age disparities within each racial/ethnic group, we reported RRs for age groups from race/ethnicity-specific Poisson models while adjusting for sex.

Pulmonary TB (PTB) often starts with minimum infiltrate and progresses to additional infiltrate; sputum smear positivity has been used previously as a proxy for delayed diagnosis (*17*). The occurrence of extrapulmonary TB (EPTB) often reflects the spread of *M. tuberculosis* outside of the lungs due to the host's inability to contain the infection (*23*). We evaluated sputum smear–positive PTB and EPTB as important indicators for advanced disease. For those 2 outcomes, we calculated RRs and adjusted RRs for the race/

ethnicity-combined variable, sex, and age group using Poisson regression.

We used the non-Hispanic White category as the reference group for race/ethnicity and female as the reference category for sex because those groups were at the lowest risk for TB compared with other variable categories. For age, no one category was at the lowest risk for TB across stratified results, so we used the ≥65 years age category as the reference group to follow how TB risk progressed with age. We determined model fit using a goodness-of-fit test. We conducted statistical analysis using the SAS OnDemand for Academics (SAS Institute Inc., https://www.sas.com).

Table 1. Demographic and clinical characteristics of 932 TB patients diagnosed in Arkansas, USA, during 2010–2021*

Characteristic	No. (%)
Diagnosis confirmation	
Bacteriologically confirmed	669 (71.78)
Clinically diagnosed	263 (28.22)
TB disease site	
Pulmonary	713 (76.50)
Extrapulmonary	164 (17.60)
Both	55 (5.90)
Sputum smear result	
Positive	333 (35.73)
Negative	473 (50.75)
Not done	126 (13.52)
Race/ethnicity	
Hispanic	125 (13.41)
Asian	109 (11.70)
Non-Hispanic Black/African American	245 (26.29)
Native Hawaiian/Pacific Islander	138 (14.81)
Non-Hispanic White	310 (33.26)
American Indian or Alaska Native	4 (0.43)
Multirace	1 (0.11)
Sex	
F	336 (36.05)
M	589 (63.20)
Unknown	7 (0.75)
Age group	
0–14 y	92 (9.87)
15–24 y	85 (9.12)
25–44 y	253 (27.15)
45–64 y	282 (30.26)
≥65 y	220 (23.61)
Origin of birth	
US born	613 (65.77)
Non-US born	319 (34.23)
Year	
2010	76 (8.15)
2011	85 (9.12)
2012	71 (7.62)
2013	72 (7.73)
2014	93 (9.98)
2015	90 (9.66)
2016	91 (9.76)
2017	85 (9.12)
2018	76 (8.15)
2019	65 (6.97)
2020	59 (6.33)
2021	69 (7.40)

*Percentages may not total 100 because of rounding. TB, tuberculosis.

Results

Characteristics of Study Sample

Among the 932 TB cases in our study, 72% were bacteriologically confirmed through either nucleic acid amplification test or positive culture (Table 1). Most TB cases (76.5%) were exclusively diagnosed as PTB patients. Among all TB patients, 35.73% had a positive sputum smear result and 43.2% of the patients with PTB diagnosis (including those with both PTB and EPTB) had a positive sputum smear result. Of the total study sample, 86.6% of TB patients identified as non-Hispanic with diverse racial categorizations; 63.2% of the study patients were male. Most case-patients among Asian (91.7%), NHPI (67.4%), and Hispanic (82.4%) persons were not US born, and all of the non–US-born NHPI TB case-patients in this study were born in the Marshall Islands. For the non-Hispanic White group, only 2.3% of TB cases were non–US born, and for the non-Hispanic Black group, only 6.1% of TB cases were non–US born.

Racial/Ethnic Disparity in TB Incidence

The overall TB incidence in Arkansas was 2.6 (95% CI 2.4–2.8) cases/100,000 population during 2010–2021 (Table 2). Upon stratifying by race/ethnicity, the NHPI persons (131.6 [95% CI 111.4–155.5] cases/100,000 population) had the highest incidence of TB followed by Asian (20.0 [95% CI 16.6–24.2] cases/100,000 population), Hispanic (4.8 [95% CI 4.0–5.7] cases/100,000 population), non-Hispanic Black (4.4 [95% CI 3.9–5.0] cases/100,000 population), and non-Hispanic White persons (1.2 [95% CI 1.0–1.3] cases/100,000 population).

Racial/Ethnic Disparity after Adjusting for Sex and Age Differences

Based on the unadjusted model (Table 3), the risk for TB was many folds higher for all racial/ethnic groups when compared with the non-Hispanic White group. The risk for TB for NHPI persons was 113 (95% CI 92.1–137.7) times the risk for non-Hispanic White persons. Asian (RR 17.1, 95% CI 13.8–21.3) Hispanic (RR 4.0, 95% CI 3.3–5.0), and non-Hispanic Black (RR 3.8, 95% CI 3.2–4.5) persons all had higher risk for TB than non-Hispanic White persons. Male persons were at an 81% (RR 1.8, 95% CI 1.6–2.1) higher risk for TB than female persons. The risk for TB was 66% (RR 0.3, 95% CI 0.3–0.4) lower for the youngest group, 0–14 years of age, compared to the oldest age group. TB risk increased with age; the ≥65-year age group had the highest risk for TB.

Table 2. Average TB incidence by race/ethnicity, Arkansas, USA, 2010–2021*

Category	Incidence (95% CI)					
	All ages	0–14 y	15–24 y	25–44 y	45–64 y	≥65 y
State	2.580 (2.42–2.76)	1.29 (1.05–1.59)	1.75 (1.42–2.17)	2.76 (2.44–3.13)	3.09 (2.75–3.48)	3.79 (3.32–4.33)
Hispanic	4.75 (3.99–5.67)	1.40 (0.80–2.47)	3.64 (2.26–5.86)	6.27 (4.76–8.28)	7.51 (5.25–10.75)	16.61 (10.02–27.56)
Asian	20.02 (16.60–24.16)	1.79 (0.45–7.14)	18.52 (11.17–30.72)	25.45 (19.29–33.59)	29.85 (21.33–41.77)	19.45 (9.73–38.90)
Non-Hispanic Black	4.42 (3.90–5.01)	1.65 (1.07–2.53)	2.98 (2.04–4.35)	4.45 (3.50–5.66)	6.34 (5.11–7.88)	8.54 (6.44–11.33)
NHPI	131.62 (111.39–155.51)	139.60 (105.51–184. 71)	108.08 (68.94–169.44)	109.27 (80.45–148.40)	206.17 (139.31–305.11)	158.67 (59.55–422.75)
Non-Hispanic White	1.17 (1.04–1.31)	0.16 (0.07–0.33)	0.22 (0.10–0.46)	0.66 (0.49–0.89)	1.50 (1.24–1.81)	2.88 (2.44–3.39)

*Incidence is no. cases/100,000 population. The table provides overall and age-stratified TB incidence for the state of Arkansas and for racial/ethnic groups as calculated by Poisson regression. NHPI, Native Hawaiian/Pacific Islander; TB, tuberculosis.

After adjusting for age group and sex, racial/ethnic disparities continued to persist. NHPI persons were at the highest risk for TB compared with non-Hispanic White persons (RR 173.6, 95% CI 140.6–214.2), followed by Asian (RR 21.6, 95% CI 17.3– 27.0), Hispanic (RR 5.9, 95% CI 4.8– 7.4), and non-Hispanic Black (RR 4.6, 95% CI 3.9–5.5) persons.

Age-Related Racial/Ethnic Disparities in TB Incidence

The statewide TB incidence was highest among the ≥65-year age group (3.8 [95% CI 3.3– 4.3] cases/100,000 population) whereas the youngest group, 0–14 years, had the lowest incidence (1.3 [95% CI 1.1–1.6] cases/100,000 population). Risk for TB increased with age in Arkansas (Table 2). The 0–14-year age group had the lowest risk for TB compared with the ≥65 year age group for non-Hispanic White (RR 0.05, 95% CI 0.02– 0.11), non-Hispanic Black (RR 0.18, 95% CI 0.11–0.30), Asian (RR 0.09, 95% CI 0.02–0.42), and Hispanic (RR 0.08, 95% CI 0.04–0.18) groups, (Table 4). We observed no significant age differences for the NHPI group (p = 0.13). NHPI persons 0–14 years of age had 888 (95% CI 403–1,962) times and NHPI persons ≥65 years of age had 55 (95% CI 20–148) times the risk of TB compared to similarly aged non-Hispanic White persons (Table 5).

Racial/Ethnic Disparity in Advanced Disease at Diagnosis

The risk for sputum smear-positive PTB was highest for NHPI persons (RR 138.8, 95% CI 94.7–203.7), followed by Asian (RR 14.4, 95% CI 9.5–22.0), Hispanic (RR 5.5, 95% CI 3.8–8.0), and non-Hispanic Black (RR 4.8, 95% CI 3.7–6.3) persons when compared with non-Hispanic White persons (Table 6). The risk for EPTB was highest for NHPI persons (RR 133.3, 95% CI 83.7–212.4), followed by Asian (RR 31.4, 95% CI 21.1–46.7), Hispanic (RR 5.3, 95% CI 3.3–8.3), and non-Hispanic Black (RR 4.5, 95% CI 3.1–6.3) persons compared to non-Hispanic White persons (Table 6).

Discussion

The TB incidence in the United States and Arkansas has been <10 cases/100,000 population for several

Table 3. Disparity in tuberculosis incidence by race, sex, and age, Arkansas, USA, 2010–2021*

Covariate	Unadjusted risk ratio (95%CI)	Age- and sex-adjusted risk ratio (95%CI)
Race/ethnicity†		
Hispanic	4.07 (3.30–5.01)	5.94 (4.79–7.37)
Asian	17.14 (13.77–21.33)	21.61 (17.32–26.98)
Non-Hispanic Black	3.78 (3.20–4.48)	4.60 (3.88–5.45)
NHPI	112.64 (92.13–137.73)	173.58 (140.64–214.24)
Non-Hispanic White	Referent	Referent
Sex‡		
F	Referent	Referent
M	1.81 (1.59–2.07)	1.88 (1.64–2.15)
Age group§		
0–14 y	0.34 (0.27–0.44)	0.16 (0.12–0.20)
15–24 y	0.46 (0.36–0.59)	0.23 (0.18–0.30)
25–44 y	0.73 (0.61–0.87)	0.36 (0.30–0.43)
45–64 y	0.82 (0.68–0.97)	0.58 (0.49–0.70)
≥65 y	Referent	Referent

*RR calculated by Poisson regression. NHPI, Native Hawaiian/Pacific Islander; RR, risk ratio.
†Using unadjusted RR model 1.
‡Using unadjusted RR model 2.
§Using unadjusted RR model 3.

Table 4. Age disparities in tuberculosis incidence across racial/ethnic groups, Arkansas, USA, 2010–2021*

	Risk ratio (95% CI)				
Age group	Non-Hispanic White, no. cases = 305	Non-Hispanic Black, no. cases = 244	Asian, no. cases = 109	NHPI, no. cases = 138	Hispanic, no. cases = 124
0–14 y	0.05 (0.02–0.11)	0.18 (0.11–0.30)	0.09 (0.02–0.42)	0.87 (0.31–2.42)	0.08 (0.04–0.18)
15–24 y	0.07 (0.03–0.15)	0.33 (0.20–0.52)	0.92 (0.39–2.16)	0.68 (0.23–1.99)	0.21 (0.11–0.43)
25–44 y	0.22 (0.15–0.31)	0.50 (0.34–0.72)	1.27 (0.60–2.68)	0.68 (0.24–1.90)	0.37 (0.21–0.65)
45–64 y	0.50 (0.39–0.64)	0.72 (0.50–1.03)	1.51 (0.70–3.26)	1.29 (0.45–3.72)	0.44 (0.24–0.82)
≥65 y	Referent	Referent	Referent	Referent	Referent

*Risk ratio calculated by Poisson regression. NHPI, Native Hawaiian/Pacific Islander.

years; however, neither the state nor the country has been able to make the final push toward preelimination and elimination targets. The underlying epidemiologic factors that drive the remaining TB epidemic in low-incidence countries differ from those in high-burden settings and also across subpopulations within low-incidence settings, which suggests the need for locally informed, context-specific TB interventions (*24*).

Our study provides an in-depth epidemiologic understanding of the concentrated TB epidemic in Arkansas that is not well captured by aggregated statewide estimates. We found remarkable disparities in TB incidence around the axes of race/ethnicity, sex, and age. Of particular importance were racial/ethnic disparities, which could not be explained by age and sex differences across racial/ethnic groups. Age-specific TB incidence and differences in clinical manifestation of TB at diagnosis across racial/ethnic categories hold important lessons for understanding the drivers of TB incidence and challenges related to health equity in Arkansas.

The racial/ethnic disparities that we observed in our study are consistent with previous studies conducted in Arkansas and the United States, which consistently reported racial disparities in risk for LTBI, recent transmission, and TB disease (*13*,*15*,*16*,*25*,*26*). In 2021, a total of 88.1% of the TB cases reported in the United States were attributable to racial/ethnic minorities (*9*,*27*). Such observed racial disparities can be explained as a consequence of structural racism that perpetuates health inequities primarily through 2 interlinked pathways: residential segregation and inadequate healthcare (*14*,*28*). Persons from racial/ethnic minority groups are more likely to live in neighborhoods with high population density, limited healthcare access, poor housing conditions, and greater air pollution, which makes them more susceptible to acquiring TB infection (*14*,*28*,*29*). Moreover, those persons are more likely to experience conditions such as diabetes, HIV, and malnutrition that can contribute toward progression to TB disease (*28*,*30*). In essence, race is associated with socioeconomic status (SES), including generational wealth, income, and education, which then mediates the relationship between race and susceptibility to infection and progression to disease through psychosocial stress, nutrition, physical environment, healthcare access, and immune function (*28*,*31*).

The NHPI persons in Arkansas had a strikingly high TB incidence of 131.6 cases/100,000 population, many times higher than their annual national-level TB incidence rate that has remained <20 cases/100,000 during 2003–2021 (*9*,*32*). Most of the TB case-patients among NHPI in our study were born in the Marshall Islands, where TB incidence was 280.6 cases/100,000 population in 2020 and 343.2 cases/100,000 population in 2021 (*9*,*32*). Decades of colonial rule and testing of nuclear weapons by the US government during 1946–1958 had socioeconomic repercussions for the health infrastructure of the Marshall Islands, where the prevalence of comorbidities that substantially increase TB risk is alarmingly high (*33*). Under the Compact of Free Association, the people of the Marshall Islands can freely travel, live, and work in the United States, where they experience language, cultural, and economic barriers when accessing health-

Table 5. Racial/ethnic disparities in tuberculosis incidence across age groups, Arkansas, USA, 2010–2021*

	Risk ratio (95% CI)				
Race/ethnicity	0–14 y, no. cases = 91	15–24 y, no. cases = 85	25–44 y, no. cases = 249	45–64 y, no. cases = 277	≥65 y, no. cases = 218
Hispanic	8.93 (3.52–22.68)	16.68 (6.92–40.22)	9.37 (6.22–14.13)	4.84 (3.23–7.26)	5.57 (3.27–9.48)
Asian	11.38 (2.36–54.78)	85.02 (34.67–208.53)	38.81 (25.75–58.50)	20.72 (14.08–30.50)	7.09 (3.48–14.46)
Non-Hispanic Black	10.50 (4.46–24.69)	13.77 (6.00–31.63)	6.83 (4.64–10.06)	4.36 (3.26–5.81)	3.06 (2.21–4.25)
NHPI	888.70 (402.55–1961.98)	496.40 (208.68–1180.84)	162.91 (105.93–250.55)	138.01 (89.26–213.38)	54.82 (20.30–148.08)
Non-Hispanic White	Referent	Referent	Referent	Referent	Referent

*RR calculated by Poisson regression. The table reports RR estimates with 95% CI while adjusting for sex. NH, non-Hispanic; NHPI, Native Hawaiian/Pacific Islander; RR, risk ratio.

Table 6. Disparities in advanced TB disease at diagnosis by race/ethnicity, sex, and age, Arkansas, USA, 2010–2021*

Covariate	RR (95% CI) for sputum smear-positive PTB		RR (95% CI) for EPTB	
	Unadjusted	Age- and sex-adjusted	Unadjusted	Age- and sex-adjusted
Race/ethnicity†				
Hispanic	3.42 (2.39–4.90)	5.54 (3.84–8.00)	3.61 (2.31–5.66)	5.26 (3.32–8.34)
Asian	11.07 (7.28–16.82)	14.43 (9.46–22.02)	25.97 (17.59–38.35)	31.37 (21.09–46.66)
Non-Hispanic Black	3.80 (2.90–4.99)	4.80 (3.65–6.31)	3.68 (2.59–5.22)	4.46 (3.13–6.34)
NHPI	78.73 (54.40–113.94)	138.84 (94.65–203.67)	89.90 (57.41–140.78)	133.32 (83.68–212.41)
Non-Hispanic White	Referent	Referent	Referent	Referent
Sex‡				
M	2.27 (1.79–2.87)	2.40 (1.89–3.05)	1.43 (1.09–1.87)	1.49 (1.14–1.95)
F	Referent	Referent	Referent	Referent
Age group§				
0–14 y	NA¶	NA	0.20 (0.11–0.36)	0.10 (0.05–0.18)
15–24 y	0.42 (0.27–0.64)	0.22 (0.14–0.34)	0.37 (0.22–0.64)	0.20 (0.11–0.35)
25–44 y	0.73 (0.54–0.99)	0.37 (0.27–0.51)	0.93 (0.66–1.31)	0.48 (0.33–0.69)
45–64 y	1.04 (0.78–1.38)	0.75 (0.56–1.00)	0.66 (0.45–0.96)	0.48 (0.33–0.71)
≥65 y	Referent	Referent	Referent	Referent

*Estimates used Poisson regression, EPTB includes cases concurrently diagnosed with PTB. EPTB, extrapulmonary tuberculosis; NA, not available; NHPI, Native Hawaiian/Pacific Islander; PTB, pulmonary tuberculosis; RR, risk ratio; TB, tuberculosis.
†Using unadjusted RR model 1.
‡Using unadjusted RR model 2.
§Using unadjusted RR model 3.
¶Not available due to small sample size.

care that can lead to infection, delayed diagnosis, and prolonged infectiousness with implications for community transmission (*34*,*35*). Despite the high incidence of TB in the Marshall Islands, persons from that country are not required to undergo screening for LTBI or active disease upon arrival to the United States (*36*). Screening those persons for TB may help in early diagnosis and treatment, thereby reducing the burden of TB in Arkansas and among NHPI persons.

TB is driven by various mechanisms, mainly by reactivation of LTBI or primary disease by a recent transmission, each of which requires specialized mitigation strategies (*37*). TB incidence was 139.6 cases/100,000 population among 0–14-year-old NHPI children in our study; incidence was<2 cases/100,000 population among all other racial/ethnic groups of similar age. The risk among 0–14-year-old NHPI children was 888 times the risk among non-Hispanic White children of similar age. Because progression from infection to disease is rapid, TB among young children is a good marker for ongoing community transmission (*38*,*39*). Given the high risk for sputum smear positive PTB and elevated TB risk among 0–14-year-olds, TB transmission appears to play a role in driving TB incidence among NHPI persons. Hence, to curtail the disproportionate TB burden for NHPI persons, mitigation strategies should focus on active case finding in addition to LTBI screening of adults to disrupt chains of transmission (*36*). Curtailing the TB epidemic will also require ramping up contact tracing based on contact disclosure from TB patients, who often hesitate to name contacts because of stigma around TB in their communities (*40*). Community-level advocacy and awareness using culturally appropriate tools can improve contact disclosure and equip the local community with the necessary information on TB diagnosis, treatment, and transmission (*40*).

For Hispanic, non-Hispanic White, and non-Hispanic Black persons, the risk for TB was highest among the oldest age group, indicating that TB is likely driven by reactivation of LTBI in those subpopulations (*41*). Two previous studies conducted in Arkansas using genotyping data from 1997–2010 demonstrated that TB incidence among ≥65-year-olds was largely driven by nonclustered TB incidence, which is indicative of reactivation of LTBI (*15*,*16*). In addition, foreign-born non-Hispanic White, non-Hispanic Black, Asian, and Hispanic persons had significantly higher risks for TB than did US-born persons (Appendix Table). The high risk among foreign-born persons likely indicates reactivation, as suggested by a previous national-level study based on genotyping data (*42*). Racial/ethnic groups with a high proportion of foreign-born TB cases can particularly benefit from TB control efforts focused on preventing reactivation of LTBI.

Sputum smear–positive PTB is highly infectious because its high bacillary load leads to an elevated risk for transmission (*43*,*44*). In addition, the increased risk of smear-positive PTB at first diagnosis in persons from racial/ethnic minority groups likely points toward differential access to timely and adequate TB care, previously supported by a study from Arkansas, and such difference can result in severe disease with poor health outcomes (*17*,*44*). Another study from Arkansas found that TB patients from rural Arkansas faced delays in receiving the correct diagnosis and were treated for other conditions for several months

(*40*). Our findings suggest the need to explore the barriers related to TB care that affect various subpopulations in Arkansas. Increasing awareness of TB among healthcare workers, especially in a time when TB incidence is low in the country can help equip them with the knowledge needed to make timely and accurate TB diagnosis (*40*).

The increased risk for EPTB, including concurrent PTB, among persons from racial/ethnic minority groups is indicative of elevated risk for advanced disease that is a diagnostic and a therapeutic challenge due to the dissemination of the disease (*45*). An increased prevalence of comorbidities such as HIV might predispose racial/ethnic minority groups to EPTB, suggesting the need for improved management of risk factors that compromise host immunity (*46*). The Arkansas Office of Minority Health and Health Disparities reported that among non-Hispanic Black persons, the mortality rate for HIV was 6 times higher and for diabetes was 2 times higher than the rates among non-Hispanic White persons during 2011–2015 (*47*). TB preventive strategies should go beyond curtailing transmission and focus on improved comanagement of noncommunicable conditions, which are often modifiable risk factors, by collaborating across health programs to provide more holistic patient-centered care (*48*).

This study relies on surveillance data that provides access to limited study variables. We used markers of advanced TB disease to make inferences related to access to timely and adequate care in Arkansas. To clarify the factors that limit access to timely care, future studies should collect qualitative data crucial for determining delays in healthcare and assessing if these delays are patient- or provider-related to bridge health inequities related to TB care. Distinguishing between ongoing community transmission and reactivation of remotely acquired TB infection is crucial when designing TB interventions, but lack of genotyping data in this study prevented reliable evaluation of the relative contribution of each of these 2 mechanisms across racial/ethnic groups (*49*). Despite those limitations, this study provides incidence and RR estimates stratified by detailed racial/ethnic categories that had not been previously reported at the population level for Arkansas using the most recent surveillance data (*11*,*15*–*17*).

The state-level estimates of TB incidence in Arkansas are misleading because the progress toward TB elimination is unequally felt across racial/ethnic subpopulations. Our findings demonstrate that drivers of TB incidence vary across subpopulations, which necessitates designing context-specific TB interventions. Although our results may not be generalizable to other low-incidence settings, the racial/ethnic disparities we observed demonstrate the need for detailed disaggregated analysis of TB surveillance data by race/ethnicity while providing a framework for such an analysis in other US states.

Acknowledgments

We thank colleagues in the Tuberculosis Control Program at the Arkansas Health Department for their assistance in the collection of the TB surveillance data used in this study.

The deidentified TB surveillance data used for this study can be shared with other research teams after the review and approval of their research proposal by the Arkansas Department of Health's Scientific Advisory Committee. The aggregated data and code generated in this study are available upon request to Zhenhua Yang, zhenhua@umich.edu.

Author contributions: M.H. contributed to the study design, data analysis, interpretation of results, and drafting of the manuscript. L.M. contributed to the data collection. W.Y. contributed to the data analysis and development of the manuscript. J.B. contributed to the development of the manuscript and interpretation of the results. Z.Y. contributed to the study design and directed the conduction of the study and the development of the manuscript. All the authors contributed to the revision of the manuscript and approved the final manuscript.

About the Author

Ms. Humayun is an PhD candidate in epidemiological science at the University of Michigan, Ann Arbor, Michigan. She received her MPH in epidemiology from University of Maryland as a Fulbright Scholar. Her research interests lie in infectious disease epidemiology, especially global tuberculosis disparities, and TB-HIV coinfection.

References

1. World Health Organization. WHO reveals leading causes of death and disability worldwide: 2000–2019. Geneva: The Organization; 2020.
2. World Health Organization. Global tuberculosis report. TB incidence. 2022 [cited 2023 Nov 28]. https://www.who.int/teams/global-tuberculosis-programme/tb-reports/global-tuberculosis-report-2022/tb-disease-burden/2-1-tb-incidence.
3. Centers for Disease Control and Prevention. Core curriculum on tuberculosis: what the clinician should know. 7th edition. 2021 [cited 2023 Nov 28]. https://www.cdc.gov/tb/education/corecurr/pdf/CoreCurriculumTB-508.pdf.
4. Houben RMGJ, Dodd PJ. The global burden of latent tuberculosis infection: a re-estimation using mathematical

modelling. PLoS Med. 2016;13:e1002152. https://doi.org/10.1371/journal.pmed.1002152
5. World Health Organization. The End TB strategy. Geneva: The Organization; 2015 [cited 2023 Nov 28]. https://cdn.who.int/media/docs/default-source/documents/tuberculosis/end-tb-brochure22cf78c9-ddf7-47df-9261-b999e8df83ba.pdf
6. Next steps in eliminating tuberculosis in the Americas. Lancet Reg Heal—Americas 2023;21:100512.
7. World Health Organization. Towards TB elimination: an action framework for low-incidence countries. 2014 [cited 2023 Nov 28]. http://apps.who.int/iris/bitstream/handle/10665/132231/9789241507707_eng.pdf
8. Lönnroth K, Migliori GB, Abubakar I, D'Ambrosio L, de Vries G, Diel R, et al. Towards tuberculosis elimination: an action framework for low-incidence countries. Eur Respir J. 2015;45:928–52. https://doi.org/10.1183/09031936.00214014
9. Filardo TD, Feng P-J, Pratt RH, Price SF, Self JL. Tuberculosis—United States, 2021. MMWR Morb Mortal Wkly Rep. 2022;71:441–6. https://doi.org/10.15585/mmwr.mm7112a1
10. Renardy ME, Gillen C, Yang Z, Mukasa L, Bates J, Butler R, et al. Disease phenotypic and geospatial features vary across genetic lineages for tuberculosis within Arkansas, 2010–2020. PLOS Glob Public Health. 2023;3:e0001580. https://doi.org/10.1371/journal.pgph.0001580
11. Arkansas Department of Health Tuberculosis Control Program. Tuberculosis morbidity annual statistical report 2016. 2016 [cited 2023 Dec 5]. https://www.healthy.arkansas.gov/images/uploads/pdf/2016_Tuberculosis_Statistical_Report_Final.pdf
12. Heuvelings CC, de Vries SG, Grobusch MP. Tackling TB in low-incidence countries: improving diagnosis and management in vulnerable populations. Int J Infect Dis. 2017;56:77–80. https://doi.org/10.1016/j.ijid.2016.12.025
13. Noppert GA, Wilson ML, Clarke P, Ye W, Davidson P, Yang Z. Race and nativity are major determinants of tuberculosis in the U.S.: evidence of health disparities in tuberculosis incidence in Michigan, 2004–2012. BMC Public Health. 2017;17:538. https://doi.org/10.1186/s12889-017-4461-y
14. Bailey ZD, Krieger N, Agénor M, Graves J, Linos N, Bassett MT. Structural racism and health inequities in the USA: evidence and interventions. Lancet. 2017;389:1453–63. https://doi.org/10.1016/S0140-6736(17)30569-X
15. Berzkalns A, Bates J, Ye W, Mukasa L, France AM, Patil N, et al. The road to tuberculosis (*Mycobacterium tuberculosis*) elimination in Arkansas; a re-examination of risk groups. PLoS One. 2014;9:e90664. https://doi.org/10.1371/journal.pone.0090664
16. France AM, Cave MD, Bates JH, Foxman B, Chu T, Yang Z. What's driving the decline in tuberculosis in Arkansas? A molecular epidemiologic analysis of tuberculosis trends in a rural, low-incidence population, 1997–2003. Am J Epidemiol. 2007;166:662–71. https://doi.org/10.1093/aje/kwm135
17. Yang ZH, Gorden T, Liu DP, Mukasa L, Patil N, Bates JH. Increasing likelihood of advanced pulmonary tuberculosis at initial diagnosis in a low-incidence US state. Int J Tuberc Lung Dis. 2018;22:628–36. https://doi.org/10.5588/ijtld.17.0413
18. Centers for Disease Control and Prevention. Report of verified case of tuberculosis, instructional manual. 2020. [cited 2021 Jan 8]. https://www.cdc.gov/tb/programs/rvct/InstructionManual.pdf
19. US Census Bureau. State population totals and components of change: 2020–2022. 2022 [cited 2022 Feb 12]. https://www.census.gov/data/tables/time-series/demo/popest/2020s-state-total.html
20. Flanagin A, Frey T, Christiansen SL, Bauchner H. The reporting of race and ethnicity in medical and science journals. JAMA. 2021;325:1049–52. https://doi.org/10.1001/jama.2021.2104
21. Wu IL, Chitnis AS, Jaganath D. A narrative review of tuberculosis in the United States among persons aged 65 years and older. J Clin Tuberc Other Mycobact Dis. 2022;28:100321. https://doi.org/10.1016/j.jctube.2022.100321
22. Shingadia D, Novelli V. Diagnosis and treatment of tuberculosis in children. Lancet Infect Dis. 2003;3:624–32. https://doi.org/10.1016/S1473-3099(03)00771-0
23. Baykan AH, Sayiner HS, Aydin E, Koc M, Inan I, Erturk SM. Extrapulmonary tuberculosıs: an old but resurgent problem. Insights Imaging. 2022;13:39. https://doi.org/10.1186/s13244-022-01172-0
24. Houben RMGJ, Menzies NA, Sumner T, Huynh GH, Arinaminpathy N, Goldhaber-Fiebert JD, et al. Feasibility of achieving the 2025 WHO global tuberculosis targets in South Africa, China, and India: a combined analysis of 11 mathematical models. Lancet Glob Health. 2016;4:e806–15. https://doi.org/10.1016/S2214-109X(16)30199-1
25. Kim S, Cohen T, Horsburgh CR Jr, Miller JW, Hill AN, Marks SM, et al. Trends, mechanisms, and racial/ethnic differences of tuberculosis incidence in the US-born population aged 50 years or older in the United States. Clin Infect Dis. 2022;74:1594–603. https://doi.org/10.1093/cid/ciab668
26. Khan A, Marks S, Katz D, Morris SB, Lambert L, Magee E, et al. Changes in tuberculosis disparities at a time of decreasing tuberculosis incidence in the United States, 1994–2016. Am J Public Health. 2018;108(S4):S321–6. 10.2105/AJPH.2018.304606 https://doi.org/10.2105/AJPH.2018.304606
27. US Centers for Disease Control and Prevention. Health disparities in TB. 2022 [cited 2023 Nov 28]. https://www.cdc.gov/tb/topic/populations/healthdisparities/default.htm
28. Noppert GA, Malosh RE, Moran EB, Ahuja SD, Zelner J. Contemporary social disparities in TB infection and disease in the USA: a review. Curr Epidemiol Rep. 2018;5:442–9. https://doi.org/10.1007/s40471-018-0171-y
29. Mathema B, Andrews JR, Cohen T, Borgdorff MW, Behr M, Glynn JR, et al. Drivers of tuberculosis transmission. J Infect Dis. 2017;216(suppl_6):S644–53. https://doi.org/10.1093/infdis/jix354
30. Lönnroth K, Jaramillo E, Williams BG, Dye C, Raviglione M. Drivers of tuberculosis epidemics: the role of risk factors and social determinants. Soc Sci Med. 2009;68:2240–6. https://doi.org/10.1016/j.socscimed.2009.03.041
31. Noppert GA, Clarke P, Hicken MT, Wilson ML. Understanding the intersection of race and place: the case of tuberculosis in Michigan. BMC Public Health. 2019;19:1669. https://doi.org/10.1186/s12889-019-8036-y
32. US Centers for Disease Control and Prevention. Reported tuberculosis in the United States, 2021. 2022 [cited 2023 Nov 28]. https://www.cdc.gov/tb/statistics/reports/2021/table2.htm
33. Ritz S. Cash DH. Republic of the Marshall Islands hybrid survey: final report. 2018 [cited 2023 Dec 5]. https://cdn.who.int/media/docs/default-source/ncds/ncd-surveillance/data-reporting/marshall-islands/rmi-report-12_july_2018.pdf
34. Riklon S, Alik W, Hixon A, Palafox NA. The "compact impact" in Hawaii: focus on health care. Hawaii Med J. 2010;69(Suppl 3):7–12.
35. McElfish PA, Post J, Rowland B. A social ecological and community-engaged perspective for addressing health disparities among Marshallese in Arkansas. Int J

Nurs Clin Pract. 2016;3. https://doi.org/10.15344/2394-4978/2016/191
36. Rothfeldt LL, Patil N, Haselow DT, Williams SH, Wheeler JG, Mukasa LN. Notes from the field: cluster of tuberculosis cases among Marshallese persons residing in Arkansas—2014–2015. MMWR Morb Mortal Wkly Rep. 2016;65:882–3. https://doi.org/10.15585/mmwr.mm6533a7
37. Pareek M, Greenaway C, Noori T, Munoz J, Zenner D. The impact of migration on tuberculosis epidemiology and control in high-income countries: a review. BMC Med. 2016;14:48. https://doi.org/10.1186/s12916-016-0595-5
38. Swaminathan S, Rekha B. Pediatric tuberculosis: global overview and challenges. Clin Infect Dis. 2010;50(Suppl 3):S184–94. https://doi.org/10.1086/651490
39. Ki HP, Shingadia D. Tuberculosis in children. Paediatrics Child Health (United Kingdom). 2017;27:109–15. https://doi.org/10.1016/j.paed.2016.12.004
40. Labuda SM, McDaniel CJ, Talwar A, Braumuller A, Parker S, McGaha S, et al. Tuberculosis outbreak associated with delayed diagnosis and long infectious periods in rural Arkansas, 2010–2018. Public Health Rep. 2022;137:94–101. https://doi.org/10.1177/0033354921999167
41. Caraux-Paz P, Diamantis S, de Wazières B, Gallien S. Tuberculosis in the elderly. J Clin Med. 2021;10:5888. https://doi.org/10.3390/jcm10245888
42. Yuen CM, Kammerer JS, Marks K, Navin TR, France AM. Recent transmission of tuberculosis—United States, 2011–2014. PLoS One. 2016;11:e0153728. https://doi.org/10.1371/journal.pone.0153728
43. Migliori GB, Nardell E, Yedilbayev A, D'Ambrosio L, Centis R, Tadolini M, et al. Reducing tuberculosis transmission: a consensus document from the World Health Organization Regional Office for Europe. Eur Respir J. 2019;53:1900391. https://doi.org/10.1183/13993003.00391-2019
44. Tedla K, Medhin G, Berhe G, Mulugeta A, Berhe N. Delay in treatment initiation and its association with clinical severity and infectiousness among new adult pulmonary tuberculosis patients in Tigray, northern Ethiopia. BMC Infect Dis. 2020;20:456. https://doi.org/10.1186/s12879-020-05191-4
45. Mbuh TP, Ane-Anyangwe I, Adeline W, Thumamo Pokam BD, Meriki HD, Mbacham WF. Bacteriologically confirmed extrapulmonary tuberculosis and treatment outcome of patients consulted and treated under program conditions in the littoral region of Cameroon. BMC Pulm Med. 2019;19:17. https://doi.org/10.1186/s12890-018-0770-x
46. Yang Z, Kong Y, Wilson F, Foxman B, Fowler AH, Marrs CF, et al. Identification of risk factors for extrapulmonary tuberculosis. Clin Infect Dis. 2004;38:199–205. https://doi.org/10.1086/380644
47. Office of Minority Health and Health Disparities and Epidemiological Branch. Disparities in diabetes mellitus mortality among Blacks in Arkansas. 2018 [cited 2023 Dec 5]. https://www.healthy.arkansas.gov/images/uploads/pdf/2018_Diabetes_Mortality_Disparity_Fact_Sheet.pdf
48. World Health Organization. Framework for collaborative action on tuberculosis and comorbidities. Geneva: The Organization; 2022.
49. Raz KM, Talarico S, Althomsons SP, Kammerer JS, Cowan LS, Haddad MB, et al. Molecular surveillance for large outbreaks of tuberculosis in the United States, 2014–2018. Tuberculosis (Edinb). 2022;136:102232. https://doi.org/10.1016/j.tube.2022.102232

Address for correspondence: Zhenhua Yang, Epidemiology Department, School of Public Health, University of Michigan, 1415 Washington Heights, Ann Arbor, MI 48105, USA; email: zhenhua@umich.edu

Reemergence of Human African Trypanosomiasis Caused by *Trypanosoma brucei rhodesiense*, Ethiopia

Adugna Abera, Tihitina Mamecha, Ebise Abose, Belachew Bokicho, Agune Ashole, Tesfahun Bishaw, Abinet Mariyo, Buzayehu Bogale, Haileyesus Terefe, Henok Tadesse, Mahlet Belachew, Hailemariam Difabachew, Araya Eukubay, Solomon Kinde, Abraham Ali, Feyesa Regasa, Fikre Seife, Zeyede Kebede, Mesfin Wossen, Getachew Tollera, Mesay Hailu, Nigus Manaye, Nick Van Reet, Gerardo Priotto, Johan van Griensven, Myrthe Pareyn, Geremew Tasew

We report 4 cases of human African trypanosomiasis that occurred in Ethiopia in 2022, thirty years after the last previously reported case in the country. Two of 4 patients died before medicine became available. We identified the infecting parasite as *Trypanosoma brucei rhodesiense*. Those cases imply human African trypanosomiasis has reemerged.

Human African trypanosomiasis (HAT), also known as African sleeping sickness, is caused by different subspecies of the blood parasite *Trypanosoma brucei*. *T. brucei rhodesiense* mainly affects livestock and wildlife but sporadically spills over into humans, causing an acute disease that progresses quickly. Without prompt appropriate treatment, patient prognosis is poor; case-fatality rate is almost 100%. Tsetse flies (*Glossina* spp.) transmit the parasites (*1*). HAT was first reported in Ethiopia in 1967 in the Gambella region (*2*). Sporadic cases were reported in that area until 1991 (*3*).

In 2022, four cases of HAT were reported from the Kucha Alfa district, Gamo zone, South Nations Nationalities Peoples' Region (SNNPR), Ethiopia. Because >3 decades had passed since the last reported case in Ethiopia, no surveillance or reporting systems existed. HAT is also not included in the national tropical diseases disease roadmap list (*4*). Necessary resources for case management were lacking at the time of the outbreak. We developed a case-series report using data from patients' hospital records to describe activities and processes used to respond to the recent cases. Each case patient provided informed written consent or assent from parents if patient was <18 years of age.

The Study

All 4 case-patients with diagnosed HAT experienced fever, headache, insomnia, and a reduced level of consciousness; all were from near the Omo River area in the Kucha Alfa district of Gamo Zone, SNNPR (Figure). We initially sought to rule out malaria by microscopy of blood film at Selamber Primary Hospital (Selamber, Ethiopia). For each case-patient, we performed a complete blood count

Authors affiliations: Ethiopia Public Health Institute, Bacterial, Parasitic, and Zoonotic Research Directorate, Addis Ababa, Ethiopia (A. Abera, M. Belachew, H. Difabachew, A. Eukubay, S. Kinde, A. Ali, G. Tasew); Selamber Primary Hospital, Kucha Alfa District, Selamber, Ethiopia (T. Mamecha, A. Mariyo, B. Bogale); Public Health Emergency Management, Ethiopia Public Health Institute, Addis Ababa (E. Abose, H. Tadesse, F. Regasa, M. Wossen); South Nations Nationalities People's Region Health Bureau, Hawassa, Ethiopia (B. Bokicho, A. Ashole, H. Terefe); Federal Ministry of Health Ethiopia, Addis Ababa (T. Bishaw, F. Seife); World Health Organization Country Office, Addis Ababa (Z. Kebede, N. Manaye); Ethiopia Public Health Institute, Addis Ababa (G. Tollera, M. Hailu); World Health Organization Center for Research and Training on Human African Trypanosomiasis Diagnostics, Antwerp, Belgium, and Trypanosoma Unit, Institute of Tropical Medicine, Antwerp, Belgium (N. Van Reet); World Health Organization, Geneva, Switzerland (G. Priotto); Unit of Neglected Tropical Diseases, Institute of Tropical Medicine, Antwerp (J. van Griensven, M. Pareyn)

DOI: https://doi.org/10.3201/eid3001.231319

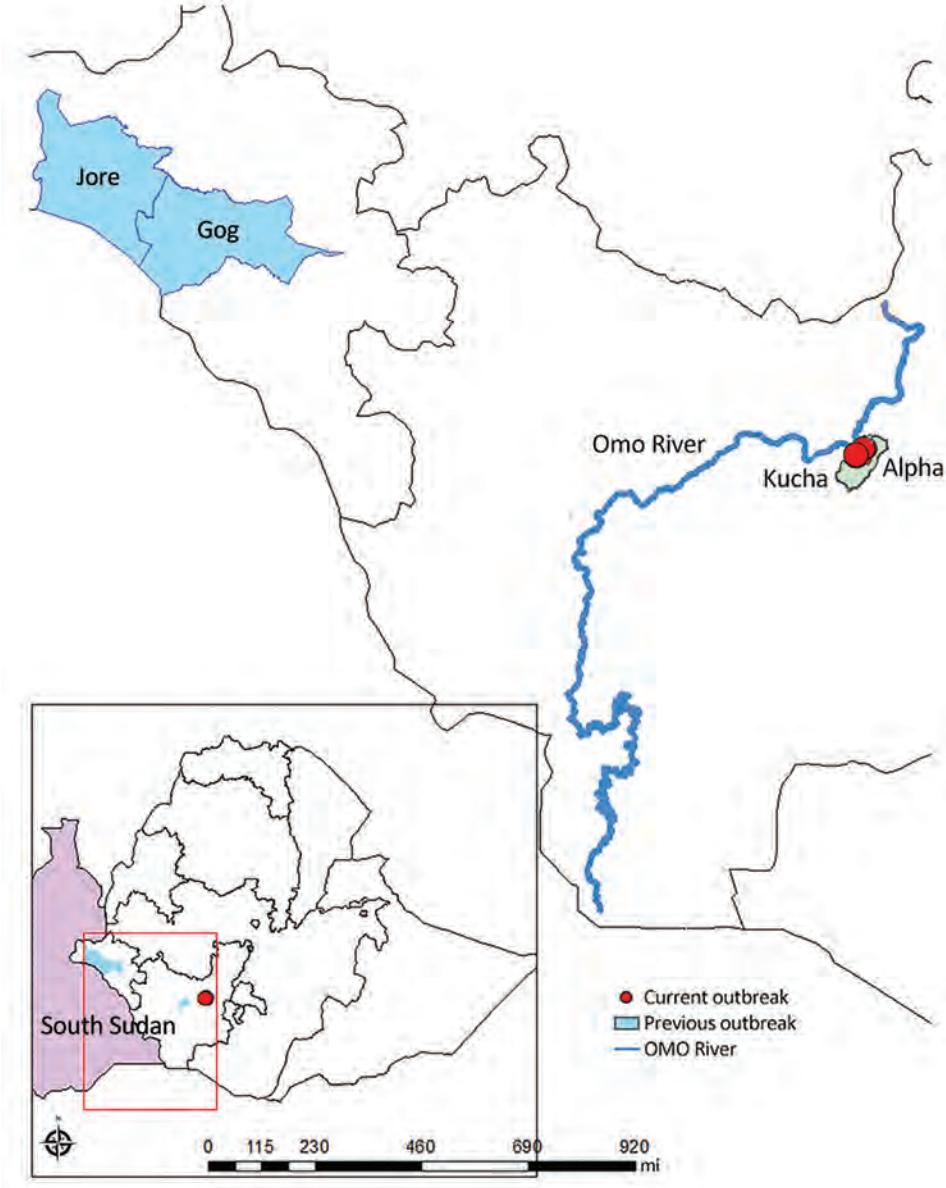

Figure. Locations of past and present human African trypanosomiasis outbreaks in Ethiopia. Areas in light blue indicate location of 1969–1970 outbreak and last case report in the Goge and Jore Districts in the Gambella region. Red dot indicates location of 2022 outbreak in Kucha Alfa District, Gamo Zone, South Nations Nationalities Peoples' Region. Inset shows location of primary map area.

and blood chemistry analysis (Table 1). Dried blood spot samples retrieved from 1 case-patient in October 2022 were sent to the Institute of Tropical Medicine in Antwerp, Belgium, where the parasite was confirmed by molecular analysis as *T. brucei rhodesiense*.

We reported the cases to the Ethiopia Public Health Institute after the second case. A working group from the Ethiopia Ministry of Health and World Health Organization Ethiopia country office was immediately established to make resources available for case management and case reporting.

Fever, headaches, and joint and muscle discomfort were the most frequently expressed clinical signs and symptoms among the 4 confirmed case-patients. All manifested acute malnutrition, loss of consciousness, and insomnia. The first 2 case-patients died because appropriate treatment was unavailable in Ethiopia at that time. By the time the third case-patient sought treatment, HAT had progressed to stage 2; after performing cerebrospinal fluid analysis, we treated the patient with melarsoprol. Unfortunately, the patient developed a drug-induced encephalopathic syndrome with high-grade fever and generalized seizures and subsequently died. The fourth patient was successfully treated (Table 2).

Responses to the outbreak, provided with World Health Organization support, included making laboratory supplies, medicines, technical guidelines,

Table 1. Laboratory data and clinical information for 4 human African trypanosomiasis case-patients, Selamber Primary Hospital, Kucha Alfa District, South Nations Nationalities Peoples' Region, Ethiopia, 2022*

Laboratory data	Case 1	Case 2	Case 3	Case 4
Leukocytes, $\times 10^9$ cells/L	4.7	5	7.5	4
Hemoglobin, g/dL	6.6	8	7.3	10
MCV, fL	88	91.3	96	89
Platelets, $\times 10^3/\mu L$	120	110	143	90
SGOT, U/L	5	3.6	83.7	21.3
SGPT, U/L	0.5	4.4	26.3	37
ALP, U/L	18.5	65	70	200
Giemsa-stained blood film	*T. brucei* spp. positive	*T. brucei* spp. positive	*T. brucei* spp. positive	*T. brucei* spp. positive
Test blood film for malaria	Yes	Yes	Yes	Yes
PCR test done	No	No	Yes	No

*ALP, alkaline phosphatase; MCV, mean corpuscular volume; SGOT, serum glutamic-oxaloacetic transaminase; SGPT, serum glutamic-pyruvic transaminase.

healthcare staff training, and job aids (e.g., fact sheets, checklists, manuals) available for clinically suspected HAT, and establishment of a surveillance system. When the outbreak began, no national guidelines, training materials, or protocols for HAT existed, meaning few disease prevention and control measures were available.

The Kucha Alfa district is surrounded by the Omo River, where tsetse flies are abundant and cattle come to drink water. Furthermore, the district is close to the Maze National Park, which is home to much wildlife and livestock. The proximity of tsetse fly habitat, animal reservoirs, and humans increases the likelihood of interaction between humans and infected wildlife and consequently the risk for infectious spillover, including from *T. brucei rhodesiense*. The areas in which the recent cases originated are rural and hard to reach, and residents have little access to medical facilities. Local persons usually first visit primary healthcare facilities in their village, then a district health center, and only after unsuccessful diagnosis or treatment do they seek care at Selamber Primary Hospital. That multistep progression substantially delays diagnosis and reduces chances for a good prognosis. Furthermore, the absence of laboratory supplies, gaps in health professionals' knowledge and expertise related to HAT, and lack of resources for active surveillance and case management further hamper timely diagnosis and treatment initiation.

According to 1 study (*5*), animal trypanosomiasis in Ethiopia poses a serious threat to livestock and agricultural productivity. SNNPR states comprise ≈75% of the area in Ethiopia conducive to tsetse fly habitat. Most risk factors enabling the transmission of HAT are present in the Kucha Alfa district. Many locations in the Gamo and Gofa zones in SNNPR, including savannah-covered national parks, river basins, and bushy land areas, together with favorable average temperatures, support tsetse fly reproduction (*6*).

Conclusions

HAT has reemerged in Ethiopia in a different geographic region from where previous cases were reported 30 years earlier. Four confirmed case-patients were recently admitted to Selamber Hospital, providing evidence of ongoing transmission of the disease. Left untreated, HAT is almost always fatal, and the prognosis is generally poor even with treatment. Resources that can be established quickly and mobilized for surveillance, detection, reporting, diagnosis, and treatment of new cases are urgently needed. It is imperative to raise awareness of HAT by including it in the list of national tropical diseases in Ethiopia. Collaborative partnerships, including with One Health programs, are critical for designing control strategies, and additional areas that might be vulnerable to HAT should be mapped using the worldwide HAT atlas (*7*).

Table 2. Sociodemographic and treatment information for 4 human African trypanosomiasis case-patients, Selamber Primary Hospital, Kucha Alfa District, South Nations Nationalities Peoples' Region, Ethiopia, 2022*

Descriptions	Case 1	Case 2	Case 3	Case 4
Age	18 mo	11 y	20 y	7 y
Sex	F	M	M	M
Date of onset	2022 Mar 20	2022 Apr 5	2022 Jul 13	2022 Sep 11
Date of diagnosis	2022 Apr 15	2022 May 28	2022 Oct 20	2022 Oct 29
CSF findings	Motile *T. brucei* spp. positive	Motile *T. brucei* spp. positive	Motile *T. brucei* spp. positive	Motile *T. brucei* spp. positive
Treatment	None	None	Melarsoprol (2.2 mg/kg/d)	Melarsoprol (2.2 mg/kg/d)
Final outcome	Died	Died	Died	Cured

*CSF, cerebrospinal fluid

Acknowledgments

We thank members of outbreak investigation and control agencies in all regional, zonal, districts, and communities and the World Health Organization Ethiopia country office for providing medications for the patients.

J.vG. and G.T. received funding from the Directorate-General Development Cooperation and Humanitarian Aid under the Framework Agreement 5 collaboration between the Institute of Tropical Medicine (Antwerp, Belgium) and Ethiopia Public Health Institute (Addis Ababa, Ethiopia).

Conception and study design: Ad.A. and G.T.; experimental laboratory work: B.B., M.B., H.D., and Nv.R.; revision and finalization: G.P., J.vG., and M.P. All authors read and approved the final manuscript.

About the Author

Mr. Abera has been a researcher at the Ethiopian Public Health Institute since 2016. He focuses on molecular epidemiology, drug resistance, diagnostics, and metagenomics research applied to malaria, NTDs, and arboviral diseases in Ethiopia.

References

1. Simarro PP, Diarra A, Ruiz Postigo JA, Franco JR, Jannin JG. The human African trypanosomiasis control and surveillance programme of the World Health Organization 2000–2009: the way forward. PLoS Negl Trop Dis. 2011;5:e1007. https://doi.org/10.1371/journal.pntd.0001007
2. Baker JR, McConnell E. Human trypanosomiasis in Ethiopia. Trans R Soc Trop Med Hyg. 1969;63:114. https://doi.org/10.1016/0035-9203(69)90075-3
3. Endeshaw T, Kebede A, Haddis M, Tilahun T, Asfaw T. The human trypanosomiasis situation in Gambella, southwestern Ethiopia. Ethiopian Journal of Health Development. 1997;11:23–8.
4. Ministry of Health of Ethiopia. The third national neglected tropical diseases strategic plan 2021–2025. Addis Ababa: Ministry of Health of Ethiopia; 2021.
5. Aki A, Dinede G. Trypanosomiasis in cattle population of Pawe district of Benishangul Gumuz regional state, western Ethiopia: anemia, vector density and associated risks. Researcher. 2016;8:60–6.
6. Zekarias T, Kapitano B, Mekonnen S, Zeleke G. The dynamics of tsetse fly in and around intensive suppression area of southern tsetse eradication project site, Ethiopia. Ethiopian J Agri Sci. 2014;24:59–67.
7. Simarro PP, Cecchi G, Paone M, Franco JR, Diarra A, Ruiz JA, et al. The atlas of human African trypanosomiasis: a contribution to global mapping of neglected tropical diseases. Int J Health Geogr. 2010;9:57. https://doi.org/10.1186/1476-072X-9-57

Address for correspondence: Adugna Abera, Malaria and Neglected Tropical Diseases Research Team, Ethiopia Public Health Institute, Arbagnoch Street, PO Box 1242, Addis Ababa, Ethiopia; email: adugnabe@yahoo.com

Helicobacter fennelliae Localization to Diffuse Areas of Human Intestine, Japan

Takashi Sakoh, Emiko Miyajima, Yusuke Endo, Kei Kono, Junichiro Sato, Mizuki Haraguchi, Sho Ogura, Masayo Morishima, Keiko Ishida, Yorinari Ochiai, Shu Hoteya, Yutaka Takazawa, Masaru Baba, Hideki Araoka

The site of enterohepatic *Helicobacter* colonization/infection in humans is still unknown. We report microbiologically and histopathologically confirmed *H. fennelliae* localization in the large intestine in an immunocompromised patient in Japan. This case contributes to better understanding of the life cycle of enterohepatic *Helicobacter* species.

Helicobacter species are classified into enterohepatic and gastric species. Human infections with enterohepatic species have been reported mainly as bloodstream infections caused by *H. cinaedi* and *H. fennelliae* in the immunocompromised patients (*1*–*3*). Intestinal localization and bacterial translocation have been suggested as the origin of those infections (*4*,*5*) because the same pathogen is detected in the stool of patients with *Helicobacter* bacteremia (*3*,*6*). However, evidence is limited regarding where enterohepatic *Helicobacter* is present in the gastrointestinal tract. We describe a confirmed human case of localization of *H. fennelliae* in crypts of the mucosal epithelium of the large intestine in a patient with recurrent *H. fennelliae* bacteremia.

The Case Study

A 62-year-old man sought treatment at Toranomon Hospital, Tokyo, Japan, for recurrence of *H. fennelliae* bacteremia, causing cellulitis of the left lower leg. He had received 3 weeks of intravenous ampicillin therapy, followed by oral doxycycline therapy, for the first episode *H. fennelliae* bacteremia, which initially resulted in a confirmed negative blood culture. However, blood culture became positive again under oral doxycycline therapy. *H. fennelliae* could be detected in stool culture before ampicillin administration, which raised suspicion of entry via the intestinal tract. However, the most recent colonoscopy (first colonoscopy) was performed before the first episode of bacteremia 5.5 weeks earlier, which showed no abnormal findings other than two 3-mm erosions in the cecum (biopsies revealed no abnormal tissue) and some small-sized adenomatous lesions in the colon (Figure 1, panels A–C). A fourth-generation HIV antigen/antibody combination assay was negative.

The blood tests we conducted at the time of recurrence showed hypogammaglobulinemia (IgG 625 mg/dL, IgA 38.6 mg/dL, IgM 1.0 mg/dL), leading us to suspect impaired intestinal immunity, which prompted a repeat colonoscopy. Gastroenterologists performed a second colonoscopy to observe the mucosal surface, taking random biopsies and tissue cultures of the cecum, ascending colon, transverse colon, descending colon, sigmoid colon, and rectum. Pathologists assessed the biopsy tissue by using hematoxylin-eosin and Warthin-Starry silver staining. Microbiologists homogenized cultured tissue specimens and suspended them in saline, and infectious disease specialists assessed Gram staining of the suspension. Laboratory staff incubated microaerobic cultures of the tissue suspension in modified Skirrow medium EX (Shimadzu Diagnostics Corporation, https://corp.sdc.shimadzu.co.jp) at 35°C. After the bacterial colony was obtained, we confirmed the pathogen by using matrix-assisted laser desorption/ionization time-of-flight (MALDI-TOF) mass spectrometry (MicroflexLT,flexcontrol3.4.135.0,MALDIBiotyper4.1.1; Bruker Daltonics, https://www.bruker.com/en.html) (Appendix https://wwwnc.cdc.gov/EID/article/30/1/23-1049-App1-pdf).

Colonoscopy confirmed that the erosions in the cecum seen at the time of the previous examination had disappeared. Overall, the colonic vascular permeability was preserved and there were no erosions, ulcers, or other findings suspicious for inflammation

Author affiliation: Toranomon Hospital, Tokyo, Japan

DOI: http://doi.org/10.3201/eid3001.231049

(Figure 1, panels D–F). Gram staining showed gram-negative spiral bacilli in the tissue obtained from the cecum and transverse colon (Figure 2, panel A). Hematoxylin and eosin staining of the biopsied tissues showed only slight inflammation with very mild edema of the mucosa in both cases, preservation of goblet cells, and mild leukocytic infiltration. In contrast, Warthin-Starry silver staining showed bacteria with spiral structures in crypts of the cecum, ascending colon, transverse colon, descending colon, and sigmoid colon but not in the rectal tissues (Figure 2, panels B–D). Culture of the tissue suspension showed bacterial growth in all tissues from the cecum, the ascending, transverse, descending, and sigmoid colon, and the rectum, which we identified as *H. fennelliae* by MALDI-TOF mass spectrometry, confirming the localization of *H. fennelliae*.

Conclusions

This study provides evidence for the localization of *H. fennelliae* in the intestinal tract. This confirmation may lead to better understanding of the life cycle of enterohepatic *Helicobacter* species. Reports of human infections with *H. cinaedi* are scarce but are gradually increasing (*3*–*5*), whereas those of *H. fennelliae* are even scarcer (*2*). Enterohepatic *Helicobacter* species cannot be identified based on biochemical characteristics alone. A definitive diagnosis requires identification by PCR, MALDI-TOF mass spectrometry, or both (*3*,*7*). Detection from stool and tissue is also difficult by routine culture methods, and many cases might have been overlooked (*3*).

Some previous reports have focused on disturbance of the intestinal tract by enterohepatic *Helicobacter* in animal models, but not in humans (*8*). Experiments conducted on pigtailed macaques given *H. cinaedi* and *H. fennelliae* orally showed that diarrhea, bacteremia, and localized inflammation of the colon were seen 3–7 days after exposure and that organisms remained detectable in stools for 3 weeks after diarrhea resolved. Researchers noted no acute inflammatory findings or microbial adherence in the small or large intestine in animals in the *H. cinaedi* group; however, they did note lymphoid hyperplasia caused by immune stimulation in the Peyer's patches. In contrast, our case of a human patient with recurrent bacteremia showed broad localization of *H. fennelliae* in the crypts of the colonic mucosa, almost without background inflammation in the intestinal tract or grossly visible disruption of the mucosal barrier.

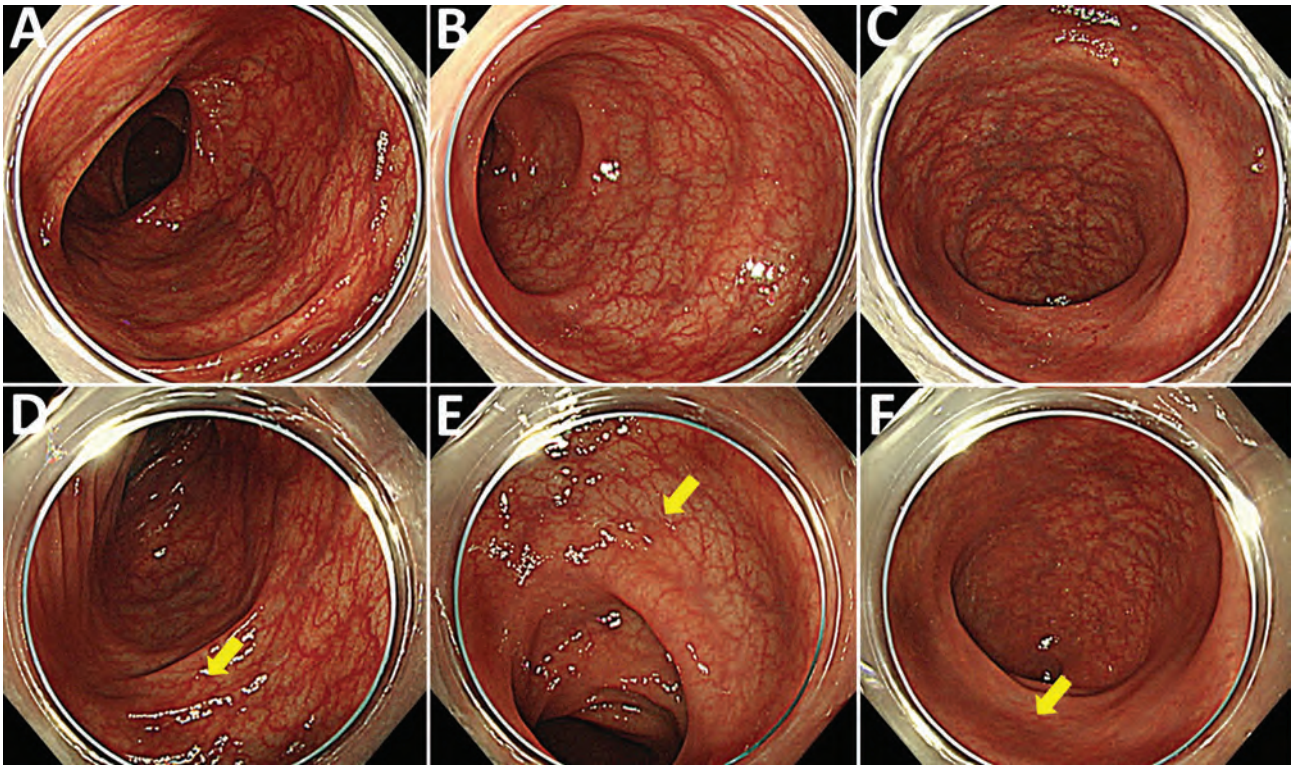

Figure 1. Colonoscopy findings from a man in Japan who had recurrent *Helicobacter fennelliae* bacteremia. A–C) First colonoscopy findings in the transverse colon (A), in the sigmoid colon (B), and in the rectum (C). D–F) Second colonoscopy findingsin the transverse colon (D), in the sigmoid colon (E), and in the rectum (F). Yellow arrows indicate randomly biopsied sites. Colonic vascular permeability was preserved, and there were no significant findings for inflammation.

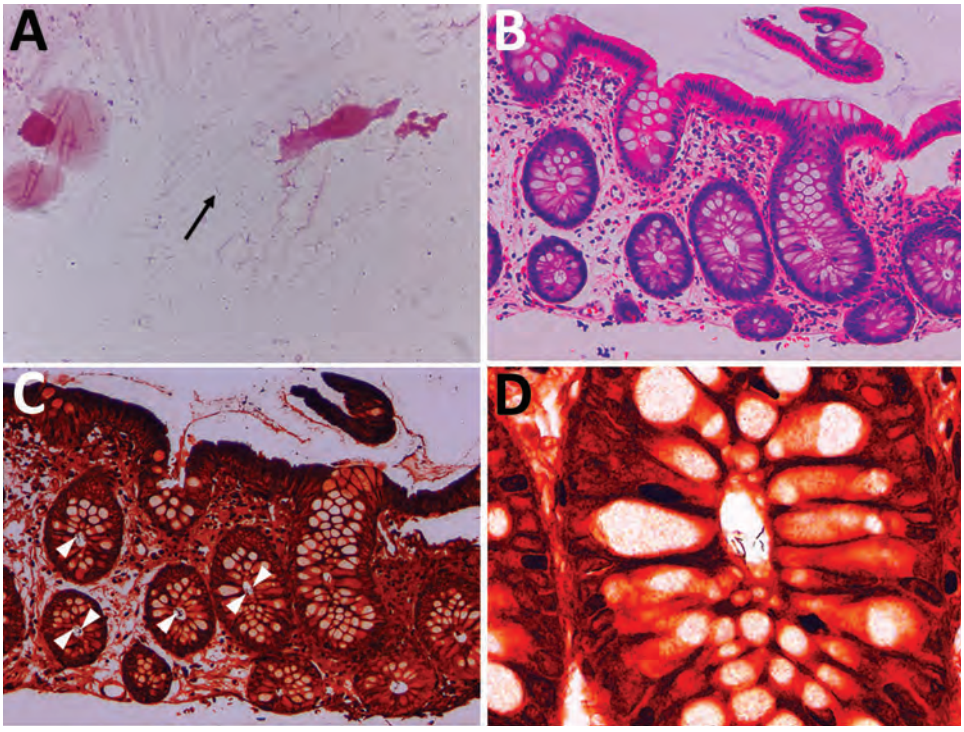

Figure 2. Microscopic findings in ileocolonic biopsy specimens (second colonoscopy) in a man in Japan who had recurrent *Helicobacter fennelliae* bacteremia. A) Morphologic features of the bacteria in a cecal tissue suspension with Gram staining (original magnification ×2,000). Arrow indicates gram-negative spiral bacilli. B) Histologic findings in a biopsy specimen taken from the transverse colon with hematoxylin-eosin staining (original magnification ×200). The colonic mucosa shows mild leukocytic infiltration. C) Histologic findings in a biopsy specimen taken from the transverse colon with Warthin-Starry silver staining (original magnification ×200). Bacteria are aggregated in crypts (arrowheads) D) Morphologic features of bacteria obtained from the transverse colon with Warthin-Starry silver staining (original magnification ×1,000). A cluster of spiral bacilli was observed.

The lack of inflammation and mucosal abnormality may reflect the fact that the patient was immunocompromised with hypogammaglobulinemia and lacked adequate intestinal immunity, which possibly caused bacteremia. Fujiya et al. described a patient with *H. fennelliae* bacteremia who had been receiving anticancer chemotherapy that included carboplatin, a possible risk factor of mucositis (*9*). They mentioned the possibility of the damaged intestinal mucosa being the route of entry for the pathogen. However, retrospective Warthin-Starry silver staining of the biopsied erosive mucosal tissue in the cecum from the first colonoscopy in the patient we describe showed no spiral bacillus-like structures in the mucosal lesions. Furthermore, we detected no gross abnormalities in the second colonoscopy. Given the absence of abnormal mucosal findings in our patient, immunoglobulin-associated impairment of intestinal immunity may be more important than damage to the intestinal mucosa in prevention of pathogen entry. This hypothesis would explain the mechanism caused in a previously reported patient with X-linked agammaglobulinemia, who developed recurrent bacteremia with persistent detection of *H. cinaedi* in stools despite repeated courses of antimicrobial therapy and selective decontamination of the digestive tract (*10*).

We report the microbiological and histopathological confirmation of *H. fennelliae* localization in the large intestine in an immunocompromised patient. Only 1 other report, regarding a patient in Japan, had enterohepatic *Helicobacter* detected pathologically (*11*). That patient contracted *Clostridioides difficile* enteritis after treatment for *H. cinaedi* bacteremia that resulted in bloody stools. Colonoscopy revealed pseudomembranous mucosal tissue in the cecum, where *H. cinaedi* was detected and confirmed pathologically. The authors stated, however, that it was impossible to determine whether the enteritis found in their patient was caused by *C. difficile* or *H. cinaedi* and whether it was localized at the time of the onset of *H. cinaedi* bacteremia. In our case, *H. fennelliae* was already present in stool culture at the time of the initial episode of bacteremia. Moreover, when the recurrent bacteremia was detected, persistence of the localized pathogen in the intestinal tract after the resolution of the first episode of bacteremia was confirmed. Both results suggest entry of *H. fennelliae* via the intestinal tract. We believe that investigating carriage rate or pathogenicity of enterohepatic *Helicobacter* in humans will help to better establish the disease concept.

This work was supported in part by a Research Grant from Okinaka Memorial Institute for Medical Research, Tokyo, Japan. Written informed consent for publication of this report and the associated images was obtained from the patient.

About the Author

Dr. Sakoh is a physician and researcher in the Department of Infectious Diseases at Toranomon Hospital, Tokyo, Japan.

References

1. Péré-Védrenne C, Flahou B, Loke MF, Ménard A, Vadivelu J. Other Helicobacters, gastric and gut microbiota. Helicobacter. 2017;22(Suppl 1):e12407. https://doi.org/10.1111/hel.12407
2. Saito S, Tsukahara M, Ohkusu K, Kurai H. *Helicobacter fennelliae* bacteremia: three case reports and literature review. Medicine (Baltimore). 2016;95:e3556. https://doi.org/10.1097/MD.0000000000003556
3. Araoka H, Baba M, Kimura M, Abe M, Inagawa H, Yoneyama A. Clinical characteristics of bacteremia caused by *Helicobacter cinaedi* and time required for blood cultures to become positive. J Clin Microbiol. 2014;52:1519–22. https://doi.org/10.1128/JCM.00265-14
4. Araoka H, Baba M, Okada C, Kimura M, Sato T, Yatomi Y, et al. First evidence of bacterial translocation from the intestinal tract as a route of *Helicobacter cinaedi* bacteremia. Helicobacter. 2018;23:e12458. https://doi.org/10.1111/hel.12458
5. Araoka H, Baba M, Okada C, Kimura M, Sato T, Yatomi Y, et al. Risk factors for recurrent *Helicobacter cinaedi* bacteremia and the efficacy of selective digestive decontamination with kanamycin to prevent recurrence. Clin Infect Dis. 2018;67:573–8. https://doi.org/10.1093/cid/ciy114
6. Burnens AP, Stanley J, Schaad UB, Nicolet J. Novel Campylobacter-like organism resembling *Helicobacter fennelliae* isolated from a boy with gastroenteritis and from dogs. J Clin Microbiol. 1993;31:1916–7. https://doi.org/10.1128/jcm.31.7.1916-1917.1993
7. Endo Y, Araoka H, Baba M, Okada C, Kimura M, Higurashi Y, et al. Matrix-assisted laser desorption ionization-time of flight mass spectrometry can be used to identify *Helicobacter cinaedi*. Diagn Microbiol Infect Dis. 2020;96:114964. https://doi.org/10.1016/j.diagmicrobio.2019.114964
8. Flores BM, Fennell CL, Kuller L, Bronsdon MA, Morton WR, Stamm WE. Experimental infection of pig-tailed macaques (Macaca nemestrina) with *Campylobacter cinaedi* and *Campylobacter fennelliae*. Infect Immun. 1990;58:3947–53. https://doi.org/10.1128/iai.58.12.3947-3953.1990
9. Fujiya Y, Nagamatsu M, Tomida J, Kawamura Y, Yamamoto K, Mawatari M, et al. Successful treatment of recurrent *Helicobacter fennelliae* bacteraemia by selective digestive decontamination with kanamycin in a lung cancer patient receiving chemotherapy. JMM Case Rep. 2016;3:e005069. https://doi.org/10.1099/jmmcr.0.005069
10. Toyofuku M, Tomida J, Kawamura Y, Miyata I, Yuza Y, Horikoshi Y. *Helicobacter cinaedi* bacteremia resulting from antimicrobial resistance acquired during treatment for X-linked agammaglobulinemia. J Infect Chemother. 2016;22:704–6. https://doi.org/10.1016/j.jiac.2016.02.008
11. Nishio H, Asagoe K. A case of *Helicobacter cinaedi* isolated from inflammatory intestinal mucosa following bacteremia with diffuse large B-cell lymphoma. [in Japanese]. Kansenshogaku Zasshi. 2018;92:133–7. https://doi.org/10.11150/kansenshogakuzasshi.92.133

Address for correspondence: Hideki Araoka, MD, PhD, Department of Infectious Diseases, Toranomon Hospital, 2-2-2 Toranomon, Minato-ku, Tokyo 105-8470, Japan; email: h-araoka@toranomon.gr.jp

Hantavirus Disease Cluster Caused by Seoul Virus, Germany

Jörg Hofmann, Rainer G. Ulrich, Calvin Mehl, Stephan Drewes, Jutta Esser, Martin Loyen, Heinz Zeichhardt, Konrad Schoppmeyer, Lioba Essen, Wolfgang Güthoff, Detlev H. Krüger

A cluster of 3 persons in Germany experienced hantavirus disease with renal insufficiency. Reverse transcription PCR–based genotyping revealed infection by Seoul hantavirus transmitted from pet rats. Seoul virus could be responsible for disease clusters in Europe, and infected pet rats should be considered a health threat.

Hantavirus disease occurs worldwide. Estimated number of cases is ≈100,000 annually; most cases are in Asia and Europe. Pathogenic hantaviruses are transmitted to humans through excreta of infected rodents. The infection can lead to renal or cardiopulmonary failure; case-fatality rates are up to 50% (*1*). Seoul virus (SEOV) is a hantavirus species for which rats (*Rattus* spp.) are natural hosts. In humans, SEOV infection causes mild to moderate disease with fever, acute kidney injury, hepatitis, and gastroenteritis; it is associated with transient thrombocytopenia and proteinuria (*2*–*4*).

Despite numerous clinical cases and local outbreaks of SEOV infection in Asia, few human cases are known in Europe (*4*–*6*). However, SEOV infections are difficult to identify by routine serodiagnosis because of high cross-reactivity with antigens of related hantaviruses, such as Hantaan virus and Dobrava-Belgrade virus. Whereas Hantaan virus is endemic in Asia, Dobrava-Belgrade virus is found in many parts of Europe (*1*).

Autochthonous human SEOV infection in Germany was described in 2020; the hantavirus type was determined by molecular analysis, and infection source was identified as a pet rat (*4*). Deeper molecular analysis found SEOV strains in several pet rats, including the animals owned by that patient (*7*). However, no clusters of human SEOV infections were reported previously from Germany or any other part of Europe.

The Study

During November–December 2021, three persons in Germany experienced typical initial signs of hantavirus disease (fever, malaise, myalgia, chills, low-back pain, nausea) (Table 1). The patients lived ≈25 km apart. All 3 patients had acute kidney injury with reduction of glomerular filtration rate, proteinuria, and microhematuria. Moreover, biochemical analysis revealed typical thrombocytopenia and signs of inflammation, including elevation of C-reactive protein and transaminases. Serum creatinine levels remained within reference ranges or were only transiently higher. The patients recovered and were discharged after 3–6 days (Table 1).

All 3 patients developed IgM and IgG against diagnostic antigens from the group of murine-associated hantaviruses, including Hantaan virus, Dobrava-Belgrade virus, and SEOV. After onset of disease, we performed panhantavirus PCR, reverse transcription PCR based on amplification of a 412-nt region of the genomic large segment (*8*), to detect hantavirus genetic material from serum samples of patients 1 and 3 (Table 2).

Patients 1 and 2 were married to each other and lived in the federal state of North Rhine-Westphalia.

Author affiliations: Charité–Universitätsmedizin Berlin, Berlin, Germany (J. Hofmann, D.H. Kruger); German Centre for Infection Research (DZIF), Partner Site Hamburg-Lübeck-Borstel-Riems, Greifswald-Insel Riems, Germany (R.G. Ulrich, C. Mehl); Friedrich-Loeffler-Institut, Greifswald-Insel Riems (R.G. Ulrich, C. Mehl, S. Drewes); Laborarztpraxis Osnabrück, Georgsmarienhütte, Germany (J. Esser); Herz-Jesu Krankenhaus, Münster-Hiltrup, Germany (M. Loyen); INSTAND e.V., Society for Promoting Quality Assurance in Medical Laboratories, Düsseldorf, Germany (H. Zeichhardt); Institut für Qualitätssicherung in der Virusdiagnostik, Berlin (H. Zeichhardt); Euregio-Klinik, Nordhorn, Germany (K. Schoppmeyer); Maria-Josef-Hospital Greven, Greven, Germany (L. Essen); Gesellschaft für Biotechnologische Diagnostik mbH, Berlin (W. Güthoff)

DOI: http://doi.org/10.3201/eid3001.230855

Table 1. Clinical characteristics of patients infected with Seoul virus, Germany*

Criteria	Patient 1	Patient 2	Patient 3
Domicile	North Rhine-Westphalia	North Rhine-Westphalia	Lower Saxony
Sex	M	F	M
Age, y	31	31	20
Duration of hospitalization, d	3	4	6
Initial fever, °C	40	39	40
Malaise, myalgia, chills, low-back pain, nausea	Y	Y	Y
Serum creatinine elevation	Y†	N	N
Thrombocytopenia	Y	Y†	Y
CRP elevation	Y	Y	Y
Liver enzyme elevation	Y	Y	Y
GFR reduction	Y	Y	N
Proteinuria	Y	Y	Y
Microhematuria	Y	Y	Y
Additional clinical findings	Splenomegaly	Splenomegaly	Lung opacity

*CRP, C-reactive protein; GFR, glomerular filtration rate; LS, Lower Saxony; NRW, North Rhine-Westphalia.
†Test result was at the cutoff between positive and negative.

Their children (persons 12a and 12b) (Table 2) remained healthy and did not seroconvert. The family was known to keep pet rats at home. Patient 3, who lived in Lower Saxony, reported that his girlfriend also kept pet rats. Investigation of his girlfriend (person 4) showed that she remained healthy; however, her hantavirus IgM negative/IgG positive serostatus suggested a previous subclinical infection (Table 2).

The family of patients 1 and 2 permitted us to test their pet rats. We amplified the corresponding region from the genomic large segment. Phylogenetic analysis of the amplified virus sequences from patients 1 and 3 and the pet rats revealed almost identical sequences (Figure). We compared them to the amplified virus sequences from a previous unrelated patient and her pet rat from Lower Saxony (*4*).

Phylogenetic analysis disclosed the detected virus sequences as SEOV and, moreover, demonstrated the high relatedness of virus sequences from patients and pet rats from North-West Germany. The high similarity of SEOV sequences from Germany to sequences derived from breeder rats in the Netherlands, France, and the United States, but not to sequences from wild rats of those countries, suggests an intensive exchange of pet rats between neighboring countries in Europe and between Europe and the United States (*7*).

Human SEOV infections might be underestimated because the nucleocapsid proteins used in serologic assays share high amino acid sequence similarity and cross-reactivity with different hantavirus species. To explore this hypothesis in an external quality assessment, we sent a serum sample from patient 3, obtained 2 months after complete recovery, to 8 expert laboratories in Europe. All laboratories analyzed the sample in their routine hantavirus diagnostics, including commercial and lab-derived enzyme immunoassays, immunofluorescence assays, rapid assays, and immunoblots for confirmation (Appendix Tables 1, 2, https://wwwnc.cdc.gov/EID/article/30/1/23-0855-App1.pdf). Results revealed strong cross-reactivities to related hantavirus nucleocapsid proteins in IgG and IgM screening and in confirmation assays, making correct serotyping impossible. Thus, in cases of unexpected pattern in serodiagnostics or cases of known contact to rats, we strongly recommend verifying positive results with molecular methods or by typing of neutralizing antibodies. Only the laboratory using a focus reduction neutralization assay identified the SEOV infection (Appendix Table 1).

Table 2. Virus diagnostics results of hantavirus patients and close contacts, Germany*

Person no.	Illness	Pan-hantavirus PCR	Hantavirus IgM†	Hantavirus IgG†
1	Y	+	+	+
2‡	Y	–	+	+
12a§	N	NA	–	–
12b§	N	NA	–	–
3	Y	+	+	+
4¶	N	–	–	+

*NA, not applicable; +, positive; –, negative.
†Tested with recomLine HantaPlus IgG and IgM (https://www.mikrogen.de).
‡Wife of patient 1.
§Children of patients 1 and 2.
¶Girlfriend of patient 3.

Conclusions

A total of 6 molecularily proven SEOV-infected patients in Germany have been described: 1 imported case (*9*), 1 autochthonous case (*4*), and the 3 symptomatic case-patients and 1 asymptomatic case-patient we described in this report. Five of these persons had been admitted to hospital for several days. In all autochthonous cases, pet rats were confirmed as source of infection, strongly suggesting a need for close cooperation between public health and animal health institutions in the One Health frame. Pet rats, in addition to wild and breeder or feeder rats, should be considered threats for SEOV infection in humans.

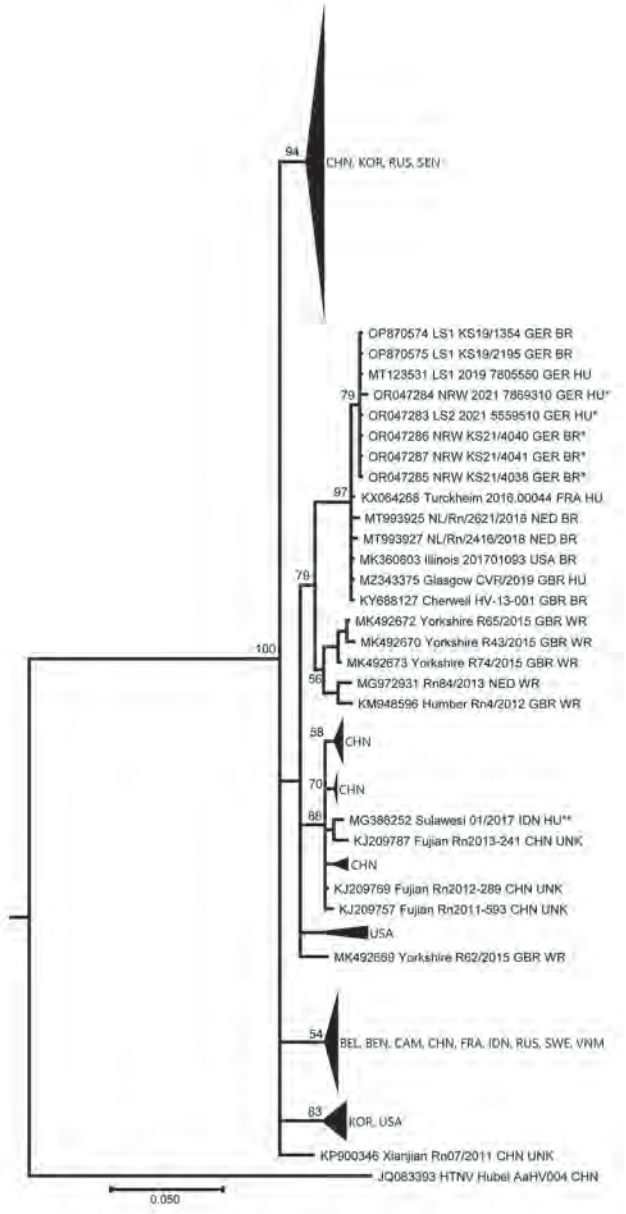

Figure. Phylogenetic tree of partial large segment Seoul virus sequences from humans and rats, Germany. Segments were 412-nt long, positions nt 2919–3330 based on reference sequence (KM948594_Cherwell_GBR_BR). The partial large segment Bayesian tree was reconstructed using 20 million generations and the Hasegawa-Kishino-Yano substitution model with gamma distribution and invariant sites. Single asterisks indicate sequences from this study, denoted by their GenBank accession numbers. Double asterisks indicate sequence from the imported Seoul virus case from Indonesia (*9*). Aa, *Apodemus agrarius*; BEL, Belgium; BEN, Benin; BR, breeder rat (includes feeder, lab, and pet rats); CAM, Cambodia; CHN, China; FRA, France; GBR, Great Britain; GER, Germany; HTNV, Hantaan virus; HU, human; IDN, Indonesia; KOR, Korea; L, large segment; NED, the Netherlands; Rn, *Rattus norvegicus*; RUS, Russia; SEN, Senegal; SEOV, Seoul virus; SWE, Sweden; UNK, unknown wild or breeder rat; USA, United States of America; VNM, Vietnam; WR, wild rat.

Acknowledgments

We thank J. Dreesman, C. Klier, and M. Oskamp from local health authorities for their support. We thank the 8 expert laboratories in Europe for analyzing the serum sample, as described in the Appendix Tables. We thank M. Raftery for critical reading of the manuscript and C. Stephan for expert technical assistance.

This work was supported by the German Centre for Infection Research, thematic translational unit Emerging Infections (grant no. 01.808 00) awarded to R.G.U.

About the Author

Dr. Hofmann is the chair of the National Consultation Laboratory for Hantaviruses, Institute of Virology, Charité University Medicine, Berlin, Germany. His primary research interest is human infections with viral pathogens.

References

1. Kruger DH, Figueiredo LT, Song JW, Klempa B. Hantaviruses—globally emerging pathogens. J Clin Virol. 2015;64:128–36. https://doi.org/10.1016/j.jcv.2014.08.033
2. Lee HW. Hemorrhagic fever with renal syndrome in Korea. Rev Infect Dis. 1989;11(Suppl 4):S864–76. https://doi.org/10.1093/clinids/11.Supplement_4.S864
3. Clement J, LeDuc JW, McElhinney LM, Reynes JM, Van Ranst M, Calisher CH. Clinical characteristics of ratborne Seoul hantavirus disease. Emerg Infect Dis. 2019;25:387–8. https://doi.org/10.3201/eid2502.181643
4. Hofmann J, Heuser E, Weiss S, Tenner B, Schoppmeyer K, Esser J, et al. Autochthonous ratborne Seoul virus infection in woman with acute kidney injury. Emerg Infect Dis. 2020;26:3096–9. https://doi.org/10.3201/eid2612.200708
5. Zhang YZ, Dong X, Li X, Ma C, Xiong HP, Yan GJ, et al. Seoul virus and hantavirus disease, Shenyang, People's Republic of China. Emerg Infect Dis. 2009;15:200–6. https://doi.org/10.3201/eid1502.080291
6. Clement J, LeDuc JW, Lloyd G, Reynes JM, McElhinney L, Van Ranst M, et al. Wild rats, laboratory rats, pet rats: global Seoul hantavirus disease revisited. Viruses. 2019;11:652. https://doi.org/10.3390/v11070652
7. Heuser E, Drewes S, Trimpert J, Kunec D, Mehl C, de Cock MP, et al. Pet rats as the likely reservoir for human Seoul orthohantavirus infection. Viruses. 2023;15:467. https://doi.org/10.3390/v15020467
8. Klempa B, Fichet-Calvet E, Lecompte E, Auste B, Aniskin V, Meisel H, et al. Hantavirus in African wood mouse, Guinea. Emerg Infect Dis. 2006;12:838–40. https://doi.org/10.3201/eid1205.051487
9. Hofmann J, Weiss S, Kuhns M, Zinke A, Heinsberger H, Kruger DH. Importation of human Seoul virus infection to Germany from Indonesia. Emerg Infect Dis. 2018;24:1099–102. https://doi.org/10.3201/eid2406.172044

Address for correspondence: Jörg Hofmann, Charité Medical School—Institute of Medical Virology, Chariteplatz 1 Berlin 10117, Germany; email: joerg.hofmann@charite.de

Tuberculosis Diagnostic Delays and Treatment Outcomes among Patients with COVID-19, California, USA, 2020

Emily Han,[1] Scott A. Nabity,[1] Shom Dasgupta-Tsinikas, Ramon E. Guevara, Marisa Moore, Ankita Kadakia, Hannah Henry, Martin Cilnis, Sonal Buhain, Amit Chitnis, Melony Chakrabarty, Ann Ky, Quy Nguyen, Julie Low, Seema Jain, Julie Higashi, Pennan M. Barry, Jennifer Flood

We assessed tuberculosis (TB) diagnostic delays among patients with TB and COVID-19 in California, USA. Among 58 persons, 43% experienced TB diagnostic delays, and a high proportion (83%) required hospitalization for TB. Even when viral respiratory pathogens circulate widely, timely TB diagnostic workup for at-risk persons remains critical for reducing TB-related illness.

California typically reports one quarter of tuberculosis (TB) cases in the United States and had a 19% case decline during 2020 (*1*). That decline paralleled national and global observations during the COVID-19 pandemic (*1*,*2*). Pandemic-related disruptions challenged healthcare systems and TB control programs by diverting staff and other resources (*3*,*4*). Pandemic effects on TB diagnostic and care delays in the United States have not been fully described. We aimed to characterize missed opportunities and diagnostic delays, hospitalizations, and treatment outcomes in a subset of patients in California who had TB and COVID-19 during 2020. The California Department of Public Health, Centers for Disease Control and Prevention, and participating local health departments reviewed and approved this activity. This study was conducted consistent with applicable federal and Centers for Disease Control and Prevention policies (Appendix, https://wwwnc.cdc.gov/EID/article/30/1/23-0924-App1.pdf).

The Study

Using surveillance records of TB and COVID-19, we used name-based probabilistic matching to find persons with diagnosed TB and COVID-19 in California (*5*). We abstracted records for 58 patients who had TB disease diagnosed in 2020 and COVID-19 diagnosed within 120 days and who resided in 6 local health jurisdictions with high TB burdens: Los Angeles, San Diego, Santa Clara, Orange, Alameda, and Sacramento Counties (Figure 1). We captured TB and COVID-19 symptom profiles and timing, chest imaging results, TB diagnostic testing, and hospitalizations from TB program, hospital, emergency department, and outpatient records, and from death certificates. We also obtained PCR and antigen-based COVID-19 test results, including negative results, beginning on March 9, 2020. We performed statistical comparisons by using 2-sided χ^2 or Fisher exact tests for categorical data and Wilcoxon 2-sample tests for continuous data ($\alpha = 0.05$) (Appendix).

Among 58 patients with COVID-19 and TB, 51 had pulmonary or pleural TB disease. The median time from symptom onset to TB diagnosis was 29.0

Author affiliations: California Department of Public Health, Richmond, California, USA (E. Han, S.A. Nabity, H. Henry, M. Cilnis, S. Jain, P.M. Barry, J. Flood); Centers for Disease Control and Prevention, Atlanta, Georgia, USA (S.A. Nabity, M. Moore); Los Angeles County Department of Public Health, Los Angeles, California, USA (S. Dasgupta-Tsinikas, R.E. Guevara, J. Higashi); San Diego County Health and Human Services Agency, San Diego, California, USA (M. Moore, A. Kadakia); Alameda County Public Health Department, San Leandro, California, USA (S. Buhain, A. Chitnis); Sacramento County Health Services, Sacramento, California, USA (M. Chakrabarty); Santa Clara County Public Health Department, San Jose, California, USA (A. Ky); Orange County Health Care Agency, Santa Ana, California, USA (Q. Nguyen, J. Low)

DOI: https://doi.org/10.3201/eid3001.230924

[1]These first authors contributed equally to this article.

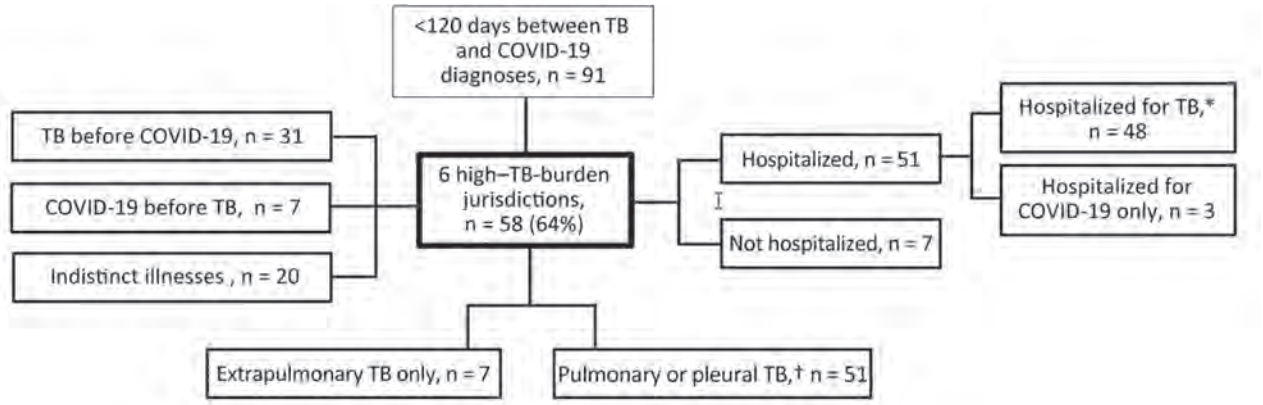

Figure 1. Flowchart of patients included in a study of TB diagnostic delays and treatment outcomes among patients with COVID-19, California, USA, 2020. TB high-burden counties included were Alameda (excluding the city of Berkeley), Los Angeles (excluding the cities of Long Beach and Pasadena), Orange, Sacramento, San Diego, and Santa Clara. Excluded cities maintain independent surveillance registries. *Includes TB patients also hospitalized for COVID-19. †Includes 3 patients with pleural TB only. TB, tuberculosis.

(interquartile range [IQR] 5.0–95.0) days. Twenty-two (43%) patients had a diagnostic delay of >30 days (median 95.0 [IQR 60.0–117.0] days) between TB symptom onset and first TB clinical consultation (Table 1; Appendix Table). Patients with diagnostic delays had indicators of more severe TB, such as

Table 1. Characteristics of 51 persons with pulmonary or pleural TB in a study of TB diagnostic delays and treatment outcomes among patients with COVID-19, California, USA, 2020*

Characteristics	Diagnostic delay†	No diagnostic delay
All pulmonary or pleural cases‡	22	29
Median days between symptom onset to first TB care visit (IQR)	95.0 (60.0–117.0)	5.5 (2.0–13.0)
Age, y (IQR)	55.5 (42.0–71.0)	58 (49.0–77.0)
Sex		
M	11 (50.0)	22 (75.6)
F	11 (50.0)	7 (24.1)
Hispanic or Latino ethnicity	13 (59.1)	17 (58.6)
Healthy Places Index score in 1st quartile§	10 (45.5)	10 (34.5)
Primary language non-English, n = 46	13 (59.1)	18 (66.7)
No health insurance	2 (9.5)	7 (28.0)
Essential worker¶	8 (36.4)	4 (14.3)
No. underlying conditions		
0–1	9 (40.9)	12 (41.4)
≥2	13 (59.1)	17 (58.6)
Smear-positive, cavitary, or disseminated pulmonary TB#	**19 (86.4)**	**16 (55.2)**
Mycobacterium tuberculosis NAAT testing done	21 (95.5)	23 (79.3)
Positive *M. tuberculosis* NAAT	18 (85.7)	16 (69.6)
M. tuberculosis NAAT done before or within 7 d of TB diagnosis	19 (90.5)	18 (78.3)
Recent secondary TB case among cases with genotype**	4 (18.2)	3 (10.3)
Diagnosed with COVID-19 during period of elevated COVID-19 incidence††	**18 (81.8)**	**16 (55.2)**
Missed opportunity for pulmonary TB diagnosis	6 (27.3)	2 (6.9)
Order of disease		
TB first	7 (31.8)	8 (27.6)
COVID-19 first	2 (9.1)	3 (10.3)
Not distinct	7 (31.8)	12 (41.4)
≥1 episode, asymptomatic or with unknown symptoms	6 (27.3)	6 (20.7)
Death	2 (9.1)	6 (20.7)
ICU and intubated while hospitalized for TB	1 (50.0)	3 (50.0)
Died in hospital	1 (50.0)	4 (66.7)

*TB–COVID-19 co-infected patients had TB and COVID-19 diagnoses within 120 d of each other, whereby ≥1 of the diseases was diagnosed in 2020. Included California jurisdictions were Alameda, Los Angeles, Orange, Sacramento, San Diego, and Santa Clara Counties. Values are no. (%) except where indicated. Bold text indicates statistical significance (p<0.05). ICU, intensive care unit; NAAT, nucleic acid amplification test; TB, tuberculosis.
†Diagnostic delay was defined as >30 d between TB symptom onset and first care visit for TB.
‡Extrapulmonary-only cases not included.
§The Healthy Places Index combines 25 community characteristics, such as access to healthcare, housing, education, and more, into a single indexed score; 1st quartile is the least advantaged score.
¶Work that must be done in person and in which the worker interacts with other workers or the public.
#Disseminated TB is defined as meningeal, miliary, positive acid-fast bacilli blood culture, or both pulmonary and extrapulmonary TB.
**Based on phylogenetic analysis (≤5 single-nucleotide polymorphisms) and timing (<3 y) or epidemiologic link.
††California 7-d average incidence of new COVID-19 cases ≥15 cases per 100,000 population.

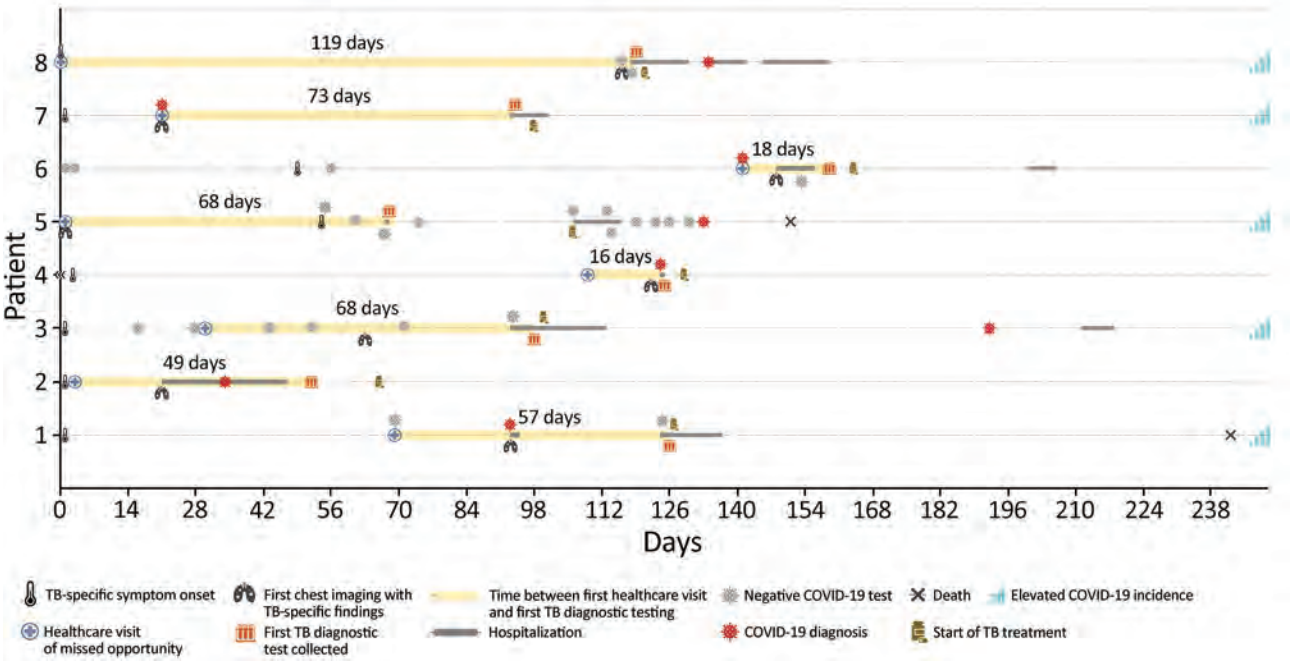

Figure 2. Timeline of 8 patients included in a study of TB diagnostic delays and treatment outcomes among patients with COVID-19, California, USA, 2020. Symptom onset is the date the first symptoms compatible with either TB or COVID-19 was identified. Symptom onset for patient 6 was in June 2019. Patient 7 was hospitalized for reasons unrelated to TB or COVID-19, and the TB diagnostic work-up was prompted by incidental findings on chest imaging. The healthcare visit of a missed opportunity to diagnose TB in a person with TB risk factors was a visit where ≥1 symptom or chest imaging finding was known. Yellow shading captures the number of days between the first missed opportunity and the first specimen collection for a TB diagnosis. Elevated COVID-19 incidence in California was considered ≥15 cases/100,000 population (7-day average rate). TB, tuberculosis.

acid-fast bacilli smear–positive sputum, cavitary imaging results, or disseminated pulmonary disease, than patients without diagnostic delays (86% vs. 55%; p = 0.02). Diagnostic delays were marginally more common among persons with COVID-19 diagnosed during periods of elevated incidence, considered the statewide 7-day average COVID-19 incidence rate of ≥15 cases/100,000 population, than persons diagnosed at periods without elevated incidence (82% vs. 55%; p = 0.05).

Among 51 patients with COVID-19 and pulmonary or pleural TB, 8 (16%) had ≥1 missed opportunity for TB diagnosis. We defined a missed opportunity as a documented clinical encounter in which a person with TB risk factors (e.g., experiencing homelessness or being non–US-born, in a correctional facility, or HIV-positive) had TB-specific symptoms but no TB diagnostic testing. TB-specific symptoms were hemoptysis, weight loss, or cough ≥3 weeks, or chest imaging of cavity, tree in bud pattern, pleural effusions, nodules, miliary, or upper lobe infiltrate; TB diagnostic testing included acid-fast bacilli smear or *Mycobacterium tuberculosis* nucleic acid amplification test. The median time between the first missed opportunity and start of TB diagnostic testing was 62.5 (IQR 33.5–70.5) days. Five (63%) missed opportunities

Table 2. Hospitalizations for 51 persons who might have experience TB diagnostic delay in a study of TB diagnostic delays and treatment outcomes among patients with COVID-19, California, USA, 2020*

Disease-associated hospitalization†	No. admissions	Median duration, d (IQR)	Range, d	Cumulative hospital days	ICU and intubation	In-hospital death‡
Total	73	12.0 (7.0–21.0)	1–139	1,324	14	6
TB only	35 (47.9)	13.0 (8.0–21.0)	1–74	634	5 (14.3)	0 (0.0)
TB and COVID-19§	23 (31.5)	10.0 (5.0–20.0)	1–139	392	5 (21.7)	4 (17.4)
COVID-19 only	15 (20.5)	12.0 (6.0–26.0)	3–68	298	4 (26.7)	2 (13.3)

*TB–COVID-19 co-infected patients had TB and COVID-19 diagnoses within 120 d of each other, whereby ≥1 of the diseases was diagnosed in 2020. Included California jurisdictions were Alameda, Los Angeles, Orange, Sacramento, San Diego, and Santa Clara Counties. Values are no. (%) except where indicated. ICU, intensive care unit; TB, tuberculosis.
†Based on the timing of hospitalization and diagnosis for each disease. Distinct TB-associated and COVID-19–associated hospitalizations must have occurred >14 d apart. Persons who were hospitalized at any point had an average 1.3 hospitalizations each.
‡Patients who died in hospital had admission durations of 10–57 d.
§Concurrent TB and COVID-19 were addressed in same hospital stay.

occurred during periods of elevated COVID-19 incidence, and 4 (50%) patients had COVID-19 testing (2 COVID-19–negative and 2 COVID-19–positive) instead of TB testing at the clinical encounter where the missed opportunity occurred (Figure 2).

Among the 58 patients, 51 (88%) were hospitalized ≥1 time (Table 2). Among 73 hospitalizations (average 1.3 per person), 35 (48%) were related to TB disease alone, 23 (32%) to indistinct (i.e., concurrent) TB and COVID-19 disease episodes, and 15 (21%) to COVID-19 alone. All 6 in-hospital deaths occurred during COVID-19–associated hospitalizations. The median overall hospital stay was 12 (IQR 7–21) days and was similar across all 3 disease-associated hospitalizations, even when we excluded in-hospital deaths.

Two patients did not start TB treatment because they died before TB diagnosis. Of the remaining 56 patients, 42 (75%) completed TB treatment within 12 months, 5 (9%) completed treatment in ≥12 months (including 1 case with rifampin resistance), 1 refused treatment, and 8 (14%) died before completing treatment. Overall, 10 (17%) patients died. Local TB programs determined that 3 (30%) deaths were definitely related to TB, 5 (50%) were possibly related, and 2 (20%) were probably not related. Of the 8 deaths definitely or possibly related to TB, 3 (38%) had TB and COVID-19 listed as contributors on the death certificate, 4 (50%) had only COVID-19, and 1 (16%) had neither term listed.

Conclusions

Delays in TB diagnosis or documentation of a missed opportunity to diagnose TB were more frequent during periods of elevated COVID-19 incidence, potentially because of pandemic-related staff and health system disruptions and community transmission mitigation policies (*6*,*7*). Approximately 1 in 6 persons in our sample had a documented clinical encounter where TB diagnostic evaluations could have been initiated earlier, which was consistent with literature published before the pandemic (*8*). Delayed diagnosis could lead to increased TB transmission and worse TB outcomes; in this analysis, delayed diagnosis appeared to be associated with more advanced TB, suggesting more infectiousness.

In our sample, 83% of patients had >1 TB-related hospitalization, which is higher than the prepandemic frequency of TB-associated hospitalization in California, which previously was reported as ≈50% (*9*). This finding might have been influenced by the slightly older age distribution of this patient cohort (median 57.5 [IQR 42–76] years) compared with pre-pandemic TB patients (median 56.0 IQR 35–70 [years]) in California from 2017–2019 (*5*). The median duration of TB-related hospital stays did not change compared with historical TB hospitalizations in California (*9*).

TB treatment completion appeared consistent with the pre–COVID-19 era in which ≈75% of patients completed TB treatment within 12 months (*10*). As we previously described, the proportion of deaths among TB patients with COVID-19 was higher than for TB patients in the recent pre-pandemic period (*5*). Most (77%) deaths were definitely or possibly TB-related but TB attribution on death certificates had poor correlation with detailed retrospective review, as has also been historically described (*11*). Thus, death certificates are unlikely to yield accurate estimates for deaths related to TB and COVID-19 co-infections.

Limitations of this study include use of observational data and lack of a comparison cohort of persons with TB who did not have COVID-19 in 2020 but had the same detailed clinical data. Our small sample size also precluded robust subgroup comparisons. The 6 participating TB programs represented 55% of California's population (*12*), 53% of reported COVID-19 (*13*), and 66% of the state's reported TB in 2020 (*1*). Nonetheless, our findings may not be generalizable to all areas of California or to other US regions.

In summary, delays in TB diagnoses continued to occur and the frequency of TB-related hospitalizations was higher for patients diagnosed with both TB and COVID-19 during the pandemic than historically observed in California. Nonetheless, the proportion of TB patients with COVID-19 completing treatment within 12 months was similar to persons with TB in the prepandemic period, suggesting TB programs managed to maintain TB treatment standards despite redirection of staff and resources. Pursuing a diagnostic workup for persons at risk of developing TB disease, even when a viral respiratory pathogen is widely circulating, remains critical for reducing TB-related illness in California.

Acknowledgments

We thank Vilma A. Contreras, Rebecca Fisher, and Jane Lam for assisting in data collection and management; Tambi Shaw for assistance estimating recent transmission; and Melissa Ehman and Joan Sprinson developing tools to assess diagnostic delays and TB-related deaths.

Author contributions: All authors contributed to study design, data collection, scientific interpretation, and review and approval of the final manuscript. S.D., R.G., M.M., A.K., S.B., A.C., M.C., A.K., Q.N., J.L., and J.H. implemented the study protocol and abstracted data. M.C. provided estimates of recent transmission. E.H. and H.H. curated and analyzed the data. E.H., S.A.N., and S.D. drafted the original manuscript. S.A.N., S.J., P.B., and J.F. coordinated the project.

About the Author

Ms. Han is an epidemiologist with California Department of Public Health (CDPH), Richmond, California, USA. Her research interests are related to TB surveillance and epidemiology. Dr. Nabity is a Centers for Disease Control and Prevention medical officer and epidemiologist affiliated with CDPH. His research interests focus on the epidemiology of infectious diseases, including TB and COVID-19.

References

1. Deutsch-Feldman M, Pratt RH, Price SF, Tsang CA, Self JL. Tuberculosis—United States, 2020. MMWR Morb Mortal Wkly Rep. 2021;70:409–14. https://doi.org/10.15585/mmwr.mm7012a1
2. World Health Organization. Global tuberculosis report 2021 [cited 2022 Apr 27]. https://www.who.int/publications/i/item/9789240037021
3. Blecker S, Jones SA, Petrilli CM, Admon AJ, Weerahandi H, Francois F, et al. Hospitalizations for chronic disease and acute conditions in the time of COVID-19. JAMA Intern Med. 2021;181:269–71. https://doi.org/10.1001/jamainternmed.2020.3978
4. Nabity SA, Fong V, Keh C, Flood J. Disruptions to TB program services and capacity during the COVID-19 response in California, January 2020–August 2021. In: Abstracts of the National TB Controllers Association/California TB Controllers Association Conference, 2022. Palm Springs, CA, USA; 2022 May 23–26. Smyrna (GA): National TB Controllers Association; 2022.
5. Nabity SA, Han E, Lowenthal P, Henry H, Okoye N, Chakrabarty M, et al. Sociodemographic characteristics, comorbidities, and mortality among persons diagnosed with tuberculosis and COVID-19 in close succession in California, 2020. JAMA Netw Open. 2021;4:e2136853. https://doi.org/10.1001/jamanetworkopen.2021.36853
6. Readhead A, Cooksey G, Flood J, Barry P. Hospitalizations with TB, California, 2009–2017. Int J Tuberc Lung Dis. 2021;25:640–7. https://doi.org/10.5588/ijtld.21.0173
7. State of California. Tracking COVID-19 in California [cited 2022 Jun 15]. https://covid19.ca.gov/state-dashboard
8. Miller AC, Polgreen LA, Cavanaugh JE, Hornick DB, Polgreen PM. Missed opportunities to diagnose tuberculosis are common among hospitalized patients and patients seen in emergency departments. Open Forum Infect Dis. 2015;2:ofv171. https://doi.org/10.1093/ofid/ofv171
9. The Commonwealth Fund. 2022 Scorecard on state health system performance [cited 2023 Oct 5]. https://www.commonwealthfund.org/publications/scorecard/2022/jun/2022-scorecard-state-health-system-performance
10. Ledesma JR, Zou L, Chrysanthopoulou SA, Giovenco D, Khanna AS, Lurie MN. Community mitigation strategies, mobility, and COVID-19 incidence across three waves in the United States in 2020. Epidemiology. 2023;34:131–9. https://doi.org/10.1097/EDE.0000000000001553
11. California Department of Public Health. Report on tuberculosis in California, 2019. Sacramento: The Department; 2020.
12. Beavers SF, Pascopella L, Davidow AL, Mangan JM, Hirsch-Moverman YR, Golub JE, et al.; Tuberculosis Epidemiologic Studies Consortium. Tuberculosis mortality in the United States: epidemiology and prevention opportunities. Ann Am Thorac Soc. 2018;15:683–92. https://doi.org/10.1513/AnnalsATS.201705-405OC
13. State of California Department of Finance. Report P-2C: population projections by sex and 5-year age group, 2010–2060: California counties (2019 baseline) [cited 2022 Apr 27]. https://covid19.ca.gov/state-dashboard

Address for correspondence: Scott A. Nabity, California Department of Public Health, 850 Marina Bay Pwky, Bldg P 2, Richmond, CA 94804, USA; email: hjq5@cdc.gov

Respiratory Viruses in Wastewater Compared with Clinical Samples, Leuven, Belgium

Annabel Rector, Mandy Bloemen, Marijn Thijssen, Bram Pussig, Kurt Beuselinck, Marc Van Ranst, Elke Wollants

In a 2-year study in Leuven, Belgium, we investigated the use of wastewater sampling to assess community spread of respiratory viruses. Comparison with the number of positive clinical samples demonstrated that wastewater data reflected circulation levels of typical seasonal respiratory viruses, such as influenza, respiratory syncytial virus, and enterovirus D68.

Since the COVID-19 pandemic began, wastewater-based surveillance has been used to track circulation levels of SARS-CoV-2 (*1*,*2*). For that purpose, we began collecting samples from a regional wastewater treatment plant in Leuven, Belgium, in December 2020. We found wastewater-based surveillance was an objective indicator of SARS-CoV-2 community circulation, which can be highly valuable when testing is limited (*3*).

Many persons with acute respiratory infections (ARI) do not seek medical care, thereby enabling those infections to go undetected. Obtaining detailed information on the circulation of respiratory viruses in the community is key to elucidating their societal burden. This knowledge could enable better prediction and management of major outbreaks and could guide physicians in diagnosis. The current approach, usually based on limited reporting by sentinel physicians and laboratories, can lead to substantial data bias. We explored whether wastewater sampling can provide an alternative method for monitoring circulation of respiratory pathogens at the population level.

The Study

We screened 112 wastewater samples collected weekly over a 2-year period at a large regional treatment plant in Leuven for the presence of respiratory pathogens with an in-house–developed multiplex quantitative PCR respiratory panel (Appendix, https://wwwnc.cdc.gov/EID/article/30/1/23-1011-App1.pdf) (*4*). We investigated whether respiratory viruses found in wastewater corresponded to their detection in samples from patients with respiratory infections at the University Hospitals Leuven (UZL) (*5*). At UZL, patient samples were only tested with the respiratory panel in case of serious lower respiratory tract infection in immunocompromised or critically ill patients. Those clinical samples are therefore not entirely representative of locally circulating respiratory pathogens, especially when those pathogens cause mainly mild infections. When possible, we supplemented clinical sample data with epidemiologic data from sentinel laboratories across Belgium reported by Sciensano, but these were only available for a limited number of viruses (*6*). Nonpharmacologic interventions during the COVID-19 pandemic affected timing and levels of virus circulation.

Influenza A was repeatedly identified during mid-February–mid-May 2022 (Figure 1, panel A). This pattern aligned with positive clinical samples at UZL, which showed an influenza A peak during March–May 2022 and few cases outside that period. It also corresponded to Sciensano data, which indicated a mild 2020–21 influenza season and a late 2021–22 season (end of February to end of April) (*6*), caused almost exclusively by influenza A (*7*). The onset of the 2022–23 influenza epidemic, with cocirculation of influenza A and B, was reflected in positive wastewater samples as of mid-December.

The off-season peak of respiratory syncytial virus (RSV) in the spring of 2021, visible in clinical samples at UZL and in data reported by Sciensano, was reflected in positive wastewater samples during March–July 2021 (Figure 1, panel B). We detected RSV in almost all wastewater samples from

Author affiliations: KU Leuven Rega Institute, Louvain, Belgium (A. Rector, M. Bloemen, M. Thijssen, M. Van Ranst, E. Wollants); KU Leuven Academic Center for General Practice, Louvain (B. Pussig); University Hospitals Leuven, Louvain (K. Beuselinck, M. Van Ranst).

DOI: https://doi.org/10.3201/eid3001.231011

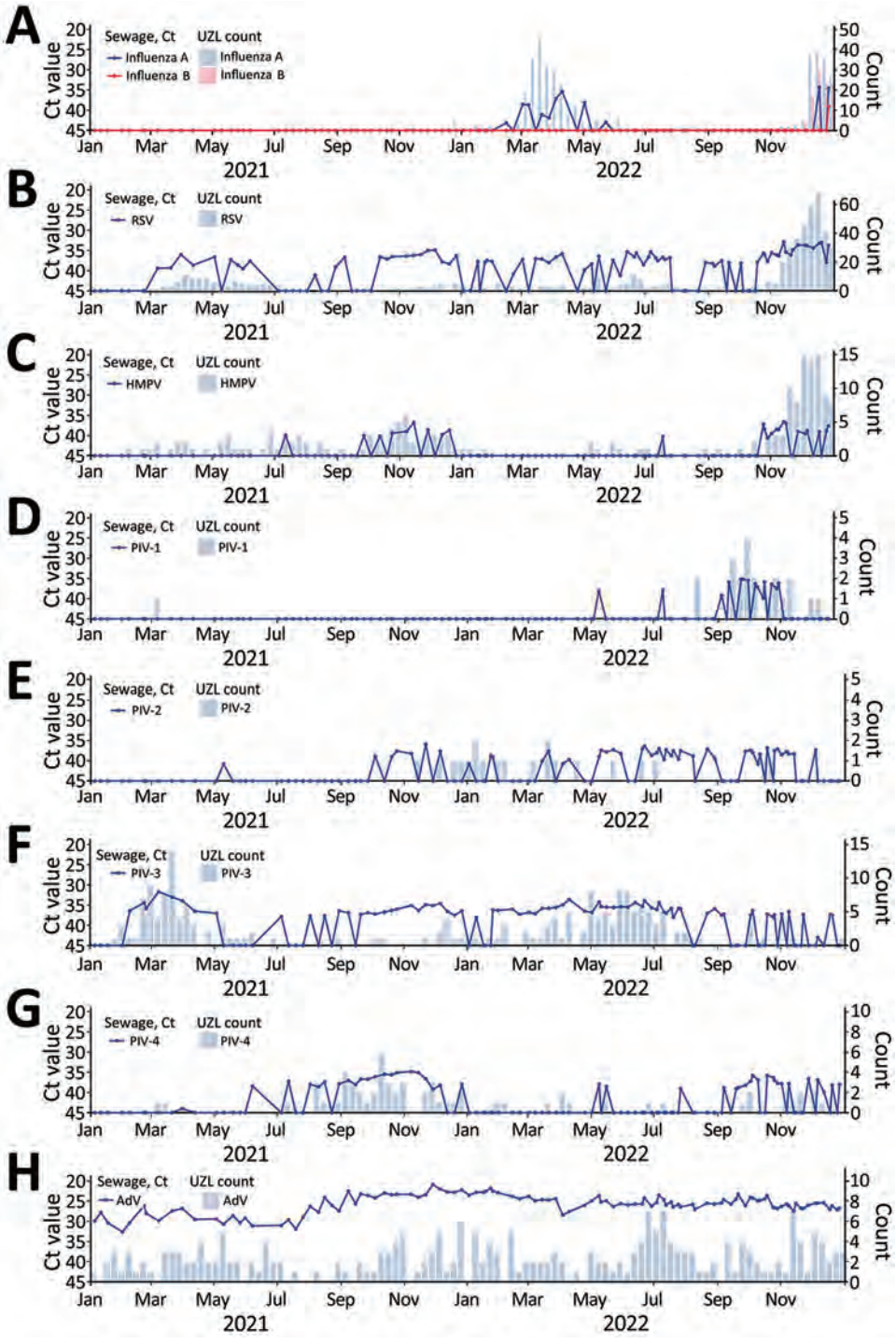

Figure 1. Respiratory viruses measured in wastewater versus positive clinical samples, Leuven, Belgium, January 2021–December 2022: A) influenza virus; B) RSV; C) HMPV; D) PIV-1; E) PIV-2; F) PIV-3; G) PIV-4; H) AdV. Graphs indicate evolution of viruses detected in wastewater by an in-house–developed multiplex quantitative PCR respiratory panel (line graphs; dots represent individual measurements) and by weekly counts of PCR-positive tests detected at UZL (bar graphs). Plots were generated using R version 4.1.1 (The R Foundation for Statistical Computing, https://www.r-project.org) and the ggplot2 package version 3.3.5 (https://ggplot2.tidyverse.org). A larger version of this figure is available at https://wwwnc.cdc.gov/EID/article/30/1/23-1011-F1.htm. AdV, adenovirus; Ct, cycle threshold; HMPV, human metapneumovirus; PIV, parainfluenzavirus; RSV, respiratory syncytial virus; UZL, University Hospitals Leuven.

mid-October 2021 until the end of July 2022. Data from Sciensano also showed a low continuous RSV presence in the 2021–22 season (*6*). After August 2022, RSV reappeared in wastewater; levels were elevated in November and December 2022. The number of positive clinical samples in UZL and sentinel laboratories remained low until the end of October 2022, followed by a strong RSV epidemic in November and December 2022.

During late September–December 2021, human metapneumovirus was almost continuously detectable in wastewater, which corresponded with high numbers of positive samples at UZL (Figure 1, panel C). Human metapneumovirus reappeared in wastewater

in late October 2022, followed by an increase in positive samples at UZL in November and December.

Parainfluenzavirus (PIV) type 1 was predominantly found in wastewater samples during fall 2022, coinciding with a rise in positive cases at UZL. PIV-2 was sporadically detected in wastewater beginning in fall 2021, corresponding with low positive case numbers at UZL during November 2021–November 2022. PIV-3 was almost always detected in wastewater samples; a clear peak occurred during February–May 2021, in concordance with positive sample numbers at UZL. PIV-4 was detectable during August–December 2021 and September–December 2022, and occurred sporadically in between. The data also demonstrated an association with numbers of positive samples at UZL (Figure 1, panels D–G).

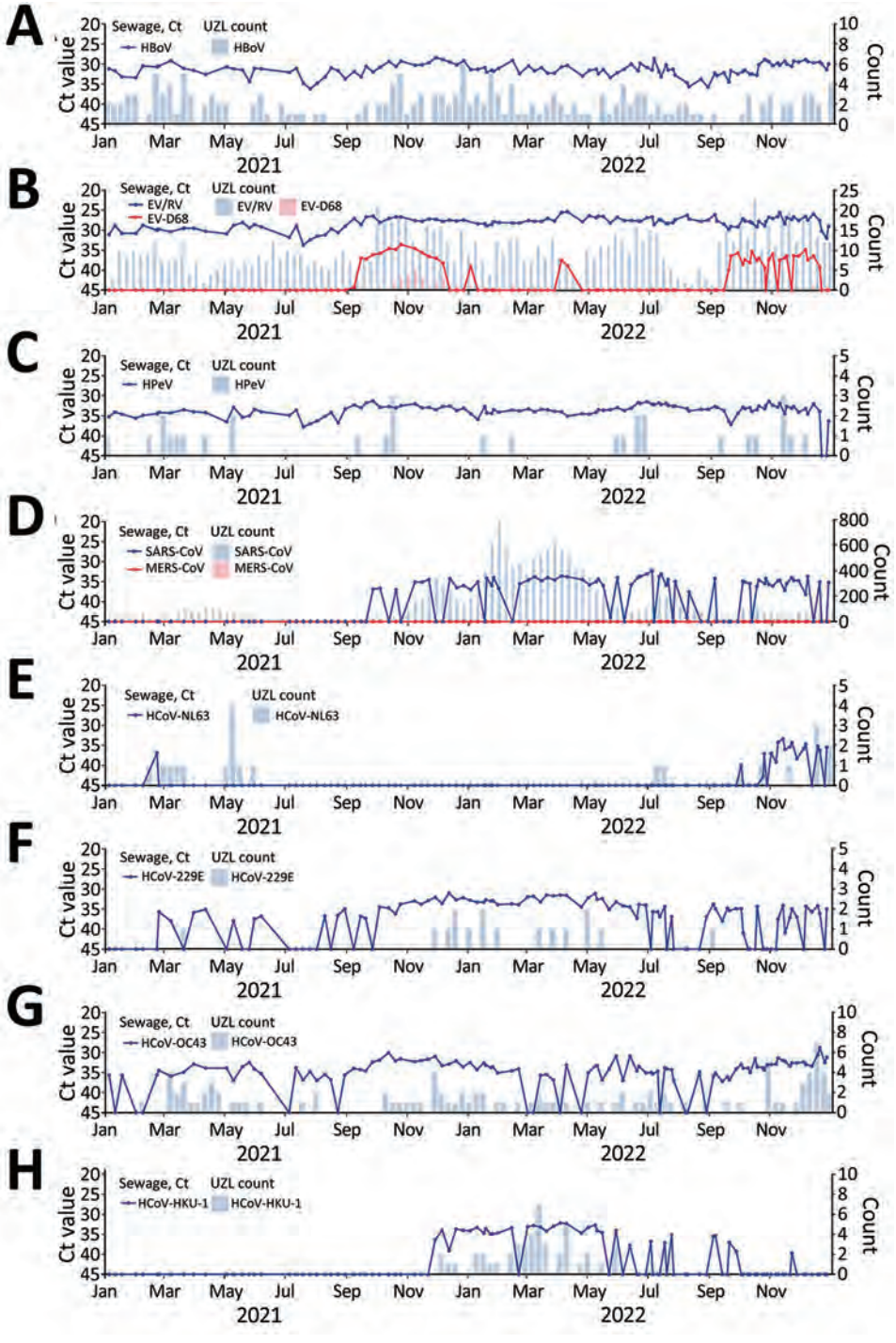

Figure 2. Respiratory viruses measured in wastewater versus number of positive clinical samples, Leuven, Belgium, January 2021–December 2022: A) HBoV; B) EV/RV and EV-D68; C) HPeV; D) SARS-CoV-1; SARS-CoV-2; and MERS-CoV; E) HCoV-NL63; F) HCoV-229E; G) HCoV-OC43; H) HCoV-HKU-1. Graphs indicate evolution of viruses detected in wastewater by an in-house–developed multiplex quantitative PCR respiratory panel (line graphs; dots represent individual measurements) and by weekly counts of PCR-positive tests detected at UZL (bar graphs). Plots were generated using R version 4.1.1 (The R Foundation for Statistical Computing, https://www.r-project.org) and the ggplot2 package version 3.3.5 (https://ggplot2.tidyverse.org). A larger version of this figure is available at https://wwwnc.cdc.gov/EID/article/30/1/23-1011-F2.htm. Ct, cycle threshold; EV, enterovirus; HBoV, bocavirus; HCoV, human coronavirus; HPeV, parechovirus; MERS-CoV, Middle East respiratory syndrome coronavirus; RV, rhinovirus; UZL, University Hospitals Leuven.

We detected adenovirus and human bocavirus (HBoV) consistently and in high concentrations in all wastewater samples (Figure 1, panel H; Figure 2, panel A). That finding is consistent with continuous adenovirus circulation in 2020–21 and 2021–22 reported by Sciensano and with our previous study on ARI samples, in which adenovirus infections were detected year-round (*8*). The continuous high-level detection of adenovirus and HBoV in wastewater does not align with the low numbers of positive samples found in ARI patients at UZL. Of the 4 HBoV genotypes, HBoV1 is mainly associated with respiratory symptoms in children with ARI and HBoV2 is linked to gastroenteritis (*9*,*10*). All HBoV genotypes are known to be present in stool and can frequently be detected in wastewater samples (*11*). Adenovirus infections can cause gastrointestinal symptoms, even when the primary site of involvement is the respiratory tract (*12*). The presence of HBoV and adenovirus in wastewater samples is likely linked to enteric rather than respiratory infections.

Enterovirus/rhinovirus were continuously detected in wastewater, but enterovirus D68 (EV-D68) was only present during early September–December 2021; the highest concentrations were detected in October 2021 (Figure 2, panel B). Those findings suggest a regional EV-D68 outbreak during fall 2021, in line with increasing EV-D68 infections in Europe in September 2021 (*13*). At UZL, 33 EV-D68–positive samples were detected during the study period, most during October 2021–January 2022. In mid-September 2022, EV-D68 reappeared in wastewater; only a small number of positive samples were reported at UZL. Detection of EV-D68 in wastewater preceded positive cases in the same region, indicating that wastewater surveillance can be used as a sensitive early warning signal for EV-D68 circulation.

Human parechovirus (HPeV) infections are common in children; illness can range from gastroenteritis and respiratory infections to neurologic disease, particularly in neonates (*14*). We detected HPeV consistently in almost all wastewater samples throughout the study but detected few positive clinical samples (Figure 2, panel C). HPeV's presence in wastewater could be associated with enteric infections or paucisymptomatic respiratory infections with limited spillover to hospitals.

The SARS-CoV assay in the respiratory panel did not detect SARS-CoV-2 until late September 2021 (Figure 2, panel D). This assay targets a conserved region in the open reading frame 1ab polyprotein gene to enable detection of SARS-CoV-1 and SARS-CoV-2, resulting in a lower sensitivity. That lower sensitivity was observed in validation experiments on clinical samples but did not negatively affect accuracy in routine clinical practice (*4*). The assay is, however, not sensitive enough for environmental surveillance. Of the 4 endemic seasonal coronaviruses infecting humans, human coronavirus (HCoV) NL63 was primarily detected in wastewater during fall and winter of 2022, whereas HCoV-229E and HCoV-OC43 were present in most samples year-round. HCoV-HKU-1 was mainly detected between winter of 2021 and summer of 2022; all positive clinical samples were also reported during this period (Figure 2, panels E–H). Low numbers of HCoV positive clinical samples were detected in UZL, particularly for HCoV-NL63 and HCoV-229E, likely because of the mild nature of endemic coronavirus infections (typically not requiring hospitalization) rather than because of absence of circulation.

Conclusions

By using an in-house respiratory panel to test a 2-year wastewater sample collection, we effectively detected the presence and seasonal variations of most tested respiratory viruses. These findings demonstrate wastewater sampling's potential for population-level pathogen monitoring and early outbreak detection, addressing limitations associated with limited sentinel laboratory data. Our study underscores the role of wastewater-based epidemiology in supplementing clinical surveillance for respiratory viruses, enhances understanding of community virus circulation, and supports public health efforts.

This article was published as a preprint at https://www.medrxiv.org/content/10.1101/2022.10.24.22281437v1.

Acknowledgments

We thank the staff of the Aquafin wastewater treatment plant in Leuven for collecting the wastewater samples.

About the Author

Dr. Rector is a senior researcher at the KU Leuven Rega Institute for Medical Research, Leuven, Belgium. Her primary research interests are the molecular evolutionary virology and epidemiology of respiratory viruses, with a focus on respiratory syncytial virus.

References

1. Agrawal S, Orschler L, Schubert S, Zachmann K, Heijnen L, Tavazzi S, et al. Prevalence and circulation patterns of

SARS-CoV-2 variants in European sewage mirror clinical data of 54 European cities. Water Res. 2022;214:118162. https://doi.org/10.1016/j.watres.2022.118162
2. Medema G, Heijnen L, Elsinga G, Italiaander R, Brouwer A. Presence of SARS-Coronavirus-2 RNA in sewage and correlation with reported COVID-19 prevalence in the early stage of the epidemic in the Netherlands. Environ Sci Technol Lett. 2020;7:511–6. https://doi.org/10.1021/acs.estlett.0c00357
3. Rector A, Bloemen M, Thijssen M, Delang L, Raymenants J, Thibaut J, et al. Monitoring of SARS-CoV-2 concentration and circulation of variants of concern in wastewater of Leuven, Belgium. J Med Virol. 2023;95:e28587. https://doi.org/10.1002/jmv.28587
4. Raymenants J, Geenen C, Budts L, Thibaut J, Thijssen M, De Mulder H, et al. Indoor air surveillance and factors associated with respiratory pathogen detection in community settings in Belgium. Nat Commun. 2023;14:1332. https://doi.org/10.1038/s41467-023-36986-z
5. UZ Leuven. Weekly detection results of respiratory pathogens at UZ Leuven [in Dutch] [cited 2023 Apr 4]. https://www.uzleuven.be/nl/laboratoriumgeneeskunde/wekelijkse-detectieresultaten-respiratoire-pathogenen
6. Sciensano. Acute respiratory infections bulletin [cited 2023 Apr 04]. https://www.sciensano.be/en/health-topics/acute-respiratory-tract-infection/numbers
7. Flu News Europe. Joint ECDC–WHO weekly influenza update, week 20/2022 [cited 2023 May 4]. https://flunewseurope.org/Archives
8. Ramaekers K, Keyaerts E, Rector A, Borremans A, Beuselinck K, Lagrou K, et al. Prevalence and seasonality of six respiratory viruses during five consecutive epidemic seasons in Belgium. J Clin Virol. 2017;94:72–8. https://doi.org/10.1016/j.jcv.2017.07.011
9. Lu QB, Wo Y, Wang HY, Huang DD, Zhao J, Zhang XA, et al. Epidemic and molecular evolution of human bocavirus in hospitalized children with acute respiratory tract infection. Eur J Clin Microbiol Infect Dis. 2015;34:75–81. https://doi.org/10.1007/s10096-014-2215-7
10. De R, Liu L, Qian Y, Zhu R, Deng J, Wang F, et al. Risk of acute gastroenteritis associated with human bocavirus infection in children: A systematic review and meta-analysis. PLoS One. 2017;12:e0184833. https://doi.org/10.1371/journal.pone.0184833
11. Booranathawornsom T, Pombubpa K, Tipayamongkholgul M, Kittigul L. Molecular characterization of human bocavirus in recycled water and sewage sludge in Thailand. Infect Genet Evol. 2022;100:105276. https://doi.org/10.1016/j.meegid.2022.105276
12. Lynch JP III, Kajon AE. Adenovirus: epidemiology, global spread of novel serotypes, and advances in treatment and prevention. Semin Respir Crit Care Med. 2016; 37:586–602.
13. Benschop KSM, Albert J, Anton A, Andrés C, Aranzamendi M, Armannsdóttir B, et al. Re-emergence of enterovirus D68 in Europe after easing the COVID-19 lockdown, September 2021. Euro Surveill. 2021;26:2100998. https://doi.org/10.2807/1560-7917.ES.2021.26.45.2100998
14. Harvala H, Simmonds P. Human parechoviruses: biology, epidemiology and clinical significance. J Clin Virol. 2009;45:1–9.

Address for correspondence: Elke Wollants, Rega Instituut, KU Leuven Campus Gasthuisberg, O&N Rega, Herestraat 49 box 1040, 3000 Leuven, Belgium; email: elke.wollants@kuleuven.be

Excess Deaths Associated with Rheumatic Heart Disease, Australia, 2013–2017

Ingrid Stacey, Rebecca Seth, Lee Nedkoff, Vicki Wade, Emma Haynes, Jonathan Carapetis, Joseph Hung, Kevin Murray, Dawn Bessarab, Judith Katzenellenbogen

During 2013–2017, the mortality rate ratio for rheumatic heart disease among Indigenous versus non-Indigenous persons in Australia was 15.9, reflecting health inequity. Using excess mortality methods, we found that deaths associated with rheumatic heart disease among Indigenous Australians were probably substantially undercounted, affecting accuracy of calculations based solely on Australian Bureau of Statistics data.

Rheumatic heart disease (RHD), caused by *Streptococcus pyogenes* infections, is driven by social determinants of health and disproportionately affects Aboriginal and Torres Strait Islanders in Australia (hereafter Indigenous Australians), causing premature illness and death (*1*–*3*). Deaths associated with RHD can be prevented by addressing poor living conditions, treatment delays, racism, and healthcare inaccessibility (*2*,*4*–*6*). Approximately 663 deaths associated with RHD among Indigenous Australians are predicted for 2016–2031 (*7*). Our previous analysis of persons from 5 jurisdictions in Australia who had RHD, were <65 years of age, and died during 2013–2017 (covering 86% of the Indigenous population) revealed that RHD was the underlying cause of death for only 15.0%; cause of death was recorded as underlying noncardiovascular for 42.7%, and cause of death among Indigenous Australians was missing for 13.7% (*2*). Thus, the burden of death associated with RHD is potentially underestimated when measured by using RHD-coded death records from the Australian Bureau of Statistics (ABS). Concerns regarding inaccurate or missing cause-of-death data can be reduced by using excess mortality methods, which measure deaths directly and indirectly attributable to RHD (*8*). Consequently, we used excess mortality methods, independent of ABS RHD-coded records, to estimate RHD-associated deaths for 2013–2017 in Australia.

Author affiliations: The University of Western Australia, Perth, Western Australia, Australia (I. Stacey, L. Nedkoff, E. Haynes, J. Carapetis, J. Hung, K. Murray, D. Bessarab, J. Katzenellenbogen); Curtin University, Perth, Western Australia (R. Seth); Victor Chang Cardiac Research Institute, Darlinghurst, New South Wales, Australia (L. Nedkoff); National Heart Foundation of Australia, East Sydney, New South Wales, Australia (V. Wade); Telethon Kids Institute, Nedlands, Western Australia, Australia (J. Carapetis, J. Katzenellenbogen)

DOI: https://doi.org/10.3201/eid3001.230905

The Study

In a cross-sectional study, we used linked administrative health and ABS data to estimate RHD-related deaths (Figure 1). We estimated observed mortality rates by age at death and Indigenous status by using data from End RHD in Australia: Study of Epidemiology (ERASE) (*9*). We used the generated excess deaths rates to calculate expected RHD-associated deaths and compared them with ABS RHD-coded death counts.

The ERASE cohort has been described (*2*). In brief, prevalent and new RHD cases were identified from the RHD register, surgical registry, and hospitalization records (*1*,*9*,*11*,*12*). ERASE included 5 jurisdictions in Australia: Northern Territory, Queensland, South Australia, Western Australia, and New South Wales (Appendix Figure 1, https://wwwnc.cdc.gov/EID/article/30/1/23-0905-App1.pdf). We obtained probabilistically linked data from jurisdiction-specific linkage units; ERASE investigators harmonized variables between jurisdictions and data sources and determined vital status.

To create the RHD study cohort, we selected ERASE cohort members who had RHD, were <65 years of age, and were alive on January 1, 2013 (Figure 1). We used broad age groups (0–24, 25–44, and 45–64 years), which corresponded to those used in

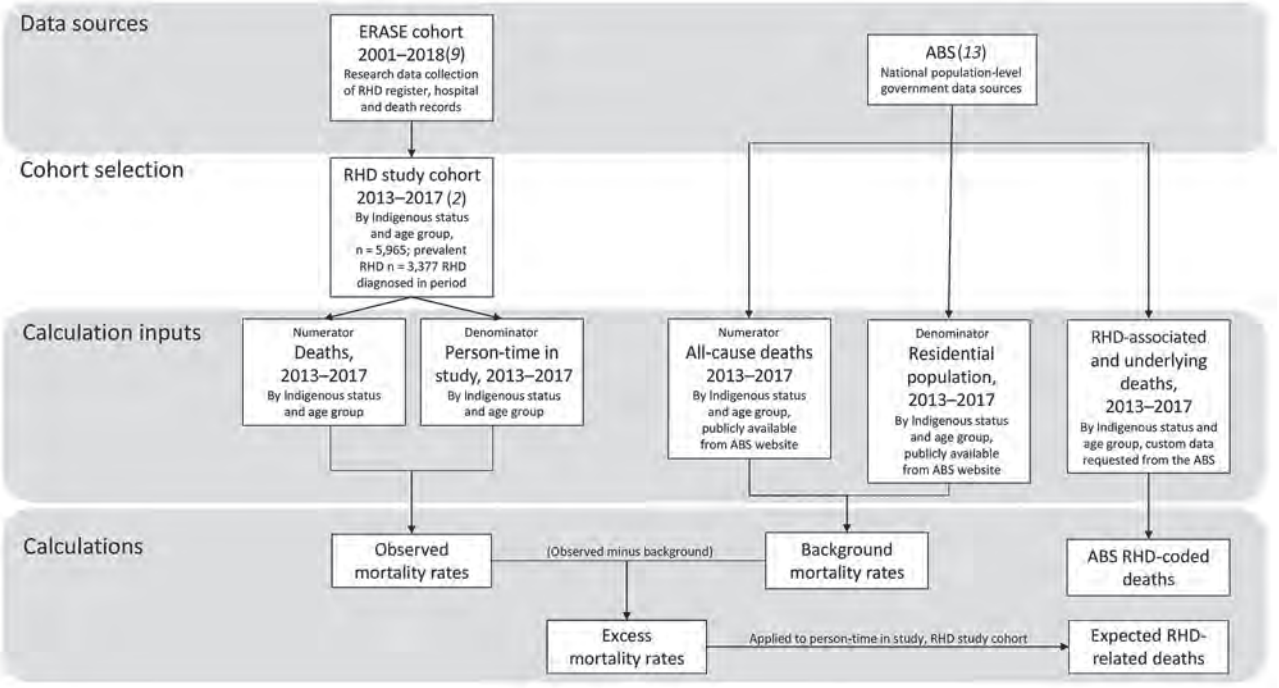

Figure 1. Data sources, cohort selection, and calculations generated in study of excess deaths associated with rheumatic heart disease, Australia, 2013–2017 (*2*,*9*,*10*). The main study outputs are observed mortality rates, excess mortality rates, and expected RHD-associated deaths (bottom row). ABS, Australian Bureau of Statistics; RHD, rheumatic heart disease.

previous RHD mortality studies (*2*,*13*). We used multiple ERASE data sources to assign Indigenous status, minimizing known underidentification (*9*). We searched all hospitalization record diagnosis fields for comorbidities (Appendix Table 1).

We calculated observed and background mortality rates (both crude and age-specific per 100,000 person-years). We calculated age-standardized mortality rates by using the direct method, standardized to World Health Organization World Standard Population 5-year age groupings for 2000–2025. For observed mortality rates (Figure 1), RHD diagnoses from January 1, 2013, through December 31, 2017, contributed person-time from whichever time was latest (denominators): first diagnosis date or January 1, 2013. Deaths during 2013–2017 contributed to observed mortality rate numerators. For background mortality rates (Figure 1), we used age group–specific deaths of Indigenous and non-Indigenous Australians (numerators) and residential population denominators from the ABS (*13*).

We calculated excess mortality rates as the difference between the observed and background mortality rates (within matched age/population stratum; Figure 1). We derived 95% CIs by using nonparametric bootstrap methods, assuming a Poisson distribution (Appendix). We calculated expected RHD-related deaths by applying excess mortality rates to person-years within the RHD study cohort age/population stratum (Appendix Table 2). We calculated observed and excess mortality rate ratios (MRRs) with 95% CIs by comparing Indigenous with non-Indigenous populations with RHD.

Epidemiologic, demographic, and clinical characteristics of this cohort are described (Appendix Table 3). Among the 9,342 persons in the RHD study cohort (65.6% female, 24.6% <25 years of age, 55.6% Indigenous), comorbidities included atrial fibrillation (30.5%), heart failure (26.0%), hypertension (23.7%), diabetes (19.4%), chronic kidney disease (17.4%), and chronic obstructive pulmonary disease (10.6%) (Appendix Table 3). The 726 observed cohort deaths occurred most frequently among persons 45–64 years of age (72.3%) and among those who were female (58.7%) (Appendix Table 3). Among the 325 non-Indigenous persons who died, 36.0% were immigrants from low/middle income countries. Metropolitan residents accounted for 14.0% (n = 56) of deaths among Indigenous and 71.4% (n = 232) among non-Indigenous persons. Detailed causes of death within the study cohort were attributed to mostly noncardiovascular causes; most frequent were cancer, diabetes mellitus, and respiratory diseases (*2*).

In 2013–2017 in Australia, the background mortality rate was 193.6 deaths/100,000 Indigenous person-years and 72.3 deaths/100,000 non-Indigenous

Table. Mortality rates associated with RHD among persons <65 years of age, Australia, 2103–2017*

Age group, y	Indigenous		Non-Indigenous		Rate ratio (95% CI)
	No.	Rate (95% CI)	No.	Rate (95% CI)	
Background mortality rates†					
0–24	1,319	70.4 (66.7–74.4)	8282	32.6 (32.0 –33.4)	2.16 (2.03–2.29)
25–44	2,302	262.87 (252.2–273.8)	17,004	74.20 (73.1– 75.3)	3.54 (3.29–3.60)
45–64	5,221	921.66 (896.8 –947.0)	69,752	344.26 (341.7–346.8)	2.68 (2.60–2.75)
Crude, 0–64	8,842	266.83 (261.3– 272.4)	95,038	138.64 (137.8–139.5)	1.92 (1.88–1.97)
ASMR, 0–64	8,842	193.55 (189.5– 197.6)	95,038	72.29 (71.8– 72.7)	2.68 (2.66–2.70)
Observed mortality rates‡					
0–24	13	204.1 (93.2–315.1)	<5	339.4 (0–723.4)	NC
25–44	112	1,238.3 (1,009.0–1,467.7)	34	858.4 (569.8–1,146.9)	1.44 (0.98–2.12)
45–64	276	4,568.6 (4,029.6–5,107.6)	288	2,140.1 (1,892.9–2,387.3)	2.13 (1.81–2.52)
Crude, 0–64	401	1,869.1 (1,687.9–2,050.4)	325	1,775.7 (1,584.4–1,967.1)	1.05 (0.91–1.22)
ASMR, 0–64	401	1,451.6 (1,307.0–1,596.2)	325	883.6 (674.3–1,092.9)	1.64 (1.42–1.9)
Excess mortality rates§					
0–24	9¶	136.7 (39.3–249.0)	<5¶	308.40 (0–751.3)	NC
25–44	88¶	1,000.2 (786.4–1230.9)	29¶	760.7 (487.8–1,047.3)	1.31 (1.02–2.31)
45–64	222¶	3,720.4 (3,184.8–4305.8)	240¶	1,817.8 (1,566.9–2,066.8)	2.05 (1.81–2.5)
Crude, 0–64	319¶	1,636.7 (1,459.8–1822.1)	272¶	1,646.7 (1,454.5–1,847.4)	0.99 (0.85–1.16)
ASMR, 0–64	319¶	1,166.0 (1,028.8–1317.6)	272¶	770.8 (584.3–989.0)	1.51 (1.14–2.02)
ABS RHD-coded mortality rates#					
0–24	8	0.43 (0.13–0.72)	7	0.03 (0.01–0.05)	15.49 (5.62–42.71)
25–44	48	5.48 (3.93–7.03)	41	0.18 (0.12–0.23)	30.64 (20.19–46.48)
45–64	89	15.71 (12.45–18.98)	252	1.24 (1.09–1.40)	12.63 (9.92–16.09)
Crude, 0–64	145	4.38 (3.66–5.09)	300	0.44 (0.39–0.49)	10.00 (8.20–12.19)
ASMR, 0–64	145	5.25 (4.40–6.11)	300	0.33 (0.29–0.37)	15.85 (13.00–19.33)

*Rates are deaths/100,000 person-years; intervals for excess mortality rates were obtained from bootstrapping of estimates (interpreted as 95% CIs).
ABS, Australian Bureau of Statistics; ASMR, age-standardized mortality rate; NC, not calculated (numbers too low for reliable estimate); RHD, rheumatic heart disease.
†Population level, n = 14,372,851.
‡Deaths from all causes within the RHD study cohort (n = 9,342).
§Observed mortality rates minus background mortality rates.
¶Expected number of deaths associated with RHD were calculated on the basis of excess mortality rate applied to person-years within appropriate age/population strata.
#Whole population. Previously published data, reproduced with permission (*2*). Population-level mortality rates based on ABS RHD-coded data (RHD as an underlying or associated cause of death).

person-years (Table). Background age-specific mortality rates increased with advancing age in both populations but were always 2- to 3-fold higher for the Indigenous than non-Indigenous population (Table, Figure 2).

In the RHD study cohort, 401 Indigenous and 325 non-Indigenous persons died, corresponding to observed mortality rates of 1,451 deaths/100,000 Indigenous person-years and 883 deaths/100,000 non-Indigenous person-years (Table). Age-specific mortality rates among Indigenous persons were highest among those 45–64 years of age (4,568 deaths/100,000 person-years; Figure 2); corresponding MRR was 2.13 (95% CI, 1.81–2.52) for Indigenous versus non-Indigenous persons (Table).

For the RHD study cohort, we estimated excess mortality rates of 1,166 deaths/100,000 Indigenous person-years and 771 deaths/100,000 non-Indigenous person-years, generating an MRR of 1.5 (Table). Excess mortality rates were highest among Indigenous persons 45–64 years of age for whom the peak excess MRR of 2.1 was observed (Table; Figure 2). Excess mortality rates applied to RHD study cohort strata estimated that 319 Indigenous and 272 non-Indigenous deaths were directly or indirectly associated with RHD (Table; Appendix Table 4). By comparison,

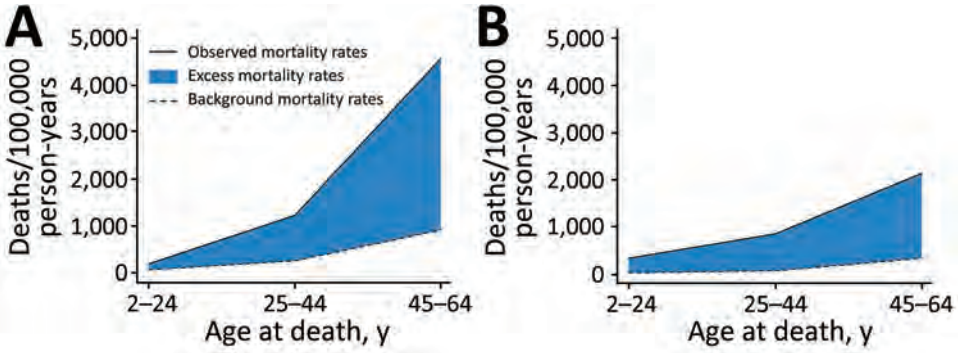

Figure 2. Excess RHD-associated mortality by Indigenous status and age at death, Australia, 2013–2017. A) Indigenous; B) non-Indigenous. Background mortality rates (from the Australian Bureau of Statistics) were subtracted from the observed mortality rates (in the RHD study cohort), generating excess mortality rates (the direct and indirect RHD-associated mortality rate). RHD, rheumatic heart disease.

ABS RHD-coded deaths captured 145 Indigenous deaths, less than half the expected cases (174 fewer than expected), but 300 non-Indigenous deaths, approximately the same as expected (28 more).

Accuracy of our estimates is limited by the quality of the coded information within source datasets and constrained by available data, including nonavailability of migrant population denominator information for rate calculations. The RHD mortality rates that we report also do not capture the profound effects that those deaths had on families, communities, and cultures.

Conclusions

After adjusting for background mortality in Indigenous and non-Indigenous populations, we found that excess deaths were higher among persons with RHD. The excess mortality method applied to the RHD study cohort estimates both direct and indirect RHD-associated deaths and reduces concerns regarding misclassified and missing cause of death arising from use of ABS RHD-coded data only. Our method is particularly useful with the Indigenous population, for whom missing ABS RHD-coded data are an issue. RHD is probably not the only underlying driver of observed excess premature deaths; rather, RHD is a potent marker of the inequities experienced by Indigenous Australians and drives excess deaths indirectly in synergy with other chronic health conditions associated with social determinants. Expected deaths among non-Indigenous persons corresponded closely to ABS RHD-coded records; however, among the Indigenous population, excess deaths were more than twice those recorded in ABS (*2*). Similar to other chronic illnesses (diabetes and dementia [*10*,*14*]), the burden of RHD-associated deaths in Australia is potentially underascertained when based exclusively on ABS RHD-coded records, especially among Indigenous persons, for whom cause-of-death data are missing for >10% and multiple comorbidities, along with underlying RHD, contribute to death (*2*). Before Australia can achieve its RHD elimination goals, improved quality of Indigenous cause-of-death data and identification of synergistic factors contributing to excess RHD-associated deaths are needed (*7*).

Acknowledgments

We thank ABS for providing the customized aggregated RHD-coded death data, in particular Lauren Moran for her expert review. We also thank the staff of the data linkage units of the state and territory governments (Western Australia, South Australia–Northern Territories, New South Wales, Queensland) for linkage of the ERASE project data. We thank the State and Territory Registries of Births, Deaths and Marriages, the State and Territory Coroners, and the National Coronial Information System and the Victorian Department of Justice for enabling Cause of Death Unit Record File data to be used for this project. Furthermore, we thank the data custodians and data managers for providing inpatient hospital and emergency department data (5 states and territories), RHD registers (5 states and territories), the Australian and New Zealand Society of Cardiac and Thoracic Surgeons Cardiac Surgery Database (single registry covering 5 states and territories), the Royal Melbourne Children's Hospital Paediatric Cardiac Surgery database (single data source for RHD pediatric patients from South Australia and Northern Territory receiving surgical intervention in Melbourne), and the Northern Territory Department of Health primary healthcare data.

The Human Research Ethics Committees of the Health Departments of participating Australian jurisdictions provided approval for the ERASE project, which is registered on the Australian New Zealand Clinical Trials Registry (ACTRN12620000981921). Aboriginal Ethics Committee approval was sought in jurisdictions where operational and support letters were received from peak bodies of the Aboriginal Community Controlled Health Services.

This work was supported by funding from the National Health and Medical Research Council through project grant no. 1146525 and seed funds from the End Rheumatic Heart Disease Centre for Research Excellence and HeartKids.

I.S. is supported by a National Health and Medical Research Council Postgraduate Scholarship (grant no. 2005398) and an ad hoc postgraduate scholarship from The University of Western Australia. J.K. and L.N. are supported by National Heart Foundation Future Leader Fellowships (nos. 102043, 105038).

About the Author

Ms. Stacey is a cardiovascular epidemiologist with a background in biostatistics and a PhD candidate within the Cardiovascular Epidemiology Research Centre, School of Population and Global Health, at the University of Western Australia. Her research interest is using linked administrative data to investigate disease progression and complications associated with acute rheumatic fever and RHD among youth in Australia.

References

1. Katzenellenbogen JM, Bond-Smith D, Seth RJ, Dempsey K, Cannon J, Stacey I, et al. Contemporary incidence and prevalence of rheumatic fever and rheumatic heart disease in Australia using linked data: the case for policy change. J Am Heart Assoc. 2020;9:e016851. https://doi.org/10.1161/JAHA.120.016851

2. Stacey I, Seth R, Nedkoff L, Hung J, Wade V, Haynes E, et al. Rheumatic heart disease mortality in Indigenous and non-Indigenous Australians between 2013 and 2017. Heart. 2023;109:1025–33. https://doi.org/10.1136/heartjnl-2022-322146
3. Stacey I, Hung J, Cannon J, Seth RJ, Remenyi B, Bond-Smith D, et al. Long-term outcomes following rheumatic heart disease diagnosis in Australia. Eur Heart J Open. 2021;1:oeab035.
4. Colquhoun SM, Condon JR, Steer AC, Li SQ, Guthridge S, Carapetis JR. Disparity in mortality from rheumatic heart disease in Indigenous Australians. J Am Heart Assoc. 2015;4:e001282. https://doi.org/10.1161/JAHA.114.001282
5. Coroners Court of Queensland. Inquest into the deaths of Yvette Michelle Wilma Booth, Adele Estelle Sandy, Shakaya George ("RHD Doomadgee Cluster") 2023 [cited 2023 Jul 1]. https://www.courts.qld.gov.au/courts/coroners-court
6. Wade V, Stewart M. Bridging the gap between science and Indigenous cosmologies: Rheumatic Heart Disease Champions4Change. Microbiol Aust. 2022;43:89–92. https://doi.org/10.1071/MA22030
7. Wyber R, Noonan K, Halkon C, Enkel S, Cannon J, Haynes E, et al.; END RHD CRE Investigators Collaborators. Ending rheumatic heart disease in Australia: the evidence for a new approach. Med J Aust. 2020;213(Suppl 10):S3–31. https://doi.org/10.5694/mja2.50853
8. Dickman PW, Adami HO. Interpreting trends in cancer patient survival. J Intern Med. 2006;260:103–17. https://doi.org/10.1111/j.1365-2796.2006.01677.x
9. Katzenellenbogen JM, Bond-Smith D, Seth RJ, Dempsey K, Cannon J, Nedkoff L, et al.; ERASE Collaboration Study Group. The End Rheumatic Heart Disease in Australia Study of Epidemiology (ERASE) Project: data sources, case ascertainment and cohort profile. Clin Epidemiol. 2019;11:997–1010. https://doi.org/10.2147/CLEP.S224621
10. Gao L, Calloway R, Zhao E, Brayne C, Matthews FE; Medical Research Council Cognitive Function and Ageing Collaboration. Accuracy of death certification of dementia in population-based samples of older people: analysis over time. Age Ageing. 2018;47:589–94. https://doi.org/10.1093/ageing/afy068
11. Bond-Smith D, Seth R, de Klerk N, Nedkoff L, Anderson M, Hung J, et al. Development and evaluation of a prediction model for ascertaining rheumatic heart disease status in administrative data. Clin Epidemiol. 2020;12:717–30. https://doi.org/10.2147/CLEP.S241588
12. Katzenellenbogen JM, Nedkoff L, Canon J, Kruger D, Pretty F, Carapetis JR, et al. Low positive predictive value of ICD-10 codes in relation to rheumatic heart disease: a challenge for global surveillance. Int Med J. 2019;49:400–3. https://doi.org/10.1111/imj.14221
13. Australian Bureau of Statistics. National, state, and territory population [cited 2020 Dec 9]. https://www.abs.gov.au/statistics/people/population/national-state-and-territory-population
14. Whittall DE, Glatthaar C, Knuiman MW, Welborn TA. Deaths from diabetes are under-reported in national mortality statistics. Med J Aust. 1990;152:598–600. https://doi.org/10.5694/j.1326-5377.1990.tb125391.x

Address for correspondence: Ingrid Stacey, Cardiovascular Epidemiology Research Centre, School of Population and Global Health, M431 Clifton Street Bldg, Clifton St, Nedlands, Western Australia 6009, Australia; email: ingrid.stacey@uwa.edu.au

Delayed *Plasmodium falciparum* Malaria in Pregnant Patient with Sickle Cell Trait 11 Years after Exposure, Oregon, USA

Wendi Drummond, Kathleen Rees, Stephen Ladd-Wilson, Kimberly E. Mace, Douglas Blackall, Melissa Sutton

Delayed *Plasmodium falciparum* malaria in immigrants from disease-endemic countries is rare. Such cases pose a challenge for public health because mosquitoborne transmission must be rigorously investigated. We report a case of delayed *P. falciparum* malaria in a pregnant woman with sickle cell trait 11 years after immigration to the United States.

Plasmodium falciparum malaria is a major cause of illness and death worldwide (*1*). In disease-hyperendemic areas, most of the population are parasitemic (*2*). Chronic exposure results in partial immunity, and sickle cell trait reduces the severity of infection (*3*,*4*). Delayed *P. falciparum* malaria after immigration to nonendemic countries has been reported in the literature, and pregnancy is the most common risk factor for this unusual presentation (*5*).

Former residents of disease-endemic areas who have *P. falciparum* malaria without recent travel risk present a public health challenge because locally acquired mosquitoborne transmission of the parasite must be ruled out, given the widespread distribution of *Anopheles* spp. mosquito vectors in the United States (*6*–*8*). We report the clinical and public health investigation of a case of delayed *P. falciparum* malaria in a pregnant woman 11 years after immigration to the United States from sub-Saharan Africa.

Author affiliations: Providence Portland Medical Center, Portland, Oregon, USA (W. Drummond); Washington County Health and Human Services, Hillsboro, Oregon, USA (K. Rees); Oregon Health Authority, Portland (S. Ladd-Wilson, M. Sutton); Centers for Disease Control and Prevention, Atlanta, Georgia, USA (K.E. Mace); Providence Oregon Core Laboratory, Portland (D. Blackall)

DOI: https://doi.org/10.3201/eid3001.231231

The Study

The patient was a 20–30-year-old multiparous pregnant woman from sub-Saharan Africa who came to an emergency department at Providence Portland Medical Center, Portland, Oregon, USA, during her third trimester; she had inadequate prenatal care and a 2-week history of loose stools and abdominal pain before defecation. She reported chills and night sweats without fevers. She denied nausea, vomiting, epigastric pain, runny nose, cough, sore throat, lymphadenopathy, dysuria, or vaginal discharge. The patient was tachycardic; fetal heart rate (FHR) tracing showed a normal FHR, moderate variability, accelerations, and late and variable decelerations. Initial laboratory evaluation on the woman showed microcytic anemia, leukocytopenia, thrombocytopenia, and an increased level of bilirubin (Table).

Testing results were negative for HIV, SARS-CoV-2, influenza, hepatitis B, hepatitis C, rubella, and syphilis. The result of a rapid point-of-care BinaxNOW malaria test (Abbott Laboratories, https://www.globalpointofcare.abbott) was positive for *P. falciparum.* Thick and thin malaria blood smears showed *P. falciparum* (Figure 1). Initial parasitemia was 0.2%. We submitted blood smears to the Division of Parasitic Diseases and Malaria diagnostic laboratory, Center for Global Health, Centers for Disease Control and Prevention, and *P. falciparum* morphologic identification was confirmed. A pretreatment blood sample was not available for molecular speciation or whole-genome sequencing.

We initiated a 3-day course of artemether/lumefantrine, and percentage parasitemia decreased to 0.1% within 24 hours. No parasites were observed by day 3 of therapy. The patient received intravenous fluids and 1 unit of packed red blood cells. Maternal tachycardia resolved, and FHR tracing displayed normal FHR with moderate variability,

Table. Pregnant patient laboratory values at initial clinical evaluation (day 0) and at discharge (day 5), Washington County, Oregon, USA, July–September 2022

Laboratory test	Day 0	Day 5
Hemoglobin	9.1 g/dL	8.8 g/dL
Hematocrit	27.9 g/dL	27.9 g/dL
Mean corpuscular volume	70.8 fL	72.5 fL
Leukocyte count	3.6 × 10^9/L	7.3 × 10^9/L
Platelet count	91.0 × 10^9/L	102.0 × 10^9/L
Total bilirubin	2.23 mg/dL	0.92 mg/dL (day 3)

accelerations, and resolution of decelerations. The patient's anemia and thrombocytopenia improved, and her leukocyte count normalized. The patient gave birth to a healthy postterm infant without evidence of placental insufficiency. Placental pathologic analysis showed sickled maternal erythrocytes, pigment in perivillous fibrin, and mild lymphocytic deciduitis without immunohistochemical evidence of parasites.

The patient immigrated to the United States with her family 11 years before she sought care. She had lived in a metropolitan area of Oregon during the 5 years before she sought care and denied any history of foreign or domestic travel. The patient reported a history of malaria during childhood 19 years earlier, for which treatment was received while living in sub-Saharan Africa. She denied any history of blood transfusions or recent insect bites. The most recent visit to the patient's home by a person from sub-Saharan Africa occurred 2 years before her illness. She had a history of anemia during previous pregnancies, and her first pregnancy was complicated by thrombocytopenia and preeclampsia. She had a history of sickle cell trait diagnosed by hemoglobin fractionation.

We explored the plausibility of local malaria transmission by evaluating current mosquito surveillance data and conducting case finding with temporospatial proximity to the case. The investigation was anchored to month of symptom onset (September 2022). We used mapping to visualize spatial associations between mosquito surveillance, malaria case reports, syndromic surveillance, and death surveillance (Figure 2).

Anopheles freeborni and *An. punctipennis* mosquitoes were identified during Washington County Public Health's 2022 Mosquito Control trapping season, May–September 2022. However, during the period of our investigation, temperatures had decreased, and *Anopheles* mosquitos were not active in the area. *P. falciparum* case finding within the statewide reportable disease database showed 1 travel-associated malaria case with an onset 2 months before this patient and ≈4 miles away. There was no epidemiologic link between the cases; whole blood was not available to identify microsatellite parasite signatures. A search of Oregon's Electronic Surveillance System for the Early Notification of Community-Based Epidemics for emergency department encounters with a discharge diagnosis of fever of unknown origin (FUO) showed greater than expected activity in the week of the patient's onset of symptoms (*9*). However, the trend was not isolated to the proximity of the case-patient, and many encounters noted manifestations consistent with viral infections.

An Early Notification of Community-Based Epidemics query for mosquito bites and arboviral diseases did not show greater than expected activity. A vital records query for deaths with an associated diagnosis of FUO showed 1 death temporospatially related to the case. Medical record review by the Malaria Branch, Center for Global Health, Division of Parasitic Diseases and Malaria, Centers for Disease Control and Prevention, ruled out the death as related to malaria due to clinical and laboratory incompatibility. Thus, there was no evidence to support local mosquitoborne transmission.

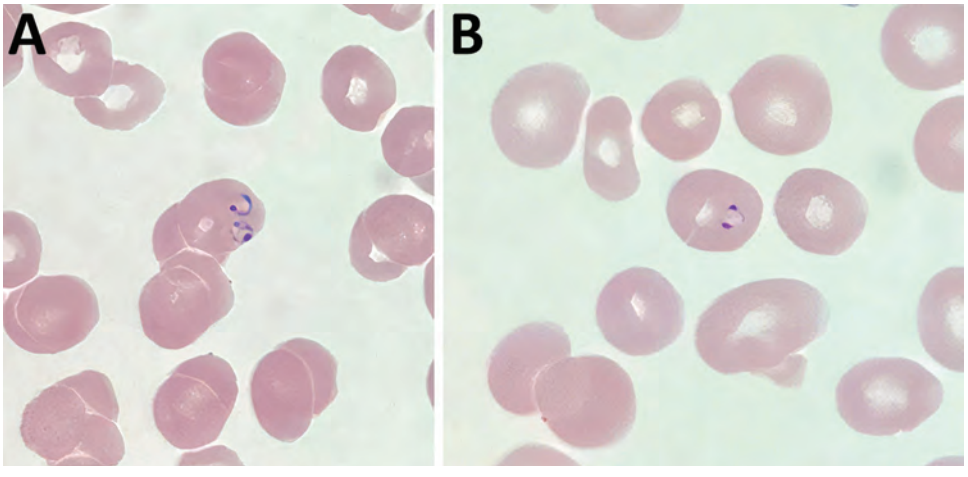

Figure 1. Representative thin blood smears showing *Plasmodium falciparum* in pregnant patient, Washington County, Oregon, USA, July–September 2022. Ring-form trophozoites, morphologically consistent with *P. falciparum*, were identified. A) Multiply-infected erythrocyte showing an applique form; B) ring form showing 2 chromatin dots (headphone form). Original magnification x1,000.

Conclusions

We report a case of *P. falciparum* malaria in a pregnant woman 11 years after immigration from sub-Saharan Africa to the United States. To assess for local mosquitoborne transmission, a joint state and local public health investigation examined mosquito surveillance data, performed case finding for additional malaria cases, and reviewed syndromic surveillance and death surveillance for FUO diagnoses with temporospatial proximity to the case. This comprehensive assessment enabled the public health departments to effectively evaluate local mosquitoborne transmission and emerging local risk.

Although delayed *P. falciparum* illness has been documented, it remains rare, and the patient's latency period was unusually long at 11 years. In 1 case series and literature review, pregnancy was the most prevalent risk factor associated with delayed presentation and reports of delayed presentation in pregnant women ranged from 3 months to 4 years (*5*). Delayed *P. falciparum* in persons from disease-endemic regions is believed to arise from persistent low-level parasitemia and decaying *P. falciparum*-specific immunity (*5*). In pregnant women, pregnancy-related immunosuppression, sequestration of *P. falciparum* parasites in the placenta, and, possibly, placental antigen expression might increase the risk for delayed *P. falciparum* presentation (*10*–*12*). The patient's sickle cell trait might have also contributed to the latency of her delayed presentation. Sickle cell trait protects against severe disease from *P. falciparum* infection and is associated with lower parasite densities and delayed malaria (*13*,*14*).

Most malaria cases in the United States are related to travel to a disease-endemic region. However, malaria can rarely be acquired locally through mosquito bite, transfusion, or other parenteral route, transplantation, or during pregnancy or childbirth (*15*). Our case-patient had no known history of transfusion or transplantation, and her infant did not show development of malaria. Although the patient denied traveling to a disease-endemic area, she was not available for follow-up, and we were unable to verify travel history through a passport review. Therefore, undisclosed travel to a malaria-endemic country remains an unlikely possibility.

Malaria should be considered in all patients from disease-endemic regions who have compatible symptoms regardless of time since exposure. Clinical suspicion should be heightened in persons who have underlying risk factors for delayed manifestation, including pregnancy, immunosuppression, and sickle cell trait. To rule out the possibility that a patient without recent travel risk acquired malaria locally, rigorous public health investigation is required. Components of an investigation might include medical and travel record review, environmental surveillance, case finding, and syndromic and death surveillance with consideration of temporospatial proximity to the case.

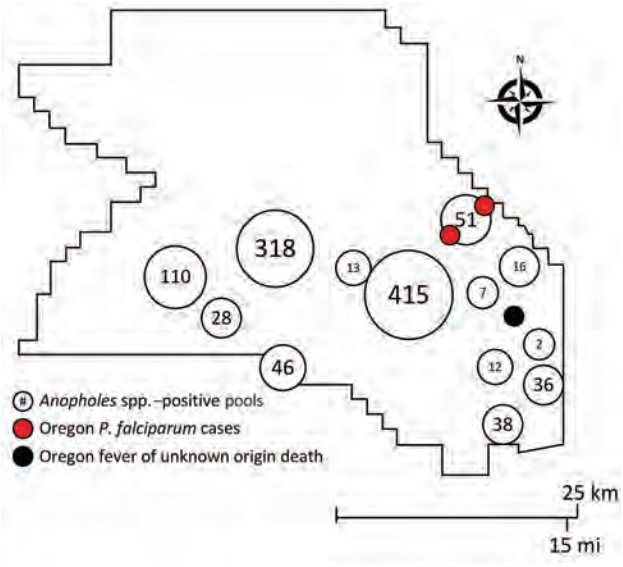

Figure 2. Number of *Anopheles* spp.–positive pools, *Plasmodium falciparum*–positive cases, and fever of unknown origin deaths, Washington County, Oregon, USA, July–September 2022.

Acknowledgment

We thank William Ryan for examining the patient's placenta and providing support in coordinating further evaluation with the Centers for Disease Control and Prevention.

About the Author

Dr. Drummond is an infectious disease specialist and a medical director for infection prevention at Providence Portland Medical Center, Portland, Oregon. Her primary research interests are management of infections in immunocompromised patients and complex pulmonary infections.

References

1. Hay SI, Guerra CA, Tatem AJ, Noor AM, Snow RW. The global distribution and population at risk of malaria: past, present, and future. Lancet Infect Dis. 2004;4:327–36. PubMed https://doi.org/10.1016/S1473-3099(04)01043-6
2. Smith DL, Guerra CA, Snow RW, Hay SI. Standardizing estimates of the *Plasmodium falciparum* parasite rate. Malar J. 2007;6:131. https://doi.org/10.1186/1475-2875-6-131
3. Doolan DL, Dobaño C, Baird JK. Acquired immunity to malaria. Clin Microbiol Rev. 2009;22:13–36. https://doi.org/10.1128/CMR.00025-08

4. Williams TN, Mwangi TW, Roberts DJ, Alexander ND, Weatherall DJ, Wambua S, et al. An immune basis for malaria protection by the sickle cell trait. PLoS Med. 2005;2:e128. https://doi.org/10.1371/journal.pmed.0020128
5. Dauby N, Figueiredo Ferreira M, Konopnicki D, Nguyen VTP, Cantinieaux B, Martin C. Case report: delayed or recurrent *Plasmodium falciparum* malaria in migrants: a report of three cases with a literature review. Am J Trop Med Hyg. 2018;98:1102–6. https://doi.org/10.4269/ajtmh.17-0407
6. Isaäcson M. Airport malaria: a review. Bull World Health Organ. 1989;67:737–43.
7. Sinka ME, Bangs MJ, Manguin S, Coetzee M, Mbogo CM, Hemingway J, et al. The dominant *Anopheles* vectors of human malaria in Africa, Europe and the Middle East: occurrence data, distribution maps and bionomic précis. Parasit Vectors. 2010;3:117. https://doi.org/10.1186/1756-3305-3-117
8. Dye-Braumuller KC, Kanyangarara M. Malaria in the USA: how vulnerable are we to future outbreaks? Curr Trop Med Rep. 2021;8:43–51. https://doi.org/10.1007/s40475-020-00224-z
9. Burkom H, Loschen W, Wojcik R, Holtry R, Punjabi M, Siwek M, et al. Electronic surveillance system for the early notification of community-based epidemics (ESSENCE): overview, components, and public health applications. JMIR Public Health Surveill. 2021;7:e26303. https://doi.org/10.2196/26303
10. Kattenberg JH, Ochodo EA, Boer KR, Schallig HD, Mens PF, Leeflang MM. Systematic review and meta-analysis: rapid diagnostic tests versus placental histology, microscopy and PCR for malaria in pregnant women. Malar J. 2011;10:321. https://doi.org/10.1186/1475-2875-10-321
11. Mayor A, Moro L, Aguilar R, Bardají A, Cisteró P, Serra-Casas E, et al. How hidden can malaria be in pregnant women? Diagnosis by microscopy, placental histology, polymerase chain reaction and detection of histidine-rich protein 2 in plasma. Clin Infect Dis. 2012;54:1561–8. https://doi.org/10.1093/cid/cis236
12. Hviid L, Staalsoe T. Late recrudescence of *Plasmodium falciparum* malaria in pregnancy. Int J Infect Dis. 2006;10:412. https://doi.org/10.1016/j.ijid.2005.10.013
13. Aidoo M, Terlouw DJ, Kolczak MS, McElroy PD, ter Kuile FO, Kariuki S, et al. Protective effects of the sickle cell gene against malaria morbidity and mortality. Lancet. 2002;359:1311–2. https://doi.org/10.1016/S0140-6736(02)08273-9
14. Crompton PD, Traore B, Kayentao K, Doumbo S, Ongoiba A, Diakite SA, et al. Sickle cell trait is associated with a delayed onset of malaria: implications for time-to-event analysis in clinical studies of malaria. J Infect Dis. 2008;198:1265–75. https://doi.org/10.1086/592224
15. Mace KE, Lucchi NW, Tan KR. Malaria surveillance—United States, 2018. MMWR Surveill Summ. 2022;71:1–35. https://doi.org/10.15585/mmwr.ss7108a1

Address for correspondence: Melissa Sutton, Public Health Division, Oregon Health Authority, 800 NE Oregon St, Ste 772, Portland, OR 97232, USA; email: melissa.sutton@oha.oregon.gov

etymologia revisited

Petri Dish

[pe'tre 'dish]

The Petri dish is named after the German inventor and bacteriologist Julius Richard Petri (1852–1921). In 1887, as an assistant to fellow German physician and pioneering microbiologist Robert Koch (1843–1910), Petri published a paper titled "A minor modification of the plating technique of Koch." This seemingly modest improvement (a slightly larger glass lid), Petri explained, reduced contamination from airborne germs in comparison with Koch's bell jar.

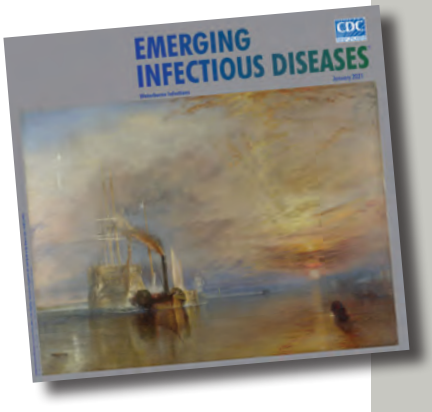

Originally published in January 2021

References

1 Central Sheet for Bacteriology and Parasite Science [in German]. Biodiversity Heritage Library. Volume 1, 1887 [cited 2020 Aug 25]. https://www.biodiversitylibrary.org/item/210666#page/313/mode/1up
2. Petri JR. A minor modification of the plating technique of Koch [in German]. Cent für Bacteriol und Parasitenkd. 1887;1:279–80.
3. Shama G. The "Petri" dish: a case of simultaneous invention in bacteriology. Endeavour. 2019;43:11–6. DOIExternal
4. The big story: the Petri dish. The Biomedical Scientist. Institute of Biomedical Science [cited 2020 Aug 25]. https://thebiomedicalscientist.net/science/big-story-petri-dish

https//wwwnc.cdc.gov/eid/article/27/1/et-2701_article

Genomic Diversity and Zoonotic Potential of *Brucella neotomae*

Gilles Vergnaud, Michel S. Zygmunt, Roland T. Ashford, Adrian M. Whatmore, Axel Cloeckaert

After reports in 2017 of *Brucella neotomae* infections among humans in Costa Rica, we sequenced 12 strains isolated from rodents during 1955–1964 from Utah, USA. We observed an exact strain match between the human isolates and 1 Utah isolate. Independent confirmation is required to clarify *B. neotomae* zoonotic potential.

The genus *Brucella* comprises a monophyletic group including 6 classical species showing clonal evolution: *B. abortus*, *B. suis*, *B. melitensis*, *B. canis*, *B. ovis*, *and B. neotomae* (*1*,*2*). The zoonotic potential of *B. melitensis*, *B. abortus*, *B. suis*, and *B. canis* (in decreasing order of disease burden in human populations) has been clinically established on the basis of numerous human cases reported over the past century.

B. neotomae was originally isolated from a single rodent species (desert woodrat, *Neotoma lepida*), in an area with low population density of other wild animals and remote from domestic livestock (*3*). Recently, 2 publications described the isolation in Costa Rica of *B. neotomae* strains from 2 human patients with brucellosis (*4*,*5*). According to those reports, the 2 human isolates, bneohCR1 and bneohCR2, differed from each other by 164 single-nucleotide polymorphisms (SNPs); bneohCR1 differed from the *B. neotomae* genome used as reference in the analysis (GenBank accession no. GCA_000742255) by 174 and bneohCR2 by 160 SNPs. Those data indicated that *B. neotomae* has zoonotic potential and is present in a much wider geographic area than previously reported.

Author affiliations: Université Paris-Saclay, Institute for Integrative Biology of the Cell, Gif-sur-Yvette, France (G. Vergnaud); Institut National de l'Agriculture, de l'Alimentation et de l'Environnement, Unité Mixte de Recherche Infectiologie et Santé Publique, Université de Tours, Nouzilly, France (M.S. Zygmunt, A. Cloeckaert); Animal and Plant Health Agency, Weybridge, UK (R.T. Ashford, A.M. Whatmore)

DOI: https://doi.org/10.3201/eid3001.221783

Because that finding was unexpected and has substantial implications regarding our understanding of *Brucella*, we further investigated available information regarding the neglected species *B. neotomae*. We reviewed the literature for previous studies in which *B. neotomae* strains were isolated and searched public sequence repositories for *B. neotomae* whole-genome sequence (WGS) datasets. In addition, we identified and sequenced available *B. neotomae* strains maintained since the 1960s in 2 *Brucella* strain collections, the UK Animal and Plant Health Agency (APHA) Weybridge collection and the *Brucella* Culture Collection Nouzilly (BCCN) of the Institut National de l'Agriculture, de l'Alimentation et de l'Environnement (INRAE; National Research Institute for Agriculture, Food and the Environment) in France. We report a comprehensive comparative analysis of all genome sequences we identified from databanks and the human cases from Costa Rica, to further shed light on the genetic relationships between those isolates.

The Study

We recovered 17 *B. neotomae* WGS datasets from public repositories as assemblies or raw reads (last accessed May 31, 2023): ERR1894830, GCA_000158715, GCA_000712255, GCA_000742255, GCA_900446125, SRR004305, SRR004306, SRR032598, SRR857216, SRR4038991 (all 10 strains 5K33), ERR2993140 (MLVA31), GCA_900446115, SRR4038990 (5E1169), GCA_900446105 (6D152), ERR473742 (babohCR62), ERR1845156 (bneohCR2), and ERR1845155 (bneohCR1) (Appendix Table 2, https://wwwnc.cdc.gov/EID/article/30/1/22-1783-App1.pdf). We merged 3 records (SRR004305, SRR004306, SRR032598) corresponding to the same biosample.

The *Brucella* strain collection maintained by APHA contained 5 and INRAE/BCCN, 7 *B. neotomae* strains (*6*,*7*). We recorded APHA and corresponding BCCN identifiers for each strain (Appendix Table 1). We produced and analyzed sequence data (Appendix). The 12 *B. neotomae* sequence datasets produced for

this report were SRR22273182–8 (BCCN collection corresponding to primary names 6G152, 5E1169, 5E1266, 7E1260, 6H8988, and 5G239 and 1 unknown primary name) and SRR22414766–70 (APHA collection corresponding to primary names 7E164 and 5E1266 and 3 unknown primary names). We deposited sequences in the National Center for Biotechnology BioProject database as PRJNA901374 (BCCN) and PRJNA905663 (APHA) (Appendix Table 2).

We generated a maximum parsimony tree from the 149 SNPs identified among the 27 *B. neotomae* sequence datasets, including 15 public and 12 newly sequenced WGS datasets (Figure 1; Appendix Tables 1, 2). The whole-genome SNP (wgSNP) genotype of the most recent common ancestor (MRCA) of known *B. neotomae* lineages descends into 2 groups (Figure 1): the group containing type strain 5K33 corresponds to sequence type (ST) 22 in the *Brucella* multilocus sequence typing scheme MLST21, the other to ST120 (*7*). The limited available information about the sampling site of each strain from rodents in the Great Salt Lake Desert in Utah, USA, is consistent with congruence between *B. neotomae* phylogeny and the geography of the Great Salt Lake region, but further data are needed to robustly test this association (Appendix).

We show a different representation of the wgSNP phylogenetic analysis after removal of duplicates and of 1 dataset with relatively lower coverage (Figure 2; GenBank accession no. GCA_900446105 from strain 6D152). Because we removed the WGS datasets with partial coverage, the new tree contained 205 SNPs. The distances from MRCA to tips were similar: maximum 76 SNPs (to strain 7E1260) and minimum 56 SNPs (to strain APHA#65–197). The 3 whole-genome datasets from Costa Rica, including the human isolates bneohCR1 and bneohCR2 and the isolate babohCR62 entered as *B. abortus* in the European Nucleotide

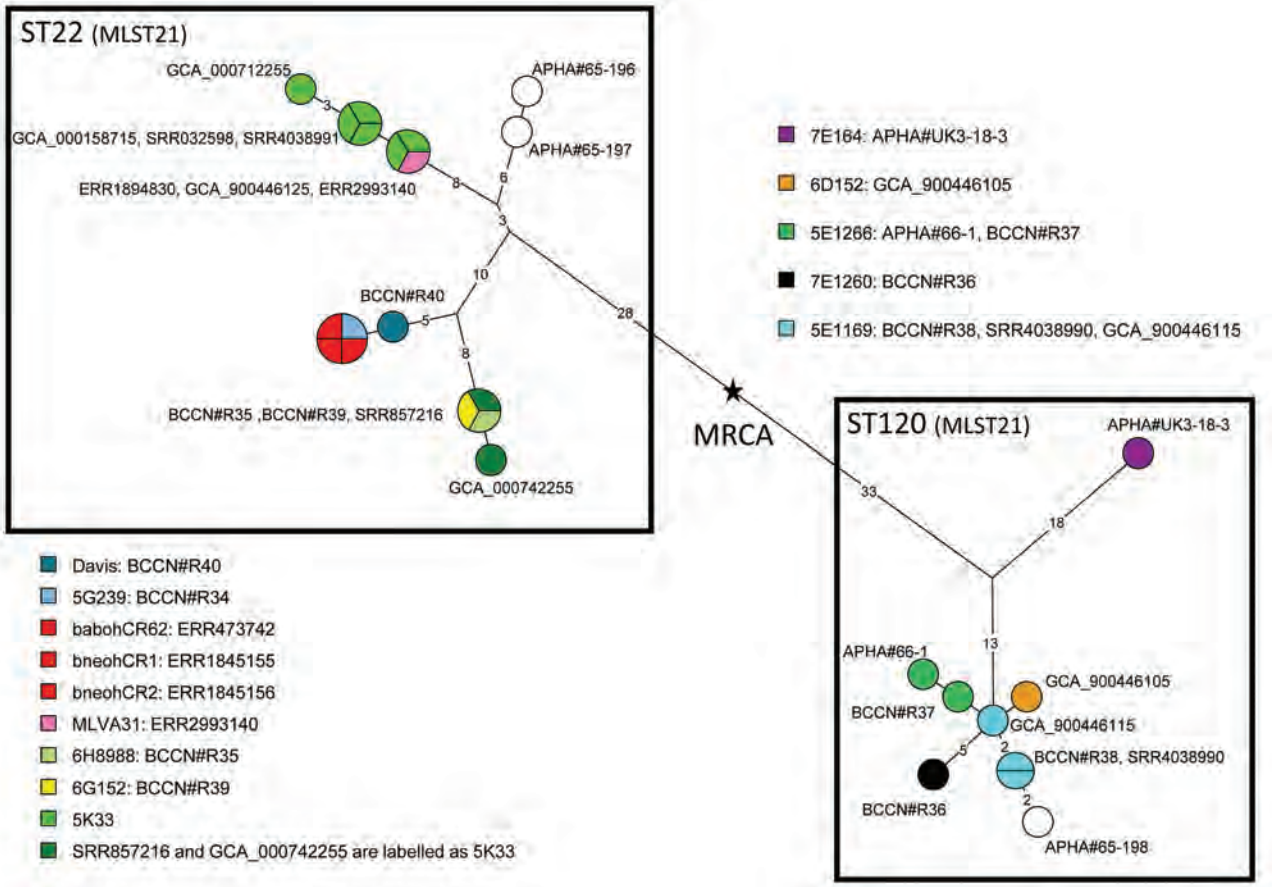

Figure 1. *Brucella neotomae* phylogeny. Maximum parsimony tree was derived from wgSNP data. We investigated 27 datasets and identified 149 SNPs; tree size is 151 substitutions (homoplasy 1.5%). Circles are colored according to primary strain identifier; red indicates the 3 datasets from Costa Rica. Circles are labeled with an accession number or collection strain identifier (*Brucella* Culture Collection Nouzilly [BCCN]) or Animal and Plant Health Agency [APHA] Weybridge collections). Branch lengths >1 substitution are indicated. Black star shows the position of the hypothetical MRCA. Box indicates the 2 MLST21 STs. MLST, multilocus sequence typing; MRCA, most recent common ancestor; SNP, single-nucleotide polymorphism; ST, sequence type; wgSNP, whole-genome single-nucleotide polymorphism.

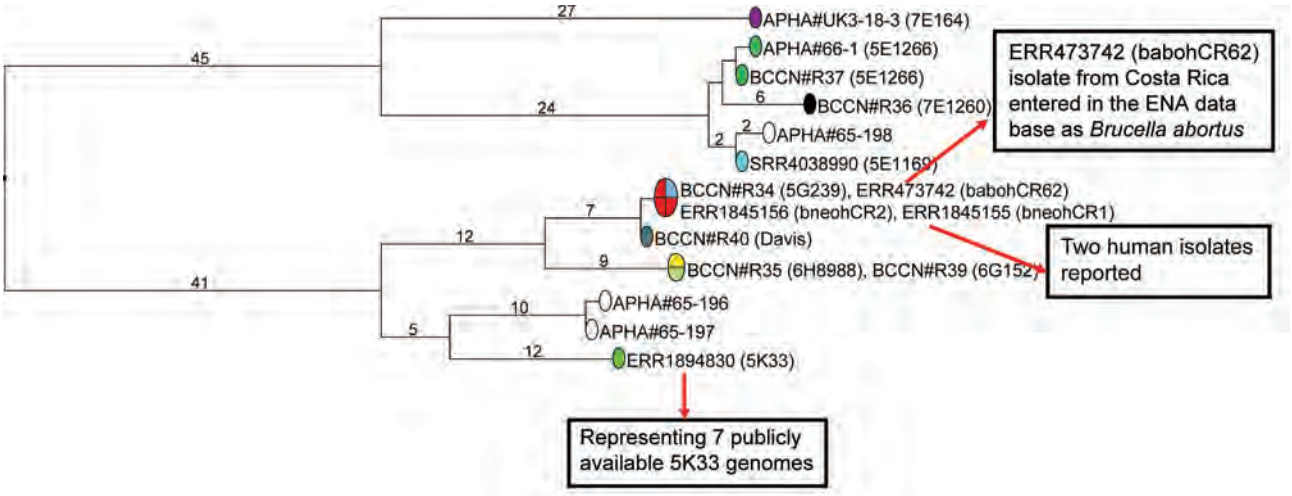

Figure 2. Rooted *Brucella neotomae* phylogeny of 16 selected datasets. Maximum parsimony tree was derived from wgSNP data; 205 SNPs in tree, tree size 207 substitutions (homoplasy 1%). Branch lengths >1 substitution are indicated. Circles are colored according to primary strain identity; red indicates the 3 datasets from Costa Rica. Circles are labeled with an accession number or collection strain identifier (*Brucella* Culture Collection Nouzilly [BCCN] or Animal and Plant Health Agency [APHA] Weybridge collections). Primary strain identifier is indicated in brackets when available. ENA, European Nucleotide Archive; SNP, single-nucleotide polymorphism; wgSNP, whole-genome SNP.

Archive database, remained identical in wgSNP genotype to strain 5G239 (BCCN#R34) in spite of the increased resolution. We still observed a coincident wgSNP genotype when we considered only these 4 strains, in sharp contrast with a report of human cases that indicated the corresponding genomes differed by 164 SNPs (*4*).

Conclusions

Our findings demonstrate that the strains isolated during 1955–1964 in the Great Salt Lake Desert in Utah display notable intraspecies genetic diversity despite being isolated from a geographically limited location, within a limited time frame, and from the same host species. In contrast, the datasets from wgSNP analysis of isolates from Costa Rica were identical despite having been isolated 4 years apart and in different areas of Costa Rica (*5*). Of note, datasets from analysis of isolates from Costa Rica were identical to data from 1 *B. neotomae* strain, 5G239, from the Great Salt Lake region. Finding an identical genotype in human cases from Costa Rica >3,000 km and >50 years apart in a different species from the Great Salt Lake discovery is remarkable in light of the diversity of strains noted in the geographically limited location in Utah and reported absence of rats of genus *Neotoma* in Costa Rica (*5*). Full understanding of the zoonotic potential of *B. neotomae* requires further exploration, including additional sampling of rodents and human cases in the US Southwest and Central America.

Work conducted at INRAE and University Paris-Saclay was supported in part by ANR (Agence Nationale de la Recherche; French National Research Agency) ASTRID-maturation project ANR-14-ASMA-0002 (Global surveillance of infectious agents: molecular typing kits and databases–MicroType). Work conducted at UK APHA was supported in part by the One Health EJP project (JRP-17–IDEMBRU: Identification of emerging Brucella species: new threats for human and animals; grant agreement no. 773830).

About the Author

Dr. Vergnaud is a research associate at University Paris-Saclay, Gif-sur-Yvette, France. His research interests currently focus on the evolution and phylogeography of a number of dangerous bacterial pathogens.

References

1. Whatmore AM, Foster JT. Emerging diversity and ongoing expansion of the genus *Brucella.* Infect Genet Evol. 2021;92:104865. https://doi.org/10.1016/j.meegid.2021.104865
2. Whatmore AM, Perrett LL, MacMillan AP. Characterisation of the genetic diversity of *Brucella* by multilocus sequencing. BMC Microbiol. 2007;7:34. https://doi.org/10.1186/1471-2180-7-34
3. Stoenner HG, Holdenried R, Lackman D, Orsborn JS Jr. The occurrence of *Coxiella burnetii*, *Brucella*, and other pathogens among fauna of the Great Salt Lake Desert in Utah. Am J Trop Med Hyg. 1959;8:590–6. https://doi.org/10.4269/ajtmh.1959.8.590
4. Suárez-Esquivel M, Ruiz-Villalobos N, Jiménez-Rojas C, Barquero-Calvo E, Chacón-Díaz C, Víquez-Ruiz E, et al. *Brucella neotomae* infection in humans, Costa Rica. Emerg Infect Dis. 2017;23:997–1000. [Erratum in Emerg Infect Dis. 2017;23:1435.] https://doi.org/10.3201/eid2306.162018

5. Villalobos-Vindas JM, Amuy E, Barquero-Calvo E, Rojas N, Chacón-Díaz C, Chaves-Olarte E, et al. Brucellosis caused by the wood rat pathogen *Brucella neotomae*: two case reports. J Med Case Reports. 2017;11:352. https://doi.org/10.1186/s13256-017-1496-8
6. Vergnaud G, Hauck Y, Christiany D, Daoud B, Pourcel C, Jacques I, et al. Genotypic expansion within the population structure of classical *Brucella* species revealed by MLVA16 typing of 1404 *Brucella* isolates from different animal and geographic origins, 1974–2006. Front Microbiol. 2018;9:1545. https://doi.org/10.3389/fmicb.2018.01545
7. Whatmore AM, Koylass MS, Muchowski J, Edwards-Smallbone J, Gopaul KK, Perrett LL. Extended multilocus sequence analysis to describe the global population structure of the genus *Brucella*: phylogeography and relationship to biovars. Front Microbiol. 2016;7:2049. https://doi.org/10.3389/fmicb.2016.02049

Address for correspondence: Gilles Vergnaud, University Paris-Saclay, Institute for Integrative Biology of the Cell (I2BC), 1 Av de la Terrasse, Blg 24, Rm 02-335, 91190 Gif-sur-Yvette, France; email: gilles.vergnaud@universite-paris-saclay.fr

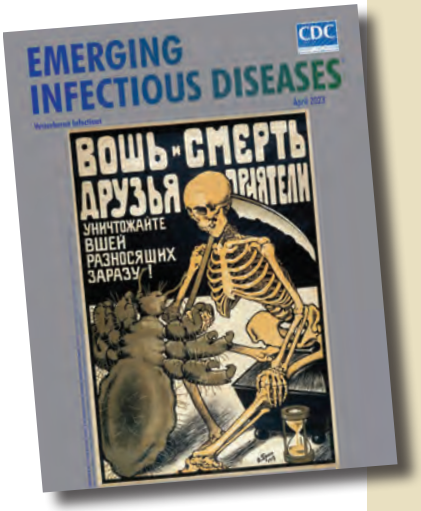

Originally published in April 2023

etymologia revisited

Haematospirillum jordania

[Hae.ma.to.spi.ril'lum jor.da'ni.ae]

For the sesquipedalian term *Haematospirillum*, *Haema* is derived from the Greek haima, meaning blood. *Spirillum* is derived from Medieval Latin in the mid-13th century Latin (*spiralis*), French in the 1550s (*spiral*), and Greek (*speira*). All suggest a winding or coil. A New Latin reference book entry in 1875 implied a little coil (Figure 1).

Isolated from human blood, Haematospirillum jordaniae was reported as a novel genus and species in 2016 by Centers for Disease Control and Prevention (CDC) scientist Ben W. Humrighouse and his laboratory team, which included Jean G. Jordan, a microbiologist (Figure 2). This gram-negative bacterium was isolated 14 times in 10 states during 2003–2012 before its identification in 2016.

H. jordaniae was previously considered an environmental bacterium with limited pathogenicity, but increasing numbers of isolates indicated a possible emerging pathogen. All cases occurred in male patients, and the pathogen showed a predilection for infecting lower leg injuries. In 2018, Hovan and Hollinger reported a case of infection in a Delaware man who, in 2016, had sepsis from a lower leg wound. The organism isolated was identified at the CDC Special Bacteriology Reference Laboratory (SBRL) in the Division of High-Consequence Pathogens and Pathology, National Center for Emerging and Zoonotic Infectious Diseases.

References

1. Hovan G, Hollinger A. Clinical isolation and identification of *Haematospirillum jordaniae*. Emerg Infect Dis. 2018;24:1955–6.
2. Humrighouse BW, Emery BD, Kelly AJ, Metcalfe MG, Mbizo J, McQuiston JR. *Haematospirillum jordaniae* gen. nov., sp. nov., isolated from human blood samples. Antonie van Leeuwenhoek. 2016;109:493–500.
3. LPSN List of prokaryotic names with standing in nomenclature. Species *Haematospirillum jordaniae* [cited 2022 May 21]. https://lpsn.dsmz.de/species/haematospirillum-jordaniae
4. Jean Jordan obituary. Published by the Atlanta Journal-Constitution on May 28, 2014 [cited 2022 Oct 17]. https://www.legacy.com/us/obituaries/atlanta/name/jean-jordan94
5. Pal E, Štrumbelj I, Kišek TC, Kolenc M, Pirš M, Rus KR, et al. *Haematospirillum jordaniae* cellulitis and bacteremia. Emerg Infect Dis. 2022;28:2116–9.
6. Persiana (1875) (Latin Edition): Heckmanns, Alexius. *Spirillum* (n.) [cited 2022 May 21]. https://www.etymoline.com/word/spirillum
7. Weyant RS, Moss CW, Weaver RE. Hollis, Jordan JG, Cook E, et al.; Centers for Disease Control and Prevention. Identification of unusual pathogenic gram-negative aerobic and facultatively anaerobic bacteria. The Orange Book, 2nd ed. Philadelphia: Lippincott Williams and Wilkins; 1996

Increased Peripheral Venous Catheter Bloodstream Infections during COVID-19 Pandemic, Switzerland

Marie-Céline Zanella,[1] Eva Pianca,[1] Gaud Catho, Basilice Obama, Marlieke E.A. De Kraker, Aude Nguyen, Marie-Noëlle Chraiti, Jonathan Sobel, Loïc Fortchantre, Stephan Harbarth, Mohamed Abbas, Niccolò Buetti

Studies suggest that central venous catheter bloodstream infections (BSIs) increased during the COVID-19 pandemic. We investigated catheter-related BSIs in Switzerland and found peripheral venous catheter (PVC) BSI incidence increased during 2021–2022 compared with 2020. These findings should raise awareness of PVC-associated BSIs and prompt inclusion of PVC BSIs in surveillance systems.

Peripheral intravenous catheters (PVCs) and central venous catheters (CVCs) are frequently used in hospitalized patients. Estimates from global device sales illustrated that ≈1.2 billion PVCs are used worldwide annually (*1*,*2*). PVC-related complications include phlebitis, hematoma, and extravasation (*3*,*4*). PVC-associated bloodstream infections (BSIs) often are disregarded in surveillance systems because of low incidence (*5*,*6*). However, because PVCs are widely used in hospitalized patients, the burden of PVC-associated or related BSIs might still be substantial. In contrast, only 10% of acute care inpatients have a CVC inserted (*7*), but the incidence of BSIs associated with CVCs is higher than that for PVCs, likely because infection prevention strategies mostly focus on CVCs.

Several studies have shown that intravascular catheter infections increased during the COVID-19 pandemic (*8*–*11*). Those studies mainly focused on BSIs associated with CVCs. COVID-19 might have substantially affected the frequency of PVC infections, but published reports are lacking. To assess the incidence of BSIs associated with or related to intravenous catheters, we used a large prospective database to study BSIs by catheter type during the COVID-19 pandemic in Switzerland.

The Study

We performed a cohort study at Geneva University Hospitals (HUG), a large network of tertiary care centers in Switzerland. HUG includes 5 rehabilitation or palliative care sites and 1 acute care, 1 geriatric, 1 pediatric, 1 gynecology-obstetrics, and 1 psychiatric site. HUG has ≈2,100 beds and receives 60,000 hospital admissions per year.

We included all patients hospitalized during January 1, 2020–December 31, 2022. All hospital-acquired BSIs during that timeframe were investigated as part of prospective hospital-wide surveillance, which has been conducted for >25 years by the HUG infection control program. We limited the analysis to catheter-related or -associated BSIs (CRABSIs), comprising catheter-related BSI (CRBSI) and catheter-associated BSI (CABSI). We classified CRABSI that were attributed to PVC, short-term CVC, and long-term CVC. The infection control program routinely collects patient data from CRABSI, including onset date, age, sex, ward of acquisition, catheter type, and microorganism identified.

The primary outcomes (i.e., CRABSI) were based on European Centre for Disease Prevention and Control definitions (*12*). A CRBSI required a positive blood culture ≤48 hours after catheter removal and

Author affiliations: Infection Control Programme and World Health Organization Collaborating Center, Geneva University Hospitals and Faculty of Medicine, Geneva, Switzerland (M.-C. Zanella, E. Pianca, G. Catho, B. Obama, M.E.A. De Kraker, A. Nguyen, M.-N. Chraiti, L. Fortchantre, S. Harbarth, M. Abbas, N. Buetti); University of Geneva, Geneva (J. Sobel); MRC Centre for Global Infectious Disease Analysis, Jameel Institute, School of Public Health, Imperial College London, London, UK (M. Abbas); Université Paris-Cité, Paris, France (N. Buetti)

DOI: https://doi.org/10.3201/eid3001.230183

[1]These authors contributed equally to this article.

the same microorganism isolated from a quantitative catheter tip culture or the same microorganism isolated in a culture from pus collected from a catheter site (Appendix, https://wwwnc.cdc.gov/EID/article/30/1/23-0183-App1.pdf). A CABSI required a positive blood culture occurring from time of insertion until 48 hours after catheter removal, resolution of symptoms within 48 hours after catheter removal, and no other infectious focus. We also tracked details of COVID-19 infections reported in the hospital system (Appendix).

We used patient-days as the main denominator, which we extracted from the electronic record system. We used a 5-step statistical plan. First, we determined the total monthly incidence of CRABSI, and CRABSI attributed to PVC, short-term CVC, and long-term CVC per 1,000 patient-days (Figure 1). Second, we evaluated incidence rate ratios (IRRs) for intravascular catheter infections stratified for catheter type for 2021 and 2022 by segmented Poisson regression models using aggregated monthly data and used 2020 as the referent and patient-days as the offset. We tested overdispersion by using the likelihood ratio test and subsequently fit a negative binomial model, if required. Third, we compared patient and microbiologic characteristics of CRABSI attributed to PVC between the different periods using χ^2 test for categorical variables and Kruskal-Wallis test for continuous variables. Fourth, we determined the number of PVCs and PVCs in situ >4 days inserted per month. Fifth, we performed a sensitivity analysis by using catheter-days as a denominator for CRABSI attributed to PVC and CVC.

We used SAS version 9.4 (SAS Institute, Inc., https://www.sas.com) to perform all analyses and considered $p<0.05$ statistically significant. This analysis complies with STROBE guidelines for observational studies (*13*).

During the study period, a total of 179,463 patients were hospitalized at HUG, corresponding to 1,978,177 patient-days. We included 249 CRABSI episodes. We observed 90 CRABSI attributed to PVC, 94 attributed to short-term CVC, 74 attributed to long-term CVC, and 9 cases were possibly attributable to >1 intravascular catheter. Overall, the median age of patients with a CRABSI was 61 (interquartile range [IQR] 47–73) years; 62.3% (n = 155) were male and 37.7% (n = 94) were female. Most (37.8%, n = 94) CRABSI were caused by coagulase-negative staphylococci (Appendix Table 1).

CRABSI incidence remained stable during the study period, but we observed peaks in CRABSI attributed to short-term and long-term CVC during November 2021–January 2022 (Appendix Figure 1). Of note, incidence of CRABSI attributed to PVC increased during late 2021 and in 2022. Similarly, the proportion of CRABSI attributed to PVC among all intravascular catheter infections increased during late 2021 and in 2022 (Figure 1).

Overall, compared with 2020, IRRs for CRABSI did not significantly increase in 2021 (IRR 1.24, 95% CI 0.91–1.71; p = 0.18) and 2022 (IRR 1.19, 95% CI 0.87–1.64; p = 0.27) (Figure 2; Appendix Table 2). By contrast, rates of CRABSI attributed to PVC significantly increased during 2021 (IRR 2.08, 95% CI 1.14–3.78; p = 0.02) and 2022 (IRR 3.23, 95% CI 1.85–5.65; p<0.01) compared with 2020. Rates of CRABSI attributed to short-term and long-term CVC did not show statistically significant changes (Figure 2; Appendix Table 2).

Among patients with CRABSI attributed to PVC, we did not observe statistically significant

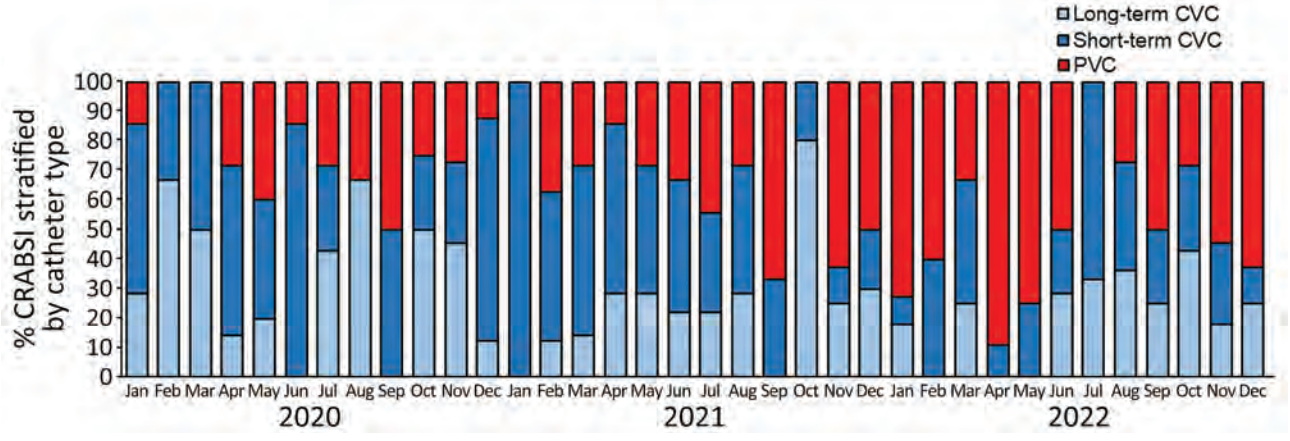

Figure 1. Percentage of intravascular catheter infections stratified by catheter type in study of intravascular catheter bloodstream infections during the COVID-19 pandemic, Switzerland, January 1, 2020–December 31, 2022. CRABSI, catheter-related or -associated bloodstream infections; CVC, central venous catheter; PVC, peripheral venous catheter.

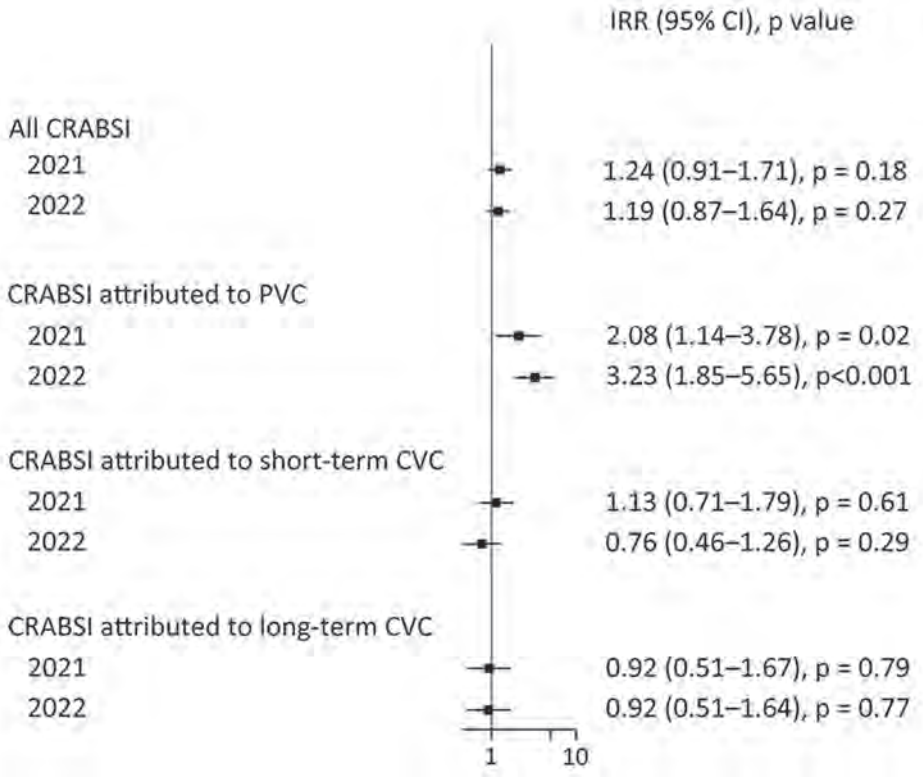

Figure 2. Incidence rate ratios per 1,000 patient days in a study of intravascular catheter bloodstream infections during the COVID-19 pandemic, Switzerland, January 1, 2020–December 31, 2022. Squares indicate IRRs, bars indicate 95% CIs. Patient-days were used as the denominator; 2020 rates were used as the referent. BSI, bloodstream infection; CRABSI, catheter related or associated bloodstream infections; CVC, central venous catheter; IRR, incidence rate ratio; PVC, peripheral venous catheter.

differences for sex, age, ward of acquisition, or microorganism distribution (Appendix Table 1). We observed similar results for short-term and long-term CVC (Appendix Table 1). Furthermore, the monthly number of CVCs and PVCs inserted, and PVCs in situ >96 hours did not change over time (Appendix Table 3, Figures 2, 3). A sensitivity analysis using catheter-days as a denominator yielded similar results (Appendix Figure 4).

Conclusions

This study showed that CRABSI attributed to PVC increased during the 2021–2022 compared with 2020. Studies in different countries showed that CVC-related BSIs increased during the COVID-19 pandemic (*10*,*11*), but no data on PVC-related infections are available.

Several hypotheses might explain these findings. First, ward of acquisition and microorganism distributions from 2020–2022 did not substantially change among PVC-related BSIs. Nevertheless, we observed a nonsignificant increase of PVC-attributed CRABSI due to coagulase-negative staphylococci in surgery wards in 2022. Moreover, we did not observe a significant increase of blood culture contaminations during 2021–2022 compared with 2020 (*14*). Second, according to our institutional recommendations, PVCs should be routinely changed every 4 days. We did not observe an increase of PVCs inserted for >96 h, suggesting adequate compliance to that preventive measure (Appendix). Recent unpublished data from France showed similar alarming results in the surveillance system of devices associated infections (*15*).

Our study's first limitation is that the study was single-center, limiting the generalizability of the results; however, HUG comprises several different sites, thus increasing the diversity of the patient population. Moreover, our data cannot be generalized to centers that routinely use midline catheters or that routinely use other infection control strategies, such as chlorhexidine-gluconate bathing post-CVC insertion or use of impregnated dressings. Second, we did not include confounders such as site of insertion, emergent versus elective insertions, immunocompromised states, chronic illnesses, body mass index, and nurse-to-patient ratio in our analysis. Third, our primary outcome, CRABSI, did not include pulmonary arterial, peripheral arterial, and umbilical arterial catheter infections.

In conclusion, our findings show that CRABSI attributed to PVC significantly increased during 2021–2022 in HUG. The observed increasing incidence of CRABSI attributed to PVC should raise awareness and warrants inclusion of PVC-related BSIs in national surveillance systems.

Acknowledgments

We thank the COVID-19 hospital-based surveillance system, jointly coordinated by the Federal Office of Public Health, the institute of global health of the University of Geneva and the Infection Prevention and Control of Geneva University Hospitals (HUG) for providing data of COVID-19 hospitalizations at HUG.

About the Author

Dr. Zanella is an infectious disease and infection prevention control specialist in the infection control program and WHO Collaborating Centre on Patient Safety, University Hospitals and Faculty of Medicine, Geneva, Switzerland. Her primary research interests are in bloodstream infection surveillance and respiratory infection surveillance and prevention.

References

1. Zingg W, Pittet D. Peripheral venous catheters: an under-evaluated problem. Int J Antimicrob Agents. 2009; 34:S38–42. https://doi.org/10.1016/S0924-8579(09)70565-5
2. PR Newswire. Global peripheral I.V. catheter market 2014–2018 [cited 2022 Jul 17]. https://www.prnewswire.com/news-releases/global-peripheral-iv-catheter-market-2014-2018-257019061.html
3. Hadaway L. Short peripheral intravenous catheters and infections. J Infus Nurs. 2012;35:230–40. https://doi.org/10.1097/NAN.0b013e31825af099
4. Buetti N, Abbas M, Pittet D, Chraiti MN, Sauvan V, De Kraker MEA, et al. Lower risk of peripheral venous catheter-related bloodstream infection by hand insertion. Antimicrob Resist Infect Control. 2022;11:80. https://doi.org/10.1186/s13756-022-01117-8
5. Buetti N, Abbas M, Pittet D, de Kraker MEA, Teixeira D, Chraiti MN, et al. Comparison of routine replacement with clinically indicated replacement of peripheral intravenous catheters. JAMA Intern Med. 2021;181:1471–8. https://doi.org/10.1001/jamainternmed.2021.5345
6. Mermel LA. Short-term peripheral venous catheter–related bloodstream infections: a systematic review. Clin Infect Dis. 2017;65:1757–62. https://doi.org/10.1093/cid/cix562
7. Zingg W, Metsini A, Balmelli C, Neofytos D, Behnke M, Gardiol C, et al. National point prevalence survey on healthcare-associated infections in acute care hospitals, Switzerland, 2017. Euro Surveill. 2019;24:1800603. https://doi.org/10.2807/1560-7917.ES.2019.24.32.1800603
8. Porto APM, Borges IC, Buss L, Machado A, Bassetti BR, Cocentino B, et al. Healthcare-associated infections on the ICU in 21 Brazilian hospitals during the early months of the COVID-19 pandemic: an ecological study. Infect Control Hosp Epidemiol. 2023;44:284–90. https://doi.org/10.1017/ice.2022.65
9. Rosenthal VD, Myatra SN, Divatia JV, Biswas S, Shrivastava A, Al-Ruzzieh MA, et al. The impact of COVID-19 on health care-associated infections in intensive care units in low- and middle-income countries: International Nosocomial Infection Control Consortium (INICC) findings. Int J Infect Dis. 2022;118:83–8. https://doi.org/10.1016/j.ijid.2022.02.041
10. Baker MA, Sands KE, Huang SS, Kleinman K, Septimus EJ, Varma N, et al.; CDC Prevention Epicenters Program. The impact of coronavirus disease 2019 (COVID-19) on healthcare-associated infections. Clin Infect Dis. 2022;74:1748–54. https://doi.org/10.1093/cid/ciab688
11. Weiner-Lastinger LM, Pattabiraman V, Konnor RY, Patel PR, Wong E, Xu SY, et al. The impact of coronavirus disease 2019 (COVID-19) on healthcare-associated infections in 2020: a summary of data reported to the National Healthcare Safety Network. Infect Control Hosp Epidemiol. 2022;43:12–25. https://doi.org/10.1017/ice.2021.362
12. European Centre for Disease Prevention and Control. Surveillance of healthcare-associated infections and prevention indicators in European intensive care units 2017 [cited 2017 May 5]. https://www.ecdc.europa.eu/sites/default/files/documents/HAI-Net-ICU-protocol-v2.2_0.pdf
13. von Elm E, Altman DG, Egger M, Pocock SJ, Gøtzsche PC, Vandenbroucke JP; STROBE Initiative. Strengthening the Reporting of Observational Studies in Epidemiology (STROBE) statement: guidelines for reporting observational studies. BMJ. 2007;335:806–8. https://doi.org/10.1136/bmj.39335.541782.AD
14. Chraiti M-N, Abbass M, Nguyen M, Zanella M-C, Catho G, Bosetti D, et al. Contamination of blood cultures before and during COVID-19 in a large tertiary-care center in Switzerland. In: Abstracts of the 7th International Conference on Prevention and Infection Control 2023; Geneva; 2023 Sep 12–15. Abstract P476. https://doi.org/10.1186/s13756-023-01276-2
15. Van der Mee-Marquet N, Goube F, Gimenes R, Valentin AS. Surveillance of infections linked to invasive devices, developments 2019–2022 [in French] [cited 2022 October 18]. https://www.santepubliquefrance.fr

Address for correspondence: Niccolò Buetti, Infection Control Programme and World Health Organization Collaborating Center, Geneva University Hospitals and Faculty of Medicine, Rue Gabrielle-Perret-Gentil 4, 1205 Geneva, Switzerland; email: niccolo.buetti@gmail.com

Emergence of Novel Norovirus GII.4 Variant

Preeti Chhabra,[1] Damien C. Tully,[1] Janet Mans, Sandra Niendorf, Leslie Barclay, Jennifer L. Cannon, Anna M. Montmayeur, Chao-Yang Pan, Nicola Page, Rachel Williams, Helena Tutill, Sunando Roy, Cristina Celma, Stuart Beard, Michael L. Mallory, Gédéon Prince Manouana, Thirumalaisamy P. Velavan, Ayola Akim Adegnika, Peter G. Kremsner, Lisa C. Lindesmith, Stéphane Hué, Ralph S. Baric, Judith Breuer, Jan Vinjé

We detected a novel GII.4 variant with an amino acid insertion at the start of epitope A in viral protein 1 of noroviruses from the United States, Gabon, South Africa, and the United Kingdom collected during 2017–2022. Early identification of GII.4 variants is crucial for assessing pandemic potential and informing vaccine development.

Norovirus is the most common cause of acute gastroenteritis (AGE) worldwide. Norovirus has an ≈7.7 kb positive-sense single-stranded RNA genome organized into 3 open reading frames (ORFs). ORF1 encodes a polyprotein that is post-translationally cleaved into 6 nonstructural (NS) proteins, including NS7, the viral RNA-dependent RNA polymerase (RdRp). ORF2 encodes the major viral protein (VP), VP1, and ORF3 encodes the minor VP2 capsid protein.

Noroviruses are genetically diverse and classified into ≥10 different genogroups. Genogroup II genotype 4 (GII.4) viruses cause most illnesses worldwide (*1*,*2*). GII.4 variants include US95–96, Farmington Hills_2002, Asia_2003, Hunter_2004, Yerseke_2006, Den Haag_2006, Osaka_2007, Apeldoorn_2007, New Orleans_2009, Sydney_2012, and HongKong_2019 (*3*). GII.4 variant emergence has been associated with changes in epitopes A–I on the surface exposed P2 subdomain of VP1 affecting interactions with histo-blood group antigens (HBGA) on host cells (*4*). Since 2012, GII.4 Sydney has been the most prevalent norovirus genotype globally (*2*). We sequenced complete genomes or VP1 of GII.4 viruses from recent outbreaks and sporadic cases that could not be genotyped to investigate genomic similarities with existing variants.

The Study

Several surveillance networks track trends in norovirus strain diversity, including CaliciNet in the United States (*5*) and NOROPATROL in the United Kingdom. In July 2017, four identical sequences from a norovirus outbreak in a childcare facility in San Francisco, California, USA, were uploaded to CaliciNet (https://www.cdc.gov/norovirus/reporting/calicinet). We genotyped those 4 sequences as GII.4 untypeable; the sequences had >2% nucleotide sequence difference in the 5′ end of ORF2 from existing GII.4 viruses. We identified genetically similar strains in stool specimens from 3 UK outbreaks: 1 strain from a hospitalized 32-year-old patient with AGE in Newcastle in 2019, 1 from

Author affiliations: Centers for Disease Control and Prevention, Atlanta, Georgia, USA (P. Chhabra, L. Barclay, J.L. Cannon, A.M. Montmayeur, J. Vinjé); London School of Hygiene & Tropical Medicine, London, UK (D.C. Tully, S. Hué); University of Pretoria, Pretoria, South Africa (J. Mans, N. Page); Robert Koch Institut, Berlin, Germany (S. Niendorf); California Department of Public Health, Richmond, California, USA (C.-Y. Pan); National Institute for Communicable Diseases, Sandringham, South Africa (N. Page); UCL Great Ormond Street Institute of Child Health, London (R. Williams, H. Tutill, S. Roy, J. Breuer); UK Health Security Agency, London (C. Celma, S. Beard); University of North Carolina, Chapel Hill, North Carolina, USA (M.L. Mallory, L.C. Lindesmith, R.S. Baric); Universitätsklinikum Tübingen, Tübingen, Germany (G.P. Manouana, T.P. Velavan, A.A. Adegnika); Centre de Recherches Médicales de Lambaréné, Lambarene, Gabon (G.P. Manouana, A.A. Adegnika, P.G. Kremsner); Vietnamese-German Center for Medical Research, Hanoi, Vietnam (T.P. Velavan); Duy Tan University, Da Nang, Vietnam (T.P. Velavan); German Center for Infection Research, Tübingen (A.A. Adegnika)

DOI: https://doi.org/10.3201/eid3001.231003

[1]These authors contributed equally to this article.

Table. List of oligonucleotide primers used to examine emergence of novel norovirus GII.4 strains on 3 continents*

Primer names	Sequence, 5′ → 3′	Orientation	Nested reverse transcription PCR
NV6e	ACC AYT WTG ATG CAG ACT A	Forward	Round 1
NV6f	ACC AYT ATG ATG CTG ATT A	Forward	Round 1
NV6g	ATC AYT ATG ATG CWG AYT A	Forward	Round 1
NV357a	CGC CAG TCC AGG AGT CCA AAA TY	Reverse	Round 1
NV378	GCT TAC GAA TGT GAG CGA A	Reverse	Round 2

*Primers were used to amplify complete ORF2 and ORF3 genes of GII.4 San Francisco strains from Gabon. ORF, open reading frame

a 1-year-old child in London in 2021, and 2 from Brighton in 2021, from a 1-year-old and a 3-year-old from the same household in an oyster-related outbreak. We also identified similar strains in sporadic samples from children with AGE in Gabon during 2018–2019 (*6*) and in children and adolescents with AGE from Western Cape and Gauteng in South Africa during 2021–2022. We sequenced 5 near-complete genomes and 10 complete VP1 sequences and compared those with existing GII.4

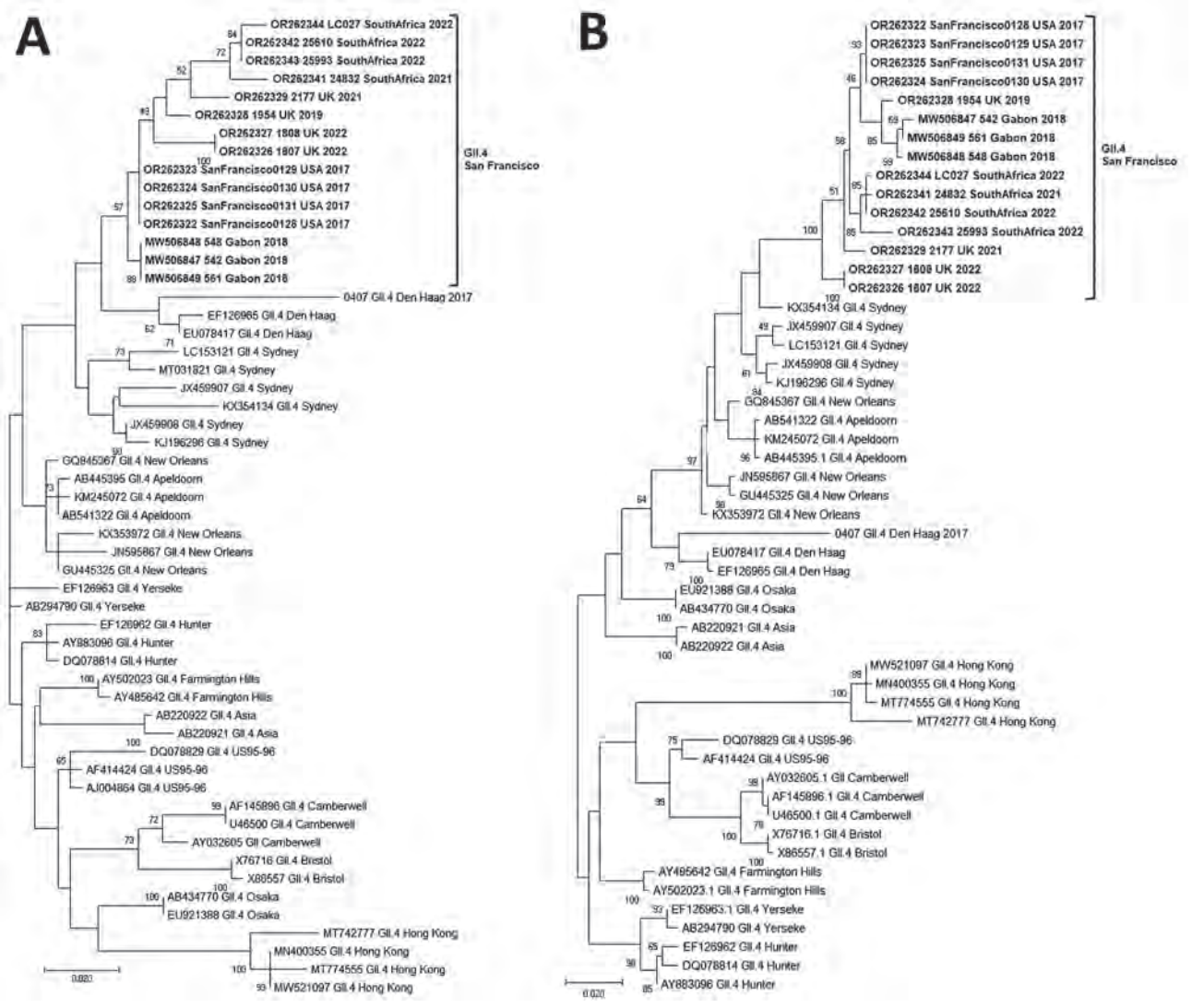

Figure 1. Phylogenetic trees of the emerging novel norovirus GII.4 strains on 3 continents. A) Common genotyping region C; 250 nt from the 5′ end of ORF2; B) complete VP1 aa sequences. Phylogenetic trees show novel GII.4 San Francisco strains and GII.4 variants, including recently identified clusters like GII.4 Hong Kong. Evolutionary analyses were conducted in MEGA X (https://www.megasoftware.net) using the maximum-likelihood method based on the Tamura-Nei model for the C region and Jones-Taylor-Thornton matrix-based model for VP1. We used a discrete gamma distribution to model evolutionary rate differences among sites; 5 categories γ parameter = 0.2174. Bootstrap (100) values are indicated at the nodes. Trees were drawn to scale. Scale bar represents nucleotide substitutions per site. ORF, open reading frame; VP1, viral protein 1.

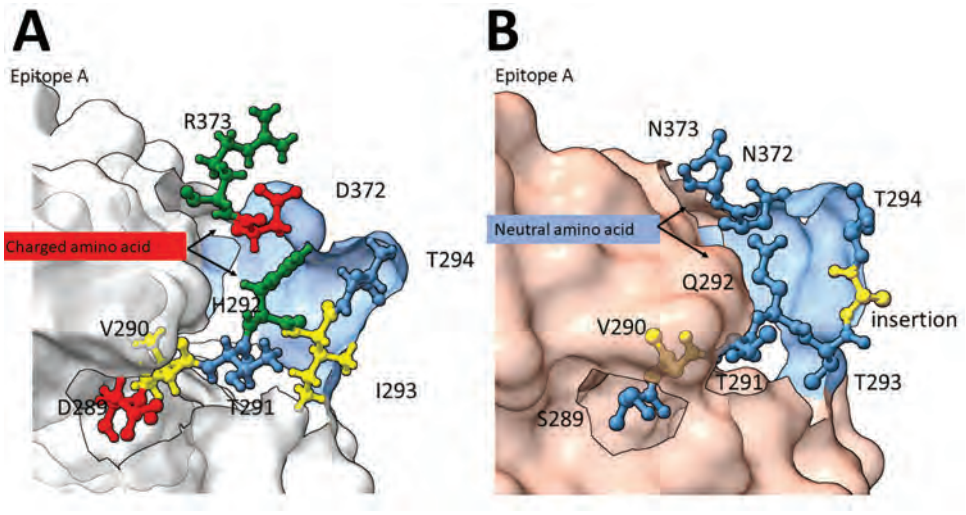

Figure 2. Structural changes of emergent novel norovirus GII.4 strains from 3 continents. A) Sydney GII.4 strain (GenBank accession no. JX459908); B) GII.4 San Francisco strain. The 3-dimensional structure models were predicted by using ChimeraX version 1.4 (*11*) and the alphafold prediction tool (*12*). Models show structural changes near and within the epitope A antigenic region on GII.4 San Francisco P-domain (panel B) are overlayed on a GII.4 Sydney 2012 backbone (Protein Data Bank, https://www.rcsb.org/structure/4OP7). Negatively (red) and positively (green) charged amino acids of GII.4 Sydney (panel A) were replaced with neutral amino acids (blue) in the GII.4 San Francisco strain and a hydrophobic (yellow) amino acid, alanine, was inserted between T293 and T294.

sequences from the Human Calicivirus Typing Tool (https://calicivirustypingtool.cdc.gov/gebali.cgi).

We extracted viral RNA and obtained complete genome or VP1 sequences for strains from the United States, United Kingdom, and South Africa according to published methods (*5*–*9*). We amplified the complete VP1 from Gabon strains by seminested reverse transcription PCR (RT-PCR) using Oligo dT and Lunascript Master Mix Kit (New England Biolabs, https://www.neb.com) for cDNA synthesis at 55°C for 30 min. We amplified complete VP1 and VP2 by using seminested RT-PCR and oligonucleotide primers designed for this study (Table). We performed RT-PCRs by using OneTaq 2X Master Mix (New England Biolabs) for 30 cycles at 94°C for 10 s, 45°C for 30 s, and 72°C for 3 min, then a final extension of 72°C for 2 min. We sequenced all amplicons.

We aligned complete VP1 amino acid sequences with GII.4 reference strains representing all known emerging and epidemic GII.4 viruses by using ClustalW in MEGA X (*10*). We computed maximum-likelihood phylogenetic trees by using the Jones-Taylor-Thornton model for amino acid sequences and Tamura-Nei model for nucleotide sequences and performed gamma distribution of evolutionary rates among sites using 100 bootstrap replications. We deposited nucleotide sequences of GII.4 San Francisco strains in GenBank (accession nos. OR262322–29, OR262341–44, and MW506847–49). We predicted 3-dimensional structures of GII.4 San Francisco viruses by using ChimeraX version 1.4 (*11*) and the alphafold prediction tool (*12*) and used the P-domain of GII.4 Sydney (Protein Data Bank no. PDB 4OP7; https://www.rcsb.org/structure/4OP7) as the backbone. To evaluate the effects of amino acid changes in P2, we synthesized virus-like particles from the codon-optimized ORF2 sequence of SF128 (GenBank accession no. OR262322) and compared ligand binding with other GII.4 virus-like particles (*4*).

We found that GII.4 San Francisco sequences from the 5′-end of ORF2 were closest to GII.4 Sydney and GII.4 Den Haag reference strains with maximum identities ranging from 91%–95% (Figure 1, panel A). Complete VP1 amino acid sequences of GII.4 San Francisco strains formed a distinct cluster with 5%–10% amino acid difference from GII.4 New Orleans and GII.4 Sydney (Figure 1, panel B). We typed RdRp sequences of all strains as GII.P31.

Of note, VP1 sequences of all GII.4 San Francisco strains had an alanine insertion at position 293/294 at the start of epitope A, coinciding with a unique SVTQTAT/A motif at positions 289–295 adjacent to epitope A (Appendix Figure 1, https://wwwnc.cdc.gov/EID/article/30/1/23-1003-App1.pdf). Compared with GII.4 Sydney_2012 and GII.4 New Orleans viruses, we observed mutations at amino acid residues 256 and 438 in the P1 region and 294, 310, 340, 341, 356, 372, 373, 377, 393, and 395 in the hypervariable region, P2 (Appendix Figure 1).

Homology modeling of the GII.4 San Francisco P-domain using GII.4 Sydney 2012 as a backbone (PDB 4OP7; GenBank accession no. JX459908) showed structural changes near and within epitope A (Figure 2). When the alanine insertion and SVTQTAT/A motif were introduced, several charged amino acids in GII.4 Sydney_2012 were replaced by neutral amino

acids (Figure 2). We also observed changes in the charge or hydrophobicity of amino acids in the monoclonal antibody binding epitope G (A356N) and within and around the HBGA binding regions D391N, S393D, and T395A, except in strains from South Africa (Appendix Figure 1). The alanine insertion in GII.4 San Francisco strains does not ablate binding to ligands found in porcine gastric mucin (Appendix Figure 2), which is consistent with ligand binding patterns known to correlate with susceptibility.

Conclusions

We report a novel norovirus GII.4 variant, named GII.4 San Francisco, detected in human stool specimens from patients with AGE on at least 3 continents during 2017–2022. The novel strains have a unique amino acid insertion in VP1 at the start of epitope A. We observed a similar unique insertion on epitope D in GII.4 variant Farmington Hills, which emerged in 2002, replacing the GII.4 US95–96 viruses, which had been circulating globally since 1995 (*13*). Whether the emerging GII.4 San Francisco strains will replace the current globally dominant GII.4 Sydney variant is not yet clear. Previous studies showed that epidemic GII.4 viruses diversified and spread over wide geographic areas for several years before epidemic emergence (*14*).

GII.4 viruses have always had strong immunodominance on epitope A, and alterations in epitope A residues has affected antibody responses (*15*). Addition of alanine at the start of epitope A and introduction of several neutral amino acids (SVTQTAT/A) before the insertion indicate major changes in the structure that could have an outsize effect on neutralizing antibody responses. GII.4 San Francisco strains showed mutations at residues S393D and T395A in epitope D. Those changes kept the ligand binding stabilizing function; epitope D also is a neutralizing epitope and an HBGA binding site (*4*). That finding further indicates that this virus has potential for increased spread and warrants additional antigenicity studies. Those data provide information for evaluation of norovirus vaccines that are currently in clinical trials.

In conclusion, the unique amino acid insertion in epitope A of VP1 together with a >5% aa difference from existing GII.4 variants confirmed that GII.4 San Francisco can be classified as a new GII.4 variant. This virus variant is circulating on at least 3 continents, North America, Europe, and Africa. Early detection and rapid assigning of an agreed upon name for future GII.4 variants will be crucial to assessing their pandemic potential.

Acknowledgments

We thank the Microscopy Services Laboratory, Department of Pathology and Laboratory Medicine, University of North Carolina Chapel Hill, for expert technical assistance.

This work was supported by the Wellcome Trust (grant 203268/Z/16/Z), National Institutes of Health (grant AI148260 to R.S.B.), and by CDCs intramural food safety program.

Biographical Sketch

Dr. Chhabra is a microbiologist at the National Calicivirus Laboratory, Division of Viral Diseases, National Center for Immunization and Respiratory Diseases, Centers for Disease Control and Prevention. Her primary research interest is molecular epidemiology of gastroenteritis viruses.

References

1. Chhabra P, de Graaf M, Parra GI, Chan MC, Green K, Martella V, et al. Updated classification of norovirus genogroups and genotypes. J Gen Virol. 2019;100:1393–406. https://doi.org/10.1099/jgv.0.001318
2. Farahmand M, Moghoofei M, Dorost A, Shoja Z, Ghorbani S, Kiani SJ, et al. Global prevalence and genotype distribution of norovirus infection in children with gastroenteritis: a meta-analysis on 6 years of research from 2015 to 2020. Rev Med Virol. 2022;32:e2237. https://doi.org/10.1002/rmv.2237
3. Parra GI, Tohma K, Ford-Siltz LA, Eguino P, Kendra JA, Pilewski KA, et.al. Minimal antigenic evolution after a decade of norovirus GII.4 Sydney_2012 circulation in humans. J Virol. 2023;97:e0171622. https://doi.org/10.1128/jvi.01716-22
4. Lindesmith LC, Boshier FAT, Brewer-Jensen PD, Roy S, Costantini V, Mallory ML, et al. Immune imprinting drives human norovirus potential for global spread. mBio. 2022;13:e0186122. https://doi.org/10.1128/mbio.01861-22
5. Cannon JL, Barclay L, Collins NR, Wikswo ME, Castro CJ, Magaña LC, et al. Genetic and epidemiologic trends of norovirus outbreaks in the United States from 2013 to 2016 demonstrated emergence of novel GII.4 recombinant viruses. J Clin Microbiol. 2017;55:2208–21. https://doi.org/10.1128/JCM.00455-17
6. Manouana GP, Nguema-Moure PA, Mbong Ngwese M, Bock CT, Kremsner PG, Borrmann S, et al. Genetic diversity of enteric viruses in children under five years old in Gabon. Viruses. 2021;13:545. https://doi.org/10.3390/v13040545
7. Brown JR, Roy S, Ruis C, Yara Romero E, Shah D, Williams R, et al. Norovirus whole-genome sequencing by SureSelect target enrichment: a robust and sensitive method. J Clin Microbiol. 2016;54:2530–7. https://doi.org/10.1128/JCM.01052-16
8. Mans J, Murray TY, Taylor MB. Novel norovirus recombinants detected in South Africa. Virol J. 2014;11:168. https://doi.org/10.1186/1743-422X-11-168
9. Parra GI, Squires RB, Karangwa CK, Johnson JA, Lepore CJ, Sosnovtsev SV, et al. Static and evolving norovirus genotypes: implications for epidemiology and immunity. PLoS Pathog. 2017;13:e1006136. https://doi.org/10.1371/journal.ppat.1006136

10. Kumar S, Stecher G, Li M, Knyaz C, Tamura K. MEGA X: Molecular Evolutionary Genetics Analysis across computing platforms. Mol Biol Evol. 2018;35:1547–9. https://doi.org/10.1093/molbev/msy096
11. Pettersen EF, Goddard TD, Huang CC, Meng EC, Couch GS, Croll TI, et al. UCSF ChimeraX: structure visualization for researchers, educators, and developers. Protein Sci. 2021;30:70–82. https://doi.org/10.1002/pro.3943
12. Jumper J, Evans R, Pritzel A, Green T, Figurnov M, Ronneberger O, et al. Highly accurate protein structure prediction with AlphaFold. Nature. 2021;596:583–9. https://doi.org/10.1038/s41586-021-03819-2
13. Widdowson MA, Cramer EH, Hadley L, Bresee JS, Beard RS, Bulens SN, et al. Outbreaks of acute gastroenteritis on cruise ships and on land: identification of a predominant circulating strain of norovirus—United States, 2002. J Infect Dis. 2004;190:27–36. https://doi.org/10.1086/420888
14. Ruis C, Lindesmith LC, Mallory ML, Brewer-Jensen PD, Bryant JM, Costantini V, et al. Preadaptation of pandemic GII.4 noroviruses in unsampled virus reservoirs years before emergence. Virus Evol. 2020;6:veaa067. https://doi.org/10.1093/ve/veaa067
15. Debbink K, Donaldson EF, Lindesmith LC, Baric RS. Genetic mapping of a highly variable norovirus GII.4 blockade epitope: potential role in escape from human herd immunity. J Virol. 2012;86:1214–26. https://doi.org/10.1128/JVI.06189-11

Address for correspondence: Preeti Chhabra, Centers for Disease Control and Prevention, Mailstop H18-7, Atlanta, GA 30329-4018, USA; email: PChhabra@cdc.gov

Avian Influenza A(H5N1) Neuraminidase Inhibition Antibodies in Healthy Adults after Exposure to Influenza A(H1N1)pdm09

Pavithra Daulagala, Samuel M.S. Cheng, Alex Chin, Leo L.H. Luk, Kathy Leung, Joseph T. Wu, Leo L.M. Poon, Malik Peiris,[1] Hui-Ling Yen[1]

We detected high titers of cross-reactive neuraminidase inhibition antibodies to influenza A(H5N1) virus clade 2.3.4.4b in 96.8% (61/63) of serum samples from healthy adults in Hong Kong in 2020. In contrast, antibodies at low titers were detected in 42% (21/50) of serum samples collected in 2009. Influenza A(H1N1) pdm09 and A(H5N1) titers were correlated.

The A/goose/Guangdong/1/1996-like (GsGD-like) highly pathogenic avian influenza A(H5N1) viruses were first identified in 1996 and have continuously evolved into antigenically distinct hemagglutinin (HA) clades that have substantially affected animal and human health. Before 2005, the GsGd-like virus mainly circulated in Asia among domestic poultry. Spillover infections from domestic poultry to wild migratory birds have enabled intercontinental spread to Europe, the Middle East, Africa, and North America, as previously observed in 2005 (clade 2.2 virus) and in 2014–2015 (clade 2.3.4.4c virus) (*1*). Since 2016, the clade 2.3.4.4b viruses have undergone a 3rd wave of intercontinental spread and have become enzootic among wild birds as of 2021 (*2*,*3*). Currently, the GsGD-like H5N1 viruses have been reported in all continents except Oceania and Antarctica. Expanded genetic diversity and geographic distribution has led to spillover events into numerous mammal species and sporadic human infections (*4*).

Highly pathogenic avian influenza A(H5N1) virus has not yet achieved efficient transmissibility in humans, but the current epidemiology of H5N1 2.3.4.4b lineage raises concerns of possible pandemic potential. Population immunity to an emerging influenza virus is one of the key parameters considered in assessing its pandemic risk according to the Centers for Disease Control and Prevention influenza risk assessment tool (https://www.cdc.gov/flu/pandemic-resources/national-strategy/risk-assessment.htm) and the World Health Organization tool for influenza pandemic risk assessment (https://www.who.int/teams/global-influenza-programme/avian-influenza/tool-for-influenza-pandemic-risk-assessment-(tipra)). Neutralizing antibodies targeting the HA receptor-binding domain and antibodies that inhibit neuraminidase (NA) activity have been shown to correlate with protection against influenza infection (*5*,*6*). We evaluated whether healthy adults possess cross-reactive hemagglutination inhibition (HAI) and neuraminidase inhibition (NAI) antibodies to H5N1 virus through previous exposure to seasonal influenza infections.

The Study

We collected serum samples from 63 healthy blood donors 18–73 years of age in 2020 in Hong Kong (HKU/HA HKW IRB #UW-132) to determine cross-reactive HAI antibodies and NAI antibodies to a clade 2.3.4.4b H5N1 virus (A/black-faced spoonbill/Hong Kong/AFCD-HKU-22-21429-01012/2022; Spoonbill/

Author affiliations: School of Public Health, The University of Hong Kong, Hong Kong, China (P. Daulagala, S.M.S. Cheng, A. Chin, L.H.L. Luk, K. Leung, J.T. Wu, L.L.M. Poon, M. Peiris, H.L. Yen); The University of Hong Kong–Shenzhen Hospital, Shenzhen, China (K. Leung); Centre for Immunology and Infection, Hong Kong Science Park, Hong Kong (L.L.M. Poon, M. Peiris)

DOI: https://doi.org/10.3201/eid3001.230756

[1]These senior authors contributed equally to this article.

HK/22), which showed high homology to the HA and NA proteins of clade 2.3.4.4b candidate vaccine viruses A/chicken/Ghana/AVL-76321VIR7050-39/2021 (98.8% [HA] and 97.3% [NA]) and A/American wigeon/South Carolina/AH0195145/2021 (98.6% [HA] and 97.2% [NA]) (*7*). For comparison, we also determined the HAI and NAI antibody responses to the 2009 pandemic influenza A(H1N1)pdm09 (pH1N1) virus (A/California/04/2009; California/09) using an HAI assay and enzyme-linked lectin assay (detection limit at 1:10) (*8*,*9*).

Among healthy adults, 56/63 (88.8%) possessed HAI antibodies to pH1N1 virus with a geometric mean titer (GMT) of 21.84; none showed detectable HAI antibodies to H5N1 virus (Figure 1, panel A). NAI antibodies against pH1N1 were detected in 57/63 (90.5%) healthy participants (GMT 41.80), and 61/63 (96.8%) also possessed cross-reactive NAI antibodies to H5N1 (GMT 41.34) (Figure 1, panel B). The NAI titers against pH1N1 and H5N1 were highly correlated (Spearman $\rho = 0.8349$; $p<0.001$) (Appendix Figure 1). Furthermore, 57 (90.5%) persons had NAI antibodies to both viruses at titers >1:10, and 32 (50.8%) persons had NAI antibodies to both viruses at titers ≥1:40. To evaluate whether the cross-reactivity extends to N1 proteins of other avian influenza viruses, we randomly selected 32 serum samples to determine NAI titers against an avian influenza A(H6N1) virus isolated from wild bird surveillance (A/environment/Hong Kong/HKU_MPT_2006/2015; Env/HK/15). DNA barcoding suggested that the specimen originated from *Platalea minor* (black-face spoonbill). Similarly, 93.75% (30/32) persons possessed cross-reactive NAI titers against H6N1 virus (GMT 26.50), and 40.6% (13/32) possessed NAI titers ≥1:40 (Appendix Figure 1). However, cross-reactivity did not extend to N4 protein of an avian influenza A(H6N4) virus isolated from wild bird surveillance (A/environment/Hong Kong/HKU_MPT_2022; Env/HK/22) originated from *Anas acuta* (northern pintail) (Appendix Figure 1). Overall, we observed high correlations between NAI titers against pH1N1 and H6N1 viruses (Spearman $\rho = 0.875$; $p<0.001$) and between H5N1 and H6N1 viruses (Spearman $\rho = 0.874$; $p<0.001$).

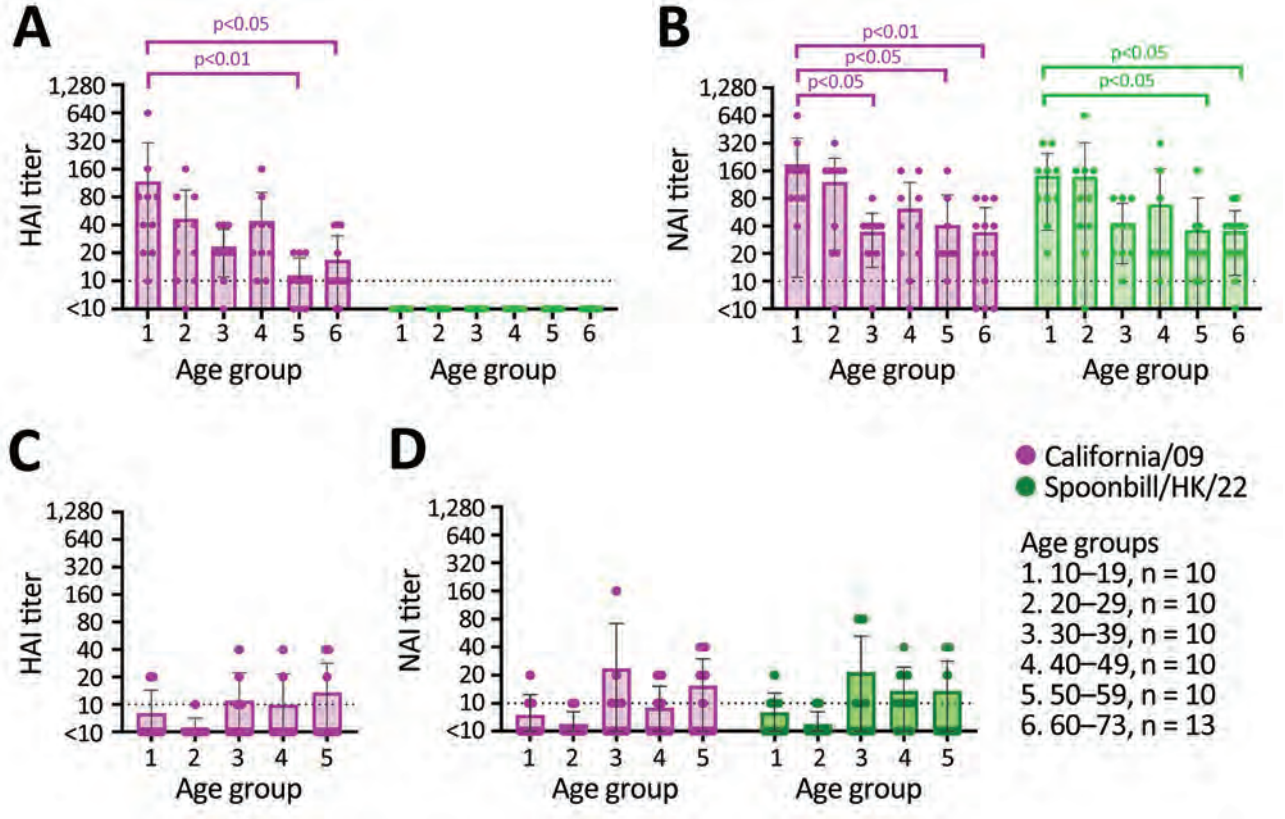

Figure. Age-stratified HAI and NAI antibody responses to influenza A(H1N1)pdm09 (California/09) and A(H5N1) (Spoonbill/HK/22) viruses in serum samples collected from healthy adults in 2020 and 2009, Hong Kong, China. A, B) Results for serum samples of 63 healthy adults collected in 2020. C, D) Results for serum samples of 50 healthy adults collected in 2009. The assay detection limit was 1:10, and samples with antibody below the detection limit were assigned an arbitrary antibody titer of 5, which is used to calculate geometric mean titer. The HAI and NAI titers across different age groups were compared using Kruskal-Wallis test and Dunn's multiple comparison test. HAI, hemagglutination inhibition; NAI, neuraminidase inhibition.

Table 1. NAI antibody titers detected in postinfection ferret antiserum against influenza A(H1N1), A(H1N1)pdm09, and A(H5N1) viruses, Hong Kong, China

Postinfection ferret antiserum†	NAI antibody titers*		
	Homologous virus	California/09 A (H1N1)pdm09	Spoonbill/HK/22 A(H5N1)
A/USSR/90/1977	320	<10	<10
A/Chile/01/1983	320	<10	<10
A/Singapore/06/1986	320	<10	<10
A/Texas/36/1991	320	<10	<10
A/Brisbane/59/2007	1,280	<10	<10
A/California/04/2009	2,560	2,560	320–640

*NAI antibody response was determined using recombinant A(H6N1) viruses carrying the N1 proteins derived from A(H1N1), A(H1N1)pdm09, or A(H5N1) viruses that were generated as described previously (*10*). Although we used recombinant H6N1 viruses in ELLA assays to avoid interference of hemagglutinin-reactive antibodies, we might not completely prevent the interference of cross-reactive antibodies that bind to the stalk of H6 protein and inhibit neuraminidase activity through stearic hindrance. NAI, neuraminidase inhibition.
†One ferret antiserum against each of the influenza A(H1N1) viruses and 6 ferret antiserum against the influenza A(H1N1)pdm09 were used.

We examined NAI titers to the homologous virus and cross-reaction to H5N1 virus in archival ferret antiserum against seasonal A(H1N1) viruses and pH1N1 (Table 1). Ferret antiserum against H1N1 viruses circulating during 1977–2007 showed no cross-reactive NAI response to H5N1 but had NAI titers at 1:320–1:1280 against the homologous viruses. Ferret antiserum against pH1N1 virus showed a homologous NAI titer of 1:2,560 and cross-reactive NAI titers to H5N1 at 1:320 to 1:640.

To further confirm whether exposure to pH1N1 virus contributed to the cross-reactive NAI antibodies, we used serum samples of 50 healthy blood donors (17–55 years of age) collected in July 2009, before pH1N1 had become widespread in Hong Kong (*11*). HAI antibodies to pH1N1 were detected in 22% (11/50) of the samples; GMT was low, at 7.07 (Figure 1, panel C). We detected NAI antibodies to pH1N1 in 44% (22/50) of healthy blood donors; GMT was low, at 8.24. NAI antibodies to H5N1 were detected in 42% (21/50) of donors; GMT was 8.35 (Figure 1, panel D). Most participants (16/20) with detectable NAI antibodies to pH1N1 also had NAI antibodies to H5N1. Overall, the cross-reactive NAI titers detected in 2009 (Figure 1, panel D) were lower than the those detected in 2020 (Figure 1, panel B). This result suggests that previous exposure to pH1N1 virus is the potential source of cross-reactive NAI antibodies to H5N1 virus. The NA protein of Spoonbill/HK/22 differed from the pH1N1 (California/09) NA by 53 aa and from the seasonal H1N1 NA proteins by 68–76 aa; most changes occurred in the NA head domain (Table 2; Appendix Figure 2).

Table 2. Comparison of the neuraminidase proteins of seasonal influenza A(H1N1) and A(H1N1)pdm09 viruses to the neuraminidase proteins of influenza A(H5N1) virus, Hong Kong, China

Viruses	No. amino acid differences compared with Spoonbill/HK/22	Amino acid homology, %
A/USSR/90/1977	70	84.08
A/Chile/01/1983	68	84.58
A/Singapore/06/1986	68	84.58
A/Texas/36/1991	69	84.33
A/Brisbane/59/2007	76	83.83
A/California/04/2009	53	88.00

Conclusion

We detected high titers of cross-reactive NAI antibodies to clade 2.3.4.4b H5N1 virus, Spoonbill/HK/22, in samples collected from healthy adults 18–73 years of age in 2020. The N1 antibody cross-reactivity also extended to an H6N1 avian influenza virus isolated from wild bird samples in Hong Kong. Our results confirm and extend the findings from a recent study reporting cross-reactive NAI antibody responses to clade 2.3.4.4b H5N1 virus in healthy blood donors (*12*). The use of monospecific archival ferret antiserum against seasonal H1N1 and pH1N1 influenza showed that cross-reactive NAI response to H5N1 were elicited by pH1N1 but not by seasonal H1N1 viruses circulating during 1977–2007. The pH1N1 virus derived its NA protein from the avian-origin Eurasian-avian swine viruses (*13*) and appeared antigenically more closely related to the N1 of H5N1 and H6N1 avian influenza viruses but not to a N4 of H6N4 avian influenza virus. The use of serum samples collected from healthy blood donors in 2009 further confirmed that exposure to pH1N1 might have contributed to the cross-reactive NAI antibodies against H5N1.

HAI titer of ≥1:40 has long been established to correspond with a 50% reduction in influenza infection risk, which might be used to model the effects of cross-reactive HAI antibody titers on reducing the basic reproduction number (R_0) of novel zoonotic viruses with pandemic potential (*14*). NAI antibodies have also been shown to protect against infection, reduce symptoms, and shorten the duration of viral shedding (*5*,*6*); however, the NAI antibody threshold that corresponds with protection has not been clearly defined.

In summary, we detected high titers of cross-reactive NAI antibodies against influenza A(H5N1)

clade 2.3.4.4b virus in serum samples collected from healthy adults in 2020 but not detected in serum samples collected in 2009. Further studies are needed to confirm whether cross-reactive NAI antibodies confer protection against H5N1 infection or modulate disease severity, but our results suggest that the antibodies against H5N1 and H6N1 viruses might derive from exposure to the conserved epitopes shared between the avian-origin pH1N1 virus and avian N1 proteins.

Acknowledgments

We thank Christopher J. Brackman and the Agriculture Fisheries and Conservation Department, Government of the Hong Kong Special Administrative Region, China, for sharing the A(H5N1) virus.

This study was supported by RGC Theme-based Research Schemes (T11-712/19-N) of the Research Grant Council and Health@InnoHK (Centre for Immunology and Infection) administered by Innovation and Technology Commission, Hong Kong, China.

About the Author

Dr. Daulagala is a researcher at the School of Public Health, University of Hong Kong. Her primary research interest is understanding the role of neuraminidase antibodies in influenza infections.

References

1. Lee DH, Bertran K, Kwon JH, Swayne DE. Evolution, global spread, and pathogenicity of highly pathogenic avian influenza H5Nx clade 2.3.4.4. J Vet Sci. 2017;18(S1):269–80. https://doi.org/10.4142/jvs.2017.18.S1.269
2. Pohlmann A, King J, Fusaro A, Zecchin B, Banyard AC, Brown IH, et al. Has epizootic become enzootic? Evidence for a fundamental change in the infection dynamics of highly pathogenic avian influenza in Europe, 2021. mBio. 2022;13:e0060922.
3. Adlhoch C, Fusaro A, Gonzales JL, Kuiken T, Mirinaviciute G, Niqueux É, et al.; European Food Safety Authority, European Centre for Disease Prevention and Control, European Union Reference Laboratory for Avian Influenza. Avian influenza overview March–April 2023. EFSA J. 2023;21:e08039 https://doi.org/10.2903/j.efsa.2023.8039
4. World Health Organization. Antigenic and genetic characteristics of zoonotic influenza A viruses and development of candidate vaccine viruses for pandemic preparedness. 2022 [cited 2023 May 18]. https://cdn.who.int/media/docs/default-source/influenza/who-influenza-recommendations/vcmnorthern-hemisphere-recommendation-2022-2023/202203_zoonotic_vaccinevirusupdate.pdf
5. Krammer F, Weir JP, Engelhardt O, Katz JM, Cox RJ. Meeting report and review: immunological assays and correlates of protection for next-generation influenza vaccines. Influenza Other Respir Viruses. 2020;14:237–43 https://doi.org/10.1111/irv.12706
6. Maier HE, Nachbagauer R, Kuan G, Ng S, Lopez R, Sanchez N, et al. Pre-existing antineuraminidase antibodies are associated with shortened duration of influenza A(H1N1) pdm virus shedding and illness in naturally infected adults. Clin Infect Dis. 2020;70:2290–7. https://doi.org/10.1093/cid/ciz639
7. World Health Organization. Summary of status of development and availability of A(H5N1) candidate vaccine viruses and potency testing reagents. 2023 [cited 2023 Jun 7]. https://cdn.who.int/media/docs/default-source/influenza/cvvs/cvv-zoonotic-northern-hemisphere-2023-2024/h5n1_summary_a_h5n1_cvv_20230225.pdf
8. World Health Organization. Manual for the laboratory diagnosis and virological surveillance of influenza. Geneva: The Organization; 2011.
9. Couzens L, Gao J, Westgeest K, Sandbulte M, Lugovtsev V, Fouchier R, et al. An optimized enzyme-linked lectin assay to measure influenza A virus neuraminidase inhibition antibody titers in human sera. J Virol Methods. 2014;210:7–14.
10. Daulagala P, Mann BR, Leung K, Lau EHY, Yung L, Lei R, et al. Imprinted Anti-Hemagglutinin and Anti-Neuraminidase Antibody Responses after Childhood Infections of A(H1N1) and A(H1N1)pdm09 Influenza Viruses. mBio. 2023;14:e00084–23.
11. Wu JT, Ho A, Ma ES, Lee CK, Chu DK, Ho PL, et al. Estimating infection attack rates and severity in real time during an influenza pandemic: analysis of serial cross-sectional serologic surveillance data. PLoS Med. 2011; 8:e1001103.
12. Kandeil A, Patton C, Jones JC, Jeevan T, Harrington WN, Trifkovic S, et al. Rapid evolution of A(H5N1) influenza viruses after intercontinental spread to North America. Nat Commun. 2023;14:3082.
13. Garten RJ, Davis CT, Russell CA, Shu B, Lindstrom S, Balish A, et al. Antigenic and genetic characteristics of swine-origin 2009 A(H1N1) influenza viruses circulating in humans. Science. 2009;325:197–201.
14. Cheung JTL, Tsang TK, Yen HL, Perera RAPM, Mok CKP, Lin YP, et al. Determining existing human population immunity as part of assessing influenza pandemic risk. Emerg Infect Dis. 2022;28:977–85. https://doi.org/10.3201/eid2805.211965

Address for correspondence: Hui-Ling Yen or Malik Peiris, L6-42, Laboratory Block, LKS Faculty of Medicine, 21 Sassoon Rd, Hong Kong, China; email: hyen@hku.hk or malik@hku.hk

Clade I–Associated Mpox Cases Associated with Sexual Contact, the Democratic Republic of the Congo

Emile M. Kibungu, Emmanuel H. Vakaniaki, Eddy Kinganda-Lusamaki, Thierry Kalonji-Mukendi, Elisabeth Pukuta, Nicole A. Hoff, Isaac I. Bogoch, Muge Cevik, Gregg S. Gonsalves, Lisa E. Hensley, Nicola Low, Souradet Y. Shaw, Erin Schillberg, Mikayla Hunter, Lygie Lunyanga, Sylvie Linsuke, Joule Madinga, Martine Peeters, Jean-Claude Makangara Cigolo, Steve Ahuka-Mundeke, Jean-Jacques Muyembe, Anne W. Rimoin,[1] Jason Kindrachuk,[1] Placide Mbala-Kingebeni,[1] Robert S. Lushima;[1] International Mpox Research Consortium

We report a cluster of clade I monkeypox virus infections linked to sexual contact in the Democratic Republic of the Congo. Case investigations resulted in 5 reverse transcription PCR–confirmed infections; genome sequencing suggest they belonged to the same transmission chain. This finding demonstrates that mpox transmission through sexual contact extends beyond clade IIb.

Human mpox, caused by monkeypox virus (MPXV), is an emerging zoonotic viral disease first identified in the Democratic Republic of the Congo (DRC) (*1*). MPXV is endemic in multiple regions of Central and West Africa (*2*,*3*). The virus is subclassified into 2 clades: clade I, formerly Congo Basin (Central Africa) clade, and clade II, formerly West African clade. Clade II is further subdivided into 2 subclades, IIa and IIb; subclade IIb was responsible for the 2022 global epidemic (*4*; https://www.who.int/news/item/12-08-2022-monkeypox--experts-give-virus-variants-new-names). Clade I infections are associated with greater disease severity and more pronounced rash and had demonstrated increased human-to-human transmission compared with clade II before the global emergence of clade IIb (*5*). Those difference are likely influenced by factors such as clade-specific genomic differences in host response modifier proteins, exposure type and dose, and vaccination status (https://www.who.int/news/item/12-08-2022-monkeypox--experts-give-virus-variants-new-names). Travel-related and animal importation–related cases have been reported in nonendemic regions (*6*). In 2022, rapid spread of MPXV to new geographic regions resulted in >86,000 confirmed infections in nonendemic regions and declaration of a public health emergency of international concern by the World Health Organization (*7*).

During the 2022 epidemic, >90% of infections were linked to secondary transmission, mainly through sexual contact among men who have sex with men (MSM) (*8*–*11*). The disease appeared to affect younger populations in endemic regions because of increased contact with zoonotic sources; the average age at infection was <25 years, and the case-fatality

Author affiliations: Ministry of Public Health, Kinshasa, Democratic Republic of the Congo (E.M. Kibungu, T. Kalonji-Mukendi, R.S. Lushima); Institut National de Recherche Biomédicale, Kinshasa (E.H. Vakaniaki, E. Kinganda-Lusamaki, E. Pukuta, L. Lunyanga, S. Linsuke, J. Madinga, J.-C. Makangara Cigolo, S. Ahuka-Mundeke, J.-J. Muyembe, P. Mbala-Kingebeni); Cliniques Universitaires de Kinshasa, Université de Kinshasa, Kinshasa (E. Kinganda-Lusamaki, J.-C. Makangara Cigolo, S. Ahuka-Mundeke, J.-J. Muyembe, P. Mbala-Kingebeni); TransVIHMI (Recherches Translationnelles sur le VIH et les Maladies Infectieuses endémiques et émergentes); University of Montpellier, French National Research Institute for Sustainable Development, INSERM, Montpellier, France (E. Kinganda-Lusamaki, M. Peeters); University of California, Los Angeles, California, USA (N.A. Hoff, A.W. Rimoin); Toronto General Hospital, University Health Network, Toronto, Ontario, Canada (I.I. Bogoch); University of St. Andrews, St. Andrews, Scotland, UK (M. Cevik); Yale School of Public Health, New Haven, Connecticut, USA (G.S. Gonsalves); USDA Agricultural Research Service, Manhattan, Kansas, USA (L.E. Hensley); University of Bern, Bern, Switzerland (N. Low); University of Manitoba, Winnipeg, Manitoba, Canada (S.Y. Shaw, E. Schillberg, M. Hunter, J. Kindrachuk)

DOI: https://doi.org/10.3201/eid3001.231164

[1]These authors contributed equally to this article.

rate was higher among children. In nonendemic regions, however, the average age at infection was >30 years, and infection occurred predominantly in men (>95%) who self-identify as MSM (>80%) (*10*,*11*). Clinical characteristics during the 2022 epidemic included fever, physical asthenia or lethargy, and lymphadenopathy with high concentrations of papules, pustules, and vesicles on the skin of the genital and perianal organs. Rectal pain, bleeding, and purulent bloody stools were also common (*12*,*13*). A recent case series assessing data from clade IIb infections in persons living with HIV demonstrated that increased disease severity and fatal disease were also linked to CD4 counts (*11*).

Although clade I–related infections can occur through close contacts, including through fomites, transmission through sexual contact has not been reported previously (*14*,*15*). However, given the high sequence homology across MPXV clades and the increased disease severity associated with clade I, clarifying whether sexual contact–related infections occur across MPXV clades is critical. We report a confirmed cluster of clade I–associated mpox associated with sexual contact.

The Study

An alert was issued by the Kwango Provincial Health Division, DRC, after reports from civil society organizations in March 2023 regarding a resident with skin rashes and pruritus. Teams from the National Programme for the Control of Monkeypox and Viral Hemorrhagic Fevers and the Institut National de Recherche Biomédicale, accompanied by members of the senior team from the Kwango Provincial Health Division, the senior team from the Kenge Health Zone, the provincial team from the National Programme for the Control of HIV, and the provincial civil society representative, conducted an investigation. During the investigation, the national and provincial health teams instituted training for local healthcare clinics to raise awareness of the clinical signs and mode of transmission for mpox and HIV, including sexual contact in MSM.

A man from DRC in his late 20s (case-patient 1) reported having 2 sexual encounters with a man (suspected primary case-patient) in Europe 1 week before returning to DRC. The suspected primary case-patient frequently visited DRC. Case-patient 1 reported that the primary case-patient had general clinical symptoms including genital pruritus, joint pain, and physical asthenia. Nine days after contact, case-patient 1 began experiencing pruritus, vesicular skin eruptions, and genital and perianal ulcerations. He contacted a local civil organization, which initiated a preliminary investigation and alerted the National Programme for the Control of Monkeypox and Viral Hemorrhagic Fevers. He had penile lesions and penile papules (Figure 1); localized redness on the lips and in the oral buccal mucosa were also noted, and he had 1 lesion on the middle finger of the right hand. Blood samples, oropharyngeal swab samples, swab samples from rectal and genital lesions, and swab samples from vesicles on the skin of the penis and pubis were taken.

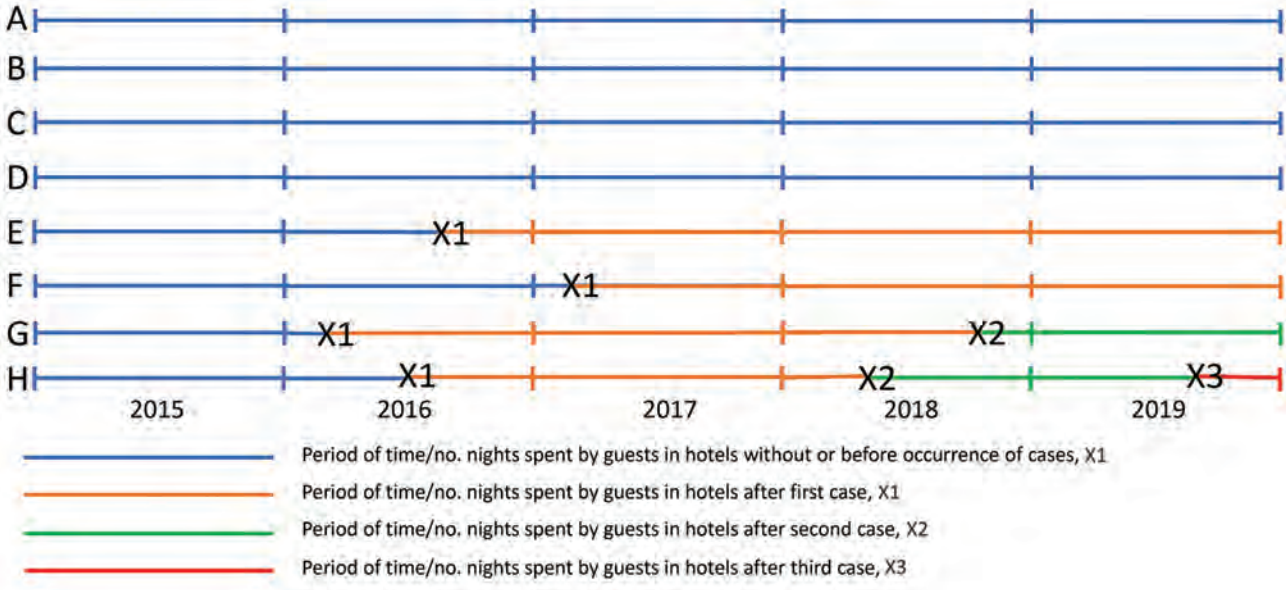

Figure 1. Penile lesions and papules associated with clade I monkeypox virus infection in a man in his late 20s who reported having 2 sexual encounters with a man in Europe 1 week before arriving in Democratic Republic of the Congo.

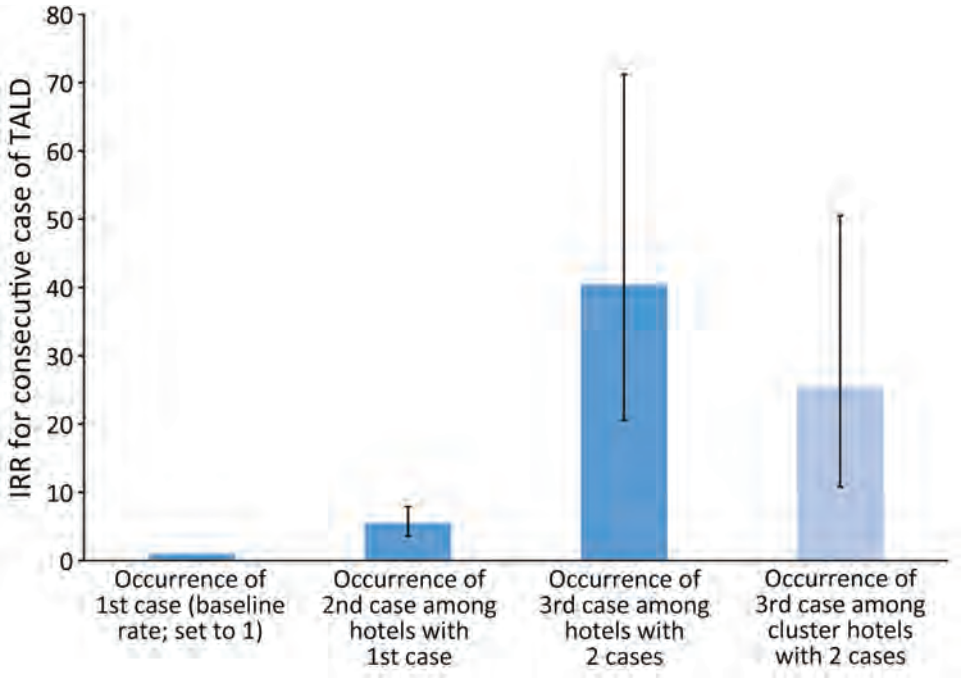

Figure 2. Phylogenetic analysis of MPXV sequences from a cluster of mpox cases described in Kwango Province, Democratic Republic of the Congo. A) MPXV global phylogeny showing that the Kwango Province outbreak cluster belongs to clade I MPXV. B) Phylogenetic analysis of MPXV genome sequences from the reported cases and clade I MPXV sequences from Central Africa. Posterior support values are shown at branch points. DNA was extracted at Institut National de Recherche Biomédicale using a QIAGEN DNA Mini Kit (https://www.qiagen.com) from blood samples and subsequently screened for MPXV with an orthopoxvirus-specific real-time PCR assay. Whole-genome sequencing was attempted on samples from the index case by next-generation sequencing. The library preparation was performed using Illumina DNA Prep with Enrichment (https://www.illumina.com), and the libraries were enriched for MPXV using biotinylated custom probes synthesized by Twist Biosciences (https://www.twistbioscience.com). Note that 23MPX098 (or 23MPX0245V) and 23MPX099 (or 23MPX0245C) are vesicle and crust samples from case-patient 1. Scale bar indicates number of substitutions per site. DRC, Democratic Republic of the Congo; hMPXV, human MPXV; MPXV, monkeypox virus.

Case-patient 1 reported having sexual contact with 9 partners (6 men and 3 women) after arriving in DRC. A prescreening of those contacts identified suspected mpox in 3 sexual contacts (2 men and 1 woman, 30–35 years of age) who had fever and lesions in the genital and perianal region. Blood samples and oropharyngeal swab samples were taken from all 9 partners; additional rectal or vaginal swab samples were taken from the men and woman suspected to be secondary case-patients. Investigation of all sexual contacts yielded an additional 36 sexual contacts. Samples from case-patient 1 and 3 suspected secondary case-patients were confirmed to be MPXV-positive by PCR using samples from vesicles, crusts, or blood. One of the 36 sexual contacts was also PCR-positive for MPXV. We performed viral genome sequencing on PCR-positive samples; phylogenetic analysis showed tight clustering among 3 positive samples, suggesting they belong to the same chain of transmission. The closest related sequence beyond this cluster was a 2022 clade I MPXV sequence from DRC (Figure 2).

We treated the 5 PCR-positive case-patients with supportive care and pain control on an outpatient basis. We performed a follow-up investigation to further investigate transmission chains and identify additional contacts; follow-up was conducted for each contact through individual case report forms. We monitored a total of 120 contacts over 21 days. The contacts were categorized into 3 groups: sexual contacts (n = 5), family members (n = 45), and persons associated with close nonsexual contact (n = 70). None of the persons monitored during the 21 days experienced clinical signs.

Conclusions

We describe a cluster of clade I MPXV–associated infections in DRC related to sexual contact, which has previously only been described for clade II MPXV. Of note, MPXV transmission through sexual contact is not exclusive to clade IIb and can occur during heterosexual and same-sex contact. This study demonstrates that MPXV infections can occur through additional exposure routes in MPXV-endemic regions and that the current understanding of mpox burden in clade I–endemic regions is based on classical transmission exclusively; recognizing those factors is critical. Our findings highlight additional considerations for MPXV circulation and transmission containment in endemic areas. Thus, increased MPXV surveillance, diagnostic testing access, and equitable access to both vaccines and therapeutics for persons at increased risk for infection are needed for ongoing

mitigation strategies. Given the increased disease severity associated with clade I MPXV, the potential implications of sexual transmission on broadening geographic distribution for MPXV across clades I and II must be considered. In addition, long-term immunity to mpox inferred by vaccination is unknown, including the role of mucosal immunity against clade I MPXV infections. This report highlights multiple critical global health considerations that must be addressed. Ongoing support for community engagement and educational efforts focusing on mpox recognition and reporting, including within sexual networks and for specific groups who might suffer from lack of care or experience stigma when seeking care.

Our findings highlight historically unrecognized MPXV transmission through sexual contact and indicate the need for increased routine screening in sexual health clinics in mpox-endemic and nonendemic regions. Population movement and previously unreported routes of transmission could exacerbate global distribution of MPXV, which could be compounded by the lack of routine diagnostic testing or inadequate access to rapid point-of-care testing. In view of this investigation, epidemiologic and genomic surveillance for MPXV, in both endemic and nonendemic regions, should be improved and strengthened.

Acknowledgments

We thank the residents of Kwango Province, DRC, and the Ministry of Health, DRC, for their cooperation and assistance during this outbreak investigation. We also thank Sophie Gabia, Franc Kasongo, Jackie Muteba, and staff from the Ministry of Health, who assisted in field investigations, as well as Eric Delaporte, Ahidjo Ayouba, and all members of the AFROSCREEN Consortium (https://www.afroscreen.org/en/network) for their work and support on genomic surveillance in DRC.

This work was supported by the International Mpox Research Consortium (IMReC) through funding from the Canadian Institutes of Health Research and International Development Research Centre (grant no. 202209MRR-489062-MPX-CDAA-168421); Department of Defense, Defense Threat Reduction Agency, Monkeypox Threat Reduction Network grant #HDTRA1-21-1-0040; and USDA Non-Assistance Cooperative Agreement #20230048. Additional laboratory support was provided by Agence Française de Développement through the PANAFPOX and AFROSCREEN project (grant agreement CZZ3209), coordinated by ANRS Maladies infectieuses émergentes in partnership with Institut de Recherche pour le Développement (IRD).

E.L. received a PhD grant from the French Foreign Office.

About the Author

Dr. Kibungu is a senior expert epidemiologist with a primary research interest in emerging infectious diseases, including response and containment efforts from the Ministry of Public Health, Hygiene and Prevention, Democratic Republic of the Congo. His primary research interests are emerging infectious diseases, including response and containment efforts.

References

1. Ladnyj ID, Ziegler P, Kima E. A human infection caused by monkeypox virus in Basankusu Territory, Democratic Republic of the Congo. Bull World Health Organ. 1972;46:593–7.
2. Breman JG, Kalisa-Ruti, Steniowski MV, Zanotto E, Gromyko AI, Arita I. Human monkeypox, 1970–79. Bull World Health Organ. 1980;58:165–82.
3. Durski KN, McCollum AM, Nakazawa Y, Petersen BW, Reynolds MG, Briand S, et al. Emergence of monkeypox—West and Central Africa, 1970–2017. MMWR Morb Mortal Wkly Rep. 2018;67:306–10. https://doi.org/10.15585/mmwr.mm6710a5
4. Ulaeto D, Agafonov A, Burchfield J, Carter L, Happi C, Jakob R, et al. New nomenclature for mpox (monkeypox) and monkeypox virus clades. Lancet Infect Dis. 2023;23:273–5. https://doi.org/10.1016/S1473-3099(23)00055-5
5. McCollum AM, Damon IK. Human monkeypox. Clin Infect Dis. 2014;58:260–7. https://doi.org/10.1093/cid/cit703
6. Reynolds MG, Yorita KL, Kuehnert MJ, Davidson WB, Huhn GD, Holman RC, et al. Clinical manifestations of human monkeypox influenced by route of infection. J Infect Dis. 2006;194:773–80. https://doi.org/10.1086/505880
7. World Health Organization. WHO Director-General declares the ongoing monkeypox outbreak a public health event of international concern [cited 2023 Nov 28]. https://www.who.int/europe/news/item/23-07-2022-who-director-general-declares-the-ongoing-monkeypox-outbreak-a-public-health-event-of-international-concern
8. Minhaj FS, Ogale YP, Whitehill F, Schultz J, Foote M, Davidson W, et al.; Monkeypox Response Team 2022. Monkeypox outbreak—nine states, May 2022. MMWR Morb Mortal Wkly Rep. 2022;71:764–9. https://doi.org/10.15585/mmwr.mm7123e1
9. Thornhill JP, Palich R, Ghosn J, Walmsley S, Moschese D, Cortes CP, et al.; Share-Net writing group. Human monkeypox virus infection in women and non-binary individuals during the 2022 outbreaks: a global case series. Lancet. 2022;400:1953–65. https://doi.org/10.1016/S0140-6736(22)02187-0
10. Thornhill JP, Barkati S, Walmsley S, Rockstroh J, Antinori A, Harrison LB, et al.; SHARE-net Clinical Group. Monkeypox virus infection in humans across 16 countries—April–June 2022. N Engl J Med. 2022;387:679–91. https://doi.org/10.1056/NEJMoa2207323
11. World Health Organization. Mpox (monkeypox) outbreak 2022 [cited 2023 Aug 25]. https://www.who.int/emergencies/situations/monkeypox-oubreak-2022
12. Girometti N, Byrne R, Bracchi M, Heskin J, McOwan A, Tittle V, et al. Demographic and clinical characteristics of confirmed human monkeypox virus cases in individuals attending a sexual health centre in London, UK: an observational analysis. Lancet Infect Dis. 2022;22:1321–8. https://doi.org/10.1016/S1473-3099(22)00411-X

13. Philpott D, Hughes CM, Alroy KA, Kerins JL, Pavlick J, Asbel L, et al.; CDC Multinational Monkeypox Response Team. Epidemiologic and clinical characteristics of monkeypox cases— United States, May 17–July 22, 2022. MMWR Morb Mortal Wkly Rep. 2022;71:1018–22. https://doi.org/10.15585/mmwr.mm7132e3
14. Van Dijck C, Hoff NA, Mbala-Kingebeni P, Low N, Cevik M, Rimoin AW, et al. Emergence of mpox in the post-smallpox era—a narrative review on mpox epidemiology. Clin Microbiol Infect. 2023. https://doi.org/10.1016/j.cmi.2023.08.008
15. Titanji BK, Tegomoh B, Nematollahi S, Konomos M, Kulkarni PA. Monkeypox: a contemporary review for healthcare professionals. Open Forum Infect Dis. 2022;9:ofac310.

Address for correspondence: Jason Kindrachuk, Department of Medical Microbiology & Infectious Diseases, Department of Internal Medicine, University of Manitoba, 523-745 Bannatyne Ave, Winnipeg, MB R3E 0J9, Canada; email: Jason.Kindrachuk@umanitoba.ca; Placide Mbala-Kingebeni, Département de Biologie Médicale, Université de Kinshasa, 5345, Ave. de la Democratie, B.P. 1187 Gombe, Kinshasa, Democratic Republic of the Congo; email: mbalaplacide@gmail.com

Macacine alphaherpesvirus 1 (B Virus) Infection in Humans, Japan, 2019

Souichi Yamada, Harutaka Katano, Yuko Sato, Tadaki Suzuki, Akihiko Uda, Keita Ishijima, Motoi Suzuki, Daigo Yamada, Shizuko Harada, Hitomi Kinoshita, Phu Hoang Anh Nguyen, Hideki Ebihara, Ken Maeda, Masayuki Saijo, Shuetsu Fukushi

Two human patients with *Macacine alphaherpesvirus* 1 infection were identified in Japan in 2019. Both patients had worked at the same company, which had a macaque facility. The rhesus-genotype B virus genome was detected in cerebrospinal fluid samples from both patients.

The herpesvirus *Macacine alphaherpesvirus* 1 (herpes B virus, or B virus) is ubiquitous in macaque monkeys. Although macaque monkeys do not usually show symptoms when infected with B virus, humans show severe disease, including encephalitis and encephalomyelitis, and death frequently results from infection with B virus from monkeys (*1*). However, B virus infection of humans is rare. Infection can occur after being bitten or scratched by a macaque monkey that is actively shedding the virus or through direct contact with bodily fluids or contaminated laboratory materials. Since B virus infection was first reported in 1934, more than 50 cases have been reported, mainly in North America, and 29 cases have been confirmed, including a recent case in China (*2*,*3*). In most cases in which a specific macaque species was identified, patients had been exposed to rhesus macaques, rather than other species of monkey (e.g., cynomolgus macaques, African green monkeys, Vervet monkeys, or Sykes monkeys) (*2*).

In this study, 2 patients in Japan with chronic and long-term neurologic diseases were tested for B virus infection; the B virus genome was detected in cerebrospinal fluid (CSF). Both patients had worked at a macaque facility in Japan. To maintain confidentiality and privacy, we report no personal information, or information about the clinical course or the working environment. All protocols and procedures were approved by the research ethics committee of the National Institute of Infectious Diseases for the use of human subjects (approval no. 1314). We confirmed B virus infection in both patients by using molecular assay and, in one patient, by also using immunohistochemical analysis. We describe molecular and immunohistochemical findings in the 2 patients.

Author affiliations: National Institute of Infectious Diseases, Tokyo, Japan (S. Yamada, H. Katano, Y. Sato, T. Suzuki, A. Uda, K. Ishijima, M. Suzuki, S. Harada, H. Kinoshita, P.H.A. Nguyen, H. Ebihara, K. Maeda, M. Saijo, S. Fukushi); Ministry of Health, Labor and Welfare, Tokyo (D. Yamada); Health and Welfare Bureau, Sapporo, Japan (M. Saijo)

DOI: https://doi.org/10.3201/eid3001.230435

The Study

Patient 1 worked in the macaque facility at a pharmaceutical research company. In 2019, the patient was hospitalized for headache, fever, and deterioration of consciousness. CSF samples were collected at the time of hospitalization and sent to the National Institute of Infectious Diseases (Tokyo, Japan), where we tested them for B virus infection. We extracted total DNA from the CSF samples and tested the samples by using real-time PCR with primers and a fluorescent probe targeting the B virus gB gene: forward primer, 5′- CGTGGCCAGGTAGTACTGCAC-3′; reverse primer, 5′- CTCGTTCCGCTTCTCCTCGTC-3′); AND fluorescent-labeled probe, 5′- FAM-TAGCGCCGGAGGAA-MGB-3′. The reaction mixture (total volume 25 μL) contained 12.5 μL TaqMan Universal PCR Master Mix (ThermoFisher, https://www.thermofisher.com), 2.0 μg/mL of sonicated salmon sperm DNA, 0.2 μmol/L of each primer and fluorescein amidite–labeled probe, and 4.0 μL of extracted DNA. We subjected the reaction mixture to real-time PCR

by using an ABI-7500 Fast Real-Time PCR System (ThermoFisher). The reaction conditions were as follows: 50°C for 2 min and 95°C for 10 min, followed by 40 cycles of 95°C for 15 s and 60°C for 60 s. We performed real-time PCR targeting the B virus gG gene as described previously (*4*). We performed conventional PCR by using primers targeting a gB gene region conserved among primate herpes viruses (herpes-PCR) as described previously (*5*). We detected the gB and gG genes in the CSF samples at a concentration of 5.1×10^5 copies/mL for gB and 7.6×10^5 copies/mL for gG. Sequencing of the 364-bp herpes-PCR product revealed 100% identity with a B virus sequence from GenBank (accession no. LC637778).

Patient 2 had been diagnosed with chronic neurologic disease. The patient was tested for B virus infection because they worked at the same facility as patient 1 and had been working with macaques. In 2014, patient 2 was admitted to hospital with fever, headache, and neurologic symptoms. Brain biopsy was performed, but no pathogen was detected at that time. In 2019, after identification of patient 1, we collected a CSF sample and tested it for B virus infection in addition to testing a paraffin-embedded section of the brain biopsy collected in 2014. Real-time PCR of the CSF detected the gB (3.5×10^5 copies/mL) and gG genes (2.0×10^6 copies/mL) of B virus. Nucleotide sequencing of the 364-bp herpes-PCR product confirmed that it had 100% identity with the sequence detected in patient 1. Furthermore, real-time PCR of the DNA extracted from the paraffin-embedded section of brain tissue biopsied in 2014 was positive for the B virus gG gene. Real-time PCR did not detect herpes simplex virus 1, herpes simplex virus 2, or varicella zoster virus. Histologic analysis of the brain biopsy revealed inflammatory cell infiltration and hemorrhage in the white matter of the cerebellum (Figure 1). Careful observation revealed the presence of inclusion bodies in the nuclei. Immunohistochemical analysis using B virus rabbit polyclonal and gB mouse monoclonal antibodies generated positive signals in cells with inclusion bodies (*6*).

Conclusions

From our results, we concluded that patients 1 and 2 had been infected with B virus. Although the 2 patients worked in the facility managing imported macaques, there was no direct evidence that they were

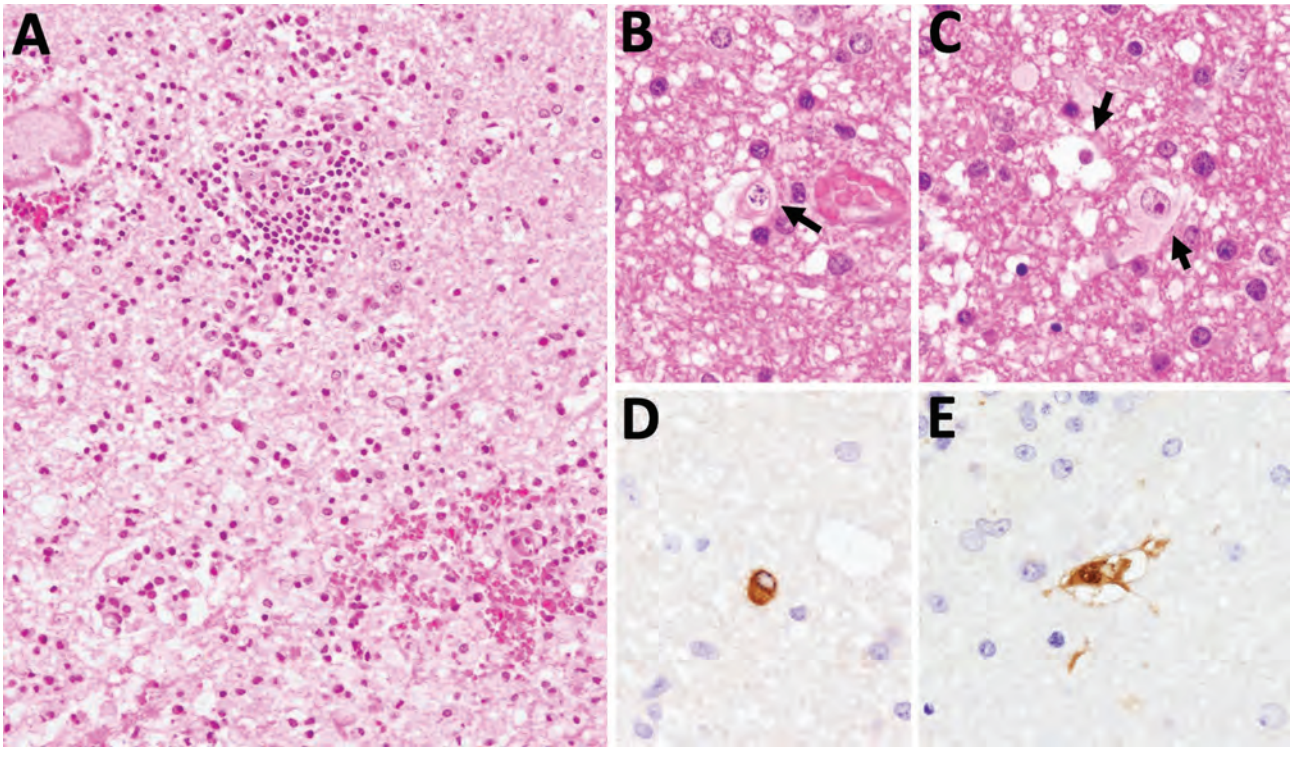

Figure 1. Brain biopsy from patient (patient 2) with *Macacine alphaherpesvirus* 1 (herpes B virus) infection, Japan, 2019. A–C) Inflammatory cell infiltration and hemorrhage observed around blood vessels in the cerebellar white matter. Arrows indicate nuclear inclusion bodies (B, C). Hematoxylin and eosin stain. D, E) Immunohistochemical analysis using B virus gB mouse monoclonal (clone 19B6) (D) and an B virus rabbit polyclonal (E) antibodies as the primary antibodies. Original magnification × 200 for all images.

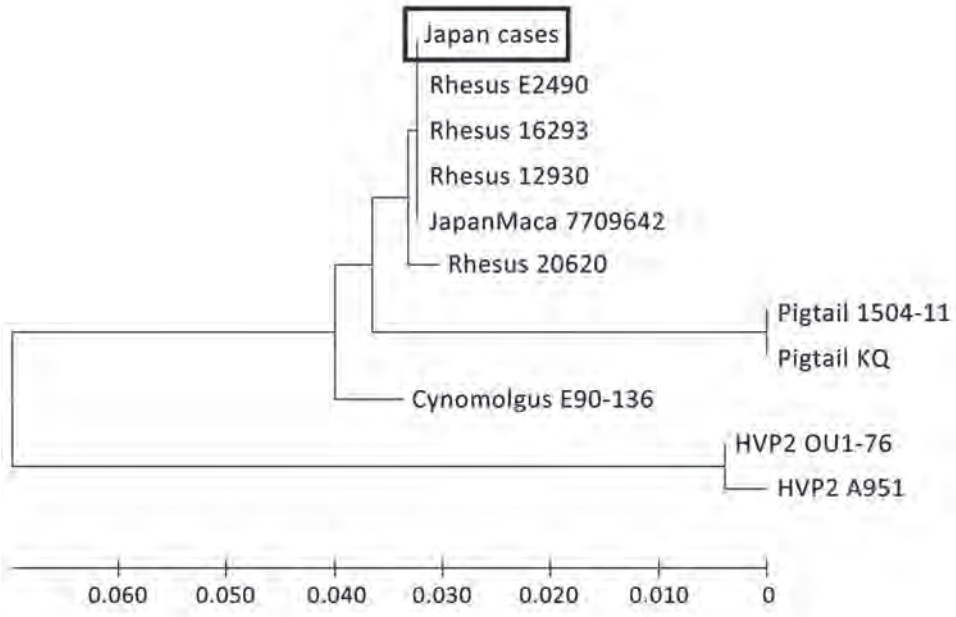

Figure 2. Phylogenetic tree of *Macacine alphaherpesvirus* 1 (herpes B virus) gB gene in 2 patients with B virus infection, Japan, 2019. Nucleotide sequences of the herpes-specific PCR products (364 bp) from the 2 patients were aligned with the corresponding region of the B virus gB gene from GenBank (accession no. LC637778 for virus from patient 1 and LC637779 for virus from patient 2). Phylogenetic tree with HVP2 as an outgroup constructed using the neighbor-joining method. Scale bar indicates number of nucleotide substitutions per site. HVP2, herpesvirus papio 2.

infected from imported macaques. Given that no epidemiologic link between the 2 patients had been recorded, it seems that they were infected independently. Nucleotide sequence analysis identified B virus genotypes known to be carried by the macaque species (*7*,*8*). Recently, a case of human B virus infection was identified in China; however, the genotype was not identified (*3*). Phylogenetic analysis of the gB gene indicated that B virus from the 2 patients in Japan clustered with the genotype in rhesus macaques (Figure 2). The full-length nucleotide sequences of the gG, gB, and gJ genes also were obtained from the CSF of patient 2 and also were classified by phylogenetic analysis as the rhesus B virus genotype (data not shown). Although there is no direct epidemiologic evidence of zoonotic transmission of rhesus B virus in the monkey facility, the results indicated that workers in such facilities are at risk for infection with rhesus B virus infection, which is pathogenic in humans.

This research was supported by AMED (grant nod. JP19fk0108097 and JP23fk0108634) and the Grant-in-Aid for Scientific Research from the Ministry of Education, Culture, Sports, Science and Technology (grant nos. 20K06404 and 21K05967).

About the Author

Dr. S. Yamada is a senior scientist in the Laboratory of Herpesviruses, Department of Virology 1, National Institute of Infectious Diseases, Japan. His research interests include virology of herpes simplex virus, human cytomegalovirus, and B virus.

References

1. Huff JL, Barry PA. B-virus (*Cercopithecine herpesvirus* 1) infection in humans and macaques: potential for zoonotic disease. Emerg Infect Dis. 2003;9:246–50. https://doi.org/10.3201/eid0902.020272
2. Jones-Engel E. Low incidence, high lethality or higher incidence, lower lethality: what we know and don't know about zoonotic *Macacine alphaherpesvirus* 1 (monkey B virus) [Chapter 8]. In: Knauf S, Jones-Engel L, editors. Neglected diseases in monkeys. Cham (Switzerland): Springer Nature Switzerland; 2020. p. 171–204.
3. Wang W, Qi W, Liu J, Du H, Zhao L, Zheng Y, et al. First human infection case of monkey B virus identified in China, 2021. China CDC Wkly. 2021;3:632–3. https://doi.org/10.46234/ccdcw2021.154
4. Perelygina L, Patrusheva I, Manes N, Wildes MJ, Krug P, Hilliard JK. Quantitative real-time PCR for detection of monkey B virus (*Cercopithecine herpesvirus* 1) in clinical samples. J Virol Methods. 2003;109:245–51. https://doi.org/10.1016/S0166-0934(03)00078-8
5. Black DH, Eberle R. Detection and differentiation of primate alpha-herpesviruses by PCR. J Vet Diagn Invest. 1997;9:225–31. https://doi.org/10.1177/104063879700900301
6. Blewett EL, Black D, Eberle R. Characterization of virus-specific and cross-reactive monoclonal antibodies to *Herpesvirus simiae* (B virus). J Gen Virol. 1996;77:2787–93. https://doi.org/10.1099/0022-1317-77-11-2787
7. Smith AL, Black DH, Eberle R. Molecular evidence for distinct genotypes of monkey B virus (*Herpesvirus simiae*) which are related to the macaque host species. J Virol. 1998;72:9224–32. https://doi.org/10.1128/JVI.72.11.9224-9232.1998
8. Ohsawa K, Black DH, Torii R, Sato H, Eberle R. Detection of a unique genotype of monkey B virus (*Cercopithecine herpesvirus* 1) indigenous to native Japanese macaques (*Macaca fuscata*). Comp Med. 2002;52:555–9.

Address for correspondence: Shuetsu Fukushi, Department of Virology 1, National Institute of Infectious Diseases, 1-23-1, Shinjuku, Tokyo 162-8640, Japan; e-mail: fukushi@niid.go.jp

Estimation of Incubation Period of Mpox during 2022 Outbreak in Pereira, Colombia

Jorge M. Estrada Alvarez, Maryluz Hincapié Acuña, Hernán F. García Arias, Franklyn E. Prieto Alvarado, Juan J. Ospina Ramírez[1]

We estimated the incubation period for mpox during an outbreak in Pereira, Colombia, using data from 11 confirmed cases. Mean incubation period was 7.1 (95% CI 4.9–9.9) days, consistent with previous outbreaks. Accurately estimating the incubation period provides insights into transmission dynamics, informing public health interventions and surveillance strategies.

Mpox, a zoonotic disease endemic to central and western Africa, is caused by monkeypox virus and transmitted primarily through person-to-person contact, secretions from skin and respiratory lesions, and fomites, such as bedding and shared utensils (*1*). Mpox manifests in a wide spectrum of signs and symptoms, including fever, headache, muscle pain, fatigue, lymphadenopathy, and a characteristic rash progressing from macules to papules, vesicles, pustules, and eventually crusts (*2*).

Since May 2022, mpox outbreaks have been reported in 109 countries, notably affecting men who have sex with men (MSM) (*3*). The atypical transmission pattern of mpox has prompted investigation into potential sexually associated routes and led to hypotheses about disease dynamics (*4*,*5*). Previous evidence suggests changes from classic clinical manifestations, which included milder symptoms and genital lesions, and alterations in transmission dynamics, particularly during the incubation period (*6*–*8*).

Author affiliations: Instituto Nacional de Salud, Bogotá, Colombia (J.M. Estrada Alvarez); Salud Comfamiliar–Caja de Compensación Familiar de Risaralda, Pereira, Colombia (J.M. Estrada Alvarez); Corporación Universitaria Minuto de Dios, Pereira (M. Hincapie Acuña); SISTEMIC Research Group, Universidad de Antioquia, Medellin, Colombia (H.F. Garcia Arias); Secretaria de Salud Pública y Seguridad Social, Pereira (J.J. Ospina Ramírez); Instituto Nacional de Salud, Bogotá (F.E. Prieto Alvarado)

DOI: https://doi.org/10.3201/eid3001.221663

Accurately estimating the mpox incubation period is crucial for implementing effective public health measures, such as quarantine and isolation during outbreaks. We attempted to estimate the distribution of the incubation period using data from the first confirmed cases among MSM identified through routine surveillance. This study was approved by the institutional committee of the Health Department of Pereira (Colombia) in accordance with Resolution 8430 of 1993.

The Study

We conducted a descriptive cross-sectional epidemiologic study using data extracted from field epidemiologic investigation of 11 reverse transcription PCR–confirmed cases of mpox in Pereira, Colombia, from the national reference laboratory of the National Institute of Health of Colombia. Case investigations were performed by a coinvestigator with training and experience in conducting epidemiologic interviews. Investigators gathered information from patients on travel history within the 21 days before symptom onset and any potential exposure events from a list of events developed from scientific publications on the 2022 mpox outbreak (*4*,*6*). Events included having multiple sexual encounters or new sexual partners, attending LGBTQ+ venues such as saunas and venues for sexual encounters involving chemsex (sexual activity while under the influence of drugs), or social gatherings involving intimate contact, including sexual activity.

We used 2 approaches to collect data on date of exposure. If during the initial interview a case-patient reported an exact date potentially related to exposure to mpox infection, we recorded that as probable date of exposure. If the case-patient identified multiple potential exposure times, we recorded the longest period of time during which visits to places or situations for potential monkeypox virus transmission. That second

[1]All authors contributed equally to this article.

approach generated censored interval data in which occurrence of the transmission event was known, but not the exact timing.

For the date of onset, we used the day in the prodromal period on which symptoms were first reported, including nonspecific symptoms such as fever, fatigue, headache, lymphadenopathy, muscle pain, sore throat, or rash. We resolved inconsistencies in dates and missing data through follow-up telephone interviews. We conducted an event-time analysis to estimate the distribution that would best fit the incubation periods of the cases. Because measurements corresponded to both interval-censored and left-censored data, as explained elsewhere (*9*), we constructed a dataset with these characteristics. We used 3 parametric distributions—gamma, Weibull, and log-normal—to determine the best fit for the analytic model. We evaluated the fitted models using the corrected Akaike information criterion (AICc) to obtain the lowest value, which indicates a better model fit. We performed all analyses in R software icenReg package version 2015 (https://cran.r-project.org/web/packages/icenReg/index.html) using the maximum-likelihood method (*10*).

All 11 mpox case-patients included in our analysis were men who reported having sexual contact with other men. Median age was 34 (range 22–53, interquartile range 27–41) years. Symptoms commonly reported were myalgia, headache, fever, and lymphadenopathy. Only 1 case-patient did not manifest genital lesions, and only 2 did not have a previous HIV diagnosis. Dates of probable exposure for the 11 patients were July 9–September 10, 2022; dates of first symptom onset were July 11–September 20, 2022. Exposure window was 1 day in 6/11 cases; maximum exposure window was 8 days (1 case) and minimum 1 day.

Visual inspection of the parametric curves confirmed that all 3 fitted parametric models provided reasonable fits for distribution of the incubation period (Figure). Based on AICc values (Table), Weibull parametric distribution (AICc = 61.18) fit the data most closely, followed by gamma (AICc = 61.64) and log-normal (AICc = 62.79) distributions. For the best-fit Weibull distribution, median incubation period was 7.1 days (95% CI 4.9–9.9 days); 95th percentile incubation period was 15 days (95% CI 10.6–22.6 days).

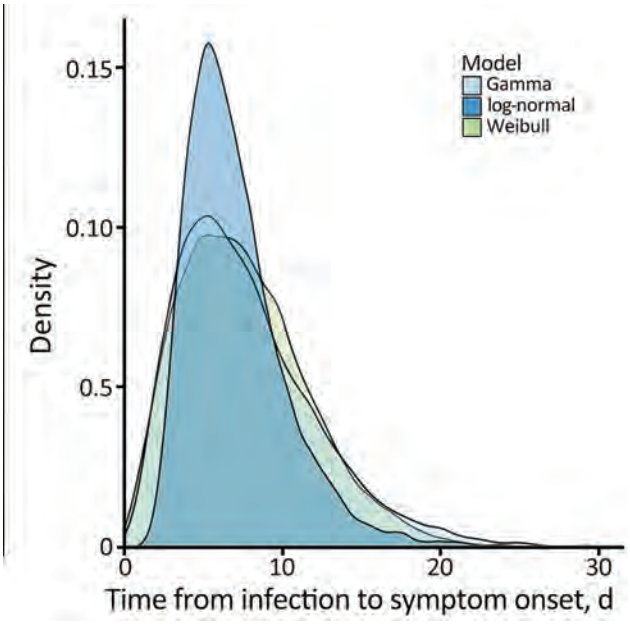

Figure. Comparison of parametric distributions from different models for the incubation period of mpox for patients in Pereira, Colombia.

Results for gamma and log-normal distributions were similar (Figure). Adjusted mean incubation period using the Weibull parametric distribution from likely exposure to onset was 7.1 days (5th–95th percentiles 1.9–15.0 days). That estimated incubation period aligns with some previous findings after considering associated uncertainty and statistical methodologies used in those studies. One study reported a mean of 8.5 days (5th–95th percentiles 4.2–17.3 days) slightly longer than in our study (*11*); another (K. Charniga, unpub. data, https://doi.org/10.1101/2022.06.22.22276713) estimated a mean 7.6 days (95% credible interval 6.2–9.7) and the 95th percentile 17.7 days (95% CrI 12.4–28.1 days), more closely consistent with our estimation and supported by data from 3 additional studies (*4*,*5*,*12*).

Mpox might exhibit a shorter incubation period in invasive or complex exposures, in which the patient experienced contact through damaged skin or mucous membranes; typical incubation period is 9 days in those exposures (*4*). Mean mpox incubation period in MSM during this outbreak was 7.1 days,

Table. Estimated mean and percentile parametric distributions for incubation period in 11 confirmed cases of mpox, Pereira, Colombia*

Model	Mean incubation, d (95% CI)			AICc
	P_{50}	P_5	P_{95}	
Gamma	6.7 (4.6–9.5)	2.0 (1.0–3.9)	15.9 (10.6–24.5)	61.64
log-normal	6.4 (4.3–9.2)	2.2 (1.0–3.9)	18.6 (10.7–37.6)	62.79
Weibull	7.1 (4.9–9.9)	1.9 (1.0–4.0)	15.0 (10.6–22.6)	61.18

*P_5, P_{50}, and P_{95} indicate the percentiles of the estimated distribution. AICc, corrected Akaike information criterion

which aligns with reports in cases with similar conditions, falling within the typical values for complex or invasive exposure (*11*; K. Charniga, unpub. data). Of the 11 case-patients, 9 had a previous HIV diagnosis; research has indicated that HIV-infected patients may experience shorter incubation periods than persons not infected with HIV (*13*). That association might be related to immunosuppression and compromised immune response in persons with HIV potentially accelerating viral replication and clinical manifestations of mpox.

Conclusions

Establishing precise and accurate estimates of the temporal distribution of incubation periods for emerging infectious diseases is crucial for case definition and to inform public health policies. Robust inference methods that account for interval censoring in the estimations are recommended. Regarding potential transmission associated with sexual contact during the mpox outbreak (*6*), the complex and varied nature of those types of exposure should be carefully considered and incorporated into epidemiologic findings. We obtained the data on which this study was based from initial epidemiologic investigations of cases during a mpox outbreak in the city of Pereira, Colombia. The small sample size (11 case-patients) was a limitation of this study.

Our study provides empirical evidence of the incubation period in the 2022 mpox outbreak, illustrated by the Weibull distribution graph, using data on exposure history and symptom onset in cases confirmed using PCR testing in Colombia and Latin America. The upper limit of the confidence interval for the estimated 95th percentile, 22.6 days, supports the recommendation of using a 21-day monitoring period for potential mpox cases involving close contact to limit further spread of the infection. Understanding the incubation period and its variability contributes to the development of targeted control strategies and enhances our knowledge of this emerging infectious disease.

Acknowledgments

We thank local public health departments in Pereira, Colombia for allowing us to use case data.

About the Author

Dr. Estrada Alvarez is part of the Fellow Training Epidemiology Program at the Instituto Nacional de Salud in Colombia and a researcher at Comfamiliar Risaralda in Pereira, Colombia. His research interests include use of healthcare statistical methods in epidemiology and data science.

References

1. Petersen E, Kantele A, Koopmans M, Asogun D, Yinka-Ogunleye A, Ihekweazu C, et al. Human monkeypox: epidemiologic and clinical characteristics, diagnosis, and prevention. Infect Dis Clin North Am. 2019;33:1027–43. https://doi.org/10.1016/j.idc.2019.03.001
2. US Centers for Disease Control and Prevention. Signs and symptoms [cited 2022 Oct 20]. https://www.cdc.gov/poxvirus/monkeypox/symptoms/index.html
3. World Health Organization. 2022 monkeypox outbreak: global trends 2022 [cited 2022 Oct 20]. https://worldhealthorg.shinyapps.io/mpx_global
4. Català A, Clavo-Escribano P, Riera-Monroig J, Martín-Ezquerra G, Fernandez-Gonzalez P, Revelles-Peñas L, et al. Monkeypox outbreak in Spain: clinical and epidemiological findings in a prospective cross-sectional study of 185 cases. Br J Dermatol. 2022;187:765–72. https://doi.org/10.1111/bjd.21790
5. Thornhill JP, Barkati S, Walmsley S, Rockstroh J, Antinori A, Harrison LB, et al.; SHARE-net Clinical Group. Monkeypox virus infection in humans across 16 countries—April–June 2022. N Engl J Med. 2022;387:679–91. https://doi.org/10.1056/NEJMoa2207323
6. Antinori A, Mazzotta V, Vita S, Carletti F, Tacconi D, Lapini LE, et al.; INMI Monkeypox Group. Epidemiological, clinical and virological characteristics of four cases of monkeypox support transmission through sexual contact, Italy, May 2022. Euro Surveill. 2022;27:2200421. https://doi.org/10.2807/1560-7917.ES.2022.27.22.2200421
7. Rodriguez-Morales AJ, Lopardo G. Monkeypox: another sexually transmitted infection? Pathogens. 2022;11:713. https://doi.org/10.3390/pathogens11070713
8. Reynolds MG, Yorita KL, Kuehnert MJ, Davidson WB, Huhn GD, Holman RC, et al. Clinical manifestations of human monkeypox influenced by route of infection. J Infect Dis. 2006;194:773–80. https://doi.org/10.1086/505880
9. Klein JP, Moeschberger ML. Survival analysis: techniques for censored and truncated data. New York: Springer; 2003.
10. Anderson-Bergman C. icenReg: regression models for interval censored data in R. J Stat Softw. 2017;81:1–23. https://doi.org/10.18637/jss.v081.i12
11. Miura F, van Ewijk CE, Backer JA, Xiridou M, Franz E, Op de Coul E, et al. Estimated incubation period for monkeypox cases confirmed in the Netherlands, May 2022. Euro Surveill. 2022;27:2200448. https://doi.org/10.2807/1560-7917.ES.2022.27.24.2200448
12. Tarín-Vicente EJ, Alemany A, Agud-Dios M, Ubals M, Suñer C, Antón A, et al. Clinical presentation and virological assessment of confirmed human monkeypox virus cases in Spain: a prospective observational cohort study. Lancet. 2022;400:661–9. https://doi.org/10.1016/S0140-6736(22)01436-2
13. Eser-Karlidag G, Chacon-Cruz E, Cag Y, Martinez-Orozco JA, Gudino-Solorio H, Cruz-Flores RA, et al. Features of mpox infection: the analysis of the data submitted to the ID-IRI network. New Microbes New Infect. 2023;53:101154. https://doi.org/10.1016/j.nmni.2023.101154

Address for correspondence: Jorge Mario Estrada Alvarez, Av. Circunvalar No. 3-01, Pereira, Risaralda, Colombia; email: jestradaa@comfamiliar.com

Autochthonous Dengue Fever in 2 Patients, Rome, Italy

Serena Vita,[1] Licia Bordi,[1] Giuseppe Sberna, Priscilla Caputi, Daniele Lapa, Angela Corpolongo, Cosmina Mija, Alessandra D'Abramo, Fabrizio Maggi, Francesco Vairo, Eliana Specchiarello, Enrico Girardi, Eleonora Lalle, Emanuele Nicastri

Author affiliation: National Institute for Infectious Diseases Lazzaro Spallanzani, Rome, Italy

https://doi.org/10.3201/eid3001.231508

Since August 2023, outbreaks of dengue virus (DENV) infection have occurred in Italy. We report 2 autochthonous case-patients and their extended follow-up. Despite persistent DENV detected in blood by PCR, results for antigenomic DENV RNA were negative after day 5, suggesting that a 5-day isolation period is adequate to avoid secondary cases.

Dengue virus (DENV) infection is the most prevalent arthropodborne viral disease in humans, caused by 4 DENV serotypes widely spread in tropical and subtropical regions and transmitted mainly by *Aedes* mosquitoes (*1*). *Aedes albopictus* mosquitoes colonizing every continent except Antarctica has led to an increase in areas of Europe at risk for *Aedes*-borne viruses (*2*,*3*). During August–October 2023, a total of 68 case-patients who had DENV infection and no travel link were reported in Italy, 36 (53%) in Lombardia and 32 (47%) in Lazio; all had a good clinical condition (*4*,*5*). We report 2 autochthonous case-patients who had DENV infection and prolonged viral shedding during a follow-up period of 28 days after symptoms onset.

On August 31, a 46-year-old man (case-patient 1) and a 48-year-old woman (case-patient 2) who were living in Rome, Italy, and had no history of recent international travel or of yellow fever vaccination were referred to the National Institute for Infectious Diseases L. Spallanzani in Rome for history of fever. Both persons were on holiday during August 14–21. On August 27, eighty km south of Rome, where 1 imported DENV case was previously reported, case-patient 1 had a 2-day history of fever with bilateral conjunctivitis and a face and trunk macular rash, and case-patient 2 had a 1-day history of fever with myalgia and arthralgia. No major concurrent illnesses were present.

[1]These authors equally contributed to this article.

At admission, we tested the 2 patients for DENV nonstructural protein 1 (NS1) and IgM and IgG by using fluorimetric rapid assays (Standard F Dengue NS1 Ag FIA and Standard F Dengue IgM/IgG FIA; SD Biosensor, https://www.sdbiosensor.com) (*6*). For both patients, rapid assays were positive for DENV NS1 antigen only, which is considered an early marker for acute DENV infection (*7*). Results for chikungunya virus, HIV, hepatitis B virus, and hepatitis C virus were negative. Hematologic analyses showed platelet values within reference limits but leukopenia (minimum 2,760 cells/mm^3 for case-patient 1 and 1,850 cells/mm^3 for case-patient 2; reference range 4,000–11,000 cells/mm^3) and lymphocytopenia (minimum 750 cells/mm^3 for case-patient 1 and 230 cells/mm^3 for case-patient 2; reference range 1,000–4,800 cells/mm^3).

Case-patient 1 had continuous fever (maximum temperature 38.5°C) until day 8, skin macular rash and lymphopenia until day 9, and lowest platelet level (98,000 cells/mm3) on day 9. Case-patient 2 had fever (maximum temperature 38.7°C), headache, myalgia, arthralgia, and lymphopenia until day 7.

We performed molecular and serologic analyses during the 28-day follow-up period (Appendix, https://wwwnc.cdc.gov/EID/article/30/1/23-1508-App1.pdf). DENV-specific reverse transcription PCR on plasma and blood samples collected within 3 days after symptom onset yielded positive results, enabling us to identify a DENV-3 infection (*8*). Plasma samples remained positive until day 9 for case-patient 1 and day 8 for case-patient 2. Blood samples were positive at day 17 for case-patient 1 and day 16 for case-patient 2. Saliva sample results were positive until day 9 for case-patient 1 and day 8 for case-patient 2. Positive urine samples were observed only at day 9 for case-patient 1 and day 16 for case-patient 2. Ocular swab specimens remained negative for both patients. At the end of the 28-day follow-up period, all samples were negative in the DENV molecular assay.

We analyzed serum and saliva samples by using an immunofluorescence assay to detect DENV-3–specific IgM, IgG, and IgA at serologic and mucosal levels (Appendix). IgM appeared in serum samples by day 6 and seroconversion of IgG by day 9 in both case-patients. In saliva, IgM, IgG, and IgA were always negative for case-patient 1, and a positive result was obtained for IgA at day 8 for case-patient 2, suggesting an absent/poor antibody response at the mucosal level for these patients.

To determine whether the DENV genome in plasma/blood samples was associated with active viral replication, we measured levels of antigenomic DENV RNA (negative-strand) (Appendix) by using a DENV type 3–specific forward primer because we considered it to be an indirect marker of ongoing viral replication (*9*). Both patients had antigenomic DENV RNA during the acute phase of infection (i.e., day 3), and case-patient 2 was positive for antigenomic DENV RNA until day 5. Thereafter, despite prolonged viral persistence detected by reverse transcription PCR in plasma/blood until day 16, the antigenomic DENV RNA test results were always negative, suggesting absence of ongoing active viral replication. Patients were discharged at day 9 (case-patient 1) and day 8 (case-patient 2) in good clinical condition.

DENV-infected patients can transmit the virus to Aedes mosquitoes if bitten after symptom onset. Therefore, patients should use precautionary measures to reduce the risk for transmission (i.e., sleeping alone) during the first 7 days of febrile illness.

Our results suggest that prolonged viral shedding is not always a marker of ongoing replication in blood, and that the 5-day isolation period might be adequate to prevent transmission (*10*). This observation is relevant for nonendemic countries to limit generation and spread of autochthonous cases.

This study was supported by the Ministero della Salute: Ricerca Corrente, Linea 1.

This study was conducted in accordance with the Declaration of Helsinki and protocol code no. 70 and approved on December 17, 2018, by the institutional review board of the National Institute for Infectious Diseases, L. Spallanzani, Istituto di Ricovero e Cura a Carattere Scientifico, according to which the study protocol did not provide informed consent by patients because no additional samples were taken other than those used for diagnostic purposes. Data for biologic samples collected for diagnostic purposes were used only after their complete anonymization. Analysis of genetic data was not provided.

L.B. and S.V. analyzed results and wrote and edited the article; C.M. and D.L. performed serologic testing; E.S. and G.S. performed molecular testing; A.D., P.C., and A.C. enrolled patients and edited the article; F.V., F.M., and E.G. reviewed and edited the article; and E.N. and E.L. conceptualized, reviewed, and edited the article.

About the Author

Dr. Vita is a research scientist at the National Institute for Infectious Diseases Lazzaro Spallanzani, Rome, Italy. Her primary research interests are chronic and emerging acute infections.

References

1. Guzman MG, Harris E. Dengue. Lancet. 2015;385:453–65. https://doi.org/10.1016/S0140-6736(14)60572-9
2. European Centre for Disease Prevention and Control. Autochthonous vectorial transmission of dengue virus in mainland EU/EEA, 2010–present. October 5, 2023 [cited 2023 Oct 31]. https://www.ecdc.europa.eu/en/all-topics-z/dengue/surveillance-and-disease-data/autochthonous-transmission-dengue-virus-eueea
3. Benedict MQ, Levine RS, Hawley WA, Lounibos LP. Spread of the tiger: global risk of invasion by the mosquito *Aedes albopictus*. Vector Borne Zoonotic Dis. 2007;7:76–85. https://doi.org/10.1089/vbz.2006.0562
4. De Carli G, Carletti F, Spaziante M, Gruber CEM, Rueca M, Spezia PG, et al.; Lazio Dengue Outbreak Group. Outbreaks of autochthonous dengue in Lazio region, Italy, August to September 2023: preliminary investigation. Euro Surveill. 2023;28:2300552. https://doi.org/10.2807/1560-7917.ES.2023.28.44.2300552
5. Cassaniti I, Ferrari G, Senatore S, Rossetti E, Defilippo F, Maffeo M, et al.; Lombardy Dengue Network. Preliminary results on an autochthonous dengue outbreak in Lombardy Region, Italy, August 2023. Euro Surveill. 2023;28:2300471. https://doi.org/10.2807/1560-7917.ES.2023.28.37.2300471
6. Matusali G, Colavita F, Carletti F, Lalle E, Bordi L, Vairo F, et al. Performance of rapid tests in the management of dengue fever imported cases in Lazio, Italy 2014–2019. Int J Infect Dis. 2020;99:193–8. https://doi.org/10.1016/j.ijid.2020.07.008
7. Huang JL, Huang JH, Shyu RH, Teng CW, Lin YL, Kuo MD, et al. High-level expression of recombinant dengue viral NS-1 protein and its potential use as a diagnostic antigen. J Med Virol. 2001;65:553–60. https://doi.org/10.1002/jmv.2072
8. Centers for Disease Control and Prevention. Molecular tests for dengue virus. June 12, 2019 [cited 2023 Oct 31]. https://www.cdc.gov/dengue/healthcare-providers/testing/molecular-tests/index.html
9. Lalle E, Colavita F, Iannetta M, Gebremeskel Teklè S, Carletti F, Scorzolini L, et al. Prolonged detection of dengue virus RNA in the semen of a man returning from Thailand to Italy, January 2018. Euro Surveill. 2018;23:18–00197. https://doi.org/10.2807/1560-7917.ES.2018.23.18.18-00197
10. Carrington LB, Simmons CP. Human to mosquito transmission of dengue viruses. Front Immunol. 2014;5:290. https://doi.org/10.3389/fimmu.2014.00290

Address for correspondence: Eleonora Lalle, Laboratory of Virology and Biosafety Laboratories, National Institute of Infectious Diseases L. Spallanzani, Via Portuense 292, Rome 00149, Italy; email: eleonora.lalle@inmi.it

Pseudomonas guariconensis Necrotizing Fasciitis, United Kingdom

Edward J. Moseley, Jian Cheng Zhang, O. Martin Williams

Author affiliations: UK Health Security Agency Specialist Microbiology and Laboratories, South West Region and Severn Infection Sciences, Bristol, UK (E.J. Moseley, J.C. Zhang, O.M. Williams); University Hospitals Bristol and Weston NHS Foundation Trust, Bristol (E.J. Moseley, O.M. Williams); Southmead Hospital, Bristol (J.C. Zhang)

DOI: https://doi.org/10.3201/eid3001.231192

We describe a case of necrotizing fasciitis in the United Kingdom in which *Pseudomonas guariconensis* was isolated from multiple blood culture and tissue samples. The organism carried a Verona integron-encoded metallo-β-lactamase gene and evidence of decreased susceptibility to β-lactam antimicrobial agents. Clinicians should use caution when treating infection caused by this rare pathogen.

A 67-year-old man in the United Kingdom was seen in the emergency department for right lower leg pain and swelling with associated fevers lasting 24 hours. He reported a right heel blister had formed 1 week earlier, after he purchased new footwear. His medical history included obesity, hypertension, atrial fibrillation, and left ventricular systolic dysfunction. He was a former smoker and had a 40 pack-year history.

On examination, the patient appeared alert and comfortable. He was febrile (38.0°C), tachycardic (124 beats/min) in atrial fibrillation, and had a stable blood pressure (108/72 mm Hg). His respiratory rate was 20 breaths/min, and oxygen saturation was 92% on room air. He had right leg swelling and erythema, extending from the blister on his heel to his mid-calf. Blood test results showed leukocyte count was 15.03 × 10^9 cells/L (reference range 4.0–11.0 cells/L), neutrophils 13.44 (reference 1.5–8.0) × 10^9 cells/L, and lymphocytes 0.38 (reference 1.0–4.0) × 10^9 cells/L. Bilirubin was 41 (reference <21) μmol/L, albumin 34 (reference 35–50) g/L, and C-reactive protein 20 (reference <6.0) mg/L.

The patient was started on intravenous flucloxacillin (1g 4×/d) for lower limb cellulitis. Aerobic blood culture samples at admission were positive at 11.5 hours' incubation and cultures collected 8 hours after admission positive at 10.5 hours' incubation by BD Bactec FX system (Becton Dickinson, https://www.bd.com). Gram stain from the samples showed gram-negative bacilli, resulting in an immediate change of therapy to intravenous amoxicillin/clavulanic acid (1.2 g 3×/d) and gentamicin (400 mg; 5 mg/kg based on patient's ideal bodyweight). Direct extract from the first sample was tested by matrix-assisted laser desorption/ionization time-of-flight (MALDI-TOF) mass spectroscopy (Bruker Corporation, https://www.bruker.com), which identified *Pseudomonas guariconensis* with a score of 1.94 within 3 hours of the initial culture report. Growth on plates from the second blood culture was subsequently confirmed to be the same organism. Samples were sent to the UK Health Security Agency Antimicrobial Resistance and Healthcare Infection reference laboratory, which also confirmed *P. guariconensis* by MALDI-TOF mass spectroscopy with a score of 2.62.

The patient's treatment was changed to intravenous piperacillin/tazobactam (4.5 g 4×/d); gentamicin was continued. On review, no local features of necrotizing fasciitis were observed, and his leg appeared improved. The patient reported that he had been applying several over-the-counter creams of uncertain age to his blister since it had developed.

Table. Antimicrobial susceptibility data for blood culture isolates in a case of *Pseudomonas guariconensis* necrotizing fasciitis, United Kingdom*

Antimicrobial agent	Admission blood culture by ViTek 2† (MIC, mg/L)	8-h blood culture		Tissue culture by disc diffusion‡
		Disc diffusion‡	Gradient strip (MIC, mg/L)	
Ceftazidime	I (4)	I	ND	I
Ciprofloxacin	I (≤0.25)	I	ND	I
Gentamicin	S (≤1)	S	ND	S
Meropenem	I (4)	I	I (4)	I
Tobramycin	S (≤1)	S	ND	S
Piperacillin/tazobactam	R (64)	I	I (16)	I
Amikacin	S (≤2)	ND	ND	ND
Cefepime	I (2)	ND	ND	ND
Imipenem	I (1)	ND	ND	ND
Levofloxacin	I (0.5)	ND	ND	ND
Ticarcillin/clavulanic acid	R (≥128)	ND	ND	ND

*All breakpoints are European Committee on Antimicrobial Susceptibility Testing (EUCAST) clinical breakpoints version 11.0, except gentamicin disk diffusion testing, for which EUCAST version 9.0 was used. I, susceptible, increased exposure; ND, not done; R, resistant; S, susceptible.
†bioMérieux, https://www.biomerieux.com.
‡Using methods from EUCAST (*1*).

Attempts were made to recover the creams for culture but were unsuccessful.

Direct disk susceptibility testing was performed by using European Committee on Antimicrobial Susceptibility Testing (EUCAST) rapid antimicrobial susceptibility testing (AST) methodology, reading plates at 16–18 hours, which showed piperacillin/tazobactam susceptibility. Although unvalidated for this organism, AST suggested piperacillin/tazobactam susceptibility at increased exposure compared with EUCAST rapid AST breakpoints for *P. aeruginosa* and standard AST clinical breakpoints for *Pseudomonas* spp. (EUCAST criteria version 11.0), which was confirmed by standard EUCAST disk diffusion testing (*1*) from the second isolate. The patient's gentamicin was stopped. However, he remained tachycardic and hypotensive.

Confirmatory AST performed by using the VITEK 2 system and software version 9.02 (bioMérieux, https://www.biomerieux.com) produced a piperacillin/tazobactam MIC of 64 mg/L and meropenem MIC of 4 mg/L (Table). Piperacillin/tazobactam MIC by gradient strip testing performed on the second isolate was increased at 16 mg/L, particularly close to the EUCAST breakpoint, and meropenem MIC was increased at 4 mg/L. The patient's therapy was changed to 2 g intravenous ceftazidime (2 g 3×/d).

In-house multiplex PCR was performed using agarose gel electrophoresis for beta-lactamase genes (Appendix, https://wwwnc.cdc.gov/EID/article/30/1/23-1192-App1.pdf), based on previously published methodology (*2*–*5*). PCR detected a Verona integron-encoded metallo-β-lactamase enzyme, consistent with previously reported strains of this species (*6*,*7*).

The patient subsequently deteriorated and required inotropic and vasopressive support. He underwent above-knee amputation and debridement after fasciotomies, and exploration confirming necrotizing fasciitis. Tissue samples isolated pure growth *P. guariconensis*, and sensitivity testing by standard EUCAST disk methodology was consistent with previous samples (Table).

The patient remained in the critical care unit for 3 days and had high vasopressor requirements despite adequate antimicrobial drug therapy. He was deemed not stable for further surgery; life-sustaining treatment was withdrawn, and he died.

P. guariconensis is a gram-negative, strictly aerobic, non–spore-forming, rod-shaped bacterium that is motile by means of 2 polar flagella, is oxidase and catalase positive, and is indole and aesculin negative. *P. guariconensis* was described in 2013, isolated from rhizospheric soil of *Vigna unguiculata* (L.) Walp. (the cowpea) in Guárico, Venezuela (*8*). Isolates of the same species producing novel carbapenemases have been reported from environmental samples taken in the Amazon Basin (*9*).

Reports of *P. guariconensis* human disease are rare; 1 case of infective endocarditis was reported in a patient with underlying lupus erythematosus (*10*). The rarity of reports likely reflects the recent description of the species and delays in updates to identification methodologies, such as MALDI-TOF databases. This case shows the pathogenic potential of *P. guariconensis* in an immunocompetent host and the degree of clinical suspicion required to exclude deep infection when isolating an unusual organism from a sterile site.

About the Author

Dr. Mosley is a specialty trainee in infectious diseases and medical microbiology in Bristol, United Kingdom. His research interests include antimicrobial stewardship, point of care testing, and medical education.

References

1. Matuschek E, Brown DFJ, Kahlmeter G. Development of the EUCAST disk diffusion antimicrobial susceptibility testing method and its implementation in routine microbiology laboratories. Clin Microbiol Infect. 2014;20:O255–66. https://doi.org/10.1111/1469-0691.12373
2. Hidalgo L, Hopkins KL, Gutierrez B, Ovejero CM, Shukla S, Douthwaite S, et al. Association of the novel aminoglycoside resistance determinant RmtF with NDM carbapenemase in Enterobacteriaceae isolated in India and the UK. J Antimicrob Chemother. 2013;68:1543–50. https://doi.org/10.1093/jac/dkt078
3. Ellington MJ, Kistler J, Livermore DM, Woodford N. Multiplex PCR for rapid detection of genes encoding acquired metallo-beta-lactamases. J Antimicrob Chemother. 2006;59:321–2. https://doi.org/10.1093/jac/dkl481
4. Poirel L, Héritier C, Tolün V, Nordmann P. Emergence of oxacillinase-mediated resistance to imipenem in *Klebsiella pneumoniae.* Antimicrob Agents Chemother. 2004;48:15–22. https://doi.org/10.1128/AAC.48.1.15-22.2004
5. Yigit H, Queenan AM, Anderson GJ, Domenech-Sanchez A, Biddle JW, Steward CD, et al. Novel carbapenem-hydrolyzing β-lactamase, KPC-1, from a carbapenem-resistant strain of *Klebsiella pneumoniae.* Antimicrob Agents Chemother. 2001;45:1151–61. https://doi.org/10.1128/AAC.45.4.1151-1161.2001
6. Public Health England. UK standards for microbiology investigations 60: detection of bacteria with carbapenem-hydrolysing β-lactamases (carbapenemases). London: Public Health England; 2020.
7. Adelowo OO, Vollmers J, Mäusezahl I, Kaster AK, Müller JA. Detection of the carbapenemase gene bla_{VIM-5} in members of the *Pseudomonas putida* group isolated from polluted Nigerian wetlands. Sci Rep. 2018;8:15116. https://doi.org/10.1038/s41598-018-33535-3
8. Toro M, Ramírez-Bahena MH, Cuesta MJ, Velázquez E, Peix A. *Pseudomonas guariconensis* sp. nov., isolated from rhizospheric soil. Int J Syst Evol Microbiol. 2013;63:4413–20. https://doi.org/10.1099/ijs.0.051193-0
9. Souza CO, Cayô R, Lima KVB, Brasiliense DM, Streling AP, Siqueira AV, et al. Genetic and biochemical characterization

of BIM-1, a novel acquired subgroup B1 MBL found in a *Pseudomonas* sp. strain from the Brazilian Amazon region. J Antimicrob Chemother. 2023;78:1359–66. https://doi.org/10.1093/jac/dkad077

10. Okano H, Okado R, Ito H, Asakawa H, Nose K, Tsuruga S, et al. Ischemic hepatitis with infectious endocarditis: A case report. Biomed Rep. 2021;15:97. https://doi.org/10.3892/br.2021.1473

Address for correspondence: Edward J. Moseley, Health Security Agency Specialist Microbiology and Laboratories, South West Region and Severn Infection Sciences, University Hospitals Bristol and Weston NHS Foundation Trust, Bristol Royal Infirmary, Zone A Queens Bldg Level 8, Upper Maudlin Street, Bristol, BS2 8HW, England; email: edward.moseley@uhbw.nhs.uk

Rare *Spiroplasma* Bloodstream Infection in Patient after Surgery, China, 2022

Ningning Xiu,[1] Chao Yang,[1] Xiaowei Chen, Jianping Long, Pinghua Qu

Author affiliations: Dongguan Kanghua Hospital, Dongguan, China (N. Xiu, J. Long); Second Clinical Medical College of Guangzhou University of Chinese Medicine, Guangzhou, China (C. Yang, X. Chen, P. Qu); The Second Affiliated Hospital of Guangzhou University of Chinese Medicine, Guangdong Provincial Hospital of Traditional Chinese Medicine, Guangzhou (P. Qu)

DOI: http://doi.org/10.3201/eid3001.230858

We report a case of *Spiroplasma* bloodstream infection in a patient in China who developed pulmonary infection, acute respiratory distress syndrome, sepsis, and septic shock after emergency surgery for type A aortic dissection. One organism closely related to *Spiroplasma eriocheiris* was isolated from blood culture and identified by whole-genome sequencing.

Spiroplasma, a genus of bacteria in the phylum *Mycoplasmatota*, is characterized by cell structures with no cell walls (*1*). *Spiroplasma* isolates have been primarily reported from plants, guts of insects, tick triturates, and crustaceans (*2*), although a few cases of *Spiroplasma* infection in humans have also been reported, causing cataracts and uveitis in infants and systemic infections in immunocompromised patients (*3*–*6*). We describe a rare *Spiroplasma* bloodstream infection in a patient after surgery for type A aortic dissection in China.

The case-patient, a 68-year-old man, underwent surgery to repair his aorta on June 3, 2022, and he developed a severe respiratory infection afterward while still hospitalized. Fibrobronchoscopy revealed extensive and severe airway erosion, with yellow and thick sputum adhering to the airway walls. A biopsy of a bronchial embolism was taken and sent for examination (Appendix Figure, panel A, https://wwwnc.cdc.gov/EID/article/30/1/23-0858-App1.pdf), and microscopic observation revealed a layered arrangement of thrombi mixed with neutrophils (Appendix Figure, panel B). On June 9, 2022, the patient's health began to deteriorate (Appendix Table). The patient was diagnosed with pulmonary infection, acute respiratory distress syndrome, sepsis, and septic shock.

Medical staff performed multiple tests on the patient to identify an infectious etiology to explain the patient's acute illness (Table). *Candida tropicalis* was cultured in bronchoalveolar lavage fluid (BALF) samples. Seven of 12 blood cultures tested positive (Bactec FX; Becton Dickinson, https://www.bd.com/en-us) for a microorganism that was isolated as rare colonies under conditions of 35°C and a 5% CO_2 atmosphere. Subcultures on Columbia blood agar showed pinpoint-size zones of hemolysis with no macroscopic colony growth at 4 days of incubation; however, Gram stain and Giemsa-Wright stain of the blood could not detect the presence of bacteria. Finally, metagenomic next-generation sequencing was performed on both the blood and BALF samples. Unique reads of *Spiroplasma eriocheiris* (n = 1,577 in BALF, n = 2,344 in blood), human alphaherpesvirus 1 (n = 66,185 in BALF, n = 1,942 in blood), and *Aspergillus fumigatus* (n = 7 in BALF, n = 12 in blood) were detected (Table). We have uploaded raw data to the National Center for Biotechnology Information Sequence Read Archive (BioProject no. PRJNA1021328).

We characterized the cultivated microorganism, designated DGKH1, by 16S rRNA gene sequencing and whole-genome sequencing analysis. Results of 16S rRNA gene phylogeny show DGKH1 is closely related to *S. eriocheiris* CCTCC M 207170^T (Figure). However, the average nucleotide identity value between the genomes of the 2 isolates was 94%, and the average digital DNA–DNA hybridization value between them was 56%, both of which were lower than

[1]These authors contributed equally to this article.

Table. Etiologic examination of a postsurgery patient with a blood infection, China, 2022*

Sampling date	Sample classification	Detection technique	Microorganism	Report date
June 11	BALF	Culture	*Candida tropicalis*	June 13
	Hydrothorax	Culture	Negative	June 17
June 12	Blood culture (2 sets)	Culture	Negative	June 18
June 15	Blood culture (2 sets)	Culture	Positive (3 bottles): *Spiroplasma eriocheiris*, identified by 16S rRNA gene sequencing	June 27
	Urine	Culture	Negative	June 18
	BALF	Culture	*Candida tropicalis*	June 17
June 19	BALF	Culture	*Candida tropicalis*	June 22
	Blood culture (2 sets)	Culture	Positive (all): *Spiroplasma eriocheiris*, identified by 16S rRNA sequencing and designated DGKH1	June 27
	Blood	mNGS†	*Spiroplasma eriocheiris* (2,344, 11.36%) Human alphaherpesvirus 1 (1,942, 84.41%) *Aspergillus fumigatus* (12, 0.00%) Human gammaherpesvirus 4 (7, 0.27%) Human betaherpesvirus 5 (3, 0.08%) Human betaherpesvirus 6B (1, 0.04%)	June 20
	BALF	mNGS†	Human alphaherpesvirus 1 (66,185, 99.49%) *Spiroplasma eriocheiris* (1,577, 0.26%) *Candida tropicalis* (42, 0.00%) *Aspergillus fumigatus* (7, 0.00%)	June 20

*BALF, bronchoalveolar lavage fluid; mNGS, metagenomic next-generation sequencing.
†Numbers in parentheses indicate unique reads and relative abundance. One set included 2 bottles (1 aerobic and 1 anaerobic).

the threshold values (95%–96% average nucleotide identity and 70% digital DNA–DNA hybridization) used for delineating prokaryotic species (*7*). Therefore, DGKH1 is represented as an unclassified species that is phylogenetically related to *S. eriocheiris*. The 16S rRNA gene sequence (accession no. OQ955597) and genomic DNA sequence (accession no. JASTWG000000000) were deposited into GenBank.

Results of serum galactomannan testing were negative, and the patient did not respond clinically to voriconazole and caspofungin treatment. We theorize that *C. tropicalis* and *A. fumigatus* played an unlikely role in the patient's infection, and their detection may reflect colonization or contamination. We postulate that *Spiroplasma* species and human alphaherpesvirus 1 were the main causes of pulmonary infection, acute respiratory distress syndrome, sepsis, and septic shock in this case. Human alphaherpesvirus 1 (previously known as herpes simplex virus 1) is a potential cause of multiorgan failure and septic shock (*8*). Although *Spiroplasma* infection is much less common, the related bacteria *Metamycoplasma hominis* (previously known as *Mycoplasma hominis* and *Mycoplasmoides pneumoniae*) can cause bloodstream infection, pneumonia, and septic shock (*9*). Unfortunately, even with the addition of acyclovir and doxycycline in the therapy, the patient developed multiple organ failure and died on June 23, 2022.

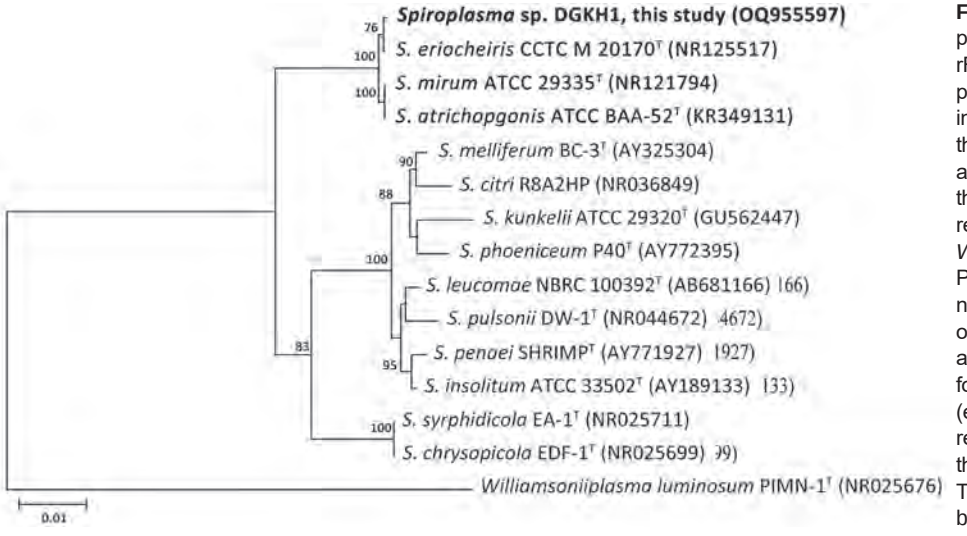

Figure. Neighbor-joining phylogenetic tree based on 16S rRNA gene sequences from a postsurgery patient with a blood infection, China, 2022. Tree shows the phylogenetic relationship among the strain DGKH1 from this study (boldface) and closely related species of *Spiroplasma*. *Williamsoniiplasma luminosum* PIMN-1T (GenBank accession no. NR025676) was used as an outgroup in the tree; GenBank accession numbers are provided for all sequences. Bootstrap values (expressed as percentages of 1,000 replications) >70% are shown at the branch points. Superscript T indicates type strains. Scale bar indicates substitutions per nucleotide position.

In conclusion, we report a rare case of *Spiroplasma* sp. blood infection in a patient after surgery for type A aortic dissection. *Spiroplasma* is an arthropod-infecting bacterium that may be part of the commensal microbiome of the human gut; there are 13 pieces of relevant information deposited into the gutMEGA database (http://gutmega.omicsbio.info) (*10*). *Spiroplasma* detection is challenging, and the discovery and diagnosis of emerging pathogens, such as the one we have described, can be aided by new technologies such as 16S rRNA gene sequencing and metagenomic next-generation sequencing.

This research was supported by the National Science and Technology Fundamental Resources Investigation Program of China (grant no. 2021FY100900).

About the Author

Dr. Ningning Xiu works in the Laboratory Department at Dongguan Kanghua Hospital, Dongguan, China. Her primary research interests are clinical microbiological laboratory diagnosis.

References

1. Gupta RS, Sawnani S, Adeolu M, Alnajar S, Oren A. Phylogenetic framework for the phylum *Tenericutes* based on genome sequence data: proposal for the creation of a new order *Mycoplasmoidales* ord. nov., containing two new families *Mycoplasmoidaceae* fam. nov. and *Metamycoplasmataceae* fam. nov. harbouring *Eperythrozoon, Ureaplasma* and five novel genera. [Erratum in: Antonie Van Leeuwenhoek. 2018; 111:2485–6.] Antonie van Leeuwenhoek. 2018;111:1583–630. https://doi.org/10.1007/s10482-018-1047-3
2. Willamson DL, Gasparich GE, Regassa LB, Saillard C, Renaudin J, Bové JM, et al. Genus Spiroplasma. In: Krieg NR, Staley JT, Brown DR, Hedlund BP, Psater BJ, Ward NL, et al. eds. Bergey's manual of systematic bacteriology, volume 4. New York: Springer; 2010. pp 654¬–86.
3. Cisak E, Wójcik-Fatla A, Zając V, Sawczyn A, Sroka J, Dutkiewicz J. Spiroplasma—an emerging arthropod-borne pathogen? Ann Agric Environ Med. 2015;22:589–93. https://doi.org/10.5604/12321966.1185758
4. Etienne N, Bret L, Le Brun C, Lecuyer H, Moraly J, Lanternier F, et al. Disseminated *Spiroplasma apis* infection in patient with agammaglobulinemia, France. Emerg Infect Dis. 2018;24:2382–6. https://doi.org/10.3201/eid2412.180567
5. Matet A, Le Flèche-Matéos A, Doz F, Dureau P, Cassoux N. Ocular *Spiroplasma ixodetis* in newborns, France. Emerg Infect Dis. 2020;26:340–4. https://doi.org/10.3201/eid2602.191097
6. Farassat N, Reich M, Serr A, Küchlin S, Erwemi M, Auw-Hädrich C, et al. *Spiroplasma* species as a rare cause of congenital cataract and uveitis: a case series. BMC Ophthalmol. 2021;21:434. https://doi.org/10.1186/s12886-021-02201-0
7. Chun J, Oren A, Ventosa A, Christensen H, Arahal DR, da Costa MS, et al. Proposed minimal standards for the use of genome data for the taxonomy of prokaryotes. Int J Syst Evol Microbiol. 2018;68:461–6. https://doi.org/10.1099/ijsem.0.002516
8. Boquet A, Boulay G, Hautin E, Mottard N. Septic shock complicated by disseminated herpes simplex virus-1 infection: a case report. J Med Case Reports. 2021;15:394. https://doi.org/10.1186/s13256-021-02985-1
9. Wang Q, Tang X, van der Veen S. *Mycoplasma hominis* bloodstream infection and persistent pneumonia in a neurosurgery patient: a case report. BMC Infect Dis. 2022;22:169. https://doi.org/10.1186/s12879-022-07137-4
10. Zhang Q, Yu K, Li S, Zhang X, Zhao Q, Zhao X, et al. gutMEGA: a database of the human gut MEtaGenome Atlas. Brief Bioinform. 2021;22:bbaa082. https://doi.org/10.1093/bib/bbaa082

Address for correspondence: Pinghua Qu, Department of Clinical Laboratory, The Second Affiliated Hospital of Guangzhou University of Chinese Medicine, Guangdong Provincial Hospital of Traditional Chinese Medicine, No.55 Neihuan West Rd, Panyu District, Guangzhou 510006, China; email: ququtdr@163.com

Emergence of Dengue Virus Serotype 2 Cosmopolitan Genotype, Colombia

David Martínez, Marcela Gómez, Carolina Hernández, Marina Muñoz, Sandra Campo-Palacio, Marina González-Robayo, Marcela Montilla, Norma Pavas-Escobar, Juan David Ramírez

Author affiliations: Universidad del Rosario, Bogotá, Colombia (D. Martínez, M. Gómez, C. Hernández, M. Muñoz, J.D. Ramírez); Universidad de Boyacá, Tunja, Colombia (M. Gómez); Centro de Tecnología en Salud (CETESA), Innovaseq SAS, Bogotá (C. Hernández); Laboratorio de Salud Pública, Secretaría de Salud Departamental Meta, Villavicencio, Colombia (S. Campo-Palacio, M. González-Robayo, M. Montilla, N. Pavas-Escobar); Universidad Cooperativa de Colombia, Villavicencio, Colombia (M. Montilla, N. Pavas-Escobar); Icahn School of Medicine at Mount Sinai, New York, New York, USA (J.D. Ramírez)

Using Oxford Nanopore technologies and phylogenetic analyses, we sequenced and identified the cosmopolitan genotype of dengue virus serotype 2 isolated from 2 patients in the city of Villavicencio, Meta department, Colombia. This identification suggests the emergence of this genotype in the country, which warrants further surveillance to identify its epidemic potential.

DOI: https://doi.org/10.3201/eid3001.230972

Dengue fever is a viral disease transmitted by *Aedes* spp. mosquitoes; the Americas are one of the most severely affected regions (*1*). The causative agent of dengue fever is the dengue virus (DENV), a positive-sense single-stranded RNA virus with a genome size of ≈10.7 kilobase. This virus is categorized into 4 distinct serotypes (DENV-1–4), classified on the basis of their surface antigens, and each serotype further consists of different genotypes that are phylogenetically distinct (*2*,*3*).

Recent epidemics in South America have been primarily attributed to the DENV-2 serotype, according to epidemiologic reports from the region (*4*). In Colombia, 70,418 cases of dengue fever have been reported as of August 2023; DENV-2 has been identified in most cases (*5*). Currently, this serotype consists of 5 genotypes named according to the region in which they circulate. Asian I and II genotypes are predominantly found in Asia, whereas the American genotype, which is no longer in circulation, was once prevalent in Central and South America. In the 1980s, the American genotype was replaced by the Asian-American genotype, which now circulates in Southeast Asia and the Americas. Last, the cosmopolitan genotype is noteworthy for its extensive global distribution, spanning 5 continents (*6*).

The cosmopolitan genotype has recently expanded in Africa and the Americas (*7*). This widespread dispersal has led to substantial intragenotype heterogeneity, reflecting the evolutionary forces acting within this genotype that are associated with its transmission. An outbreak attributed to the cosmopolitan genotype was reported in Madre de Dios Province, Peru, in 2019, coinciding with its recent expansion in Africa (*8*,*9*). In 2021, an additional 2 reports were documented in the states of Acre and Goiás in Brazil (*4*). Those reports shed light on a potential introduction route of the genotype into Brazil, specifically from the border with Peru (*4*). In 2023, the World Health Organization reported an outbreak in Latin America, generating a state of alert because of the increase in DENV cases (*10*). The genetic characteristics acquired during the extensive dissemination of the cosmopolitan genotype emphasize the need for further research into its diversity, evolution, and transmission dynamics within DENV-endemic areas.

In this report, we discuss 2 cases of the cosmopolitan genotype DENV-2 identified in Villavicencio, a city in the Meta department of Colombia. Of note, this department had the highest number of DENV cases in Colombia in 2023, accounting for 15.4% (10,859 cases) of total cases reported nationwide as of August (*5*). The 2 cases involved 2 young men with no travel history residing in suburban neighborhoods in southern Villavicencio (Figure, panel A). Both patients exhibited symptoms of fever, headache, myalgia, intense and continuous abdominal pain, and a platelet count of <100,000. Those symptoms align with the classification of DENV infection with warning signs, and dates of symptom onset were April 26, 2023, and

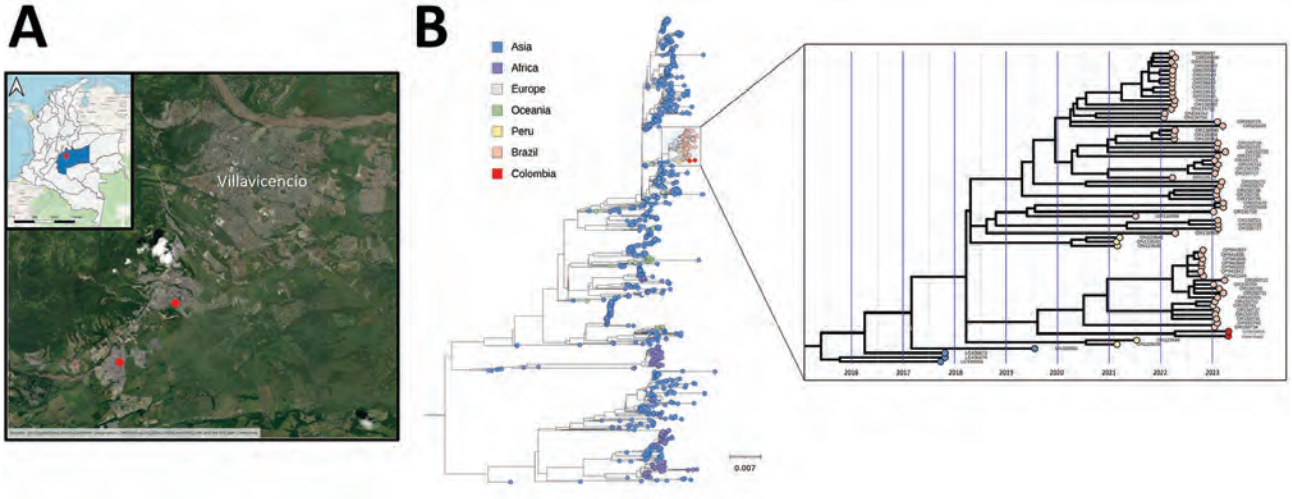

Figure. Phylogenetic analysis of dengue virus 2 cosmopolitan genotype, Colombia. A) Geographic location of the neighborhoods where the patients' residences are situated. B) Maximum-likelihood tree rooted at the midpoint depicts the evolutionary relationships of the complete genome sequence of the dengue virus 2 cosmopolitan genotype identified in 2 patients from the city of Villavicencio in Meta department, Colombia (red circles), along with 1,001 publicly available sequences from GenBank. The highlighted blue area is shown in a time-resolved maximum-likelihood tree in expanded panel; colors represent different sampling locations. Scale bar indicates number of substitutions per site.

April 29, 2023.

Serum samples were collected and sent to the microbiology laboratory at Universidad del Rosario in Bogotá, Colombia for processing. We extracted viral RNA using the Quick-RNA Viral Kit (Zymo Research, https://zymoresearch.eu). The infection was confirmed to be caused by the DENV-2 serotype using the previously described protocol (Appendix, https://wwwnc.cdc.gov/EID/article/30/1/23-0972-App1.pdf). We performed whole-genome sequencing using MinION (Oxford Nanopore Technology, https://nanoporetech.com) to determine the corresponding genotype classification and to conduct subsequent analysis of the local distribution of DENV (Appendix). The Technical Research Committee and Ethics Research Board from Universidad del Rosario in Bogotá, Colombia approved the protocol implemented in this study (approval no. DVO005 1585-CV142).

We conducted an initial maximum-likelihood phylogenetic analysis to identify the genotype. The analysis revealed that the sequences obtained from the patients were closely related, belonged to the DENV-2 cosmopolitan genotype, and were placed within the South America sequences found in Tefé and Tabatinga, Brazil, and Madre de Dios in Peru (Figure, panel B).

Further examination using a time-resolved maximum-likelihood tree demonstrated that those sequences were closely related to sequences reported in the Tabatinga province in Brazil. The bootstrap support for this relationship was 95% (Figure, panel B). This finding suggests potential cross-border transmission in the Tabatinga province, highlighting the possibility of viral spread across borders.

In conclusion, although genetic data alone cannot provide conclusive evidence about the directionality of the introduction of the DENV-2 cosmopolitan genotype, insights gained from phylogenetic reconstruction and temporal information suggest a potential introduction from Tabatinga, Brazil, with subsequent spread northwards in Colombia. Tabatinga is located in the tripartite border region between Brazil, Colombia, and Peru adjacent to the Amazonas department in southern Colombia. Because of the limited research available on the cosmopolitan genotype, our understanding of its effects on dengue disease dynamics in Colombia remains incomplete. Further investigations are required to gain a more comprehensive insight into its potential for local, regional, and global epidemics. Our findings highlight the importance of implementing robust genomic surveillance in the region, especially considering the ongoing outbreak in Latin America.

This work was supported by the Colombian Ministerio de Ciencia, Tecnología e Innovación Minciencias (grant no. 143889685192-2021).

D.M. and J.D.R. conceived the study; M.G., C.H., and M.M. analyzed the data; and S.C.P., M.G.R., M.M., and N.P.E. collected the samples. All authors have read and agreed to the published version of the manuscript.

About the Author

Mr. Martínez is a biologist and master's student in natural sciences at Universidad del Rosario, Bogotá, Colombia. His primary research interest is the genomic surveillance of dengue virus. Dr. Ramírez is an associate professor at Universidad del Rosario and the Icahn School of Medicine at Mount Sinai. His primary research interests are the genomic surveillance and evolution of viruses and parasites.

References

1. Islam MT, Quispe C, Herrera-Bravo J, Sarkar C, Sharma R, Garg N, et al. Production, transmission, pathogenesis, and control of dengue virus: a literature-based undivided perspective. Biomed Res Int. 2021;2021:4224816.
2. Pollett S, Melendrez MC, Maljkovic Berry I, Duchêne S, Salje H, Cummings DAT, et al. Understanding dengue virus evolution to support epidemic surveillance and counter-measure development. Infect Genet Evol. 2018; 62:279–95. https://doi.org/10.1016/j.meegid.2018.04.032
3. Rico-Hesse R. Molecular evolution and distribution of dengue viruses type 1 and 2 in nature. Virology. 1990; 174:479–93. https://doi.org/10.1016/0042-6822(90)90102-W
4. Amorim MT, Hernández LHA, Naveca FG, Essashika Prazeres IT, Wanzeller ALM, Silva EVPD, et al. Emergence of a new strain of DENV-2 in South America: introduction of the cosmopolitan genotype through the Brazilian-Peruvian border. Trop Med Infect Dis. 2023;8:325. https://doi.org/10.3390/tropicalmed8060325
5. Instituto nacional de salud. Weekly epidemiological bulletin: epidemiological week 33 [in Spanish] [cited 2023 Oct 2]. https://www.ins.gov.co/buscador-eventos/BoletinEpidemiologico/2023_Bolet%C3%ADn_epidemiologico_semana_33.pdf
6. Letizia AG, Pratt CB, Wiley MR, Fox AT, Mosore M, Agbodzi B, et al. Retrospective genomic characterization of a 2017 dengue virus outbreak, Burkina Faso. Emerg Infect Dis. 2022;28:1198–210. https://doi.org/10.3201/eid2806.212491
7. Yenamandra SP, Koo C, Chiang S, Lim HSJ, Yeo ZY, Ng LC, et al. Evolution, heterogeneity and global dispersal of cosmopolitan genotype of dengue virus type 2. Sci Rep. 2021;11:13496. https://doi.org/10.1038/s41598-021-92783-y
8. García MP, Padilla C, Figueroa D, Manrique C, Cabezas C. Emergence of the Cosmopolitan genotype of dengue virus serotype 2 (DENV2) in Madre de Dios, Peru, 2019. Rev Peru Med Exp Salud Publica. 2022;39:126–8. https://doi.org/10.17843/rpmesp.2022.391.10861
9. Fourié T, El Bara A, Dubot-Pérès A, Grard G, Briolant S, Basco LK, et al. Emergence of dengue virus serotype 2 in Mauritania and molecular characterization of its

circulation in West Africa. PLoS Negl Trop Dis. 2021;15:e0009829. https://doi.org/10.1371/journal.pntd.0009829
10. World Health Organization. Dengue—region of the Americas [cited 2023 Nov 29]. https://www.who.int/emergencies/disease-outbreak-news/item/2023-DON475

Address for correspondence: Juan David Ramírez, Department of Pathology, Molecular and Cell Based Medicine, Icahn School of Medicine at Mount Sinai, 1428 Madison Ave, Atran building B2-18, New York, NY 10029-6574, USA; email: juand.ramirez@urosario.edu.co, juan.ramirezgonzalez@mssm.edu

Mycobacterium senegalense Infection in Kidney Transplant Patient with Diabetes, Memphis, Tennessee, USA

Nupur Singh, Reeti Khare, Shirin Mazumder

Author affiliations: University of Tennessee Health Science Center, Memphis, Tennessee, USA (N. Singh, S. Mazumder); National Jewish Health, Denver, Colorado, USA (R. Khare); Methodist University Hospital, Memphis (S. Mazumder)

DOI: https://doi.org/10.3201/eid3001.231013

Fewer than 30 cases of *Mycobacterium senegalense* infection have been reported. We report a complicated case of *M. senegalense* infection in Memphis, Tennessee, in the southeastern United States. The patient's comorbidities of past organ transplant and insulin-dependent diabetes required delicate consideration of those health conditions to guide treatment.

Mycobacterium senegalense, also referred to as *M. conceptionense*, is a nonpigmented rapid-growing mycobacterium belonging to the *M. fortuitum* group, which was first isolated in 2006 from a posttraumatic osteitis inflammation in France (*1*,*2*). Only a handful of *M. conceptionense* cases are readily identifiable in existing literature. Infections can manifest with pulmonary involvement but more commonly manifest as skin or subcutaneous infection, such as after face rejuvenation surgery, breast augmentation surgery, gastric carcinoma resection, or subcutaneous ankle infection (*3*–*6*). Mycobacterial species like *M. senegalense* have been found in irrigation systems, soil, domestic and wild animals, and dairy products (*7*,*8*). Cases of *M. senegalense* infection have been observed in France, Iran, Taiwan, South Korea, Japan, and the United States, demonstrating an unidentifiable pattern of regional bacterial prevalence.

Establishing an accurate diagnosis of *M. senegalense* infection is incredibly difficult, requiring histological examination and extensive mycobacterial cultures (*9*). The limited susceptibility data also mean an optimal therapy has not been completely established, which leaves certain patient populations, particularly the elderly and immunocompromised, susceptible to increased illness and death from *M. senegalense* infection (*10*). We report a complicated case of *M. senegalense* infection in a patient with a previous kidney transplant and insulin-dependent diabetes mellitus in Memphis, Tennessee, USA.

A 70-year-old Black woman with end-stage kidney disease sought care for a painful, swollen, abdominal wall abscess. She had first noticed the lesion ≈3 weeks before in the left mid-abdomen, where she frequently injected insulin. The patient denied any recent travel, drainage at the site, or fever. The 7- × 4-cm abscess was drained the next day without complications, and we sent the custard-like purulent material for laboratory testing.

The patient had undergone a right-sided cadaveric renal transplant 8 years before; her immunosuppressive regimen consisted of tacrolimus, mycophenolate, and prednisone. The patient's past diagnoses at the time of infection included type 2 diabetes mellitus, lupus, hypertension, hyperlipidemia, sleep apnea, and coronary artery disease. Insulin injections create small open wounds where pathogens can enter and cause infection. An environmental source of the infection was not sought. The hospital microbiology laboratory detected acid-fast bacilli on direct AFB smear. The patient immediately began empiric antimicrobial drugs, including doxycycline (100 mg 2×/d) and levofloxacin (250 mg 1×/d), adjusted for her creatinine clearance.

The isolate was sent to the National Jewish Mycobacteriology Reference Laboratory (Denver, Colorado, USA) for confirmation and susceptibility testing. Sanger sequencing analysis was performed; BLAST (https://blast.ncbi.nlm.nih.gov/Blast.cgi) testing of the *rpoB* sequence results against the public GenBank database identified *M. senegalense* (>99% homology to existing sequences). A line probe assay for common nontuberculous mycobacteria, GenoType NTM-DR (Hain Lifescience, https://www.hain-lifescience.de),

was performed first to differentiate qualitatively and in vitro species of several strains of mycobacteria, such as *M. avium* complex, *M. abscessus*, *M. chelonae*, *M. intracellulare*, *M. chimaera*, *M. massiliense*, *M. bolletii*, and *M. chelonae*, but did not yield a species-level identification. Those tests supported identification as *M. senegalense,* and the sequence was deposited in GenBank (accession no. OR644277). In vitro susceptibility testing demonstrated the antibiotics to which the isolate was susceptible, intermediate, and resistant, according to Clinical and Laboratory Standards Institute guidelines (https://clsi.org) (Table).

The patient continued taking doxycycline. Levofloxacin was stopped after the patient reported nausea and vomiting. Because of increasing creatinine levels, trimethoprim/sulfamethoxazole was not used. The isolate was susceptible to clarithromycin, but it was not selected because of ongoing tacrolimus treatment. Amoxicillin/clavulanate was chosen, despite the isolate's intermediate susceptibility, because of better patient tolerance. The final drug regimen was doxycycline (100 mg 2×/d) and amoxicillin/clavulanate (250/125 mg 2×/d) adjusted for renal function; expected treatment course was 4–6 months. At the 3-month clinic follow-up, the lesion had notably shrunk to a 3- × 0.8-cm open wound with no drainage, foul odor, or tenderness. By 6-month follow-up, the lesion had closed and was hyperpigmented and flat, without fluctuance or signs of active infection.

Table. Antibiotic susceptibility testing for *Mycobacterium conceptionense* sample from kidney transplant patient with diabetes, Memphis, Tennessee, USA*

Antibiotic	MIC, µg/mL	Interpretation
Amikacin IV	≤8	S
Amoxicillin/clavulanate	8/4	NI
Azithromycin	≤16	NI
Cefepime	>32	NI
Cefotaxime	>64	NI
Cefoxitin	≤16	S
Ceftriaxone	>64	NI
Ciprofloxacin	≤1	S
Clarithromycin	≤0.25	S
Clofazimine	≤0.5	NI
Clofazimine/amikacin†	≤0.5/2	NI
Doxycycline	≤1	S
Gentamicin	≤2	NI
Imipenem	≤2	S
Kanamycin	≤8	NI
Linezolid	4	S
Minocycline	≤1	NI
Moxifloxacin	≤0.5	S
Tigecycline	≤0.25	NI
Tobramycin	4	I
Trimethoprim/sulfamethoxazole	1/19	S

*I, intermediate; NI, no Clinical Laboratory Standards Institute guidelines for this antibiotic/organism combination; R, resistant; S, susceptible.
†Clofazimine is not available as a combined medication commercially in the United States. It is available in the National Jewish Mycobacteriology Reference Laboratory for testing purposes only.

We achieved identification of *M. senegalense* through *rpoB* gene sequencing, and treatment was guided by antibiotic susceptibility options. Separating *M. senegalense* from the rest of the *M. fortuitum* complex species helps guide appropriate treatment and epidemiologic analysis of mycobacterial species by geographic location. This patient presented a unique and delicate case in which adequate treatment required thorough consideration of other medications, diagnoses, and comorbidities. Overall, this complicated, interesting case of *M. senegalense* infection at the site of insulin injections for a diabetic patient in the southeastern United States adds to the limited body of *M. senegalense* infection and treatment knowledge. This case highlights that *M. senegalense* is present in this region, suggesting a higher index of suspicion is needed for patients in those areas.

R.K. has laboratory-contracted research with Insmed, Paratek Pharmaceuticals, AN2 Therapeutics, Spero Therapeutics, and Mannkind Corporation.

About the Author

Ms. Singh is a third-year medical student at the University of Tennessee whose research interests include topics in dermatology or specialties of internal medicine, particularly infectious disease, rheumatology, and oncology. Dr. Mazumder is an associate professor of medicine in the Division of Infectious Diseases, Department of Internal Medicine, at the University of Tennessee Health Science Center, and the laboratory director at the Methodist LeBonheur Healthcare Ambulatory Clinics. Her research interests include infectious diseases, particularly HIV, transplant infections, and fungal infections.

References:

1. Adékambi T, Stein A, Carvajal J, Raoult D, Drancourt M. Description of *Mycobacterium conceptionense* sp. nov., a *Mycobacterium fortuitum* group organism isolated from a posttraumatic osteitis inflammation. J Clin Microbiol. 2006;44:1268–73. https://doi.org/10.1128/JCM.44.4.1268-1273.2006
2. Tortoli E, Meehan CJ, Grottola A, Fregni Serpini G, Fabio A, Trovato A, et al. Genome-based taxonomic revision detects a number of synonymous taxa in the genus *Mycobacterium*. Infect Genet Evol. 2019;75:103983. https://doi.org/10.1016/j.meegid.2019.103983
3. Liao C-H, Lai C-C, Huang Y-T, Chou C-H, Hsu H-L, Hsueh P-R. Subcutaneous abscess caused by *Mycobacterium conceptionense* in an immunocompetent patient. J Infect. 2009;58:308–9. https://doi.org/10.1016/j.jinf.2009.02.012
4. Yaita K, Matsunaga M, Tashiro N, Sakai Y, Masunaga K, Miyoshi H, et al. *Mycobacterium conceptionense* bloodstream infection in a patient with advanced gastric carcinoma.

Jpn J Infect Dis. 2017;70:92–5. https://doi.org/10.7883/yoken.JJID.2015.626
5. Kim SY, Kim MS, Chang HE, Yim JJ, Lee JH, Song SH, et al. Pulmonary infection caused by *Mycobacterium conceptionense*. Emerg Infect Dis. 2012;18:174–6. https://doi.org/10.3201/eid1801.110251
6. Thibeaut S, Levy PY, Pelletier ML, Drancourt M. *Mycobacterium conceptionense* infection after breast implant surgery, France. Emerg Infect Dis. 2010;16:1180–1. https://doi.org/10.3201/eid1607.090771
7. Gonzalez-Santiago TM, Drage LA. Nontuberculous mycobacteria: skin and soft tissue infections. Dermatol Clin. 2015;33:563–77. https://doi.org/10.1016/j.det.2015.03.017
8. Faria S, Joao I, Jordao L. General overview on nontuberculous mycobacteria, biofilms, and human infection. J Pathogens. 2015;2015:809014. https://doi.org/10.1155/2015/809014
9. Covert TC, Rodgers MR, Reyes AL, Stelma GN Jr. Occurrence of nontuberculous mycobacteria in environmental samples. Appl Environ Microbiol. 1999;65:2492–6. https://doi.org/10.1128/AEM.65.6.2492-2496.1999
10. Prevots DR, Marras TK. Epidemiology of human pulmonary infection with nontuberculous mycobacteria: a review. Clin Chest Med. 2015;36:13–34. https://doi.org/10.1016/j.ccm.2014.10.002

Address for correspondence: Nupur Singh, University of Tennessee Health Science Center, 910 Madison Ave, Memphis, TN, 38103, USA; email: nsingh8@uthsc.edu, nupursingh2799@gmail.com

Acute Gastroenteritis Associated with Norovirus GII.8[P8], Thailand, 2023

Watchaporn Chuchaona, Sompong Vongpunsawad, Weerasak Lawtongkum, Nattawan Thepnarong, Yong Poovorawan

Author affiliations: Chulalongkorn University, Bangkok, Thailand (W. Chuchaona, S. Vongpunsawad, Y. Poovorawan); Vachira Phuket Hospital, Phuket, Thailand (W. Lawtongkum, N. Thepnarong)

DOI: https://doi.org/10.3201/eid3001.231264

Acute gastroenteritis associated with human norovirus infection was reported in Phuket, Thailand, in June 2023. We amplified GII.8[P8] from the outbreak stool specimens. Retrospective sample analysis identified infrequent GII.8[P8] in the country beginning in 2018. In all, the 10 whole-genome GII.8[P8] sequences from Thailand we examined had no evidence of genotypic recombination.

Norovirus is the most common cause of acute viral gastroenteritis among adults and children and has no currently approved vaccine (*1*). Norovirus is genetically diverse and is classified into 10 genogroups (GI–GX) representing ≈50 genotypes, of which GI and GII predominantly infect humans (*2*). Currently, dual-typing of the RNA-dependent RNA polymerase (RdRp) gene in the open reading frame 1 region and the major capsid protein (VP1) gene in the open reading frame 2 region is required for proper genotype assignment and detection of viral recombinants (*3*).

In June 2023, health officials in Thailand were investigating diarrheal outbreaks that occurred on Phuket Island in southern Thailand, which is frequented by international travelers (https://www.bangkokpost.com/thailand/general/2592541/phukets-diarrhoea-outbreak-wanes-cause-still-unknown). Two stool specimens were eventually sent to our laboratory at the Center of Excellence in Clinical Virology at Chulalongkorn University (Bangkok) for molecular typing. The study was approved by Chulalongkorn University Institutional Review Board (approval no. 549/62). After viral RNA extraction from the stool specimens, quantitative real-time reverse transcription PCR (*4*) identified GII norovirus in both specimens. Confirmation assays using conventional reverse transcription PCR (*5*) with additional primers (Appendix 1 Table 1) and nucleotide sequencing yielded near-complete genomes, which we subjected to the norovirus genotyping tools of the Netherlands' National Institute for Public Health and the Environment (https://www.rivm.nl/mpf/norovirus/typingtool) and the US Centers for Disease Control and Prevention (https://calicivirustypingtool.cdc.gov).

Both specimens from Phuket were human norovirus GII.8[P8]. Because GII.8[P8] is relatively uncommon and rarely linked to large outbreaks, we retrospectively examined archived stool specimens dating back to 2018 to determine the frequency of past infection in the country. We identified 8 additional GII.8 strains (Table), all of which were GII.8[P8]. We deposited these complete genome sequences in GenBank (accession nos. OR546391–OR546400).

All 10 patients who tested positive for GII.8[P8] were relatively young (age range 3–29 years, mean age 10.8 years ± 7.1 SD). Five patients had vomiting and diarrhea, 3 had vomiting only, and 2 had diarrhea only (Appendix 1 Table 2, https://wwwnc.cdc.gov/EID/article/30/1/23-1264-App1.pdf). Minor symptoms were nausea, abdominal pain, fever, and headaches. All but 1 patient required 1–2 nights of hospital stay.

Table. Human norovirus GII.8[P8] strains identified in Thailand, 2018–2023

Collection date	Specimen ID	Patient age, y/Sex	Location	Specimen type
2018 Feb 2	B4899	5/M	Saraburi	Stool
2018 Feb 18	B5182	7/M	Bangkok	Stool
2018 Sep 18	B6213	6/F	Nonthaburi	Stool
2019 Jul 30	B6941	12/M	Nonthaburi	Stool
2020 Feb 04	B7634	29/F	Bangkok	Stool
2023 Feb 22	B9202	3/M	Bangkok	Stool
2023 Feb 27	B9256	12/F	Chaiyaphum	Stool
2023 Apr 19	B9804	10/M	Bangkok	Stool
2023 Jun 14	B10039	12/F	Phuket	Rectal swab
2023 Jun 13	B10069	7/F	Phuket	Stool

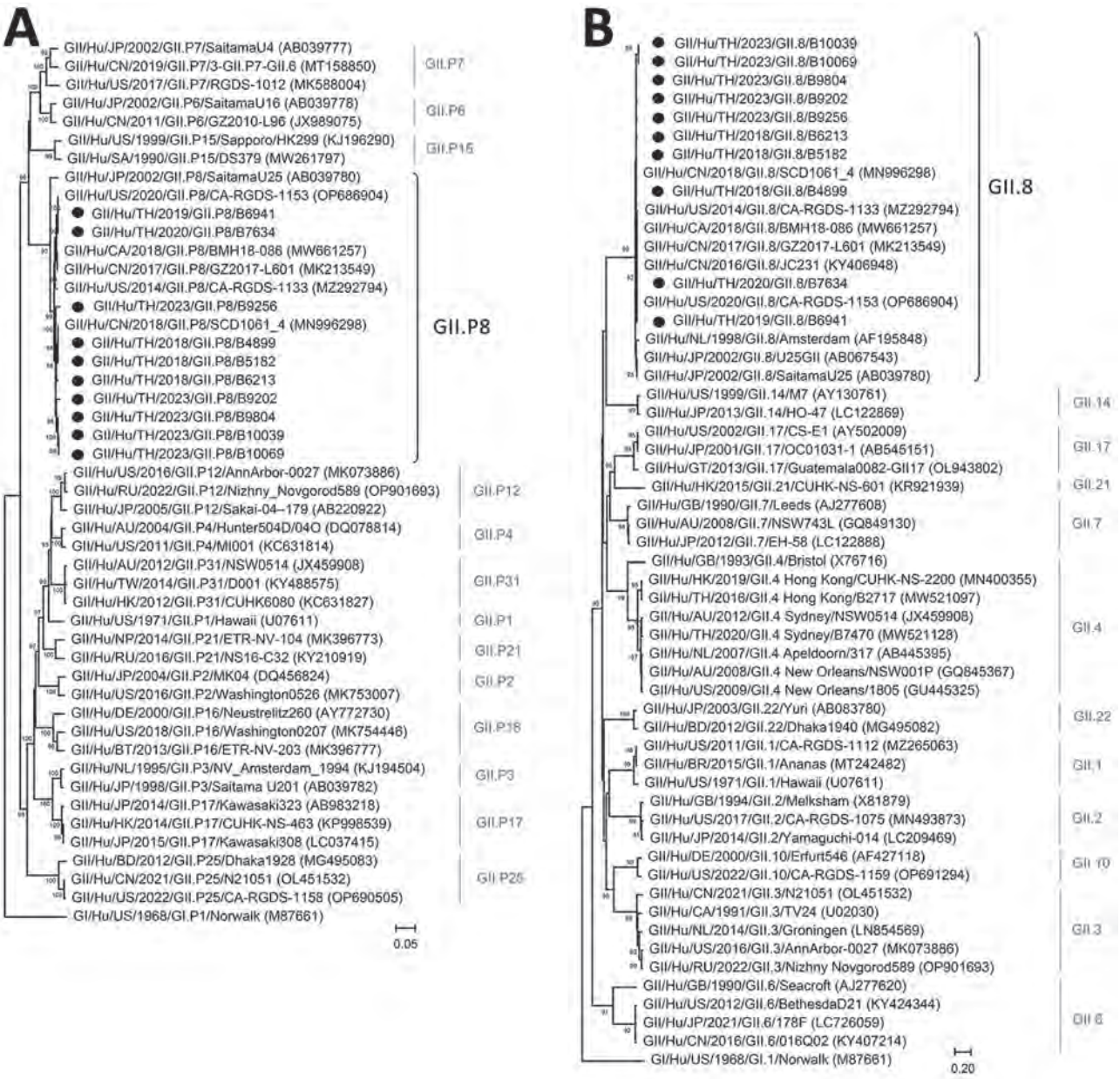

Figure. Phylogenetic analysis of the complete nucleotide sequences of noroviruses identified in Thailand, 2018–2023 (black dots), and reference sequences. A) RNA-dependent RNA polymerase (RdRp) region; B) major capsid protein (VP1) region. Trees were generated using the maximum-likelihood method based on the general time reversible model, with 1,000 bootstrap replications for branch support as implemented in MEGA software version 11 (http://www.megasoftware.net). Bootstrap values ≥80 are indicated at the branch nodes. GenBank accession numbers for reference sequences are provided in parentheses. Scale bar indicates nucleotide substitutions per site.

From the complete nucleotide sequences of the RdRp and VP1 genes, the GII.8[P8] strains from Thailand phylogenetically clustered with strains identified in Canada (GenBank accession no. MW661257), China (GenBank accession nos. MK213549 and MN996298), and the United States (GenBank accession nos. MZ292794 and OP686904) during the previous 10 years (Figure). Collectively, nucleotide sequence identities of GII.8[P8] strains from Thailand and other strains were 85%–99% over the entire genome compared with the prototypic GII.8[P8] SaitamaU25 (GenBank accession no. AB039780) (Appendix 1 Figure). However, Phuket GII.8[P8] appeared to diverge most from other GII.8[P8] strains in parts of the nonstructural protein 1–2 (p48), nonstructural protein 3 (NTPase), and VP1 shell domain.

To address whether Phuket GII.8[P8] strains had developed notable amino acid changes on its genome, we compared their deduced residues to other GII.8[P8] strains. Phuket GII.8[P8] shared many unique residue changes with the most recent strain from Thailand (B9804) identified in Bangkok 2 months prior (Appendix 2 Table, https://wwwnc.cdc.gov/EID/article/30/1/23-1264-App2.xlsx). No apparent mutations to suggest increased virulence or viral transmissibility were obvious, although ≥10 residue positions scattered throughout the GII.8[P8] genome identified in Thailand in 2023 were not shared by other known GII.8[P8] sequences. Most residue variations were conservative changes; however, T479S on VP1 is a highly conserved position among GII noroviruses.

The potential for GII.8[P8] to cause the recent norovirus outbreak in Phuket was unexpected given that the last reported outbreak in Thailand wad caused by a novel GII.3[P25] recombinant in Chanthaburi Province (*6*). Of note, GII.8[P8] outbreaks are infrequent (*7*), and the most recent occurrence was foodborne (through contaminated raspberries) (*8*). No specific food source was identified and laboratory-confirmed for norovirus, and anecdotal evidence suggests probable person-to-person norovirus transmission in the Phuket outbreak. Reports of GII.8[P8] infection in the literature have not identified RpRp–VP1 recombinants, and comprehensive historical analysis of norovirus sequences suggests that GII.8 RdRp and VP1 rarely recombine with other genotypes (*9*).

Molecular analysis in this study was limited because <40 complete GII.8[P8] genomes were available in the public database. This study was also constrained by the scarcity of specimens sent for laboratory testing, which underscored limited awareness and importance placed by health officials toward timely etiologic diagnosis. A study suggests that antibodies elicited by GI.1 and GII.4 (2 genotypes in the norovirus vaccine candidate under consideration) minimally block the binding of GII.8 VLPs to histo–blood group antigens (*10*). Although unlikely, any potential increase in the prevalence of GII.8[P8] could affect real-world norovirus vaccine effectiveness. In summary, GII.8[P8] genomes identified in this study are expected to contribute to the ongoing molecular and epidemiologic surveillance of community-acquired norovirus infection, which could benefit the tracking of global norovirus transmission.

This study was supported by the Center of Excellence in Clinical Virology of Chulalongkorn University and Hospital. Support for W.C. was provided by the Second Century Fund of Chulalongkorn University.

About the Author

Dr. Chuchaona is a postdoctoral fellow at the Center of Excellence in Clinical Virology in the Faculty of Medicine at Chulalongkorn University. Her primary research interests are molecular epidemiology and evolution of human noroviruses.

References

1. Ahmed SM, Hall AJ, Robinson AE, Verhoef L, Premkumar P, Parashar UD, et al. Global prevalence of norovirus in cases of gastroenteritis: a systematic review and meta-analysis. Lancet Infect Dis. 2014;14:725–30. https://doi.org/10.1016/S1473-3099(14)70767-4
2. Chhabra P, de Graaf M, Parra GI, Chan MC, Green K, Martella V, et al. Updated classification of norovirus genogroups and genotypes. J Gen Virol. 2019;100:1393–406. https://doi.org/10.1099/jgv.0.001318
3. Kroneman A, Vega E, Vennema H, Vinjé J, White PA, Hansman G, et al. Proposal for a unified norovirus nomenclature and genotyping. Arch Virol. 2013;158:2059–68. https://doi.org/10.1007/s00705-013-1708-5
4. Debbink K, Costantini V, Swanstrom J, Agnihothram S, Vinjé J, Baric R, et al. Human norovirus detection and production, quantification, and storage of virus-like particles. Curr Protoc Microbiol. 2013;31:15K.1.1–15K.1.45.
5. Chhabra P, Browne H, Huynh T, Diez-Valcarce M, Barclay L, Kosek MN, et al. Single-step RT-PCR assay for dual genotyping of GI and GII norovirus strains. J Clin Virol. 2021;134:104689. https://doi.org/10.1016/j.jcv.2020.104689
6. Chuchaona W, Khongwichit S, Luang-On W, Vongpunsawad S, Poovorawan Y. Norovirus GII.3[P25] in patients and produce, Chanthaburi Province, Thailand, 2022. Emerg Infect Dis. 2023;29:1067–70. https://doi.org/10.3201/eid2905.221291
7. Eftekhari M, Kachooei A, Jalilvand S, Latifi T, Habib Z, Ataei-Pirkoohi A, et al. The predominance of recombinant norovirus GII.4Sydney[P16] strains in children less than 5 years of age with acute gastroenteritis in Tehran, Iran, 2021–2022. Virus Res. 2023;334:199172. https://doi.org/10.1016/j.virusres.2023.199172
8. Lysén M, Thorhagen M, Brytting M, Hjertqvist M, Andersson Y, Hedlund KO. Genetic diversity among food-borne and

waterborne norovirus strains causing outbreaks in Sweden. J Clin Microbiol. 2009;47:2411–8. https://doi.org/10.1128/JCM.02168-08
9. Kendra JA, Tohma K, Parra GI. Global and regional circulation trends of norovirus genotypes and recombinants, 1995–2019: a comprehensive review of sequences from public databases. Rev Med Virol. 2022;32:e2354. https://doi.org/10.1002/rmv.2354
10. Gao J, Xue L, Liang Y, Wang L, He F, Meng L, et al. Receptor profile and immunogenicity of the non-epidemic norovirus GII.8 variant. Virus Res. 2021;306:198603. https://doi.org/10.1016/j.virusres.2021.198603

Address for correspondence: Yong Poovorawan, Center of Excellence in Clinical Virology, Faculty of Medicine, Chulalongkorn University, 1873 Rama 4 Rd, Pathumwan, Bangkok 10330, Thailand; e-mail: yong.p@chula.ac.th

Use of Doxycycline to Prevent Sexually Transmitted Infections According to Provider Characteristics

William S. Pearson, Brian Emerson, Matthew Hogben, Lindley Barbee

Author affiliation: Centers for Disease Control and Prevention, Atlanta, Georgia, USA

DOI: https://doi.org/10.3201/eid3001.231152

Use of doxycycline to prevent sexually transmitted infections (STIs) may lead to antimicrobial resistance. We analyzed attitudes toward this practice between US providers who commonly and less commonly treat STIs. Providers who more commonly treat STIs are more likely to prescribe prophylactic doxycycline and believe that benefits outweigh potential for increased antimicrobial resistance.

Reports of bacterial sexually transmitted infections (STIs) (e.g., chlamydia, gonorrhea, and syphilis) in the United States are at the highest level in several decades (*1*). A useful tool for preventing STIs may be prophylactic use of doxycycline taken within 72 hours after a sexual encounter (*2*–*5*). However, concerns about development of antimicrobial resistance (AMR) (e.g., in *Neisseria gonorrhea*, which is listed by the Centers for Disease Control and Prevention as an urgent AMR threat), may affect provider attitudes toward prophylactic use of doxycycline (*6*). To determine differences in the practices and beliefs of providers who work with STI patients (STI providers) and do not work with STI patients (non–STI providers) with regard to prophylactic use of doxycycline for STIs and their concerns about potential AMR consequences, we analyzed survey responses.

We analyzed data from the DocStyles panel survey (https://styles.porternovelli.com/docstyles) conducted by SERMO, a social network platform for physicians (https://www.sermo.com) in conjunction with Porter Novelli during September 9–November 3, 2022. Of 1,755 US healthcare providers who responded (response rate 67.0%), we focused on a sample of 1,504 healthcare providers, including family physicians (457, 30.4%), internists (545, 36.2%), obstetrician/gynecologists (251, 16.7%), and nurse practitioners/physician assistants (251, 16.7%). We excluded 251 pediatricians.

We further stratified analyses by the percentage of the providers' practice focused on clinical management of STIs. Providers were asked, "What proportion of your visits include screening for, diagnosing, or treating sexually transmitted infections?"; the 5 possible responses were "none," "some, but less than 10%," "more than 10% up to 25%," "more than 25% up to 50%," or "more than 50%." The 743 respondents whose practice consisted of <10% STI management were considered non–STI providers, and the 761 others were considered STI providers. We further ascertained provider age, sex, specialty, and number of years in practice.

We asked 4 questions about use and beliefs with regard to doxycycline prophylaxis and antimicrobial resistance (Figure), and the 5 response choices were "strongly disagree," "somewhat disagree," "neither agree nor disagree," "somewhat agree," or "strongly agree." We used χ^2 tests to compare the percentage of respondents who chose "strongly agree," and "agree" between STI providers and non–STI providers. We further tested those differences by using adjusted logistic regression models controlling for provider age, sex, number of years in practice, and specialty (Table).

Among STI providers, 41.9% said that they had ever prescribed doxycycline for STI prophylaxis, compared with 21.0% non–STI providers ($p<0.01$). Among STI providers, 57.4% either strongly agreed or agreed with the statement, "I have seen an increase in antibiotic resistant infections among my patients over the past 5 years," compared with 57.6% of non–STI providers ($p = 0.94$). Among STI providers, 63.5% either strongly agreed or agreed with the statement,

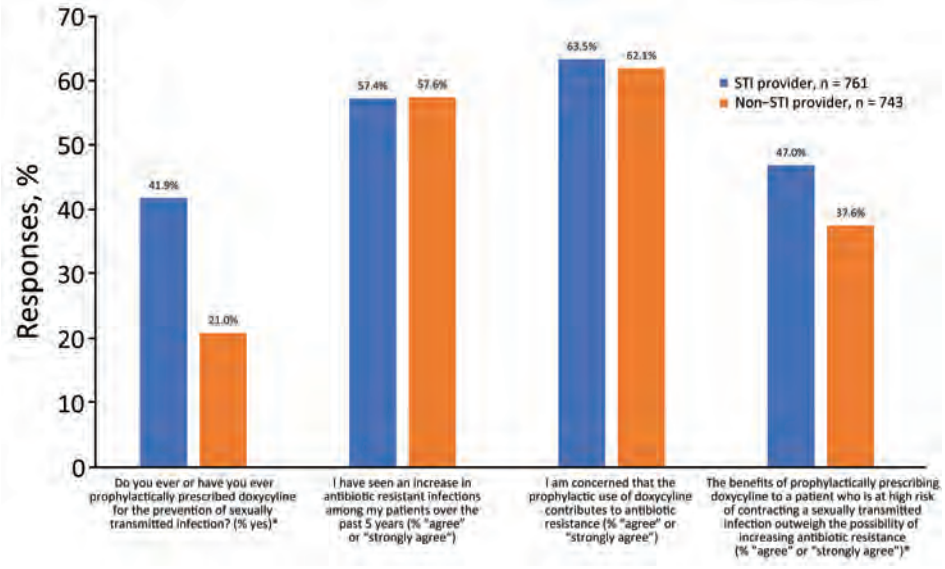

Figure. Comparison of prophylactic use of doxycycline and beliefs about antimicrobial resistance among US STI providers and non-STI providers. *Indicates a statistical difference ($p<0.05$) according to χ^2 analyses.

"I am concerned that the prophylactic use of doxycycline contributes to antibiotic resistance," compared with 62.1% of non–STI providers (p = 0.57). Among STI providers, 47.0% either strongly agreed or agreed with the statement, "The benefits of prophylactically prescribing doxycycline to a patient who is at high risk of contracting a sexually transmitted infection outweigh the possibility of increasing antibiotic resistance," compared with 36.6% of non–STI providers (p<0.01) (Figure).

When we used adjusted logistic regression models to control for provider age, sex, specialty, and number of years in practice, STI providers were >2.5 times more likely to have used doxycycline prophylactically for STI prevention (adjusted odds ratio [aOR] 2.76, 95% CI 2.20–3.48) compared with non–STI providers. STI providers were no more likely than non–STI providers to agree that they had seen an increase in AMR among their patients over the past 5 years (aOR 1.00, 95% CI 0.81–1.23) or that the prophylactic use of doxycycline contributes to AMR (aOR 1.09, 95% CI 0.88–1.35). STI providers had ≈50% greater odds than non-STI providers to agree that the benefits of prophylactically prescribing doxycycline for a patient who is at high risk of contracting an STI outweigh the possibility of increasing AMR (aOR 1.54, 95% CI 1.24–1.89).

Our findings suggest that providers whose practice includes ≥10% STI care are more likely to use doxycycline prophylactically for STI prevention and to believe that the benefits of doxycycline as STI postexposure prophylaxis outweigh the potential for increased AMR compared with providers who do not routinely care for patients with STIs. However, similar proportions of both groups reported concern about the role of prophylactic doxycycline in increasing AMR. Data on the effects that prophylactic use of doxycycline may have on development

Table. Logistic regression models comparing STI providers with non–STI providers on practices regarding prophylactic use of doxycycline and beliefs about antimicrobial resistance, United States*

Question/response	Likelihood
Do you ever or have you ever prophylactically prescribed doxycycline for the prevention of a sexually transmitted infection? By prophylactic use, we mean taking doxycycline to prevent infection ahead of or immediately after exposure risk; response: "yes"	
STI provider	aOR 2.76, 95% CI 2.20–3.48
Non–STI provider	Referent
I have seen an increase in antibiotic resistant infections among my patients over the past 5 years; response "agree" or "strongly agree"	
STI provider	aOR 1.00, 95% CI 0.81–1.23
Non–STI provider	Referent
I am concerned that the prophylactic use of doxycycline contributes to antibiotic resistance; response: "agree" or "strongly agree"	
STI provider	aOR 1.09, 95% CI 0.88–1.35
Non–STI provider	Referent
The benefits of prophylactically prescribing doxycycline to a patient who is at high risk of contracting a sexually transmitted infection outweigh the possibility of increasing antibiotic resistance; response: "agree" or "strongly agree"	
STI provider	aOR 1.53, 95% CI 1.25–1.89
Non–STI provider	Referent

*STI providers, n = 761; non–STI providers, n = 743. Controlled for age of provider, sex of provider, specialty of provider, and number of years in practice. aOR, adjusted odds ratio; STI, sexually transmitted infection.

of AMR are limited (*5*), although antimicrobial use can contribute to the development of AMR (*7*). Additional education on this topic for providers who routinely treat STIs and for providers who routinely prescribe doxycycline will help minimize any potential AMR threats.

About the Author

Dr. Pearson is a senior health scientist working in the Division of STD Prevention, National Center for HIV/AIDS, Viral Hepatitis, STD, and TB Prevention, Centers for Disease Control and Prevention, Atlanta, Georgia, USA. His research is focused on the organization, financing, and delivery of health services.

References

1. Centers for Disease Control and Prevention. Sexually transmitted disease surveillance 2021 [cited 2023 Aug 9]. https://www.cdc.gov/std/statistics/2021/default.htm
2. Molina JM, Charreau I, Chidiac C, Pialoux G, Cua E, Delaugerre C, et al.; ANRS IPERGAY Study Group. Post-exposure prophylaxis with doxycycline to prevent sexually transmitted infections in men who have sex with men: an open-label randomised substudy of the ANRS IPERGAY trial. Lancet Infect Dis. 2018;18:308–17. https://doi.org/10.1016/S1473-3099(17)30725-9
3. Siguier M, Molina JM. Doxycycline prophylaxis for bacterial sexually transmitted infections: promises and perils. ACS Infect Dis. 2018;4:660–3. https://doi.org/10.1021/acsinfecdis.8b00043
4. Grant JS, Stafylis C, Celum C, Grennan T, Haire B, Kaldor J, et al. Doxycycline prophylaxis for bacterial sexually transmitted infections. Clin Infect Dis. 2020;70:1247–53. https://doi.org/10.1093/cid/ciz866
5. Luetkemeyer AF, Donnell D, Dombrowski JC, Cohen S, Grabow C, Brown CE, et al.; DoxyPEP Study Team. Postexposure doxycycline to prevent bacterial sexually transmitted infections. N Engl J Med. 2023;388:1296–306. https://doi.org/10.1056/NEJMoa2211934
6. Centers for Disease Control and Prevention. Antibiotic resistance threats in the United States, 2019 [cited 2023 Aug 10]. https://www.cdc.gov/drugresistance/pdf/threats-report/2019-ar-threats-report-508.pdf
7. Ramblière L, Guillemot D, Delarocque-Astagneau E, Huynh BT. Impact of mass and systematic antibiotic administration on antibiotic resistance in low- and middle-income countries. A systematic review. [Erratum in: Int J Antimicrob Agents. 2021;58:106396.] Int J Antimicrob Agents. 2021;58:106364. https://doi.org/10.1016/j.ijantimicag.2021.106364

Address for correspondence: William S. Pearson, Centers for Disease Control and Prevention, 1600 Clifton Rd NE, Mailstop H24-4, Atlanta, GA 30329-4018, USA; email: wpearson@cdc.gov

Shiga Toxin–Producing *Escherichia coli* Diagnoses from Health Practitioners, Queensland, Australia

Ashish C. Shrestha, Russell Stafford, Robert Bell, Amy V. Jennison, Rikki M.A. Graham, Emma Field, Stephen B. Lambert

Author affiliations: Queensland Health, Brisbane, Queensland, Australia (A.C. Shrestha, R. Stafford, R. Bell, A.V. Jennison, R.M.A. Graham, S.B. Lambert); Australian National University, Canberra, Australian Capital Territory, Australia (A.C. Shrestha, E. Field)

DOI: https://doi.org/10.3201/eid3001.231202

In Queensland, Australia, 31 of 96 Shiga toxin–producing *Escherichia coli* cases during 2020–2022 were reported by a specialty pathology laboratory servicing alternative health practitioners. Those new cases were more likely to be asymptomatic or paucisymptomatic, prompting a review of the standard public health response.

Shiga toxin–producing *Escherichia coli* (STEC) cause gastrointestinal illness and can result in hemolytic uremic syndrome (HUS) (*1*). Asymptomatic STEC infections can occur and might remain undetected (*2*,*3*), making the population incidence of STEC higher than reported through routine surveillance. In Australia, laboratory-confirmed STEC, based on isolation by culture or detection of *stx* gene(s) by nucleic acid testing of feces, is a nationally notifiable condition (*4*). In 2022, the national notification rate was 3.2 cases/100,000 population/year in Australia and 0.6 cases/100,000 population/year in Queensland (*5*).

The frequency of asymptomatic STEC cases increased in Queensland from 2% in 2018–2019 to 29% in 2022. We reviewed the reports for 2020–2022 and found that an increasing number of STEC cases had been reported from a specialty pathology laboratory (SPL) in the state of Victoria that services healthcare providers, including alternative health practitioners (naturopaths and nutritionists).

We undertook further analysis to clarify the reason for increasing case numbers. This analysis involved descriptive analysis of STEC case data extracted from the Queensland Health Notifiable Conditions System database and case report forms for January 2020–December 2022. Ethics approval for this study

Table. Characteristics of 31 STEC cases diagnosed by the specialty pathology laboratory and other pathology laboratories, Queensland, Australia, 2020–2022*

Characteristics	Specialty pathology laboratory		Other pathology laboratories		p value
	Value	% (95% CI)	Value	% (95% CI)	
Sex, no. (%)					
M	6	19 (9–38)	37/65	57 (44–69)	0.001
F	25	81 (62–91)	28/65	43 (31–55)	
Median age, y (range)	35 (1–65)		31 (<1–90)		
Clinical manifestation					
Symptomatic†	16/29 (55)	36–73	56/64	88 (77–94)	0.001
Bloody diarrhea	1/29 (3)	0–22	37/64	58 (45–69)	<0.001
HUS (% of all cases)	0	0	9/64	14 (7–25)	0.024
Hospitalized	0	0	27/62	4 (32–56)	<0.001
Household contacts‡	0	0	6/65	9 (4–19)	0.174
Laboratory culture positive	20/30	67 (47–83)	27/65	42 (29–54)	0.023
stx genes					
stx1 positive, *stx2* negative	6/26	23 (9–44)	14/65	22 (12–33)	0.873
stx2 positive, *stx1* negative	9/26	35 (17–56)	33/65	51 (38–63)	0.059
stx1 positive, *stx2* positive	11/26	42 (23–63)	18/65	28 (17–40)	0.176
eaeA (intimin) positive	1/5	20 (1–72)	20/39	51 (35–68)	0.348
ehxA (enterohemolysin) positive	4/4	100 (40–100)	26/36	72 (55–86)	0.558
Serotypes known to cause severe disease					
O111	1/20	5 (1–25)	2/28	7 (1–24)	0.762
O157	0	0	6/28	21 (8–41)	0.034
O26	0	0	2/28	7 (1–24)	0.504
O145	0	0	2/28	7 (1–24)	0.504

*Values are no. cases or no. positive/no. tested except as indicated. Denominators reflect total cases where the relevant field was completed. HUS, hemolytic uremic syndrome; STEC, Shiga toxin–producing *Escherichia coli.*
†Gastrointestinal symptoms.
‡Includes contacts of a case and are cases of the study population.

was obtained from the Australian National University (protocol 2017/909).

SPL diagnosed STEC by performing multiplex PCR for enteric pathogens on fecal samples from patients. STEC confirmation and characterization of culture-positive isolates were performed subsequently by the Microbiology Diagnostic Unit Public Health Laboratory (Doherty Institute, University of Melbourne, Melbourne, Victoria, Australia). Other STEC cases referred to in this study were tested by pathology laboratories or the Queensland STEC reference laboratory (Public Health Microbiology, Forensic and Scientific Services, Queensland Health) by using PCR or culture. Additional confirmatory testing (culture, PCR, serotyping, genomic analysis) were performed by the reference laboratory.

STEC was reported from an SPL to Queensland Health on March 13, 2020. During 2020–2022, a total of 96 STEC cases were reported, 31 (32%) from the SPL and 65 (68%) from other pathology laboratories that provide services for medical practitioners only (Table; Figure). SPL-reported case-patients were more commonly female (81%) compared with other pathology laboratories (43%) (Table). Of the SPL-diagnosed cases, 85% (23/27) had stool testing requested by alternative health practitioners, naturopath

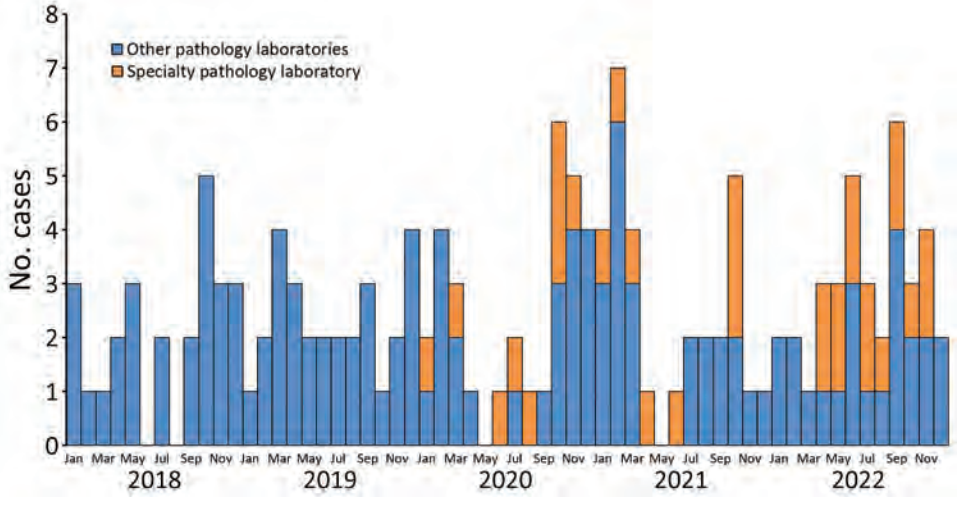

Figure. Shiga toxin–producing *Escherichia coli* cases by month and year of episode date (earliest of specimen collection/onset dates) and reporting laboratories, Queensland, Australia, 2018–2022.

(n = 19) or nutritionist (n = 4); 15% (4/27) were requested by medical practitioners, and the request source was unknown for 4 other cases. Of the case-patients diagnosed by pathology laboratories other than SPL, 92% (60/65) consulted medical practitioners, 6% (4/65) were identified during public health follow-up as a close contact of a previously reported case-patient, and 2% (1/65) were diagnosed after fecal donor screening.

More case-patients given a diagnosis by other pathology laboratories were symptomatic, experienced bloody diarrhea, and were hospitalized than were SPL-diagnosed case-patients (Table). HUS was reported in case-patients given a diagnosis by other pathology laboratories, among children and older adults (age range <1–85 years). Serotypes (O111, O157, O26, O145) and genes (*stx2* only detection and *eaeA* detection) known to cause severe disease (*6*,*7*), were higher for cases diagnosed by other pathology laboratories (Table). Data on subtypes of *stx* were available for 4 SPL and 14 other laboratory cases. *stx2a*, the toxin gene variant reported as being associated with severe disease, was detected only among cases diagnosed by other pathology laboratories (n = 6); all of those cases were symptomatic.

Consistent with current Queensland Health guidelines, all reported STEC cases are investigated and followed up to identify a source of infection (*1*). Case-patients are excluded from working in high-risk settings, and all case-patients, household contacts, and other symptomatic contacts are followed until evidence of microbiological clearance (2 successive negative stool samples 24 hours apart) (*1*). Although asymptomatic case-patients can infect other persons, evidence and guidance for managing asymptomatic cases is varied and less clear (*8*). In low-risk settings, treatment and exclusion of asymptomatic cases might not be necessary (*8*).

stx genes can be detected in stool specimens even when bacterial culture is negative (*9*). Use of higher sensitivity PCRs for STEC screening can result in an increase in notifications. A range of STEC virulence factors and host factors can influence clinical manifestations and outcome of infection, and it has been proposed that certain profiles could be useful predictors of strains associated with causing severe illness (*10*). Although causal inference of these factors with severity of disease could not be established, this investigation provided insight into the observation of increasing detection of mild STEC infection and changes in laboratory testing practices, including testing requests by alternative health practitioners.

Management of STEC cases requires resources for follow-up and testing of both symptomatic and asymptomatic case-patients and their contacts. Therefore, reports of asymptomatic cases and changes in testing practices, as shown by this study, suggest a need to revise existing guidelines for the management of STEC cases on the basis of clinical manifestations, laboratory testing, identification of risk-groups, and available resources.

Acknowledgment

We thank Queensland Health public health units and pathology diagnostic laboratories for providing case information and diagnosis results and for their public health activities for management of reported cases.

About the Author

Dr. Shrestha is a scholar in applied epidemiology at Queensland Health, Brisbane, Australia, and the Australian National University, Canberra, Australia. His primary research interests are infectious diseases epidemiology and vaccinology.

References

1. Queensland Health. Shiga toxin-producing *Escherichia coli* (STEC) infection. 2014 Dec 2 [cited 2022 Jul 20]. https://www.health.qld.gov.au/cdcg/index/stec
2. Morita-Ishihara T, Iyoda S, Iguchi A, Ohnishi M. Secondary Shiga toxin-producing *Escherichia coli* infection, Japan, 2010–2012. Emerg Infect Dis. 2016;22:2181–4. https://doi.org/10.3201/eid2212.160783
3. De Rauw K, Jacobs S, Piérard D. Twenty-seven years of screening for Shiga toxin-producing *Escherichia coli* in a university hospital. Brussels, Belgium, 1987–2014. PLoS One. 2018;13:e0199968. https://doi.org/10.1371/journal.pone.0199968
4. Australian Government Department of Health and Aged Care. Shiga toxin-producing *Escherichia coli* (STEC) infection. 2016 Apr [cited 2022 Jul 31]. https://www.health.gov.au/sites/default/files/documents/2022/06/shiga-toxin-producing-escherichia-coli-stec-infection-surveillance-case-definition.pdf
5. Australian Government Department of Health and Aged Care. National notifiable disease surveillance system: national communicable disease surveillance dashboard. 2022 [cited 2023 Aug 11]. https://nindss.health.gov.au/pbi-dashboard
6. UK Health Security Agency. Public health operational guidance for Shiga toxin-producing *Escherichia coli* (STEC). 2023 Jan [cited 2023 Apr 4]. https://assets.publishing.service.gov.uk/government/uploads/system/uploads/attachment_data/file/1127818/health-guidance-shiga-toxin-producing-escherichia-coli.pdf
7. Persson S, Olsen KE, Ethelberg S, Scheutz F. Subtyping method for *Escherichia coli* Shiga toxin (verocytotoxin) 2 variants and correlations to clinical manifestations. J Clin Microbiol. 2007;45:2020–4. https://doi.org/10.1128/JCM.02591-06
8. Shane AL, Mody RK, Crump JA, Tarr PI, Steiner TS, Kotloff K, et al. 2017 Infectious Diseases Society of America

clinical practice guidelines for the diagnosis and management of infectious diarrhea. Clin Infect Dis. 2017;65:e45–80. https://doi.org/10.1093/cid/cix669
9. Macori G, McCarthy SC, Burgess CM, Fanning S, Duffy G. Investigation of the causes of shigatoxigenic *Escherichia coli* PCR positive and culture negative samples. Microorganisms. 2020;8:587. https://doi.org/10.3390/microorganisms8040587
10. FAO/WHO STEC EXPERT GROUP. Hazard identification and characterization: criteria for categorizing Shiga toxin-producing *Escherichia coli* on a risk basis. J Food Prot. 2019;82:7–21. https://doi.org/10.4315/0362-028X.JFP-18-291

Address for correspondence: Ashish C. Shrestha, Communicable Diseases Branch, Queensland Health, PO Box 2368, Fortitude Valley BC, Queensland 4006, Australia; email: ashish.shrestha@anu.edu.au

Frequency of Children Diagnosed with Perinatal Hepatitis C, United States, 2018–2020

Suzanne M. Newton, Kate R. Woodworth, Daniel Chang, Lindsey Sizemore, Heather Wingate, Leah Pinckney, Anthony Osinski, Lauren Orkis, Bethany D. Reynolds, Cynthia Carpentieri, Umme-Aiman Halai, Caleb Lyu, Nicole Longcore, Nadia Thomas, Aprielle Wills, Amanda Akosa, Emily O'Malley Olsen, Lakshmi Panagiotakopoulos, Nicola D. Thompson, Suzanne M. Gilboa, Van T. Tong

Author affiliations: Centers for Disease Control and Prevention, Atlanta, Georgia, USA (S.M. Newton, K.R. Woodworth, E.O. Olsen, L. Panagiotakopoulos, N.D. Thompson, S.M. Gilboa, V.T. Tong); Eagle Global Scientific, LLC, San Antonio, Texas, USA (D. Chang, A. Akosa); Tennessee Department of Health, Nashville, Tennessee, USA (L. Sizemore, H. Wingate); Massachusetts Department of Public Health, Boston, Massachusetts, USA (L. Pinckney, A. Osinski); Pennsylvania Department of Health, Pittsburgh, Pennsylvania, USA (L. Orkis, B.D. Reynolds); Chickasaw Nation Industries, Norman, Oklahoma, USA (C. Carpentieri); Los Angeles County Department of Health, Los Angeles, California, USA (U-A. Halai, C. Lyu); New York State Department of Health, Albany, New York, USA (N. Longcore, N. Thomas); New York City Department of Health and Mental Hygiene, New York City, New York (A. Wills)

DOI: http://doi.org/10.3201/eid3001.230315

We describe hepatitis C testing of 47 (2%) of 2,266 children diagnosed with perinatal hepatitis C who were exposed during 2018–2020 in 7 jurisdictions in the United States. Expected frequency of perinatal transmission is 5.8%, indicating only one third of the cases in this cohort were reported to public health authorities.

Hepatitis C virus (HCV) can be transmitted perinatally (*1*). Rates of acute HCV infection have increased recently (*2*), but few children perinatally exposed to HCV are tested and referred to care (*3*). As of November 2023, the Centers for Disease Control and Prevention recommends testing of all perinatally exposed infants for detection of HCV RNA at age 2–6 months, which is earlier than previous recommendations of ≥18 months of age for HCV antibody testing (*4*). There may be advantages to performing HCV RNA testing earlier, before children might become lost to follow-up (*5*). A prior analysis found only 16% of children perinatally exposed to hepatitis C in Philadelphia, Pennsylvania, USA, received HCV testing (*6*). Limited data are available from larger surveillance cohorts about current testing patterns of children perinatally exposed to HCV.

Positive HCV test results are nationally notifiable in the United States, but negative HCV test results are not. To identify potential gaps in testing and surveillance, we used positive HCV test results to describe testing and frequency of children diagnosed with perinatal hepatitis C during 2018–2020 compared with the expected frequency of perinatal transmission in 7 US jurisdictions. This activity was deemed as public health surveillance and not research at Centers for Disease Control and Prevention, thus exempt from institutional review board review.

We assembled a retrospective cohort from surveillance data of pregnant women. The exposure of interest was prenatal exposure to HCV, and perinatal hepatitis C was the outcome. The Surveillance for Emerging Threats to Pregnant People and Infants Network conducts surveillance of pregnant women with HCV infection and their children (*7*). As of September 9, 2022, seven US jurisdictions (Georgia, Los Angeles County, Massachusetts, New York City, New York State, Pennsylvania, Tennessee) had contributed data on persons with HCV RNA detected during or within 1 year before pregnancy who had no evidence of treatment or clearance and who had live births during January 1, 2018–October 9, 2020. Children were determined to have perinatal hepatitis C if HCV RNA was detected or they had a reactive HCV antibody test during the recommended window (RNA at ≥2 months of age or antibody at ≥18 months

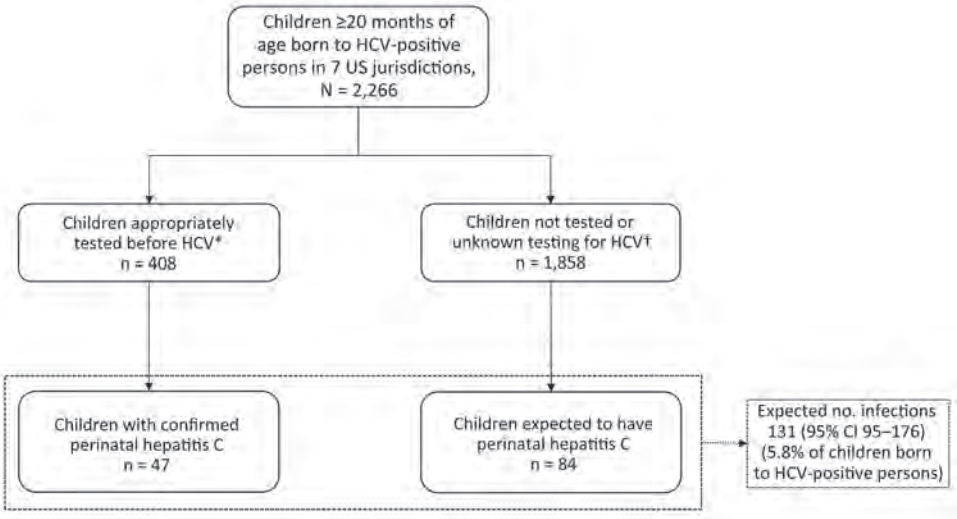

Figure. Observed and expected HCV infections among children with perinatal hepatitis C exposure in 7 US jurisdictions, 2018–2020. *Appropriate testing is considered test conducted at ≥2 months for HCV RNA or ≥18 months for HCV antibody. †May include children who tested negative for HCV, children whose tests were not reported to the health department, or children tested at an inappropriate age (<2 months for HCV RNA; <18 months for HCV antibody). HCV, Hepatitis C virus.

of age) (*4*). Collection of data is ongoing to provide a complete picture of testing practices, including distinguishing those who were not tested from those who tested negative. We determined the expected number of children with perinatal hepatitis C by estimating 5.8% (95% CI 4.2%–7.8%) of live births exposed to HCV from included jurisdictions on the basis of a published estimate (*1*).

A total of 2,266 children were born to pregnant women with hepatitis C during the surveillance period (Figure). Among those children, 408 (18%) were tested for HCV infection within the recommended window and 19 (1%) outside it. Forty-seven children (2%) had perinatal hepatitis C. Median age at initial positive test was 18.6 months. Perinatal HCV infection was detected at <18 months of age for 17 (36%) children and ≥18 months of age for 30 (64%) (Table). Of the 47 children with perinatal hepatitis C, 18 (38%) had a reactive HCV antibody test and HCV RNA detected on the same day, likely reflecting reflex laboratory testing.

Table. Characteristics of 47 children with perinatal hepatitis C in a cohort of 2,266 children from 7 United States jurisdictions, by timing of test, 2018–2020

Characteristics	Children with perinatal hepatitis C	
	First positive test <18 months of age,* n = 17 (36%)	First positive test ≥18 months of age,† n = 30 (64%)
Pregnant persons		
Age at HCV infection in pregnancy, y, median (IQR)	30 (24–33)	27 (23–32)
Race/ethnicity		
White, Non-Hispanic	15 (88)	27 (90)
Other	2 (12)	3 (10)
Education		
High school graduate and below	7 (41)	21 (70)
Some college and higher	6 (35)	9 (30)
Missing	4 (24)	0
Health insurance at delivery		
Public	13 (76)	28 (93)
Private/other/none	4 (24)	2 (7)
Substance use		
Any‡	10 (59)	22 (73)
None	2 (12)	2 (7)
Missing	5 (29)	6 (20)
Infants		
Neonatal abstinence syndrome§	4 (24)	12 (40)
Missing data	8 (47)	11 (37)
Neonatal intensive care unit admission	6 (35)	12 (40)
Missing data	1 (6)	0 (0)
Age at first positive test, mo, median (IQR)	7.3 (3.6–11.6)	19.4 (18.7–24.4)

*Values are no. (%) except as indicated. All tests were done by HCV RNA. HCV, hepatitis C virus.
†Two infants first tested by positive HCV RNA at ≥18 mo; 28 infants first tested positive by HCV antibody at ≥18 mo.
‡Substance use includes alcohol, tobacco, cannabis, illicit use of opioids, and other illicit substances (eg, methamphetamines, cocaine).
§Includes a diagnosis of neonatal abstinence syndrome or drug withdrawal syndrome in infant of dependent pregnant person (ICD-10 code P96.1) during the birth hospitalization.

The expected number (*1*) of children with perinatal hepatitis C by 20 months of age was 131 (95% CI 95–176), suggesting there were an additional 84 children with unidentified perinatal hepatitis C in this cohort. Therefore, only 36% (47/131) of children by 20 months of age who were expected to have perinatal hepatitis C within our cohort were reported to public health authorities. Potential reasons for this discrepancy include loss to follow-up (e.g., patients did not attend follow-up appointments), lack of awareness of the need for testing, delayed testing or testing too early, not completing ordered tests (*8*), or lack of reporting positive tests to health departments.

Limitations of this report include the fact that negative tests are not uniformly reportable across the jurisdictions we studied. However, medical record abstraction is ongoing to be able to describe testing practices, including those who were not tested or tested negative. In addition, the number of children included in this analysis may be underestimated if confirmatory testing occurred outside of the jurisdiction for the pregnant person or they were lost to follow-up before delivery. Last, although 5.8% is a pooled estimate for risk of vertical HCV infection, underlying differences between the prior study population and the population included in this analysis could affect risk (*1*).

This report identified more positive infants than a previous study (36% vs. 16%) (*6*), but both indicate that most children perinatally exposed to hepatitis C are not tested for infection. Understanding testing patterns among children with perinatal HCV exposure and current gaps in perinatal HCV testing and surveillance will help serve as a baseline for improving testing and surveillance to identify children with perinatal hepatitis C, connect them to the appropriate care, and move toward hepatitis C elimination.

Acknowledgments

We acknowledge the following persons and organizations for their contributions to this report: Laura Price, Tennessee Department of Health; Cynthia Brooks, Chickasaw Nation Industries; Hanna Shephard, Susan Soliva, Mahsa M. Yazdy, and Catherine M. Brown, Massachusetts Department of Public Health; Katherine Barter, Allison Longenberger, and Sharon Watkins, Pennsylvania Department of Health; Allegheny County Health Department; J. Michael Bryan, Jerusha Barton, Teri Willabus, Victoria Sanon, Michael Andrews, Nehali Shah, Tracy Kavanaugh, and Ami Gandhi, Georgia Department of Public Health; Prabhu Gounder, Raiza Amiling, Bonnie Dao, Nina Mykhaylov, Van Ngo, and Clara Chang, Los Angeles County Department of Health; and Lucila Zamboni, New York State Department of Health.

This study was performed as regular work of the Centers for Disease Control and Prevention. This work is supported by the Epidemiology and Laboratory Capacity for Prevention and Control of Emerging Infectious Diseases Cooperative Agreement (CK19-1904) and contractual mechanisms, including the Local Health Department Initiative to Chickasaw Health Consulting (200-2021-F-12655). Staffing support for this work was funded by CDC to a contract to Eagle Global Scientific (200-2019-06754).

About the Author

Ms. Newton is an epidemiologist with the National Center on Birth Defects and Developmental Disabilities at the Centers for Disease Control and Prevention, Atlanta, Georgia. Her main areas of study include infections during pregnancy and short- and long-term impact to the child.

References

1. Benova L, Mohamoud YA, Calvert C, Abu-Raddad LJ. Vertical transmission of hepatitis C virus: systematic review and meta-analysis. Clin Infect Dis. 2014;59:765–73. https://doi.org/10.1093/cid/ciu447
2. Centers for Disease Control and Prevention. Viral hepatitis surveillance report—United States, 2020. 2022 Sep [cited 2022 Nov 8]. https://www.cdc.gov/hepatitis/statistics/2020surveillance/index.htm
3. Lopata SM, McNeer E, Dudley JA, Wester C, Cooper WO, Carlucci JG, et al. Hepatitis C testing among perinatally exposed infants. Pediatrics. 2020;145:e20192482. https://doi.org/10.1542/peds.2019-2482
4. Panagiotakopoulos L, Sandul AL, Conners E, Foster M, Nelson N, Wester C, et al. CDC recommendations for hepatitis C testing among perinatally exposed infants and children—United States, 2023. MMWR Recomm Rep 2023;72(No. RR-4):1–19. PubMed http://dx.doi.org/10.15585/mmwr.rr7204a1
5. Bhardwaj AM, Mhanna MJ, Abughali NF. Maternal risk factors associated with inadequate testing and loss to follow-up in infants with perinatal hepatitis C virus exposure. J Neonatal Perinatal Med. 2021;14:123–9. https://doi.org/10.3233/NPM-190264
6. Kuncio DE, Newbern EC, Johnson CC, Viner KM. Failure to test and identify perinatally infected children born to hepatitis C virus–infected women. Clin Infect Dis. 2016;62:980–5. https://doi.org/10.1093/cid/ciw026
7. Woodworth KR, Reynolds MR, Burkel V, Gates C, Eckert V, McDermott C, et al. A preparedness model for mother-baby linked longitudinal surveillance for emerging threats. Matern Child Health J. 2021;25:198–206. https://doi.org/10.1007/s10995-020-03106-y
8. Reynolds B. Birth and infant outcomes in pregnancies affected by hepatitis C-SETNET, Allegheny County, PA. Abstract presented at: Council of State and Territorial Epidemiologists Annual Conference. June 19–23, 2022; Louisville, KY, USA.

Address correspondence to: Suzanne M. Newton, MPH, Centers for Disease Control and Prevention, 4770 Buford Hwy, Mailstop S106-3, Atlanta, GA 30341, USA: email: snewton@cdc.gov

Use of Zoo Mice in Study of Lymphocytic Choriomeningitis Mammarenavirus, Germany

Joëlle Goüy de Bellocq, Stuart J.E. Baird, Alena Fornůskova

Author affiliation: Institute of Vertebrate Biology of the Czech Academy of Sciences, Brno, Czech Republic

DOI: http://doi.org/10.3201/eid2912.230334

To the Editor: Mehl et al. (*1*) report high prevalence of lymphocytic choriomeningitis mammarenavirus (LCMV) in mice captured in a zoo in Germany; mice were screened after detection of LCMV in a golden lion tamarin. Similarly high LCMV prevalences have been detected in mouse breeding facilities (MBFs) (*2*). Mehl et al. suggested the zoo LCMV strains do not support the biogeographic hypothesis for LCMV distribution proposed by Fornůsková et al. (*3*). We feel obliged to point out that data collected from zoos cannot inform regarding biogeographic hypotheses, either way.

Fornůsková et al. (*3*) surveyed LCMV in natural (low-prevalence) house mouse populations. Their findings showed that an apparently random distribution of LCMV lineages in human infections, taken from public databases, is resolved by tracing viral origins not to diagnosing institutes, but instead through patient history. With origin tracing, most current data are consistent with the hypothesis that LCMV lineage I (sensu; *4*) originates in the range of *Mus musculus domesticus* mice, whereas LCMV lineage II originates in the range of *M. m. musculus* mice.

Regarding the infected lion tamarin (*1*), numerous LCMV infections have been reported in zoo primates (*5*); zoos in Europe exchange primates, including lion tamarins. Regarding the zoo-captured mice, zoos either maintain their own MBFs or receive live mice from external MBFs to feed reptiles, raptors, and other small carnivores. Presence of MBF mice in zoos breaks origin tracing of wild mouse pathogens because domesticated mice are crosses of 3 wild subspecies; origins of strains used to mass-produce animal food are unregulated. Mehl et al. (*1*) found multiple LCMV strains in a high-density host-pathogen transport hub. Whether such hubs might in the future lead to a breakdown in the current biogeographic pattern of LCMV lineages remains an open question.

The Czech Science Foundation supports the authors' work on house mouse viruses (grant no. 22-32394S).

References

1. Mehl C, Wylezich C, Geiger C, Schauerte N, Mätz-Rensing K, Nesseler A, et al. Reemergence of lymphocytic choriomeningitis mammarenavirus, Germany. Emerg Infect Dis. 2023;29:631–4. https://doi.org/10.3201/eid2903.221822
2. Knust B, Ströher U, Edison L, Albariño CG, Lovejoy J, Armeanu E, et al. Lymphocytic choriomeningitis virus in employees and mice at multipremises feeder-rodent operation, United States, 2012. Emerg Infect Dis. 2014;20:240–7. https://doi.org/10.3201/eid2002.130860
3. Fornůsková A, Hiadlovská Z, Macholán M, Piálek J, Goüy de Bellocq J. New perspective on the geographic distribution and evolution of lymphocytic choriomeningitis virus, Central Europe. Emerg Infect Dis. 2021;27:2638–47. https://doi.org/10.3201/eid2710.210224
4. Albariño CG, Palacios G, Khristova ML, Erickson BR, Carroll SA, Comer JA, et al. High diversity and ancient common ancestry of lymphocytic choriomeningitis virus. Emerg Infect Dis. 2010;16:1093–100. https://doi.org/10.3201/eid1607.091902
5. Childs JE, Klein SL, Glass GE. A case study of two rodent-borne viruses: not always the same old suspects. Front Ecol Evol. 2019;7:35. https://doi.org/10.3389/fevo.2019.00035

Address for correspondence: Joëlle Goüy de Bellocq, Czech Academy of Sciences—Institute of Vertebrate Biology, Studenec 122 Konesin 67502, Czech Republic; email: joellegouy@gmail.com

Calvin Mehl, Claudia Wylezich, Christina Geiger, Nicole Schauerte, Kerstin Mätz-Rensing, Anne Nesseler, Dirk Höper, Miriam Linnenbrink, Martin Beer, Gerald Heckel, Rainer G. Ulrich

Author affiliations: Friedrich-Loeffler-Institut, Greifswald–Insel Riems, Germany (C. Mehl, C. Wylezich, D. Höper, M. Beer, R.G. Ulrich); German Center for Infection Research, Hamburg–Lübeck–Borstel–Riems, Germany (C. Mehl, R.G. Ulrich); Zoo Frankfurt, Frankfurt, Germany (C. Geiger, N. Schauerte); German Primate Center, Leibniz Institute for Primate Research, Göttingen, Germany (K. Mätz-Rensing); Landeslabor Hessen, Giessen, Germany (A. Nesseler); Max Planck Institute for Evolutionary Biology, Plön, Germany (M. Linnenbrink); University of Bern, I nstitute of Ecology and Evolution, Bern, Switzerland (G. Heckel)

DOI: http://doi.org/10.3201/eid3001.231521

In Response: Gouy de Bellocq et al. question in their letter whether data from zoos can be used to test a biogeographic hypothesis regarding lymphocytic choriomeningitis mammarenavirus (LCMV) (*1*). We agree that this should be done with caution because zoos may act as hubs for pathogen transfer through captive animal transfer and the use of feeder rodents. As we stated in our article (*2*), the occurrence of LCMV in house mice in western Germany was already described in the 1960s, although

genetic information is not available (*3*). The detection of LCMV lineage I in house mice from this zoo and the previous detection of a closely related strain in another zoo in this part of Germany (*4*) is in line with a biogeographic pattern.

We note that we made no claims toward the biogeography of LCMV lineages or of the wild house mice in the zoo. Rather, the study provided multiple evidence that did not support the subspecies host specificity because both LCMV lineages were found in the same population of wild *Mus musculus domesticus* mice in the zoo. The high similarity between LCMV genome sequences from a primate and a wild house mouse suggests a transmission link between captive and wild animals in the zoo. The primate was born in the zoo, and the zoo did not breed mice and has not fed mice to primates for decades; thus, the route through which LCMV might have entered the zoo remains unknown. More detailed analyses will be necessary to test the association of LCMV lineages with their reservoir hosts. The scarcity of LCMV detection in wild rodent populations and pet rodents (*5*) and the co-detection of both LCMV lineages (*2*,*6*) will continue to pose a challenge to biogeographic hypothesis testing.

References

1. Goüy de Bellocq J, Baird SJE, Fornůsková A. Use of zoo mice in study of lymphocytic choriomeningitis mammarenavirus, Germany. Emerg Infect Dis. 2024;30:XXX. https://doi.org/10.3201/eid3001.230334
2. Mehl C, Wylezich C, Geiger C, Schauerte N, Mätz-Rensing K, Nesseler A, et al. Reemergence of lymphocytic choriomeningitis mammarenavirus, Germany. Emerg Infect Dis. 2023;29:631–4. https://doi.org/10.3201/eid2903.221822
3. Ackermann R, Bloedhorn H, Küpper B, Winkens I, Scheid W. Über die Verbreitung des Virus der lymphocytären Choriomeningitis unter den Mäusen in Westdeutschland. *Zentralblatt* für *Bakteriologie, Parasitenkunde*. I nfektionskrankheiten und Hygiene. 1964;194:407–30.
4. Asper M, Hofmann P, Osmann C, Funk J, Metzger C, Bruns M, et al. First outbreak of callitrichid hepatitis in Germany: genetic characterization of the causative lymphocytic choriomeningitis virus strains. Virology. 2001;284:203–13. https://doi.org/10.1006/viro.2001.0909
5. Fornůsková A, Hiadlovská Z, Macholán M, Piálek J, de Bellocq JG. New perspective on the geographic distribution and evolution of lymphocytic choriomeningitis virus, central Europe. Emerg Infect Dis. 2021;27:2638–47. https://doi.org/10.3201/eid2710.210224
6. Pankovics P, Nagy A, Nyul Z, Juhász A, Takáts K, Boros Á, et al. Human cases of lymphocytic choriomeningitis virus (LCMV) infections in Hungary. Arch Virol. 2023;168:275. https://doi.org/10.1007/s00705-023-05905-4

Address for correspondence: Rainer G. Ulrich, Friedrich-Loeffler-Institut, Bundesforschungsinstitut fur Tiergesundheit, Greifswald–Insel Riems, Germany; email: rainer.ulrich@fli.de

SARS-CoV-2 Incubation Period during Omicron BA.5–Dominant Period, Japan

Hao-Yuan Cheng, Andrei R. Akhmetzhanov, Jonathan Dushoff

Author affiliations: Taiwan Centers for Diseases Control, Taipei, Taiwan (H.-Y. Cheng); National Taiwan University, Taipei (A.R. Akhmetzhanov); McMaster University, Hamilton, Ontario, Canada (J. Dushoff)

DOI: https://doi.org/10.3201/eid3001.230208

To the Editor: Ogata and Tanaka (*1*) estimated the mean incubation period was 2.9 (95% CI 2.6–3.2) days for SARS-CoV-2 strain Omicron BA.1 and 2.6 (95% CI 2.5–2.8) days for Omicron BA.5 during the Omicron-dominant period in Japan. Their earlier study reported a similar mean incubation period of 3.1 days for BA.1 (*2*). Their findings were derived from data collected through contact tracing efforts in Ibaraki Prefecture, Japan, which provided high accuracy in determining exposure time windows.

A potential concern is that their study only included cases that had a single exposure event and a 1-day exposure window. Although this concern was recognized by the authors as a study limitation, we emphasize that those criteria might bias results downward, especially when the disease is widespread. Persons that had longer incubation periods might have more opportunity for contacts or multiple exposure dates; thus, those with shorter incubation periods would be favored for inclusion. A more flexible case-selection approach might reduce bias, even though this approach would require methods to address uncertainty in actual infection timing.

In Taiwan, we collected data from the first 100 local symptomatic cases during the BA.1–dominant period (December 25, 2021–January 18, 2022), which were characterized by intensive case finding and contact tracing (A. Akhmetzhanov et al., unpub. data, https://doi.org/10.1101/2023.07.20.23292983. Among 69 cases with an identified exposure, only 4 had a 1-day exposure window. Using more comprehensive exposure windows, the estimated mean incubation period in Taiwan was 3.5 (95% CI 3.1–4.0) days, longer than Tanaka et al.'s estimates (*1*,*2*) but similar to estimates of 3.5 days from Italy (data collected during January 2022) (*3*) and South Korea (data collected during November–December 2021) (*4*) and estimates from a systematic review (3.6 days) (*5*). The estimates from Japan (*2*) appear to be the shortest periods reported across previously reviewed studies (*5*).

References

1. Ogata T, Tanaka H. SARS-CoV-2 incubation period during the Omicron BA.5–dominant period in Japan. Emerg Infect Dis. 2023;29:595–8. https://doi.org/10.3201/eid2903.221360
2. Tanaka H, Ogata T, Shibata T, Nagai H, Takahashi Y, Kinoshita M, et al. Shorter incubation period among COVID-19 cases with the BA.1 Omicron variant. Int J Environ Res Public Health. 2022;19:6330. https://doi.org/10.3390/ijerph19106330
3. Manica M, De Bellis A, Guzzetta G, Mancuso P, Vicentini M, Venturelli F, et al.; Reggio Emilia COVID-19 Working Group. Intrinsic generation time of the SARS-CoV-2 Omicron variant: an observational study of household transmission. Lancet Reg Health Eur. 2022;19:100446. https://doi.org/10.1016/j.lanepe.2022.100446
4. Liu Y, Zhao S, Ryu S, Ran J, Fan J, He D. Estimating the incubation period of SARS-CoV-2 Omicron BA.1 variant in comparison with that during the Delta variant dominance in South Korea. One Health. 2022;15:100425. https://doi.org/10.1016/j.onehlt.2022.100425
5. Du Z, Liu C, Wang L, Bai Y, Lau EHY, Wu P, et al. Shorter serial intervals and incubation periods in SARS-CoV-2 variants than the SARS-CoV-2 ancestral strain. J Travel Med. 2022;29:taac052. https://doi.org/10.1093/jtm/taac052

Address for correspondence: Andrei R. Akhmetzhanov, National Taiwan University, College of Public Health, No. 17 Xuzhou Rd., Zhongzheng District, Taipei 10055, Taiwan; email: akhmetzhanov@ntu.edu.tw

Tsuyoshi Ogata, Hideo Tanaka

Author affiliations: Itako Public Health Center of Ibaraki Prefectural Government, Ibaraki, Japan (T. Ogata); Public Health Center of Neyagawa City, Osaka, Japan (H. Tanaka)

DOI: https://doi.org/10.3201/eid3001.231487

In Response: We thank Dr. Cheng and colleagues (*1*) for their valuable comments regarding our study of incubation periods observed for the SARS-CoV-2 Omicron BA.5 subvariant in Japan (*2*). As we indicated in our study limitations paragraph, "patient pairs with long incubation periods might be censored during observational periods, and selection bias might result in underestimation" (*2*). We have several other comments to make regarding our study. First, our previous study during the increasing dominance of the Omicron BA.1 subvariant only included patients who had 1 exposure day; we reported incubation periods of 3.0 days for L452R mutation–negative patients and 3.3 days for unvaccinated patients (*3*), which was similar to 3.2 days reported in a study of patients with BA.1 infections who had multiple exposure days (*4*). Therefore, the effect of only including patients who had 1 exposure day should be further evaluated. Second, the incubation period for the BA.5 subvariant in our study was 3.0 days for patients with infectors who were ≤19 years of age and 2.1 days for patients with infectors who were ≥60 years of age (*2*). Because those data are considerably different, adjustment for demographic factors for both infectors and infectees might be necessary to compare incubation periods. Third, although including patients with multiple exposure days decreases selection bias, it might increase uncertainty regarding the actual time of infection (*5*). Therefore, comparing incubation periods in studies that use various methods and evaluating corresponding study limitations are useful for review and discussion.

References

1. Cheng HY, Akhmetzhanov AR, Dushoff J. SARS-CoV-2 incubation period during Omicron BA.5–dominant period, Japan. Emerg Infect Dis. 2024 Jan [*date* cited]. https://doi.org/10.3201/eid3001.230208
2. Ogata T, Tanaka H. SARS-CoV-2 incubation period during the Omicron BA.5–dominant period in Japan. Emerg Infect Dis. 2023;29:595–8. https://doi.org/10.3201/eid2903.221360
3. Tanaka H, Ogata T, Shibata T, Nagai H, Takahashi Y, Kinoshita M, et al. Shorter incubation period among COVID-19 cases with the BA.1 Omicron variant. Int J Environ Res Public Health. 2022;19:6330. https://doi.org/10.3390/ijerph19106330
4. Park SW, Sun K, Abbott S, Sender R, Bar-On YM, Weitz JS, et al. Inferring the differences in incubation-period and generation-interval distributions of the Delta and Omicron variants of SARS-CoV-2. Proc Natl Acad Sci USA. 2023;120:e2221887120. https://doi.org/10.1073/pnas.2221887120
5. McAloon C, Collins Á, Hunt K, Barber A, Byrne AW, Butler F, et al. Incubation period of COVID-19: a rapid systematic review and meta-analysis of observational research. BMJ Open. 2020;10:e039652. https://doi.org/10.1136/bmjopen-2020-039652

Address for correspondence: Tsuyoshi Ogata, Itako Public Health Center of Ibaraki Prefectural Government, Osu1446-1, Itako, Ibaraki 311-2422, Japan; email: kenkoukikikanri@gmail.plala.or.jp

Jan Verkolje (1650–1693), ***Portrait of Anthonie van Leeuwenhoek, Natural Philosopher and Zoologist in Delft*** (detail)**, 1680–1686.** Oil on canvas, 22 in x 18.7 in/56 cm × 47.5 cm. Public domain image courtesy of Rijksmuseum, Amsterdam, Netherlands.

From Observing Little Animalcules to Detecting Fastidious Bacteria

Byron Breedlove and Clyde Partin

We still think of human disease as the work of an organized, modernized kind of demonology, in which the bacteria are the most visible and centrally placed of our adversaries. We assume that they must somehow relish what they do.

— Lewis Thomas, *The Lives of a Cell: Notes of a Biology Watcher*. Chapter 15: Germs

Pictured on this month's cover is a portrait of Anthonie van Leeuwenhoek (sometimes spelled Antony or Antoni), born October 24, 1632, in Delft, the Netherlands, and among the earliest observers of bacteria. A brief biography on the University of California Museum of Paleontology website describes Leeuwenhoek as "an unlikely scientist" who "succeeded in making some of the most important discoveries in the history of biology." During his younger years, he received no advanced education that would presage his future scientific accomplishments. Leeuwenhoek became a fabric merchant and ran a haberdashery in Delft, where he also held sev-

Author affiliation: Centers for Disease Control and Prevention, Atlanta, Georgia, USA (B. Breedlove); Emory University School of Medicine, Atlanta (C. Partin)

DOI: https://doi.org/10.3201/eid3001.AC3001

eral appointed positions as a surveyor and as a minor city official. At age 16, Leeuwenhoek moved to Amsterdam for 6 years, where, according to infectious disease specialist Robert P. Gaynes, he "became acquainted with Jan Swammerdam, a man known in later years to have fashioned early microscopes." In the course of his work, Leeuwenhoek used a simple microscope to inspect fabrics used in his drapery and clothing business.

Although he could not read English, Leeuwenhoek's interest in microscopy was piqued by *Micrographia* (1665), the popular book by Robert Hooke that detailed and illustrated his microscopic observations. Historian Frank N. Egerton noted that Leeuwenhoek started grinding his own lenses and assembling simple microscopes in 1673 and, during the next 50 years, crafted an estimated 500 microscopes. At the time of Leeuwenhoek's death, noted Meyer Friedman and Gerald W. Friedland, he had a collection of 247 microscopes and 172 lenses mounted in various precious metals. In 1745, Leeuwenhoek's daughter Maria auctioned these items, netting 61 pounds. Fewer than 10 of his microscopes are extant.

The portrait by Dutch artist Jan (Johannes) Verkolje depicts Leeuwenhoek splendidly dressed, wearing a frilled shirt, a fashionably swathed scarf, and an elegant satin robe, perhaps perks of his profession. The text accompanying the painting at the Rijksmuseum states that Leeuwenhoek "is sitting at a writing table on which is a certificate of his appointment as a member of the Royal Society in London by Charles II." Curiously, no microscopes are featured in this depiction.

As recounted in *A Brief History of Bacteriology*, Leeuwenhoek was "able to see objects which he called 'animalcules' in rain water, and in scrapings from his teeth. He noted that some specimens were motile, and described stick-like shapes and spirals. He did not associate his animalcules with disease. The animalcules have become variously known as germs, microbes, bacteria, micro-organisms or simply 'organisms.'" Leeuwenhoek's descriptions represent the primordial steps down a path that eventually proved the role of his "little creatures" to be the etiologic agents of infectious disease.

Friedman and Friedland also explain that Leeuwenhoek was later puzzled to discover that the plaque on his front teeth had quit harboring his little animals, yet his molars still hosted them. In the interim, he had taken up the habit of drinking scalding coffee, which he realized cleansed his anterior teeth but did not affect his molars. The famous French scientist Louis Pasteur, when he developed his method of pasteurization, would remind us of this theme of utilizing heat as a strategy for managing bacteria.

Eminent scientists continued the arc of Leeuwenhoek's discovery. In 1678, Robert Hooke, at the request of the Royal Society, confirmed Leeuwenhoek's "epochal observations." Leeuwenhoek's glittering star dimmed after his death in 1723. Four decades after Leeuwenhoek's death, Austrian Marc von Plenciz resurrected Leeuwenhoek's investigations and "declared flatly that contagious diseases were caused by the Dutchman's small animalcules." The Italian Agostino Bassi "demonstrated experimentally in 1835 that silk worm disease was caused by bacteria." The anatomist and physician from Bavaria, Friedrich Henle, promoted Leeuwenhoek's investigations and, as Friedman and Friedland noted, "impressed on his most brilliant student, Robert Koch, the earthshaking implications of Bassi's work." Although Pasteur and Koch were frequently at odds with each other, their contributions were the final act in the living drama that connected Leeuwenhoek's tiny creatures to the unrelenting scourge of infectious diseases. Their work occurred in a lingering milieu of spontaneous generation theory, a concept Leeuwenhoek found ludicrous, and he was incredulous that the idea was still sundering scientific thought. He wrote, "Can there even now be people who still hang on to the ancient belief that living creatures are generated out of corruption?" Pasteur dismissed the notion of spontaneous generation, especially the arguments of Félix Pouchet, as "merely betrayed shoddy lab techniques," according to medical historian Roy Porter.

More than 350 years after Leeuwenhoek first glimpsed bacteria, a report published in *Lancet* by the Global Burden of Disease 2019 Antimicrobial Resistance Collaborators, which focused on 33 bacterial pathogens and 11 infectious syndromes (excluding tuberculosis), provides global estimates for the horrendous burden of bacterial infections. Key findings include that in 2019, bacterial infections of all types were linked to 7.7 million deaths globally and that after ischemic heart disease, those infections were the second most common cause of death. Deaths from COVID-19 infection add a complex layer to the accounting of deaths associated with infectious disease. The World Health Organization reported, "On 30 January 2020 COVID-19 was declared a Public Health Emergency of International Concern (PHEIC) with an official death toll of 171. By 31 December 2020, this figure stood at 1,813,188. Yet preliminary estimates suggest the total number of global deaths attributable to the COVID-19 pandemic in 2020 is at least 3 million, representing 1.2 million more deaths than officially reported."

The 2019 study reported that 5 bacteria caused half of the non–COVID-19 deaths: *Staphylococcus aureus*, *Escherichia coli*, *Streptococcus pneumoniae*, *Klebsiella pneumoniae*, and *Pseudomonas aeruginosa.* Three types of bacterial infections—lower respiratory tract infections, bloodstream infections, and peritoneal and intraabdominal infection—were responsible for more than 75% of the fatalities reported in that study. Despite effective available antibiotics for treating the 33 culprit bacteria identified in that study, the gravest and most complex threats to global public health are access to and distribution of those treatments, lack of consistent surveillance and diagnostic abilities, and antimicrobial resistance.

Traditionally, most bacteria have been propagated on culture plates or other culture media, though some bacteria do not grow well or as quickly by those methods. Recalcitrant bacteria are known collectively as fastidious bacteria,[1] and they have a predilection to cause, although not limited to, endocarditis. Ensuing infections create a disproportionate amount of human suffering and death. Examples of fastidious bacteria include *Neisseria gonorrhoeae*, *Campylobacter* spp., and *Helicobacter* spp.

Although Koch and Pasteur did much to develop the germ theory and the cultivation of bacteria in broth and culture media, both significant gifts to science and humanity, fastidious bacteria have continued to present challenges. The problem has been partially solved by recognizing that culturing these organisms requires patience and culture media fortified with certain nutrients. Even those approaches have been supplanted by advanced identification techniques involving genomic sequencing. This issue of EID features articles that describe newer methods for detecting other fastidious bacteria, including *Auritidibacter ignavus*, *Legionella pneumophila*, *Helicobacter fennelliae*, and *Brucella neotomae.* More than 3 centuries later, the foundation laid by Leeuwenhoek steadfastly endures.

[1]The classically recognized fastidious bacteria of clinical concern are known as the HACEK group. The K stands for *Kingella kingae*, named for CDC microbiologist Elizabeth King.

Bibliography

1. Egerton FN. A history of the ecological sciences, part 19: Leeuwenhoek's microscopic natural history. Bull Ecol Soc Am. 2006;87:47–58. https://doi.org/10.1890/0012-9623(2006)87[47:AHOTES]2.0.CO;2
2. Friedman M, Friedland GW. Chapter 3. Antony Leeuwenhoek and bacteria. In: Medicine's 10 greatest discoveries. New Haven and London: Yale University Press; 1998. p. 37–64.
3. Gaynes RP. Chapter 5. Antony van Leeuwenhoek and the birth of microscopy. In: Germ theory: medical pioneers in infectious diseases. Washington (DC): ASM Press, 2011. p. 65. [Quoting Dobell C. Anthony Van Leeuwenhoek and his little animals. New York: Harcourt, Brace and Company; 1932.]
4. Global Burden of Disease 2019 Antimicrobial Resistance Collaborators. Global mortality associated with 33 bacterial pathogens: a systematic analysis for the Global Burden of Disease Study 2019. Lancet. 2022;400:2221–48. https://doi.org/10.1016/S0140-6736(22)02185-7
5. Mauritshuis. Jan Verkolje. The Messenger [cited 2023 Nov 16]. https://www.mauritshuis.nl/en/our-collection/artworks/865-the-messenger
6. Porter R. The greatest benefit to mankind: a medical history of humanity. New York and London: W.W. Norton & Company; 1997.
7. Rijksmuseum. Portrait of Anthonie van Leeuwenhoek, natural philosopher and zoologist in Delft [cited 2023 Nov 16]. https://www.rijksmuseum.nl/en/collection/SK-A-957
8. Robertson LA. Antoni van Leeuwenhoek 1723–2023: a review to commemorate Van Leeuwenhoek's death, 300 years ago: for submission to Antonie van Leeuwenhoek journal of microbiology. Antonie van Leeuwenhoek. 2023;116:919–35. https://doi.org/10.1007/s10482-023-01859-4
9. Simmons NA. An introduction to microbiology for nurses. Oxford: Butterworth-Heinemann; 1980. p. 1–5.
10. Smith KP. Who are the HACEK organisms? [cited 2023 Dec 3]. https://asm.org/Articles/2019/February/WhL-are-the-HACEK-organisms
11. Thomas L. Chapter 15: Germs. In: The lives of a cell: notes of a biology watcher. New York: Penguin Books; 1978. [Originally published by Viking Press; 1974.]
12. University of California Museum of Paleontology. Antony van Leeuwenhoek (1632–1723) [cited 2023 Nov 16]. https://ucmp.berkeley.edu/history/leeuwenhoek.html
13. World Health Organization. The true death toll of COVID-19: estimating global excess mortality [cited 2023 Dec 2]. https://www.who.int/data/stories/the-true-death-toll-of-covid-19-estimating-global-excess-mortality

Address for correspondence: Byron Breedlove, EID Journal, Centers for Disease Control and Prevention, 1600 Clifton Rd NE, Mailstop H16-2, Atlanta, GA 30329-4018, USA; email: wbb1@cdc.gov

EMERGING INFECTIOUS DISEASES®

Upcoming Issue
Vectors

- Multicenter Retrospective Study of Invasive Fusariosis in Intensive Care Units, France
- Overview of Parechovirus A Circulation and Testing Capacities in Europe, 2015–2021
- Rapid Detection of Ceftazidime/Avibactam Susceptibility/Resistance in Enterobacterales by Rapid CAZ-AVI NP Test
- Adapting COVID-19 Contact Tracing Protocols to Accommodate Resource Constraints, Philadelphia, Pennsylvania, USA, 2021
- Invasive Meningococcal Disease Caused by Neisseria meningitidis Serogroup W Sequence Type 11, Western Australia, Australia
- Identification of Large Adenovirus Infection Outbreak at University by Using Multipathogen Testing, South Carolina, USA, 2022
- Lymphocytic Choriomeningitis Virus Lineage V in Wood Mice, Germany
- Post-COVID Rebound of Gonorrhea in England
- Emerging Enterovirus A71 Subgenogroup B5 Causing Severe Hand, Foot, and Mouth Disease, Vietnam, 2023
- Inferring Incidence of Unreported SARS-CoV-2 Infections Using Seroprevalence of ORF8 Antigen
- Phylogenomics of Dengue Virus Isolates Causing Dengue Outbreak, São Tomé and Príncipe, 2022
- Integrating Veterinary Diagnostic Laboratories for Emergency Use Testing during Pandemics
- Nonnegligible Seroprevalence and Predictors of Murine Typhus, Japan
- Nonnegligible Seroprevalence and Predictors of Murine Typhus, Japan• Key Challenges for Respiratory Virus Surveillance: Transitioning out of Acute Phase of SARS-CoV-2 Pandemic
- Residual Immunity to Smallpox Vaccination and Possible Protection from Mpox, China

Complete list of articles in the February issue at https://wwwnc.cdc.gov/eid/#issue-306

Earning CME Credit

To obtain credit, you should first read the journal article. After reading the article, you should be able to answer the following, related, multiple-choice questions. To complete the questions (with a minimum 75% passing score) and earn continuing medical education (CME) credit, please go to http://www.medscape.org/journal/eid. Credit cannot be obtained for tests completed on paper, although you may use the worksheet below to keep a record of your answers.

You must be a registered user on http://www.medscape.org. If you are not registered on http://www.medscape.org, please click on the "Register" link on the right hand side of the website.

Only one answer is correct for each question. Once you successfully answer all post-test questions, you will be able to view and/or print your certificate. For questions regarding this activity, contact the accredited provider, CME@medscape.net. For technical assistance, contact CME@medscape.net. American Medical Association's Physician's Recognition Award (AMA PRA) credits are accepted in the US as evidence of participation in CME activities. For further information on this award, please go to https://www.ama-assn.org. The AMA has determined that physicians not licensed in the US who participate in this CME activity are eligible for AMA PRA Category 1 Credits™. Through agreements that the AMA has made with agencies in some countries, AMA PRA credit may be acceptable as evidence of participation in CME activities. If you are not licensed in the US, please complete the questions online, print the AMA PRA CME credit certificate, and present it to your national medical association for review.

Article Title

Auritidibacter ignavus, an Emerging Pathogen Associated with Chronic Ear Infections

CME Questions

1. Which of the following statements regarding the microbiology of *Auritidibacter ignavus* is most accurate?

A. It is an aerobic, gram-positive cocci
B. It is an aerobic, gram-positive rod
C. It is an anaerobic, gram-negative cocci
D. It is an aerobic, gram-negative rod

2. Which of the following risk factors for A. ignavus otitis was most salient among the 3 cases in the current study?

A. Immunocompromised status
B. Male sex
C. Multiple prior episodes of otitis media
D. None of the above

3. A. ignavus otitis was most associated with resistance to which of the following antibiotics in the current study?

A. Ciprofloxacin
B. Amoxicillin/clavulanate
C. Azithromycin
D. Gentamicin

4. Which of the following physical findings was noted in all 3 cases of *A. ignavus* otitis in the current study?

A. Spore formation on the tympanic membrane
B. Pre-auricular and postauricular lymphadenopathy
C. Temperature greater than 38.5 °C on clinical presentation
D. Stenosis of the external auditory canal

Earning CME Credit

To obtain credit, you should first read the journal article. After reading the article, you should be able to answer the following, related, multiple-choice questions. To complete the questions (with a minimum 75% passing score) and earn continuing medical education (CME) credit, please go to http://www.medscape.org/journal/eid. Credit cannot be obtained for tests completed on paper, although you may use the worksheet below to keep a record of your answers.

You must be a registered user on http://www.medscape.org. If you are not registered on http://www.medscape.org, please click on the "Register" link on the right hand side of the website.

Only one answer is correct for each question. Once you successfully answer all post-test questions, you will be able to view and/or print your certificate. For questions regarding this activity, contact the accredited provider, CME@medscape.net. For technical assistance, contact CME@medscape.net. American Medical Association's Physician's Recognition Award (AMA PRA) credits are accepted in the US as evidence of participation in CME activities. For further information on this award, please go to https://www.ama-assn.org. The AMA has determined that physicians not licensed in the US who participate in this CME activity are eligible for AMA PRA Category 1 Credits™. Through agreements that the AMA has made with agencies in some countries, AMA PRA credit may be acceptable as evidence of participation in CME activities. If you are not licensed in the US, please complete the questions online, print the AMA PRA CME credit certificate, and present it to your national medical association for review.

Article Title

Early-Onset Infection Caused by *Escherichia coli* ST1193 in Late Preterm and Full-Term Neonates

CME Questions

1. Which of the following statements regarding early-onset neonatal sepsis (EOS) is most accurate?

A. EOS is defined by a positive blood or cerebrospinal fluid culture within 36 hours after birth
B. EOS affects approximately 1 in 1000 live births
C. Meningitis complicates nearly 50% of cases of EOS
D. EOS due to either Streptococcus agalactiae or E coli can be prevented through peripartum prophylaxis with antibiotics

2. Which of the following statements regarding virulence factors and antibiotic resistance among E coli isolates in the current study is most accurate?

A. Virulence factors and antibiotic resistance were more common in EOS vs healthy vaginal carriage (HVC) isolates
B. Virulence factors, but not antibiotic resistance, were more common in EOS vs HVC isolates
C. Antibiotic resistance, but not virulence factors, was more common in EOS vs HVC isolates
D. Virulence factors and antibiotic resistance were more common in HVC vs EOS isolates

3. Which of the following statements regarding sequence type (ST)1193 E coli EOS isolates in the current study is most accurate?

A. All cases were diagnosed in a single hospital
B. All cases had a preterm delivery
C. None of the mothers had received peripartum antibiotics
D. All strains were resistant to fluoroquinolones

4. Which of the following statements regarding EOS among term vs preterm infants in the current study is most accurate?

A. Type A was found significantly more frequently among preterm infants
B. Type F was found significantly more frequently among term infants
C. ST95 was found significantly more frequently among preterm infants
D. Generally, phylogenetic groups and ST/sequence type complex (STc) were similar in term and preterm infants

Emerging Infectious Diseases
Photo Quiz Articles

Volume 14, Number 9
September 2008

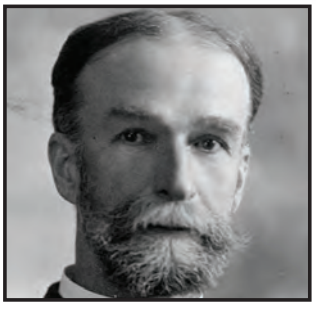

Volume 14, Number 12
December 2008

Volume 15, Number 9
September 2009

Volume 15, Number 10
October 2009

Volume 16, Number 6
June 2010

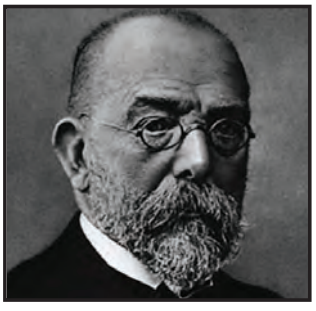

Volume 17, Number 3
March 2011

Volume 17, Number 12
December 2011

Volume 19, Number 4
April 2013

Volume 20, Number 5
May 2014

Volume 21, Number 9
September 2015

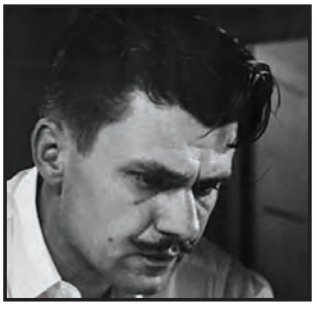

Volume 22, Number 8
August 2016

Volume 28, Number 3
March 2022

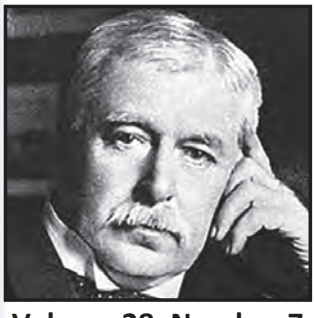

Volume 28, Number 7
July 2022

Click on the link below to read about the people behind the science.

https://bit.ly/3LN02tr

See requirements for submitting a photo quiz to EID.

https://bit.ly/3VUPqfj

EID Journal